

CHAMBER STUDIES OF SECONDARY ORGANIC AEROSOL FORMATION

Thesis by
Nga Lee Ng

In Partial Fulfillment of the Requirements for the
Degree of Doctor of Philosophy



California Institute of Technology

Pasadena, California

2007

(Defended May 22, 2007)

© 2007

Nga Lee Ng

All Rights Reserved

學貴有恆

“Perseverance is the key to learning.” – Chinese proverb

Acknowledgements

Looking back at my years at Caltech, I feel blessed every step along the way. It has been such a wonderful journey, not just because of all the great science in the roof lab, but also the many wonderful people that I got to know and become friends with.

I would like to express my sincere gratitude to my advisors, Professor John Seinfeld and Professor Richard Flagan, for their continuous trust, support, and guidance throughout the years. Their scientific insights are invaluable, and their enthusiasm about science is especially inspiring. I thank them for giving me the opportunity to join the lab. Despite their busy schedules, John and Rick are always there when I need guidance. They have been truly supportive and understanding and I could not ask for better advisors. I would also like to thank my thesis committee members, Professor Paul Wennberg and Professor Michael Hoffmann, for their valuable time and comments. I also thank my undergrad advisor, Professor Chak Chan, for introducing me to the field of atmospheric science and for his constant support.

I have been very fortunate to be part of such a supportive, friendly, and fun research group. I would like to thank the past and present group members, especially the lab people for making every day in the lab so enjoyable: Tomtor Varutbangkul, Roya Bahreini, Melita Keywood, Tracey Rissman, Song Gao, Jesse Kroll, Jason Surratt, Shane Murphy, Armin Sorooshian, Harmony Gates, Arthur Chan, and Puneet Chhabra. Because of the collaborative nature of our work, I could not have got all the work done without their help. They are also a constant source of laughter and encouragement; with them even the most stressful periods in the lab seem more manageable. I also thank the

“modelers” of the group, Philip Stier, Daven Henze, Anne Chen, Candy Tong, Amir Hakami, and Julia Lu for their support.

I am especially grateful to Tomtor and Roya for their patience in teaching me so many things in the lab, from little things like “the difference between a back ferrule and a front ferrule”, to how to operate the many instruments, and for always being there to help me even when they were overwhelmed with their own work. The two and a half years with Jesse in the lab have been incredible. We built our friendship through running hundreds and hundreds of chamber experiments (final checks!), and together we survived the ups and downs of the experiments. Jesse taught me so much about atmospheric chemistry and I am grateful for his patience and guidance. I considered myself extraordinarily lucky to have the opportunity to work so closely with such a great scientist and I treasure our friendship dearly.

I am grateful to Nathan Dalleska for his help with GC troubleshooting, Richard Gerhart for fixing/making the numerous glasswares for us, to Mike Vondrus for his help in machining various parts of the experimental setup. I would also like to thank Ann Hilgenfeldt and Yvette Grant for placing endless orders for repairs and parts. A big thanks also goes to Kathy Bubash for her administrative help.

I am glad to have met so many wonderful friends outside the lab who made my time here enjoyable, especially Joyce Poon, Michelle Friedman, Marcelo Guzman, Peter Leong, Shahin Rahman, Tonci Crmaric, Nikoo Saber, Mike Rubel, Anita Lee, as well as my “Hong Kong friends” at Caltech. I enjoyed all the fun activities we had. Fourth year is an especially fun-filled year for me, because of some very special friends, Tracey Rissman, Adam Olsen, Philip Stier, and Marco Seidel. I will always remember all the

happy times we shared. I would also like to thank Jang Wook Choi, whether we were working on problem sets or studying for quals, I really appreciate his companionship and support.

Even though I am thousands of miles away from home, my friends on the other side of the ocean keep showering me with their support and encouragement throughout the years and I am very grateful for that. A very special thanks goes to Yee Man Lai, for being such a great friend for almost twenty years and for always sharing my dreams with me.

Finally, I thank my parents, my sister, and my brother for their love and support. I am grateful to my parents for instilling within me the importance of learning and to never to give up, for their unwavering trust in my abilities, and for understanding my move far away from home to follow my own path. I could not have finished this without the unceasing support and encouragement they have given me throughout my life.

Abstract

Atmospheric oxidation of volatile organic compounds leads to the formation of secondary organic aerosol (SOA). Laboratory chambers provide a controlled environment for investigating aerosol formation and evolution. This thesis presents results on aerosol formation from a wide range of parent organic compounds under a variety of experimental conditions.

The effect of particle-phase acidity on aerosol formation is explored in a series of alkene ozonolysis experiments. Oligomeric species are detected regardless of the particle-phase acidity, indicating the ubiquitous existence of particle-phase reactions. As acidity increases, larger oligomers are formed more abundantly and aerosol yields also increase. Volatile organic compounds generally not considered to be SOA precursors, including isoprene and glyoxal, have been shown to lead to aerosol formation. Uptake of glyoxal into particles is evidence that small molecules can potentially produce aerosol via reactive absorption. Although there is strong evidence that heterogeneous reactions play an important role in SOA formation, the detailed mechanisms remain poorly understood. In a comprehensive study on aerosol formation from biogenic hydrocarbons, it is found that data on aerosol growth as a function of the amount of hydrocarbon reacted provide important insights into the general aerosol formation mechanisms by identifying rate-determining steps and whether SOA is formed from first- or second-generation products.

The mechanism of aerosol formation by isoprene is specifically investigated over a range of NO_x concentrations. Aerosol yields are found to decrease substantially with increasing NO_x . The same NO_x dependence is observed for monoterpenes (α -pinene), as well as aromatic hydrocarbons (*m*-xylene, toluene, and benzene). It is suggested that

peroxy radical chemistry plays the central role in the observed NO_x dependence. The NO_x dependence for larger compounds is, however, different from that of isoprene, monoterpenes, and aromatics. For sesquiterpenes such as longifolene and aromadendrene, aerosol yields increase with increasing NO_x concentration. The reversal of the NO_x dependence of SOA formation for the sesquiterpenes appears to be the result of formation of relatively nonvolatile organic nitrates, and/or the isomerization of large alkoxy radicals that leads to less volatile products.

Table of Contents

Acknowledgements.....	iv
Abstract.....	vii
List of Tables	xv
List of Figures.....	xvii
Chapter 1: Introduction.....	1
Chapter 2: Contribution of First- versus Second-Generation Products to Secondary Organic Aerosols Formed in the Oxidation of Biogenic Hydrocarbons.....	5
2.1 Abstract.....	6
2.2 Introduction.....	7
2.3 Experimental.....	11
2.4 Results.....	15
2.4.1 Ozonolysis studies	15
2.4.2 Photooxidation studies.....	16
2.5 Discussion.....	17
2.5.1 Time-dependent vs. final SOA growth	19
2.5.1.1 α -pinene ozonolysis (one double bond).....	19
2.5.1.2 Terpinolene ozonolysis (more than one double bond).....	20
2.5.2 Chemistry of individual compounds.....	22
2.5.2.1 α -pinene ozonolysis.....	22
2.5.2.2 α -pinene photooxidation.....	23
2.5.2.3 Terpinolene ozonolysis	24
2.5.2.4 Terpinolene and limonene photooxidation	26

2.5.2.5 Isoprene photooxidation.....	27
2.5.2.6 Other compounds with multiple double bonds	28
2.5.2.7 β -caryophyllene ozonolysis	29
2.5.2.8 Longifolene photooxidation.....	30
2.6 Implications for aerosol formation.....	31
2.7 Acknowledgements.....	33
2.8 References.....	34
Chapter 3: Particle Phase Acidity and Oligomer Formation in Secondary Organic Aerosol	70
3.1 Abstract.....	71
3.2 Introduction.....	71
3.3 Experimental.....	73
3.4 Results and discussion	75
3.5 Acknowledgements.....	80
3.6 References.....	80
Chapter 4: Chamber Studies of Secondary Organic Aerosol Growth by Reactive Uptake of Simple Carbonyls	90
4.1 Abstract.....	91
4.2 Introduction.....	91
4.3 Experimental.....	97
4.4 Results and discussion	103
4.4.1 Uptake of organics: carbonyl compounds other than glyoxal	103
4.4.2 Uptake of organics: glyoxal.....	105

4.5 Implications.....	109
4.6 Acknowledgements.....	115
4.7 References.....	115
Chapter 5: Secondary Organic Aerosol Formation from Isoprene Photooxidation under High-NO _x Conditions.....	131
5.1 Abstract.....	132
5.2 Introduction.....	132
5.3 Experimental.....	135
5.4 Results and discussion	136
5.5 Acknowledgements.....	141
5.6 References.....	141
Chapter 6: Secondary Organic Aerosol Formation from Isoprene Photooxidation.....	148
6.1 Abstract.....	149
6.2 Introduction.....	149
6.3 Experimental.....	153
6.4 Results.....	155
6.4.1 Blank Runs.....	155
6.4.2 Low-NO _x experiments	155
6.4.3 High-NO _x experiments.....	157
6.4.4 Isoprene oxidation products.....	159
6.5 Discussion.....	159
6.5.1 General mechanism of aerosol growth	159
6.5.2 Role of NO _x	162

6.5.3 Rapid photochemical loss of SOA.....	166
6.6 Acknowledgements.....	168
6.7 References.....	168
Chapter 7: Effect of NO _x on Secondary Organic Aerosol (SOA) Formation from Photooxidation of Terpenes	188
7.1 Abstract.....	189
7.2 Introduction.....	189
7.3 Experimental Section.....	191
7.4 Aerosol Yields	196
7.4.1 α -pinene photooxidation.....	196
7.4.2 Longifolene photooxidation.....	197
7.4.3 Aromadendrene photooxidation.....	198
7.5 Chemical composition of SOA	199
7.5.1 Aerosol Mass Spectrometer (Q-AMS) measurements.....	199
7.5.2 Offline chemical analysis.....	201
7.6 Discussion.....	203
7.6.1 Effect of hydrocarbon size on NO _x dependence	203
7.6.2 General mechanisms of aerosol growth.....	207
7.6.2.1 Loss of semivolatiles.....	207
7.6.2.2 SOA formation from higher generation products	209
7.7 Implications.....	210
7.8 Appendix: Description of PTR-MS technique.....	212
7.9 Acknowledgements.....	214

7.10 References.....	214
Chapter 8: Secondary Organic Aerosol Formation from <i>m</i> -xylene, toluene, and benzene	241
8.1 Abstract.....	242
8.2 Introduction.....	242
8.3 Experimental.....	245
8.4 Results.....	248
8.4.1 High-NO _x conditions	248
8.4.2 Low-NO _x conditions	251
8.4.3 SOA yield parameters	252
8.5 Discussion.....	254
8.5.1 Effect of NO _x on SOA yields.....	254
8.5.2 Effect of oxidation rate	257
8.5.3 General mechanism of SOA formation.....	260
8.5.4 Effect of seed acidity	262
8.6 Implication for SOA growth from aromatic hydrocarbons.....	263
8.7 Acknowledgements.....	264
8.8 References.....	265
Chapter 9: Conclusions.....	290
Appendix A: Reactions of Semivolatile Organics and Their Effects on Secondary Organic Aerosol Formation	295
Appendix B: Low-Molecular-Weight and Oligomeric Components in Secondary Organic Aerosol from the Ozonolysis of Cycloalkenes and α -Pinene.....	302

Appendix C: Chemical Composition of Secondary Organic Aerosol Formed from the Photooxidation of Isoprene	321
Appendix D: Evidence for Organosulfates in Secondary Organic Aerosol	348
Appendix E: Characterization of 2-Methylglyceric Acid Oligomers in Secondary Organic Aerosol Formed from the Photooxidation of Isoprene Using Trimethylsilylation and Gas Chromatography/Ion Trap Mass Spectrometry	360
Appendix F: Measurements of Secondary Organic Aerosol from Oxidation of Cycloalkenes, Terpenes, and <i>m</i> -xylene Using an Aerodyne Aerosol Mass Spectrometer	377
Appendix G: Secondary Aerosol Formation from Atmospheric Reactions of Aliphatic Amines	393
Appendix H: Hygroscopicity of Secondary Organic Aerosols Formed by Oxidation of Cycloalkenes, Monoterpenes, Sesquiterpenes, and Related Compounds.....	419
Appendix I: Gas-Phase Products and Secondary Aerosol Yields from the Ozonolysis of Ten Different Terpenes	442
Appendix J: Gas-Phase Products and Secondary Aerosol Yields from the Photooxidation of 16 Different Terpenes.....	461

List of Tables

Table 2. 1. Parent hydrocarbon studied	43
Table 2. 2. Initial conditions and data for ozonolysis experiments	46
Table 2. 3. Initial conditions and data for photooxidation experiments	47
Table 2. 4. Ozonolysis - major first-generation products and their molar yields	48
Table 2. 5. Photooxidation - major first-generation products and their molar yields	49
Table 4. 1. Experimental conditions and measured particle growth for glyoxal uptake experiments ^A	126
Table 5. 1. Experimental conditions and results	145
Table 6. 1. Experimental conditions and results for NO _x -free experiments. ¹	177
Table 6. 2. Experimental conditions and results for high-NO _x experiments. ¹	178
Table 7. 1. Parent hydrocarbons studied	220
Table 7. 2. Initial conditions and data for α -pinene experiments	221
Table 7. 3. Initial conditions and data for longifolene experiments	222
Table 7. 4. Initial conditions and data for aromadendrene experiments	223
Table 7. 5. Estimated effective SOA densities	224
Table 7. 6. α -Pinene acidic SOA components detected by the UPLC/ESI-TOFMS instrument	225
Table 7. 7. Longifolene SOA components detected by the UPLC/ESI-TOFMS instrument	226
Table 8. 1. Aromatic hydrocarbons studied	272
Table 8. 2. Initial conditions and data for high-NO _x (HONO) experiments	273
Table 8. 3. Initial conditions and data for low-NO _x (H ₂ O ₂) experiments	274

Table 8. 4. Initial conditions and data for acid/nonacid experiments	275
Table 8. 5. Estimated effective SOA densities	276
Table 8. 6. Aerosol yield parameters	277

List of Figures

Figure 2. 1. α -pinene ozonolysis and aerosol mass formation	50
Figure 2. 2. Terpinolene ozonolysis and aerosol mass formation.....	51
Figure 2. 3. Time-dependent growth curves for all compounds studied in ozonolysis experiments (except linalool, which does not have significant aerosol growth), note that the axes have different scales.....	52
Figure 2. 4. Time-dependent growth curves for all compounds studied in photooxidation experiments (except longifolene, which is shown in Figure 2.20), note that the axes have different scales.....	53
Figure 2. 5. Time-dependent and final growth curves for α -pinene ozonolysis. The large diamonds represent final growth data through which the yield curve has been fit.....	54
Figure 2. 6. AMS relative delta time series plot for α -pinene ozonolysis. Unsaturated organics yield delta values ≤ 0 , and oxygenated organics yield delta values ≥ 2	55
Figure 2. 7. Time-dependent and final growth curves for terpinolene ozonolysis. The large diamonds represent final growth data through which the yield curve has been fit.	56
Figure 2. 8. Time evolution of pinonaldehyde in α -pinene ozonolysis. The concentration of pinonaldehyde is the average of the upper and lower limits measured by PTR-MS (20).	57

Figure 2. 9. Time evolution of pinonaldehyde in α -pinene photooxidation. The concentration of pinonaldehyde is the mid-range mixing ratio measured by PTR-MS (21).	58
Figure 2. 10. Time evolution of m/z 93 and m/z 111 ions for terpinolene ozonolysis; m/z 93 is the dehydrated fragment of m/z 111.	59
Figure 2. 11. The amount of the intermediate product m/z 111 (including the dehydrated fragment m/z 93) measured, formed and reacted over time for terpinolene ozonolysis	60
Figure 2. 12. SOA mass formed as a function of the amount of the intermediate product m/z 111 reacted for terpinolene ozonolysis	61
Figure 2. 13. SOA mass formed as a function of the amount of the intermediate product m/z 111 reacted for terpinolene photooxidation	62
Figure 2. 14. SOA mass formed as a function of the amount of the intermediate product m/z 169 (including its fragments and isotopes) reacted for limonene photooxidation	63
Figure 2. 15. Time evolution of methacrolein + methyl vinyl ketone for isoprene photooxidation	64
Figure 2. 16. SOA mass formed as a function of the amount of the methacrolein + methyl vinyl ketone reacted for isoprene photooxidation	65
Figure 2. 17. β -caryophyllene ozonolysis and aerosol mass formation	66
Figure 2. 18. β -caryophyllene and ozone reacted over the course of the experiment (Table 2.2: Experiment on 3/21/2003)	67

Figure 2. 19. AMS relative delta time series plot for β -caryophyllene ozonolysis.

Unsaturated organics yield delta values ≤ 0 , and oxygenated organics yield delta values ≥ 2 68

Figure 2. 20. Growth curve for longifolene photooxidation..... 69

Figure 3. 1. The relative yield difference (RYD) of SOA between the acid and nonacid

cases for seven pairs of α -pinene ozonolysis experiments on MgSO_4 seeds, two pairs on $(\text{NH}_4)_2\text{SO}_4$ seeds, as well as two pairs of terpinolene ozonolysis experiments on MgSO_4 seeds. The absolute SOA yield is defined as the mass of SOA produced relative to the mass of hydrocarbon consumed. The RYD is defined as the difference in the absolute SOA yield between the acid and nonacid cases normalized to the nonacid-case yield. Corresponding to the seven α -pinene mixing ratios shown (i.e., 12ppb, 25ppb, 48ppb, 52ppb, 96ppb, 120ppb and 135ppb), the absolute SOA yields are 0.30, 0.32, 0.35, 0.38, 0.46, 0.52 and 0.53, respectively, for the nonacid cases, and are 0.41, 0.43, 0.44, 0.47, 0.53, 0.57, 0.57, respectively, for the acid cases..... 82

Figure 3. 2. Ion trap mass spectrum (+ ion mode) of the extract of SOA from the

ozonolysis of (a) 120 ppb α -pinene on MgSO_4 -only seed (RH = 55%). In the m/z range up to 1600, the average background ion intensity is ~ 400000 , which is labeled as the dashed line in this and the following MS, unless noted otherwise. See Supporting Information, Figure 3.S3, for a typical background MS. (b) 120 ppb α -pinene on MgSO_4 - H_2SO_4 seed. Other experimental conditions are identical to (a). (c) 72 ppb α -pinene on $(\text{NH}_4)_2\text{SO}_4$ -only seed.

Other experimental conditions are identical to (a). (d) 72 ppb α -pinene on $(\text{NH}_4)_2\text{SO}_4$ - H_2SO_4 seed. Other experimental conditions are identical to (a). . 83

- Figure 3. 3. MS/MS (- ion mode) of (a) 357 ion in the SOA from the same α -pinene ozonolysis experiment as in Figure 3.2(a), its likely structure and fragmentation (hydrogen rearrangement and dehydrogenation not shown), and the structure of the monomer. See Supporting Information, Figure 3.S5 for the detailed structures of fragment ions. (b) 245 ion in the SOA from 1-methyl cyclopentene ozonolysis, its likely structures and fragmentation, and the structures of the monomers. 86
- Figure 3. 4. Ion trap mass spectrum (+ ion mode) of the extract of SOA from the ozonolysis of 180ppb α -pinene in the presence of dry $(\text{NH}_4)_2\text{SO}_4$ -only seed. Large amounts of both small and large oligomers are present in this SOA. .. 88
- Figure 3. 5. Ion trap mass spectrum (+ ion mode) of the extract of SOA from the ozonolysis of 50ppb α -pinene in the absence of seed particles. This IT-MS is similar to that of the SOA from its parallel ozonolysis experiment in the presence of MgSO_4 seed particles, and is also similar to that of the SOA from other α -pinene ozonolysis experiments, such as the one shown in Figure 3.2(a). The background ion intensities are lower than 5% of the maximum intensity ($m/z = 381.0$, designated as 100%). 89
- Table 4. 1. Experimental conditions and measured particle growth for glyoxal uptake experiments^A. 126
- Figure 4. 1. Structures of the carbonyls studied in this work. 127

- Figure 4. 2. Sample DMA volume data for chamber experiments. Introduction of inorganic seed corresponds to $t=0$; the gradual decrease in volume is a result of particle loss to the chamber walls. Grey circles: inorganic seed only. Black circles: inorganic seed (ammonium sulfate/sulfuric acid), followed by introduction of 500 ppb 2,4-hexadienal at $t=50$ min (dashed line). Data are scaled so that starting particle volumes are equivalent. 128
- Figure 4. 3. DMA volume data growth for a glyoxal + inorganic seed experiment. As in Figure 4.2, introduction of inorganic seed corresponds to $t=0$. Grey circles: inorganic seed only. Black circles: inorganic seed (ammonium sulfate/sulfuric acid), followed by introduction of 200 ppb glyoxal at $t=53$ min (dashed line). Data are scaled so that starting particle volumes are equivalent. 129
- Figure 4. 4. Particle growth as a function of gas-phase glyoxal concentration and initial seed volume, assuming unit density of the organic fraction of the aerosol. Black circles: ammonium sulfate seed. Grey squares: mixed ammonium sulfate/sulfuric acid seed. The fit shown is to the ammonium sulfate data only. The dashed line near the bottom of the figure is the growth expected using the measured Henry's Law constant (in seawater) of 3.6×10^5 M/atm [Zhou and Mopper, 1990]. 130
- Figure 5. 1. A typical experiment (no. 6 in Table 5.1), showing [isoprene] (black circles), $[O_3]$ (dark gray lines), $[NO]$ (light gray lines), $[NO_2]$ (black lines), and particle volume increase (black dots) as a function of reaction time. Gaps in the O_3 and NO_x data are a result of switching between chambers. 146
- Figure 5. 2. Aerosol growth as a function of concentration of isoprene reacted. 147

Figure 6. 1. Structures and measured yields of first-generation products of the OH-initiated oxidation of isoprene under high-NO _x conditions. ^a Tuazon and Atkinson (5). ^b Paulson et al. (6). ^c Miyoshi et al. (7). ^d Sprengnether et al. (8). ^e Chen et al. (9). ^f Zhao et al. (10). ^g Baker et al. (11).....	179
Figure 6. 2. Reaction profile of a typical isoprene photooxidation experiment under NO _x -free conditions (Experiment 5).	180
Figure 6. 3. Typical AMS spectrum (m/z ≥ 40) of SOA formed from isoprene photooxidation under low-NO _x conditions. For clarity, masses in which the organics overlap with peaks from sulfate (m/z 48-50, 64-66, 80-83, 98-100) and tungsten (from the filament; m/z 182, 184-186) have been omitted. Light gray bars correspond to negative values after data analysis.	181
Figure 6. 4. Measured SOA growth versus isoprene reacted (low-NO _x conditions). Gray circles: maximum growth; black circles: final growth, after photochemical loss of SOA (see text for details). Each pair of points (at a single value of isoprene reacted) corresponds to one experiment. Data are taken from Table 6.1; SOA mass is calculated using a density of 1.25 g/cm ³	182
Figure 6. 5. Reaction profile of a typical isoprene photooxidation experiment under high-NO _x conditions (Experiment 11). Decay of isoprene is rapid, with most consumed in the first 30 minutes of reaction, so is omitted for clarity.....	183
Figure 6. 6. Typical AMS spectrum of SOA formed from isoprene photooxidation under high-NO _x conditions. See description of Figure 6.3 for details.	184

Figure 6. 7. SOA growth as a function of initial NO _x concentration, for a fixed isoprene concentration (45 ± 4 ppb). Results shown are from Table 6.2; the NO _x -free point is final growth from Experiment 2, Table 6.1.	185
Figure 6. 8. AMS spectrum of SOA formed from methacrolein photooxidation under high-NO _x conditions. See description of Figure 6.3 for details. The spectrum shown is similar to that of isoprene photooxidation (Figure 6.6), with the same major peaks, suggesting the importance of methacrolein as an intermediate in SOA formation from isoprene oxidation under high-NO _x conditions.	186
Figure 6. 9. Reaction mechanism of isoprene oxidation, showing the formation of first-generation products. For clarity, only one of four possible alkyl radicals and one of six possible hydroperoxy radicals are shown. The first-generation reaction products are all unsaturated so may be rapidly oxidized to second-generation products.	187
Figure 7. 1. Time-dependent growth curves for α-pinene photooxidation under different NO _x conditions.	227
Figure 7. 2. Time-dependent growth curves for longifolene photooxidation under high- and low-NO _x conditions. The mixing ratios in the legend refer to the amount of longifolene reacted in each experiment.	228
Figure 7. 3. Time-dependent growth curves for longifolene photooxidation with H ₂ O ₂ as an OH precursor. Aerosol growth in the presence of ~300 ppb NO (Experiment 7 in Table 7.3) exceeds that without NO.	229
Figure 7. 4. SOA growth as a function of initial NO _x concentrations, for a fixed longifolene concentration (~4.3 ppb). Results shown are from Table 7.3.	230

- Figure 7. 5. SOA growth as a function of initial NO_x concentration, at a fixed initial aromadendrene concentration (~5 ppb). Results shown are from Table 7.4. 231
- Figure 7. 6. AMS high-NO_x spectra signal versus low-NO_x spectra signal for α-pinene photooxidation. Each mass fragment is normalized by the total signal. The solid black line is the one-to-one line. The spectra are taken when all hydrocarbon has been consumed. 232
- Figure 7. 7. AMS high-NO_x spectra signal versus low-NO_x spectra signal for longifolene photooxidation. Each mass fragment is normalized by the total signal. The solid black line is the 1:1 line. The spectra are taken when all hydrocarbon has been consumed..... 233
- Figure 7. 8. Ratio of the sum of masses at *m/z* 30 and 46 to total organic mass as a function of organic mass as measured by the AMS for α-pinene photooxidation. The higher ratio for high- NO_x experiments suggests the formation of nitrate species..... 234
- Figure 7. 9. Ratio of the sum of masses at *m/z* 30 and 46 to total organic mass as a function of organic mass as measured by the AMS for longifolene photooxidation. The higher ratio for high- NO_x experiments suggests the formation of nitrate species..... 235
- Figure 7. 10. Changes in AMS spectrum over the course of longifolene photooxidation under high-NO_x conditions. Top panel: Fractional contribution of each mass fragment to the total organic and nitrate signal during the growth phase of the experiment. Bottom panel: Percentage change of each mass fragment from the growth phase to the point at which all of the hydrocarbon is consumed..... 236

Figure 7. 11. Changes in AMS spectrum over the course of longifolene photooxidation under low-NO_x conditions. Top panel: Fractional contribution of each mass fragment to the total organic and nitrate signal during the growth phase of the experiment. Bottom panel: Percentage change of each mass fragment from the growth phase to the point at which all of the hydrocarbon is consumed..... 237

Figure 7. 12. UPLC/ESI-TOFMS extracted ion chromatograms (EICs) (m/z 346 + 374 + 390) for longifolene photooxidation experiments. The even $[M - H]^-$ ions listed above the chromatographic peaks correspond to organic nitrates detected in longifolene SOA. No organic nitrates are detected in the H₂O₂ experiment. The HONO experiment has the widest array of organic nitrates detected (as shown in Table 7.7), as well as the largest chromatographic peaks; m/z 372 is the only exception, and is most abundant in the “H₂O₂ + NO” experiment. These EICs are directly comparable as the volume of chamber air sampled is approximately the same (2 m³). 238

Figure 7. 13. General schematic of gas-phase peroxy radical chemistry in SOA formation. 239

Figure 7. 14. A kinetic scheme depicting the competition between gas-particle partitioning and irreversible loss of the gas-phase semivolatiles. X represents the product of generic loss of semivolatile species A_g by chemical reaction, and/or loss to chamber walls. k' is the pseudo-first-order rate constant ($k' = k_{OH}[OH]$) for photooxidation of the parent hydrocarbon; k_g is the first-order rate constant of loss of semivolatiles..... 240

Figure 8. 1. Typical reaction profile of a high-NO _x experiment in which HONO is used as the OH precursor (initial conditions: 89.3 ppb of <i>m</i> -xylene, 470 ppb NO, and 473 ppb NO ₂).	278
Figure 8. 2 (a). Reaction profile of a typical classical photooxidation experiment (initial conditions: 101.6 ppb <i>m</i> -xylene, 97 ppb NO, and 26 ppb NO ₂). (b) Reaction profile of a classical photooxidation experiment in the presence of ~1 ppm NO _x (initial conditions: 94.8 ppb <i>m</i> -xylene, 878 ppb NO, and 65 ppb NO ₂). A negligible amount of ozone is formed during the experiment, and no SOA is formed.	279
Figure 8. 3. Time-dependent growth curves for <i>m</i> -xylene photooxidation under high-NO _x conditions. The concentrations in the legend refer to the amount of <i>m</i> -xylene reacted in each experiment.	281
Figure 8. 4. Time-dependent growth curves for toluene photooxidation under high-NO _x conditions. The concentrations in the legend refer to the amount of toluene reacted in each experiment.	282
Figure 8. 5. Time-dependent growth curves for benzene photooxidation under high- and low-NO _x conditions. Under high-NO _x conditions, the initial benzene concentration is 337 ppb (12% reacted). Under low-NO _x conditions, the initial benzene concentration is 395 ppb (16% reacted) and the system has a constant yield of 37%.	283
Figure 8. 6. Time-dependent growth curves for <i>m</i> -xylene photooxidation under low-NO _x conditions. The concentrations in the legend refer to the amount of <i>m</i> -xylene reacted in each experiment. The system exhibits a constant yield of 36%...	284

- Figure 8. 7. Time-dependent growth curves for toluene photooxidation under low-NO_x conditions. The concentrations in the legend refer to the amount of toluene reacted in each experiment. The system exhibits a constant yield of 30%... 285
- Figure 8. 8. Yield curves for toluene and *m*-xylene under high-NO_x conditions. The parameters for fitting the yield curves are, toluene: $\alpha_1 = 0.058$, $K_{om,1} = 0.430$, $\alpha_2 = 0.113$, and $K_{om,2} = 0.047$; *m*-xylene: $\alpha_1 = 0.031$, $K_{om,1} = 0.761$, $\alpha_2 = 0.090$, and $K_{om,2} = 0.029$ 286
- Figure 8. 9. Time-dependent growth curves for toluene photooxidation in the presence of neutral seed versus acidic seed. 287
- Figure 8. 10. A simplified SOA formation mechanism for toluene photooxidation. X represents the generic non particle-phase product from all gas-phase loss processes. 288
- Figure 8. 11. Comparison of *m*-xylene high-NO_x yield curve obtained in the current work to that from Odum et al. (1996). The yield curve from Odum et al. (1996) has been corrected for the temperature (25°C) of this study and density (1.48 g cm⁻³) of the SOA..... 289

Chapter 1

Introduction

Introduction

Aerosols are suspended solid or liquid particles and they affect air quality, human health and the earth's climate. Aerosols can be classified into two main categories according to their formation processes. Primary aerosols are emitted directly from different sources into the atmosphere, while the oxidation of organic gases leads to the formation of low-volatility products that partition into the condensed phase and result in the formation of secondary organic aerosol (SOA). Biogenic hydrocarbons emitted by vegetation and aromatics from anthropogenic sources are important precursors for SOA formation. The main oxidants in the atmosphere are ozone (O_3), hydroxyl radical (OH), and nitrate radical (NO_3). SOA contributes significantly to the total ambient organic aerosols in urban areas, as well as regionally and globally.

Laboratory chambers provide a controlled environment to study the formation and evolution of secondary organic aerosol, by isolating specific compounds of interest and controlling the oxidation environment. Since identification and quantification of all oxidation products from parent hydrocarbons are difficult, aerosol yields have been used in the study of secondary precursor organics. Aerosol yields indicate the aerosol-forming potential of various precursor organics. Yield is defined as the ratio of the mass concentration of aerosol formed from the oxidation of a given parent hydrocarbon to that of the hydrocarbon reacted: $Y = \Delta M_o / \Delta HC$, where ΔM_o ($\mu g m^{-3}$) is the organic aerosol mass produced for a certain reacted amount of hydrocarbon ΔHC ($\mu g m^{-3}$). While yield curves (Y plotted against ΔM_o) have proven to be useful in representing SOA formation, the general mechanisms of SOA formation cannot be readily inferred. In chapter 2 it is shown that this model can be extended for interpretation of laboratory SOA growth data

in terms of underlying chemistry, by plotting experimentally measured aerosol growth, ΔM_o , as a function of the amount of hydrocarbon reacted, ΔHC (growth curve). The growth curve approach is applied in a comprehensive study on aerosol formation from biogenic hydrocarbons to study the general aerosol formation mechanisms.

In chapter 3 the effect of particle-phase acidity on aerosol formation is explored in a series of alkene ozonolysis experiments, including α -pinene and 6 cycloalkenes of various carbon numbers and substitutions. The aerosol yields from α -pinene ozonolysis are systematically studied over a range of initial hydrocarbon concentrations, in the presence of seed particles of differing acidity. The composition of the aerosols formed are presented.

Volatile organic compounds previously not considered to be SOA precursors, including glyoxal and isoprene, are shown to lead to aerosol formation. In chapter 4 the potential for aerosol growth via heterogeneous reactions for a number of small carbonyls is examined by measuring changes in particle volume and composition when inorganic seed and gas-phase carbonyls are introduced into the chambers. Glyoxal is the only single carbonyl that leads to substantial aerosol growth and this reactive uptake is discussed in detail. Chapter 5 presents the results on the first study on secondary organic aerosol formation from isoprene photooxidation under high- NO_x conditions in which HONO is used as the OH precursor. In chapter 6 the mechanism of aerosol formation by isoprene photooxidation is comprehensively investigated over a range of experimental conditions, namely isoprene and NO_x concentrations. The effect of NO_x concentration on aerosol yields and composition is discussed. In chapter 7 the effect of NO_x levels on SOA formation from photooxidation of larger biogenic hydrocarbons such as monoterpenes

(α -pinene) and sesquiterpenes (longifolene and aromadendrene) are investigated by performing experiments under two limiting NO_x conditions, as well as varying the amount of NO_x present systematically. The SOA yields and composition under different NO_x conditions is presented.

Besides biogenic compounds, aerosol formation from aromatic hydrocarbons, including *m*-xylene, toluene, and benzene are investigated under different NO_x conditions. The results are presented in chapter 8. Additionally, the effect of seed aerosol acidity on SOA formation is studied under both high- and low-NO_x conditions. The SOA yield parameters obtained at the two NO_x limits allow one to parameterize the NO_x dependence of SOA formation for use in atmospheric models.

Finally, chapter 9 summarizes the findings presented in the previous seven chapters. Appendix A presents results from a kinetic model of the behavior of a semivolatile compound which may undergo irreversible reactions in both the gas and particle phases in addition to partitioning. The effect of such loss processes on aerosol yields is discussed. Appendices B-J present results on studies of SOA composition and formation mechanisms with a wide range of instruments and analytical techniques, including filter sample analysis (Appendices B-E), Aerosol Mass Spectrometer (AMS, Appendices F and G), and Hygroscopicity Tandem Differential Mobility Analyzer (HTDMA, Appendix H). The gas-phase composition from the ozonolysis and photooxidation of various biogenic hydrocarbons are studied in detail with a Proton Transfer Reaction Mass Spectrometer (PTR-MS) and the results are presented in Appendices I and J.

Chapter 2

Contribution of First- versus Second-Generation Products to Secondary Organic Aerosols Formed in the Oxidation of Biogenic Hydrocarbons*

*This chapter is reproduced by permission from “Contribution of first- versus second-generation products to secondary organic aerosols formed in the oxidation of biogenic hydrocarbons” by N. L. Ng, J. H. Kroll, M. D. Keywood, R. Bahreini, V. Varutbangkul, R. C. Flagan, J. H. Seinfeld, A. Lee., and A. H. Goldstein, *Environmental Science and Technology*, 40, 2283-2297, 2006. Copyright 2006. American Chemical Society.

2.1 Abstract

Biogenic hydrocarbons emitted by vegetation are important contributors to secondary organic aerosol (SOA), but the aerosol formation mechanisms are incompletely understood. In this study, the formation of aerosols and gas-phase products from the ozonolysis and photooxidation of a series of biogenic hydrocarbons (isoprene, 8 monoterpenes, 4 sesquiterpenes and 3 oxygenated terpenes) are examined. By comparing aerosol growth (measured by Differential Mobility Analyzers, DMAs) and gas-phase concentrations (monitored by a Proton Transfer Reaction Mass Spectrometer, PTR-MS), we study the general mechanisms of SOA formation. Aerosol growth data are presented in terms of a “growth curve”, a plot of aerosol mass formed versus the amount of hydrocarbon reacted. From the shapes of the growth curves, it is found that all the hydrocarbons studied can be classified into two groups based entirely on the number of double bonds of the hydrocarbon, regardless of the reaction systems (ozonolysis or photooxidation) and the types of hydrocarbons studied: compounds with only one double bond and compounds with more than one double bond. For compounds with only one double bond, the first oxidation step is rate-limiting and aerosols are formed mainly from low volatility first-generation oxidation products; whereas for compounds with more than one double bond, the second oxidation step may also be rate-limiting and second-generation products contribute substantially to SOA growth. This behavior is characterized by a vertical section in the growth curve, in which continued aerosol growth is observed even after all the parent hydrocarbon is consumed.

2.2 Introduction

Organic aerosols are a significant contributor to the total particulate matter in the troposphere, and a full understanding of their sources and properties is necessary to evaluate their impacts on visibility, climate, and human health. Secondary organic aerosols (SOA), formed from production of low-volatility species from the oxidation of gas-phase organic compounds, contribute a significant fraction of fine particulate matter, as high as 50-80 % in polluted regions (1).

The oxidation of biogenic non-methane hydrocarbons (NMHCs) emitted by vegetation, such as isoprene (C_5H_8), monoterpenes ($C_{10}H_{16}$), sesquiterpenes ($C_{15}H_{24}$) and oxygenated terpenes (e.g. $C_{10}H_{18}O$, $C_{10}H_{12}O$) are especially important to the total atmospheric burden of SOA. Because of their large global emissions and high reactivity with the major atmospheric oxidants, ozone (O_3), hydroxyl radical (OH) and nitrate radical (NO_3) (2), they are believed to be the dominant contributors to global SOA formation (3).

Despite considerable study of the oxidation mechanisms of these biogenic compounds (4-16), the basic underlying mechanisms of SOA formation and growth from biogenic precursors remain poorly understood. Numerous gas-phase and aerosol-phase oxidation products have been identified, but carbon balances are poorly constrained and the formation mechanisms for such products remain speculative. With the possibility of multiple oxidation steps, a particular condensable compound may be formed by the direct oxidation of the parent hydrocarbon, or through the further oxidation of first-generation gas-phase products (7, 17-24). In addition, the formation of oligomers in SOA adds complexity to the overall SOA forming reaction mechanism (25-29). Furthermore, it is

unclear whether the rate-determining step to SOA formation is the first oxidation step or the further oxidation steps (in either the gas or aerosol phase). Identifying the rate-determining step can certainly constrain the SOA formation mechanisms, as well as provide the important kinetic information in modeling SOA formation.

Laboratory-determined SOA yield, defined as the ratio of the mass concentration of aerosol formed to that of the hydrocarbon reacted, is widely used as a quantitative measure of the SOA-forming potential of a parent hydrocarbon. The aerosol yield may be described by a semi-empirical model developed by Odum et al. (30) based on absorptive gas-particle partitioning (31, 32) of two reaction products, representing compounds of differing volatility:

$$Y = \Delta M_o \left[\frac{\alpha_1 K_{om,1}}{1 + K_{om,1} \Delta M_o} + \frac{\alpha_2 K_{om,2}}{1 + K_{om,2} \Delta M_o} \right] \quad (2.1)$$

in which Y is the aerosol yield, ΔM_o is the organic aerosol mass produced, α_i is the mass-based gas-phase stoichiometric fraction for species i , and $K_{om,i}$ is the gas-particle partitioning coefficient for species i . With this two-product model, equation (2.1) can be fit to experimental yield data to determine values for α_i and $K_{om,i}$, and the resulting plot (Y versus ΔM_o) is generally referred to as a “yield curve”. Over the years, yield curves have proven to be useful in representing SOA formation (9, 17, 30, 33-36), allowing the contribution of SOA to the particulate burden in the atmosphere to be estimated, even when the detailed SOA component speciation is not available (37).

Recently it has been shown that this model may be used for the interpretation of laboratory SOA growth data in terms of underlying chemistry (38, 39). By rewriting Y in

equation (2.1) as $\Delta M_o/\Delta HC$ and assuming no absorbing organic aerosol is present initially, an expression for ΔM_o as a function of ΔHC may be obtained:

$$\Delta M_o = \frac{1}{2} \left(\Delta HC(\alpha_1 + \alpha_2) - \frac{1}{K_{om,1}} - \frac{1}{K_{om,2}} \right) + \frac{\sqrt{4K_{om,1}K_{om,2}(K_{om,1}\alpha_1\Delta HC + K_{om,2}\alpha_2\Delta HC - 1) + (K_{om,1} + K_{om,2} - K_{om,1}K_{om,2}\Delta HC(\alpha_1 + \alpha_2))^2}}{2K_{om,1}K_{om,2}} \quad (2.2)$$

As written, equations (2.1) and (2.2) are only valid when there is no absorbing organic mass present initially and that the absorbing medium is produced completely by the oxidation of the parent hydrocarbon. In the above equations, ΔM_o is defined as $M_o - M_{o,initial}$. For chamber experiments, there is no absorbing organic mass present initially and so $M_{o,initial} = 0$ and $\Delta M_o = M_o$. By plotting experimentally measured aerosol growth, ΔM_o , as a function of the amount of hydrocarbon reacted, ΔHC (hereafter referred to as a “growth curve”), it is found that the effects of heterogeneous chemistry and gas-phase reactions of oxidation products can be inferred (38). For example, it is clear that secondary reactions (further oxidation of first-generation products) play an important role in SOA growth for the oxidation of both biogenic and anthropogenic precursors (7, 17-19); however, the relative contribution of first- and second-generation products to SOA formation and growth is still unclear.

It has been generally assumed that both the yield curve expression (equation 2.1) and growth curve expression (equation 2.2) are only valid for the final SOA growth, i.e. the amount of SOA formed once the hydrocarbon is all reacted, gas-particle equilibrium is established and aerosol growth has completed. Therefore, a series of experiments with different initial hydrocarbon concentrations have traditionally been carried out for each

parent hydrocarbon to establish the yield curve/growth curve. However, one can still plot the growth curve for a single experiment over the course of the experiment (the “time-dependent growth curve”). Time-dependent aerosol formation and growth data have been examined in a few studies (7, 17, 19, 39); however, it has not been established whether it is appropriate to use time-dependent growth data to understand SOA formation in terms of the equilibrium expressions above.

In this study, the SOA formation and gas-phase oxidation products from the ozonolysis and photooxidation of a series of biogenic compounds are investigated. Overall SOA yields, gas-phase oxidation products and yields, as well as detailed multistep oxidation mechanisms from these experiments are presented in Lee et al. (20, 21). Many of these oxidation products have been observed in the Ponderosa pine canopy at Blodgett Forest in California (40). The focus here is the general mechanisms of SOA growth. By comparing gas-phase concentrations and aerosol volume in real time over the course of each experiment, we are able to study the kinetics and mechanisms of SOA formation. In particular, we focus on the contribution of secondary reactions to SOA growth in both the ozonolysis and photooxidation systems, by constructing a time-dependent growth curve for each experiment. The shapes of the growth curves reveal clearly the importance and the relative contribution of secondary reactions to SOA growth in different systems. We show that the biogenic hydrocarbons studied can be classified into two main groups based on the number of double bonds of the parent hydrocarbon. For compounds with only one double bond, the first oxidation step is the rate-determining step, and SOA is formed from the condensation of first-generation products. However, for compounds with more than one double bond, the further

oxidation of first-generation products appears to be rate-determining as well, and secondary reactions contribute substantially to SOA growth.

2.3 Experimental

Experiments are performed in Caltech's indoor, dual 28 m³ Teflon environmental chambers. Details of the facilities have been described elsewhere (36, 41) so will only be described briefly here. Before each experiment, the chambers are flushed continuously with purified air for ~32 hours.

Each chamber has a dedicated Differential Mobility Analyzer (DMA, TSI model 3081) coupled with a condensation nucleus counter (TSI model 3760) for measuring aerosol size distribution, number concentration, and total volume. Separate CPCs (TSI models 3010 and 3025) are used to monitor the total number of particles in each chamber as an additional check. All aerosol growth data are corrected for wall loss, in which size-dependent coefficients are determined from wall loss experiments and applied to the aerosol volume data (36). Temperature and relative humidity (RH) are continuously monitored using combined temperature and RH probes (Vaisala HMP233 series transmitters, Woburn, MA).

For experiments with isoprene, monoterpenes, and oxygenated terpenes, seed aerosols are introduced into the chamber to act as a substrate onto which the gas-phase products may condense. Seed aerosols are generated by atomizing an aqueous ammonium sulfate solution with a constant-rate atomizer. The aerosol stream is passed through two ²¹⁰Po neutralizers to reduce charges and minimize loss in the lines. The initial particle number concentration is about 20,000 particles cm⁻³, with a geometric mean diameter of 80-100 nm. Sesquiterpenes react with ozone and OH radicals at sufficiently fast rates that

nucleation occurs despite the presence of seed aerosols, resulting in two modes (nucleation mode and condensation mode), making data analysis (particularly the wall loss calculation) difficult. Thus, for sesquiterpene experiments no seed particles are added.

After atomization, a known volume of the parent hydrocarbon is injected into a glass bulb, and introduced into the chambers by gentle heating. The concentration of the parent hydrocarbons is monitored using two instruments, a Hewlett Packard gas chromatograph with flame ionization detection, GC-FID (Hewlette-Packard, 5890), and a Proton Transfer Reaction Mass Spectrometer, PTR-MS (Ionicon Analytik, Innsbruck, Austria) (42). The PTR-MS calibrations and measurements are described in more detail in Lee et al. (20, 21). The PTR-MS monitors concentrations of both the parent hydrocarbon and various gas-phase intermediates and products continuously over the course of the experiments. The PTR-MS is operated in mass scan mode, with each cycle completed in ~3 minutes; this time scale is much shorter than that of the GC-FID, allowing the evolution of gas-phase products to be well-captured. Together, the PTR-MS and DMA allow for simultaneous measurements of gas-phase product concentrations and aerosol growth. Aerosol mass and chemical composition are monitored with an Aerodyne quadrupole aerosol mass spectrometer (AMS). Details on the operation of AMS and its data analysis have been described elsewhere (43-46). The hygroscopicity of the aerosol is measured by a Tandem Differential Mobility Analyzer (TDMA).

For ozonolysis experiments, the temperature of the chamber is maintained at 20°C and the RH is <10%. Seed aerosols are generated by atomizing a 0.03 M (NH₄)₂SO₄ solution. The particles also pass through a silica gel diffusion dryer before they enter the

chamber. Cyclohexane is used to scavenge OH radicals formed from the hydrocarbon-O₃ reaction and to ensure ozone is the only oxidant present in the chamber. Enough cyclohexane is injected such that the reaction rate of OH radicals with cyclohexane is 100 times greater than that with parent hydrocarbon. Once the chamber contents are well mixed and GC-FID and PTR-MS readings are stabilized, ozone is injected into the chambers at 5 L min⁻¹. Ozone is generated with a UV lamp ozone generator (EnMet Corporation, MI). The amount of ozone injected is 3 times the concentration of the parent hydrocarbon. Ozone concentration is measured by a commercial ozone monitor (Horiba APOA-360 CE, Irvine, CA). The beginning of ozone injection marks the start of each experiment.

For several α -pinene ozonolysis experiments, the experimental conditions are slightly different, as described by Gao et al. (27, 28). Those experiments are carried out at ~55% RH by passing dry purified air through a bubbler prior to introduction into the chamber. The seed particles are generated by atomizing a 0.03 M MgSO₄ solution and they are not passed through the diffusion dryer prior to introduction into the chamber. Ozone is injected at twice the concentration of the parent hydrocarbon. Hydrocarbon concentration is monitored by GC-FID only.

For photooxidation studies, the experiments are conducted at 20-22°C and ~50% RH. Seed particles are generated by atomizing a 0.015 M aqueous (NH₄)₂SO₄ solution. For isoprene and monoterpenes, the parent hydrocarbon concentration is measured by both GC-FID and PTR-MS, while only PTR-MS is used for experiments with sesquiterpenes and oxygenated terpenes. After injection of seed (for the isoprene, monoterpene and oxygenated terpene experiments) and parent hydrocarbon, the OH

precursor, nitrous acid (HONO), is introduced. HONO is prepared by dropwise addition of 2 mL of 1% NaNO₂ into 15 mL of 10% H₂SO₄ in a glass bulb. The bulb is then attached to the chamber and a stream of dry air is passed through the bulb, introducing HONO into the chamber. NO and NO₂, measured by a commercial NO_x monitor (Horiba APNA-360, Irvine, CA), form as side products in the preparation of HONO, and are also introduced into the chamber. HONO is observed by PTR-MS as the dehydrated form of HONOH⁺ at *m/z* 30, and also appears to be detected by the NO_x monitor. However, since HONO calibration is not performed, its concentration in the chamber is not well-constrained.

Once the seed, parent hydrocarbon, and NO_x concentrations have stabilized, reaction is initiated by irradiating the chamber with blacklights. The blacklights used are centered at 354 nm, efficiently photolyzing HONO to OH and NO. Only 10% of the lights are used to minimize temperature increases. Over the course of the experiments, the temperature of the chambers increases by only 1-2°C and RH drops accordingly. However, RH never drops below 40%, the efflorescence RH of ammonium sulfate.

The chemicals used and their stated purities are: isoprene (Aldrich, 99.8%), α-pinene (Aldrich, ≥99%), β-pinene (Fluka, ≥99%), Δ³-carene (Aldrich, 99%), α-terpinene (Fluka, ≥97%), γ-terpinene (Fluka, ≥98.5%), terpinolene (Fluka, ≥97%), limonene (Aldrich, 97%), myrcene (Fluka, 90%), α-humulene (Sigma, purity not specified), β-caryophyllene (Aldrich, purity not specified), aromadendrene (Fluka, ≥97%), longifolene (Fluka, ≥99%), methyl chavicol (Fluka, ≥98.5%), verbenone (Fluka, 99%), and linalool (Fluka, 97%).

Table 2.1 lists the structures of the parent hydrocarbons studied and the rate constants of the compounds for reaction with ozone (k_{ozone}) and OH radicals (k_{OH}). The experimental conditions for ozonolysis and photooxidation experiments are given in Tables 2.2 and 2.3 respectively.

2.4 Results

2.4.1 Ozonolysis studies

The compounds studied in the ozonolysis experiments are α -pinene, β -pinene, Δ^3 -carene, α -terpinene, terpinolene, myrcene, α -humulene, β -caryophyllene, methyl chavicol, and linalool. Once ozone is introduced into the chamber, the parent hydrocarbon concentration is observed to decay, and various gas-phase oxidation products are formed accordingly. SOA growth typically begins within 30 minutes after reaction initiation, except for methyl chavicol, in which no SOA growth is observed until an hour after ozone injection. No significant SOA growth is observed from linalool ozonolysis. By comparing volume distributions from the DMA and mass distributions from the AMS, the effective densities for the SOA formed in ozonolysis may be estimated (46). Overall, an average effective density of 1.25 g cm^{-3} is used to convert the total aerosol volume measured by DMA to total mass for both ozonolysis and photooxidation experiments.

A typical reaction profile for α -pinene ozonolysis is shown in Figure 2.1. This profile exemplifies that for all parent compounds with a single double bond. Once ozone is injected, α -pinene begins to be oxidized, its concentration decreases, and the aerosol mass starts to increase. Aerosol growth reaches its maximum when all α -pinene is

consumed and remains constant thereafter. A typical reaction profile for terpinolene is shown in Figure 2.2; terpinolene exemplifies the behavior of compounds with more than one double bond. Unlike α -pinene, in which aerosol growth stops at the time when the hydrocarbon is consumed, the aerosol mass generated in the ozonolysis of terpinolene reaches its maximum well after the terpinolene is completely consumed (this will be discussed further in Section 2.5.2.3). The SOA growth in the ozonolysis studies is seen more directly by plotting organic aerosol mass as a function of the hydrocarbon reacted over the course of the experiment (time-dependent growth curve). The time-dependent growth curves for all compounds studied in ozonolysis experiments (except linalool, which does not produce significant SOA) are shown in Figure 2.3.

2.4.2 Photooxidation studies

In the photooxidation experiments, initiated by the irradiation of hydrocarbon/HONO/NO_x mixtures, the OH radical is the dominant oxidant. Ozone and NO₃ radicals are also formed during the experiments, so their chemistry may play a role as well. Based on the decay of the parent hydrocarbon and the measured ozone level in the chamber, O₃ and NO₃ account only for a very small fraction of the parent hydrocarbon consumption; however, we cannot rule out the possible role of O₃ or NO₃ reactions with the oxidation products. The compounds studied in the photooxidation experiments are isoprene, α -pinene, β -pinene, Δ^3 -carene, α -terpinene, γ -terpinene, limonene, terpinolene, myrcene, α -humulene, β -caryophyllene, aromadendrene, longifolene, methyl chavicol, verbenone, and linalool. Once the chamber irradiation begins, the hydrocarbon concentration decreases and various gas-phase products are formed accordingly. SOA growth typically begins 10 minutes after reaction initiation.

The time-dependent growth curves for the compounds studied (except longifolene, discussed subsequently) are shown in Figure 2.4.

2.5 Discussion

Based on Figures 2.3 and 2.4, we can classify all the compounds studied into two different groups based entirely on the shapes of the growth curves: compounds for which SOA growth stops once all the parent hydrocarbon is consumed, and compounds for which SOA growth continues even after all the hydrocarbon is consumed. The latter case is characterized by a vertical section in the growth curves. Such classifications are independent of the reaction system studied (ozonolysis or photooxidation) as well as the class of compounds studied (isoprene, monoterpene, sesquiterpene or oxygenated terpene). All compounds in the first group have one double bond while compounds in the second group have more than one double bond.

The first group of compounds includes α -pinene, β -pinene, Δ^3 -carene, aromadendrene, longifolene, methyl chavicol, and verbenone. The fact that aerosol growth stops once all hydrocarbon is consumed indicates that the first oxidation reaction is the rate-determining step in SOA formation. In this case, either the condensable products are the initial reaction products of the parent hydrocarbon oxidation (first-generation products), or subsequent reactions (in either the gas or aerosol phase) also contribute to aerosol growth, but proceed at very fast rates.

The second group of compounds includes isoprene, α -terpinene, γ -terpinene, limonene, terpinolene, myrcene, α -humulene, β -caryophyllene, and linalool. For these compounds, the growth curve can be divided into two regions. We can see that more SOA is formed as the parent hydrocarbon reacts (region I). Even after all the hydrocarbon

is completely consumed, aerosol mass continues to increase, resulting in a vertical section of the growth curve (region II). The delay in aerosol production for this group of compounds may be a result of either of the following two factors: there is delay in mass transfer, in which the partitioning of condensable products into the aerosol phase is extremely slow, or condensable products are formed from the further oxidation of first-generation products, and this second oxidation step also determines the rate of SOA formation. However, a delay in mass transfer is not observed for all compounds with only one double bond, hence it seems unlikely that SOA formation for compounds with more than one double bond will be mass-transfer limited. For this group of compounds, the first-generation products formed are still unsaturated, thus will react further with the oxidants (OH, O₃ or NO₃) to yield compounds more highly oxidized than the first-generation products. As a result, for this group of compounds there are significant contributions from secondary reactions to SOA growth. In many cases, good correlations exist between the extent to which intermediate gas-phase products react and aerosol growth; these will be discussed subsequently. There is a possibility that the first step is rate-limiting, and the second step is fast and only the second step leads to SOA growth, then the growth curve will look like compounds with only one double bond (i.e. no vertical section). However, for all the 9 compounds with more than one double bond we have studied, we found that all the growth curves exhibit a vertical section. Therefore, this scenario is unlikely to be the case, and for compounds with more than one double bond, both oxidation steps are rate-limiting, allowing one to infer the importance of the different generation products based upon these kinetic arguments.

In the following sections, the two classes of compounds will be examined in greater detail. We select one compound from each class: α -pinene ozonolysis as a representative of SOA formation from compounds with one double bond and terpinolene ozonolysis as representing the behavior of compounds with more than one double bond. The time-dependent growth curves and final SOA concentrations for each system will be discussed. From the shapes of the growth curves of these two systems, two different general SOA formation mechanisms can be inferred. Based on this analysis, we will discuss the underlying chemistry of SOA formation of individual compounds.

2.5.1 Time-dependent vs. final SOA growth

2.5.1.1 α -pinene ozonolysis (one double bond)

Substantial insight can be gained by examining time-dependent SOA growth over a range of hydrocarbon concentrations. Here we re-examine α -pinene ozonolysis experiments previously reported by Gao et al. (27, 28). The data set includes 7 α -pinene ozonolysis experiments, with initial α -pinene concentrations ranging from 12 to 135 ppb. These experiments were carried out at slightly different reaction conditions than those shown in Figures 2.3 and 2.4, as described in the Experimental section.

Based on the final SOA growth data from these 7 α -pinene experiments, a yield curve may be generated using the two-product model derived by Odum et al. (30, 33), and converted to a growth curve by using equation (2.2). For clarification, this growth curve is referred to as the “final SOA growth curve” as each data point represents the final aerosol mass resulting from the complete oxidation of a certain amount of parent hydrocarbon. The time-dependent growth curves from these experiments are shown

together with the final SOA growth curve in Figure 2.5. It can be seen that the individual data points for each α -pinene experiment overlap remarkably well not only with each other, but also with the final SOA growth curve, suggesting that for compounds with only one double bond such as α -pinene, both equations (2.1) and (2.2) are valid for the final SOA growth as well as the time-dependent growth data. It also suggests that the chemical composition of the aerosol remains essentially constant over the course of the oxidation. This constancy is confirmed by AMS measurements; it has been shown through delta series analysis of mass spectra that one can obtain information about the general oxidation state of particle-phase compounds (46). It is observed that unsaturated organics yield delta values ≤ 0 while oxygenated organics yield delta values ≥ 2 (46, 47). The delta values over the course of an α -pinene experiment are shown in Figure 2.6. The different delta values stay relatively constant after the reaction starts, suggesting no substantial changes in the degree of oxidation of SOA composition over time. This observation is also in agreement with the study by Yu et al. (7), who found that the time-dependent yield curve agrees well with that generated by experimentally determined α_i and $K_{om,i}$, which are obtained from the analysis of the denuder/filter samples collected at the end of the experiment.

2.5.1.2 Terpinolene ozonolysis (more than one double bond)

For behavior characteristic of SOA formation from a precursor hydrocarbon with more than one double bond, we examine the terpinolene ozonolysis experiments reported previously by Keywood et al. (36) (the experiment on 3/31/03 in Table 2 of Keywood et al. is the same as that shown in Figure 2.2 of this paper). We note that the yields reported in Keywood et al. (36) are based on GC-FID measurements, which are typically 10-15%

higher than those based on PTR-MS measurements; since we use mainly PTR-MS for gas-phase measurements here, we scale up accordingly the parent hydrocarbon concentrations for those experiments in which only GC-FID was used. We have recalculated the aerosol yields for these 8 experiments, obtaining a new set of aerosol yield parameters for the two-product model: $\alpha_1 = 0.243$, $\alpha_2 = 0.03$, $K_{om,1} = 0.014$ and $K_{om,2} = 0.927$. This scaling changes the parameters from Keywood et al. (36) only slightly, and has no effect on the conclusions from either work.

Shown in Figure 2.7 are the time-dependent growth data for the 8 terpinolene ozonolysis experiments, together with the growth curve based on the final data for each experiment. Unlike the case for α -pinene (Figure 2.5), the time-dependent growth curves and final SOA growth curve for terpinolene are all dramatically different. While the time-dependent growth curves for individual experiments clearly show the contribution of the secondary reactions, this information is not evident by considering just the final SOA growth curve. Therefore, in the case when secondary reactions play a role in SOA production, one cannot use the time-dependent growth data from a single experiment to represent final growth conditions. Moreover, the time-dependent growth curve for a single experiment cannot be fitted to the two-product model, indicating that for compounds with more than one double bond, this model is valid only when the data represent final SOA growth, when all the hydrocarbon is reacted, secondary reactions are complete and gas-particle equilibrium is reached.

Using α -pinene and terpinolene as model systems, we now extend our analysis to other compounds to study the underlying mechanisms of SOA formation.

2.5.2 Chemistry of individual compounds

2.5.2.1 α -pinene ozonolysis

The growth curves of α -pinene ozonolysis and photooxidation indicate that in these systems the first oxidation step is the rate-determining step as aerosol growth stops when the hydrocarbon is completely consumed. In these systems SOA is formed from the condensable first-generation products. The identification of the rate-determining step and that SOA are formed from first-generation products allow us to constrain the reaction mechanism substantially.

Much effort has been expended in identifying the oxidation products of α -pinene ozonolysis and a number of organic acids have been identified as major products: oxocarboxylic acids (pinonic acid and norpinonic acid), dicarboxylic acids (pinic acid and norpinic acid), and hydroxy pinonic acid (4-8, 10-12). According to Yu et al. (7), these compounds account for about 73% of the total aerosol mass. Different mechanisms leading to the formation of organic acids have been proposed. Pinonic acid is generally thought to be a first-generation product, either by rearrangement of a Criegee intermediate to a carboxylic acid (4, 10, 48), or by reaction of the stabilized Criegee intermediates with water (6, 49). Most studies suggest that other acids are formed from the further oxidation of their corresponding aldehydes (4, 6, 10, 12, 48). In our ozonolysis experiments, OH radicals are scavenged by cyclohexane, and so ozone is the only gas-phase oxidant. It is found that the molar ratio of ozone consumed to α -pinene reacted is 1:1, suggesting that ozone reacts only with the parent hydrocarbon and that there are no further oxidation steps in the gas phase. These data indicate that the ozone-alkene reaction is the rate-determining step, and that the condensable products are first-

generation products. Thus, mechanisms speculating that acids are formed by multiple oxidation steps in the gas phase are not consistent with the data. Our study does not exclude the formation of individual components of SOA through heterogeneous reactions; however, it would suggest that these reactions, if they do contribute to aerosol growth on the timescale of our experiments, proceed at very fast rates. The PTR-MS data show that the pinonaldehyde concentration stays constant after α -pinene is completely consumed (Figure 2.8), indicating that pinonaldehyde is not further oxidized to form significant amounts of condensable products, and that it is unlikely to be involved in heterogeneous reactions (such as oligomerization) to contribute substantially to additional aerosol mass as suggested by Tolocka et al. (25) and Iinuma et al. (26). On the other hand, mechanisms involving formation of organic acids as first-generation reaction products, such as those put forth by Jenkin et al. (49) for pinic acid and hydroxyl pinonic acid, are consistent with the data.

2.5.2.2 α -pinene photooxidation

As in the case of ozonolysis, for the photooxidation of α -pinene, carboxylic acids have been found to be predominant in the aerosol phase (13-16). Most suggested mechanisms involve multiple oxidation steps; for example, the oxidation of pinonaldehyde may form pinonic acid, which could then react further to form pinic and norpinic acids (13, 15, 16). In the present experiments, pinonaldehyde is indeed observed to decrease when α -pinene is almost completely consumed (Figure 2.9), likely a result of reaction with OH and photodissociation (50). However, the loss of pinonaldehyde is not accompanied by further aerosol growth, so the formation of low volatility organic acids through the further oxidation of pinonaldehyde seems unlikely. This is consistent with the

observation by Hatakeyama et al. (51), in which the pinonaldehyde yield and SOA yield are not well-correlated. Therefore, the acids are likely formed as first-generation products, as suggested by Larsen et al. (13), or else by oxidation reactions of species already in the particle phase.

2.5.2.3 Terpinolene ozonolysis

The growth curve for terpinolene ozonolysis indicates that the further oxidation of first-generation products contributes significantly to SOA growth and that the second oxidation step may also be rate-limiting. Unlike the case for α -pinene ozonolysis, ozone concentration is observed to decrease even after all the terpinolene is consumed, indicating there is further alkene oxidation. The PTR-MS measures the concentrations of different gas-phase products over the course of the each experiment, including some of the first-generation oxidation products. From the time evolution of these first-generation products, aerosol growth can be correlated with the further oxidation of these products. The time evolution of two intermediate ions (m/z 111 and m/z 93), corresponding to first-generation oxidation products (of mass 110 and 92 amu) is shown in Figure 2.10. At $t \cong 50$ min, all the terpinolene is consumed and yet the aerosol growth continues, with a slightly different rate (This difference in the rate of aerosol growth is much more pronounced in the case for β -caryophyllene, which is discussed below). As shown in Figure 2.10, both the m/z 111 and m/z 93 peaks start to decrease when terpinolene is totally consumed. The similar time evolution of these compounds and the 18 amu difference suggests that the m/z 93 ion is a dehydrated fragment of the m/z 111 ion (20). The m/z 111 peak is likely to be the protonated form of 4-methyl-3-cyclohexen-1-one (MW=110), known to be a major product of terpinolene ozonolysis (52, 53). The molar

yield of this product (taken from summing the calculated yields from m/z 111 and m/z 93) is 0.53. Based on this molar yield, we can calculate the amount of the product formed over the course of the experiment, and from the time-dependent PTR-MS data we can estimate the amount reacted away over time; these are shown in Figure 2.11. Figure 2.12 shows the SOA mass formed as a function of the amount of the intermediate product reacted. There is a clear correlation between the two, suggesting a contribution from the further oxidation of the intermediate product to the SOA formed. The intercept corresponding to the amount of aerosol mass already formed before any of the first-generation product has reacted away, is $\sim 70 \mu\text{g m}^{-3}$. This is similar to the amount of SOA formed before terpinolene is fully consumed (Figure 2.3). We do not quantify the contribution of second-generation products to total SOA growth, as this percentage is likely to be a function of the amount of organic matter present. Nevertheless, we can still infer from these results that a large fraction of SOA produced is from second-generation chemistry.

The remainder of the SOA formed is mostly from the condensation of relatively nonvolatile first-generation products (in the first 50 minutes of the experiment), likely from the attack of ozone on the endo-double bond, which results in larger, multifunctional molecular weight products. Only when terpinolene is completely consumed does the reaction of relatively volatile first-generation species with ozone become important. For terpinolene, it appears that the reaction of the intermediate corresponding to the m/z 111 ion (likely 4-methyl-3-cyclohexen-1-one) is largely responsible for this additional aerosol growth. We do not observe a correlation between the decay of other products and aerosol growth.

2.5.2.4 Terpinolene and limonene photooxidation

As in the ozonolysis case, for terpinolene photooxidation, we observe the m/z 111 and m/z 93 ions start to decrease when the parent hydrocarbon is consumed; again the same time evolution of these two products suggests that the m/z 93 ion is the dehydrated fragment of m/z 111. These are likely to correspond to the same compound, 4-methyl-3-cyclohexen-1-one, a known product of the OH+terpinolene reaction (52, 53). We measure the total molar yield to be 0.47 (sum of the molar yields from the m/z 93 and m/z 111 ions). Aerosol growth as a function of the amount of the m/z 111 ion reacted is shown in Figure 2.13. Again a good correlation is observed, suggesting the further oxidation of 4-methyl-3-cyclohexen-1-one contributes to aerosol growth in the photooxidation system.

The photooxidation of limonene, which is structurally similar to terpinolene, shows a substantially lower contribution from secondary products to total SOA formed. The major product ion observed to decrease when limonene is almost all consumed is m/z 169, likely to be limononaldehyde (MW=168) (52). Limononaldehyde is not calibrated in the PTR-MS, however, by analogy to the fragmentation of pinonaldehyde, limononaldehyde can be expected to fragment not only at m/z 151, the dehydrated fragment of m/z 169, but also at m/z 107, 123, 133, and 151, with a molar yield of 0.61 from the sum of all limononaldehyde-associated ions and their isotopes. The correlation of the m/z 169 ion (including the fragmented ions and isotopes) reacted and aerosol growth is shown in Figure 2.14.

Differences in the vertical section of the growth curves indicate that secondary reactions contribute to SOA production to a larger extent in the case of terpinolene than

limonene. The large difference between the importance of secondary products from terpinolene and limonene can be explained in terms of their oxidation mechanisms, particularly the importance of oxidative attack on the exo versus endo double bonds. It is estimated that OH attack on the endo double bond accounts for only 44% of the OH-terpinolene reaction but 63% of the OH-limonene reaction (54), due to differing levels of alkyl substitution of each. As described above, the contribution of second-generation products to total SOA growth is smaller for limonene than for terpinolene. This suggests that the higher percentage of OH attack at the endo double bond results in more nonvolatile first-generation products, and hence a smaller contribution of second-generation products to total SOA formed. This is intuitive as radical attack at the endo double bond results in ring opening, forming multifunctional products with no loss of carbon. Hence, attack at the endo site is more likely to lead to the formation of condensable species. By contrast, attack at the exo double bond typically leads to fragmentation, reducing the number of carbons in the molecule and adding only one polar group. Hence the relative rates of attack at the endo and exo sites can play a major role in determining the importance of first versus second-generation products in SOA formation.

2.5.2.5 Isoprene photooxidation

It has recently been shown that isoprene photooxidation produces SOA in low yields under high NO_x conditions and that the SOA formation proceeds from the further reaction of first-generation products (55, 56). We can gain insights into the isoprene SOA formation mechanism by examining the growth curve of isoprene photooxidation as shown in Figure 2.4. It is clear that $\sim 290 \mu\text{g m}^{-3}$ (~ 100 ppb) of isoprene has reacted before aerosol growth commences. This time delay in SOA formation, as well as the

continuous aerosol growth after isoprene is completely consumed, suggests that isoprene SOA is indeed a result of further oxidation of first-generation products and this step may also be rate-limiting. Methacrolein, a first-generation product of isoprene oxidation, can lead, upon photooxidation, to aerosol growth (55). Indeed, in Figure 2.15 it is shown that the total concentration of methacrolein and methyl vinyl ketone (which are isomers so cannot be distinguished in the PTR-MS) starts to decrease when isoprene is almost completely consumed. Shown in Figure 2.16 is the correlation between the amount of SOA formed and methacrolein + methyl vinyl ketone reacted. The plot has an intercept of $4.8 \mu\text{g m}^{-3}$, suggesting that this small amount of SOA is possibly formed from some more nonvolatile first-generation products and SOA is mainly formed from second-generation products. It has been shown that methyl vinyl ketone does not lead to aerosol growth (55), thus a large fraction of SOA growth is likely related to the oxidation of methacrolein.

2.5.2.6 Other compounds with multiple double bonds

Good correlations between aerosol growth and the amount of reacted intermediate products are also observed in the following systems: myrcene ozonolysis, myrcene photooxidation, γ -terpinene photooxidation, and linalool photooxidation. Tables 2.4 and 2.5 summarize the major first-generation products that are well-correlated with aerosol growth in these systems. Plots of aerosol growth versus the amount of reacted intermediates are presented in the Supporting Information. Other than the major first-generation products, certain products are also observed to decrease when the parent hydrocarbon is almost consumed; however, their concentrations are too low to obtain a

precise correlation between aerosol growth and the amount of these intermediates reacted.

For compounds such as α -terpinene, α -humulene, and β -caryophyllene, we could not identify any major intermediate products that are well-correlated with SOA growth (in both ozonolysis and photooxidation). It is possible that the first-generation products are not detected by the PTR-MS. In any case, we still observe a change in the rate of aerosol production for these compounds once the parent hydrocarbon is consumed. This suggests the occurrence of further reactions, as revealed by the continuously changing AMS delta time series after the complete consumption of the parent hydrocarbon – negative delta values continue to decrease while positive delta values continue to increase, suggesting the SOA is being further oxidized.

2.5.2.7 β -caryophyllene ozonolysis

As noted above, there is a slight difference in the aerosol growth rate before and after the parent hydrocarbon is used up. This difference is very pronounced in the case of β -caryophyllene. Figure 2.17 shows the decay of the parent hydrocarbon and the corresponding aerosol growth. Due to the high reactivity of β -caryophyllene and ozone, a rapid decay of the parent hydrocarbon is observed; ~65% of the parent hydrocarbon is reacted in the first 25 minutes and the organic mass increases rapidly. When all β -caryophyllene is consumed at $t = 50$ min, we observe a different slope in the rate of aerosol formation. This change in the rate of aerosol growth is likely due to the different mechanisms of aerosol formation. From $t = 0$ min to $t = 25$ min, the organic mass is most likely the nonvolatile first-generation products; from $t = 25$ min to $t = 50$ min, it is a mix of primary and secondary products; from $t = 50$ min onwards, the reaction of first-

generation products with ozone becomes important, and so the aerosol growth results from the nonvolatile products that are formed from this further oxidation; Hoffmann et al. (17) observed evidence for aerosol growth from secondary products from this reaction as well. The amount of β -caryophyllene and ozone reacted over time is shown in Figure 2.18. The molar ratio of β -caryophyllene reacted to ozone consumed is almost 1:1 up to $t = 25$ min, at which time β -caryophyllene is almost completely consumed, but ozone consumption continues to increase. The final amount of ozone consumed is approximately twice that of β -caryophyllene reacted, indicating that both double bonds are fully oxidized. The corresponding AMS delta series plot is shown in Figure 2.19. The fact that the negative delta values continue to decrease when all parent hydrocarbon is consumed indicates that the compounds are becoming increasingly oxidized.

2.5.2.8 Longifolene photooxidation

The growth curve from the photooxidation of longifolene, shown in Figure 2.20, appears to be anomalous. Aerosol mass increases as more longifolene is consumed; however, it appears that towards the end of the experiment aerosol growth stops even though the longifolene continues to be consumed. This atypical growth curve behavior is likely due to difficulties in obtaining good parent hydrocarbon and aerosol mass measurements. Products, or fragments of products, with the same mass to charge ratio as longifolene may be formed and interfere with the PTR-MS measurements. Another possibility is a change in the density of the aerosol over the course of the experiment, so that an accurate aerosol mass cannot be obtained from the DMA volumes and a fixed density. This is supported by our TDMA measurements, in which the increase in hygroscopic growth factor with RH is not monotonic (57) for longifolene photooxidation.

This could be indicative of large void volumes in the particles, potentially leading to large changes in the apparent density of the particles over the course of the experiment.

2.6 Implications for aerosol formation

We report a series of chamber experiments investigating the formation of aerosols from the oxidation of a suite of biogenic hydrocarbons. Two main sets of experiments are performed: the ozonolysis of hydrocarbons in the dark and photooxidation experiments in which HONO is used as an OH precursor. Instead of the normal yield curve approach of plotting SOA yield as a function of the amount of aerosol formed, we present the data in terms of a growth curve, in which aerosol mass is plotted against the amount of hydrocarbon reacted over the course of the experiments. It is found that based on the shapes of these time-dependent growth curves, we can classify the compounds into two different groups based entirely on the number of double bonds of the parent hydrocarbon, regardless of their molecular formulas (isoprene, monoterpenes, sesquiterpenes or oxygenated terpenes). For compounds with only one double bond, aerosol mass increases as more hydrocarbon is consumed, and reaches a maximum when all the hydrocarbon is consumed, implying that the first oxidation step is rate-limiting and the aerosols are formed from nonvolatile first-generation products that partition into the aerosol phase once they are formed. For compounds with more than one double bond, aerosol mass continues to increase even after all hydrocarbon is consumed, resulting in a vertical section in the growth curve. This continuation in aerosol growth indicates the aerosol is formed from the further oxidation of first-generation products by ozone, and/or OH and NO₃ radicals in photooxidation experiments, and that this second oxidation step may also be rate-limiting. This work shows that the growth curve approach is a valuable means of

understanding the mechanisms of SOA formation by providing important information on the rate-determining steps and whether SOA is formed from first- or second-generation products.

Particularly revealing are the time-dependent growth curves for a number of experiments carried out over a range of initial hydrocarbon concentrations, and comparison of those curves with the final SOA growth curve allows us to examine whether it is appropriate to use time-dependent data to understand total SOA formation. It is found that for α -pinene, the time-dependent growth curves describe the final growth data well, suggesting the parameters (α_i and $K_{om,i}$) can be determined from time-dependent data. This is likely the case for other compounds with only one double bond. Our observation implies that if the parent hydrocarbon has only one double bond, then instead of performing chamber experiments over a wide range of initial concentrations, one can simply carry out one experiment, and the time-dependent growth curve from that experiment will represent the final growth data. For terpinolene, the time-dependent growth curves and final SOA growth curve have dramatically different shapes. Therefore, for compounds with more than one double bond, the SOA is likely to have significant contributions from secondary products, and so one cannot simply use the time-dependent data to represent final growth data; instead we need to employ the standard approach, by carrying out experiments over a range of initial concentrations, until gas-phase oxidation is complete and gas-particle equilibrium is established. Thus, one has to be cautious when applying the SOA growth parameters (α_i and $K_{om,i}$) for systems with more than one double bond, making sure the data are obtained at final SOA growth conditions.

The experiments presented in this paper are performed at relatively high initial hydrocarbon concentrations; however, the same analysis should still be valid for lower SOA loadings, which are more atmospherically relevant. For the ozonolysis of both α -pinene (compound with only one double bond) and terpinolene (compound with more than one double bond), we have shown that the time-dependent growth curves have the same general shape regardless of the initial hydrocarbon concentrations. Even with a M_o as low as $20 \mu\text{g m}^{-3}$ such as in the ozonolysis of 12 pbb α -pinene, the time-dependent growth curve still has the same shape as in the ozonolysis of 135 ppb α -pinene. This suggests that the results described here should also apply to the atmospheric conditions in which organic aerosols loadings are smaller.

We have shown that for unsaturated biogenic hydrocarbons, the oxidative attack of each double bond determines the rate of SOA formation. Thus, in atmospheric models of SOA formation from compounds with more than one double bond, it is important that the first-generation products to be explicitly included. This requires the direct study of the chemistry of such intermediates, which presents a number of substantial experimental challenges. Donahue et al. (58) has recently developed a “basis-set” formalism to represent multiple oxidation stages in SOA formation; such an approach may be extremely useful for the inclusion of key intermediates, such as unsaturated oxidation products of biogenic hydrocarbons, in atmospheric models of SOA formation and growth.

2.7 Acknowledgements

This research was funded by the U. S. Environmental Protection Agency Science to Achieve Results (STAR) Program grant number RD-83107501-0, managed by EPA's

Office of Research and Development (ORD), National Center for Environmental Research (NCER), and by U.S. Department of Energy Biological and Environmental Research Program DE-FG02-05ER63983. The University of California contribution to this material is based upon work supported by the National Science Foundation under Grant No. 0443448 and 0119510, and the California Air Resources Board (Contract 00-732). The authors would like to thank Neil M. Donahue for helpful discussions.

2.8 References

- (1) Turpin, B. J.; Huntzicker, J. J. Identifications of secondary organic aerosol episodes and quantification of primary and secondary organic aerosol concentration. *Atmos. Environ.* **1995**, *29*, 3527-3544.
- (2) Atkinson, R.; Arey, J. Gas-phase tropospheric chemistry of biogenic volatile organic compounds: a review. *Atmos. Environ.* **2003**, *37*, S197-S219.
- (3) Kanakidou, M. et al. Organic aerosol and global climate modelling: a review. *Atmos. Chem. Phys.*, **2005**, *5*, 1053-1123.
- (4) Hatakeyama, S; Izumi, K.; Fukuyama, T.; Akimoto, H. Reactions of ozone with α -pinene and β -pinene in air: yields of gaseous and particulate products. *J. Geophys. Res.* **1989**, *94*, 13013-13024.
- (5) Christoffersen, T. S. et al. cis-pinic acid, a possible precursor for organic aerosol formation from ozonolysis of α -pinene. *Atmos. Environ.* **1998**, *32*, 1657-1661.
- (6) Yu, J.; Flagan, R. C.; Seinfeld, J. H. Identification of products containing $-\text{COOH}$, $-\text{OH}$, and $-\text{C}=\text{O}$ in atmospheric oxidation of hydrocarbons. *Environ. Sci. Technol.* **1998**, *32*, 2357-2370.

- (7) Yu, J.; Cocker III, D. R.; Griffin, R. J.; Flagan, R. C.; Seinfeld, J. H. Gas-phase ozone oxidation of monoterpenes: gaseous and particulate products. *J. Atmos. Chem.* **1999**, *34*, 207-258.
- (8) Hoffmann, T.; Bandur, R.; Marggraf, U.; Linscheid, M. Molecular composition of organic aerosols formed in α -pinene/O₃ reaction: implications for new particle formation process. *J. Geophys. Res.* **1998**, *103*, 25569-25578.
- (9) Griffin, R. J.; Cocker III, D.R.; Flagan, R. C.; Seinfeld, J. H. Organic aerosol formation from the oxidation of biogenic hydrocarbons. *J. Geophys. Res.* **1999**, *104*, 3555-3567.
- (10) Jang, M.; Kamens, R. M. Newly characterized products and composition of secondary aerosols from the reaction of α -pinene with ozone. *Atmos. Environ.* **1999**, *33*, 459-474.
- (11) Glasius, M.; Lahaniati, M.; Calogirou, A.; Di Bella, D.; Jensen, N. R.; Hjorth, J.; Kotzias, D.; Larsen, B. R. Carboxylic acids in secondary aerosols from oxidation of cyclic monoterpenes by ozone. *Environ. Sci. Technol.* **2000**, *34*, 1001-1010.
- (12) Koch, S.; Winterhalter, R.; Uherek, E.; Kolloff, A.; Neeb, P.; Moortgat, G. K. Formation of new particles in the gas-phase ozonolysis of monoterpenes. *Atmos. Environ.* **2000**, *34*, 4031-4042.
- (13) Larsen, B. R.; Di Bella, D.; Glasius, M.; Winterhalter, R.; Jensen, N. R.; Hjorth, J. Gas-phase OH oxidation of monoterpenes: gaseous and particulate products. *J. Atmos. Chem.* **2001**, *38*, 231-276.

- (14) Kamens, R. M.; Jaoui, M. Modeling aerosol formation from α -pinene+NO_x in the presence of natural sunlight using gas-phase kinetics and gas-particle partitioning theory. *Environ. Sci. Technol.* **2001**, *35*, 1394-1405.
- (15) Jaoui, M.; Kamens, R. M. Mass balance of gaseous and particulate products analysis from α -pinene/ NO_x/air in the presence of natural sunlight. *J. Geophys. Res.* **2001**, *106*, 12541-12558.
- (16) Librando, V.; Tringali, G. Atmospheric fate of OH initiated oxidation of terpenes. Reaction mechanism of α -pinene degradation and secondary organic aerosol formation. *J. Environ. Manage.* **2005**, *75*, 275-282.
- (17) Hoffmann, T.; Odum, J. R.; Bowman, F.; Collins, D.; Klockow, D.; Flagan, R. C.; Seinfeld, J. H. Formation of organic aerosols from the oxidation of biogenic hydrocarbons. *J. Atmos. Chem.* **1997**, *26*, 182-222.
- (18) Izumi, K.; Fukuyama, T. Photochemical aerosol formation from aromatic hydrocarbons in the presence of NO_x. *Atmos. Environ.* **1990**, *24A*, 1433-1441.
- (19) Hurley, M. D.; Sokolov, O.; Wallington, T. J.; Takekawa, H.; Karasawa, M.; Klotz, B.; Barnes, I.; Becker, K. H. Organic aerosol formation during the atmospheric degradation of toluene. *Environ. Sci. Technol.* **2001**, *35*, 1358-1366.
- (20) Lee, A.; Goldstein, A.; Keywood, M. D.; Gao, S.; Ng, N. L.; Varutbangkul, V.; Bahreini, R.; Flagan, R. C.; Seinfeld, J. H. Gas-phase products and secondary aerosol yields from the ozonolysis of ten different terpenes. *J. Geophys. Res.* **2006**, in press.
- (21) Lee, A.; Goldstein, A.; Ng, N. L.; Kroll, J. H.; Varutbangkul, V.; Bahreini, R.; Flagan, R. C.; Seinfeld, J. H. Gas-phase products and secondary aerosol yields from the photooxidation of sixteen different terpenes. *J. Geophys. Res.* **2006**, submitted.

- (22) Presto, A. A.; Huff Hartz, K. E.; Donahue, N. M. Secondary organic aerosol production from terpene ozonolysis. 1. Effect of UV radiation. *Environ. Sci. Technol.* **2005**, *39*, 7036-7045.
- (23) Presto, A. A.; Huff Hartz, K. E.; Donahue, N. M. Secondary organic aerosol production from terpene ozonolysis. 2. Effect of NO_x concentration. *Environ. Sci. Technol.* **2005**, *39*, 7046-7054.
- (24) Donahue, N. M.; Huff Hartz, K. E.; Chuong, B.; Preston, A. A.; Stanier, C. O.; Rosenhørn, T.; Robinson, A. L.; Pandis, S. N. Critical factors determining the variation in SOA yields from terpene ozonolysis: A combined experimental and computational study. *Faraday Discuss.* **2005**, *130*, 295-309.
- (25) Tolocka, M. P.; Jang, M.; Ginter, J. M.; Cox, F. J.; Kamens, R. M.; Johnston, M. V. Formation of oligomers in secondary organic aerosol. *Environ. Sci. Technol.* **2004**, *38*, 1428-1434.
- (26) Iinuma, Y.; Böge, O.; Gnauk, T.; Herrmann, H. Aerosol-chamber study of the α -pinene/O₃ reaction: influence of particle acidity on aerosol yields and products. *Atmos Environ.* **2004**, *38*, 761-773.
- (27) Gao, S. et al. Particle phase acidity and oligomer formation in secondary organic aerosol. *Environ. Sci. Technol.* **2004**, *38*, 6582-6589.
- (28) Gao, S.; Keywood, M. D.; Ng, N. L.; Surratt, J. D.; Varutbangkul, V.; Bahreini, R.; Flagan, R.C.; Seinfeld, J.H. Low-molecular weight and oligomeric components in secondary organic aerosol from the ozonolysis of cycloalkenes and α -pinene. *J. Phys. Chem. A*, **2004**, *108*, 10147-10164.

- (29) Kalberer, M.; Paulsen, D.; Sax, M.; Steinbacher, M.; Dommen, J.; Prevot, A. S. H.; Fisseha, R.; Weingartner, E.; Frankevich, V.; Zenobi, R.; Baltensperger, U. Identification of polymers as major components of atmospheric organic aerosols. *Science* **2004**, *303*, 1659-1662.
- (30) Odum J. R.; Hoffmann, T.; Bowman, F.; Collins, D.; Flagan, R. C.; Seinfeld, J. H. Gas/particle partitioning and secondary organic aerosol yields. *Environ. Sci. Technol.* **1996**, *30*, 2580-2585.
- (31) Pankow, J. F. An absorption-model of gas-particle partitioning of organic-compounds in the atmosphere. *Atmos. Environ.* **1994**, *28A*, 185-188.
- (32) Pankow, J. F. An absorption-model of the gas aerosol partitioning involved in the formation of secondary organic aerosol. *Atmos. Environ.* **1994**, *28A*, 189-193.
- (33) Odum, J. R.; Jungkamp, T. P. W.; Griffin, R. J.; Forstner, H. J. L.; Flagan, R. C.; Seinfeld, J. H. Aromatics, reformulated gasoline, and atmospheric organic aerosol formation. *Environ. Sci. Technol.* **1997**, *31*, 1890-1897.
- (34) Cocker III, D. R.; Clegg, S. L.; Flagan, R. C.; Seinfeld, J. H. The effect of water on gas-particle partitioning of secondary organic aerosol. Part 1: α -pinene/ozone system. *Atmos. Environ.* **2001**, *35*, 6049-6072.
- (35) Cocker III, D. R.; Mader, B. T.; Kalberer, M.; Flagan, R. C.; Seinfeld, J. H. The effect of water on gas-particle partitioning of secondary organic aerosol. II: *m*-xylene and 1,3,5-trimethybenzene photooxidation systems. *Atmos. Environ.* **2001**, *35*, 6073-6085.
- (36) Keywood, M. D.; Varutbangkul, V.; Bahreini, R.; Flagan, R. C.; Seinfeld, J. H. Secondary organic aerosol formation from the ozonolysis of cycloalkenes and related compounds. *Environ. Sci. Technol.* **2004**, *38*, 4157-4164.

- (37) Chung, S. H.; Seinfeld, J. H. Global distribution and climate forcing of carbonaceous aerosols. *J. Geophys. Res.* **2002**, *107*, 4407, doi10.1029/2001JD001397.
- (38) Kroll, J. H.; Seinfeld, J. H. Representation of secondary organic aerosol (SOA) laboratory chamber data or the interpretation of mechanisms of particle growth. *Environ. Sci. Technol.* **2005**, *39*, 4159-4165.
- (39) Song, C.; Na, K.; Cocker III, D. R. Impact of the hydrocarbon to NO_x ratio on secondary organic aerosol formation. *Environ. Sci. Technol.* **2005**, *39*, 3143-3149.
- (40) Holzinger, R.; Lee, A.; Paw U, K. T.; Goldstein, A. H. Observation of oxidation products above a forest imply biogenic emissions of very reactive compounds. *Atmos. Chem. Phys.* **2005**, *5*, 67-75.
- (41) Cocker III, D. R.; Flagan, R. C.; Seinfeld, J. H. State-of-the-art chamber facility for studying atmospheric aerosol chemistry. *Environ. Sci. Technol.* **2001**, *35*, 2594-2601.
- (42) Lindinger, W.; Hansel, A.; Jordan, A. Proton-transfer-reaction mass spectrometry (PTR-MS): on-line monitoring of volatile organic compounds at pptv levels. *Chem. Soc. Rev.* **1998**, *27*, 347-354.
- (43) Jayne, J. T.; Leard, D. C.; Zhang, X.; Davidovits, P.; Smith, K. A.; Kolb, C. E.; Worsnop, D. W. Development of an Aerosol Mass Spectrometer for size and composition analysis of submicron particles. *Aerosol Sci. and Technol.* **2000**, *33*, 49-70.
- (44) Allan, J. D.; Jimenez, J. L.; Coe, H.; Bower, K. N.; Williams, P. I.; Worsnop, D. R. Quantitative sampling using an Aerodyne Aerosol Mass Spectrometer. Part 1: Techniques of data interpretation and error analysis. *J. Geophys. Res.* **2003**, *108*, 4090, doi:4010.1029/2002JD002358.

- (45) Allan, J. D.; Bower, K. N.; Coe, H.; Boudries, H.; Jayne, J. T.; Canagaratna, M. R.; Millet, D. B.; Goldstein, A. H.; Quinn, P. K.; Weber, R. J.; Worsnop, D. R. Submicron aerosol composition at Trinidad Head, California, during ITCT 2K2: Its relationship with gas phase volatile organic carbon and assessment of instrument performance. *J. Geophys. Res.*, **2004**, *109*, D23S24, doi:10.1029/2003JD004208.
- (46) Bahreini, R.; Keywood, M. D.; Ng, N. L.; Varutbangkul, V.; Gao, S.; Flagan, R. C.; Seinfeld, J. H. Measurements of secondary organic aerosol (SOA) from oxidation of cycloalkenes, terpenes, and *m*-xylene using an Aerodyne aerosol mass spectrometer. *Environ. Sci. Technol.* **2005**, *39*, 5674-5688.
- (47) McLafferty, F. W.; Turecek, F. *Interpretation of Mass Spectra*; University Science Books; Sausalito, 1993.
- (48) Kamens, R. M.; Jang, M.; Chien, C. J.; Leach, K. Aerosol formation from the reaction of α -pinene and ozone using a gas-phase kinetics-aerosol partition model. *Environ. Sci. Technol.* **1999**, *33*, 1430-1438.
- (49) Jenkin, M. E.; Shallcross, D. E.; Harvey, J. N. Development and application of a possible mechanism for the generation of cis-pinic acid from the ozonolysis of α - and β -pinene. *Atmos. Environ.* **2000**, *34*, 2837-2850.
- (50) Hallquist, M.; Wängberg, I.; Ljungström, E. Atmospheric fate of carbonyl oxidation products originating from α -pinene and Δ^3 -carene: determination of rate of reaction with OH and NO₃ radicals, UV absorption cross sections, and vapor pressures. *Environ. Sci. Technol.* **1997**, *31*, 3166-3172.

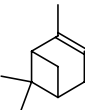
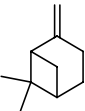
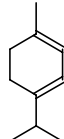
- (51) Hatakeyama, S; Izumi, K.; Fukuyama, T.; Akimoto, H.; Washida, N. Reactions of OH with α -pinene and β -pinene in air: estimate of global CO production from the atmospheric oxidation of terpenes. *J. Geophys. Res.* **1991**, *96*, 947-958.
- (52) Hakola, H.; Arey, J.; Aschmann, S. M.; Atkinson, R. Product formation from the gas-phase reactions of OH radicals and O₃ with a series of monoterpenes. *J. Atmos. Chem.* **1994**, *18*, 75-102.
- (53) Reissell, A.; Harry, C.; Aschmann, S. M.; Atkinson, R.; Arey, J. Formation of acetone from the OH radical- and O₃-initiated reactions of a series of monoterpenes. *J. Geophys. Res.* **1999**, *104*, 13869-13879.
- (54) Kwok, E. S. C.; Atkinson, R. Estimation of hydroxyl radical reaction rate constants for gas-phase organic compounds using a structure-reactivity relationship: an update. *Atmos. Environ.* **1995**, *29*, 1685-1695.
- (55) Kroll, J. H.; Ng, N. L.; Murphy, S. M.; Flagan, R. C.; Seinfeld, J. H. Secondary organic aerosol formation from isoprene photooxidation under high-NO_x conditions. *Geophys. Res. Lett.* 2005, *32*, L18808, doi:10.1029/2005GL023637.
- (56) Kroll, J. H.; Ng, N. L.; Murphy, S. M.; Flagan, R. C.; Seinfeld, J. H. Secondary organic aerosol formation from isoprene photooxidation. *Environ. Sci. Technol.* **2006**, in press.
- (57) Varutbangkul, V. et al. Hygroscopicity of secondary organic aerosols formed by oxidation of cycloalkenes, monoterpenes, sesquiterpenes and related compounds, *Atmos. Chem. Phys.* **2006**, submitted.

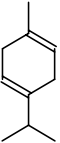
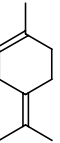
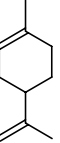
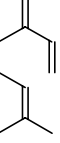
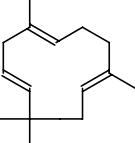
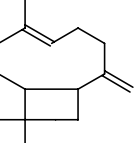
(58) Donahue, N. M.; Robinson, A. L.; Stanier, C. O.; Pandis, S. N. The coupled partitioning, dilution, and chemical aging of semivolatile organics. *Environ. Sci. Technol.* **2006**, in press.

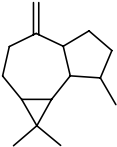
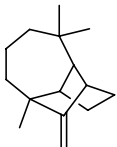
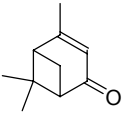
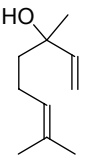
(59) Reissell, A.; Aschmann, S. M.; Atkinson, R.; Arey, J. Products of the OH radical- and O₃-initiated reactions of myrcene and ocimene. *J. Geophys. Res.* **2002**, *107*, 4138, doi:10.1029/2001JD001234.

(60) Shu, Y.; Kwok, E. S. C.; Tuazon, E. C.; Atkinson, R.; Arey, J. Products and gas-phase reactions of linalool with OH radicals, NO₃ radicals, and O₃. *Environ. Sci. Technol.* **1997**, *31*, 896-904.

Table 2. 1. Parent hydrocarbon studied

Parent Hydrocarbon	Structure	Formula (MW)	$k_{\text{Ozone}} (\text{cm}^3 \text{ molec}^{-1} \text{ s}^{-1})^a$	$k_{\text{OH}} (\text{cm}^3 \text{ molec}^{-1} \text{ s}^{-1})^a$
isoprene		C_5H_8 (68)	NS	9.9×10^{-11}
α -pinene		$\text{C}_{10}\text{H}_{16}$ (136)	8.4×10^{-17}	5.3×10^{-11}
β -pinene		$\text{C}_{10}\text{H}_{16}$ (136)	1.5×10^{-17}	7.7×10^{-11}
Δ^3 -carene		$\text{C}_{10}\text{H}_{16}$ (136)	3.7×10^{-17}	8.7×10^{-11}
α -terpinene		$\text{C}_{10}\text{H}_{16}$ (136)	2.1×10^{-14}	3.6×10^{-10}

γ -terpinene		$C_{10}H_{16}$ (136)	NS	1.8×10^{-10}
terpinolene		$C_{10}H_{16}$ (136)	1.9×10^{-15}	2.3×10^{-10}
limonene		$C_{10}H_{16}$ (136)	NS	1.7×10^{-10}
myrcene		$C_{10}H_{16}$ (136)	4.7×10^{-16}	2.1×10^{-10}
α -humulene		$C_{15}H_{24}$ (204)	1.17×10^{-14}	3.0×10^{-10}
β -caryophyllene		$C_{15}H_{24}$ (204)	1.16×10^{-14}	2.0×10^{-10}

aromadendrene		$C_{15}H_{24}$ (204)	NS	N/A
longifolene		$C_{15}H_{24}$ (204)	NS	4.8×10^{-11}
methyl chavicol		$C_{10}H_{12}O$ (148)	$1.7 \times 10^{-17}{}^b$	N/A
verbenone		$C_{10}H_{14}O$ (150)	NS	N/A
linalool		$C_{10}H_{18}O$ (154)	$6 \times 10^{-16}{}^b$	1.6×10^{-10}

a: Rate constants obtained from Atkinson and Arey (2) and references therein

b: Rate constants estimated from the rate of hydrocarbon decay

NS: Compounds not studied in ozonolysis experiments; N/A: Data not available

Table 2. 2. Initial conditions and data for ozonolysis experiments

Date	Parent Hydrocarbon	T (K)	RH (%)	Seed	ΔHC (ppb)	ΔM_o ($\mu\text{g}/\text{m}^3$)
3/24/2003	α -pinene	292	4.1	$(\text{NH}_4)_2\text{SO}_4$	186	419
3/12/2003	β -pinene	293	6.3	$(\text{NH}_4)_2\text{SO}_4$	180	174
4/4/2003	Δ^3 -carene	293	6.5	$(\text{NH}_4)_2\text{SO}_4$	90	273
3/31/2003	α -terpinene	293	3.4	$(\text{NH}_4)_2\text{SO}_4$	61	160
3/31/2003	terpinolene	293	5.5	$(\text{NH}_4)_2\text{SO}_4$	112	124
4/2/2003	myrcene	293	6.7	$(\text{NH}_4)_2\text{SO}_4$	98	61
3/28/2003	α -humulene	293	4.5	None	111	416
3/21/2003	β -caryophyllene	293	6.2	None	88	336
4/4/2003	methyl chavicol	292	4.0	$(\text{NH}_4)_2\text{SO}_4$	101	40
4/2/2003	linalool	292	4.0	$(\text{NH}_4)_2\text{SO}_4$	106	8

Table 2. 3. Initial conditions and data for photooxidation experiments

Date	Parent Hydrocarbon	T (K)	RH (%)	Seed	ΔHC (ppb)	ΔM_0 ($\mu\text{g}/\text{m}^3$)	$\frac{\text{ppbHC}}{\text{ppbNO}_x}$
3/4/2005	isoprene	294	54	(NH ₄) ₂ SO ₄	506	26	1.8
3/9/2005	α -pinene	293	43	(NH ₄) ₂ SO ₄	108	198	1.1
3/9/2005	β -pinene	293	50	(NH ₄) ₂ SO ₄	170	293	2.1
3/12/2005	Δ^3 -carene	294	52	(NH ₄) ₂ SO ₄	109	236	0.8
3/24/2005	α -terpinene	293	47	(NH ₄) ₂ SO ₄	103	145	0.9
3/21/2005	γ -terpinene	294	48	(NH ₄) ₂ SO ₄	119	193	1.1
3/23/2005	terpinolene	294	50	(NH ₄) ₂ SO ₄	110	190	1.1
3/25/2005	limonene	294	45	(NH ₄) ₂ SO ₄	120	394	1.1
3/22/2005	myrcene	294	53	(NH ₄) ₂ SO ₄	112	272	0.9
3/16/2005	α -humulene	294	53	None	46	254	1.4
3/14/2005	β -caryophyllene	295	56	None	37	212	1.3
3/15/2005	aromadendrene	294	47	None	34	107	1.4
3/19/2005	longifolene	294	49	None	34	186	0.8
3/26/2005	methyl chavicol	294	49	(NH ₄) ₂ SO ₄	79	194	0.8
3/31/2005	verbenone	294	46	(NH ₄) ₂ SO ₄	105	127	1.1
4/1/2005	linalool	295	40	(NH ₄) ₂ SO ₄	124	104	1.0

Table 2. 4. Ozonolysis - major first-generation products and their molar yields

Date	Parent Hydrocarbon (more than one double bond)	m/z of major first-generation products	Product Molar Yield
3/31/2003	α -terpinene	N/A	N/A
3/31/2003	terpinolene	111 (4-methyl-3-cyclohexen-1-one) ^a	0.58 ^b
4/2/2003	myrcene	111 (4-vinyl-4-pentenal) ^c	0.53 ^b
3/28/2003	α -humulene	N/A	N/A
3/21/2003	β -caryophyllene	N/A	N/A

N/A: No major first-generation products are observed to correlate with aerosol growth

a: Previously identified by Hakola et al. (52) and Reissell et al. (53)

b: Sum of yields of m/z 111 and m/z 93, the dehydrated fragment of m/z 111

c: Previously identified by Reissell et al. (59)

Table 2. 5. Photooxidation - major first-generation products and their molar yields

Date	Parent Hydrocarbon (more than one double bond)	m/z of major first-generation products	Product Molar Yield
3/4/2005	isoprene	71 (methacrolein + MVK)	0.79
3/24/2005	α -terpinene	N/A	N/A
3/21/2005	γ -terpinene	153	0.05
		169 (γ -terpinaldehyde)	0.58 ^a
3/23/2005	terpinolene	111 (4-methyl-3-cyclohexen-1-one) ^b	0.47 ^c
3/25/2005	limonene	169 (limononaldehyde) ^d	0.61 ^e
3/22/2005	myrcene	93	0.34
		113	0.36
3/16/2005	α -humulene	N/A	N/A
3/14/2005	β -caryophyllene	N/A	N/A
4/1/2005	linalool	129 (4-hydroxy-4-methyl-5-hexen-1-al) ^f	0.74 ^g

N/A: No major first-generation products are observed to correlate with aerosol growth

a: Sum of yields of all fragments and isotopes of m/z 169 (i.e. m/z 107, m/z 123, m/z 124, m/z 151, m/z 152 and m/z 170)

b: Previously identified by Hakola et al. (52) and Reissell et al. (53)

c: Sum of yields of m/z 111 and m/z 93, the dehydrated fragment of m/z 111

d: Previously identified by Hakola et al. (52)

e: Sum of yields of all fragments and isotopes of m/z 169 (i.e. m/z 107, m/z 108, m/z 123, m/z 124, m/z 133, m/z 151, m/z 152 and m/z 170)

f: Previously identified by Shu et al. (60)

g: Sum of yields of m/z 129, m/z 111 and m/z 93, the dehydrated fragments of m/z 129

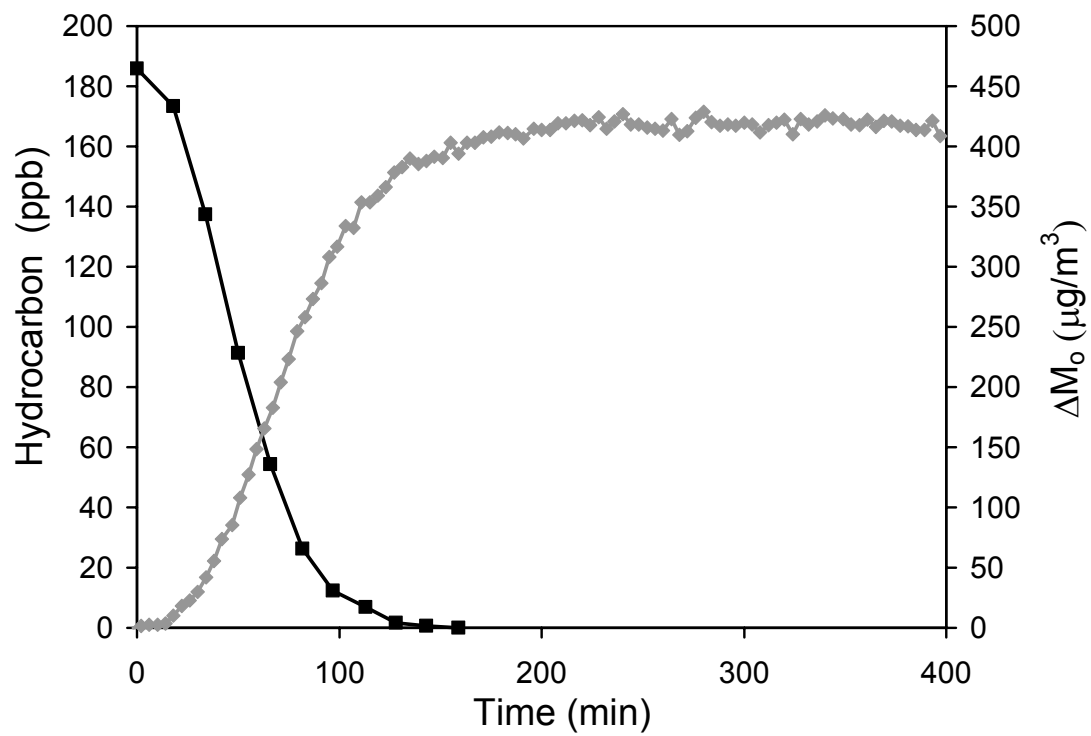
Figure 2. 1. α -pinene ozonolysis and aerosol mass formation

Figure 2. 2. Terpinolene ozonolysis and aerosol mass formation

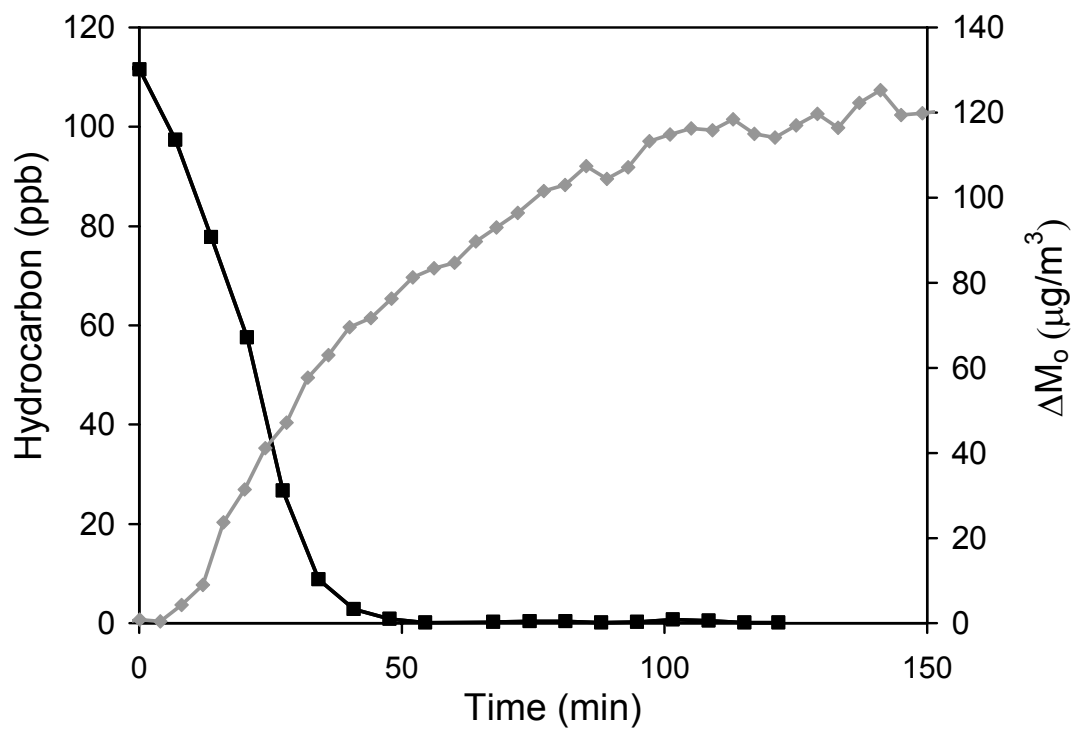


Figure 2. 3. Time-dependent growth curves for all compounds studied in ozonolysis experiments (except linalool, which does not have significant aerosol growth), note that the axes have different scales.

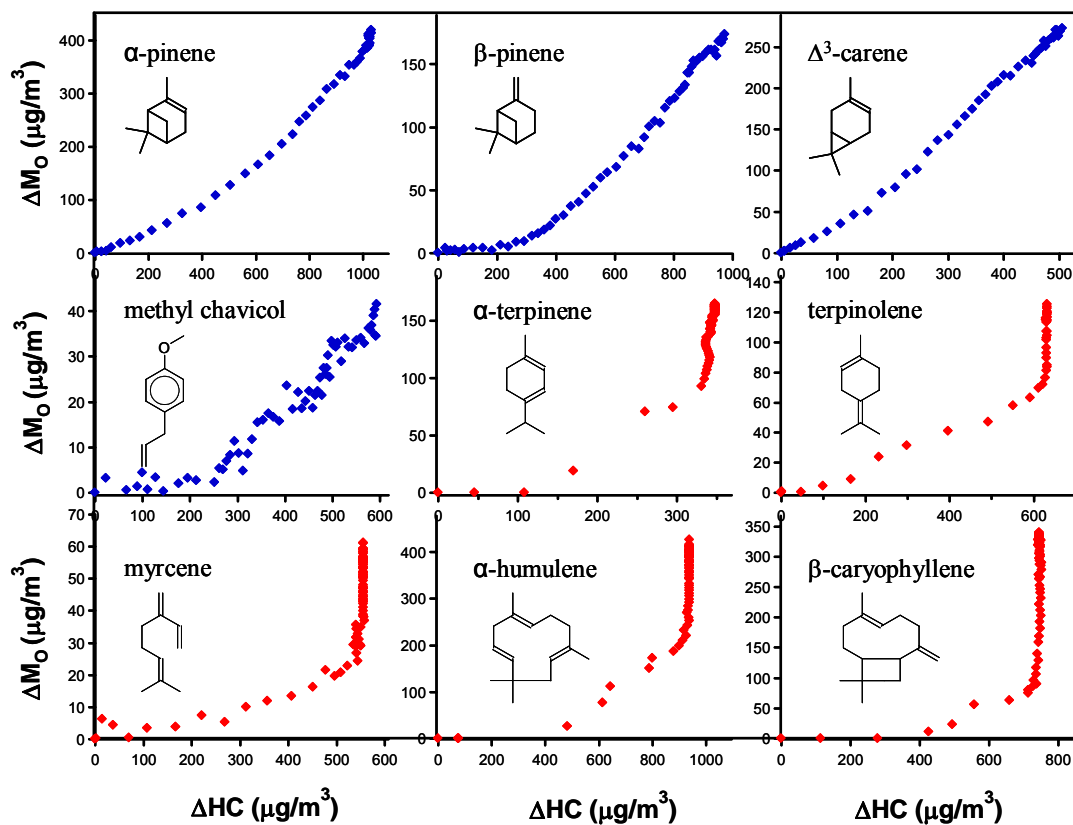


Figure 2. 4. Time-dependent growth curves for all compounds studied in photooxidation experiments (except longifolene, which is shown in Figure 2.20), note that the axes have different scales.

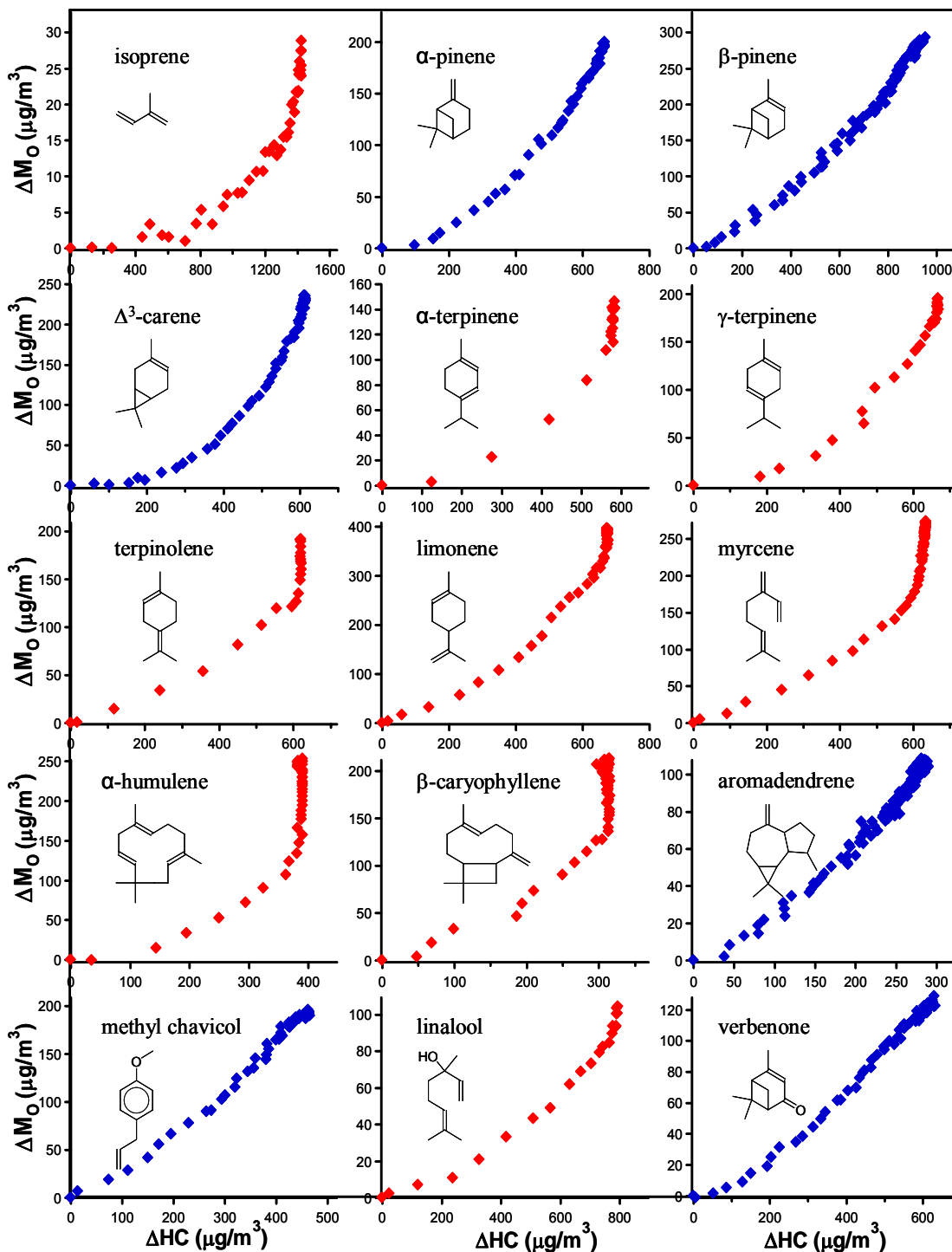


Figure 2. 5. Time-dependent and final growth curves for α -pinene ozonolysis. The large diamonds represent final growth data through which the yield curve has been fit.

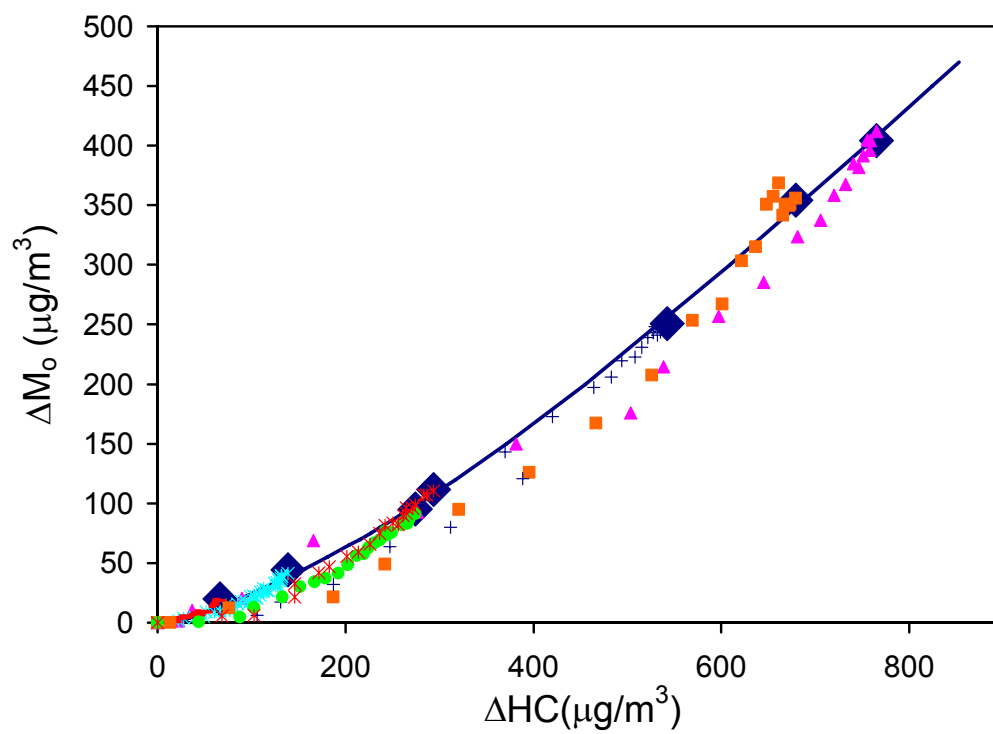


Figure 2. 6. AMS relative delta time series plot for α -pinene ozonolysis. Unsaturated organics yield delta values ≤ 0 , and oxygenated organics yield delta values ≥ 2 .

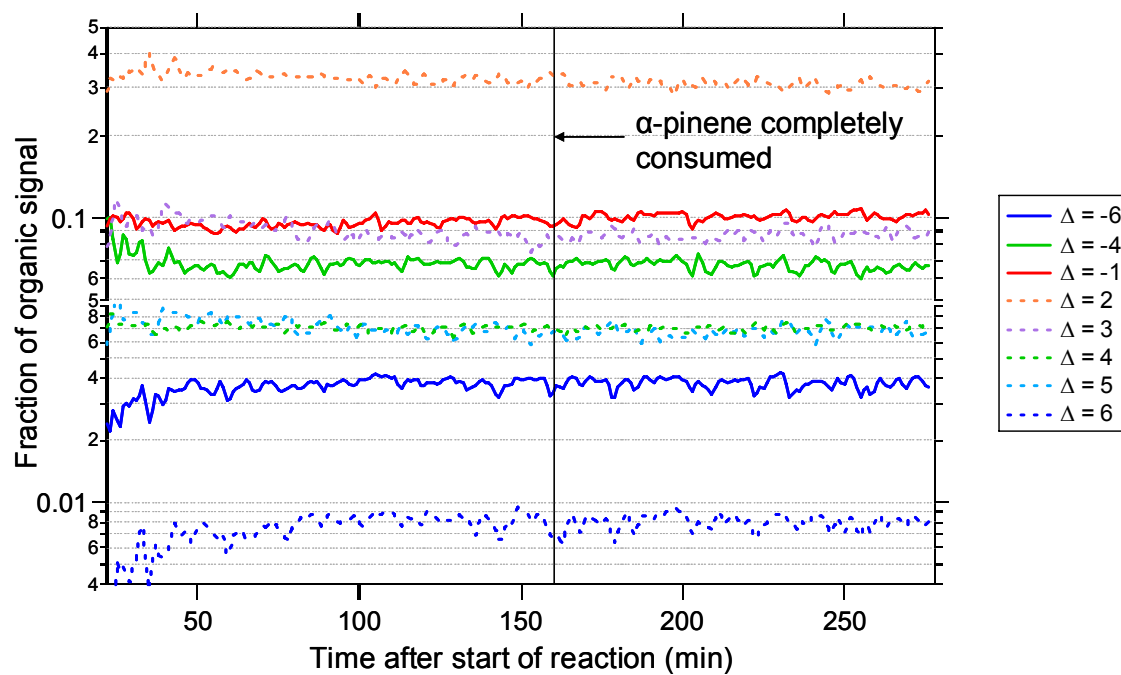


Figure 2. 7. Time-dependent and final growth curves for terpinolene ozonolysis. The large diamonds represent final growth data through which the yield curve has been fit.

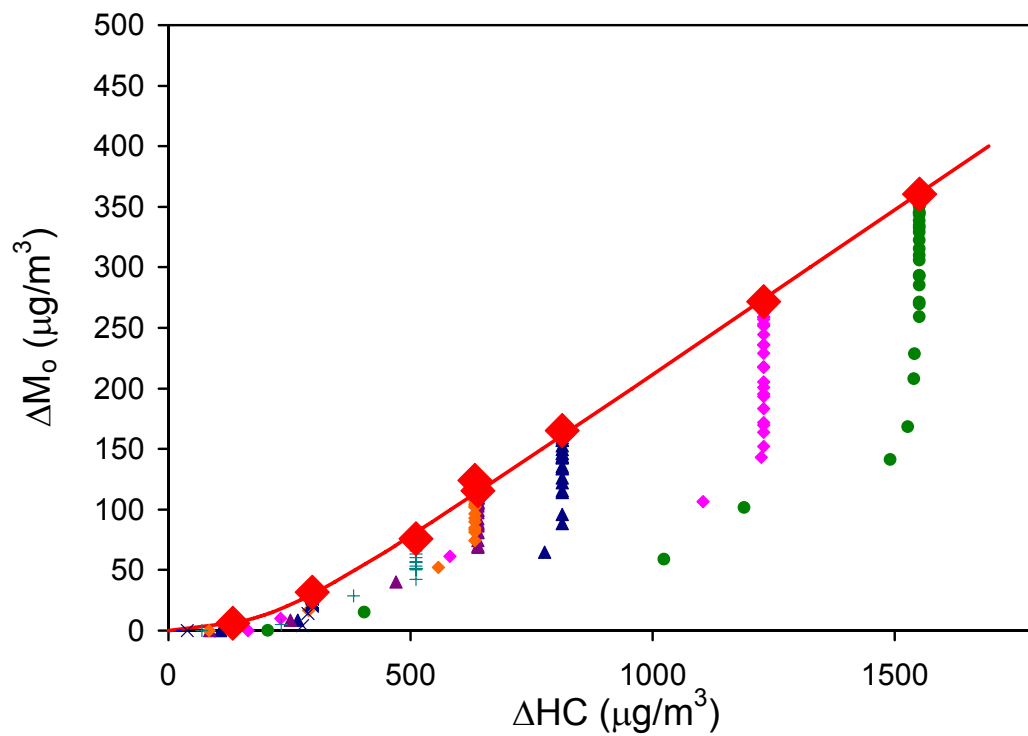


Figure 2. 8. Time evolution of pinonaldehyde in α -pinene ozonolysis. The concentration of pinonaldehyde is the average of the upper and lower limits measured by PTR-MS (20).

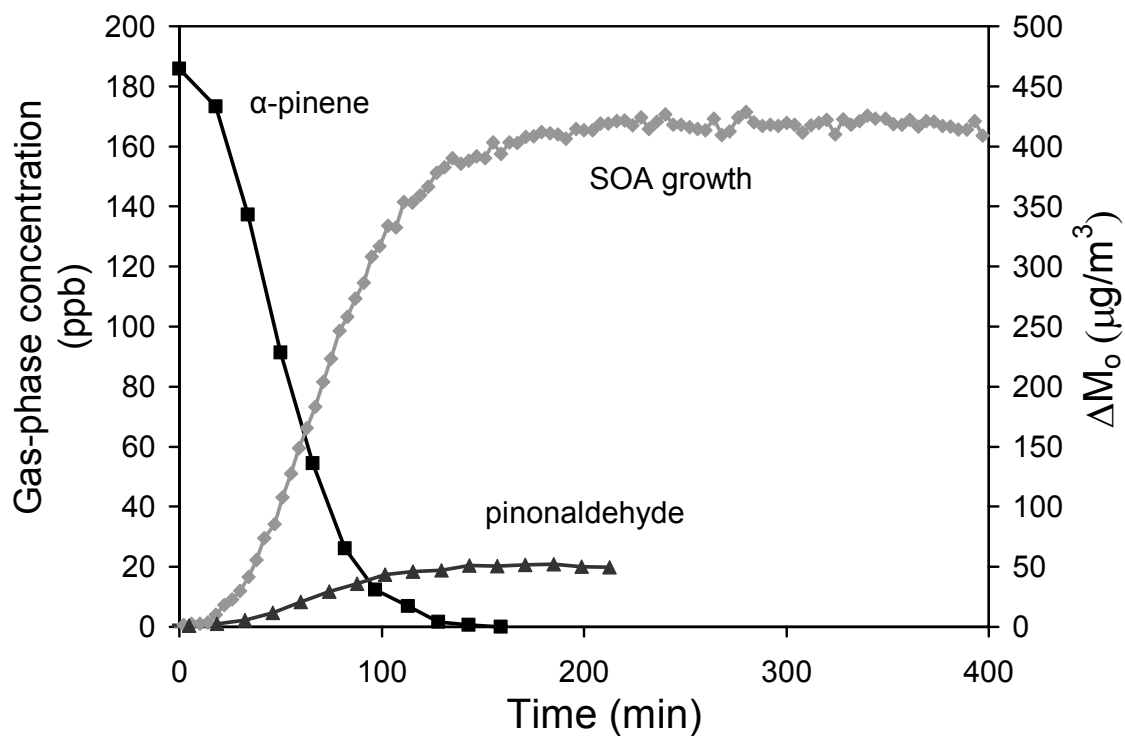


Figure 2. 9. Time evolution of pinonaldehyde in α -pinene photooxidation. The concentration of pinonaldehyde is the mid-range mixing ratio measured by PTR-MS (21).

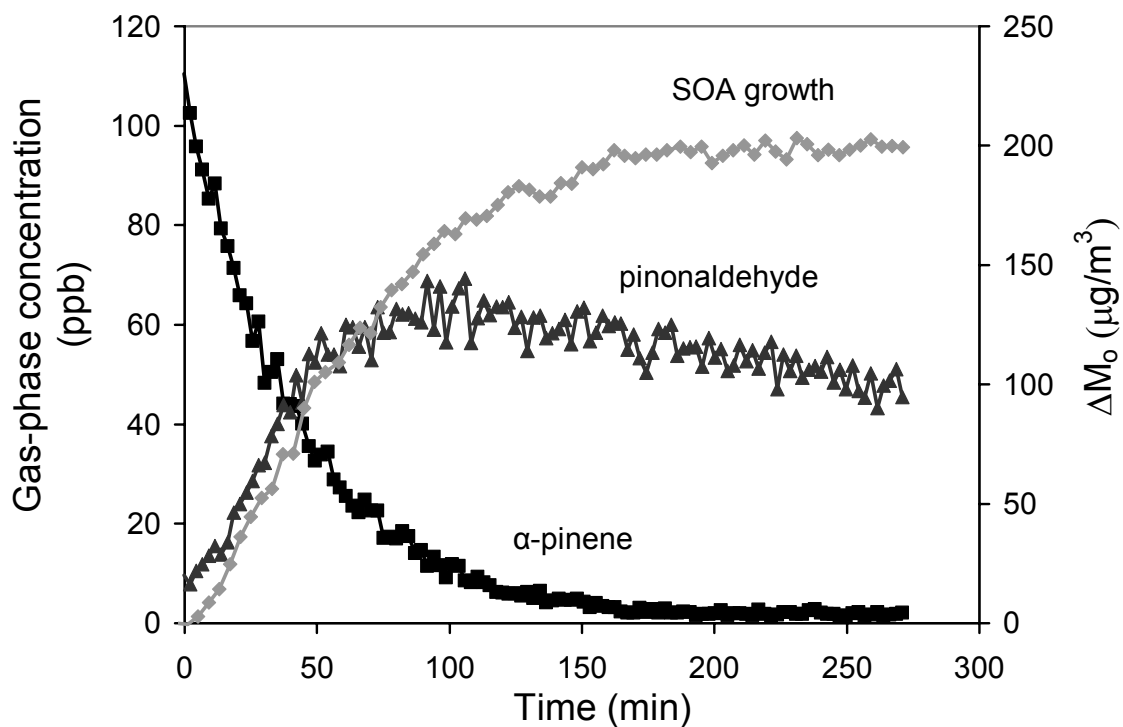


Figure 2. 10. Time evolution of m/z 93 and m/z 111 ions for terpinolene ozonolysis; m/z 93 is the dehydrated fragment of m/z 111.

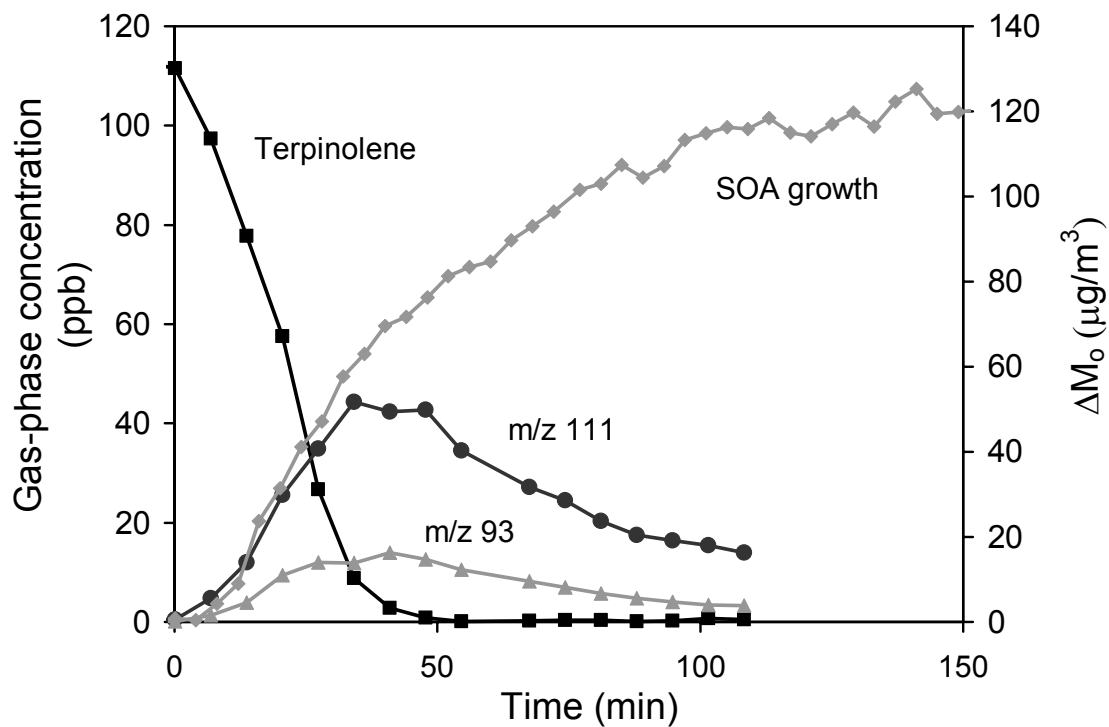


Figure 2. 11. The amount of the intermediate product m/z 111 (including the dehydrated fragment m/z 93) measured, formed and reacted over time for terpinolene ozonolysis

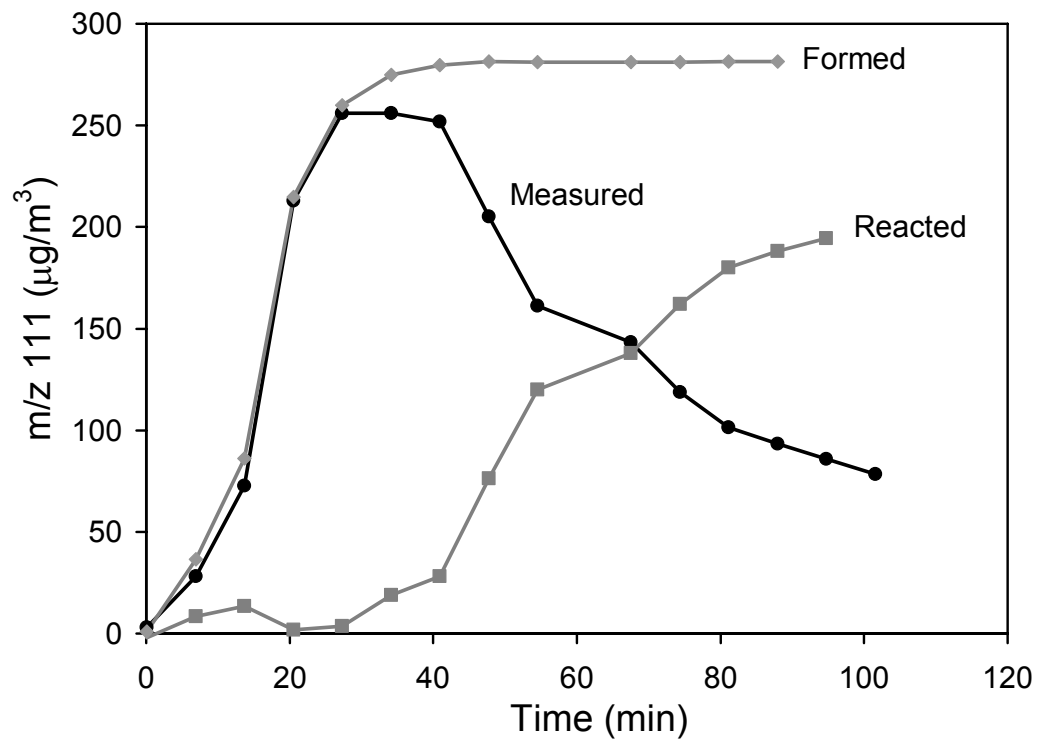


Figure 2. 12. SOA mass formed as a function of the amount of the intermediate product m/z 111 reacted for terpinolene ozonolysis

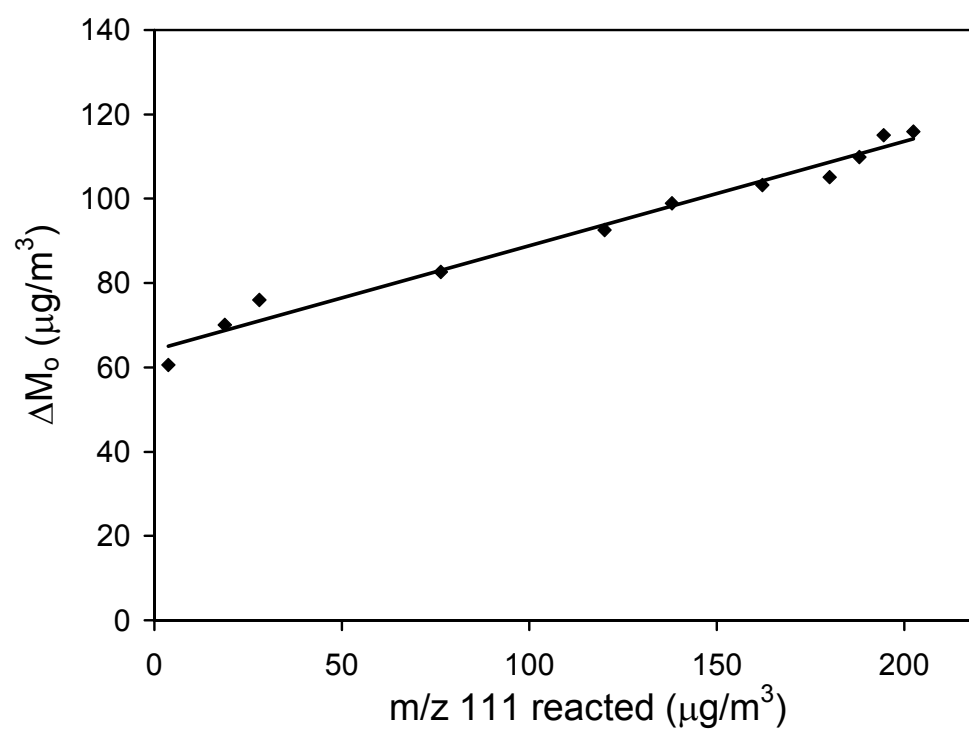


Figure 2. 13. SOA mass formed as a function of the amount of the intermediate product m/z 111 reacted for terpinolene photooxidation

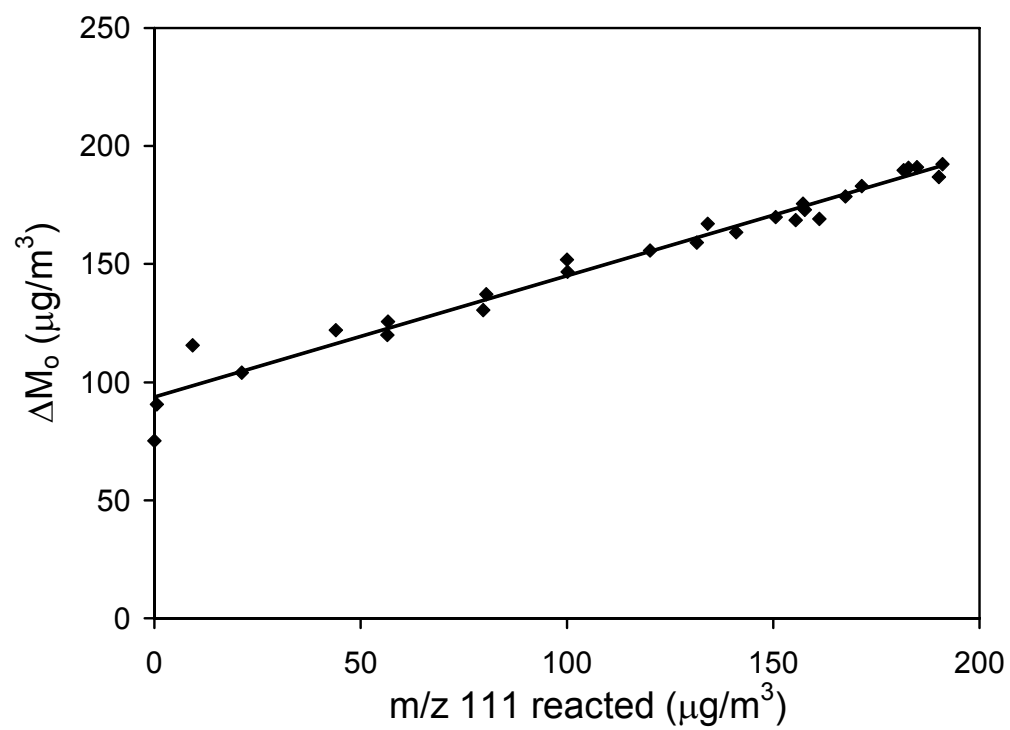


Figure 2. 14. SOA mass formed as a function of the amount of the intermediate product m/z 169 (including its fragments and isotopes) reacted for limonene photooxidation

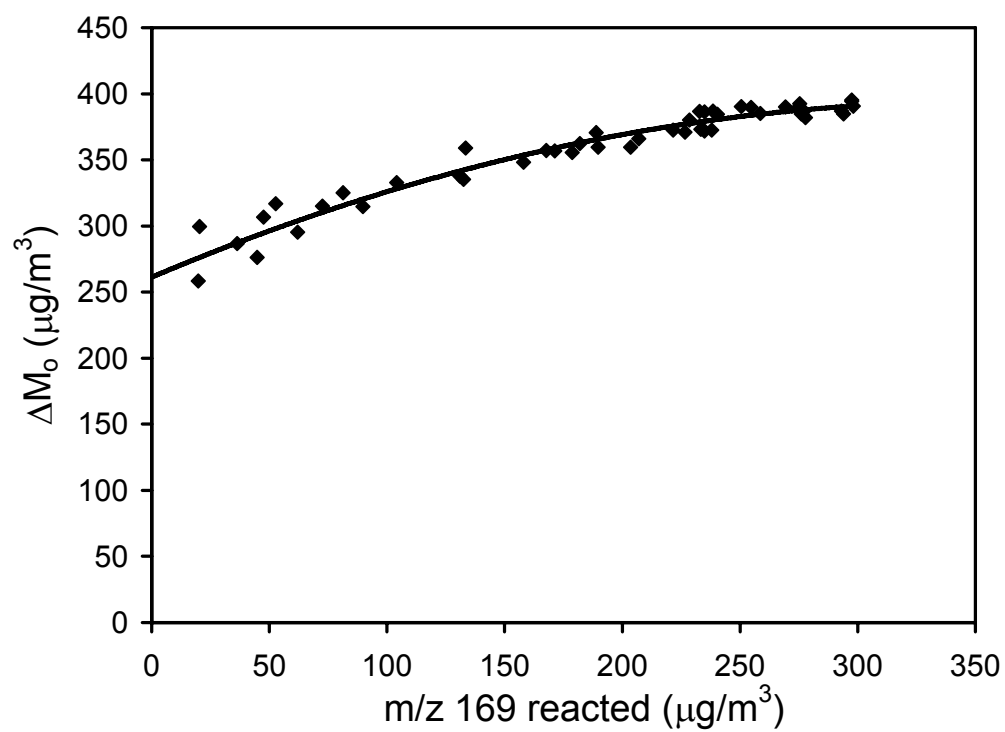


Figure 2. 15. Time evolution of methacrolein + methyl vinyl ketone for isoprene photooxidation

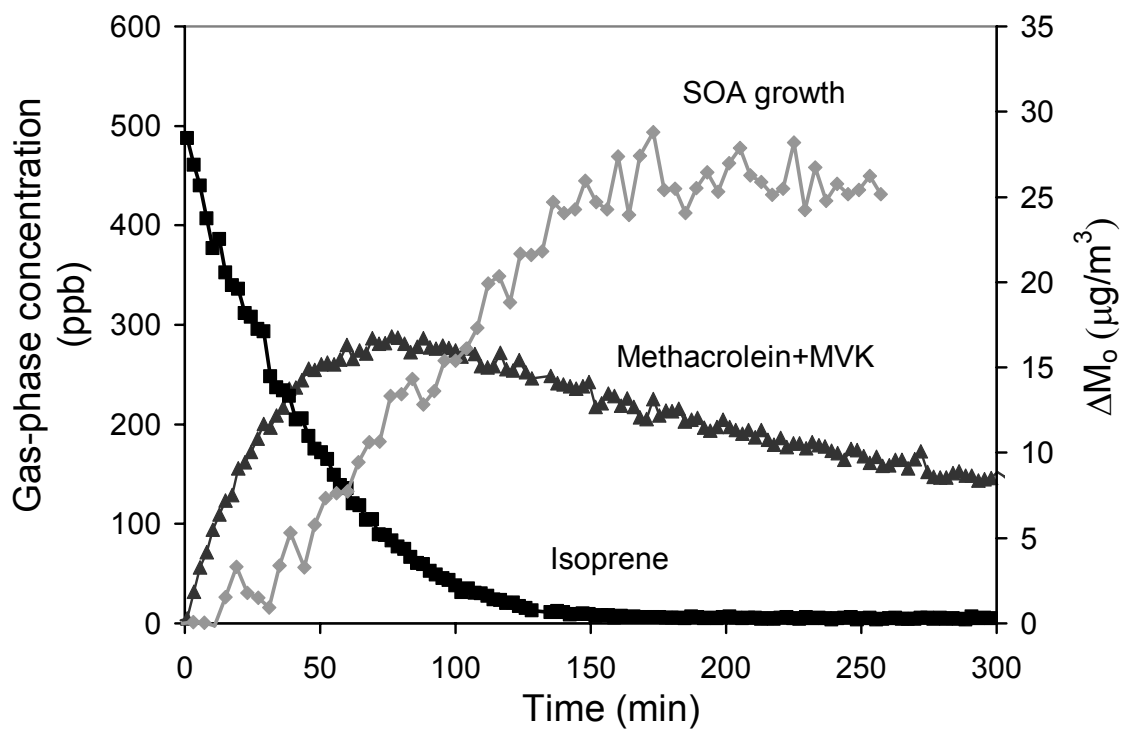


Figure 2. 16. SOA mass formed as a function of the amount of the methacrolein + methyl vinyl ketone reacted for isoprene photooxidation

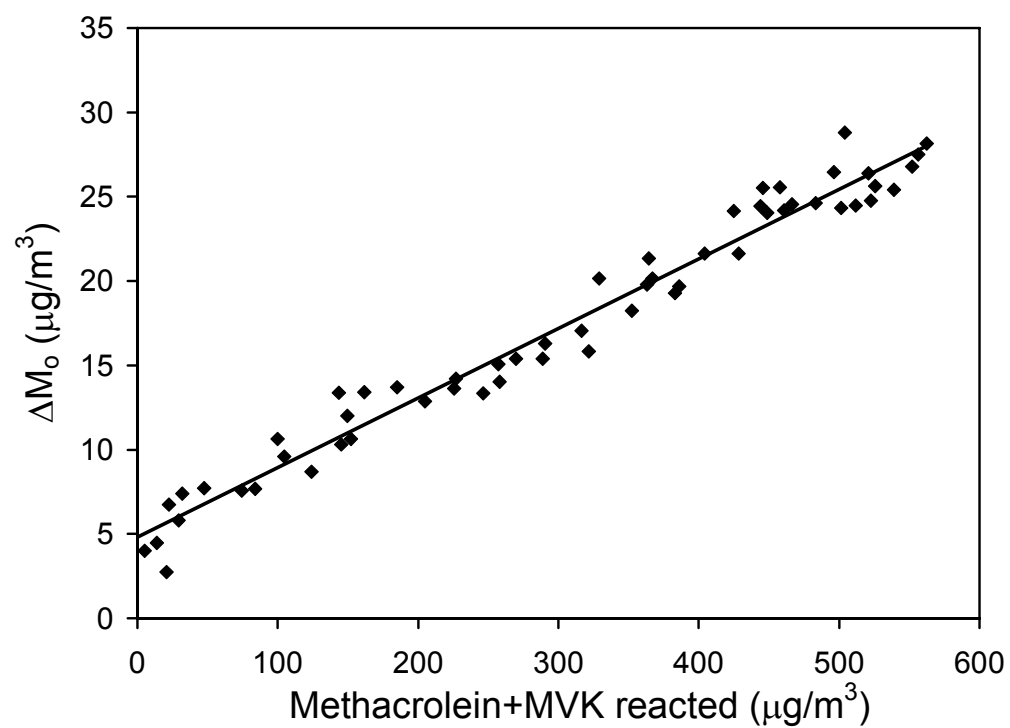


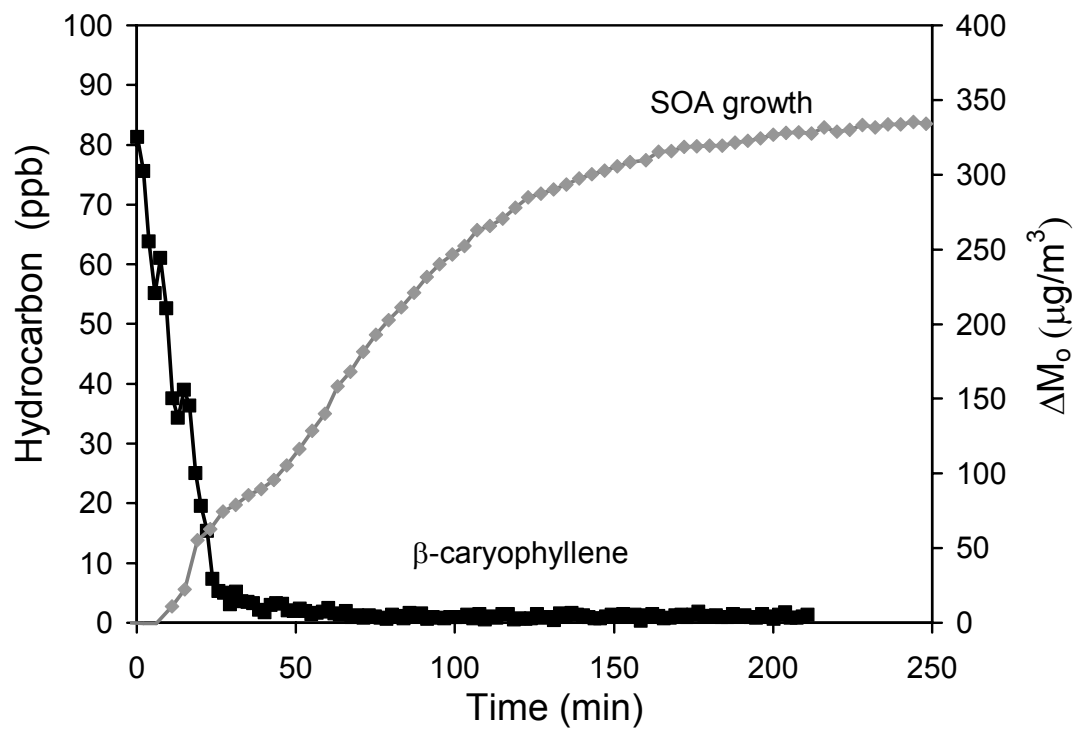
Figure 2. 17. β -caryophyllene ozonolysis and aerosol mass formation

Figure 2. 18. β -caryophyllene and ozone reacted over the course of the experiment (Table 2.2: Experiment on 3/21/2003)

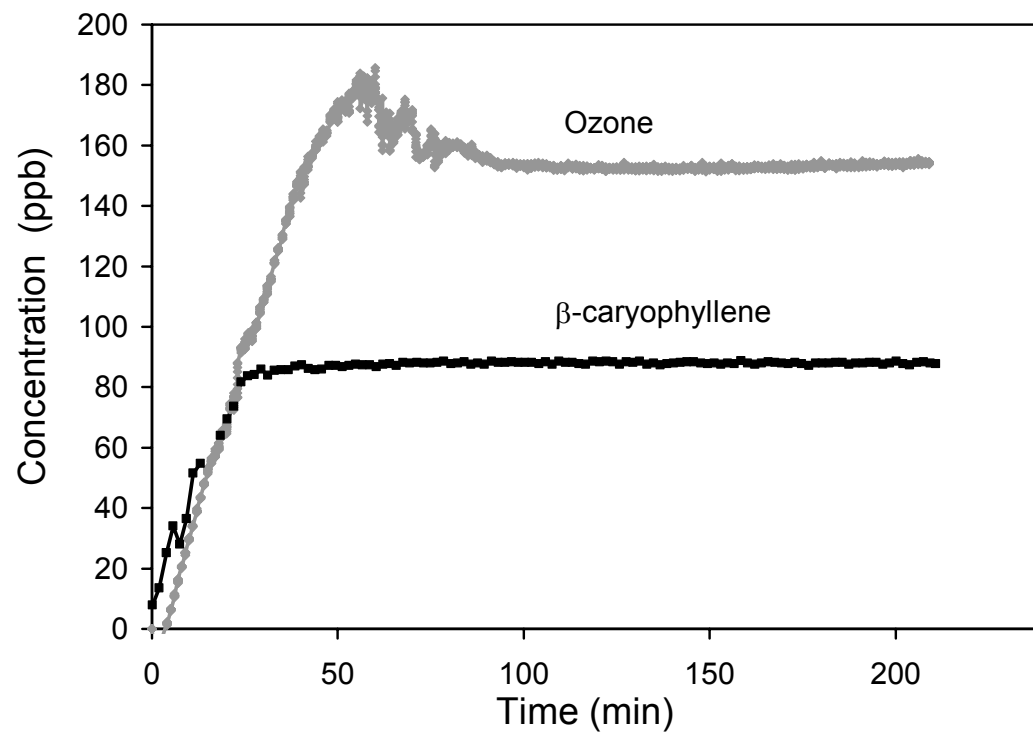


Figure 2. 19. AMS relative delta time series plot for β -caryophyllene ozonolysis. Unsaturated organics yield delta values ≤ 0 , and oxygenated organics yield delta values ≥ 2 .

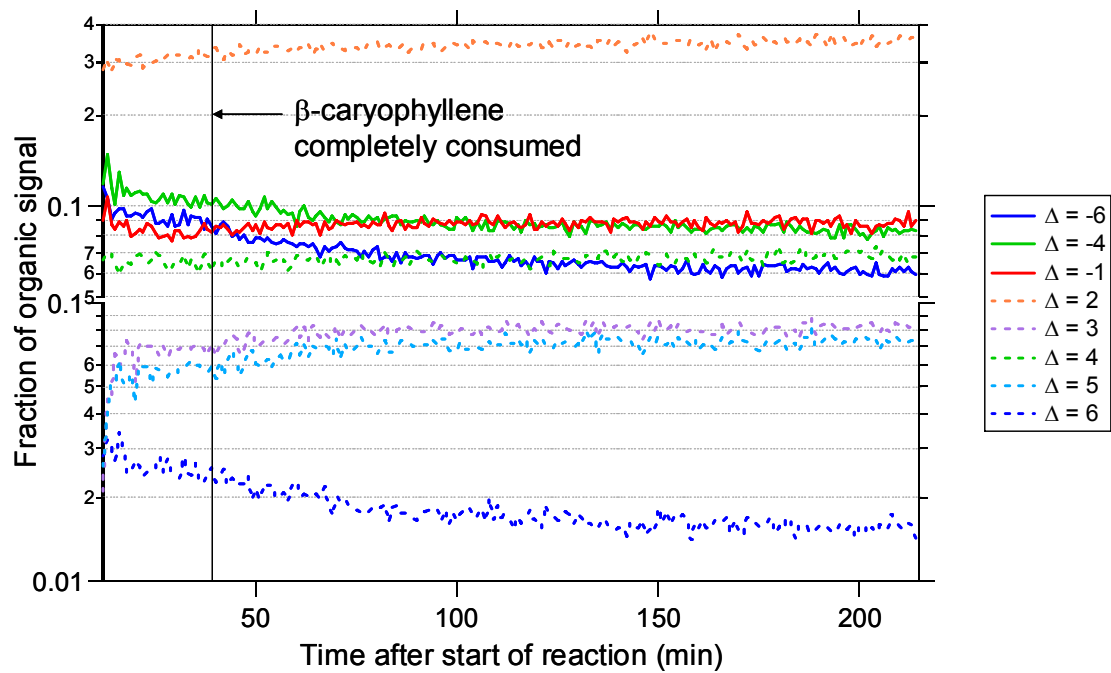
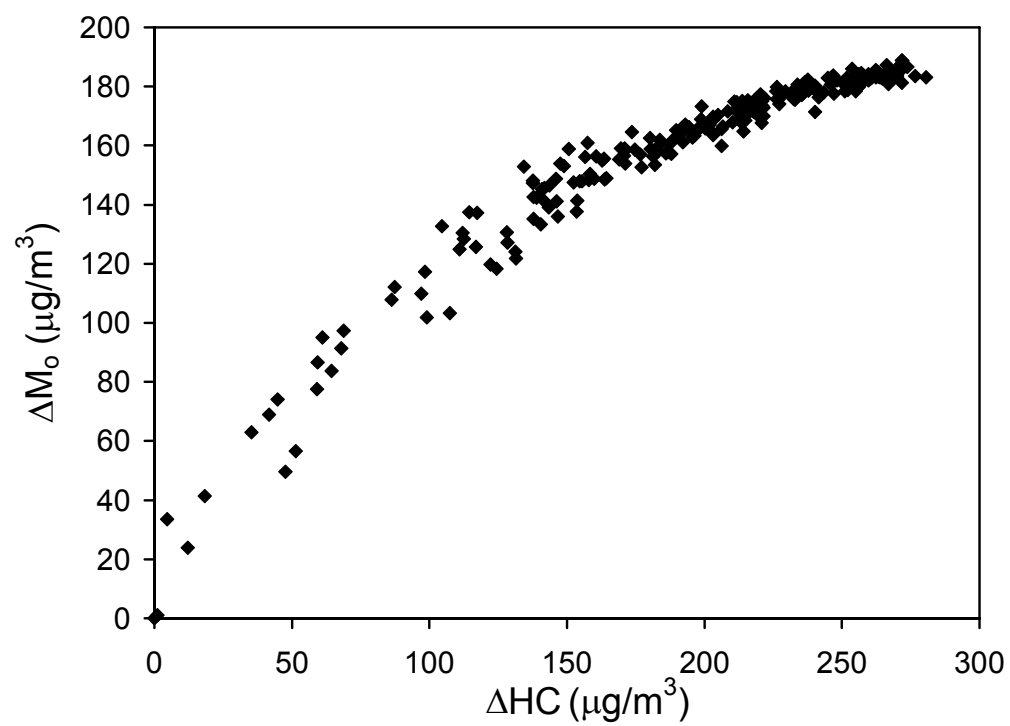


Figure 2. 20. Growth curve for longifolene photooxidation



Chapter 3

Particle Phase Acidity and Oligomer Formation in Secondary Organic Aerosol*

*This chapter is reproduced by permission from “Particle phase acidity and oligomer formation in secondary organic aerosol” by S. Gao, N. L. Ng, M. D. Keywood, V. Varutbangkul, R. Bahreini, A. Nenes, J. He, K. Y. Yoo, J. L. Beauchamp, R. P. Hodyss, R. C. Flagan, and J. H. Seinfeld, *J. Phys Chem.*, 10.1021/jp047466e, 2004. Copyright 2004, American Chemical Society.

3.1 Abstract

A series of controlled laboratory experiments are carried out in dual teflon chambers to examine the presence of oligomers in secondary organic aerosols (SOA) from hydrocarbon ozonolysis as well as to explore the effect of particle phase acidity on SOA formation. In all seven hydrocarbon systems studied, i.e., α -pinene, cyclohexene, 1-methyl cyclopentene, cycloheptene, 1-methyl cyclohexene, cyclooctene, and terpinolene, oligomers with MW from 250 to 1600 are present in the SOA formed, both in the absence and presence of seed particles and regardless of the seed particle acidity. These oligomers are comparable to, and in some cases, exceed the low-MW species (MW < 250) in ion intensities in the ion trap mass spectra, suggesting they may comprise a substantial fraction of the total aerosol mass. It is possible that oligomers are widely present in atmospheric organic aerosols, formed through acid- or base-catalyzed heterogeneous reactions. In addition, as the seed particle acidity increases, larger oligomers are formed more abundantly in the SOA; consequently, the overall SOA yield also increases. This explicit effect of particle phase acidity on the composition and yield of SOA may have important climatic consequences and need to be considered in relevant models.

3.2 Introduction

Organic compounds are a major component of atmospheric aerosols and are important contributors to the climate forcing and human health effects of airborne particles (1). A significant fraction of atmospheric organic aerosols are formed through in-situ oxidation of precursor hydrocarbons in the gas phase followed by partitioning of low-volatility products into the aerosol phase (2). These are referred to as secondary

organic aerosols (SOA). Recently, higher-molecular-weight species beyond the first-generation oxidation products have been identified in SOA (3-6). An increase in the yield of SOA formed on acidic seed particles has also been reported (3, 7, 8). In the previous conceptual model for atmospheric formation of SOA (2), once the oxidation products are in the aerosol phase, no further chemical reaction is assumed to occur. However, with aerosol-phase reactions occurring as suggested by recent studies, the overall yield of aerosol from precursor oxidation would increase beyond that resulting from pure equilibrium partitioning. The consequence is that the amount of SOA in the atmosphere may substantially exceed that predicted by current models used in global climate assessments (9).

Several fundamental questions arise. What is the increase in SOA yield in the presence of an acidic substrate for precursor hydrocarbons at or near ambient mixing ratios? Is an acidic substrate required for oligomer formation? What is the chemical nature of these oligomers and what reactions produce them? Is oligomer formation the primary cause for the increased yield of SOA formed on more acidic particles? Is there a quantitative relationship among particle phase acidity, oligomer formation and SOA yield? And finally, is oligomer formation in SOA a ubiquitous phenomenon?

Recent work has addressed some of these questions. Kalberer et al. (5) focused on the photolysis of 1,3,5-trimethylbenzene in the absence of seed particles while Tolocka et al. (6) concentrated on the ozonolysis of α -pinene in the presence of acidic inorganic seed particles. Uncertainties still exist when results from different work are compared, such as whether a pre-existing, acidic substrate is necessary for oligomer formation. To fully assess the roles of oligomers in SOA formation as well as in the

broader atmospheric chemistry, a wide variety of SOA-forming systems need to be studied. This work addresses the above questions through an extensive series of dual-chamber laboratory experiments. We consider the ozonolysis of α -pinene (mixing ratio from 12 to 135 ppb), one of the most common biogenic hydrocarbons, and of six cycloalkenes, i.e., cyclohexene, 1-methyl cyclopentene, cycloheptene, 1-methyl cyclohexene, cyclooctene, and terpinolene (mixing ratio from 25 to 300 ppb), serving as model compounds for many atmospheric hydrocarbons bearing similar molecular skeletons, in the absence or presence of seed particles of controlled acidity. We demonstrate and explain the explicit effect of particle-phase acidity on the amounts and composition of SOA formed. Moreover, we find that oligomers are present in each system studied regardless of the initial particle acidity, and speculate that oligomer formation is a ubiquitous phenomenon in ambient aerosols. These results have important implications for predicting the amounts and composition of SOA in the atmosphere.

3.3 Experimental

All experiments were carried out under dark conditions in Caltech's dual 28 m³ teflon chambers. In most experiments, seed solutions were first nebulized into the clean chamber to form seed particles (wet seeds for most α -pinene experiments and dry seeds for cycloalkene experiments). To examine the effect of seed particle acidity on SOA formation, we used two "nonacid" seeds, containing either MgSO₄ or (NH₄)₂SO₄, and two "acid" seeds, containing either [MgSO₄+H₂SO₄] or [(NH₄)₂SO₄+H₂SO₄]. The salt-only solutions were 0.03M each, and acidified solutions contained 0.03M salt and 0.05M H₂SO₄. Cyclohexane was then injected to act as a hydroxyl radical scavenger, followed by hydrocarbon and ozone injection. Relative humidity and temperature were controlled

(e.g., at 55% and 20 °C for the α -pinene ozonolysis experiments). Aerosol number concentration, size distribution, hygroscopic growth, and hydrocarbon mixing ratio were continuously measured. Aerosol loss to the chamber wall was accounted for in data analysis.

In each pair of “nonacid” and “acid” experiments, filter samples (47mm teflon membrane filters) were collected at nearly the same elapsed time (5~7 h) from the onset of reaction for nearly the same duration (1~2 h). Each filter was extracted in HPLC-grade methanol by sonication. The extract was then blown dry under a gentle N₂ stream and reconstituted by an acetic acid solution/methanol mixed solvent. A portion of the filter extract was analyzed by a Hewlett-Packard 1100 series Liquid Chromatography – Mass Spectrometry (LC-MS) system to identify and quantify low-molecular-weight species (MW < 250 Da). Another portion of the filter extract was analyzed by an LCQ classic ion trap mass spectrometer (IT-MS) to identify SOA components with molecular weights ranging from 80 to 1600 Da. Both negative and positive (Na⁺ added) ion modes of the IT-MS detection were carried out, so that compounds of different acidity and polarity could be detected. In addition, some specific ions were isolated and further fragmented by collision-induced dissociation to produce so-called tandem MS. Most of the MS/MS in this work were produced under the negative ion mode, since the isolated ions had less interference and the backgrounds were cleaner than the positive ion mode.

We carried out each pair of “nonacid” and “acid” experiments in the two chambers in parallel, with all other conditions held identical. Thermodynamic calculations (10) show that the four seed particles, once stabilized in the chamber, had distinct pH values. For example, at the RH = 55% for α -pinene ozonolysis experiments,

the pH values for [MgSO₄-only] seed and [MgSO₄+H₂SO₄] seed were 6.5 and -0.3, respectively. The pH values for [(NH₄)₂SO₄-only] seed and [(NH₄)₂SO₄+H₂SO₄] seed were 4.6 and 2.4, respectively. The acidity increase from the “nonacid” to the “acid” seed in the MgSO₄ case exceeded that of the (NH₄)₂SO₄ case by 4.6 pH units.

3.4 Results and discussion

Figure 3.1 shows the relative yield difference (RYD) of SOA between the acid and nonacid cases for seven pairs of α -pinene ozonolysis experiments on MgSO₄ particles, two pairs on (NH₄)₂SO₄ particles, as well as two pairs of terpinolene ozonolysis experiments on MgSO₄ particles. Within the range of α -pinene mixing ratios studied, the SOA yield increases by about 10 ~ 40% on the acidic MgSO₄ seed over the MgSO₄-only seed. The linear decrease in the RYD with increasing initial α -pinene may be related to the decreasing amount of H₂SO₄ in the particles. Initial SOA growth rates for the acid and nonacid cases at two α -pinene mixing ratios are shown by the two insets in Figure 3.1. By comparison, the SOA yield only increases by about 5% on acidic (NH₄)₂SO₄ particles over pure (NH₄)₂SO₄ particles. This is likely due to the markedly smaller acidity difference between the nonacid and acid particles of (NH₄)₂SO₄, as compared with MgSO₄.

The SOA composition difference between nonacid and acid cases is consistent with the overall yield difference. Our LC-MS analyses have identified a number of low-molecular-weight (low-MW) species (MW < 250), containing carbonyl, hydroxyl, and carboxyl groups, in the SOA from the ozonolysis of cycloalkenes and α -pinene, consistent with other studies (11 – 14). In the C₅ – C₈ cycloalkene-ozone systems, diacids, carbonyl acids, hydroxylated diacids, and diacid alkyl esters are consistently the

most abundant low-MW SOA components. In the α -pinene-ozone system, regardless of the seed, cis-pinic acid, norpinic acid and hydroxy pinonic acid, detected with m/z of 185, 171 and 199 (in the negative ion mode), respectively, are the most abundant low-MW SOA components (all may have isomers present; see Supporting Information, Figure 3.S1). These three acidic species are also consistently detected by the ion trap mass spectrometry (IT-MS) in the negative ion mode (see Supporting Information, Figure 3.S2). However, negative ions with m/z of 329, 343, 357, 371 and 385 are also detected by the IT-MS (see Supporting Information, Figure 3.S2). The presence of these high-MW species is confirmed by the detection of ions with m/z of 353, 367, 381, 395 and 409 in the positive ion mode IT-MS, as shown in Figure 3.2(a). These ions are pseudomolecular ions $[M+23]^+$, formed by the addition of a Na^+ to the neutral molecules. A broad range of compounds can be detected as their Na^+ adducts in the positive ion mode IT-MS, thus better reflecting the overall composition of SOA. Figure 3.2(a) illustrates that in the SOA formed on the nearly neutral MgSO_4 seed, small oligomers (MW from 250 to 450) are the most abundant species. These species are separated regularly by mass units such as 14, 16, 18 and 30, which is characteristic of a co-polymer system (15), indicating the difference of CH_2 , O, H_2O groups, or a combination of them, among monomers and oligomers. It is striking that the low-MW species (MW < 250) comprise only a minor fraction of the total ion signals in the mass spectrum. In previous studies, high-MW species may have decomposed during sample preparation or instrumental analyses (such as in a GC oven) (16), resulting in a possible overestimation of low-MW species. The ion trap MS employs an electrospray ionization source that better preserves molecular integrity by soft ionization (17).

When the seed becomes much more acidic ($\text{MgSO}_4\text{-H}_2\text{SO}_4$), as shown in Figure 3.2(b), the resultant SOA comprises many more large oligomers (MW from 450 to 950), most of which have higher ion intensities; thus, mass concentrations of these species exceed by at least a factor of 2 those in the SOA formed on MgSO_4 -only seed. Some even larger oligomers (MW from 950 to 1600) are now detected (with signal-to-noise ratios larger than 3) in the SOA formed on the acidic seed. On the other hand, the mass distribution of small oligomers remains roughly in the same pattern, with a slight decrease in some ion intensities. A similar difference in SOA composition between nonacid and acid MgSO_4 seeds is consistently observed in all other six pairs of experiments on the α -pinene system (see Supporting Information, Figure 3.S4, for the MS of another pair). Our hygroscopicity measurements (18) show that these SOA contained approximately 10 – 20 % water at the time of filter collection; thus, the increased types and amounts of oligomers formed on the more acidic seed are the primary cause for the increased SOA yield (see Figure 3.1).

By comparison, the composition difference between SOA formed on $(\text{NH}_4)_2\text{SO}_4$ -only seed and $(\text{NH}_4)_2\text{SO}_4\text{-H}_2\text{SO}_4$ seed is less pronounced than on the corresponding MgSO_4 seeds. As shown in Figures 3.2(c) and 2(d), there is only a modest increase in the types and amounts of small oligomers in the SOA formed on the more acidic seed, and there is essentially no change in the mass distribution of the large oligomers. This is consistent with the very small yield increase observed. The composition and yield differences between the two sets of nonacid vs. acid seeds clearly demonstrate that seed acidity has a direct impact on the composition and amounts of SOA formed.

That the higher-MW species (MW > 250) shown in Figure 3.2 are indeed oligomers is confirmed from the tandem MS of these ions. For example, Figure 3.3 shows the MS/MS (negative ion mode) of 357 and 245 ions in SOA from the ozonolysis of α -pinene and 1-methyl cyclopentene, respectively. The molecular structures shown alongside the MS/MS explain all major and some minor fragments. Their corresponding monomers are norpinonic acid, C₅, C₆ carbonyl acids and C₅ diacid-- all first-generation oxidation products. There are at least three possible structures for the 245 ion, illustrating the complexity of the oligomeric system in the SOA. Similar to the 357 ion, other higher-MW species in the SOA from α -pinene ozonolysis, such as the 329, 343, 371 and 385 ions, correspond to the possible combination of first-generation ozonolysis products (see Supporting Information, Figure 3.S2, for detail). Overall, our MS/MS results confirm that oligomers originate from low-MW SOA species in all the systems studied. For the α -pinene ozonolysis system, with the monomers having MW centered about 180 Da (13), the small oligomers (MW from 250 to 450) are probably dimers, whereas larger oligomers (MW from 450 to 950) are likely trimers, tetramers, and pentamers, consistent with the discussion in Tolocka et al. (6). Based on the structures of oligomers and corresponding monomers, we propose three possible reaction pathways in the aerosol phase: aldol reaction between carbonyls, gem-diol reaction between carbonyls with the participation of a water molecule, and acid dehydration with the loss of a water molecule. The first two reactions have been discussed in some recent works (3, 5, 6, 7, 8). All three reactions require acid or base catalysis. Detailed reaction mechanisms are well established in organic chemistry literature. We note that since many of the low-MW

SOA species have functional groups in branched positions, the oligomers eventually formed may contain both straight-chain and cross-linked sections.

The SOA composition difference between nonacid and acid cases actually reflects the kinetics of these acid-catalyzed reactions. As seed acidity increases, oligomer formation accelerates, and larger oligomers form within the same experimental time frame than form on less acidic seed. The slight decrease in the ion intensities of some small oligomers, as shown in Figures 3.2(a) and 3.2(b), may actually reflect their transformation into larger oligomers, at roughly 5 h from the onset of ozonolysis. In similar experiments on dry $(\text{NH}_4)_2\text{SO}_4$ seed, abundant small and large oligomers are detected in SOA from α -pinene ozonolysis, even without H_2SO_4 in the seed, as shown in Figure 3.4. Apparently, the higher acidity of the dry seed, as compared with the wet seed, facilitates faster formation of large oligomers.

Despite the sensitivity of SOA formation to the particle phase acidity, we find that oligomers (MW from 250 up to 1600) are present in SOA in all of the systems studied, regardless of seed pH. As an example of the cycloalkene ozonolysis system, Figure 3.S6 (Supporting Information) shows the presence of oligomers with MW up to 700 (i.e., structurally up to possibly pentamers) in the SOA from cycloheptene ozonolysis. Of particular importance, in the α -pinene ozonolysis system where a variety of seed particles are examined, similar types of oligomers are present in SOA, both in the presence and absence of seed particles (see Figure 3.5 for the latter case). This suggests that organic acids produced from the gas-phase hydrocarbon oxidation itself may actually provide necessary acidity for catalytic reactions. No pre-existing, acidic substrate is required for oligomer formation, consistent with the finding by Kalberer et al. (5). Since ambient

aerosols tend to be somewhat acidic, we speculate that oligomers are widely present in atmospheric organic aerosols, and they may comprise a substantial fraction of the total aerosol mass. Since the proposed heterogeneous reactions take place readily under base catalysis as well, the ubiquity of oligomers in ambient aerosols appears all the more likely.

3.5 Acknowledgements

This work was supported by U.S. Department of Energy Biological and Environmental Research Program DE-FG03-01ER63099, Electric Power Research Institute, and U.S. Environmental Protection Agency RD-83107501-0.

3.6 References

- (1) IPCC. *Climate change: contribution of working group I to the third assessment report of the intergovernmental panel on climate change*, **2001**, Cambridge Univ. Press.
- (2). Seinfeld, J. H.; Pankow, J. F. *Annual Rev. Phys. Chem.* **2003**, *54*, 121 – 140.
- (3). Iinuma, Y.; Böge, O.; Gnauk, T.; Herrmann, H. *Atmos. Environ.* **2004**, *38*, 761 – 773.
- (4). Limbeck, A.; Kulmala, M.; Puxbaum, H. *Geophys. Res. Letters* **2003**, *30* (19), doi:10.1029/2003GL017738.
- (5). Kalberer, M.; Paulsen, D.; Sax, M.; Steinbacher, M.; Dommen, J.; Prevot, A. S. H.; Fisseha, R.; Weingartner, E.; Frankevich, V.; Zenobi, R.; Baltensperger, U. *Science* **2004**, *303*, 1659 - 1662.
- (6). Tolocka, M. P.; Jang, M.; Ginter, J. M.; Cox, F. J.; Kamens, R. M.; Johnston, M. V. *Environ. Sci. Technol.* **2004**, *38*, 1428 – 1434.
- (7). Jang, M.; Czoschke, N.; Lee, S.; Kamens, R. M. *Science* **2002**, *298*, 814 – 817.

- (8). Czoschke, N.; Jang, M.; Kamens, R. *Atmos. Environ.* **2003**, *37*, 4287 – 4299.
- (9). Chung, S. H.; Seinfeld, J. H. *J. Geophys. Res.* **2002**, *107* (D19), 4407, doi:10.1029/2001JD001397.
- (10). Nenes, A.; Pandis, S. N.; Pilinis, C. *Aquatic Geochem.* **1998**, *4*, 123 – 152.
- (11). Yu, J.; Cocker III, D. R.; Griffin, R. J.; Flagan, R. C.; Seinfeld, J. H. *J. Atmos. Chem.* **1999**, *34*, 207 – 258.
- (12). Koch, S.; Winterhalter, R.; Uherek, E.; Kolloff, A.; Neeb, P.; Moortgat, G. K. *Atmos. Environ.* **2000**, *34*, 4031 – 4042.
- (13). Winterhalter, R.; Dingenen, R. V.; Larsen, B. R.; Jensen, N. R.; Hjorth, J. *Atmos. Chem. Phys. Discuss.* **2003**, *3*, 1 – 39.
- (14). Kalberer, M.; Yu, J.; Cocker, D. R.; Flagan, R. C.; Seinfeld, J. H. *Environ. Sci. Technol.* **2000**, *34*, 4894 – 4901.
- (15). Zoller, D. L.; Johnston, M. V. *Macromolecules* **2000**, *33*, 1664 – 1670.
- (16). Tobias, H. J.; Ziemann, P. J. *Anal. Chem.* **1999**, *71*, 3428 – 3435.
- (17). Gaskell, S. J. *J. Mass Spectrom.* **1997**, *32*, 677 – 688.
- (18). Cocker III, D. R.; Flagan, R. C.; Seinfeld, J. H. *Environ. Sci. Technol.* **2001**, *35*, 2594 – 2601.

Figure 3. 1. The relative yield difference (RYD) of SOA between the acid and nonacid cases for seven pairs of α -pinene ozonolysis experiments on MgSO_4 seeds, two pairs on $(\text{NH}_4)_2\text{SO}_4$ seeds, as well as two pairs of terpinolene ozonolysis experiments on MgSO_4 seeds. The absolute SOA yield is defined as the mass of SOA produced relative to the mass of hydrocarbon consumed. The RYD is defined as the difference in the absolute SOA yield between the acid and nonacid cases normalized to the nonacid-case yield. Corresponding to the seven α -pinene mixing ratios shown (i.e., 12ppb, 25ppb, 48ppb, 52ppb, 96ppb, 120ppb and 135ppb), the absolute SOA yields are 0.30, 0.32, 0.35, 0.38, 0.46, 0.52 and 0.53, respectively, for the nonacid cases, and are 0.41, 0.43, 0.44, 0.47, 0.53, 0.57, 0.57, respectively, for the acid cases.

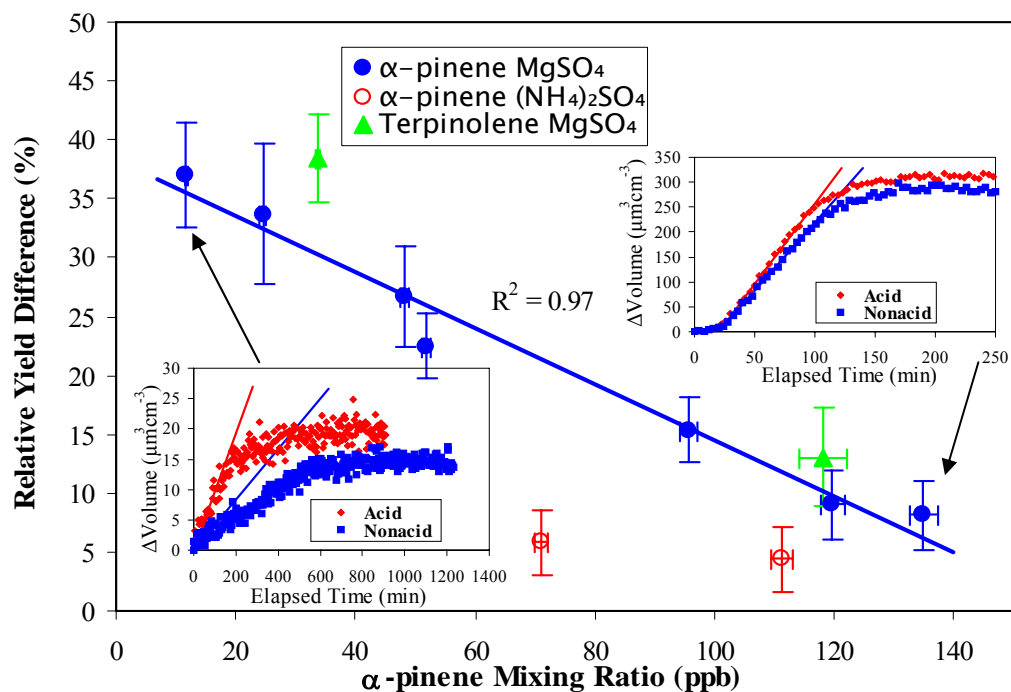
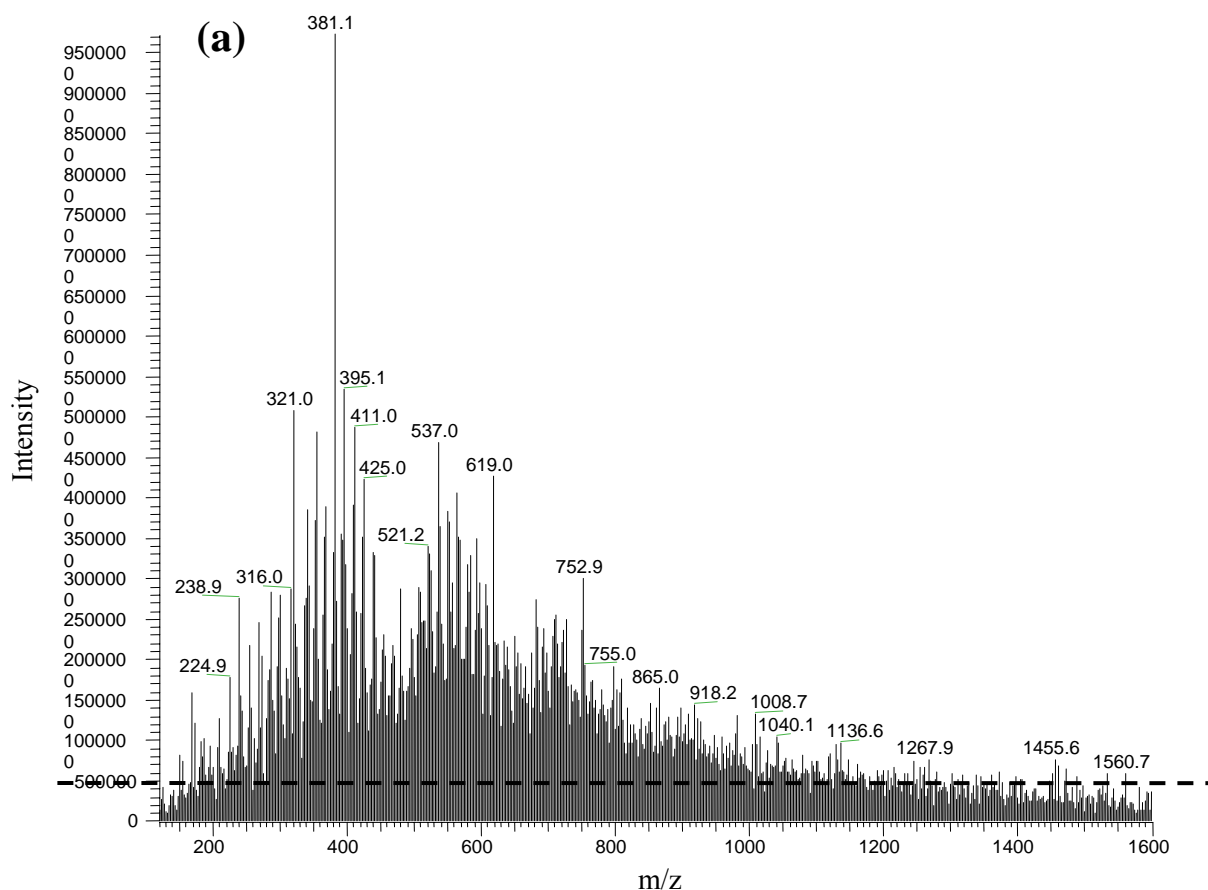
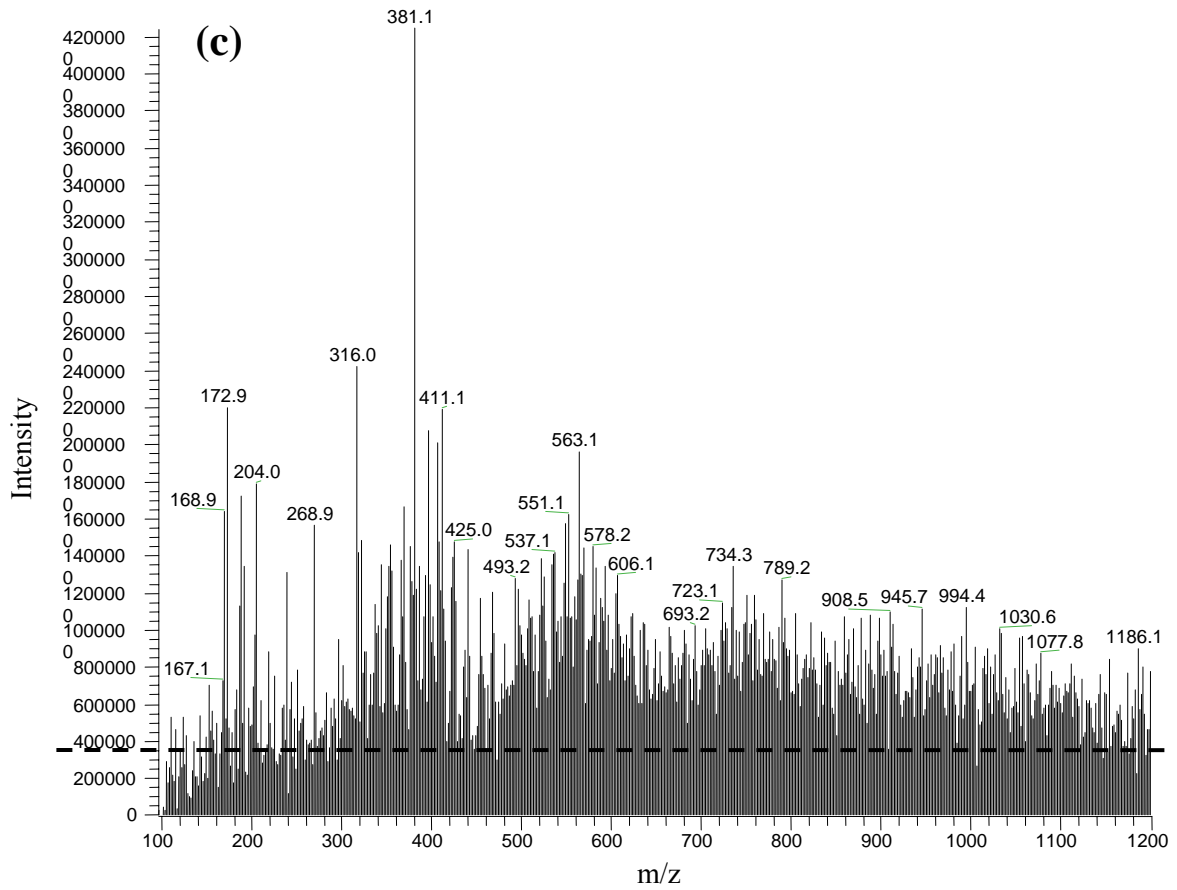
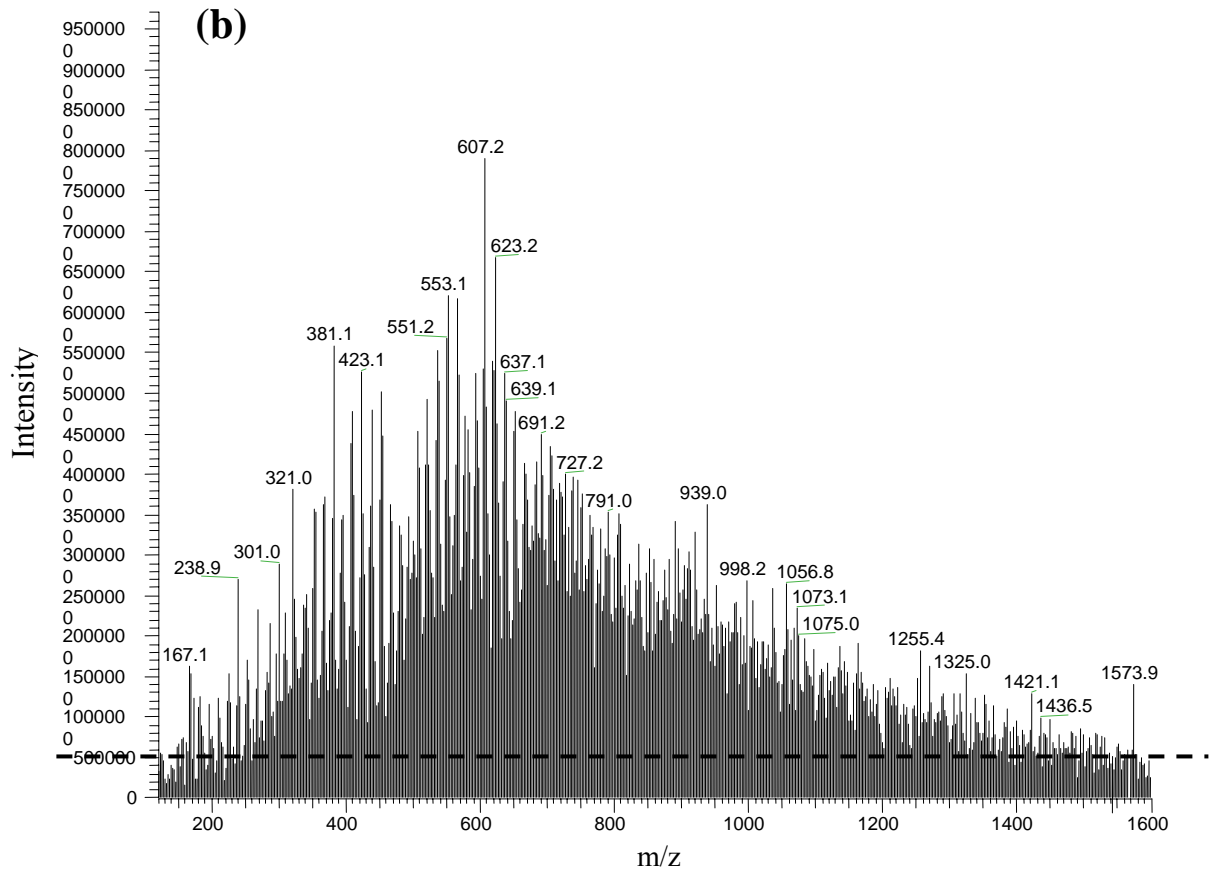


Figure 3. 2. Ion trap mass spectrum (+ ion mode) of the extract of SOA from the ozonolysis of (a) 120 ppb α -pinene on MgSO_4 -only seed (RH = 55%). In the m/z range up to 1600, the average background ion intensity is ~ 400000 , which is labeled as the dashed line in this and the following MS, unless noted otherwise. See Supporting Information, Figure 3.S3, for a typical background MS. (b) 120 ppb α -pinene on MgSO_4 - H_2SO_4 seed. Other experimental conditions are identical to (a). (c) 72 ppb α -pinene on $(\text{NH}_4)_2\text{SO}_4$ -only seed. Other experimental conditions are identical to (a). (d) 72 ppb α -pinene on $(\text{NH}_4)_2\text{SO}_4$ - H_2SO_4 seed. Other experimental conditions are identical to (a).





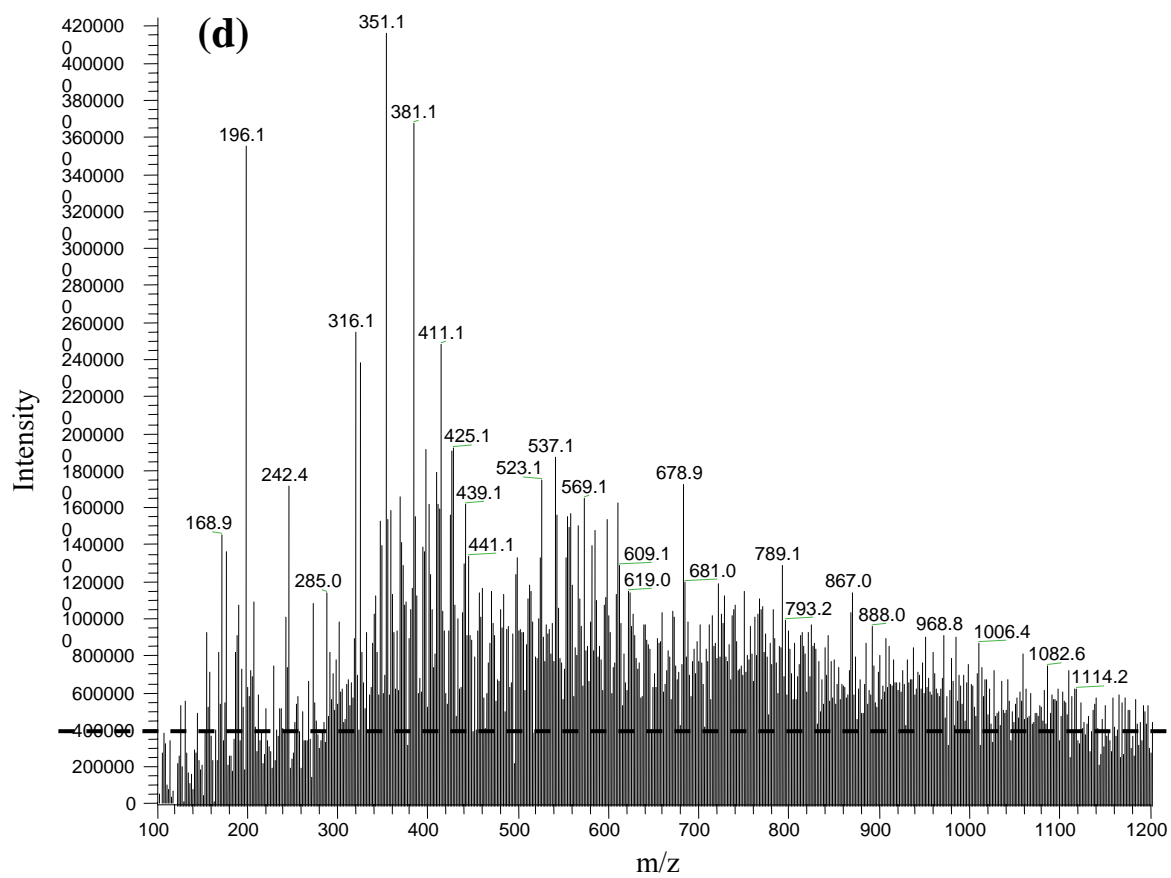
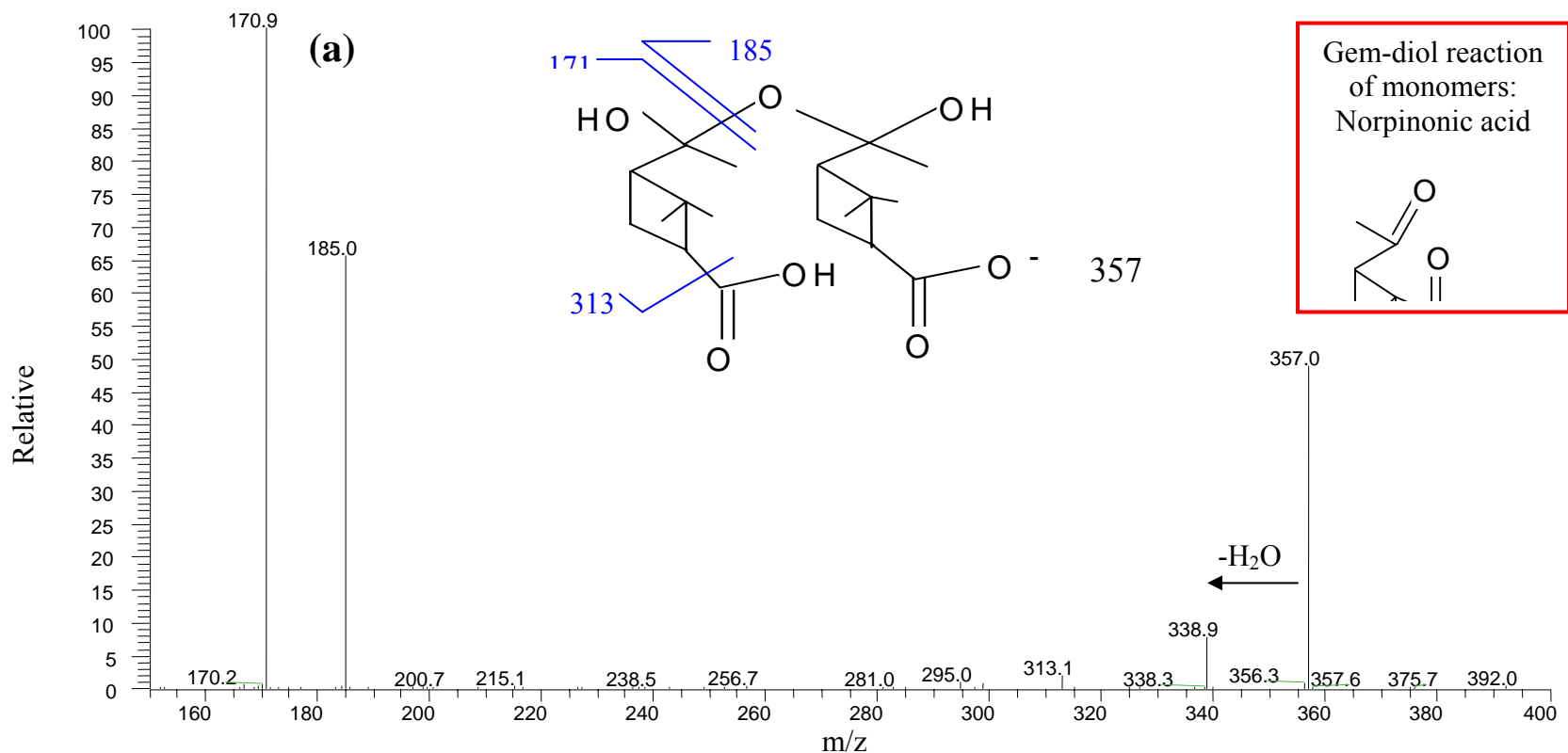


Figure 3. 3. MS/MS (- ion mode) of (a) 357 ion in the SOA from the same α -pinene ozonolysis experiment as in Figure 3.2(a), its likely structure and fragmentation (hydrogen rearrangement and dehydrogenation not shown), and the structure of the monomer. See Supporting Information, Figure 3.S5 for the detailed structures of fragment ions. (b) 245 ion in the SOA from 1-methyl cyclopentene ozonolysis, its likely structures and fragmentation, and the structures of the monomers.



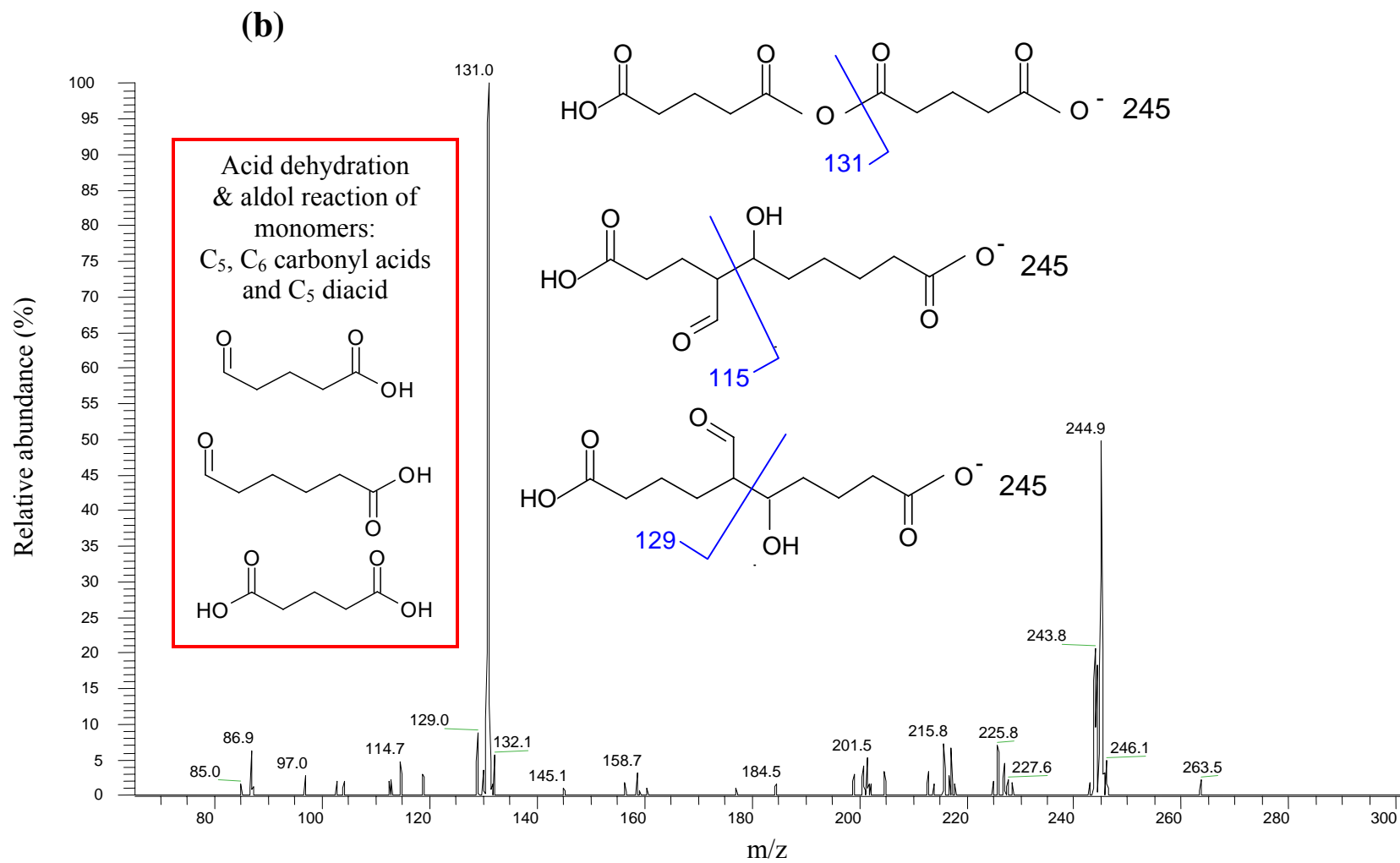


Figure 3. 4. Ion trap mass spectrum (+ ion mode) of the extract of SOA from the ozonolysis of 180ppb α -pinene in the presence of dry $(\text{NH}_4)_2\text{SO}_4$ -only seed. Large amounts of both small and large oligomers are present in this SOA.

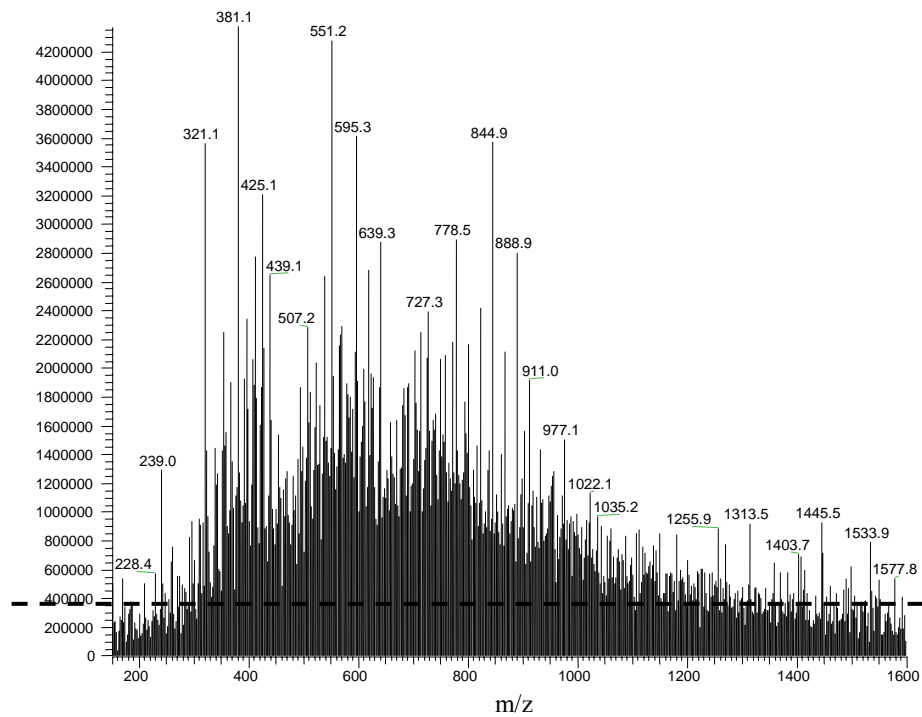
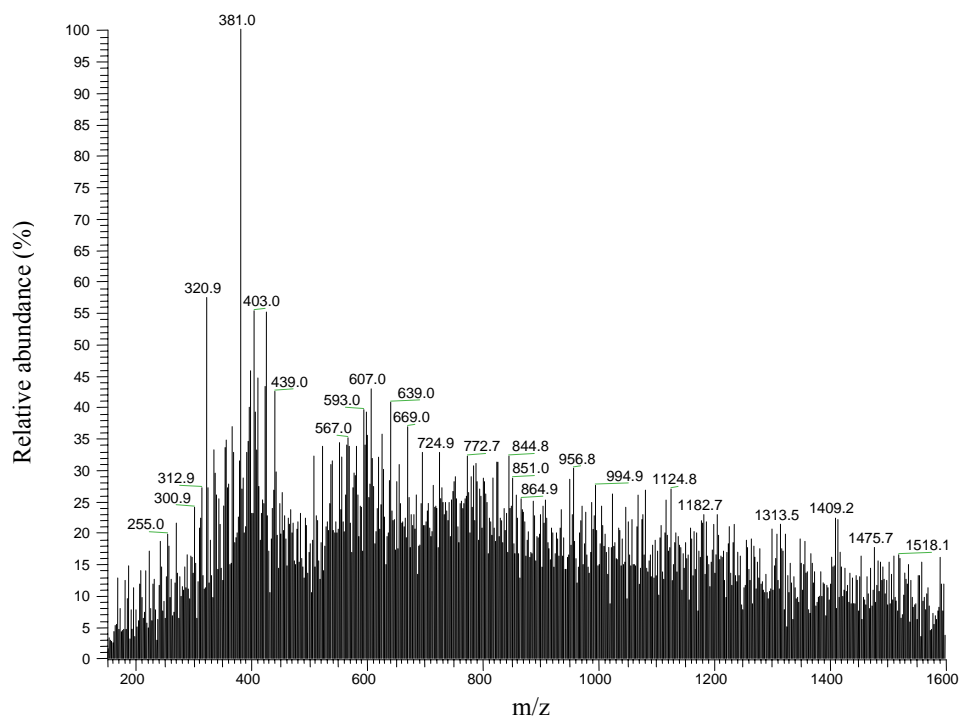


Figure 3. 5. Ion trap mass spectrum (+ ion mode) of the extract of SOA from the ozonolysis of 50ppb α -pinene in the absence of seed particles. This IT-MS is similar to that of the SOA from its parallel ozonolysis experiment in the presence of MgSO_4 seed particles, and is also similar to that of the SOA from other α -pinene ozonolysis experiments, such as the one shown in Figure 3.2(a). The background ion intensities are lower than 5% of the maximum intensity ($m/z = 381.0$, designated as 100%).



Chapter 4

Chamber Studies of Secondary Organic Aerosol Growth by Reactive Uptake of Simple Carbonyls^{*}

^{*}This chapter is reproduced by permission from “Chamber studies of secondary organic aerosol growth by reactive uptake of simple carbonyl compounds” by J. H. Kroll, N. L. Ng, S. M. Murphy, V. Varutbangkul, R. C. Flagan, and J. H. Seinfeld, *Journal of Geophysical Research-Atmosphere*, 110, D 23207, doi:10.1029/2005JD006004, 2005. Copyright 2005, American Geophysical Union.

4.1 Abstract

Recent experimental evidence indicates that heterogeneous chemical reactions play an important role in the gas-particle partitioning of organic compounds, contributing to the formation and growth of secondary organic aerosol (SOA) in the atmosphere. Here we present laboratory chamber studies of the reactive uptake of simple carbonyl species (formaldehyde, octanal, *trans,trans*-2,4-hexadienal, glyoxal, methylglyoxal, 2,3-butanedione, 2,4-pentanedione, glutaraldehyde, and hydroxyacetone) onto inorganic aerosol. Gas-phase organic compounds and aqueous seed particles (ammonium sulfate or mixed ammonium sulfate/sulfuric acid) are introduced into the chamber, and particle growth and composition are monitored using a differential mobility analyzer and an Aerodyne Aerosol Mass Spectrometer. No growth is observed for most carbonyls studied, even at high concentrations (500 ppb-5 ppm), in contrast with the results from previous studies. The single exception is glyoxal (CHOCHO), which partitions into the aqueous aerosol much more efficiently than its Henry's Law constant would predict. No major enhancement in particle growth is observed for the acidic seed, suggesting that the large glyoxal uptake is not a result of particle acidity but rather of ionic strength of the seed. This increased partitioning into the particle phase still cannot explain the high levels of glyoxal measured in ambient aerosol, indicating that additional (possibly irreversible) pathways of glyoxal uptake may be important in the atmosphere.

4.2 Introduction

Organic compounds are a significant component of total particulate matter (PM) in the troposphere, so that the characterization of sources and composition of organic aerosols is important to our understanding of the potential climate forcing and human

health effects of atmospheric PM. In particular, secondary organic aerosols (SOA), formed by the condensation of gas-phase oxidation products of volatile organic compounds (VOC's), constitute a substantial fraction of total organic PM, yet details of SOA formation and evolution remain poorly constrained. Understanding such processes poses a number of experimental and theoretical challenges, due to the large number of condensable products in SOA, the structural complexity of such components, and the importance of short-lived and/or highly nonvolatile intermediates in aerosol formation. Nonetheless, absorptive models of gas-particle partitioning [e.g., *Pankow* 1994a, 1994b; *Odum et al.*, 1996] have generally been successful in describing the total aerosol growth observed in laboratory studies of SOA formation. Such models describe particle growth not in terms of all condensable reaction products but rather in terms of a small number of model semivolatile products. Aerosol growth may then be described by such products' stoichiometric yields and absorptive gas-particle partitioning constants.

However, recent experimental work indicates that in addition to physical absorption, gas-to-particle partitioning also occurs via particle-phase chemical reactions. High-molecular weight compounds have been observed in laboratory studies of SOA formation from the ozonolysis of large alkenes [*Tobias and Ziemann*, 2001; *Ziemann*, 2002; *Tolocka et al.*, 2004; *Iinuma et al.*, 2004; *Gao et al.*, 2004a, 2004b; *Bahreini et al.*, 2005] and the photooxidation of aromatic compounds [*Kalberer et al.*, 2004]. Such products have masses significantly greater than those of their VOC precursors, indicating the formation of oligomers of VOC oxidation products in the aerosol phase. These additional particle-phase reactions are expected to have a significant influence on gas-particle partitioning, resulting in greater SOA mass than would be expected from the

vapor pressures of the VOC oxidation products alone. In addition, total SOA growth is found, in some cases, to be dependent on the chemical composition of the inorganic seed aerosol used, with enhanced aerosol growth when the seed is acidic [*Jang et al.*, 2002; *Czoschke et al.*, 2003; *Iinuma et al.*, 2004; *Gao et al.*, 2004a, 2004b]; since seed composition does not affect the gas-phase chemistry, these results indicate the importance of heterogeneous chemistry in gas-to-particle conversion. Such increases in aerosol growth by reactive uptake may still be described within the context of gas-particle partitioning models, by inclusion of heterogeneous reactions into gas-particle partitioning coefficients [*Kroll and Seinfeld*, 2005].

In order to separate the complex gas-phase chemistry of VOC oxidation from gas-particle partitioning, recent experimental studies have also investigated the SOA-forming potential of individual compounds (or analogs thereof) produced by VOC oxidation. *Jang et al.* [2001a, 2002, 2003a, 2003b, 2005] observed significant aerosol growth when inorganic seed is exposed to a wide variety of organic species; compounds studied include simple C₄-C₁₀ aldehydes, unsaturated carbonyl compounds, and dicarbonyl compounds. Growth was generally observed to be greater when the seed acidity was increased. The authors suggested that these carbonyls may undergo acid-catalyzed oligomerization reactions, including hemiacetal (or acetal) formation and aldol condensation. Subsequent theoretical calculations, however, indicated that for many of the compounds studied, such reactions may not be thermodynamically favorable [*Barsanti and Pankow*, 2004].

Reactions of a number of simple (C₁-C₃) gas-phase carbonyls in concentrated sulfuric acid solutions have also been studied, largely to understand the importance of

such reactions in the upper troposphere and lower stratosphere. While reactive uptake has been observed for formaldehyde [Tolbert *et al.*, 1993; Jayne *et al.*, 1996; Iraci and Tolbert, 1997], acetaldehyde [Michelsen *et al.*, 2004], and acetone [Duncan *et al.*, 1998, 1999; Klassen *et al.*, 1999; Kane *et al.*, 1999; Imamura and Akiyoshi, 2000], and even the larger aldehydes octanal and 2,4-hexadienal [Zhao *et al.*, 2005], reactions were generally carried out under highly acidic conditions (>50 wt% H₂SO₄) and at sub-ambient temperatures, conditions not generally relevant for SOA formation in the troposphere. Nozière and coworkers found that 2,4-pentanedione may oligomerize via the aldol condensation under tropospheric conditions (297 K, 20 wt% H₂SO₄) [Nozière and Riemer, 2003], but also that under such conditions, aldol condensation reactions are too slow to contribute significantly to SOA growth [Esteve and Nozière, 2005].

Very recently, Liggio *et al.* [2005a, 2005b] studied aerosol growth by heterogeneous reaction of gas-phase glyoxal (CHOCHO), using aerosol mass spectrometry to observe aerosol growth by oligomer formation. Glyoxal, one of the compounds observed to contribute to aerosol growth by Jang *et al.* [2001a, 2002], is formed in a number of VOC oxidation processes, such as the photooxidation of aromatic compounds [Volkamer *et al.*, 2001; Calvert *et al.*, 2002], the ozonolysis of alkenes [Calvert *et al.*, 2000], and the OH + acetylene reaction [Hatakeyama *et al.*, 1986; Yeung *et al.*, 2005], and has recently been used as a tracer for VOC oxidation in urban areas [Volkamer *et al.*, 2005]. The boiling point of glyoxal is 51°C, suggesting it is far too volatile to be physically absorbed into an organic aerosol phase to any appreciable extent. However, Liggio *et al.* [2005a] observed organics in the particle phase of mass greater than that of monomeric glyoxal, strongly suggesting the importance of reactive uptake of

glyoxal, which leads to the formation of oligomers (as well as organic sulfates) in the aerosol phase. Rate of glyoxal uptake was also measured [Liggio *et al.*, 2005b], and was found to be somewhat higher when seed particles were acidic. Heterogeneous reaction of a similar compound, methylglyoxal, has also been suggested as a pathway for oligomer formation in SOA from the photooxidation of aromatic compounds [Kalberer *et al.*, 2004]. Evidence for this was based on comparison of mass spectra of aerosol samples with those from bulk-phase methylglyoxal solutions, so reactive uptake of methylglyoxal leading to SOA growth has not yet been explicitly examined.

There thus exists clear and compelling evidence that heterogeneous reactions play an important role in the formation of secondary organic aerosol, via the increase in partitioning of gas-phase organics into the aerosol phase. The formation of oligomeric products may also be important in that it might influence the CCN activation ability [VanReken *et al.*, 2005] or optical properties [Nozière and Riemer, 2003] of the aerosol. However, the detailed chemistry, and even the basic mechanism, of such reactions remain poorly understood. The overall, quantitative effect of heterogeneous chemistry on the gas-particle partitioning of organics in the atmosphere is largely unknown, especially since it is likely to be dependent on a large number of factors, including temperature, relative humidity, particle size, and particle composition. Understanding such effects is necessary for the interpretation of mechanisms of aerosol growth as measured in the laboratory, as well as for the accurate modeling of SOA formation and evolution in the atmosphere.

In particular, the role of seed acidity in SOA growth remains poorly constrained. While an increased rate of aerosol-phase chemical reactions (acid catalysis) may explain

observed increases in uptake coefficients, it does not explain observed increases in total (equilibrium) aerosol yields in the presence of acidic seed [Czoschke *et al.*, 2003, Iinuma *et al.* 2004; Gao *et al.*, 2004a, 2004b; Jang *et al.*, 2005]. Henry's Law coefficients of many carbonyls are known to increase dramatically at high acidities [e.g., Kane *et al.*, 1999; Nozière and Riemer, 2003; Michelsen *et al.*, 2004], but it is not clear whether this is also the case for the absorptive gas-particle partitioning coefficients which govern SOA formation. And while reactions which occur within acidic particles may not be accessible under milder conditions, such differences in chemistry have not been conclusively identified; formation of oligomers has been observed even in the absence of inorganic seed [Kalberer *et al.*, 2004; Gao *et al.*, 2004a, 2004b]. Few studies of ambient aerosols have examined the relationship between acidity and organic content of aerosols, though recent measurements made in Pittsburgh reveal no significant enhancement of the organic fraction in acidic particles [Zhang *et al.*, 2005]. Therefore both the chemical mechanism and the atmospheric significance of increased uptake of organics by acidic particles are at present poorly understood.

The role of reactive uptake by small, volatile carbonyls (such as glyoxal [Liggio *et al.*, 2005a, 2005b], methylglyoxal [Kalberer *et al.*, 2004], and short-chain aldehydes [Jang and Kamens, 2001a]) in SOA formation is also not well-established. If such chemistry results in significant particle growth, then SOA may be formed by a much wider range of VOC oxidation processes than is currently believed, and the oxidation of simple, short-chain hydrocarbons may even contribute to global SOA. It is therefore especially important to understand whether heterogeneous reactions lead to the partitioning of these smaller carbonyls into the particle phase.

In this study, we examine the potential for SOA growth via heterogeneous reactions for a number of such compounds (shown in Figure 4.1), by measuring changes in particle volume and composition when inorganic seed and gas-phase carbonyls are introduced into an environmental chamber. We observe no significant growth for most compounds studied, in contrast with the results from previous studies. We do, however, observe substantial growth by gas-phase glyoxal, consistent with the results of *Liggio et al.* [2005a]. Whereas the work of *Liggio et al.* investigated the mechanism and kinetics of the oligomerization reactions [2005a] and rate of reactive uptake [2005b], here we focus on the equilibrium partitioning of glyoxal between the gas and particle phases. Total (equilibrium) aerosol growth is measured as a function of glyoxal concentration, initial inorganic seed volume, and seed acidity, and from these data a gas-particle partitioning coefficient is determined. This coefficient is then compared to ambient measurements of glyoxal in the gas and particle phases, as a test of our understanding of atmospheric gas-particle partitioning.

4.3 Experimental

Experiments are carried out in the Caltech Indoor Chamber Facility; instrumentation and methods have been described in detail elsewhere [*Cocker et al.*, 2001; *Keywood et al.*, 2004], so will be described only briefly here. The facility consists of two indoor 28 m³ Teflon (PFE) chambers, designed for the minimization of wall loss and for the control of temperature, relative humidity, and photolytic conditions. For experiments described here, temperature is held at 20 (± 1) °C; relative humidity (RH) is controlled by sending clean air through large bubblers prior to introduction into the chamber. Temperature and RH are continually monitored. For a few initial experiments

(particle growth by uptake of simple carbonyls), studies were carried out in a smaller, 3 m³ chamber; for these studies, experimental protocols and instruments used are the same as used in the larger chambers. All experiments were carried out under dark conditions, to avoid unwanted photolysis of reactants and products.

Particle volume is continually monitored by a differential mobility analyzer (DMA, TSI 3081) coupled to a condensation particle counter (CPC, TSI 3760), with settings identical to those described by *Keywood et al.* [2004]. All aerosol volume data are corrected for wall loss; standard correction techniques (application of the number concentration decay constant to total particle volume) cannot be used, as the implicit assumption that size distribution remains constant introduces errors which are too large for the small growths measured here. Instead, size-dependent decay coefficients are determined from “wall-loss” experiments, in which the exponential loss of seed aerosol under clean (organic-free) conditions is measured. Application of these decay coefficients leads to an overcorrection, due to deviations from the exponential fit, as well as the effect of coagulation, which leads to changes in number concentration but not in total particle volume. This overcorrection, empirically determined to be $\sim 9 \mu\text{m}^3/\text{cm}^3$, is subtracted from all measurements of particle growth presented here. This subtraction is valid as long as the time-dependent size distributions in particle growth experiments are similar to those in the “wall-loss” experiments. This is the case for the present experiments, as organic growth is small relative to the initial seed volume. As an additional check of total aerosol number concentration, particle number is monitored in each chamber by separate CPC’s (TSI 3010 and 3025).

For most experiments, particle composition and mass are monitored using an Aerodyne Aerosol Mass Spectrometer (AMS). Operation and calibration of this instrument have been described elsewhere [*Jayne et al.*, 2000; *Allan et al.*, 2003, 2004; *Bahreini et al.*, 2005] and will not be discussed here. The AMS allows for the quantitative measurement of inorganic (ammonium and sulfate) and organic mass within the aerosol. Organic species undergo decomposition in the vaporizer (~600 °C) and fragmentation during electron impact ionization (70 eV) so cannot be identified individually. Nonetheless, it has been shown that fragmentation patterns of organic aerosols may be useful for understanding details of particle-phase oligomerization reactions [*Liggio et al.*, 2005a; *Bahreini et al.*, 2005].

For most carbonyl + seed experiments (with the exception of glyoxal; see below), the inorganic seed is introduced into the chamber prior to introduction of the organic. Polydispersed seed particles are generated by atomization (at 30 psi) of dilute salt solutions; in all experiments described here the seed used is either ammonium sulfate (0.03M) or mixed ammonium sulfate/sulfuric acid (0.03M/0.1M).

Structures of the organic compounds studied in this work are shown in Figure 4.1. Most are introduced into the gas phase by sending air over a measured volume of the pure compound and into the chamber, though the less volatile compounds (boiling point > 120°C) require gentle heating for efficient evaporation. Care is taken to keep this heating to a minimum, as overheating was found to lead to new particle formation, presumably due to supersaturation of the gas-phase organic in the injection line; this causes a significant increase in particle number and sometimes particle volume. Compounds used are all from Aldrich and are: octanal (99%), *trans-trans*-2,4-hexandienal (95%), 2,3-

butanedione (97%), 2,4-pentanedione (99+%), glutaraldehyde (25% in water), and hydroxyacetone ($\geq 90\%$). Concentrations of these compounds are estimated by volume of hydrocarbon injected, and monitored with gas chromatography with flame ionization detection (GC-FID). For initial tests of whether these compounds contribute to aerosol growth, high concentrations (500ppb-5ppm) are used, and no calibrations of GC-FID response were made.

The three smallest compounds shown in Figure 4.1, formaldehyde, glyoxal, and methylglyoxal, could not be introduced efficiently into the gas phase by the above method, nor could they be detected with simple GC-FID. Instead, gas-phase monomers are prepared from the commercially-available polymeric (formaldehyde and glyoxal) or aqueous (glyoxal and methylglyoxal) forms. The aqueous compounds are dried down first: aqueous glyoxal or methylglyoxal (both 40 wt%, Aldrich) is evaporated under vacuum until it becomes a white crystalline solid (glyoxal) or viscous yellow liquid (methylglyoxal). After addition of P_2O_5 , the dried compound is gently heated under vacuum until it starts bubbling, indicating the release of gas-phase monomer. The monomer passes through an LN_2 trap, where it is collected as a solid. The same procedure, minus the initial drying step, is used to prepare formaldehyde from the solid paraformaldehyde (Aldrich, $\geq 95\%$) or glyoxal from solid trimeric glyoxal dihydrate (Aldrich, $\geq 97\%$). To obtain a fixed amount of gaseous compound, the LN_2 is removed, allowing the frozen monomer to slowly vaporize into a 500 mL glass bulb to a desired pressure, as measured with a capacitance manometer (MKS); care is taken to allow any CO_2 collected in the trap to escape first. FTIR measurements of the collected gas-phase glyoxal confirm that the glyoxal is pure, with minimal CO and CO_2 impurities, and is

present only in monomeric form: its spectrum matches that published previously [Niki *et al.*, 1985], and has no observable C-O or O-H features, which would suggest polymerization and/or hydration. Further, both FTIR and bulb pressure measurements indicate that, under dry conditions, glyoxal is not lost in significant amounts to glass surfaces. Under humid conditions, however, rapid loss of gas-phase glyoxal is observed, as is the formation of polymers on the walls of the vessel. Finally, the glass bulb is attached to the chamber and a stream of dry air is passed through the bulb, introducing the carbonyl into the chamber.

Formaldehyde, glyoxal, and methylglyoxal are measured by solid-phase microextraction (SPME) with on-fiber derivatization, using *o*-(2,3,4,5,6-pentafluorobenzyl) hydroxylamine (PFBHA, Aldrich, 98+%) [Martos and Pawliszyn, 1998; Reisen *et al.*, 2003]. The SPME sampler used in this study is a 65 μm poly(dimethylsiloxane)/divinylbenzene (PDMS/DVB) fiber mounted in a portable syringe holder (Supelco). After conditioning at 250°C for at least half an hour, the fiber is coated with PFBHA by exposing it to the headspace of aqueous PFBHA (17 mg/mL) for 30 minutes. The coated fiber is then exposed to the chamber through a septum for 15 minutes. Introduction of the fiber into the GC injection port at 250°C desorbs the resulting oximes (formed by the reaction of PFBHA + aldehyde) onto the column, through which they readily elute, allowing for detection by FID. For each experiment, 3-4 SPME measurements are made per chamber; values obtained generally agree to within 10-15%.

While this technique allows for the detection of formaldehyde, glyoxal, and methylglyoxal, we calibrate it only for glyoxal, the focus of this work (concentrations of

the other compounds are estimated by pressure in the glass collection bulb). To calibrate, 5.2 Torr of gas-phase glyoxal is introduced into a 2 L glass bulb, which is brought to atmospheric pressure by addition of nitrogen. A fixed volume (0.5-2.0 mL) of the gas-phase sample is removed using an airtight syringe, and added to a sealed Teflon bag containing 40 L of dry air. The resulting glyoxal concentrations (85-340 ppb) are used as calibration standards. FID signal is linear with glyoxal at these concentrations; any losses of glyoxal to surfaces (in the collection bulb, syringe, or Teflon bag) during calibration will affect the accuracy but not the precision of the measurements. We are unable to perform calibrations at higher relative humidity, due to the loss of glyoxal on surfaces at high RH (see below); however changes in RH are not expected to affect the SPME calibration significantly [Reisen *et al.*, 2005].

At values of RH above 30%, and especially at higher humidity, rapid loss of glyoxal, presumably uptake to the chamber walls, is observed: upon introduction of 500 ppb glyoxal into the 28 m³ chamber at 51% RH, approximately half is depleted after 6 hours. After several more hours the concentration eventually stabilizes, reaching equilibrium between glyoxal on the walls and in the gas phase. Equilibrium concentrations can be as high as 200 ppb, significantly higher than the 3.6-5.4 ppb concentration observed by Liggio *et al.* [2005a]; the reason for this discrepancy is not clear. To ensure constant levels of gas-phase glyoxal over the course of an experiment, the inorganic seed is introduced only after the glyoxal concentrations are observed to stabilize. As noted by Liggio *et al.* [2005a], glyoxal tends to be persistent on Teflon surfaces, so flushing the chamber for a few hours after the experiment is not sufficient to remove all glyoxal from the system. By flushing the chambers for ~36 hours between

experiments, enough glyoxal has been removed so that its equilibrium gas-phase concentration is measurably lower, and an experiment at the new concentration may be performed. Thus, a number of measurements may be made over the few days following a single glyoxal injection.

4.4 Results and discussion

4.4.1 Uptake of organics: carbonyl compounds other than glyoxal

For all the carbonyl compounds studied (Figure 4.1), with the exception of glyoxal, we observe no aerosol growth, in either the DMA or the AMS. In some experiments carried out overnight, DMA particle volume is observed to level out somewhat (or in one case, to increase slightly) for a period of a couple hours; the resulting calculated growth after correction for wall loss is small ($0\text{-}5\ \mu\text{m}^3/\text{cm}^3$). However, in these instances no organic growth is observed in the AMS (detection limit of $\sim 0.5\ \mu\text{g}/\text{m}^3$, with 2 minute averaging), and the period of leveling off coincides with a decrease in temperature (and therefore an increase in RH), presumably arising from temperature changes outside and/or poor thermostating of the room. Therefore the small growth observed is from water uptake by the inorganic seed rather than uptake of the organic compound. Such fluctuations were not observed for the glyoxal experiments.

Shown in Figure 4.2 are the raw DMA particle volume data (not corrected for wall loss) from a typical experiment, 500 ppb of 2,4-hexadienal in the presence of acidic seed (54-56% RH). Also shown is a “seed-only experiment”, in which seed but no organic is introduced. Both experiments were carried out in the same $28\ \text{m}^3$ chamber, and data are scaled to the same initial seed volume. No substantial difference in particle volume is observed between runs with and without 2,4-hexadienal. Similarly,

introduction of ~960 ppb methylglyoxal, which has been implicated in oligomer formation during photooxidation of aromatic compounds [Kalberer *et al.*, 2004], results in negligible growth: volume measured by the DMA, after correction for wall loss, shows a small ($<5 \mu\text{m}^3/\text{cm}^3$) volume increase, but no organic growth is observed by the AMS. Similar results are obtained for the other carbonyls studied (save glyoxal): no growth is observed for formaldehyde (5 ppm), octanal (500 ppb), 2,3-butanedione (500 ppb), glutaraldehyde (500 ppb), 2,4-pentanedione (5 ppm), and hydroxyacetone (3 ppm), all at 50-55% RH.

The lack of growth at these high concentrations, when scaled to tropospheric carbonyl concentrations, suggests that reactive uptake of these species onto inorganic aerosols is not significant in the troposphere. These results are in stark contrast to those of Jang *et al.* [2001a, 2002, 2003a, 2003b, 2005], who report significant aerosol growth for a number of carbonyl compounds. While it is difficult to compare the present chamber data with their flow reactor measurements [Jang *et al.*, 2003a, 2003b], which involve shorter experimental timescales and much higher carbonyl concentrations, their chamber experiments [Jang *et al.*, 2001a, 2003a, 2005] may be directly compared to ours, as both are carried out with ammonium sulfate or mixed ammonium sulfate/sulfuric acid seed and gas-phase carbonyl concentrations of 100's-1000's of ppb. Using octanal as an example, we observe no growth at 500 ppb, whereas Jang *et al.* find that concentrations of 1.7-3.4 ppm lead to particle growths of $59\text{-}581 \mu\text{m}^3/\text{cm}^3$ [Jang and Kamens, 2001a], and that 295 ppb octanal leads to $44\text{-}137 \mu\text{m}^3/\text{cm}^3$ growth [Jang *et al.*, 2005]. Similar differences arise for 2,4-hexadienal: we observe no growth at 500 ppb, while they measure $118 \mu\text{m}^3/\text{cm}^3$ growth at 2.4 ppm [Jang and Kamens, 2003a] and $15\text{-}65 \mu\text{m}^3/\text{cm}^3$

growth at 328 ppb [*Jang et al.*, 2005]. Hence even at lower carbonyl concentrations than are used in this study they measure significant aerosol growth. They observe particle growth to be immediate (occurring within 3 minutes of introduction of the carbonyl), and, in some instances at least, accompanied by an increase in particle number concentration [*Jang and Kamens*, 2001a], which is inconsistent with heterogeneous reaction. Further research is needed to understand the source of this discrepancy.

4.4.2 Uptake of organics: glyoxal

By contrast, using both the DMA and AMS we observe significant particle growth with glyoxal in the presence of aqueous seed, consistent with the results of *Liggio et al.* [2005a]. Shown in Figure 4.3 are aerosol volume data (before wall-loss correction) for an experiment in which first acidic seed and then 200 ppb glyoxal are added to the chamber at 48% RH. This figure is for illustrative purposes only; since glyoxal is rapidly lost to the walls, the integrated glyoxal concentration may be lower than 200 ppb. As discussed in the Experimental section, for quantitative measurements of particle growth, glyoxal is added first and seed is added only after the glyoxal concentration has stabilized. In all experiments, particle volume is observed to level out after a few hours, though gas-phase glyoxal concentrations remain high.

Aerosol mass spectra of the organic fraction of the aerosols are in agreement with those measured by *Liggio et al.* [2005a] and so are not discussed here. Ion fragments of masses greater than $m/z=58$ (the molecular weight of glyoxal) indicate the presence of hydrates and oligomers of glyoxal, and observed masses and relative intensities match those measured by *Liggio et al.* [2005a] well.

Table 4.1 summarizes experimental conditions and aerosol growth (ΔM) for all glyoxal experiments carried out for glyoxal concentrations ≤ 200 ppb. Total aerosol volume is measured by the DMA and converted to mass by assuming unit density. Uncertainties in ΔM arise from signal-to-noise of the DMA volume measurement ($\sigma \approx 2.0 \mu\text{m}^3/\text{cm}^3$) and do not include uncertainties inherent in the wall-loss correction, which are difficult to quantify. Water content of the seed aerosol is estimated using molalities of aqueous solutions at the experimental RH, as obtained from the ISORROPIA aerosol thermodynamic equilibrium model database [Nenes *et al.*, 1998]; for the mixed ammonium sulfate/sulfuric acid seed, water content of the individual components is assumed to add linearly, based on the relative ratios (0.3:1.0) in the seed solution.

Aerosol growth is observed for all experiments shown in Table 4.1. Considerably larger growth is observed at even higher glyoxal concentrations. Glyoxal uptake may be accompanied by loss of water in the seed, or may occur as the seed particles are still mixing (first 30 minutes of the experiment); such effects would lead to an underestimate of organic growth. Comparison of organic mass measured by the AMS with particle volume measured by the DMA suggests these are relatively minor effects, and any errors introduced are proportional to total growth. Only a small fraction of the aerosol volume (at the start and end of the experiment) is from particles larger than the DMA cutoff (~ 820 nm); neglect of such large particles therefore has minimal effect on measured aerosol growth.

Tests in the 3 m^3 chamber using dry ammonium sulfate seed (12% RH) show zero growth, even at glyoxal concentrations as high as ~ 1 ppm, consistent with the results of Liggi *et al.* [2005a]. This strongly suggests that glyoxal first partitions into the aerosol

phase by dissolution into the aqueous seed, so a Henry's Law treatment of glyoxal uptake is appropriate:

$$\Delta M = [\text{Gly}_A] = 10^{-12} K_H^* mw V [\text{Gly}_G] \quad (4.1)$$

in which ΔM is change in aerosol mass, $[\text{Gly}_A]$ is the mass concentration of glyoxal in the aerosol phase ($\mu\text{g}/\text{m}^3$), $[\text{Gly}_G]$ is the glyoxal concentration in the gas phase (ppb), K_H^* is the effective Henry's Law constant of glyoxal (M/atm), mw is the molecular weight of glyoxal (g/mol), and V is the volume concentration of aqueous seed ($\mu\text{m}^3/\text{cm}^3$) (the 10^{-12} is for units conversion). This relation assumes that gas-phase glyoxal concentration $[\text{Gly}_G]$ is constant, and becomes somewhat more complex if gas-phase glyoxal decreases during gas-particle partitioning [*Kroll and Seinfeld, 2005*]; however no significant decrease is observed.

By Equation 4.1, aerosol growth is expected to be linear with concentration of gas-phase glyoxal ($[\text{Gly}_G]$) as well as the volume of aqueous seed (V). While linear relationships between concentrations of a condensable compound in the gas and particle phases are not typical in SOA formation [*Odum et al., 1996*], they may occur in systems in which the absorbing medium is inorganic, so that uptake of the organic does not affect the amount of absorbing medium [*Kroll and Seinfeld, 2005*]. Shown in Figure 4.4 is a plot of aerosol growth ΔM vs. the product of gas-phase glyoxal concentration $[\text{Gly}_G]$ and volume of aqueous seed V . The linearity is clear, with the exception of one large outlier (experiment 7; 174 ppb glyoxal, acidic seed). The data collected in that experiment do not seem particularly anomalous, so the source of the large discrepancy is not clear. We therefore first examine only the ammonium sulfate data; the effect of particle acidity will be discussed subsequently.

Linear fitting to the data from the experiments with ammonium sulfate seed (experiments 1-5), yields an effective Henry's Law constant of 2.6×10^7 M/atm (the same value is obtained by fitting all data except experiment 7). This value scales linearly with our glyoxal calibration, so any glyoxal losses that may have occurred during calibration (namely surface losses) would lead to an underestimate of the actual value. Moreover, this value depends on the density of the organic fraction of the aerosol, which we assume to be unity; while it is likely to be somewhat greater, it is difficult to estimate. Additionally, the high organic content (up to 20% by volume) may lead to deviations from Henry's Law behavior, but the linearity seen in Figure 4.4 suggests this is not a major effect. Other possible errors in our organic growth measurements (such as those described above) are expected to be proportional to glyoxal uptake, and so do not affect the linearity shown in Figure 4.4. These potential errors in our calculated effective Henry's Law constant are all expected to be relatively small, and do not affect our conclusions substantially.

The dashed line near the bottom of Figure 4.4 represents the expected amount of aerosol growth based on the measured effective Henry's Law constant for glyoxal (in seawater) of 3.6×10^5 M/atm [Zhou and Mopper, 1990]. While there are no measurements of the Henry's Law constant for glyoxal in pure water (Betterson and Hoffmann [1988] determined a lower limit of 3.0×10^5 M/atm), it is unlikely to be significantly different from this value. Comparison of the two lines indicates that glyoxal uptake on ammonium sulfate aerosols is far higher (by a factor of ~ 70) than glyoxal uptake by water.

The source of this very large increase in partitioning coefficient is not immediately clear. While Jang and Kamens [2001a] observed aerosol growth by glyoxal

uptake to increase with particle acidity, we do not observe this effect. In fact, measured growth in mixed ammonium sulfate/sulfuric acid seed may be even lower than that in ammonium sulfate seed. Therefore we conclude that increased particle acidity does not promote partitioning of glyoxal into the aerosol phase appreciably. Instead, this partitioning may be controlled by the ionic strength of the seed aerosol (“salting in”). Ammonium sulfate and sulfuric acid are fairly concentrated in the particles (total concentrations of 6.5-7.5 M), leading to high ionic strengths. The higher water content of mixed ammonium sulfate/sulfuric acid seed leads to a somewhat lower (~10-15%) ionic strength than in ammonium sulfate. *Liggio et al.* [2005a] observed significant growth using neutral seeds (sea salt and sodium nitrate), which also suggests high ionic strength (rather than high acidity) leads to increased uptake. Therefore the factors that control reactive uptake of glyoxal are apparently different than those controlling uptake of condensable species formed in α -pinene ozonolysis, in which growth is higher in the presence of acidic seed [*Czoschke et al.*, 2003; *Iinuma et al.*, 2004; *Gao et al.*, 2004a, 2004b]. The effect of seed composition on gas-particle partitioning may thus be extremely complex. Further research on the effect of the seed particle identity and concentration, including measurements of glyoxal uptake in the bulk phase, may be useful for understanding this effect.

4.5 Implications

We have shown that reactive uptake of glyoxal on aqueous seed aerosols may lead to significant particle growth, consistent with the results of *Liggio et al.* [2005a]. Results from this study also indicate that reactive uptake of other small, volatile carbonyls (shown in Figure 4.1) onto inorganic seed is not important under most

tropospheric conditions and therefore does not contribute significantly to global SOA production. Most important is the lack of uptake of formaldehyde, the most abundant carbonyl in the troposphere. Further studies are certainly necessary, as results of similar experiments reported by *Jang et al.* [2001a, 2002, 2003a, 2003b, 2005] do not agree with our observations. From our experiments we cannot rule out the possibility that uptake of such simple carbonyls may occur on highly acidic (i.e., $\geq 50\%$ H₂SO₄) particles. Such high acidities are not common in tropospheric particles but may occur in plumes from coal-burning power plants [e.g., *Brock et al.*, 2002], or by freshly-nucleated particles [*Zhang et al.*, 2004]; ambient measurements of the organic fraction of such particles are at present scarce.

We emphasize that the present work focuses only on small, relatively volatile (bp < 200°C) carbonyl compounds. It is expected that reactive uptake by larger carbonyls contribute to SOA; the combination of low volatility and high reactivity may lead to effective gas-particle partitioning coefficients large enough to lead to significant particle growth. Heterogeneous reactions of such compounds have been implicated in oligomer formation in SOA from α -pinene ozonolysis [*Tolocka et al.*, 2004; *Iinuma et al.*, 2004; *Gao et al.*, 2004a, 2004b]. Additionally, the potential role of cross-reactions, such as the reaction of a low-volatility compound in the particle phase with a more volatile gas-phase carbonyl, has yet to be explored in detail.

In contrast to the other carbonyls studied in this work, glyoxal is found to contribute substantially to aerosol growth. The adjacent electron-poor aldehydic carbons contribute to high water solubility and reactivity of glyoxal, making hydration and oligomerization relatively facile. However, no growth is observed from gas-phase

methylglyoxal, presumably due to its more stable (less electron-deficient) ketone moiety. From these results the gas-particle partitioning constant for methylglyoxal is at least 30 times lower than that of glyoxal; this is consistent with determinations of effective Henry's Law constants for the two compounds, which find methylglyoxal to be 10-100 times less soluble than glyoxal in water [Betterton and Hoffman, 1988; Zhou and Mopper, 1990]. Similarly, we observe no particle growth from 2,3-butanedione, an α -diketone with a still lower Henry's Law constant [Snider and Dawson, 1985; Betterton, 1991]. Hence, the observed reactive uptake of glyoxal cannot be generalized to all other atmospheric α -dicarbonyls. It seems likely, however, that more highly functionalized carbonyl compounds, such as the polycarbonyls produced in the photooxidation of aromatic compounds [Yu *et al.*, 1997; Jang and Kamens, 2001b; Edney *et al.*, 2001] may undergo significant reactive uptake similar to that observed for glyoxal.

Our measurements of the reactive uptake of glyoxal are in qualitative agreement with those by Liggio *et al.* [2005a]. However it is difficult to compare the results from these two studies directly. In Liggio *et al.* [2005a], equilibrium had not yet been reached by the end of the experiments (the organic:sulfate ratio continued to increase), perhaps a result of the chamber walls serving as a continual source of gas-phase glyoxal (organic aerosol growth exceeded initial amount of gas-phase glyoxal). Such conditions allow for the study of the kinetics, but not the thermodynamics, of glyoxal uptake. By contrast, the long mixing timescales of the present chamber experiments (there is no active mixing within our chambers) preclude the study of uptake kinetics. However, in these studies gas-particle equilibrium is reached, as particle volume stops increasing after an initial period of growth. Thus these two studies address different characteristics of glyoxal

uptake (kinetics and thermodynamics), which likely explains the observed differences in the role of seed acidity in particle growth.

Our observation that particle growth stops even while glyoxal is still present in the gas phase indicates that the reactive uptake of glyoxal is fully reversible. This conclusion is also supported by observations of equilibrium between glyoxal in the gas phase and on chamber walls, both in the present work and in *Liggio et al.* [2005a]. Further, in laboratory studies of aqueous glyoxal, equilibrium between gas-phase and aqueous-phase glyoxal has been observed [*Zhou and Mopper*, 1990], as has equilibrium between hydrated glyoxal monomer and dimer (the dominant forms of aqueous glyoxal at concentrations below 10M) [*Whipple*, 1970; *Fratzke and Reilly*, 1986]; such experiments also strongly suggest the reversibility of glyoxal uptake.

By treating glyoxal uptake as reversible, with gas-phase and particle-phase glyoxal in equilibrium, concentrations of particulate glyoxal in the troposphere may be estimated, based upon measurements of ambient gas-phase glyoxal in the gas phase, the effective Henry's Law constant, and the water content of tropospheric aerosols. This equilibrium approach yields calculated particle-phase glyoxal concentrations which are significantly lower than if glyoxal uptake were assumed to be irreversible. The assumption of irreversibility, in which aerosol growth is determined only by the kinetics of glyoxal uptake, was found to lead to unreasonably high aerosol mass, particularly in urban areas [*Liggio et al.*, 2005b].

Ambient measurements of glyoxal concentrations in urban areas, using sampling and derivatization techniques, indicate that glyoxal levels can be highly variable, ranging from 10 ppt to 1 ppb, with more polluted areas typically having higher levels [*Lee et al.*,

1998; Kawamura *et al.*, 2000; Jing *et al.*, 2001; Grosjean *et al.*, 2002, Ho and Yu, 2004]. Recent spectroscopic measurements of ambient glyoxal in Mexico City show significantly higher concentrations, often exceeding 1 ppb in the daytime [Volkamer *et al.*, 2005]. Using our measured effective Henry's Law coefficient of 2.6×10^7 M/atm, and assuming 100 ppt gas-phase glyoxal and $10 \mu\text{m}^3/\text{cm}^3$ of aqueous aerosol (corresponding to $10 \mu\text{g}/\text{m}^3$ of ammonium sulfate at 50% RH) in urban air, $1.5 \text{ ng}/\text{m}^3$ of glyoxal will be in the particle phase; at the highest measured concentration (1.82 ppb in Mexico City [Volkamer *et al.*, 2005]), particle-phase concentration will be $27 \text{ ng}/\text{m}^3$. In rural areas, gas-phase glyoxal concentrations are somewhat lower, varying from 10-100 ppt [Lee *et al.*, 1995; Grossmann *et al.*, 2003; Matsunaga *et al.*, 2004], so even lower aerosol-phase glyoxal concentrations are predicted.

There exist few measurements of particulate glyoxal concentrations to which these estimates may be compared, and in only one study [Matsunaga *et al.*, 2004] have both gas- and particle-phase glyoxal concentrations been measured. Such a comparison is also made difficult by the fact that glyoxal oligomers may revert to monomeric form during sampling and derivatization [Jang and Kamens, 2001a], and derivatization conditions such as temperature, choice of solvent, and pH may affect the extent of this reversion. Still, measurements of particle-phase glyoxal made in British Columbia, Canada by Liggio and McLaren [2003] are generally in agreement with these predictions, with concentrations of $0.47\text{-}1.4 \text{ ng}/\text{m}^3$ in Vancouver and $0.43\text{-}3.3 \text{ ng}/\text{m}^3$ in rural areas. However, comparison with other studies shows poorer agreement: particulate glyoxal concentrations as high as $46 \text{ ng}/\text{m}^3$ [Kawamura, 1993] and $73 \text{ ng}/\text{m}^3$ [Kawamura and Yasui, 2005] have been measured in and near Tokyo, and concentrations measured by

Matsunaga et al. [2004] in Hokkaido Island, Japan (a rural site) averaged 32 ng/m^3 (and were as high as 154 ng/m^3). In that study, glyoxal was found to partition roughly equivalently between the gas and particle phases, suggesting a gas-particle partitioning coefficient orders of magnitude higher than what we determine.

Hence, while ambient measurements are scarce, it appears that in some cases more glyoxal partitions into the particle phase than would be expected from the results of this study. Particulate glyoxal has even been measured in polar regions, in which gas-phase glyoxal concentrations are expected to be close to zero [*Kawamura et al.*, 1996]. One possible explanation for such discrepancies is the incorporation of glyoxal (as well as methylglyoxal, etc.) into the aerosol phase via heterogeneous reactions with other, less volatile organic compounds already in the aerosol phase. Complexation of glyoxal with inorganic aerosol components (such as metals) may also contribute. Alternately, rapid evaporation of liquid water within aerosols (or cloud droplets) may drive dissolved glyoxal towards higher-order oligomers. Any of these particle-phase processes may be effectively irreversible under tropospheric conditions, and if glyoxal reverts back to its monomer form during sample preparation and/or derivatization, this may lead to measured particulate glyoxal concentrations which are higher than predicted. Further laboratory studies using a wide range of reaction conditions (in particular, using different seed particle compositions) are necessary to understand the importance of such processes.

Moreover, this work underscores the need for ambient measurements of individual compounds in both the gas and particle phases simultaneously. Comparison of partitioning coefficients measured in the atmosphere with those measured in the laboratory provides a powerful test of our understanding of gas-particle partitioning

processes in the atmosphere, and in particular our understanding of the role of heterogeneous chemistry in SOA formation and growth.

4.6 Acknowledgements

This research was funded by the U. S. Environmental Protection Agency Science to Achieve Results (STAR) Program grant number RD-83107501-0, managed by EPA's Office of Research and Development (ORD), National Center for Environmental Research (NCER), and by U.S. Department of Energy Biological and Environmental Research Program DE-FG03-01ER63099. The authors are grateful to R. Bahreini for assistance with operation of the aerosol mass spectrometer; to A. Nenes for aid in calculating water content of the inorganic seed; to J. D. Crounse, C. M. Roehl, and P. O. Wennberg for the use of and aid with their FTIR spectrometer for the characterization of gas-phase glyoxal; and to B. Nozière and R. Volkamer for helpful discussions.

4.7 References

- Allan, J. D., J. L. Jimenez, H. Coe, K. N. Bower, P. I. Williams, and D. R. Worsnop (2003), Quantitative sampling using an Aerodyne Aerosol Mass Spectrometer. Part 1: Techniques of data interpretation and error analysis, *J. Geophys. Res.*, *108* (D3), 4090, doi:4010.1029/2002JD002358
- Allan, J. D., A. E. Delia, H. Coe, K. N. Bower, M. R. Alfarra, J. L. Jimenez, A. M. Middlebrook, F. Drewnick, T. B. Onasch, M. R. Canagaratna, J. T. Jayne, and D. R. Worsnop (2004), A generalized method for the extraction of chemically resolved mass spectra from aerodyne aerosol mass spectrometer data, *J. Aerosol Science*, *35*, 909-922

- Atkinson, R., and S. M. Aschmann (1984), Rate constants for the reactions of O₃ and OH radicals with a series of alkynes, *Int. J. Chem. Kinet.*, *16*, 259-268.
- Bahreini R., M. D. Keywood, N. L. Ng, V. Varutbangkul, S. Gao, R. C. Flagan, J. H. Seinfeld (2005), Measurements of secondary organic aerosol (SOA) from oxidation of cycloalkenes, terpenes, and *m*-xylene using an Aerodyne aerosol mass spectrometer, *Environ. Sci. Technol.*, *39*, 5674-5688.
- Barsanti K. C., and J. F. Pankow (2004), Thermodynamics of the formation of atmospheric matter by accretion reactions—Part 1: aldehydes and ketones, *Atmos. Environ.*, *38*, 4371-4382.
- Betterton, E. A., and M. R. Hoffmann (1988), Henry's Law constants of some environmentally important aldehydes, *Environ. Sci. Technol.*, *22*, 1415-1418.
- Betterton, E. A (1991). The partitioning of ketones between the gas and aqueous phases, *Atmos. Environ.*, *25A*, 1473-1577.
- Brock, C. A., R. A. Washenfelder, M. Trainer, T. B. Ryerson, J. C. Wilson, J. M. Reeves, L. G. Huey, J. S. Holloway, D. D. Parrish, G. Hübler, and F. C. Fehsenfeld (2002), Particle growth in the plumes of coal-fired power plants, *J. Geophys. Res.*, *107* (D12), 4155, doi:10.1029/2001JD001062.
- Calvert, J. G., R. Atkinson, J. A. Kerr, S. Madronich, G. K. Moortgat, T. J. Wallington, G. Yarwood (2000), *The Mechanisms of the Atmospheric Oxidation of the Alkenes*, 552 pp., Oxford University Press, Oxford.
- Calvert, J. G., R. Atkinson K. H. Becker R. M. Kamens, J. H. Seinfeld, T. J. Wallington, G. Yarwood (2002), *The Mechanisms of the Atmospheric Oxidation of Aromatic Hydrocarbons*, 566 pp., Oxford University Press, Oxford.

- Canosa-Mas. C., S. J. Smith, S. Toby, R. P. Wayne (1988), Reactivity of the nitrate radical towards alkynes and some other molecules, *J. Chem. Soc. Far. Trans. II*, *84*, 247-262.
- Cocker III, D. R., R. C. Flagan, and J. H. Seinfeld (2001), State-of-the-art chamber facility for studying atmospheric aerosol chemistry, *Environ. Sci. Technol.*, *35*, 2594-2601.
- Czoschke, N. M., M. Jang, and R. M. Kamens (2003), Effect of acidic seed on biogenic secondary organic aerosol growth, *Atmos. Environ.*, *37*, 4287-4299.
- Duncan, J. L., L. R. Schindler, and J. T. Roberts (1998), A new sulfate-mediated reaction: Conversion of acetone to trimethylbenzene in the presence of liquid sulfuric acid, *Geophys. Res. Lett.*, *25*, 631-634.
- Duncan, J. L., L. R. Schindler, and J. T. Roberts (1999), Chemistry at and near the surface of liquid sulfuric acid: a kinetic, thermodynamic, and mechanistic analysis of heterogeneous reactions of acetone, *J. Phys. Chem. B*, *103*, 7247-7259.
- Edney, E. O., D. J. Driscoll, W. S. Weathers, T. E. Kleindienst, T. S. Conner, C. D. McIver, and W. Li (2001), Formation of polyketones in irradiated toluene/propylene/NO_x/air mixtures, *Aerosol Sci. Technol.*, *35*, 998-1008.
- Esteve W., and B. Nozière (2005), Uptake and reaction kinetics of acetone, 2-butanone, and 2,4-pentanedione in sulfuric acid solutions, *J. Phys. Chem. A*, submitted.
- Fratzke, A. R., and P. J. Reilly (1986), Thermodynamic and kinetic analysis of the dimerization of aqueous glyoxal, *Int. J. Chem. Kin.*, *18*, 775-589.

- Gao, S., N. L. Ng, M. Keywood, V. Varutbangkul, R. Bahreini, A. Nenes, J. He, K. Y. Yoo, J. L. Beauchamp, R. P. Hodyss, R. C. Flagan, and J. H. Seinfeld (2004), Particle phase acidity and oligomer formation in secondary organic aerosol, *Environ. Sci. Technol.*, *38*, 6582-6589.
- Gao, S., M. Keywood, N. L. Ng, J. Surratt, V. Varutbangkul, R. Bahreini, R. C. Flagan, and J. H. Seinfeld (2004), Low-molecular weight and oligomeric components in secondary organic aerosol from the ozonolysis of cycloalkenes and α -pinene, *J. Phys. Chem. A*, *108*, 10147-10164.
- Grosjean, D., E. Grosjean, and L. F. R. Moreira (2002), Speciated ambient carbonyls in Rio de Janeiro, Brazil, *Environ. Sci. Technol.*, *36*, 1389-1395.
- Grossmann, D., G. K. Moortgat, M. Kibler, S. Schlomski, K. Bächmann, B. Alicke, A. Geyer, U. Platt, M.-U. Hammer, B. Vogel, D. Mihelcic, A. Hofzumahaus, F. Holland, and A. Volz-Thomas (2003), Hydrogen peroxide, organic peroxides, carbonyl compounds, and organic acids measured and Pabstthum during BERLIOZ, *J. Geophys. Res.*, *108* (D4), 8250, doi:10.1029/2001JD001096.
- Hatakeyama, S., N. Washida, and H. Akimoto (1986), Rate constants and mechanisms for the reaction of OH (OD) radicals with acetylene, propyne, and 2-butyne in air at 297 ± 2 K, *J. Phys. Chem.*, *90*, 173-178.
- Ho, S. S. H., and J. Z. Yu (2004), Determination of airborne carbonyls: Comparison of a thermal desorption/GC method with the standard DNPH/HPLC method, *Environ. Sci. Technol.*, *38*, 862-870.

- Iinuma, Y., O. Böge, T. Gnauk, and H. Herrmann (2004), Aerosol-chamber study of the α -pinene/O₃ reaction: influence of particle acidity on aerosol yields and products, *Atmos. Environ.*, *38*, 761-773.
- Imamura T., and H. Akiyoshi (2000), Uptake of acetone into sulfuric-acid solutions, *Geophys. Res. Lett.*, *27*, 1419-1422.
- Iraci L. T., and M. A. Tolbert (1997), Heterogeneous interaction of formaldehyde with cold sulfuric acid: Implications for the upper troposphere and lower stratosphere, *J. Geophys. Res.*, *102* (D13), 16,099-16,107.
- Jang, M., and R. M. Kamens (2001a), Atmospheric secondary aerosol formation by heterogeneous reactions of aldehydes in the presence of a sulfuric acid aerosol catalyst, *Environ. Sci. Technol.*, *35*, 4758-4766.
- Jang, M., and R. M. Kamens (2001b), Characterization of secondary organic aerosol from the photooxidation of toluene in the presence of NO_x and 1-propene, *Environ. Sci. Technol.*, *35*, 4758-4766.
- Jang, M., N. M. Czoschke, S. Lee, and R. M. Kamens (2002), Heterogeneous atmospheric aerosol production by acid-catalyzed particle-phase reactions, *Science*, *298*, 814-817.
- Jang, M., M. Carroll, B. Chandramouli, and R. M. Kamens (2003a), Particle growth by acid-catalyzed heterogeneous reactions of organic carbonyls on preexisting aerosols, *Environ. Sci. Technol.*, *37*, 3828-3837.
- Jang, M., S. Lee, and R. M. Kamens (2003b), Organic aerosol growth by acid-catalyzed heterogeneous reactions of octanal in a flow reactor, *Atmos. Environ.*, *37*, 2125-2138.

- Jang, M., N. M. Czoschke, and A. L. Northcross (2005), Semiempirical model for organic aerosol growth by acid-catalyzed heterogeneous reactions of organic carbonyls, *Environ. Sci. Technol.*, *39*, 164-174.
- Jayne, J. T., D. R. Worsnop, C. E. Kolb, E. Swartz, and P. Davidovitz (1996), Uptake of gas-phase formaldehyde by aqueous acid surfaces, *J. Phys. Chem.*, *100*, 8015-8022.
- Jayne, J. T., D. C. Leard, X. Zhang, P. Davidovits, K. A. Smith, C. E. Kolb, and D. R. Worsnop (2000), Development of an Aerosol Mass Spectrometer for size and composition analysis of submicron particles, *Aerosol Sci. and Technol.*, *33*, 49-70.
- Jing, L., S. M. Steinberg, and B. J. Johnson (2001), Aldehyde and monocyclic aromatic hydrocarbon mixing ratios at an urban site in Las Vegas, Nevada, *J. Air & Waste Manage. Assoc.*, *51*, 1359-1366.
- Kalberer, M., S. Paulsen, M. Sax, M. Steinbacher, J. Dommen, A. S. H. Prevot, R. Fisseha, E. Weingartner, V. Frankevich, R. Zenobi, U. Baltensperger (2004), Identification of polymers as major components of atmospheric organic aerosols, *Science*, *303*, 1659-1662.
- Kane, S. M., R. S. Timonen, and M.-T. Leu (1999), Heterogeneous chemistry of acetone in sulfuric acid solutions: Implications for the upper troposphere, *J. Phys. Chem. A*, *103*, 9259-9265.
- Kawamura, K. (1993), Identification of C₂-C₁₀ ω-oxocarboxylic acids, pyruvic acid, and C₂-C₃ α-dicarbonyls in wet precipitation and aerosol samples by capillary GC and GC/MS, *Anal. Chem.*, *65*, 3505-3511.

- Kawamura, K., H. Kasukabe, and L. A. Barrie (1996), Source and reaction pathways of dicarboxylic acids, ketoacids and dicarbonyls in arctic aerosols: One year of observations, *Atmos. Environ.*, *30*, 1709-1722.
- Kawamura K., S. Steinberg, and I. R. Kaplan (2000), Homologous series of C1-C10 monocarboxylic acids and C1-C6 carbonyls in Los Angeles air and motor vehicle exhausts, *Atmos. Environ.*, *34*, 4175-4191.
- Kawamura, K., and O. Yasui (2005), Diurnal changes in the distribution of dicarboxylic acids, ketocarboxylic acids and dicarbonyls in the urban Tokyo atmosphere, *Atmos. Environ.*, *39*, 1945-1960.
- Keywood, M. D., V. Varutbangkul, R. Bahreini, R. C. Flagan, J. H. Seinfeld (2004), Secondary organic aerosol formation from the ozonolysis of cycloalkenes and related compounds, *Environ. Sci. Technol.*, *38*, 4157-4164.
- Klassen, J. K., J. Lynton, D. M. Golden, and L. R. Williams (1999), Solubility of acetone in low-temperature (210-240 K) sulfuric acid solutions, *J. Geophys. Res.*, *104* (D21), 26,355-26,361.
- Kroll, J. H., and J. H. Seinfeld (2005), Representation of secondary organic aerosol laboratory chamber data for the interpretation of mechanisms of particle growth, *Env. Sci. Technol.*, *39*, 4159-4165.
- Lee, Y.-N., X. Zhou, and K. Hallock (1995), Atmospheric carbonyl compounds at a rural southeastern United States site, *J. Geophys. Res.*, *100* (D12), 25,933-25,944.
- Lee, Y.-N., X. Zhou, L. I. Kleinman, L. J. Nunnermacker, S. R. Springston, P. H. Daum, L. Newman, W. G. Keigley, M. W. Holdren, C. W. Spicer, V. Young, B. Fu, D. D. Parrish, J. Holloway, J. Williams, J. M. Roberts, T. B. Ryerson, and F. C. Fehsenfeld

- (1998), Atmospheric chemistry and distribution of formaldehyde and several multioxygenated carbonyl compounds during the 1995 Nashville/Middle Tennessee Ozone Study, *J. Geophys. Res.*, *103* (D17), 22,449-22462.
- Liggio J., and R. McLaren (2003), An optimized method for the determination of volatile and semi-volatile aldehydes and ketones in ambient particulate matter, *Int. J. Environ. Anal. Chem.*, *83*, 819-835.
- Liggio, J., S.-M. Li, and R. McLaren (2005a), Heterogeneous reactions of glyoxal on particulate matter: Identification of acetals and sulfate esters, *Environ. Sci. Technol.*, *39*, 1532-1541.
- Liggio, J., S-M. Li, and R. McLaren (2005b), Reactive uptake of glyoxal by particulate matter, *J. Geophys. Res.*, *110* (D103), doi:10.1029/2004JD005113.
- Martos, P. A., and J. Pawliszyn (1998), Sampling and determination of formaldehyde using solid-phase microextraction with on-fiber derivatization, *Anal. Chem.*, *70*, 2311-2320.
- Matsunaga, S., M. Mochida, and K. Kawamura (2004), Variation on the atmospheric concentrations of biogenic carbonyl compounds and their removal processes in the northern forest at Moshiri, Hokkaido Island in Japan, *J. Geophys. Res.*, *109*, D04302, doi:10.1029/2003JD004100.
- Michelsen, R. R., S. F. M. Ashbourn, and L. T. Iraci (2004), Dissolution, speciation, and reaction of acetaldehyde in cold sulfuric acid, *J. Geophys. Res.*, *109*, D23205, doi:10.0129/2004JD005041.

- Niki, H., P. D. Maker, C. M. Savage, and L. P. Breitenbach (1985), An FTIR study of the Cl-initiated reaction of glyoxal, *Int. J. Chem. Kinet.*, *17*, 547–558.
- Nozière, B., and D. D. Riemer (2003), The chemical processing of gas-phase carbonyl compounds by sulfuric acid aerosols: 2,4-pentanedione, *Atmos. Environ.*, *37*, 841-851.
- Odum J. R., T. Hoffmann, F. Bowman, D. Collins, R. C. Flagan, and J. H. Seinfeld (1996), Gas/particle partitioning and secondary organic aerosol yields, *Environ. Sci. Technol.*, *30*, 2580-2585.
- Pankow, J. F. (1994a), An absorption-model of gas-particle partitioning of organic-compounds in the atmosphere, *Atmos. Environ.*, *28A*, 185-188.
- Pankow, J. F. (1994b), An absorption-model of the gas aerosol partitioning involved in the formation of secondary organic aerosol, *Atmos. Environ.*, *28A*, 189-193.
- Reisen F., S. M. Aschmann, R. Atkinson, and J. Arey (2003), Hydroxyaldehyde products from hydroxyl radical reactions of Z-3-hexen-1-ol and 2-methyl-3-buten-2-ol quantifies by SPME and API-MS, *Environ. Sci. Technol.*, *37*, 4664-4671.
- Reisen, F., S. M. Aschmann, R. Atkinson, and J. Arey (2005), 1,4-Hydroxycarbonyl products of the OH radical initiated reactions of C₅-C₈ n-alkanes in the presence of NO, *Env. Sci. Technol.*, *39*, 4447-4453.
- Snider, J. R., and G. A. Dawson (1985), Tropospheric light alcohols, carbonyls, and acetonitrile: Concentrations in the southwestern United States and Henry's Law data, *J. Geophys. Res.*, *90* (D2), 3797-3805.

- Tobias H. J., and P. J. Ziemann (2001), Kinetics of the gas-phase reactions of alcohols, aldehydes, carboxylic acids, and water with the C13 stabilized Criegee intermediate formed from the ozonolysis of 1-tetradecene, *J. Phys. Chem. A*, *105*, 6129-6135.
- Tolbert, M. A., J. Pfaff, I. Jayaweera, and M. J. Prather (1993), Uptake of formaldehyde by sulfuric acid solutions: Impact on stratospheric ozone, *J. Geophys. Res.*, *98* (D2), 10,563-10,571.
- Tolocka, M. P., M. Jang, J. M. Ginter, F. J. Cox, R. M. Kamens, and M. V. Johnston (2004), Formation of oligomers in secondary organic aerosol, *Environ. Sci. Technol.*, *38*, 1428-1434.
- VanReken, T. M., N. L. Ng, R. C. Flagan, and J. H. Seinfeld (2005), Cloud condensation nuclei (CCN) activation properties of biogenic secondary organic aerosol, *J. Geophys. Res.*, in press.
- Volkamer R., U. Platt, and K. Wirtz (2001), Primary and secondary glyoxal formation of aromatics: experimental evidence for the bicycloalkyl-radical pathway from benzene, toluene, and *p*-xylene, *J. Phys. Chem. A*, *105*, 7865-7874.
- Volkamer, R., L. T. Molina, M. J. Molina, T. Shirley, and W. H. Brune, (2005), DOAS measurements of glyoxal as an indicator for fast VOC chemistry in urban air, *Geophys. Res. Lett.*, *32*, L08806, doi:10.1029/2005GL022616.
- Whipple, E. B. (1970), The structure of glyoxal in water, *J. Am. Chem. Soc.*, *92*, 7183-7186.

- Yeung, L. Y., M. J. Pennino, A. M. Miller, and M. J. Elrod (2005), Kinetics and mechanistic studies of the atmospheric oxidation of alkynes, *J. Phys. Chem. A*, *109*, 1879-1889.
- Yu, J., H. E. Jeffries, and K. G. Sexton (1997), Atmospheric Photooxidation of alkylbenzenes—I. Carbonyl product analyses, *Atmos. Environ.*, *31*, 2261-2280.
- Zhang, Q., C. O. Stanier, M. R. Canagaranta, J. T. Jayne, D. R. Worsnop, S. N. Pandis, and J. L. Jimenez (2004), Insights into the chemistry of new particle formation and growth events in Pittsburgh based on aerosol mass spectrometry, *Environ. Sci. Technol.*, *38*, 4797-4809.
- Zhang, Q., M. R. Canagaranta, J. T. Jayne, D. R. Worsnop, and J. L. Jimenez (2005), Time- and size-resolved chemical composition of submicron particles in Pittsburgh: Implications for aerosol sources and processes, *J. Geophys. Res.*, *110*, D07S09, doi:10.1029/2004JD004649.
- Zhao, J., N. P. Leavitt, and R. Zhang (2005), Heterogeneous chemistry of octanal and 2,4-hexadienal with sulfuric acid, *Geophys. Res. Lett.*, *32*, L09802, doi:10.1029/2004GL022200.
- Zhou, X., and K. Mopper (1990), Apparent partition coefficients of 15 carbonyl compounds between air and seawater and between air and freshwater, Implications for air-sea exchange, *Environ. Sci. Technol.*, *24*, 1864-1869.
- Ziemann, P. J. (2002), Evidence for low-volatility diacyl peroxides as a nucleating agent and major component of aerosol formed from reactions of O₃ with cyclohexene and homologous compounds, *J. Phys. Chem. A*, *106*, 4390-4402.

Table 4. 1. Experimental conditions and measured particle growth for glyoxal uptake experiments^A.

Exp. No.	Seed ^B	[Glyoxal] (ppb)	RH	Seed volume V ($\mu\text{m}^3/\text{cm}^3$)	Water content of seed ^C	ΔM ($\mu\text{g}/\text{m}^3$) ^D
1	AS	55 ± 7	47.5%	65.3 ± 1.5	31%	5.8 ± 2.0
2	AS	153 ± 7	54.5%	86.8 ± 1.8	36%	18.8 ± 2.8
3	AS	126 ± 5	53.5%	86.5 ± 2.6	35%	14.5 ± 3.1
4	AS	110 ± 4	44.5%	68.5 ± 2.1	30%	7.6 ± 2.4
5	AS	158 ± 20	54.5%	91.7 ± 2.2	36%	21.3 ± 3.3
6	AS/SA	25 ± 3	31.0%	77.4 ± 2.0	42%	0.7 ± 2.5
7	AS/SA	174 ± 8	48.5%	115.4 ± 1.9	51%	11.8 ± 2.7
8	AS/SA	93 ± 12	50.0%	97.3 ± 1.7	52%	10.7 ± 2.5
9	AS/SA	60 ± 7	52.5%	97.6 ± 1.9	53%	10.3 ± 3.0

^AReported uncertainties of 1σ . ^BAS=ammonium sulfate (seed solution 0.03 M), AS/SA=mixed ammonium sulfate/sulfuric acid seed (seed solution 0.03M/0.1M). ^Cpercent water by mass. ^DAssuming unit density of the organic aerosol.

Figure 4. 1. Structures of the carbonyls studied in this work.

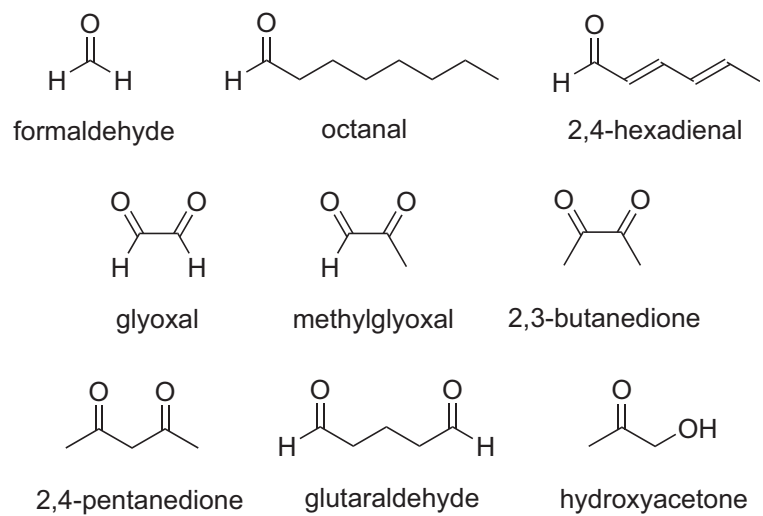


Figure 4. 2. Sample DMA volume data for chamber experiments. Introduction of inorganic seed corresponds to $t=0$; the gradual decrease in volume is a result of particle loss to the chamber walls. Grey circles: inorganic seed only. Black circles: inorganic seed (ammonium sulfate/sulfuric acid), followed by introduction of 500 ppb 2,4-hexadienal at $t=50$ min (dashed line). Data are scaled so that starting particle volumes are equivalent.

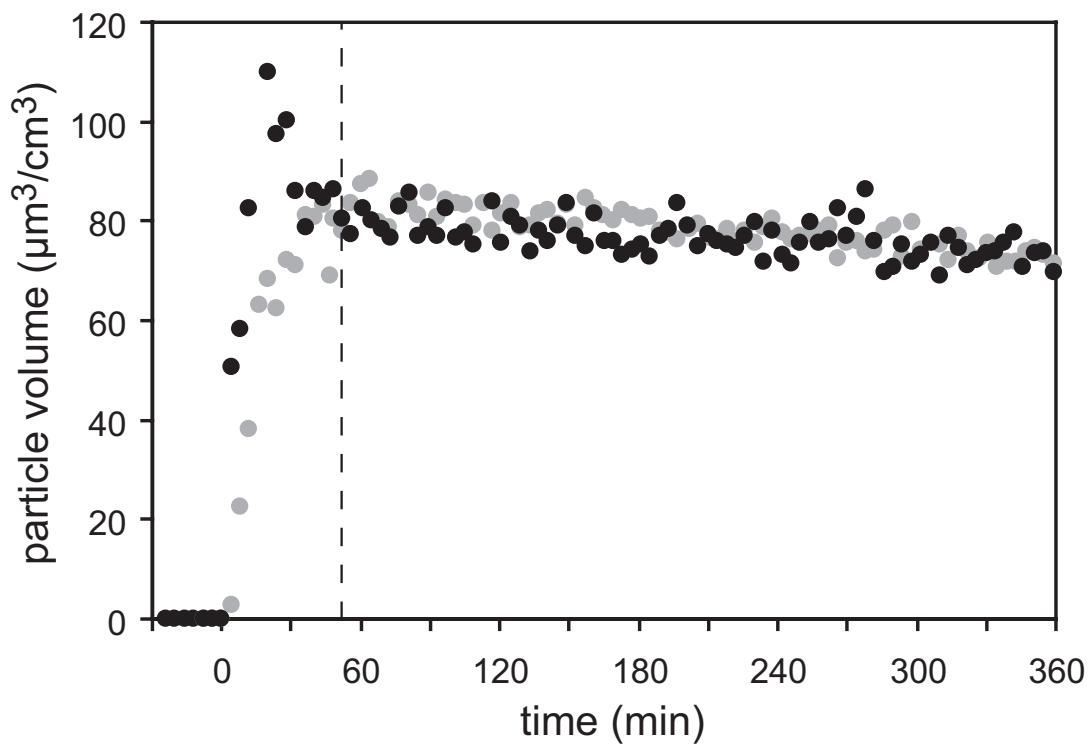


Figure 4. 3. DMA volume data growth for a glyoxal + inorganic seed experiment. As in Figure 4.2, introduction of inorganic seed corresponds to $t=0$. Grey circles: inorganic seed only. Black circles: inorganic seed (ammonium sulfate/sulfuric acid), followed by introduction of 200 ppb glyoxal at $t=53$ min (dashed line). Data are scaled so that starting particle volumes are equivalent.

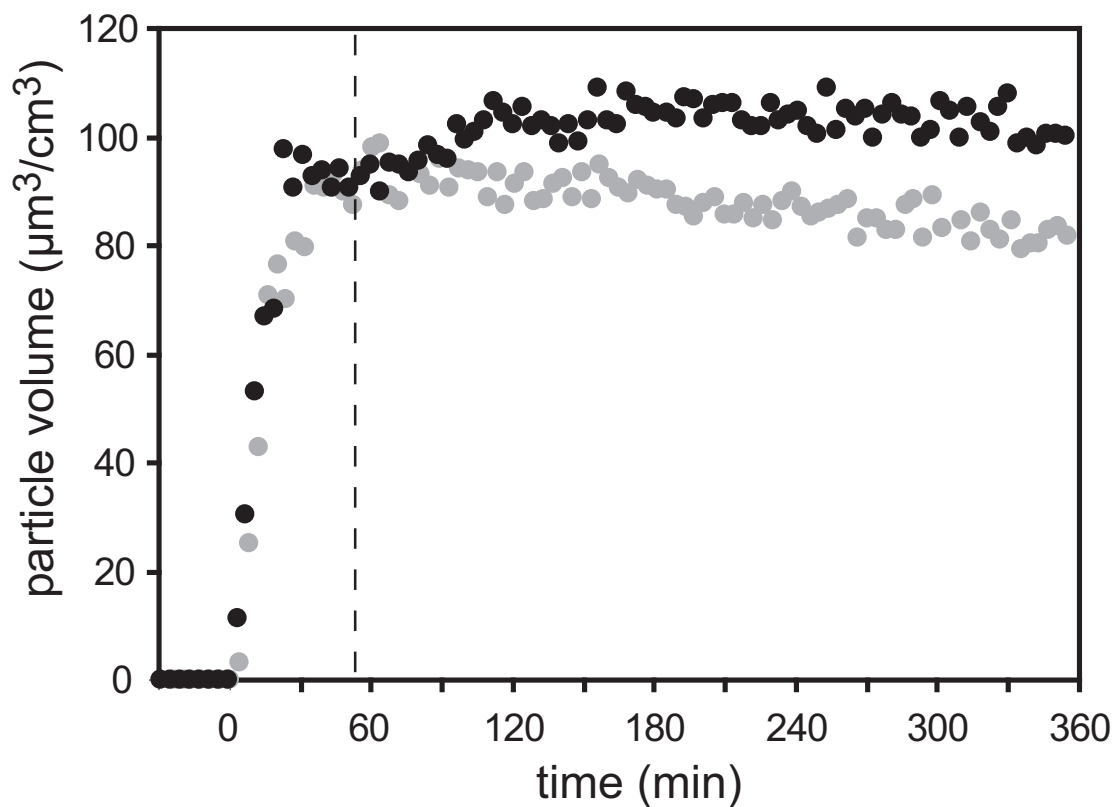
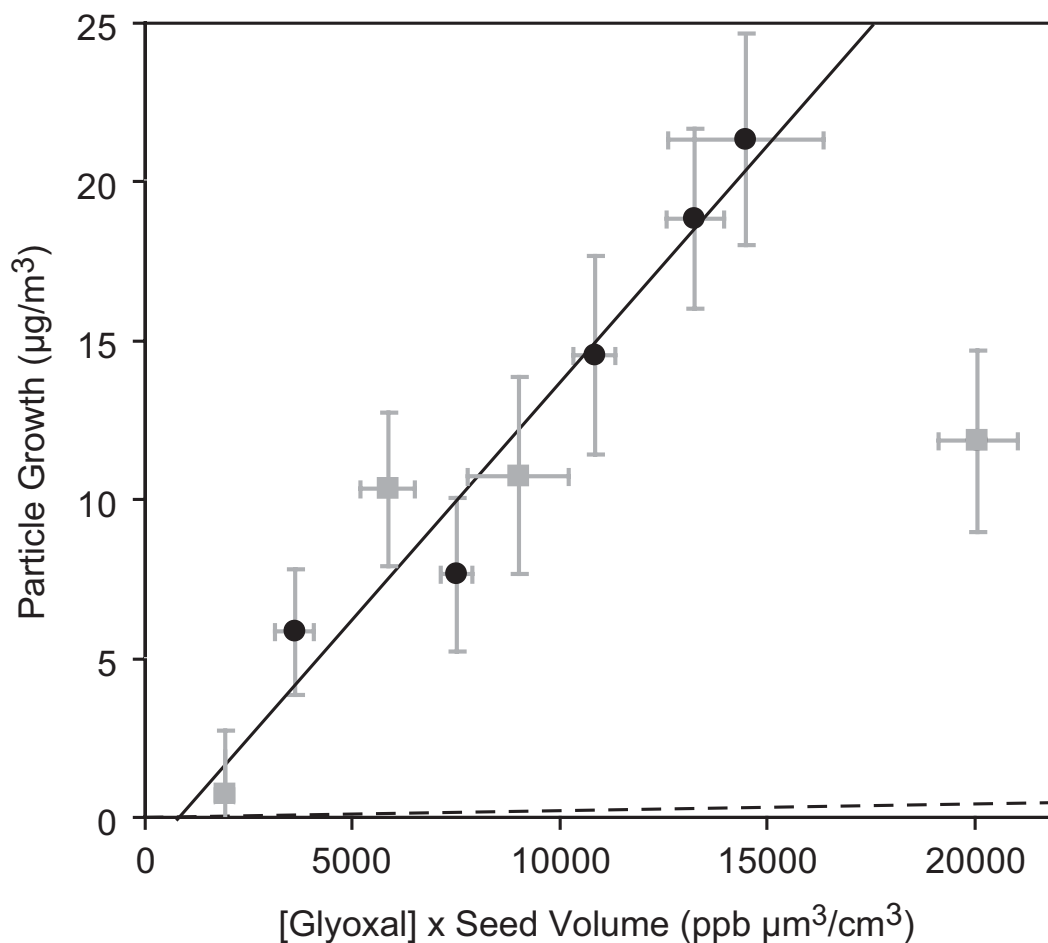


Figure 4. 4. Particle growth as a function of gas-phase glyoxal concentration and initial seed volume, assuming unit density of the organic fraction of the aerosol. Black circles: ammonium sulfate seed. Grey squares: mixed ammonium sulfate/sulfuric acid seed. The fit shown is to the ammonium sulfate data only. The dashed line near the bottom of the figure is the growth expected using the measured Henry's Law constant (in seawater) of 3.6×10^5 M/atm [Zhou and Mopper, 1990].



Chapter 5

Secondary Organic Aerosol Formation from Isoprene

Photooxidation under High-NO_x Conditions*

*This chapter is reproduced by permission from “Secondary organic aerosol formation from isoprene photooxidation under high-NO_x conditions” by J. H. Kroll, N. L. Ng, S. M. Murphy, R. C. Flagan, J. H. Seinfeld, *Geophysical Research Letters*, 32, L18808, doi:10.1029/2005GL023637, 2005. Copyright 2005, American Geophysical Union.

5.1 Abstract

The oxidation of isoprene (2-methyl-1,3-butadiene) is known to play a central role in the photochemistry of the troposphere, but is generally not considered to lead to the formation of secondary organic aerosol (SOA), due to the relatively high volatility of known reaction products. However, in the chamber studies described here, we measure SOA production from isoprene photooxidation under high-NO_x conditions, at significantly lower isoprene concentrations than had been observed previously. Mass yields are low (0.9-3.0%), but because of large emissions, isoprene photooxidation may still contribute substantially to global SOA production. Results from photooxidation experiments of compounds structurally similar to isoprene (1,3-butadiene and 2- and 3-methyl-1-butene) suggest that SOA formation from isoprene oxidation proceeds from the further reaction of first-generation oxidation products (i.e., the oxidative attack of both double bonds). The gas-phase chemistry of such oxidation products is in general poorly characterized and warrants further study.

5.2 Introduction

Isoprene (2-methyl-1,3-butadiene, C₅H₈) is the most abundant non-methane hydrocarbon emitted into the troposphere. Global emissions are estimated at 500 Tg/year [Guenther *et al.*, 1995], and concentrations of several ppb are routinely measured in deciduous forests. Because of its large concentrations and high reactivity with the hydroxyl radical (OH), isoprene can have a major impact on tropospheric photochemistry, and in particular regional ozone production, in both rural and urban environments [e.g., Trainer *et al.*, 1987; Biesenthal *et al.*, 1997].

The initial steps of the OH-isoprene reaction (under high-NO_x conditions) are generally well understood. While product yields vary somewhat among different laboratory studies, and structures of all products are not fully established, total carbon balance is close to 100% [Zhao *et al.*, 2004]. Fragmentation to C4 compounds, most importantly methyl vinyl ketone and methacrolein, accounts for ~50-70% of the reacted isoprene; the remainder leads to multifunctional C5 products, hydroxynitrates (4-14%), hydroxycarbonyls (15-19%), 3-methylfuran (<2-5%), and carbonyls (8%) [Tuazon and Atkinson 1990; Paulson *et al.*, 1992; Miyoshi *et al.*, 1994; Chen *et al.*, 1998; Sprengnether *et al.*, 2002; Zhao *et al.*, 2004; Baker *et al.* 2005]. Because of the relatively high volatility of these products, oxidation of isoprene is generally not considered to contribute significantly to the formation of secondary organic aerosol (SOA) in the troposphere. Indeed, chamber studies by Pandis *et al.* [1991] and Edney *et al.* [2005] found that the photooxidation of isoprene (at concentrations below a few hundred ppb) leads to insignificant SOA growth, suggesting that condensable compounds are not formed in sufficient concentrations to partition into the aerosol phase.

Recent work suggests isoprene may instead contribute to organic aerosol via routes other than the gas-phase formation of condensable oxidation products. Tetrols with the same carbon backbone as isoprene have recently been measured in ambient aerosols [Claeys *et al.*, 2004a] and are believed to be formed by the heterogeneous acid-catalyzed oxidation of isoprene in the presence of peroxides [Claeys *et al.*, 2004b]. Edney *et al.* [2005] observed aerosol growth from isoprene photooxidation when SO₂ was added to the chamber, acidifying the aerosol seed; tetrols and related compounds accounted for 6% of aerosol mass. Heterogeneous reaction of isoprene under highly

acidic conditions was also observed to lead to the formation of polymeric, humic-like substances [Limbeck *et al.*, 2003]. Uptake of volatile, water-soluble isoprene oxidation products (such as glycolaldehyde and hydroxyacetone [Matsunaga *et al.*, 2003]) may also contribute to aerosol growth, though laboratory studies on such a mechanism are scarce. Polymerization of methylglyoxal, a second-generation product, has been suggested to contribute to SOA growth [Kalberer *et al.*, 2004]; however, growth from methylglyoxal uptake was not observed in recent chamber experiments [Kroll *et al.*, 2005]. Finally, models [Ervens *et al.*, 2004; Lim *et al.*, 2005] predict that cloud processing of water-soluble isoprene oxidation products may also lead to the formation of low-volatility SOA components.

Thus isoprene might contribute to the organic fraction of tropospheric aerosol via a number of pathways, though most are poorly understood or await experimental verification. To our knowledge, only the studies of Pandis *et al.* [1991] and Edney *et al.* [2005] have investigated whether SOA is formed directly from condensable isoprene photooxidation products. In the present work, we investigate the gas-phase oxidation of isoprene under different reaction conditions (at lower temperatures and with a different radical precursor), observing SOA formation at lower isoprene concentrations than have been observed previously. Aerosol yield is small compared to that of other SOA-forming reactions, but given the large source strength of isoprene, isoprene may still have an impact on SOA production on both the local and global scales. We show that the SOA is likely formed from the oxidation of first-generation oxidation products, the chemistry of which is generally poorly understood.

5.3 Experimental

Experiments are carried out in 28 m³ Teflon chambers [Cocker *et al.*, 2001; Keywood *et al.*, 2004] at ~20°C and 40-50% relative humidity. Aqueous ammonium sulfate seed particles, providing surface area for the initial condensation of condensable products, are introduced into the chamber (at volume concentrations of 10-25 µm³/cm³) by atomization of a 0.03 M salt solution. A known concentration of isoprene is then introduced by sending air over a measured volume of the pure compound (Aldrich, 99.8%) and into the chamber. Nitrous acid (HONO) is used as the OH precursor. HONO is prepared by dropwise addition of 1% NaNO₂ into 10% H₂SO₄ and introduced by blowing dry air over the mixture and into the chamber; this also introduces NO_x as a side product. Reaction is initiated by irradiation of the chamber with blacklights centered at 354 nm, efficiently photolyzing HONO to OH and NO; only 10% of available lights are used to minimize temperature increases. After ~3 hours of irradiation, the chamber temperature rises by 1-2°C, and relative humidity decreases correspondingly (RH never drops below 40%, the efflorescence point of ammonium sulfate). Isoprene decay is monitored using GC-FID, and commercial monitors (Horiba) are used to measure O₃ (by UV absorption) and NO_x (by conversion to NO by activated carbon, followed by NO+O₃ chemiluminescence). HONO is not measured directly but might be detected by the NO_x monitor as NO₂ (or NO); consideration of the rate of isoprene decay after reaction initiation suggests [HONO] is unlikely to be significantly greater than measured [NO₂]. Aerosol growth is monitored using two instruments, a differential mobility analyzer (DMA, for the measurement of aerosol volume) and an Aerodyne aerosol mass

spectrometer (AMS, for the measurement of aerosol mass and composition [Jayne *et al.*, 2000]).

5.4 Results and discussion

Prior to irradiation, isoprene concentrations are stable and no organic growth is observed, indicating that heterogeneous reaction of isoprene (or reaction with HONO) does not contribute to aerosol growth. Once the lights are turned on, isoprene is observed to decay immediately, and is consumed within 120 minutes (at the highest concentration studied). Measured NO_x increases slightly from the photolysis of HONO, reaches a maximum after 25-35 minutes, and then decreases throughout the remainder of the experiment due to chain-termination ($\text{HO}_x + \text{NO}_x$) reactions. The evolution of concentrations during a typical experiment is shown in Figure 5.1.

Aerosol growth, measured by both the DMA and the AMS, is observed at all isoprene concentrations studied. Growth typically begins 20-30 minutes after reaction initiation, corresponding approximately to when NO approaches zero and the formation of O_3 begins. AMS spectra indicate the growth is indeed by condensation of organic matter, rather than by uptake of inorganic nitrate, water, etc. At the highest isoprene concentrations (≥ 250 ppb), additional particle formation is even observed. By contrast, no growth is observed from the photooxidation of 500 ppb propene under similar conditions.

Experimental conditions and results are given in Table 5.1. All growth data reported are from DMA measurements; growth measurements from the AMS are in general agreement. SOA growth is corrected for loss to the walls by applying a size-dependent first-order loss coefficient [Keywood *et al.*, 2004], with typical corrections of

1.5-5.0 $\mu\text{m}^3/\text{cm}^3$ over the course of a 3-hour experiment. At the lowest concentrations studied (25 and 50 ppb), particle growth is of the same order as loss to the chamber walls, so further work is necessary to determine whether SOA growth occurs at concentrations typical for the troposphere (<10 ppb). Shown in Figure 5.2 is particle growth as a function of isoprene reacted; the nonlinear relationship is typical for SOA-forming reactions [Kroll and Seinfeld, 2005]. Comparison of DMA and AMS data indicates the organic aerosol has a density of $\sim 1.4 \text{ g/cm}^3$, leading to mass yields (ratios of organic aerosol formed to amount of hydrocarbon reacted) of 0.9-3.0%. There is no obvious dependence of aerosol growth on initial seed particle volume.

Our observation of aerosol growth from the photooxidation of isoprene, even at relatively low concentrations, is in contrast with the results of *Pandis et al.* [1991] and *Edney et al.* [2005]. *Pandis et al.* [2005] observed no growth at <120 ppb isoprene, and mass yields never exceeding 1.4% (0.8% carbon yield) at high (ppm) concentrations; *Edney et al.* [2005] observed even less growth (yield of 0.2% at 1.6 ppm isoprene reacted). Such differences likely arise from differing experimental conditions: for example, in our experiments RH and ammonium sulfate seed loadings are higher than those of the previous studies. Moreover, those experiments were carried out at temperatures of $\sim 30^\circ\text{C}$, about 10 degrees warmer than the present experiments. Such a temperature difference is expected to have a large effect on gas-particle partitioning.

In addition, the oxidative conditions in those studies are different from those of the present experiments. In the studies by *Pandis et al.* [1991] and *Edney et al.* [2005], reaction was initiated by irradiation of NO_x /isoprene mixtures. The hydroxyl radical is formed from a number of secondary reactions, including ozone photolysis to form $\text{O}(^1\text{D})$,

heterogeneous production of HONO, isoprene ozonolysis, and the $O(^3P)+\text{isoprene}$ reaction [Paulson *et al.*, 1992]. In the present study, OH is produced directly from the photolysis of HONO, and J_{NO_2} is a factor of 3-10 lower, leading to the lower ozone levels in our experiments. Based upon the measured ozone production and rate of isoprene decay in our experiments (Figure 5.1), the O_3 -isoprene reaction cannot account for more than a small fraction of the total isoprene reacted; it is likely to be more important in isoprene/ NO_x photooxidation experiments. In addition, the NO concentrations reported in those experiments do not approach zero, in contrast to the present experiments. High concentrations (10's of ppb or more) of NO may have the effect of suppressing SOA growth [e.g., Johnson *et al.*, 2005], which might explain the lack of observed growth in the previous studies.

As noted above, condensable compounds partitioning into the aerosol phase are unlikely to be any of the known first-generation products of OH+isoprene, as they are all relatively volatile. It is possible that a minor, as yet unidentified, product (yield $\leq 2\%$) may be responsible for SOA production. However, the observed time lag between the decay of isoprene and particle growth (Figure 5.1) suggests SOA is instead formed by the further oxidation of first-generation oxidation products [Bowman *et al.*, 1997]. The role of second-generation oxidation products in SOA formation is also suggested by measurements of aerosol growth from the photooxidation of compounds structurally similar to isoprene. No growth was observed from the photooxidation experiments of monoalkene C5 analogs of isoprene (500 ppb of 2- and 3-methyl-1-butene). Such compounds are expected to undergo only one oxidation step under our reaction conditions: first-generation reaction products are expected to be unreactive towards NO_3

and O₃, and to react with OH slowly (at a rate 10-100 times slower than if a second double bond were present). By contrast, photooxidation of the C₄ analog of isoprene, 1,3-butadiene, was observed to lead to aerosol growth, though in lower yields (1.5% at 560 ppb).

Thus the aerosol formation we observe is likely the result of oxidation of both double bonds of isoprene. This can lead to a complex array of reaction products, with up to four functional (hydroxy, carbonyl, carboxylic acid, or nitrate) groups; such tetrasubstituted compounds are likely to be of sufficiently low volatility to partition efficiently into the aerosol phase. Their formation route may be complex, due to the number of potential oxidation routes available to first-generation oxidation products. While the loss of isoprene is dominated by reaction with OH, ozone and the nitrate radical (NO₃) are formed over the course of the experiment and so may react with OH-isoprene oxidation products to form condensable compounds; photolysis of such products may also play a role. The importance of these different oxidation pathways and the product yields of each are for the most part poorly constrained, as the atmospheric fates of first-generation isoprene oxidation products (other than methacrolein and methyl vinyl ketone) have received little study. Measurements of rates and products of the gas-phase oxidation of these compounds would be very useful.

In preliminary photooxidation experiments of isoprene oxidation products, we observe no aerosol growth from methyl vinyl ketone (500 ppb) but do from methacrolein (2.2% yield at 100 ppb). Oxidation of 3-methylfuran was also observed to lead to SOA formation (3.5% yield at 100 ppb); the oxidation of other multifunctional products of OH+isoprene are also likely candidates for SOA formation.

We note that from the AMS spectra we do not observe significant organic signal at high masses ($m/z > 130$), which might suggest that particle-phase oligomers, observed in other SOA-forming reactions [e.g., *Kalberer et al.*, 2004], are not major components of SOA produced from isoprene oxidation. However, it is possible that oligomers are formed but are not detected by the AMS, due to fragmentation and the relatively small total organic signal. Further study of the chemical composition of SOA and the effects of seed composition and loading on particle growth is required to understand the role of particle-phase reactions.

The photooxidation of isoprene, even with small (<1%) SOA yields, may be an important contributor to global SOA production, given the large source strength of isoprene (~500 Tg/year); global production of SOA from other precursor VOC's is estimated at 12-70 Tg/year [*Kanakidou et al.*, 2005]. From the present results alone it is difficult to estimate global SOA production from isoprene oxidation, as these measurements are only at high concentrations of isoprene and NO_x . Very recent results from our laboratory show that aerosol is formed from isoprene photooxidation initiated by H_2O_2 photolysis as well, indicating that isoprene may also serve as a source of SOA in low- NO_x (remote) regions, and that oxidation of isoprene by OH alone (with no O_3 or NO_3 present) leads to aerosol formation. In a forthcoming paper we will discuss the NO_x dependence of the aerosol yield, and the chemical composition of the SOA produced, in order to better understand the chemical mechanism of aerosol growth by isoprene photooxidation.

5.5 Acknowledgements

This work was supported by the Department of Energy, Award DE-FG02-05ER63983, and the U.S. Environmental Protection Agency, grant RD-83107501-0; it has not been subjected to the EPA's required peer and policy review and therefore does not necessarily reflect the views of the Agency and no official endorsement should be inferred.

5.6 References

- Baker, J., J. Arey, and R. Atkinson, Formation and reaction of hydroxycarbonyls from the reaction of OH radicals with 1,3-butadiene and isoprene (2005), *Environ. Sci. Technol.*, *39*, 4091-4099.
- Biesenthal, T. A., Q. Wu, P. B. Shepson, H. A. Wiebe, K. G. Anlauf, and G. I. Mackay (1997), A study of relationships between isoprene, its oxidation products, and ozone in the Lower Fraser Valley, BC, *Atmos. Environ.*, *31*, 2049–2058.
- Bowman, F. M., J. R. Odum, J. H. Seinfeld, and S. N. Pandis (1997), Mathematical model for gas-particle partitioning of secondary organic aerosols, *Atmos. Environ.*, *31*, 3921-3931.
- Chen, X., D. Hulbert, and P. B. Shepson (1998), Measurement of the organic nitrate yield from OH reaction with isoprene, *J. Geophys. Res.*, *103*, 25,563–25,568.
- Claeys, M. et al. (2004a), Formation of secondary organic aerosol through photooxidation of isoprene, *Science*, *303*, 1173-1176.
- Claeys, M. W. Wang, A. C. Ion, I. Kourttchev, A. Gelencsér, W. Maenhaut (2004b), Formation of secondary organic aerosols from isoprene and gas-phase oxidation products through reaction with hydrogen peroxide, *Atmos. Environ.*, *38*, 4093-4098.

- Cocker III, D. R., R. C. Flagan, and J. H. Seinfeld (2001), State-of-the-art chamber facility for studying atmospheric aerosol chemistry, *Environ. Sci. Technol.*, *35*, 2594-2601.
- Edney, E. O., T. E. Kleindienst, M. Jaoui, M. Lewandowski, J. H. Offenberg, W. Wang, and M. Claeys (2005), Formation of 2-Methyl Tetrols and 2-Methylglyceric Acid in Secondary Organic Aerosol from Laboratory Irradiated Isoprene/NO_x/SO₂/Air Mixtures and Their Detection in Ambient PM_{2.5} Samples Collected in the Eastern United States, *Atmos. Environ.*, in press.
- Ervens, B., G. Feingold, G. J. Frost, and S. M. Kreidenweis (2003), A modeling study of aqueous production of dicarboxylic acids: 1. Chemical pathways and speciated organic mass production, *J. Geophys. Res.*, *109* (D15205), doi: 10.1029/2003JD004387.
- Guenther A. et al. (1995), A global model of natural volatile organic compound emissions, *J. Geophys. Res.*, *100*, 8873-8892.
- Jayne, J. T., D. C. Leard, X. Zhang, P. Davidovits, K. A. Smith, C. E. Kolb, and D. R. Worsnop (2000), Development of an Aerosol Mass Spectrometer for size and composition analysis of submicron particles, *Aerosol Sci. and Technol.*, *33*, 49-70.
- Johnson, D., M. E. Jenkin, K. Wirtz, and M. Martin-Reviejo (2005), Simulating the formation of secondary organic aerosol from the photooxidation of aromatic hydrocarbons, *Environ. Chem.*, *2*, 35-48.
- Kalberer M., et al. (2004), Identification of polymers as major components of atmospheric organic aerosols, *Science*, *303*, 1659-1662.

- Kanakidou, M. et al. (2005), Organic aerosol and global climate modelling: a review, *Atmos. Chem. Phys.*, 5, 1053-1123.
- Keywood, M. D., V. Varutbangkul, R. Bahreini, R. C. Flagan, and J. H. Seinfeld (2004), Secondary organic aerosol formation from the ozonolysis of cycloalkenes and related compounds, *Environ. Sci. Technol.*, 38, 4157-4164.
- Kroll, J. H., and J. H. Seinfeld (2005), Representation of secondary organic aerosol (SOA) laboratory chamber data or the interpretation of mechanisms of particle growth, *Env. Sci. Technol.*, 39, 4159-4165.
- Kroll, J. H., N. L. Ng, S. M. Murphy, V. Varutbangkul, R. C. Flagan, and J. H. Seinfeld (2005), Chamber studies of secondary organic aerosol growth by reactive uptake of simple carbonyl compounds, *J. Geophys. Res.*, submitted.
- Lim, H.-J., A. G. Carlton, and B. J. Turpin (2005), Isoprene forms secondary organic aerosol through cloud processing: Model simulations, *Environ. Sci. Technol.*, 39, 4441-4446.
- Limbeck, A., M. Kulmala, and H. Puxbaum (2003), Secondary organic aerosol formation in the atmosphere via heterogeneous reaction of gaseous isoprene on acidic particles, *Geophys. Res. Lett.*, 30, 1996-1999.
- Matsunaga, S., M. Mochida, and K. Kawamura (2003), Growth of organic aerosols by biogenic semi-volatile carbonyls in the forestal atmosphere, *Atmos. Environ.*, 37, 2045-2050.
- Miyoshi, A., S. Hatakeyama, and N. Washida (1994), OH radical-initiated photooxidation of isoprene: An estimate of global CO production, *J. Geophys. Res.*, 99, 18,779-18,787.

- Pandis, S. N., S. E. Paulson, J. H. Seinfeld, and R. C. Flagan (1991), Aerosol formation in the photooxidation of isoprene and β -pinene, *Atmos. Environ.*, *25A*, 997-1008.
- Paulson, S. E., R. C. Flagan, and J. H. Seinfeld (1992), Atmospheric photooxidation of isoprene, Part I: The hydroxyl radical and ground state atomic oxygen reactions, *Int. J. Chem. Kinet.*, *24*, 79– 101.
- Sprengnether, M., K. L. Demerjian, N. M. Donahue, and J. G. Anderson (2002), Product analysis of the OH oxidation of isoprene and 1,3-butadiene, *J. Geophys. Res.*, *107* (D15), 4268, doi: 10.1029/2001JD000716.
- Trainer, M., E. J. Williams, D. D. Parrish, M. P. Buhr, E. J. Allwine, H. H. Westberg, F. C. Fehsenfeld, and S. C. Liu (1987), Models and observations of the impact of natural hydrocarbons on rural ozone, *Nature*, *329*, 705-707.
- Tuazon, E. C., and R. Atkinson (1990), Product study of the gas-phase reaction of isoprene with the OH radical in the presence of NO_x, *Int. J. Chem. Kinet.*, *22*, 1221– 1236.
- Zhao, J., R. Zhang, E. C. Fortner, and S. W. North, Quantification of hydroxycarbonyls from OH-isoprene reactions (2004), *J. Am. Chem. Soc.*, *126*, 2686-2687.

Table 5. 1. Experimental conditions and results.

Exp. No.	Isoprene (ppb)	Seed volume ($\mu\text{m}^3/\text{cm}^3$) ^a	[NO] ₀ (ppb)	[NO ₂] ₀ (ppb) ^b	[NO _x] _{max} (ppb) ^b	[O ₃] _{max} (ppb)	T (°C) ^c	RH ^c	SOA volume ($\mu\text{m}^3/\text{cm}^3$) ^a	SOA yield ^d
1	500	11.0 ± 0.7	138	124	280	n.m. ^e	20.3	43.9%	30.4 ± 2.0	3.0%
2	250	10.0 ± 0.6	85	147	242	70	20.1	42.4%	11.9 ± 1.2	2.3%
3	100	14.8 ± 0.6	85	136	240	4	19.9	47.3%	4.4 ± 0.8	2.2%
4	50	17.4 ± 1.0	100	98	213	10	20.8	46.6%	0.9 ± 1.6	0.9%
5	25	12.2 ± 0.9	87	102	202	25	20.9	41.1%	0.5 ± 1.3	1.1%
6	175	17.1 ± 1.3	107	120	240	119	20.2	44.2%	5.5 ± 2.1	2.1%
7	375	25.6 ± 0.9	~107 ^f	~120 ^f	239	213	20.5	49.5%	16.3 ± 1.7	1.6%
8	75	17.4 ± 0.8	75	165	255	32	21.9	48.1%	2.3 ± 1.3	1.5%
9	60	13.2 ± 0.7	83	139	249	24	21.2	43.1%	1.5 ± 1.4	1.2%

^a Stated uncertainties (2σ) are from noise in the DMA measurements. ^b May include contribution from HONO. ^c Averaged over the course of the experiment. ^d Assuming a density of 1.4 g/cm³. ^e Not measured. ^f Accurate initial values of NO_x were not obtained for this experiment but are expected to be similar to those of Expt. 6

Figure 5. 1. A typical experiment (no. 6 in Table 5.1), showing [isoprene] (black circles), [O₃] (dark gray lines), [NO] (light gray lines), [NO₂] (black lines), and particle volume increase (black dots) as a function of reaction time. Gaps in the O₃ and NO_x data are a result of switching between chambers.

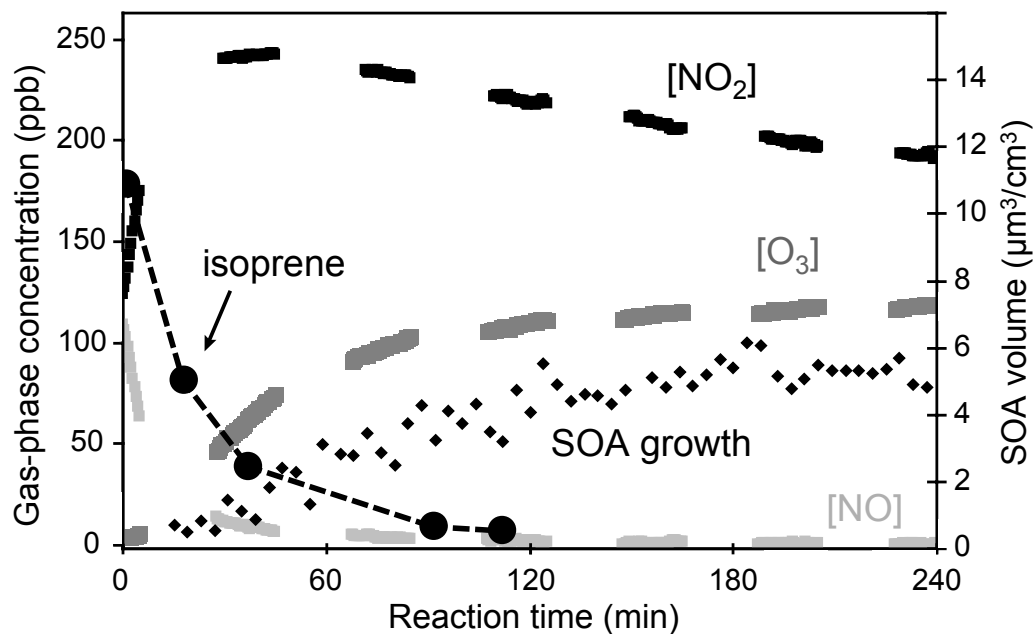
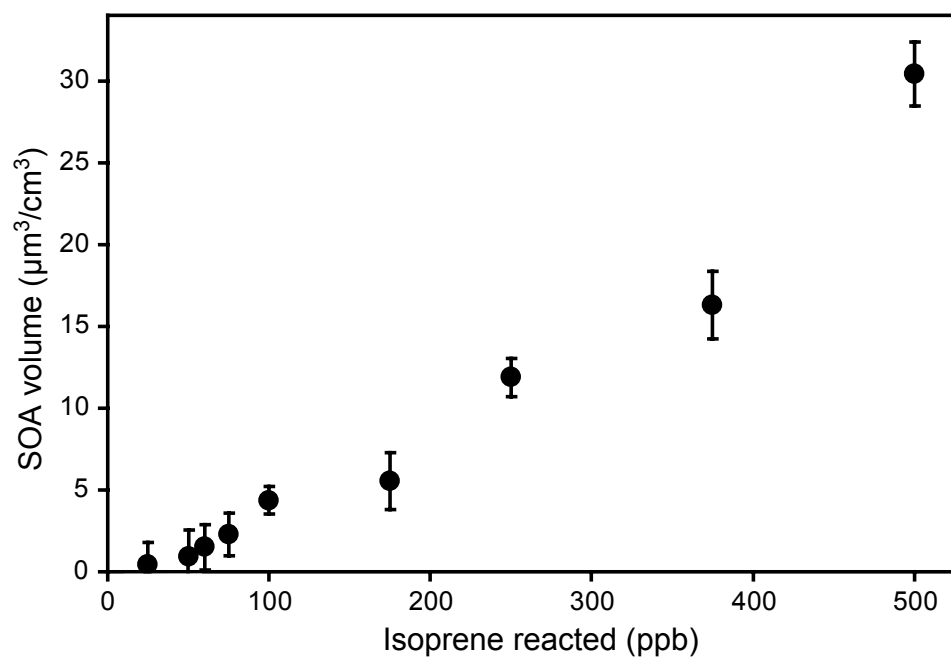


Figure 5. 2. Aerosol growth as a function of concentration of isoprene reacted.



Chapter 6

Secondary Organic Aerosol Formation from Isoprene Photooxidation*

*This chapter is reproduced by permission from “Secondary organic aerosol formation from isoprene photooxidation” by J. H. Kroll, N. L. Ng, S. M. Murphy, R. C. Flagan, J. H. Seinfeld, A. Lee., and A. H. Goldstein, *Environmental Science and Technology*, 40, 1869-1877, 2006. Copyright 2006. American Chemical Society.

6.1 Abstract

Recent work has shown that the atmospheric oxidation of isoprene (2-methyl-1,3-butadiene, C₅H₈) leads to the formation of secondary organic aerosol (SOA). In this study, the mechanism of SOA formation by isoprene photooxidation is comprehensively investigated, by measurements of SOA yields over a range of experimental conditions, namely isoprene and NO_x concentrations. Hydrogen peroxide is used as the radical precursor, constraining the observed gas-phase chemistry substantially: all oxidation is dominated by the OH radical, and organic peroxy radicals (RO₂) react only with HO₂ (formed in the OH + H₂O₂ reaction) or NO, depending on relative concentrations. SOA formation is observed over a wide range of NO_x concentrations, including NO_x-free conditions. At high NO_x, yields are found to decrease substantially with increasing [NO_x], indicating the importance of RO₂ chemistry in SOA formation. Under low-NO_x conditions, SOA mass is observed to decay rapidly, a result of chemical reactions oxidizing semivolatile SOA components, most likely organic hydroperoxides.

6.2 Introduction

As a substantial fraction of tropospheric particulate matter (PM) is composed of organic material, a detailed understanding of the sources and sinks of condensed organic compounds in the atmosphere is necessary to understand the effects of PM on the earth's climate and human health. A major source of uncertainty is the formation of secondary organic aerosol (SOA), particulate matter that is not emitted into the troposphere directly but rather is formed by gas-to-particle conversion of the oxidation products of volatile organic compounds (VOC's). At present, the global formation of SOA is poorly constrained, with estimates from modeling studies ranging from 12-70 Tg/year (1). Such

estimates rely critically on laboratory measurements of the amount of SOA produced by individual SOA precursors, typically carried out in large environmental (“smog”) chambers. From these yield measurements, coupled with atmospheric models, it is now understood that the dominant contributors to global SOA are biogenic hydrocarbons (terpenes and sesquiterpenes), which form SOA primarily by reaction with the hydroxyl radical (OH) and ozone (O₃) (2). Anthropogenic hydrocarbons (most notably aromatic compounds) are also believed to make a minor contribution to SOA on a global scale (3).

The global emission of biogenic terpenes and anthropogenic hydrocarbons is far lower than that of isoprene (2-methyl-1,3-butadiene, C₅H₈), estimated at ~500 Tg/year (4). Despite this large flux, isoprene has generally not been considered to be an SOA precursor, owing to the high volatility of its known reaction products. First-generation reaction products of the OH-isoprene reaction (under high-NO_x conditions) are well-characterized, with a measured carbon balance approaching 100%; structures and yields are shown in Figure 6.1. These products are too volatile to partition appreciably into the aerosol phase, and on this basis, isoprene is not expected to form SOA. Pandis et al. (12) and Edney et al. (13), for example, observed no aerosol growth from the photooxidation of isoprene under high-NO_x conditions.

Recent work suggests that isoprene may contribute to organic aerosol formation via heterogeneous reactions. Claeys and coworkers (14-16) have recently measured tetrols with the same carbon backbone as isoprene (as well as related compounds) in a number of atmospheric samples. Such species are likely to be formed by heterogeneous reactions: formation of tetrols has been observed in the aqueous-phase oxidation of isoprene in the presence of acid and hydrogen peroxide (17), as well as in the gas-phase

photooxidation of isoprene in the presence of NO_x , SO_2 , and ammonium sulfate seed (13). In the latter study only ~6% of the SOA mass observed could be identified (as tetrols and related products), suggesting the formation of other low-volatility compounds. In fact, Limbeck et al. showed (18) that polymeric, humic-like substances are formed when isoprene is passed through filters impregnated with sulfuric acid. Czoschke et al. (19) reported that the (very small) SOA yields from the ozonolysis of isoprene were enhanced in the presence of acidic seed particles, suggesting the polymerization of gas-phase oxidation reaction products as well. Matsunaga et al. (20,21) measured high concentrations of second-generation isoprene oxidation products (hydroxyacetone, methylglyoxal, and glycolaldehyde) in aerosol samples, which may also suggest heterogeneous reactions leading to enhanced uptake. Additionally, modeling studies (22,23) predict that water-soluble isoprene oxidation products will be scavenged by clouds, where they may be oxidized to lower-volatility compounds that remain in the condensed phase after droplet evaporation. Thus, isoprene may contribute to SOA via a number of heterogeneous chemical reactions, involving either polymerization or oxidation of isoprene and its reaction products.

In a recent chamber study (24), we showed that the gas-phase oxidation of isoprene indeed forms SOA. Isoprene oxidation was initiated by the photolysis of nitrous acid (HONO) in the presence of NO_x and ammonium sulfate seed, with SOA (yields of 0.9-3.0%) detected from isoprene concentrations as low as 60 ppb. At smaller concentrations, SOA yields could not be determined, due to loss of particles to the walls, so SOA formation from isoprene oxidation under tropospheric conditions could not be determined. The difference in these results from those of Pandis et al. (12) and Edney et

al. (13) likely arose from lower temperatures (20°C vs. 30°C) and differences in oxidative conditions. SOA was shown to be formed from the oxidation of first-generation reaction products, but details of the underlying chemistry remain unclear. Many factors that may play a role in SOA formation have yet to be examined, such as reactions by different oxidants (OH, O₃ and NO₃), heterogeneous reactions (such as those outlined above), and NO_x concentration.

In the present study we examine SOA formation from isoprene in greater detail, in order to better understand the chemical mechanism of particle growth. The focus of this study is total SOA growth under varying reaction conditions (in particular NO_x and isoprene concentrations); the chemical composition of the SOA is beyond the scope of this work, and will be discussed in detail in a forthcoming paper. In these experiments, hydrogen peroxide (H₂O₂) is used as the radical precursor. H₂O₂ photolysis continually produces OH and HO₂ (from the OH + H₂O₂ reaction) over the course of the experiments, greatly simplifying the gas-phase chemistry. Gas-phase oxidation is dominated by reaction with OH (the primary oxidant of isoprene in the troposphere), with minimal interference by O₃ or NO₃; NO_x can be systematically varied over a wide range of concentrations by addition of NO; and peroxy radical (RO₂) chemistry is relatively straightforward, as any RO₂ formed will react only with HO₂ or NO. Additionally, here we use much lower seed particle loadings than in previous experiments, allowing for the precise measurement of small SOA volumes. From these measurements we are able to better constrain the chemical mechanism of SOA formation from isoprene oxidation, particularly the role of peroxy radicals.

6.3 Experimental

Experiments are carried out in Caltech's dual 28 m³ Teflon chambers, described in detail elsewhere (25,26). The chambers are surrounded by banks of blacklights (276 GE350BL) and aluminum sheets for maximum reflectivity. Numerous ports allow both for the introduction of clean air, gas-phase reagents, and inorganic seed, and for various gas-phase and particulate measurements. A differential mobility analyzer (DMA, TSI 3760) measures the size distribution and hence volume concentration of particles inside the chambers; settings are the same as described in Keywood et al. (26). In most experiments, an Aerodyne Time-of-Flight Aerosol Mass Spectrometer (AMS, described in detail in ref. 27) is also used, for the measurement of mass distributions of particulate organics, sulfate, nitrate, and ammonium. A gas chromatograph coupled with flame ionization detection (GC-FID, HP 5890) allows for the measurement of gas-phase isoprene. GC-FID response is calibrated by sampling from a 60 L Teflon bag into which known volumes of isoprene have been introduced. Temperature, relative humidity (RH), O₃, NO, and NO_x are all continually monitored. Experiments are run in each chamber on alternating days; the chamber that is not in use on a given day is repeatedly flushed with clean air and irradiated with UV light for cleaning.

The radical precursor used in the present experiments is hydrogen peroxide. H₂O₂ is introduced by bubbling 5 L/min of humidified room temperature air for 2 ½ hours through a 50% H₂O₂ solution (Aldrich), through a particle filter to avoid the introduction of droplets, and finally into the chamber. The concentration of H₂O₂ is not measured directly, but from the rate of isoprene decay during irradiation, and literature values of $\sigma_{\text{H}_2\text{O}_2}$, $k_{\text{OH}+\text{isoprene}}$, and $k_{\text{OH}+\text{H}_2\text{O}_2}$ (28,29), [H₂O₂] is estimated to be ~3-5 ppm; this may

decrease somewhat over the course of the experiment due to wall loss, photolysis, and reaction with OH. To minimize potential uptake of H₂O₂ into the particle phase, all experiments are run under dry (RH<10%) conditions. These conditions are substantially drier than those of the troposphere; the dependence of SOA growth on RH is beyond the scope of this work but warrants future investigation.

After introduction of H₂O₂, ammonium sulfate seed (if used) is introduced, by atomization of a 0.015 M solution of (NH₄)₂SO₄ at 30 psi; initial volume concentrations are 4.6-7.1 μm³/cm³. For high-NO_x experiments, a known quantity of NO is then introduced from a 500 ppm gas cylinder (in N₂, Scott Specialty Gases). Typically some fraction (20-40 ppb) is immediately converted to NO₂, likely from reactions with residual O₃ and NO₃/N₂O₅ in the chamber, so the chamber is free of any oxidants when hydrocarbon is added. Isoprene (12-90 ppb) is introduced by sending air over a measured volume of the pure compound (Aldrich, 99.8%) and into the chamber.

When all components are well-mixed (measured values of [isoprene], [NO_x], and seed particle volume are constant), the blacklights are turned on, initiating photooxidation and beginning the experiment. Output from the lights in the ultraviolet is between 300 and 400 nm, with a maximum at 354 nm. The very weak absorption cross section of H₂O₂ in this range necessitates the use of more lights than in our prior study using HONO (24); half the available lights are used in the present experiments. Using measurements of photon flux inside the chamber enclosure, and known absorption cross sections (28), we calculate J_{NO₂} and J_{H₂O₂} to be 0.29 min⁻¹ and 0.00029 min⁻¹, respectively; hence ppm concentrations of H₂O₂ are required. Heating from the lights leads to a temperature increase inside the chamber, approximately 5°C over the course of the experiment. The

DMA and AMS are both located outside the chamber enclosure, so are at the temperature of the surrounding room (~20-22°C). Thus, the air may cool slightly as it is sampled from the chamber and into the instruments, and the measured aerosol is likely to correspond to gas-particle partitioning at the temperature of the room rather than the temperature at which the gas-phase chemistry occurs. Such temperature differences ($\leq 5^\circ\text{C}$) are unlikely to affect results significantly.

6.4 Results

6.4.1 Blank Runs

In order to ensure that all SOA growth observed is indeed from isoprene photooxidation, “blank” runs are performed regularly over the course of the data collection. Minimal growth ($< 0.1 \mu\text{g}/\text{m}^3$) is observed from irradiation of mixtures of H_2O_2 , NO_x , and/or inorganic seed (with no isoprene present). In addition, from the measured SOA yields and mass spectra, the particle growth observed cannot be the result of a small terpene impurity (~0.2%) in the isoprene. These results are described in detail in the Supporting Information.

6.4.2 Low- NO_x experiments

Shown in Figure 6.2 is a typical low- NO_x experiment ($[\text{NO}_x] < 1 \text{ ppb}$), in which 63.6 ppb isoprene is oxidized in the absence of inorganic seed. Particles are detected after ~40 minutes of irradiation; aerosol growth is measured using both the DMA and AMS, and occurs mostly after all the isoprene has been reacted. AMS data confirm that the new particle mass is organic, with a typical mass spectrum shown in Figure 6.3. Ozone formation (not shown in Figure 6.2) of a few ppb is observed, possibly due to

residual NO_x emitted by the chamber walls; such small O_3 concentrations are unlikely to have any appreciable effect on the gas-phase chemistry. After an initial period of aerosol growth, aerosol mass and volume are observed to decrease rapidly to lower final values. This is not a result of loss of particles to the walls, as it is characterized by a shrinking of the aerosol size distribution rather than a decrease in number concentration. The loss of aerosol mass stops immediately when the lights are turned off, and resumes when the lights are turned back on, suggesting it is not caused by gradual changes in temperature or RH. Possible mechanisms are examined in the Discussion section.

Aerosol growth from isoprene photooxidation is also observed at lower isoprene concentrations (and hence smaller organic aerosol loadings). The DMA detects SOA from isoprene concentrations as low as 12.2 ppb; below that, the signal-to-noise is too poor for the detection of growth. Aerosol growth is detected at still lower isoprene concentrations (~ 8 ppb) by the AMS. The mass spectra of the SOA, at maximum growth and at the end of the experiment, are similar to those from the higher-concentration experiments, indicating that SOA formation is indeed significant even at such low isoprene concentrations and particulate loadings.

Experimental conditions and results from all low- NO_x experiments are given in Table 6.1. For all these experiments, no inorganic seed is added: the small size of nucleated particles leads to good signal-to-noise of the DMA volume measurement, so that very small growths ($< 1 \mu\text{m}^3/\text{cm}^3$) can be measured. Measured increases in aerosol volume are found to be largely insensitive to the presence of ammonium sulfate seed. Two values for the increase in aerosol volume are given in Table 6.1: “maximum growth” (before the rapid loss of SOA dominates) and “final growth” (once SOA volume

and mass have leveled out). All volumes are corrected for losses to the chamber walls, by applying size-dependent first-order loss coefficients, estimated by running “seed-only” experiments in the absence of hydrocarbon (26). SOA yield, defined as the ratio of mass concentration of SOA formed to mass concentration of isoprene reacted, is given for the final growth only. This requires knowledge of the SOA density, determined by comparison of aerosol volume (from the DMA) and aerosol mass (from the AMS), as described by Bahreini et al. (30). Density is determined to be $1.25 (\pm 0.1) \text{ g/cm}^3$ for SOA formed under low NO_x conditions. As is typical for SOA-forming reactions, yields are found to vary with the amount of hydrocarbon reacted (31,32); the dependence of aerosol growth (both maximum and final growth) on the amount of isoprene reacted is illustrated in Figure 6.4.

6.4.3 High- NO_x experiments

The addition of NO to the reaction mixture has a large effect on the gas-phase chemistry, as illustrated in Figure 6.5 for a typical experiment (42.7 ppb isoprene, 98 ppb NO, 31 ppb NO_2 , $6.4 \mu\text{m}^3/\text{m}^3$ seed). Isoprene decay is far faster than in the low- NO_x case, due to regeneration of OH from the $\text{HO}_2 + \text{NO}$ reaction. This reaction also rapidly converts NO to NO_2 . Ozone formation, from NO_2 photolysis, begins once [NO] falls below ~ 50 ppb. When [NO] approaches zero (concentrations of a few ppb), aerosol growth is observed. Aerosol mass and volume typically reach a maximum after ~ 4 hours into the reaction; unlike in the low- NO_x case, no rapid loss of SOA is observed.

The mass spectrum of SOA formed from isoprene under typical high- NO_x conditions is shown in Figure 6.6. SOA composition is clearly different from that formed under NO_x -free conditions (Figure 6.3), with mass fragments displaying a more ordered,

repetitive pattern. Aerosol growth is also observed from the oxidation of ~8 ppb isoprene (with 280 ppb NO); the mass spectrum is again the same as that from higher concentrations of isoprene (see Supporting Information).

Measurements of aerosol growth and SOA yield over a range of isoprene concentrations were not carried out for the high-NO_x case, as we have presented such results previously (24). Instead we focus on the dependence of SOA growth on NO_x concentration, in which initial isoprene concentrations are held essentially constant (45 ± 4 ppb). Shown in Table 6.2 are experimental conditions and results for the high-NO_x experiments. Ammonium sulfate seed is used in all cases, to provide surface area onto which semivolatile products may condense. Running the reaction in the absence of seed leads to the formation of large number concentrations (50,000-150,000 particles/cm³) of very small particles, due to the fast rate of formation of condensable products. Such small particles are lost to the walls very quickly, precluding accurate (wall-loss-corrected) volume measurements, so seed particles are necessary. Under high-NO_x conditions, SOA density is determined to be 1.35 (± 0.05) g/cm³. Shown in Figure 6.7 is SOA growth versus initial NO_x concentration. The SOA yields measured in these experiments are somewhat higher than reported in our previous study (24); this may be a result of differences in gas-phase chemistry (such as initial [NO_x], rate of change of [NO_x], and the [NO]:[NO₂] ratio), photolytic conditions, and/or RH. Understanding these possible effects requires further study; we note that in one previous photooxidation study (33), no RH-dependence of SOA yields was observed.

6.4.4 Isoprene oxidation products

Two additional studies are carried out in which methacrolein (500 ppb, Aldrich, 95%) and methyl vinyl ketone (500 ppb, Aldrich, 99%) are photooxidized under high- NO_x conditions (initial $[\text{NO}_x] = 860$ ppb). While the oxidation of methyl vinyl ketone produces no SOA, methacrolein oxidation produces substantial SOA ($170 \pm 1 \mu\text{m}^3/\text{cm}^3$), as reported previously in an experiment using HONO as the radical precursor (24). The AMS spectrum of SOA from methacrolein oxidation is shown in Figure 6.8.

6.5 Discussion

6.5.1 General mechanism of aerosol growth

In both the low- and high- NO_x experiments, SOA growth does not begin until a significant fraction ($>50\%$) of the isoprene is consumed, and SOA growth continues even after the isoprene is fully consumed. This implies the existence of a rate-limiting step in SOA formation following the initial OH-isoprene reaction. As discussed in previous work (24), this step is likely the oxidation of first-generation reaction products: both double bonds of isoprene must be oxidized, resulting in the addition of up to four polar functional groups to the carbon skeleton. This conclusion is strongly supported by the observation of SOA production from the oxidation of methacrolein, a major first-generation isoprene oxidation product. The role of second-generation products in SOA formation (from the oxidation of isoprene and other biogenic hydrocarbons) is discussed in detail by Ng et al. (34).

Shown in Figure 6.9 is the simplified mechanism of the initial steps of the OH + isoprene reaction, leading to the formation of first-generation molecular products. The

hydroxyl radical adds to one of the double bonds, primarily at the 1- or 4-position, and the subsequent addition of O₂ leads to the formation of six possible isoprene hydroperoxy radicals (for simplicity, only one is shown in Figure 6.9). The fate of this radical depends on the level of ambient NO_x. At high NO_x ([NO] >> [HO₂] + [RO₂]), peroxy radicals primarily react with NO. They may also react with NO₂ to form peroxy nitrates (RO₂NO₂), but these are thermally unstable, with lifetimes shorter than 1s, so are generally unimportant under most conditions. Isoprene hydroxyperoxy radicals plus NO forms either hydroxynitrates or hydroxyalkoxy radicals, the latter of which undergo decomposition, isomerization, or hydrogen abstraction by O₂ to form methacrolein, methyl vinyl ketone, and other first-generation isoprene oxidation products shown in Figure 6.1.

As noted previously (24), the rates and products of the oxidation reactions of many of these first-generation products are poorly constrained. The oxidation reactions of methacrolein and methyl vinyl ketone are well-studied, with known products accounting for >90% of the total reaction (35-37). Based on our observation of SOA production from methacrolein oxidation, it is clear that some products of the OH-methacrolein reaction (possibly minor, previously undetected species) are condensable. The similarity between the mass spectrum of SOA from methacrolein oxidation (Figure 6.8) and that of isoprene oxidation (Figure 6.6) strongly suggests that methacrolein is a principal intermediate in SOA formation from isoprene photooxidation under high-NO_x conditions. It is not straightforward to quantify the contribution of methacrolein oxidation products to SOA from isoprene oxidation, due to the dependence of gas-particle partitioning on available organic particulate matter (31, 34). Products of the

oxidation of other first-generation products, accounting for 20-40% of the OH + isoprene reaction, have for the most part not been measured, but may also play a role in SOA formation.

The oxidation of isoprene under low-NO_x conditions has received far less study and so is more uncertain. When concentrations of peroxy radicals (HO₂ and RO₂) approach the concentration of NO, RO₂ + HO₂ and RO₂ + RO₂ reactions become competitive with RO₂ + NO, so a different product distribution is expected (lower half of Figure 6.9). The reaction of isoprene hydroxyperoxy radicals with other RO₂ radicals is expected to lead to a mixture of hydroxycarbonyls, diols, and products from alkoxy radical reactions, such as methacrolein and methyl vinyl ketone, all of which have been detected in the laboratory (7,38-40); yields and hence carbon balance are not fully established. The hydroxyhydroperoxides expected from the reaction of HO₂ with isoprene RO₂ radicals have not been conclusively identified in the laboratory, though have been tentatively identified in the troposphere (41). Miyoshi et al. (7) found that under conditions in which the HO₂ + RO₂ reaction dominates, organic hydroperoxides are formed in high concentrations, with no other identifiable gas-phase products. The further reactions of these oxidation products have not been studied. In particular, the tropospheric fate of isoprene hydroxyhydroperoxides is highly uncertain; the relative importance of photolysis and reaction with OH is largely unknown, as is the product distribution from each channel.

In summary, the lack of experimental data on the second-generation products (and, at low NO_x, even the first generation products) of isoprene oxidation makes it difficult to know the exact chemical mechanism of SOA formation. Under high-NO_x

conditions, methacrolein is certainly an important intermediate in the production of SOA. Numerous pathways may be put forth which lead to the formation of relatively nonvolatile second-generation oxidation products, with 4-5 carbon atoms and 3-4 polar functional (carbonyl, hydroxy, hydroperoxy, nitrate, or acid) groups. Further studies of the gas- and particle-phase products of isoprene oxidation would be useful for identifying the detailed chemistry of SOA formation.

In addition, particle-phase reactions of these products are likely to contribute to SOA formation. From the aerosol mass spectra (Figures 6.3, 6.6, and 6.8), it is clear that oligomers are formed. At both high- and low- NO_x , a significant fraction of the organic mass is from fragments of high molecular weight ($m/z > 200$), corresponding to species with more than five carbon atoms (C5 products will have masses ≤ 226 , the mass of the dihydroxy-dinitrate). An important role of such reactions in SOA formation may explain why methacrolein oxidation forms SOA but methyl vinyl ketone oxidation does not, as aldehydes are substantially more susceptible to nucleophilic attack (and hence oligomerization reactions) than are ketones (42). The chemical composition of the SOA, and oligomer formation in particular, will be discussed in detail in a forthcoming publication.

6.5.2 Role of NO_x

Despite uncertainties in the detailed chemical mechanism of isoprene oxidation, the dependence of SOA growth on NO_x level (Figure 6.7) provides some insight into the underlying chemistry of SOA formation. At high NO_x (> 200 ppb), SOA yield is found to decrease with increasing NO_x ; similar decreases have been observed in a number of SOA yield measurements (12,43-49). This dependence has been attributed to two effects:

(1) relative levels of different oxidants (OH, NO₃, and O₃) present in the reaction system (45), and (2) the chemistry of peroxy radicals (43,46,49). In the present study, OH is the dominant oxidant throughout the course of the experiment, due to the continual production of OH radicals from H₂O₂ photolysis. The O₃ and NO₃ produced in the high-NO_x experiments account for a negligible fraction of the isoprene reacted, as they are only formed once NO concentration is near zero, typically after all isoprene has been reacted away. Isoprene oxidation products may react with O₃ or NO₃, but for major oxidation products such reactions are slow (29) and so are expected to be unimportant. There may, however, be exceptions (for example, 3-methyl-furan reacts rapidly with NO₃ (50)), so we cannot rule out the possibility that reactions of O₃ or NO₃ may be sinks for minor isoprene oxidation products.

Nonetheless, all of the oxidation of isoprene, and the oxidation of most of its reaction products, is initiated by the OH radical, so the observed NO_x dependence of SOA yields is likely a result not of differences in OH, O₃, and NO₃ reactions but of rather differences in peroxy radical chemistry. In the present experiments, organic peroxy radicals will react with either HO₂ (formed in the OH + H₂O₂ reaction) or NO. RO₂ + RO₂ reactions are relatively unimportant, as the concentration of H₂O₂ (which reacts with OH to form HO₂) is much higher than that of isoprene (which reacts with OH to form RO₂), and HO₂ + RO₂ reactions are significantly faster than RO₂ self-reactions (51). As mentioned above, peroxy nitrates formed from RO₂ + NO₂ serves as only as a short-lived reservoir of RO₂. Thus the fate of RO₂ radicals depends on the relative concentrations of HO₂ and NO. At high [NO], alkoxy radicals and organic nitrates will be formed from the RO₂ + NO reaction; small alkoxy radicals are expected to fragment, and organic nitrates

may be relatively volatile (49). On the other hand, at low [NO], $\text{RO}_2 + \text{HO}_2$ reactions form hydroperoxides, recently shown in both experimental (52) and modeling (46,53,54) studies to be important components of SOA. High concentrations of NO therefore appear to suppress the formation of SOA by suppressing hydroperoxide formation, consistent with the conclusions of other studies of the NO_x -dependence of SOA formation (43,46,49). This also explains our observations that SOA growth begins only when NO concentrations approach zero, which appears to be a general feature of chamber measurements of SOA formation from hydrocarbon photooxidation (e.g., 45-47,54). As discussed previously (24), in the studies of Pandis et al. (12) and Edney et al. (13), [NO] did not fall below ~ 30 ppb, so no SOA was produced. Thus the formation of hydroxyhydroperoxides is likely to play an important role in SOA formation from isoprene photooxidation. This is consistent with the results of Miyoshi et al. (7), who report the formation of both gas-phase hydroperoxides and particles from the $\text{OH} +$ isoprene reaction at low NO_x (and high HO_2). In the particle phase, hydroperoxides may react further, oxidizing organics or reacting with aldehydes to form peroxyhemiacetals (55), oligomeric species which may account for some of the high-MW peaks seen in AMS spectra of SOA (Figure 6.6).

However, the suppression of SOA formation by NO does not fully explain the observed NO_x -dependence of aerosol yields from isoprene photooxidation, as yields increase with NO_x at low NO concentrations (Figure 6.7). Similar NO_x -dependences of aerosol yield have been observed in the photooxidation of α - and β -pinene (12,44); however, those experiments were carried out under very different oxidative conditions than in the present study and so may not be directly comparable. The increase in SOA

growth with NO_x may be the result of changes in reaction conditions over the course of the experiments: over time the $[\text{NO}]/[\text{HO}_2]$ ratio decreases (as NO is converted to NO_2 and suppression of HO_2 by NO decreases), which may lead to a switch from high- NO_x to low- NO_x conditions. This could lead to a complex dependence of SOA formation on NO_x : peroxy radicals formed in the first oxidation step ($\text{OH} + \text{isoprene}$) react with NO , whereas peroxy radicals formed by the oxidation of isoprene reaction products react with HO_2 . Such a change in NO_x conditions may be relevant in the troposphere during transport from a polluted to an unpolluted region, but it would be preferable to measure SOA yields under conditions in which the $[\text{NO}]/[\text{HO}_2]$ ratio, and thus the fate of organic peroxy radicals, stays constant over the course of the entire experiment. More generally, in order to apply chamber results to atmospheric conditions, it is important that the $[\text{NO}]/[\text{HO}_2]$ ratio be well-constrained: in our experiments, SOA is suppressed by 100's of ppb of NO , though in the atmosphere this is likely to occur at lower NO concentrations, due to elevated HO_2 concentrations (estimated at 100's of ppt) in the chamber. Thus, reaction conditions need to be better controlled and characterized before parameterizations of SOA yields as a function of $[\text{NO}_x]$ may be obtained.

It should be noted that the NO_x -dependence of SOA growth measured in this work may not apply generally to all SOA-forming reactions. For example, Edney et al. (13) showed that in the presence of SO_2 , isoprene oxidation forms SOA even in the presence of NO , suggesting that enhanced reactive uptake by acidic aerosol particles may counteract the reduced production of condensable species at high NO_x . Additionally, the reaction of NO with large peroxy radicals will form alkoxy radicals which may isomerize rather than fragment, forming large, multifunctional products which may efficiently

partition into the aerosol phase. Thus hydrocarbons substantially larger than isoprene are expected to form SOA even under high-NO_x conditions. Indeed, recently SOA formation from the OH-initiated oxidation of long-chain alkanes has been observed in the presence of several ppm of NO (56). In such cases SOA yields may even be higher at high NO_x. Thus SOA formation may be a complex function of NO_x level, and future study is required.

6.5.3 Rapid photochemical loss of SOA

As noted earlier, under low-NO_x conditions ($[\text{NO}_x] < 1$ ppb), initial SOA growth from isoprene oxidation is large (sometimes reaching yields of >10%), but is followed by a rapid decrease in aerosol volume as the reaction progresses (Figure 6.2). To our knowledge such an effect has not been reported in previous chamber studies of SOA formation. The decrease in SOA, characterized by a shrinking of particles rather than a reduction in particle number, is a photochemical effect, as it occurs only during chamber irradiation (when UV photons and OH radicals are present), ceasing immediately when the chamber lights are turned off. Therefore this may be an example of photochemical “aging”, or oxidative processing, of the SOA. We do not observe rapid loss of SOA formed in the low-NO_x photooxidation of β -pinene (140 ppb), indicating that it is not a general feature of the irradiation of all hydrocarbon/H₂O₂ mixtures.

The photochemical mechanism of volatilization is not at present clear. Recent experimental evidence shows that the reaction of gas-phase OH radicals with condensed organics may lead to efficient volatilization of organic compounds, thereby serving as a sink for SOA in the troposphere (57). However, such a mechanism probably cannot account for the fast rate of SOA loss observed, and we observe no obvious dependence of

rate of SOA loss on surface area, which would be expected for reactions of gas-phase oxidants with condensed-phase organics.

Instead, the SOA loss may be a result of gas-phase or particle-phase oxidation reactions continuing after particle formation. Once semivolatile compounds reach gas-particle equilibrium, any further gas-phase losses (by reaction with OH or photolysis) of those compounds may drive equilibrium away from the particle phase, leading to a decrease in SOA mass. If all losses are from such gas-phase reactions, and these reactions (rather than gas-particle partitioning) are the rate-limiting step, then the SOA loss ($0.006\text{--}0.018\text{ min}^{-1}$) is consistent with reaction with OH ($k_{\text{OH}} = 4.0 \times 10^{-11}\text{--}1.2 \times 10^{-10}\text{ cm}^3\text{ molec}^{-1}\text{ s}^{-1}$ for $[\text{OH}] = 2.5 \times 10^6/\text{cm}^3$), photolysis ($J=0.006\text{--}0.018\text{ min}^{-1}$), or some combination of the two. Given that this effect is seen only at low NO_x , these reactive compounds are likely to be organic hydroperoxides. If loss is by photolysis, the inferred J value is significantly larger (by 1 or 2 orders of magnitude) than that of the simplest organic peroxide, CH_3OOH (29). The efficient photolysis of organic hydroperoxides has been put forth as an explanation for discrepancies between measured rates of tropospheric ozone production and modeled HO_x chemistry (58), as well as for the observation that SOA yields from α -pinene ozonolysis are lower under UV irradiation than under dark conditions (59). In the latter case, the underlying chemistry (and inferred photolytic lifetime) is substantially different than in the present study, but it is clear that the detailed photochemistry of structurally complex organic peroxides deserve further study.

However, gas-phase reaction is unlikely to account for all of the observed loss, as AMS results show that the chemical composition of the SOA changes over the course of the decrease: a number of high-MW organic fragments are observed to increase in

intensity even during the rapid loss of organic aerosol mass. This may be a result of particle-phase reactions, such as the photolysis of condensed-phase hydroperoxides. Such reactions would form OH and alkoxy radicals within the aerosol, which would serve to rapidly oxidize other SOA components; products of such reactions may be quite volatile, leading to loss of SOA mass, or oligomeric and hence highly nonvolatile. In a forthcoming publication, in which we focus on the chemical composition of SOA from isoprene oxidation, the chemistry of this photochemical aging process will be explored in greater detail.

6.6 Acknowledgements

This research was funded by the U. S. Environmental Protection Agency Science to Achieve Results (STAR) Program grant number RD-83107501-0, managed by EPA's Office of Research and Development (ORD), National Center for Environmental Research (NCER), and by U.S. Department of Energy Biological and Environmental Research Program DE-FG03-01ER63099; this work has not been subjected to the EPA's required peer and policy review and therefore does not necessarily reflect the views of the Agency and no official endorsement should be inferred.

6.7 References

- (1) Kanakidou, M.; et al. Organic aerosol and global climate modelling: a review. *Atmos. Chem. Phys.* **2005**, *5*, 1053-1123.
- (2) Chung, S. H.; Seinfeld, J. H. Global distribution and climate forcing of carbonaceous aerosols. *J. Geophys. Res.* **2002**, *107*, 4407, doi10.1029/2001JD001397.

- (3) Tsigaridis, K.; Kanakidou, M. Global modelling of secondary organic aerosol in the troposphere: a sensitivity analysis. *Atmos. Chem. Phys.* **2003**, *3*, 1849-1869.
- (4) Guenther, A.; et al. A global model of natural volatile organic compound emissions. *J. Geophys. Res.* **1995**, *100*, 8873-8892.
- (5) Tuazon, E. C.; Atkinson, R. Product study of the gas-phase reaction of isoprene with the OH radical in the presence of NO_x. *Int. J. Chem. Kinet.* **1990**, *22*, 1221– 1236.
- (6) Paulson, S. E.; Flagan, R. C.; Seinfeld, J. H.. Atmospheric photooxidation of isoprene, Part I: The hydroxyl radical and ground state atomic oxygen reactions. *Int. J. Chem. Kinet.* **1992**, *24*, 79– 101.
- (7) Miyoshi, A.; Hatakeyama, S.; Washida, N. OH radical-initiated photooxidation of isoprene: An estimate of global CO production. *J. Geophys. Res.* **1994**, *99*, 18,779– 18,787.
- (8) Sprengnether, M.; Demerjian, K. L.; Donahue, N. M.; Anderson, J. G. Product analysis of the OH oxidation of isoprene and 1,3-butadiene. *J. Geophys. Res.* **2002**, *107*, D15, 4268, doi: 10.1029/2001JD000716.
- (9) Chen, X.; Hulbert, D.; Shepson, P. B. Measurement of the organic nitrate yield from OH reaction with isoprene. *J. Geophys. Res.* **1998**, *103*, 25,563–25,568.
- (10) Zhao, J.; Zhang, R.; Fortner, E. C.; North, S. W. Quantification of hydroxycarbonyls from OH-isoprene reactions. *J. Am. Chem. Soc.* **2004**, *126*, 2686-2687.
- (11) Baker, J.; Arey, J.; Atkinson, R. Formation and reaction of hydroxycarbonyls from the reaction of OH radicals with 1,3-butadiene and isoprene. *Environ. Sci. Technol.* **2005**, *39*, 4091-4099.

- (12) Pandis, S. N.; Paulson, S. E.; Seinfeld, J. H.; Flagan, R. C. Aerosol formation in the photooxidation of isoprene and β -pinene, *Atmos. Environ.*, **1991** 25A, 997-1008.
- (13) Edney, E. O.; Kleindienst, T. E.; Jaoui, M.; Lewandowski, M.; Offenberg, J. H.; Wang, W.; Claeys, M. Formation of 2-methyl tetrols and 2-methylglyceric acid in secondary organic aerosol from laboratory irradiated isoprene/NO_x/SO₂/air mixtures and their detection in ambient PM_{2.5} samples collected in the eastern United States. *Atmos. Environ.* **2005**, 39, 5281-5289.
- (14) Claeys, M., et al. Formation of secondary organic aerosol through photooxidation of isoprene. *Science* **2004**, 303, 1173-1176.
- (15) Ion, A. C.; Vermeylen, R.; Kourtchev, I.; Cafmeyer, J.; Chi, X.; Gelencsér, A.; Maenhaut, W.; Claeys, M. Polar organic compounds in rural PM_{2.5} aerosols from Kpuszta, Hungary, during a 2003 summer field campaign: sources and diurnal variations. *Atmos. Chem. Phys. Discuss.* **2005**, 5, 1863-1889.
- (16) Kourtchev, I.; Ruuskanen, T.; Maenhaut, W.; Kulmala, M.; Claeys, M. Observation of 2-methyltetrols and related photo-oxidation products of isoprene in boreal forest aerosols from Hyytiälä, Finland. *Atmos. Chem. Phys. Discuss.* **2005**, 5, 2947-2971.
- (17) Claeys, M.; Wang, W.; Ion, A. C.; Kourtchev, I.; Gelencsér, A.; Maenhaut, W. Formation of secondary organic aerosols from isoprene and gas-phase oxidation products through reaction with hydrogen peroxide. *Atmos. Environ.* **2004**, 38, 4093-4098.

- (18) Limbeck, A.; Kulmala, M.; Puxbaum, H. Secondary organic aerosol formation in the atmosphere via heterogeneous reaction of gaseous isoprene on acidic particles. *Geophys. Res. Lett.* **2003**, *30*, 1996-1999.
- (19) Czoschke, N. M.; Jang, M.; Kamens, R. M. Effect of acidic seed on biogenic secondary organic aerosol growth. *Atmos. Environ.* **2003**, *37*, 4287-4299.
- (20) Matsunaga, S.; Mochida, M.; Kawamura, K. Growth of organic aerosols by biogenic semi-volatile carbonyls in the forestal atmosphere. *Atmos. Environ.* **2003**, *37*, 2045-2050.
- (21) Matsunaga, S.; Mochida, M.; Kawamura, K. Variation on the atmospheric concentrations of biogenic compounds and their removal processes in the northern forest at Moshiri, Hokkaido Island in Japan. *J. Geophys. Res.* **2004**, *109*, D04302, doi:10.1029/2003JD004100.
- (22) Ervens, B.; Feingold, G.; Frost, G. J.; Kreidenweis, S. M. A modeling study of aqueous production of dicarboxylic acids: 1. Chemical pathways and speciated organic mass production. *J. Geophys. Res.* **2003**, *109*, D15205, doi: 10.1029/2003JD004387.
- (23) Lim, H.-J., A. G. Carlton, and B. J. Turpin (2005), Isoprene forms secondary organic aerosol through cloud processing: model simulations, *Environ. Sci. Technol.* **2005**, *39*, 4441-4446.
- (24) Kroll, J. H.; Ng, N. L.; Murphy, S. M.; Flagan, R. C.; Seinfeld, J. H. Secondary organic aerosol formation from isoprene photooxidation under high-NO_x conditions. *Geophys. Res. Lett.* **2005**, *32*, L18808, doi:10.1029/2005GL023637.

- (25) Cocker, D. R. III; Flagan, R. C.; Seinfeld, J. H. State-of-the-art chamber facility for studying atmospheric aerosol chemistry. *Environ. Sci. Technol.* **2001**, *35*, 2594-2601.
- (26) Keywood, M. D.; Varutbangkul, V.; Bahreini, R.; Flagan, R. C.; Seinfeld, J. H. Secondary organic aerosol formation from the ozonolysis of cycloalkenes and related compounds. *Environ. Sci. Technol.* **2004**, *38*, 4157-4164.
- (27) Drewnick F.; et al. A new time-of-flight aerosol mass spectrometer (TOF-AMS)—Instrument description and first field deployment. *Aerosol Sci. Technol.* **2005**, *39*, 637-658.
- (28) Atkinson, R.; et al. Evaluated kinetic and photochemical data for atmospheric chemistry: volume 1 – gas phase reactions of O_x, HO_x, NO_x, and SO_x species. *Atmos. Chem. Phys.* **2004**, *4*, 1461-1738.
- (29) Atkinson, R.; et al. Evaluated kinetic and photochemical data for atmospheric chemistry: Supplement VII, Organic species, *J. Phys. Chem. Ref. Data* **1999**, *28*, 191-393.
- (30) Bahreini, R.; Keywood, M. D.; Ng, N. L.; Varutbangkul, V.; Gao, S.; Flagan, R. C.; Seinfeld, J. H. Measurements of secondary organic aerosol (SOA) from oxidation of cycloalkenes, terpenes, and *m*-xylene using an Aerodyne aerosol mass spectrometer. *Environ. Sci. Technol.* **2005**, *39*, 5674-5688.
- (31) Odum J. R.; Hoffmann, T.; Bowman, F.; Collins, D.; Flagan, R. C.; Seinfeld, J. H. Gas/particle partitioning and secondary organic aerosol yields. *Environ. Sci. Technol.* **1996**, *30*, 2580-2585.

- (32) Kroll, J. H.; Seinfeld, J. H. Representation of secondary organic aerosol (SOA) laboratory chamber data or the interpretation of mechanisms of particle growth. *Environ. Sci. Technol.* **2005**, *39*, 4159-4165.
- (33) Cocker, D. R. III; Mader B. T.; Kalberer, M.; Flagan, R. C.; Seinfeld, J. H. The effect of water on gas-particle partitioning of secondary organic aerosol: II. *m*-xylene and 1,3,5-trimethylbenzene photooxidation systems. *Atmos. Environ.* **2001**, *35*, 6073-6085.
- (34) Ng, N. L.; Kroll, J. H.; Keywood, M. D.; Bahreini, R.; Varutbangkul, V.; Flagan, R. C.; Seinfeld, J. H.; Lee, A.; Goldstein, A. H. Contribution of first- versus second-generation products to secondary organic aerosols formed in the oxidation of biogenic hydrocarbons. *Environ. Sci. Technol.* **2006**, submitted.
- (35) Tuazon, E. C.; Atkinson, R. A product study of the gas-phase reaction of methyl vinyl ketone with the OH radical in the presence of NO_x. *Int. J. Chem. Kinet.* **1989**, *21*, 1141– 1152.
- (36) Tuazon, E. C.; Atkinson, R. A product study of the gas-phase reaction of methacrolein with the OH radical in the presence of NO_x. *Int. J. Chem. Kinet.* **1990**, *22*, 591– 602.
- (37) Orlando, J. J.; Tyndall, G. S; Paulson, S. E. Mechanism of the OH-initiated oxidation of methacrolein. *Geophys. Res. Lett.* **1999**, *26*, 2191-2194.
- (38) Ruppert, L.; Becker, K. H. A product study of the OH radical-initiated oxidation of isoprene: formation of C₅-unsaturated diols. *Atmos. Environ.* **2000**, *34*, 1529-1542.

- (39) Benkelberg, H.-J.; Böge, O.; Seuwen, R.; Warneck, P. Product distributions from the OH radical-induced oxidation of but-1-ene, methyl-substituted but-1-enes and isoprene in NO_x-free air. *Phys. Chem. Chem. Phys.* **2000**, *2*, 4029-4039.
- (40) Lee, W.; Baasandorj, M.; Stevens, P. S.; Hites, R. A. Monitoring OH-initiated oxidation kinetics of isoprene and its products using online mass spectrometry. *Environ. Sci. Technol.* **2005**, *39*, 1030-1036.
- (41) Warneke, C., et al. Isoprene and its oxidation products methyl vinyl ketone, methacrolein, and isoprene related peroxides measured online over the tropical rain forest of Surinam in March 1998. *J. Atmos. Chem.* **2001**, *38*, 167-185.
- (42) McMurry, J. *Organic Chemistry*, 4th ed., 1243 pp. Brooks/Cole: Pacific Grove, CA, 1995.
- (43) Hatakeyama, S.; Izumi, K.; Fukuyama, T.; Akimoto, H.; Washida, N. Reactions of OH with α -pinene and β -pinene in air: estimates of global CO production from the atmospheric oxidation of terpenes. *J. Geophys. Res.* **1991**, *96*, D1, 947-958.
- (44) Zhang, S.-H.; Shaw, M.; Seinfeld, J. H.; Flagan, R. C. Photochemical aerosol formation from α -pinene and β -pinene. *J. Geophys. Res.* **1992**, *92*, D18, 20,717-20,729.
- (45) Hurley, M. D.; Sokolov, O.; Wallington, T. J.; Takekawa H.; Karasawa M.; Klotz B.; Barnes I.; Becker, K. H. Organic aerosol formation during the atmospheric degradation of toluene. *Environ. Sci. Technol.* **2001**, *35*, 1358-1366.

- (46) Johnson, D.; Jenkin, M. E.; Wirtz, K.; Martín-Reviejo, M. Simulating the formation of secondary organic aerosol from the photooxidation of toluene. *Environ. Chem.* **2004**, *1*, 150-165.
- (47) Martin-Reviejo, M.; Wirtz, K. Is benzene a precursor for secondary organic aerosol? *Environ. Sci. Technol.* **2005**, *39*, 1045-1054.
- (48) Song, C.; Na, K.; Cocker, D. R. III Impact of the hydrocarbon to NO_x ratio on secondary organic aerosol formation. *Environ. Sci. Technol.* **2005**, *39*, 3143-3149.
- (49) Presto, A. A.; Huff Hartz, K. E.; Donahue, N. M. Secondary organic aerosol production from ozonolysis: 2. Effect of NO_x concentration. *Environ. Sci. Technol.* **2005**, *39*, 7046.
- (50) Alvarado, A.; Atkinson, R.; Arey, J. Kinetics of the gas-phase reactions of NO₃ radicals and O₃ with 3-methylfuran and the OH radical yield from the O₃ reaction. *Int. J. Chem. Kinetics* **1996**, *28*, 905-909.
- (51) Jenkin, M. E.; Boyd, A. A.; Lesclaux, R. Peroxy radical kinetics resulting from the OH-initiated oxidation of 1,3-butadiene, 2,3-dimethyl-1,3-butadiene and isoprene. *J. Atmos. Chem.* **1998**, *29*, 267-298.
- (52) Docherty, K. S.; Wu, W.; Lim, Y. B.; Ziemann, P. J. Contributions of organic peroxides to secondary organic aerosol formed from reactions of monoterpenes with O₃. *Environ. Sci. Technol.* **2005**, *39*, 4049-4059.
- (53) Bonn, B.; von Kuhlmann, R.; Lawrence, M. G. High contribution of biogenic hydroperoxides to secondary organic aerosol formation. *Geophys. Res. Lett.* **2004**, *31* L10108, doi:10.1029/2003GL019172.

- (54) Johnson, D.; Jenkin, M. E.; Wirtz, K.; Martín-Reviejo, M. Simulating the formation of secondary organic aerosol from the photooxidation of aromatic hydrocarbons. *Environ. Chem.* **2005**, *2*, 35-48.
- (55) Tobias, H. J.; Ziemann, P. J. Thermal desorption mass spectrometric analysis of organic aerosol formed from reactions of 1-tetradecene and O₃ in the presence of alcohols and carboxylic acids. *Environ. Sci. Technol.* **2000**, *34*, 2105-2115.
- (56) Lim, Y. B.; Ziemann, P. J. Products and mechanism of secondary organic aerosol formation from reactions of *n*-alkanes with OH radicals in the presence of NO_x. *Environ. Sci. Technol.* **2005**, *39*, 9229-9236.
- (57) Molina, M. J.; Ivanov, A. V.; Trakhtenberg, S.; Molina, L. T. Atmospheric evolution of organic aerosol. *Geophys. Res. Lett.* **2004**, *31*, L22104, doi:10.1029/2004GL020910.
- (58) Thornton, J. A.; et al. Ozone production rates as a function of NO_x abundances and HO_x production rates in the Nashville urban plume. *J. Geophys. Res.* **2002**, *107*, D12, doi:10.1029/2001JD000932.
- (59) Presto, A. A.; Huff Hartz, K. E.; Donahue, N. M. Secondary organic aerosol production from terpene ozonolysis. 1. Effect of UV radiation. *Environ. Sci. Technol.* **2005**, *39*, 7036-7045.

Table 6. 1. Experimental conditions and results for NO_x-free experiments.¹

Expt. No.	Isoprene reacted (ppb)	ΔM_o (max) (μg/m³)²	ΔM_o (final) (μg/m³)²	SOA Yield (%)³	T_{max} (°C)
1	90.0	27.0 ± 0.5	9.3 ± 0.4	3.6 ± 0.1	25.4
2	46.1	13.5 ± 0.6	3.8 ± 0.5	2.9 ± 0.3	25.6
3	23.0	2.3 ± 0.5	0.6 ± 0.3	0.9 ± 0.4	26.0
4	12.2	0.7 ± 0.1	0.3 ± 0.1	1.0 ± 0.3	25.7
5	63.6	17.8 ± 0.5	5.0 ± 0.5	2.8 ± 0.3	26.7
6	29.4	6.2 ± 0.8	2.2 ± 0.5	2.6 ± 0.6	28.7
7	47.8	11.1 ± 0.5	3.0 ± 0.4	2.2 ± 0.3	26.6
8	41.6	8.4 ± 0.4	2.4 ± 0.5	2.1 ± 0.5	26.4

¹ Stated uncertainties (2σ) are from scatter in particle volume measurements. ² Assuming an SOA density of 1.25 g/cm³. ³ SOA yields from final growth only.

Table 6. 2. Experimental conditions and results for high-NO_x experiments.¹

Expt. No.	Isoprene reacted (ppb)	Initial [NO] (ppb)	Initial [NO _x] (ppb)	(NH ₄) ₂ SO ₄ volume (μm ³ /cm ³)	Maximum [O ₃] (ppb)	ΔM ₀ (μg/m ³) ²	SOA Yield (%)	T _{max} (°C)
9	46.7	242	266	4.6 ± 0.2	342	6.3 ± 1.0	4.7 ± 0.7	28.3
10	43.5	496	526	7.1 ± 0.3	389	2.9 ± 1.2	2.3 ± 0.9	28.3
11	42.7	98	129	6.4 ± 0.7	245	6.7 ± 1.3	5.5 ± 1.0	28.1
12	49.1	51	78	6.5 ± 0.3	256	5.6 ± 1.3	4.0 ± 0.9	28.2
13	42.7	337	405	4.8 ± 0.2	508	4.6 ± 1.0	3.8 ± 0.8	28.3
14	42.0	708	745	4.7 ± 0.3	492	1.7 ± 1.1	1.4 ± 0.9	27.5

¹ Stated uncertainties (2σ) are from scatter in particle volume measurements. ² Assuming an SOA density of 1.35 g/cm³.

Figure 6. 1. Structures and measured yields of first-generation products of the OH-initiated oxidation of isoprene under high-NO_x conditions. ^aTuazon and Atkinson (5). ^bPaulson et al. (6). ^cMiyoshi et al. (7). ^dSprenghether et al. (8). ^eChen et al. (9). ^fZhao et al. (10). ^gBaker et al. (11).

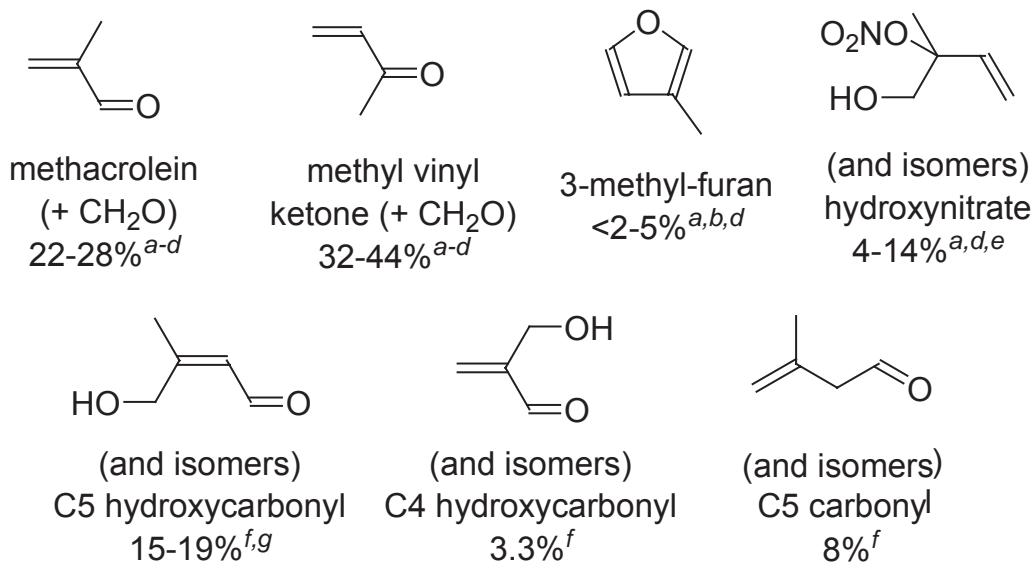


Figure 6. 2. Reaction profile of a typical isoprene photooxidation experiment under NO_x -free conditions (Experiment 5).

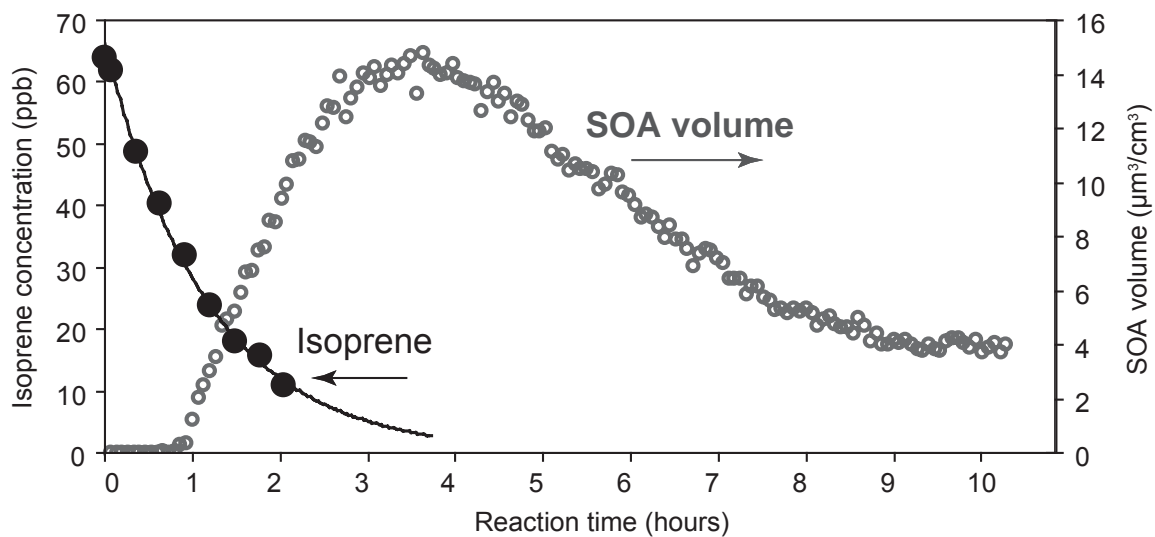


Figure 6. 3. Typical AMS spectrum ($m/z \geq 40$) of SOA formed from isoprene photooxidation under low- NO_x conditions. For clarity, masses in which the organics overlap with peaks from sulfate (m/z 48-50, 64-66, 80-83, 98-100) and tungsten (from the filament; m/z 182, 184-186) have been omitted. Light gray bars correspond to negative values after data analysis.

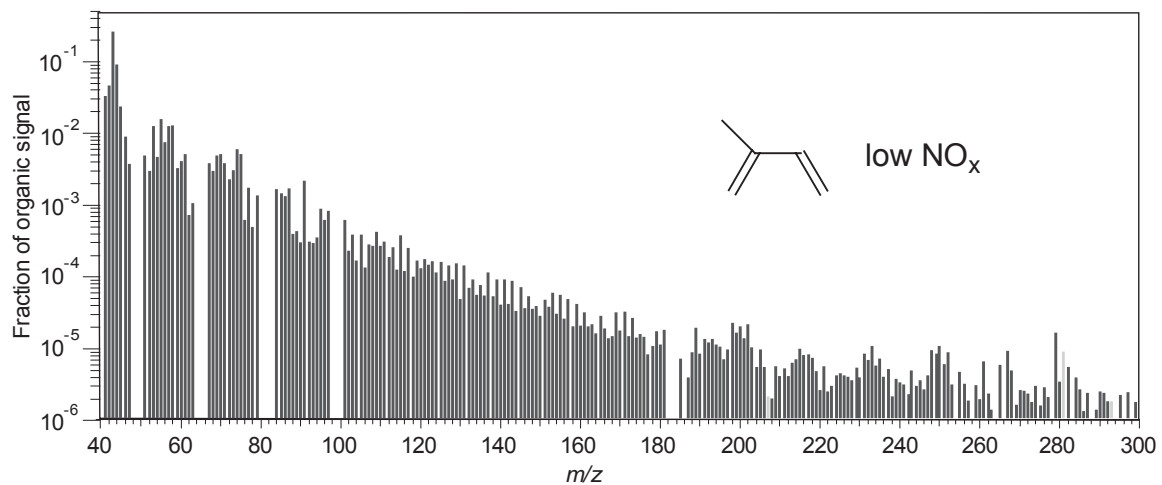


Figure 6. 4. Measured SOA growth versus isoprene reacted (low-NO_x conditions). Gray circles: maximum growth; black circles: final growth, after photochemical loss of SOA (see text for details). Each pair of points (at a single value of isoprene reacted) corresponds to one experiment. Data are taken from Table 6.1; SOA mass is calculated using a density of 1.25 g/cm³.

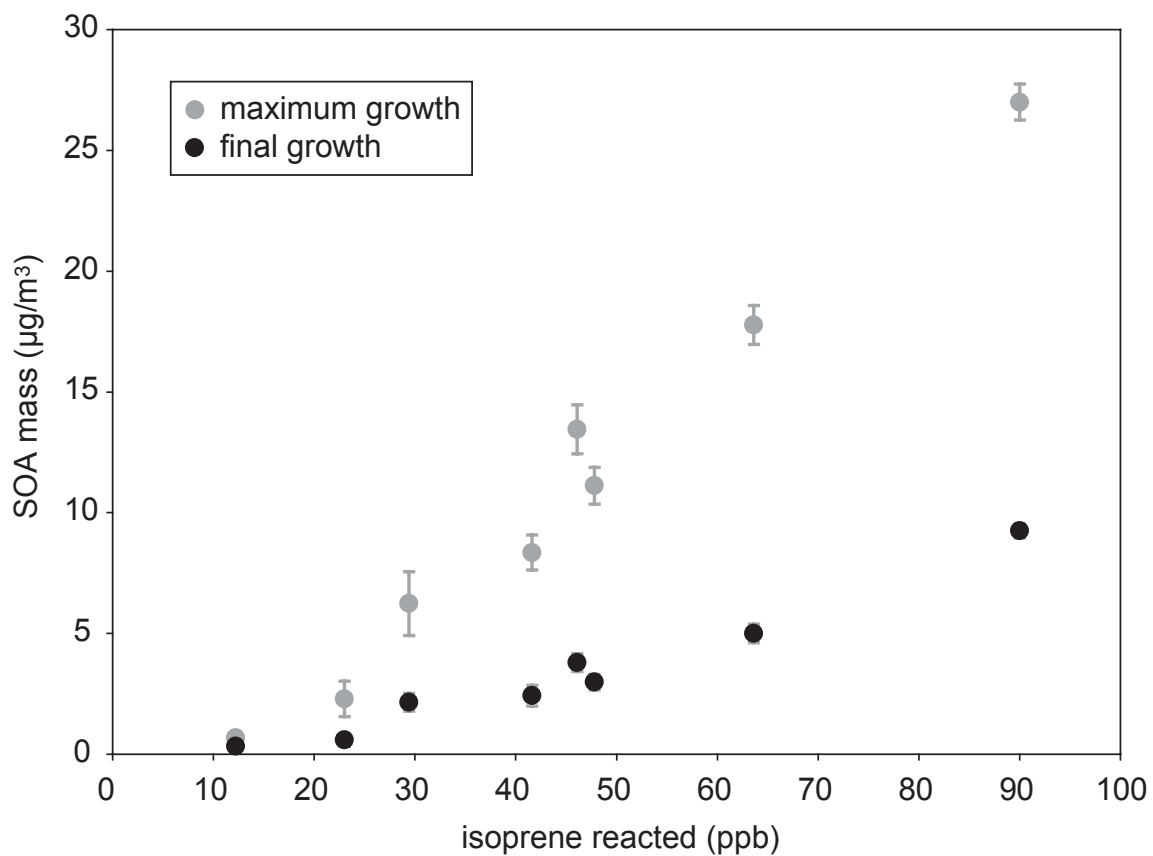


Figure 6. 5. Reaction profile of a typical isoprene photooxidation experiment under high- NO_x conditions (Experiment 11). Decay of isoprene is rapid, with most consumed in the first 30 minutes of reaction, so is omitted for clarity.

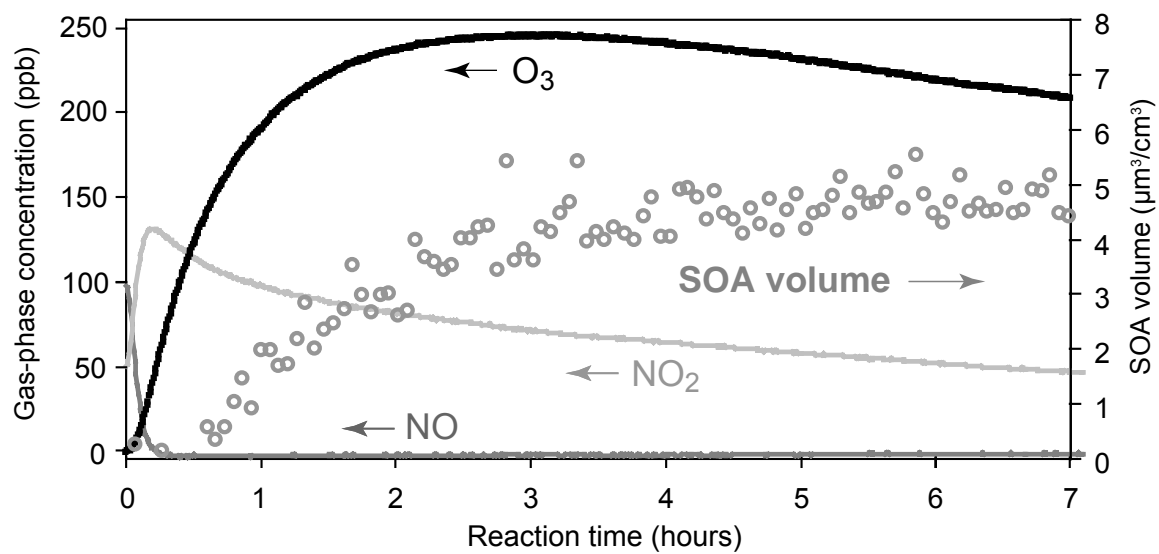


Figure 6. 6. Typical AMS spectrum of SOA formed from isoprene photooxidation under high- NO_x conditions. See description of Figure 6.3 for details.

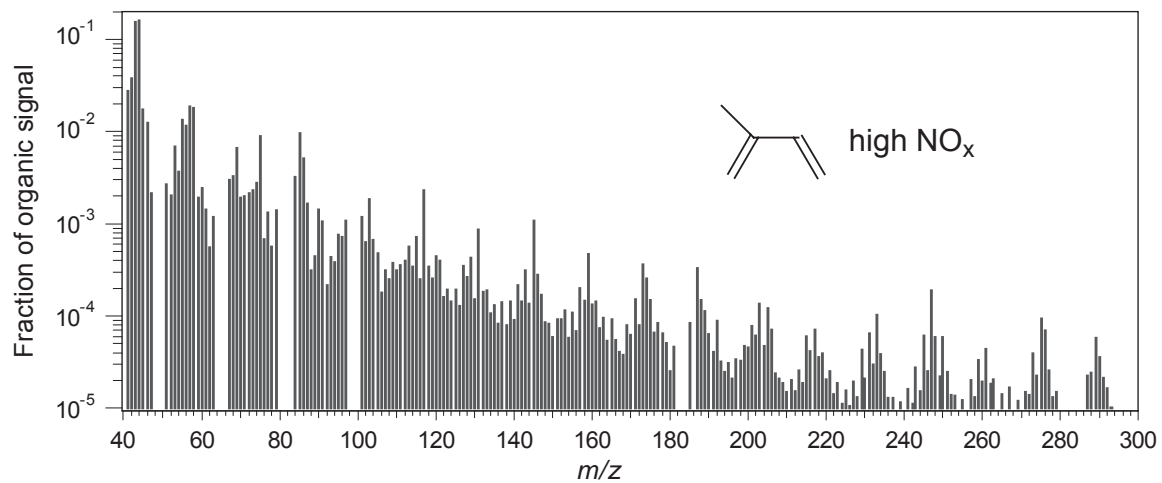


Figure 6. 7. SOA growth as a function of initial NO_x concentration, for a fixed isoprene concentration (45 ± 4 ppb). Results shown are from Table 6.2; the NO_x -free point is final growth from Experiment 2, Table 6.1.

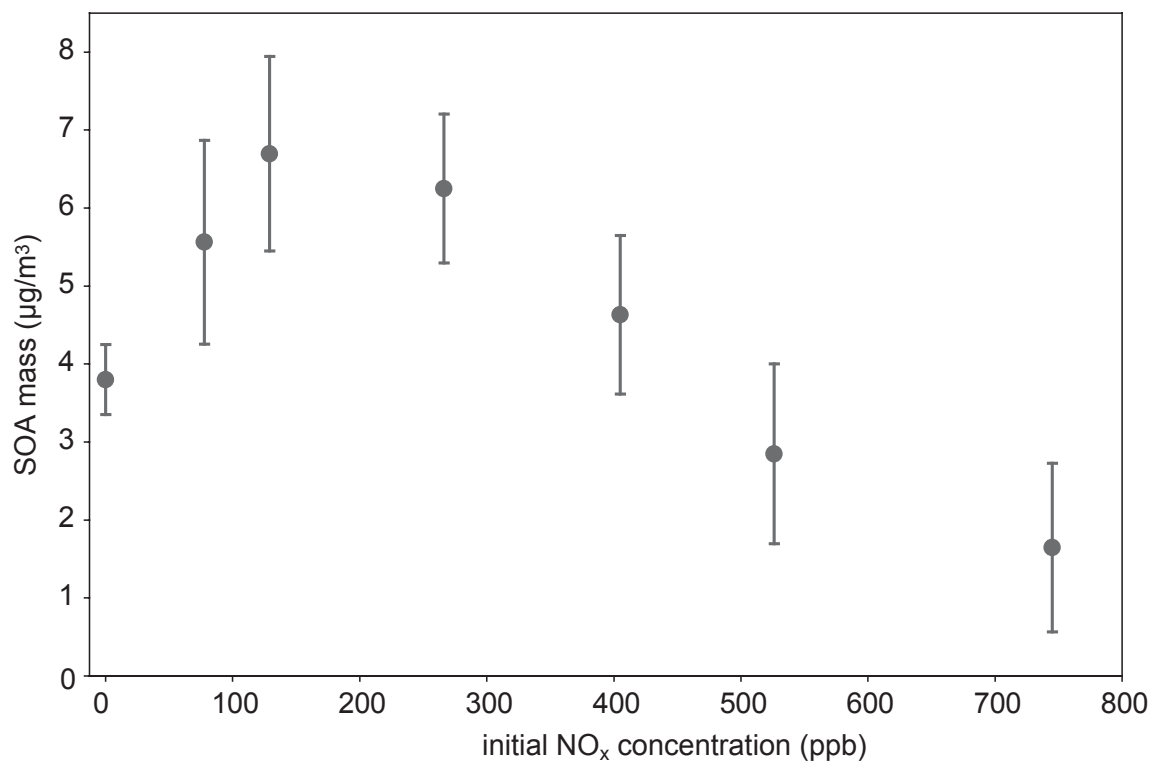


Figure 6. 8. AMS spectrum of SOA formed from methacrolein photooxidation under high- NO_x conditions. See description of Figure 6.3 for details. The spectrum shown is similar to that of isoprene photooxidation (Figure 6.6), with the same major peaks, suggesting the importance of methacrolein as an intermediate in SOA formation from isoprene oxidation under high- NO_x conditions.

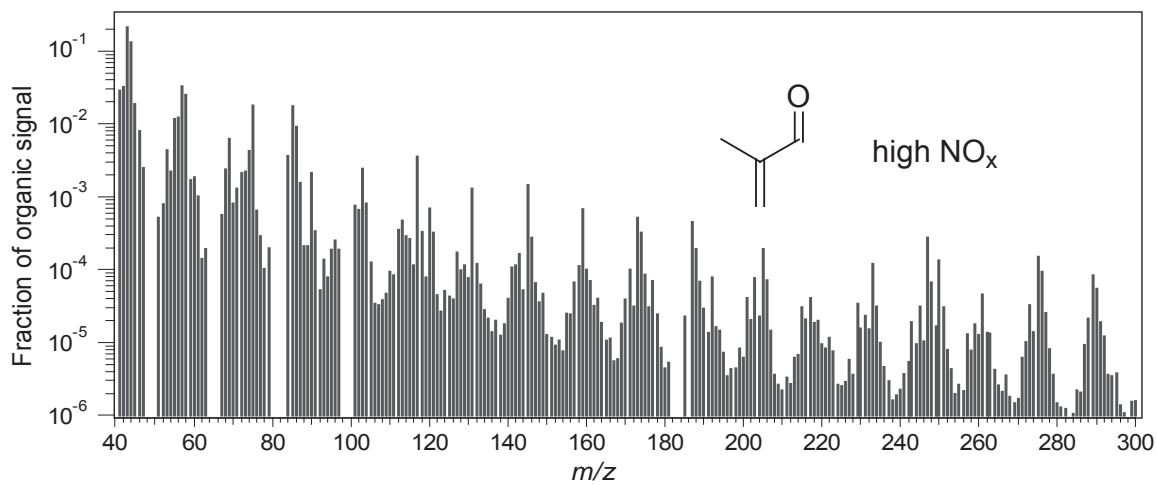
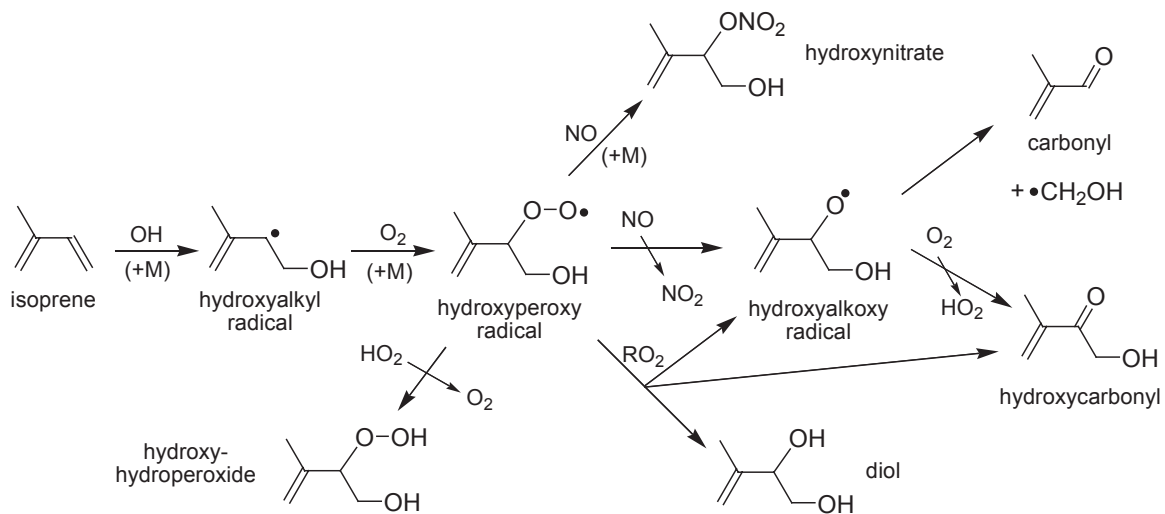


Figure 6. 9. Reaction mechanism of isoprene oxidation, showing the formation of first-generation products. For clarity, only one of four possible alkyl radicals and one of six possible hydroperoxy radicals are shown. The first-generation reaction products are all unsaturated so may be rapidly oxidized to second-generation products.



Chapter 7

Effect of NO_x on Secondary Organic Aerosol (SOA) Formation from Photooxidation of Terpenes*

*This chapter is prepared for journal submission as “Effect of NO_x on secondary organic aerosol (SOA) formation from photooxidation of terpenes” by N. L. Ng, P. S. Chhabra, A. W. H. Chan, J. D. Surratt, J. H. Kroll, A. J. Kwan, D. C. McCabe, P. O. Wennberg, A. Sorooshian, S. M. Murphy, N. F. Dalleska, R. C. Flagan, and J. H. Seinfeld.

7.1 Abstract

Secondary organic aerosol (SOA) formation from the photooxidation of one monoterpene (α -pinene) and two sesquiterpenes (longifolene and aromadendrene) is investigated in the Caltech environmental chambers. By performing photooxidation experiments under varying NO_x conditions, the effect of NO_x on SOA formation for these biogenic hydrocarbons is evaluated. The NO_x dependence of α -pinene SOA formation follows the same trend as that of isoprene (Kroll et al., 2006), in which SOA yield (defined as the ratio of the mass of organic aerosol formed to the mass of parent hydrocarbon reacted) decreases as NO_x level increases. The NO_x dependence of SOA yield for the sesquiterpenes, longifolene and aromadendrene, however, differs from that determined for isoprene and α -pinene; the aerosol yield under high- NO_x conditions substantially exceeds that under low- NO_x conditions. The reversal of the NO_x dependence of SOA formation for the sesquiterpenes is consistent with formation of relatively nonvolatile organic nitrates, and/or the isomerization of large alkoxy radicals that leads to less volatile products. Analysis of the aerosol chemical composition for longifolene confirms the presence of organic nitrates under high- NO_x conditions. Consequently the formation of SOA from certain biogenic hydrocarbons such as sesquiterpenes may be more efficient in polluted air.

7.2 Introduction

Atmospheric oxidation of certain volatile organic compounds (VOCs) leads to the formation of low volatility species that partition into the condensed phase and form secondary organic aerosol (SOA). Biogenic hydrocarbons, such as isoprene (C_5H_8), monoterpenes ($\text{C}_{10}\text{H}_{16}$), and sesquiterpenes ($\text{C}_{15}\text{H}_{24}$), are important contributors to the

total atmospheric burden of SOA owing to their large global emissions and high reactivity with hydroxyl radicals (OH), ozone (O₃), and nitrate radicals (NO₃) (Guenther et al., 1995; Griffin et al., 1999a; Geron et al., 2000; Owen et al., 2001; Atkinson and Arey, 2003; Seinfeld and Pankow, 2003; Kanakidou et al., 2005).

Over the last two decades, numerous laboratory chamber experiments have been conducted to study aerosol formation from biogenic hydrocarbons. The NO_x level has been found to be highly influential in SOA production for a variety of compounds. Recent studies on isoprene photooxidation, α -pinene ozonolysis, limonene ozonolysis, and benzene, toluene, and *m*-xylene photooxidation have demonstrated that a larger aerosol yield is observed under low-NO_x conditions (Kroll et al., 2005, 2006; Presto et al., 2005; Zhang et al., 2006; Ng et al., 2007). Competitive chemistry of peroxy radicals between NO and HO₂, with the HO₂ reaction route producing products of lower volatility, seems consistent with these observations (Hatakeyama et al., 1991; Johnson et al., 2004, 2005; Kroll et al., 2005, 2006; Presto et al., 2005; Ng et al., 2007). For example, in α -pinene ozonolysis Presto et al. (2005) observed relatively volatile organic nitrates under high-NO_x conditions, while less volatile products, such as 10-hydroxypinonic acid, were more abundant under low-NO_x conditions. Although the increase in SOA yield at low-NO_x conditions has now been well-established for isoprene, α -pinene, limonene, and benzene, toluene, and *m*-xylene, a key question is – do larger molecules, especially the sesquiterpenes, exhibit a similar NO_x-dependence of SOA yield?

In the present study, we focus on two sesquiterpenes, longifolene and aromadendrene, and compare the NO_x-dependence of their SOA formation with that of

α -pinene. Longifolene reacts very slowly with ozone (Atkinson and Arey, 2003), making it ideal for study of OH photooxidation. Moreover, both longifolene and aromadendrene have only a single double bond; one can infer more easily the general oxidation mechanisms in SOA formation than when multiple double bonds are present (Ng et al., 2006). Experiments are conducted under limiting NO_x conditions (high-NO_x conditions in which HONO is used as the OH precursor, and low-NO_x conditions in which H₂O₂ is used as the OH precursor), as well as by systematically varying the level of NO_x, using well-established protocols for studying SOA formation.

7.3 Experimental Section

Experiments are performed in Caltech's dual 28 m³ Teflon environmental chambers. Details of the facilities have been given elsewhere (Cocker et al., 2001; Keywood et al., 2004). Before each experiment, the chambers are flushed continuously with dry purified air for ~24 h. Each chamber has a dedicated Differential Mobility Analyzer (DMA, TSI model 3081) coupled with a condensation nucleus counter (TSI model 3760) for measuring aerosol size distribution, number concentration, and volume concentration. All aerosol growth data are corrected for wall loss, in which size-dependent coefficients determined from inert particle wall loss experiments are applied to the aerosol volume data (Keywood et al., 2004). Temperature, relative humidity (RH), O₃, NO, and NO_x are continuously monitored. The initial temperature of the chamber is ~20°C. Heating from the lights leads to a temperature increase of approximately 5°C inside the chamber over the course of the experiment. The analytical instruments are located outside the chamber enclosure and are at the temperature of the surrounding room (~20-22°C). The air may cool slightly as it is sampled from the chamber into the

instruments, and the measured aerosol likely corresponds to the gas-particle partitioning at the temperature of the surrounding room rather than the chamber enclosure. Such small temperature difference is unlikely to affect the results significantly.

Seed particles are introduced into the chamber to act as a substrate onto which the gas-phase semivolatile products may condense. Seed aerosols are generated from a 0.015M aqueous ammonium sulfate solution with a constant-rate atomizer, producing initial particle number concentrations of about 25,000 particles cm^{-3} , with a geometric mean diameter of about 50 nm, and initial aerosol seed volume of $\sim 10\text{-}15 \mu\text{m}^3 \text{cm}^{-3}$. After introduction of the seed aerosol, a known volume of the parent hydrocarbon is injected into a glass bulb, and then introduced into the chambers by an air stream. For experiments with α -pinene and longifolene, the concentration (mixing ratio) of the parent hydrocarbon is monitored with a Hewlett Packard gas chromatograph (model 5890) with flame ionization detection (GC-FID). Owing to the difficulties in measuring aromadendrene with GC-FID, its concentration is measured with a Proton Transfer Reaction Mass Spectrometer (PTR-MS), a custom-modified Varian 1200 system (see the Appendix). Under typical chamber conditions aromadendrene concentrations are measured with an uncertainty of about $\pm 22\%$.

In the high- NO_x experiments nitrous acid (HONO) serves as the OH precursor. It is introduced into the chamber after injection of the seed aerosol and parent hydrocarbon. HONO is prepared by dropwise addition of 15 mL of 1% NaNO_2 into 30 mL of 10% H_2SO_4 in a glass bulb. The bulb is then attached to the chamber and a stream of dry air is passed through the bulb into the chamber. NO and NO_2 , formed as side products in the preparation of HONO, are also introduced into the chamber, and are measured by a

commercial NO_x monitor (Horiba APNA-360, Irvine, CA). Additional NO from a 500 ppm gas cylinder (Scott Marrin, Inc.) is introduced into the chamber after the addition of HONO to achieve a target NO_x level in the chamber of about 1 ppm (upper detection limit of the NO_x monitor).

For low-NO_x experiments, H₂O₂ serves as the OH precursor. The background NO_x level in the chamber during such experiment is ≤ 2 ppb. About 3 ppm H₂O₂ is introduced into the chamber (prior to introduction of seed particles and parent hydrocarbon) by bubbling air through a 50% H₂O₂ solution for 2.5 h at 5 L/min. The air stream then passes through a particle filter to remove any droplets. Variable NO experiments are also carried out, in which a known quantity of NO is introduced into the chamber after the addition of H₂O₂.

Once the seed, parent hydrocarbon, and NO_x concentrations stabilize, reaction is initiated by irradiating the chamber with blacklights. Output from the lights is between 300 and 400 nm, with a maximum at 354 nm. Half of the available black lights are used in the experiments. At these wavelengths HONO efficiently photolyzes to OH and NO. By contrast, H₂O₂ absorbs only weakly in this wavelength range, requiring the use of ppm mixing ratios of H₂O₂ to achieve target levels of OH.

A comprehensive range of measurements are employed to study the chemical composition of the SOA formed. Real-time particle mass spectra are obtained with an Aerodyne quadrupole Aerosol Mass Spectrometer (Q-AMS) (Jayne et al., 2000; Bahreini et al., 2005). A Particle-Into-Liquid Sampler (PILS, Brechtel Manufacturing, Inc.) is employed for quantitative measurements of water-soluble ions in the aerosol phase (Sorooshian et al., 2006). For offline chemical analysis, Teflon filters (PALL Life

Sciences, 47-mm diameter, 1.0- μm pore size, teflo membrane) are collected at the point when aerosol volume reaches its maximum value. Depending on the total chamber volume concentration of aerosol, the filter sampling time is 2-4 h, which results in $\sim 1.5\text{-}6\text{ m}^3$ of total chamber air sampled. Teflon filter extraction protocols in HPLC-grade methanol have been described previously (Surratt et al., 2006). The resultant filter extracts are then analyzed by the following suite of analytical techniques: high performance liquid chromatography/electrospray ionization-quadrupole mass spectrometry (HPLC/ESI-MS), electrospray ionization-ion trap mass spectrometry (ESI-ITMS), and matrix-assisted laser desorption ionization-time-of-flight mass spectrometry (MALDI-TOFMS); details of the protocols are described elsewhere (Surratt et al., 2006).

In addition to the above analytical techniques, filter extracts (in 1:1 (v/v) solvent mixture of methanol and 0.1% aqueous acetic acid solution) are also analyzed by a Waters ACQUITY ultra performance liquid chromatography (UPLC) system, coupled with a Waters LCT Premier time-of-flight (TOF) mass spectrometer (MS) equipped with an electrospray ionization (ESI) source. The ESI source on this instrument contains two individual sprays; one spray is for the eluent and the other is for the lock-mass correction. Optimum ESI conditions are found using a 2.5 kV capillary voltage, 40 V sample cone voltage, 350°C desolvation temperature, 130°C source temperature, 20 L hr⁻¹ cone gas flow rate, and a 650 L hr⁻¹ desolvation gas flow rate. Data are collected from m/z 50-1000 in the negative (-) ionization mode using the TOFMS operated in the W geometry reflectron mode. The W reflectron mode offers the highest mass resolution, which is approximately 12000, and allows for exact mass measurements to be conducted on detected SOA components. The chromatographic separations are carried out on a Waters

ACQUITY HPLC HSS (high strength Silica) column (2.1 x 100 mm, 1.8 μm particle size) at 45°C using a gradient elution scheme. The eluent composition is (A) 0.1% acetic acid in water and (B) 0.1% acetic acid in methanol; both eluents are high purity solvents (LC-MS ChromaSolv Grade, Sigma-Aldrich). In the 12-min gradient elution program used, the concentration of eluent B is 0% for the first 2 min, increased to 90% from 2 to 10 min, held at 90% from 10 to 10.2 min; and then decreased back to 0% from 10.2 to 12 min. The flow rate of the eluent is 0.3 mL min⁻¹ and the sample injection volume is 2 μL . At the beginning of each analysis period, the TOFMS is calibrated using a 1:1 (v/v) solvent mixture of acetonitrile and 0.1% phosphoric acid aqueous solution. During each chromatographic run, 2 ng/ μL of leucine enkephalin (MW = 555) is used for the lock-mass spray for lock-mass correction to obtain accurate masses for each SOA component eluting from the column. The lock-mass syringe pump is operated at 20 $\mu\text{L min}^{-1}$. In addition to the lock-mass spray, the dynamic range enhancement feature of this mass spectrometer is applied to prevent dead time, which affects mass accuracy, from occurring. As confirmation of the UPLC/ESI-TOFMS technique, a standard sample containing known isoprene and α -pinene sulfate esters previously characterized by Surratt et al. (2007) are analyzed. The known elemental compositions (i.e. molecular formulas) of the previously characterized sulfate esters (Surratt et al., 2007) are in excellent agreement with their measured exact masses (i.e. within ± 2 mDa or ± 2 ppm). In addition to exact mass measurements, further insights into the structures of the SOA components is obtained by generating tandem MS data, which are generated by increasing the first aperture voltage on the TOFMS from 10 V to 25 V.

The parent aromatics studied (shown in Table 7.1) and their stated purities are as follows: α -pinene (Aldrich, 99+%), longifolene (Aldrich, >99%), and aromadendrene (Aldrich, >97%). Experimental conditions and results for each of the parent hydrocarbons studied are given in Tables 7.2, 7.3, and 7.4. In calculating SOA yield, knowledge of the SOA density is required. By comparing volume distributions from the DMA and mass distributions from the Q-AMS, effective densities for the SOA formed can be estimated (Bahreini et al., 2005, Alfarra et al., 2006). The estimated densities of the SOA formed from different parent hydrocarbons are given in Table 7.5.

7.4 Aerosol Yields

7.4.1 α -pinene photooxidation

Under high-NO_x conditions, the efficient photolysis of HONO generates relatively high concentrations of OH ($\sim 2 \times 10^7$ molecules cm⁻³ initially), leading to rapid α -pinene decay. Aerosol growth occurs essentially immediately even when [NO] is high (100's of ppb). With the high NO concentration throughout the entire experiment, formation of ozone (and also NO₃) is suppressed.

Under low-NO_x conditions, aerosol growth is also observed immediately after initiation of irradiation. The α -pinene decays at a slower rate than under high-NO_x conditions, owing to the relatively slow production of OH radicals by H₂O₂ photolysis. Ozone formation is observed at an increasing concentration over time (~ 30 ppb at the peak of aerosol growth). Based on the reaction rate constants of α -pinene + O₃ (k_{ozone}) and α -pinene + OH (k_{OH}), and an inferred OH concentration of 3×10^6 molecules cm⁻³, it is estimated that an ozone source of ~ 0.1 ppb/min would be required to produce the

observed α -pinene decay. It is estimated that only about 35% of the α -pinene reacts by ozonolysis at the point of maximum growth. Therefore, while α -pinene ozonolysis accounts for some of the SOA yield under low- NO_x conditions, it is highly unlikely that the observed yield difference between high- and low- NO_x arises solely from the presence of ozone.

Figure 1 shows the time-dependent growth curves (organic aerosol generated, denoted as ΔM_o , as a function of hydrocarbon reacted ΔHC) for α -pinene under different NO_x conditions. As hydrocarbon measurements are made with a lower frequency than those of particle volume, the α -pinene concentrations shown are obtained by interpolating the GC measurements. In all cases, the initial mixing ratio of α -pinene was about 15 ppb, all of which was consumed by the end of the experiment. It is clear that the aerosol growth under low- NO_x (H_2O_2) conditions substantially exceeds that under high- NO_x (HONO) conditions, while the intermediate NO_x (" $\text{H}_2\text{O}_2 + \text{NO}$ ") experiment exhibits an aerosol yield between those of the two extremes. The time-dependent growth curve of the " $\text{H}_2\text{O}_2 + \text{NO}$ " experiment exhibits a vertical section at the end, indicating that further reactions are contributing to aerosol growth after the α -pinene is consumed. We return to this observation in Section 7.6.2.2.

7.4.2 Longifolene photooxidation

For longifolene, a series of high- NO_x (HONO) experiments and low- NO_x (H_2O_2) experiments with varying initial hydrocarbon concentrations were carried out. The time-dependent growth curves for 3 high- NO_x and 3 low- NO_x experiments, with initial longifolene mixing ratios ranging from ~ 10 to 30 ppb, are shown in Fig. 2. In contrast to α -pinene photooxidation, longifolene aerosol yields under high- NO_x conditions exceed

those under low-NO_x conditions. Under high-NO_x conditions, the maximum SOA yield (about ~100-130%; note that yield is defined on a mass basis) is reached in ~10 min after initiation of the experiments, with the yield decreasing after that point. Under low-NO_x conditions, SOA yield continues to increase over the course of the experiment, reaching a maximum when all the longifolene is consumed. The final SOA yields of each longifolene low-NO_x experiment actually lie on a straight line that passes through the origin, indicating that under low-NO_x conditions SOA yield is constant, at ~75%. Based on the observed longifolene decay and k_{OH} for longifolene, the chamber OH concentration under low-NO_x conditions is estimated to be $\sim 3 \times 10^6$ molecules cm⁻³.

The effect of NO_x on longifolene aerosol formation is further illustrated by the time-dependent growth curves in Fig. 3. In both experiments H₂O₂ is used as the OH precursor and the initial longifolene mixing ratio is ~4.3 ppb, with only the amount of NO differing; in one experiment no extra NO is added, while in the other experiment about 300 ppb of NO is introduced into the chamber after the addition of H₂O₂. Aerosol growth in the presence of ~300 ppb NO is substantially higher. A series of experiments with the same initial longifolene concentration but different initial NO concentrations (~100-600 ppb) are also carried out. Figure 4 shows the final aerosol yield as a function of the initial NO_x concentration. The amount of aerosol formed is highly dependent on the level of NO_x present initially; with ~600 ppb NO, the ultimate aerosol yield is twice that at low-NO_x conditions.

7.4.3 Aromadendrene photooxidation

Figure 5 shows the final aerosol yield as a function of initial NO_x concentration for aromadendrene photooxidation. The OH precursor used in these experiments is H₂O₂

and the initial aromadendrene mixing ratio is ~ 5 ppb. In these experiments the concentration of aromadendrene is monitored with the PTR-MS with an uncertainty of about $\pm 22\%$. Despite uncertainties in the aromadendrene measurements, it is clear that aromadendrene aerosol yield increases with NO_x concentration; similarly to longifolene, with ~ 500 ppb NO, the aerosol yield is doubled over that at low- NO_x conditions.

7.5 Chemical composition of SOA

In this section, the chemical composition of α -pinene and longifolene SOA are presented. The aromadendrene experiments are performed mainly to verify the observed NO_x dependence for longifolene, in which SOA yield is higher under high- NO_x conditions. Thus, detailed analysis of the chemical composition of aromadendrene SOA is not pursued.

7.5.1 Aerosol Mass Spectrometer (Q-AMS) measurements

Figures 6 and 7 show the AMS high- NO_x versus low- NO_x spectrum signal for α -pinene and longifolene photooxidation, respectively. Each mass fragment is normalized by the total signal. All spectra have prominent signals at m/z 43 (CH_3CO^+) and m/z 44 (CO_2^+), indicating that the aerosols are highly oxidized and are dominated by carbonyl-containing compounds and multifunctional carboxylic acids. Mass fragment 29 can arise from C_2H_5^+ or CHO^+ , and mass fragment 41 can arise from C_3H_5^+ or C_2HO^+ ; given the highly oxidized nature of the aerosols, they are more likely to be the latter. Though the above mass fragments are prominent in all spectra, the relative contribution of each m/z is different for low- and high- NO_x spectra for both α -pinene and longifolene, suggesting that aerosol compositions are different under different NO_x conditions. The common

feature in the α -pinene and longifolene spectra is that there is a significant contribution from m/z 30 and m/z 46 under high-NO_x conditions for both compounds.

The contribution of m/z 30 and m/z 46 to the total organic mass under different NO_x conditions can be examined more directly by examining $[m/z$ 30 + m/z 46]/[Organic mass] as a function of the total organic mass. As seen in Figs. 8 and 9, for both α -pinene and longifolene, respectively, this ratio is very small under low-NO_x conditions (~2%) and ~15-25% under high-NO_x conditions. The m/z 30 (NO⁺) and m/z 46 (NO₂⁺) signals are commonly associated with nitrate species; the significance of these mass fragments will be discussed further in Section 7.6.1.

Changes in AMS spectra over the course of the experiment for longifolene under high- and low-NO_x conditions are shown in Figs. 10 and 11, respectively, for which the corresponding growth curves appears in Fig. 2 (the pair of experiments with ~30 ppb of longifolene injected). In Figs. 10 and 11, the top panel shows the fractional contribution of each mass fragment to the total organic and nitrate signal during the growth phase of the experiment (Δ H_C~100 μ g m⁻³ in Fig. 2); the bottom panel shows the percentage change of each mass fragment from the growth phase to the point at which all of the hydrocarbon is consumed (Δ H_C~200 μ g m⁻³ in Fig. 2). Under high-NO_x conditions, changes in mass fractions of different fragments during aerosol growth are minimal, indicating that the aerosol composition is not changing significantly over time. Under low-NO_x conditions, however, the mass fraction of m/z 44 increases by 93% as the oxidation progresses, while those for higher m/z 's are observed to decrease. The mass fractions of m/z 44 and higher m/z 's continue to change even after the aerosol growth

levels off, suggesting the presence of further chemistry (either gas-phase or particle-phase) even after all the initial hydrocarbon is consumed.

7.5.2 Offline chemical analysis

All of the ions detected by the UPLC/ESI-TOFMS instrument from α -pinene and longifolene photooxidation under different NO_x conditions are listed in Tables 7.6 and 7.7, respectively. The tables list the exact masses and their likely molecular formulas that corresponding to each of the $[\text{M} - \text{H}]^-$ ions detected, where M is the molecular weight of the compound. The error between the measured mass and theoretical mass is reported in two different ways, ppm and mDa. For most of the ions observed, the error between the measured and theoretical masses is less than ± 2 mDa and ± 5 ppm, which is considered as excellent resolution for small molecules (i.e. compounds less than 1000 Da). Solvent blanks and control filters were also run on the UPLC/ESI-TOFMS instrument; none of the listed ions is observed in either of these control samples, indicating that these ions are not contaminant ions introduced during sample workup. The ions listed in Tables 7.6 and 7.7 are also detected by HPLC/ESI-MS and ESI-ITMS, confirming that these compounds are not the result of artifact formation in a specific mass spectrometer.

Acidic compounds, such as carboxylic acids and sulfate esters, readily ionize under (-)ESI-MS techniques (Gao et al., 2004; Surratt et al., 2006; Surratt et al., 2007). Hydroxylated compounds, as well as ketones and aldehydes, however, are not ionizable unless carboxylic acid and/or sulfate ester moieties are also present within the same molecule. Therefore, it is expected that the UPLC/ESI-TOFMS data are sensitive only to acidic compounds. For the SOA formed in the presence of NO_x , (HONO and “ $\text{H}_2\text{O}_2 + \text{NO}$ ” experiments), even $[\text{M} - \text{H}]^-$ ions are observed in ESI mass spectra, indicating the

compound has an odd number of organic nitrate functional groups, as previously observed in isoprene SOA formed under high-NO_x conditions (both HONO and ‘H₂O₂ + NO’) (Surratt et al. 2006). For α -pinene, only one acidic organic nitrate (m/z 322) is detected in the HONO experiment and none is detected in H₂O₂ and intermediate NO_x experiments. Most of these ions detected in the α -pinene experiments have been identified in previous laboratory work (Glasius et al., 1999; Glasius et al., 2000; Larsen et al., 2001) and field studies (Gao et al., 2006). For longifolene, a much wider array of acidic organic nitrates is detected by the UPLC/ESI-TOFMS instrument in both HONO and ‘H₂O₂ + NO’ experiments.

Figure 12 shows the extracted ion chromatograms (EICs) of m/z 346, 374, and 390 from longifolene oxidation under different NO_x conditions. These m/z values correspond to acidic organic nitrates, as confirmed by the exact mass data (Table 7.7) and by their even $[M - H]^-$ ions. The chromatographic peaks are much larger in the highest NO_x experiment than those in the ‘H₂O₂ + NO’ experiment (except m/z 372); no chromatographic peaks are observed under low-NO_x (H₂O₂) conditions. Besides the detection of more organic nitrates in the highest NO_x experiment, for several $[M - H]^-$ ions (e.g. m/z 374 and 390) there are more structural isomers present. When comparing the chromatographic peaks for the non-organic nitrate species (e.g. m/z 223, 239, 253, 255, 267, 269, and 283), it is found that these peaks are larger under low-NO_x conditions, indicating differing SOA composition in the absence of NO_x.

7.6 Discussion

7.6.1 Effect of hydrocarbon size on NO_x dependence

It has been established that NO_x levels exert a major influence on SOA formation (Hatakeyama et al., 1991; Pandis et al., 1991; Zhang et al., 1992; Hurley et al., 2001; Johnson et al., 2004, 2005; Song et al., 2005; Presto et al., 2005; Kroll et al., 2005, 2006; Zhang et al., 2006; Ng et al., 2007). For photooxidation of isoprene, SOA yields increase as the NO_x level decreases (Kroll et al., 2006). The proposed mechanism for this observed NO_x dependence is the competitive chemistry of organic peroxy radicals between NO and HO₂, in which the semivolatile products formed via the RO₂ + HO₂ path are less volatile than those formed via the RO₂ + NO route (Hatakeyama et al., 1991; Johnson et al., 2004, 2005; Presto et al., 2005; Kroll et al., 2006; Zhang et al., 2006; Ng et al., 2007). A similar yield dependence on NO_x is observed here for photooxidation of α -pinene as for isoprene (Fig. 1). For an initial α -pinene concentration of \sim 15 ppb, the SOA yield under low-NO_x conditions is about a factor of 3 higher than that under high-NO_x conditions. The observed NO_x dependence is consistent with that of previous studies on α -pinene photooxidation (Hatakeyama et al., 1991; Zhang et al., 1992).

The observed NO_x dependence of SOA yield for the sesquiterpenes is, however, different from that of isoprene and α -pinene. For longifolene and aromadendrene, aerosol yield increases with increasing NO_x concentration (Figs. 2-5). This reversal of the NO_x dependence of SOA formation could be the result of a number of factors. Figure 13 shows a simplified reaction mechanism involving peroxy radical chemistry. At the two limiting NO_x conditions of this study, the peroxy radical chemistry is relatively well-defined; under high-NO_x conditions, peroxy radicals react virtually entirely with NO,

while under low-NO_x conditions, RO₂ reacts predominantly with HO₂. One of the possible explanations for the higher SOA yield under high-NO_x conditions is the formation of large alkoxy radicals that isomerize rather than fragment. Isomerization is plausible if the alkoxy radical has four or more carbon atoms and can form a 6-membered transition state (Baldwin et al., 1977; Carter and Atkinson, 1985). The isomerization pathway leads to the formation of larger, multifunctional products that are likely less volatile. The relative importance of isomerization increases with the size of alkoxy radicals (Atkinson, 1994, 1997a, 1997b; Atkinson et al., 1995; Atkinson et al., 1999), and larger compounds could exhibit increasing SOA yields under high-NO_x conditions as a consequence of this mechanism. For example, Lim et al. (2005) measured SOA yields up to ~50% for C₁₅ alkanes in the presence of ppm levels of NO_x. In their study, multiple isomerization steps have been proposed to lead to the formation of multifunctional compounds including nitrooxy, hydroxyl, and carbonyl groups, and it is suggested that the hydroxycarbonyls formed isomerize to form furan species that can undergo further reaction (Lim et al., 2005). Gas-phase products that are consistent with the isomerization mechanism have been observed in α -pinene photooxidation but this pathway does not appear to dominant SOA formation under high-NO_x conditions (Aschmann et al., 1998, 2002). Such a mechanism is consistent with the observed NO_x dependence of SOA yield for longifolene and aromadendrene.

Higher sesquiterpene SOA yields observed under high-NO_x conditions may, secondly, be a result of the formation of relatively nonvolatile organic nitrates, evidence for which appears in both Q-AMS data and filter sample data. As shown in Figs. 8 and 9, for both α -pinene and longifolene, the ratio of the sum of m/z 30 (NO⁺) and m/z 46

(NO₂⁺) to the total organic mass is higher under high-NO_x conditions. The ratio $[m/z\ 46]/[\text{Organic mass}]$ follows the same trend as that of $[m/z\ 30 + m/z\ 46]/[\text{Organic mass}]$ as a function of organic mass, indicating that $m/z\ 30$ and $m/z\ 46$ are correlated. It is possible that the signal at $m/z\ 30$ could be the result of a non-nitrogen containing organic fragment ion; however, given the observed correlation between $m/z\ 30$ and $m/z\ 46$, the unlikely case of an organic fragment ion at $m/z\ 46$, and the small signals under low-NO_x conditions, it appears that there is little interference from organics at these signals and their presence is indicative of nitrate formation. Under high-NO_x conditions, PILS/IC analysis, which measures only inorganic ions, shows that $\sim 10\ \mu\text{g m}^{-3}$ of nitrates are present in the aerosol. These inorganic nitrates may arise from the partitioning of gas-phase HNO₃ into the aerosol phase, and they will contribute to some of the AMS signals at $m/z\ 30$ and 46 . Assuming no non-nitrate contribution to $m/z\ 30$ and 46 , the total nitrate content of the SOA is estimated as the sum of the signals at each fragment. It is found that the calculated nitrate content exceeds that measured by PILS/IC, suggesting the presence of organic nitrates. It is emphasized that $m/z\ 30$ and $m/z\ 46$ are used only as a qualitative indication of the presence of organic nitrates.

The filter sample data provide a more direct comparison on the amount of organic nitrates formed in α -pinene and longifolene photooxidation under different NO_x conditions. For both α -pinene and longifolene, no acidic nitrates are observed under low-NO_x conditions, consistent with the prevalent RO₂ + HO₂ reaction in this case. Organic nitrate yield from the RO₂ + NO reaction increases with increasing carbon number (Atkinson et al., 1987; Carter and Atkinson, 1989; O'Brien et al., 1998; Arey et al., 2001; Aschmann et al., 2001; Zhang et al., 2004), and with the larger carbon chain the organic

nitrates formed are likely to be less volatile, an observation that is consistent with the much wider array and larger quantities of acidic nitrates detected in longifolene photooxidation under high-NO_x conditions. Hence for photooxidation of larger compounds such as sesquiterpenes, the nitrate formation channel may play an important role in SOA formation under high-NO_x conditions. With the addition of atoms such as O and N, mass-based SOA yields from longifolene photooxidation under high-NO_x conditions actually exceed 100%. Tandem MS data (generated by increasing the aperture voltage from 10 to 25 V on the UPLC/ESI-TOFMS instrument) for the C₁₇ acidic organic nitrates (i.e. *m/z* 342, 374, and 390) from longifolene photooxidation reveal a common neutral loss of 60 Da, which possibly corresponds to an acetic acid monomer. Surratt et al. (2006) and Szmigielski et al. (2007) have recently shown that particle-phase esterification occurs in isoprene SOA formed under high-NO_x conditions; specifically a 2-methylglyceric acid monomer (known isoprene ambient SOA tracer compound) can react with an acetic acid monomer to create a 2-methylglyceric acid dimer mono-acetate derivative. The observed neutral loss of 60 Da for these C₁₇ acidic organic nitrates suggests that these compounds may be dimers formed by particle-phase esterification.

Lacking appropriate analytical techniques for the detection of non-acidic nitrates, the contribution of these species under high-NO_x conditions cannot be assessed. In α -pinene photooxidation, hydroxynitrates have been identified in the gas phase using mass spectrometry (Aschmann et al., 1998, 2002). In SOA formation from alkanes under high-NO_x conditions, Lim et al. (2005) found that, while SOA from oxidation of C₁₀ alkane contains no δ -hydroxynitrates, such compounds contribute ~40% of the SOA mass for

reactions of the C₁₅ alkane. It is likely that a larger quantity of hydroxynitrates are present also in the longifolene system, as compared to α -pinene.

7.6.2 General mechanisms of aerosol growth

7.6.2.1 Loss of semivolatiles

Substantial insights into the general mechanism of SOA formation and growth kinetics can be gained by examining so-called growth curves (Ng et al., 2006, 2007). Figure 2 shows the time-dependent growth curves from longifolene photooxidation under high- and low-NO_x conditions. The high-NO_x growth curves have a “convex” shape, indicating that aerosol growth slows down as longifolene approaches complete reaction. Similar behavior for longifolene growth was observed by Ng et al. (2006), who suggested that this atypical growth behavior may have been spurious, as a result of inaccuracies in PTR-MS measurements, owing to interference from products, or fragments of products with the same mass to charge ratio as longifolene; or a change in the aerosol density over the course of the experiment. In this study, in those experiments in which the longifolene concentration was monitored by both GC-FID and PTR-MS, the shape of PTR-MS hydrocarbon decay agrees with that measured by GC-FID. The density of the aerosol is estimated during oxidation by comparing Q-AMS and DMA data. It is found that the SOA density decreases slightly (<5%) over the course of the experiment, however, such a small decrease in density is within experimental uncertainty and cannot account for the observed atypical growth behavior.

Deceleration in SOA growth can arise from the loss of semivolatiles by photolysis, further reaction with OH to form volatile products, or deposition loss to

chamber walls. When fitting the observed aerosol growth with a simple kinetic system that accounts for gas-phase loss of semivolatile oxidation products (Fig. 14), it is estimated that the first-order gas-phase loss rate constant (k_g) is about 5 times larger than the pseudo-first-order oxidation rate of the parent hydrocarbon ($k'_{OH} = k_{OH}[OH]$). At the estimated OH concentration of $\sim 2 \times 10^7$ molecules cm^{-3} under high- NO_x conditions, k'_{OH} for longifolene is $\sim 9.6 \times 10^{-4} \text{ s}^{-1}$. Under high- NO_x conditions, the loss of organic nitrates (among other gas-phase species) may play a role in the observed deceleration in aerosol growth. The reaction rate constants of small alkyl nitrates with OH are generally of the order of $10^{-13} \text{ cm}^3 \text{ molecule}^{-1} \text{ s}^{-1}$ (hence pseudo-first-order reaction rate of $\sim 10^{-6} \text{ s}^{-1}$) and their photolysis rates have been measured to be $\sim 1 \times 10^{-6} \text{ s}^{-1}$ (Talukdar et al., 1997; Finlayson-Pitts and Pitts, 2000). Although the OH reaction rate and photolysis rate of organic nitrates are much slower than the oxidation rate of longifolene, both rates are expected to increase with carbon number (Talukdar et al., 1997; Finlayson-Pitts and Pitts, 2000; Treves et al., 2003). Hence, it is possible that gas-phase reaction of C_{15} organic nitrates may be occurring at an appreciable rate. From the change in AMS spectra from longifolene photooxidation under high- NO_x conditions (Fig. 10), it is found that both m/z 30 and 46 decrease by $\sim 10\%$ over the course of the photooxidation. Further study on the OH reaction rate constant and photolysis rate of larger nitrates would be useful in evaluating the importance of gas-phase nitrate chemistry in aerosol formation.

As a possible explanation of decreasing SOA volume during the photooxidation of isoprene under low- NO_x conditions, Kroll et al. (2006) suggest photolysis of organic hydroperoxides in the gas phase, and/or particle-phase photolysis, or further reactions of OH radicals to form products of higher volatility that partition back to the gas phase may

be occurring. From the AMS data on the percentage change in the mass fraction of different mass fragments under low-NO_x conditions (Fig. 11), it is found that m/z 44 increases over the course of the oxidation while other higher m/z values decrease. The signal at m/z 44 (CO₂⁺) is often used as a tracer for oxidized aerosol (Zhang et al., 2005); thus, an increase in m/z 44 may be indicative of further oxidization of SOA. In comparison to the dramatic decrease in SOA volume observed in isoprene photooxidation, the compounds formed from further oxidations of longifolene products are still sufficiently nonvolatile that they do not repartition back into the gas phase. Also the photolysis and the OH reaction rate constants for larger hydroperoxides may not be as rapid as those formed in the isoprene system. While no gas-phase data regarding the photolysis and OH reaction rate for larger organic peroxides are available, a recent study on the photooxidation of methyhydroperoxide and ethylhydroperoxide in the aqueous phase indicates that the photolysis and OH reaction rates for the latter are indeed slower than those of methyhydroperoxide (Monod et al., 2007). The photochemistry of larger and more complex hydroperoxides merits further investigation.

7.6.2.2 SOA formation from higher generation products

In Figs. 1 and 3, the growth curves of α -pinene and longifolene photooxidation exhibit a “hook” at the end of the intermediate NO_x experiments, indicating that aerosol growth continues after the complete consumption of the parent hydrocarbon. Organic mass measured by the Q-AMS increases even after all the hydrocarbon is consumed, indicating that this additional aerosol growth is not a result of condensation of inorganic nitrate. Continued aerosol growth can arise from further gas-phase reactions of reactive oxidation products, such as aldehydes and furans, etc, or from further particle-phase

reactions. In the intermediate NO_x experiments, the NO concentration goes to zero about 30 min after the commencement of photooxidation, owing to the rapid reaction of NO and peroxy radicals (HO_2 and other peroxy radicals). As a result, a transition from high- NO_x to low- NO_x conditions occurs over the course of the experiment, and the final aerosol formed is potentially a mixture of the products formed under both conditions. Johnson et al. (2004, 2005) proposed the formation of peroxyhemiacetals from hydroperoxides and aldehyde species as an effective mechanism for the higher aerosol yield observed from photooxidation of aromatics under low- NO_x conditions. Such type of particle-phase reactions may be contributing to the further aerosol growth observed in the intermediate NO_x experiments.

7.7 Implications

A series of chamber experiments investigating the NO_x dependence of SOA formation from the photooxidation of one monoterpene and two sesquiterpenes is reported here. Monoterpene SOA formation, such as from α -pinene, is found to follow the same NO_x dependence as isoprene, in which the aerosol yields are substantially higher under low- NO_x conditions. The NO_x dependence of SOA formation from the two sesquiterpenes is, however, markedly different from those of isoprene and α -pinene; for longifolene and aromadendrene, aerosol yields are at their maximum under high- NO_x conditions. The reason for this reversal of the NO_x dependence of SOA formation for the sesquiterpenes, while not unequivocally established here, may be the result of production of highly nonvolatile organic nitrates, the existence of which is suggested by both Q-AMS and filter sample data. Since larger alkoxy radicals can isomerize more readily, the

higher SOA yields observed under high-NO_x conditions suggests also that isomerization may be an effective channel for SOA production for larger hydrocarbon precursors.

The increase in SOA yield from photooxidation of the larger biogenic hydrocarbons under high-NO_x conditions could have implications in terms of the effect of anthropogenically influenced air masses on biogenic SOA formation. In the recent study of de Gouw et al. (2005), it is suggested that over the western Atlantic the majority of the measured organic aerosol is from secondary anthropogenic sources, a conclusion that is not consistent with the radiocarbon measurements that indicate high fractions of “modern”, biogenic carbon (e. g. Klinedinst and Currie, 1999). If the production of SOA from biogenic hydrocarbons is enhanced in the presence of NO_x, observations of enhanced SOA correlated with anthropogenic sources can occur, even for organic carbon of biogenic origin. Large anthropogenic hydrocarbons may exhibit a similar NO_x behavior as that of the sesquiterpenes studied, as suggested by the substantial SOA yields from the OH-initiated reaction of large alkanes in the presence of ppm levels of NO_x (Lim et al., 2005). If the NO_x behavior observed for longifolene and aromadendrene extends to other sesquiterpenes as well as larger alkanes, the contribution to the total SOA from these compounds in polluted air may actually be higher than already estimated (Griffin et al., 1999ab; Carreras-Sospedra et al., 2005; de Gouw et al. 2005).

In this study, we have investigated only the NO_x dependence of SOA formation from photooxidation of the monoterpene α -pinene and two sesquiterpenes, each containing only one double bond. SOA formation from compounds with two or more double bonds can exhibit characteristics that suggest significant contributions from multiple generation products (Ng et al., 2006) and this may have impacts on the NO_x

dependence. It is clear that the effect of NO_x on SOA yields from the complete suite of ambient aerosol-forming hydrocarbons should be evaluated thoroughly.

7.8 Appendix: Description of PTR-MS technique

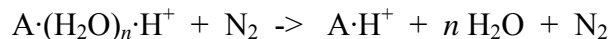
For PTR-MS sampling, a constant flow of ~ 2.5 standard liters per minute (slm) is drawn from the chamber through PFA tubing. The residence time in the inlet tubing is roughly 1 s. A small portion of the flow, 93 standard cubic centimeters per minute [sccm], is pulled through a glass critical orifice into a 2.54-cm diameter glass flow tube, in which this sample flow is diluted with dry N_2 (1.6 slm) to maintain the flow tube pressure at 35 mbar. This dilution minimizes confounding effects owing to large concentrations of hydrogen peroxide and other compounds typically used or produced in chamber experiments.

In the flow tube, analyte ionization occurs in a manner similar to that described by Crouse et al. (2006) for negative ionization. N_2 (400 sccm) flows through an ion source cup composed of a cylindrical silver foil lined with ^{210}Po and sealed with gold. α bombardment from the ^{210}Po , coupled with trace water present in the N_2 , leads to the formation of positively charged clusters, e.g., $(\text{H}_2\text{O})_n\text{H}^+$. The electric potentials of the ion source components are set such that these positively charged clusters then pass through a 6.35 mm aperture into the 35 mbar flow tube, flowing perpendicular to the sample flow. The clusters then react via proton transfer with the analyte, in the present case aromadendrene, in the sample flow to form aromadendrene- H^+ and higher order water clusters.

Across the flow tube from the ion source, a pinhole aperture (diameter 0.34 mm) allows a portion of the ions and neutral gas (~ 30 sccm) to flow into the mass

spectrometer, a Varian 1200 tandem mass spectrometer. The spectrometer was modified by removing the electron impact source and extending the hexapole ion guide that leads to the quadrupole mass analyzer to the pinhole aperture. For these measurements, the mass spectrometer was operated exclusively in one-dimensional mass spectrometry mode.

In order to simplify the mass spectra, a DC potential of -10 V (relative to the pinhole aperture) is applied to the hexapole. This offset pulls ions into the hexapole, where the pressure is relatively high owing to the neutral gas flow (chiefly N₂) through the pinhole. The ions therefore undergo high energy collisions with the neutral gas molecules which dissociate water clusters of analyte A:



Thus, species are predominantly observed at $m/z = M + 1$, where M is the molecular mass of the species. Hydrates, $A \cdot (H_2O)_m \cdot H^+$, particularly $m = 1$, are also observed for some species, though not for aromadendrene.

Each day, the PTR-MS sensitivity towards aromadendrene was determined by sampling standard mixtures of aromadendrene in teflon bags filled with 50 L zero air. The sensitivity was determined to be linear from 0 ppb to at least 5 ppb. Also, because of the large amounts of H₂O₂ utilized in the experiments, the sensitivity as a function of H₂O₂ was determined, with [H₂O₂] measured by operating the Varian 1200 in negative ionization mode, exploiting the reaction of CF₃O⁻ with H₂O₂ (Crouse et al., 2006). Thus, the sensitivity determined from H₂O₂-free standards was corrected for sampling from the chamber when H₂O₂ was present.

The uncertainty of aromadendrene measurements using PTR-MS is estimated to be $\sim \pm 22\%$, based on the scatter of replicate data and background measurements and uncertainties in the H_2O_2 correction.

7.9 Acknowledgements

This research was funded by U.S. Department of Energy Biological and Environmental Research Program grant DE-FG02-05ER63983. This material is based in part on work supported by the National Science Foundation under grant ATM-0432377. Alan J. Kwan acknowledged the support of NSF graduate research fellowship.

7.10 References

- Alfarra, M. R., Paulsen, D., Gysel, M., Garforth, A. A., Dommen, J., Prevot, A. S. H., Worsnop, D. R., Baltensperger, U., Coe, H.: A mass spectrometric study of secondary organic aerosols formed from the photooxidation of anthropogenic and biogenic precursors in a reaction chamber, *Atmos. Chem. Phys.*, 6, 5279-5293, 2006.
- Arey, J., Aschmann, S. M., Kwok, E. S. C., Atkinson, R.: Alkyl nitrates, hydroxyalkyl nitrates and hydroxycarbonyl formation from the NO_x – air photooxidation of C_5 - C_8 n-alkanes, *J. Phys. Chem. A*, 105, 1020-1027, 2001.
- Aschmann, S. M., Arey, J., Atkinson, R.: Atmospheric chemistry of three C_{10} alkanes. *J. Phys. Chem. A*, 105, 7598-7606, 2001.
- Aschmann, S. M., Atkinson, R., Arey, J.: Products of reaction of OH radicals with α -pinene, *J. Geophys. Res.*, 107, D14, 4191, doi: 10.1029/2001JD001098, 2002.
- Aschmann, S. M., Reissell, A., Atkinson, R., Arey, J.: Products of the gas phase reactions of the OH radical with α - and β -pinene in the presence of NO, *J. Geophys. Res.*, 103, D19, 4191, 25553-25561, 1998.
- Aschmann, S. M., Reissell, A., Atkinson, R., Arey, J.: Products of the gas phase reactions of the OH radical with a- and b-pinene in the presence of NO, *J. Geophys. Res.*, 103, D19, 25553-25561, 1998.
- Atkinson, R. Kwok, E. S. C., Arey, J., Aschmann, S. M.: Reactions of alkoxy radicals in the atmosphere, *Faraday Discuss.*, 100, 23-37, 1995.

- Atkinson, R., Arey, J.: Gas-phase tropospheric chemistry of biogenic volatile organic compounds: a review, *Atmos. Environ.*, 37, S197-S219, 2003.
- Atkinson, R., Aschmann, S. M., Winer, A. M.: Alkyl nitrate formation from the reaction of a series of branched RO₂ radicals with NO as a function of temperature and pressure, *J. Phys. Chem.*, 5, 91-102, 1987.
- Atkinson, R., Baulch, D. L., Cox, R. A., Hampson, R. F., Kerr, J. A., Rossi, M. J., Troe, J.: Evaluated kinetic and photochemical data for atmospheric chemistry, organic species, supplement VII, *J. Phys. Chem. Ref. Data.*, 28, 2, 1999.
- Atkinson, R.: Atmospheric reactions of alkoxy and β -hydroxyalkoxy radicals, *Int. J. Chem. Kinet.*, 29, 99-111, 1997a.
- Atkinson, R.: Gas phase tropospheric chemistry of organic compounds, *J. Phys. Chem. Ref. Data, Monogr, No. 2*, 11-216, 1994.
- Atkinson, R.: Gas phase tropospheric chemistry of volatile organic compounds: 1. Alkanes and Alkenes, *J. Phys. Chem. Ref. Data.*, 215-290, 1997b.
- Baldwin, A. C., Barker, J. R., Golden, D. M., Hendry, D. G.: Photochemical smog – rate parameter estimates and computer simulations, *J. Phys. Chem.*, 81, 2483-2492, 1977.
- Bahreini, R., Keywood, M. D., Ng, N. L., Varutbangkul, V., Gao, S., Flagan, R. C., Seinfeld, J. H. Measurements of secondary organic aerosol (SOA) from oxidation of cycloalkenes, terpenes, and m-xylene using an Aerodyne aerosol mass spectrometer. *Environ. Sci. Technol.*, 39, 5674-5688, 2005.
- Carreras-Sospedra, M., Griffin, R. J., Dabdub, D.: Calculations of incremental secondary organic aerosol reactivity, *Environ. Sci. Technol.*, 39, 1724-1730, 2005.
- Carter, W. P. L., Atkinson, R.: Alkyl nitrate formation from the atmospheric photooxidation of alkanes; a revised estimation, *J. Phys. Chem.*, 8, 165-173, 1989.
- Carter, W. P. L., Atkinson, R.: Atmospheric chemistry of alkanes, *J. Atmos. Chem.* 3, 377-405, 1985.
- Cocker III, D. R., Flagan, R. C., Seinfeld, J. H.: State-of-the-art chamber facility for studying atmospheric aerosol chemistry, *Environ. Sci. Technol.*, 35, 2594-2601. 2001.
- Crounse, J. D., McKinney, K. A., Kwan, A. J., Wennberg, P. O.: Measurements of gas-phase hydroperoxides by chemical ionization mass spectrometry, *Anal. Chem.*, 78, 6726-6732, 2006.

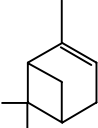
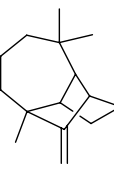
- de Gouw, J. A., Middlebrook, A. M., Warneke, C., Goldan, P. D., Kuster, W. C., Roberts, J. M., Fehsenfeld, F. C., Worsnop, D. R., Canagaratna, M. R., Pszenny, A. A. P., Keene, W. C., Marchewka, M., Bertman, S. B., and Bates, T. S.: Budget of organic carbon in a polluted atmosphere: Results from the New England Air Quality Study in 2002, *J. Geophys. Res.*, 110, D16305, doi: 10.1029/2004JD005623, 2005.
- Finlayson-Pitts, B. J., Pitts, J. N.: *Chemistry of the upper and lower atmosphere: theory, experiments and applications*, Academic Press, San Diego, 2000.
- Gao, S., Keywood, M. D., Ng, N. L., Surratt, J. D., Varutbangkul, V., Bahreini, R., Flagan, R. C. and Seinfeld, J. H.: Low-molecular weight and oligomeric components in secondary organic aerosol from the ozonolysis of cycloalkenes and α -pinene, *J. Phys. Chem. A*, 108, 10147-10164, 2004.
- Gao, S., Surratt, J. D., Kinipping, E. M., Edgerton, E. S., Shahgholi, M. Seinfeld, J. H.: Characterization of polar organic components in fine aerosols in the southeastern United States: Identity, origin, and evolution, *J. Geophys. Res.*, 111, D14314, doi:10.1029/2005JD006601, 2006.
- Geron, C., Rasmussen, R., Arnts, R. R., Guenther, A.: A review and synthesis of monoterpene speciation from forests in the United States, *Atmos. Environ.*, 34, 1761-1781, 2000.
- Glasius, M., Duane, M., Larsen, B. R.: Determination of polar terpene oxidation products in aerosols by liquid chromatography-ion trap mass spectrometry, *J. Chrom. A.*, 833, 121-135, 1999.
- Glasius, M., Lahaniati, M., Calogirou, A., Di Bella, D., Jensen, N. R., Hjorth, J., Kotzias, D., Larsen, B. R.: Carboxylic acids in secondary aerosols from oxidation of cyclic monoterpenes by ozone, *Environ. Sci. Technol.*, 34, 1001-1010, 2000.
- Griffin, R. J., Cocker, D. R., Flagan, R. C., Seinfeld, J. H., Dabdub, D.: Estimate of global atmospheric organic aerosol formation from the oxidation of biogenic hydrocarbons, *Geophys. Res. Lett.*, 26, 17, 2721-2724, 1999a.
- Griffin, R. J., Cocker, D. R., Flagan, R. C., Seinfeld, J. H.: Organic aerosol formation from the oxidation of biogenic hydrocarbons, *J. Geophys. Res.*, 104, D3, 3555-3567, 1999b.
- Guenther, A., Hewitt, C. N., Erickson, D., Fall, R., Geron, C., Graedel, T., Harley, P., Klinger, L., Lerdau, M., McKay, W. A., Pierce, T., Scholes, B., Steinbrecher, R., Tallamraju, R., Taylor, T., Zimmerman, P.: A global model of natural volatile organic compound emission, *J. Geophys. Res.*, 100, D5, 8873-8892, 1995.

- Hatakeyama, S., Izumi, K., Fukuyama, T., Akimoto, H., Washida, N.: Reactions of OH with α -pinene and β -pinene in air: Estimates of global CO production from the atmospheric oxidation of terpenes, *J. Geophys. Res.*, 96, D1, 947-958, 1991.
- Hurley, M. D., Sokolov, O., Wallington, T. J., Takekawa, H., Karasawa, M., Klotz, B., Barnes, I., Becker, K. H.: Organic aerosol formation during the atmospheric degradation of toluene, *Environ. Sci. Technol.*, 35, 1358-1366, 2001.
- Jayne, J. T., Leard, D. C., Zhang, X., Davidovits, P., Smith, K. A., Kolb, C. E., Worsnop, D. W.: Development of an Aerosol Mass Spectrometer for size and composition analysis of submicron particles, *Aerosol Sci. and Technol.*, 33, 49-70, 2000.
- Johnson, D., Jenkin, M. E., Wirtz, K., Martín-Reviejo, M. Simulating the formation of secondary organic aerosol from the photooxidation of aromatic hydrocarbons, *Environ. Chem.*, 2, 35-48, 2005.
- Johnson, D., Jenkin, M. E., Wirtz, K., Martín-Reviejo, M.: Simulating the formation of secondary organic aerosol from the photooxidation of toluene, *Environ. Chem.*, 1, 150-165, 2004.
- Kanakidou, M., Seinfeld, J. H., Pandis, S. N., Barnes, I., Dentener, F. J., Facchini, M. C., Van Dingenen, R., Evers, B., Nenes, A., Swietlicki, E., Pautaud, J. P., Balkanski, Y., Fuzzi, S., Horth, J., Moortgat, G. K., Winterhalter, R., Myhre, C. E. L., Tsigaridis, K., Vignati, E., Stephanou, E. G., Wilson, J.: Organic aerosol and global climate modeling: a review, *Atmos. Chem. Phys.*, 5, 1053-1123, 2005.
- Keywood, M. D., Varutbangkul, V., Bahreini, R., Flagan, R. C., Seinfeld, J. H.: Secondary organic aerosol formation from the ozonolysis of cycloalkenes and related compounds, *Environ. Sci. Technol.*, 38, 4157-4164, 2004.
- Klinedinst, D. B., Currie, L. A.: Direct quantification of PM_{2.5} fossil and biomass carbon within the northern front range air quality study's domain, *Environ. Sci. Technol.*, 33, 4146-4154, 1999.
- Kroll, J. H., Ng, N. L., Murphy, S. M., Flagan, R. C., Seinfeld, J. H.: Secondary organic aerosol formation from isoprene photooxidation under high-NO_x conditions, *J. Geophys. Res.*, 32, L18808, doi: 10.1029/2005GL023637, 2005.
- Kroll, J. H., Ng, N. L., Murphy, S. M., Flagan, R. C., Seinfeld, J. H.: Secondary organic aerosol formation from isoprene photooxidation, *Environ. Sci. Technol.*, 40, 1869-1877, 2006.
- Larsen, B. R., Di Bella, D., Glasius, M., Winterhalter, R., Jensen, N. R., Hjorth, J.: Gas-phase OH oxidation of monoterpenes: Gaseous and particulate products, *J. Atmos. Chem.*, 38, 2310276, 2001.

- Lim, Y. B, Ziemann, P. J.: Products and mechanism of secondary organic aerosol formation from reactions of *n*-alkanes with OH radicals in the presence of NO_x, *Environ. Sci. Technol.*, 39, 9229-9236, 2005.
- Monod, A., Chevallier, E., Durand Jolibois, R., Doussin, J. F., Picquet-Varrault, B., Carlier, P. : Photooxidation of methylhydroperoxide and ethylhydroperoxide in the aqueous phase under simulated cloud droplet conditions, *Atmos., Environ.*, 41, 2412-2426, 2007.
- Ng, N. L., Kroll, J. H., Keywood, M. D., Bahreini, R., Varutbangkul, V., Flagan, R. C., Seinfeld, J. H., Lee, A., and Goldstein, A. H.: Contribution of first- versus second-generation products to secondary organic aerosols formed in the oxidation of biogenic hydrocarbons, *Environ. Sci. Technol.*, 40, 2283-2297, 2006.
- Ng, N. L., Kroll, J. H., Chan, A. W. H., Chhabra, P. S., Flagan, R. C. and Seinfeld, J. H.: Secondary organic aerosol formation from *m*-xylene, toluene, and benzene, *Atmos. Chem. Phys. Discuss.*, 7, 4085-4126, 2007.
- O'Brien, J. M., Czuba, E., Hastie, D. R., Francisco, J. S., Shepson, P. B.: Determination of the hydroxy nitrate yields from the reaction of C₂-C₆ alkenes with OH in the presence of NO, *J. Phys. Chem.*, 102, 8903-8908, 1998.
- Odum, J. R., Hoffmann, T., Bowman, F., Collins, D., R. C. Flagan, R. C., and Seinfeld, J. H.: Gas/particle partitioning and secondary organic aerosol yields, *Environ. Sci. Technol.*, 30, 2580-2585, 1996.
- Odum, J. R., Jungkamp, T. P. W., Griffin, R. J., Forstner, H. J. L., Flagan, R. C., and Seinfeld, J. H.: Aromatics, reformulated gasoline and atmospheric organic aerosol formation, *Environ. Sci. Technol.*, 31, 1890-1897, 1997.
- Owen, S. M., Boissard, C., Hewitt, C. N.: Volatile organic compounds (VOCs) emitted from 40 Mediterranean plant species: VOC speciation and extrapolation to habitat scale, *Atmos. Environ.*, 35, 5393-5409, 2001.
- Pandis, S. N., Paulson, S. E., Seinfeld, J. H., Flagan, R. C.: Aerosol formation in the photooxidation of isoprene and β -pinene, *Atmos. Environ.*, 25A, 997-1008, 1991.
- Presto, A. A., Huff Hartz, K. E., Donahue, N. M.: Secondary organic aerosol production from ozonolysis: 2. Effect of NO_x concentration, *Environ. Sci. Technol.*, 39, 7046-7054, 2005.
- Seinfeld, J., Pankow, J. F.: Organic atmospheric particulate material, *Annu. Rev. Phys. Chem.*, 54, 121-140, 2003.
- Song, C., Na, K., Cocker III, D. R.: Impact of the hydrocarbon to NO_x ratio on secondary organic aerosol formation, *Environ. Sci. Technol.*, 39, 3143-3149, 2005.

- Sorooshian, A., Brechtel F. J., Ma, Y. L., Weber R. J., Corless, A., Flagan, R. C. and Seinfeld, J. H.: Modeling and characterization of a particle-into-liquid sampler (PILS), *Aerosol Sci. and Technol.*, 40, 396-409, 2006.
- Surratt, J. D., Kroll, J. H., Kleindienst, T. E., Edney, E. O., Claeys, M., Sorooshian, A., Ng, N. L., Offenberg, J. H., Lewandowski, M., Jaoui, M., Flagan, R. C. and Seinfeld, J. H.: Evidence for organosulfates in secondary organic aerosol, *Environ. Sci. Technol.*, 41, 517-527, 2007.
- Surratt, J. D., Murphy, S. M., Kroll, J. H., Ng, N. L., Hildebrandt, L., Sorooshian, A., Szmigielski, R., Vermeylen, R., Maenhaut, W., Claeys, M., Flagan, R. C. and Seinfeld, J. H.: Chemical composition of secondary organic aerosol formed from the photooxidation of isoprene, *J. Atmos. Chem.*, 31, 9665-9690, 2006.
- Szmigielski, R., Surratt, J. D., Vermeylen, R., Szmigielska, K., Kroll, J. H., Ng, N. L., Murphy, S. M., Sorooshian, A., Seinfeld, J. H., Claeys, M.: Characterization of 2-methylglyceric acid oligomers in secondary organic aerosol formed from the photooxidation of isoprene using trimethylsilylation and gas chromatography/ion trap mass spectrometry, *J. Mass Spectrom.*, 42, 101-116, 2007.
- Talukar, R. K., Herndon, S. C., Burkholder, J. B., Roberts, J. M., Ravishankara, A. R.: Atmospheric fate of several alkyl nitrates, *J. Chem. Soc., Faraday Trans.*, 93, 2787-2796, 1997.
- Treves, K., Rudich, Y.: The atmospheric fate of C₃-C₆ hydroxyalkyl nitrates, *J. Phys. Chem. A*, 107, 7809-7817, 2003.
- Zhang, J., Dransfield, T., Donahue, N. M.: On the mechanism for nitrate formation via the peroxy radical + NO reaction, *J. Phys. Chem. A*, 108, 9082-9095, 2004.
- Zhang, J., Hartz, K. E. H., Pandis, S. N., and Dohanue, N. M.: Secondary organic aerosol formation from limonene ozonolysis: Homogeneous and heterogeneous influences as a function of NO_x, *J. Phys. Chem., A*, 110, 11053-11063, 2006.
- Zhang, S. H., Shaw, M., Seinfeld, J. H., Flagan, R. C.: Photochemical aerosol formation from α -pinene and β -pinene, *J. Geophys. Res.*, 97, D18, 20717-20729, 1992.

Table 7. 1. Parent hydrocarbons studied

Parent Hydrocarbon	Structure	Formula (MW)	k_{OH} ($\text{cm}^3 \text{molec}^{-1} \text{s}^{-1}$)
α -pinene		$\text{C}_{10}\text{H}_{16}$ (136)	$5.3 \times 10^{-11} \text{ a}$
longifolene		$\text{C}_{15}\text{H}_{24}$ (204)	$4.8 \times 10^{-11} \text{ a}$
aromadendrene		$\text{C}_{15}\text{H}_{24}$ (204)	$1.5 \times 10^{-10} \text{ b}$

a: Rate constants were obtained from Atkinson et al. (2003)

b: Rate constant was estimated from the rate of aromadendrene decay (experiment 1 in Table 7.4), assuming an OH concentration of $3 \times 10^6 \text{ molecule cm}^{-3}$ and that aromadendrene reacts with OH only

Table 7. 2. Initial conditions and data for α -pinene experiments

Expt. No.	NO _x Condition	NO (ppb)	NO ₂ (ppb)	T (K)	RH (%)	Δ H _C (ppb) ^a	Δ M ₀ (μ g/m ³) ^b	SOA Yield (%) ^c
1	H ₂ O ₂	0	0	298	5.3	13.8 \pm 0.2	29.3 \pm 2.4	37.9 \pm 3.2
2	H ₂ O ₂	0	1	298	6.2	47.5 \pm 0.8	121.3 \pm 9.4	45.8 \pm 3.6
3	H ₂ O ₂ + NO	198	0	296	6.4	13.1 \pm 0.2	15.6 \pm 1.4	21.2 \pm 2.0
4	HONO	475	463	299	3.3	12.6 \pm 0.2	4.5 \pm 0.9	6.6 \pm 1.4
5	HONO	390	578	298	3.7	46.6 \pm 0.8	40.8 \pm 3.8	15.8 \pm 1.5

a: Stated uncertainties include scatter in GC measurements and GC calibration errors

b: Stated uncertainties are from scatter in particle volume measurements

c: Stated uncertainties are propagated from errors in Δ H_C and Δ M₀

Table 7. 3. Initial conditions and data for longifolene experiments

Expt. No.	NO_x Condition	NO (ppb)	NO₂ (ppb)	T (K)	RH (%)	ΔHC (ppb)^b	ΔM_o (μg/m³)^c	SOA Yield (%)^d
1	H ₂ O ₂	0	0	298	5.8	4.5 ± 0.2	28.5 ± 2.4	75.7 ± 7.0
2	H ₂ O ₂	0	2	297	6.0	8.4 ± 0.4	52.5 ± 4.2	74.4 ± 6.7
3	H ₂ O ₂	0	2	297	6.3	19.4 ± 0.8	117.1 ± 9.3	72.1 ± 6.5
4	H ₂ O ₂	0	2	299	5.7	24.8 ± 1.1	148.4 ± 11.6	71.8 ± 6.4
5	H ₂ O ₂ + NO	70	31 ^a	297	6.2	3.8 ± 0.2	35.8 ± 2.9	111.7 ± 10.2
6	H ₂ O ₂ + NO	209	26 ^a	297	8.0	4.7 ± 0.2	43.4 ± 3.5	110.2 ± 10.0
7	H ₂ O ₂ + NO	316	0	298	6.4	4.1 ± 0.2	43.4 ± 3.5	127.2 ± 11.5
8	H ₂ O ₂ + NO	394	0	297	6.1	4.8 ± 0.2	50.0 ± 4.1	124.9 ± 11.5
9	H ₂ O ₂ + NO	564	0	297	6.2	3.9 ± 0.2	51.6 ± 4.1	157.0 ± 14.1
10	HONO	428	550	298	3.7	9.7 ± 0.4	68.3 ± 5.1	84.0 ± 7.1
11	HONO	469	502	298	3.7	19.6 ± 0.9	141.9 ± 10.3	86.8 ± 7.3
12	HONO	394	577	299	3.2	26.6 ± 1.2	213.6 ± 15.3	96.3 ± 8.0

a: NO₂ formed due to NO reacting with residual ozone in the chamber

b: Stated uncertainties include scatter in GC measurements and GC calibration errors

c: Stated uncertainties are from scatter in particle volume measurements

d: Stated uncertainties are propagated from errors in ΔHC and ΔM_o

Table 7. 4. Initial conditions and data for aromadendrene experiments

Expt. No.	NO_x Condition	NO (ppb)	NO₂ (ppb)	T (K)	RH (%)	ΔHC (ppb)^a	ΔM₀ (μg/m³)^b	SOA Yield (%)
1	H ₂ O ₂	0	0	299	5.5	5.7 ± 1.2	19.7 ± 2.0	41.7 ± 10
2	H ₂ O ₂ + NO	120	0	298	9.3	5.3 ± 1.2	23.1 ± 2.2	52.0 ± 12.4
3	H ₂ O ₂ + NO	195	0	298	7.7	6.0 ± 1.4	29.3 ± 2.6	58.8 ± 14.4
4	H ₂ O ₂ + NO	517	0	299	7.4	3.2 ± 0.7	22.6 ± 2.2	84.7 ± 20.0

a: Stated uncertainties include scatter in CIMS measurements and CIMS calibration errors

b: Stated uncertainties are from scatter in particle volume measurements

Table 7. 5. Estimated effective SOA densities

Parent Hydrocarbon	NO _x Condition	Effective Density (g cm ⁻³) ^a
α-pinene	H ₂ O ₂	1.32 ± 0.10
α-pinene	H ₂ O ₂ + NO	1.32 ± 0.10
α-pinene	HONO	1.33 ± 0.10
longifolene	H ₂ O ₂	1.29 ± 0.10
longifolene	H ₂ O ₂ + NO	1.30 ± 0.10
longifolene	HONO	1.40 ± 0.10
aromadendrene	H ₂ O ₂	1.20 ± 0.10
aromadendrene	H ₂ O ₂ + NO	1.35 ± 0.10

a: Stated uncertainties (1σ) are from repeated measurements of ammonium sulfate seed densities

Table 7. 6. α -Pinene acidic SOA components detected by the UPLC/ESI-TOFMS instrument

Experiment	Measured [M - H] ⁻ ion (<i>m/z</i>)	TOFMS suggested molecular formula	Error (mDa)	Error (ppm)	Retention Time
H ₂ O ₂	157.0497	C ₇ H ₉ O ₄ ⁻	-0.4	-2.5	5.09
	169.0873	C ₉ H ₁₃ O ₃ ⁻	0.8	4.7	6.89
	171.0654	C ₈ H ₁₁ O ₄ ⁻	-0.3	-1.8	5.61
	183.1027	C ₁₀ H ₁₅ O ₃ ⁻	0.6	3.3	7.50
	185.0821	C ₉ H ₁₃ O ₄ ⁻	0.7	3.8	6.85
	199.0983	C ₁₀ H ₁₅ O ₄ ⁻	1.3	6.5	6.17
	199.0982	C ₁₀ H ₁₅ O ₄ ⁻	1.2	6.0	6.29
	199.0976	C ₁₀ H ₁₅ O ₄ ⁻	0.6	3.0	6.34
	215.0923	C ₁₀ H ₁₅ O ₅ ⁻	0.4	1.9	5.99
	215.0930	C ₁₀ H ₁₅ O ₅ ⁻	1.1	5.1	7.18
	231.0885	C ₁₀ H ₁₅ O ₆ ⁻	1.6	6.9	6.80
H ₂ O ₂ + NO	157.0499	C ₇ H ₉ O ₄ ⁻	-0.2	-1.3	5.08
	171.0655	C ₈ H ₁₁ O ₄ ⁻	-0.2	-1.2	5.60
	183.1025	C ₁₀ H ₁₅ O ₃ ⁻	0.4	2.2	7.49
	185.0812	C ₉ H ₁₃ O ₄ ⁻	-0.2	-1.1	6.86
	197.0814	C ₁₀ H ₁₃ O ₄ ⁻	0.0	0.0	8.09
	199.0971	C ₁₀ H ₁₅ O ₄ ⁻	0.1	0.5	6.36
	203.0557	C ₈ H ₁₁ O ₆ ⁻	0.1	0.5	5.50
	215.0925	C ₁₀ H ₁₅ O ₅ ⁻	0.6	2.8	6.23
	229.0718	C ₁₀ H ₁₃ O ₆ ⁻	0.6	2.6	6.17
231.0856	C ₁₀ H ₁₅ O ₆ ⁻	-1.3	-5.6	6.79	
HONO	171.0649	C ₈ H ₁₁ O ₄ ⁻	-0.8	-4.7	5.60
	183.1022	C ₁₀ H ₁₅ O ₃ ⁻	0.1	0.5	7.49
	185.0457	C ₈ H ₉ O ₅ ⁻	0.7	3.8	6.63
	187.0606	C ₈ H ₁₁ O ₅ ⁻	0.0	0.0	5.65
	197.0819	C ₁₀ H ₁₃ O ₄ ⁻	0.5	2.5	8.09
	203.0546	C ₈ H ₁₁ O ₆ ⁻	-1.0	-4.9	5.50
	213.0781	C ₁₀ H ₁₃ O ₅ ⁻	1.8	8.4	5.26
	231.0883	C ₁₀ H ₁₅ O ₆ ⁻	1.4	6.1	6.80
	259.1182	C ₁₂ H ₁₉ O ₆ ⁻	0.0	0.0	5.85
	322.1148	C ₁₂ H ₂₀ NO ₉ ⁻	1.0	3.1	7.62

Table 7. 7. Longifolene SOA components detected by the UPLC/ESI-TOFMS instrument

Experiment	Measured [M - H] ⁻ ion (m/z)	TOFMS suggested molecular formula	Error (mDa)	Error (ppm)	Retention Time (min)
H ₂ O ₂	223.1344	C ₁₃ H ₁₉ O ₃ ⁻	1.0	4.5	8.92
	237.1500	C ₁₄ H ₂₁ O ₃ ⁻	0.9	3.8	9.06
	239.1651	C ₁₄ H ₂₃ O ₃ ⁻	0.4	1.7	10.50
	253.1445	C ₁₄ H ₂₁ O ₄ ⁻	0.5	2.0	9.36
	249.1499	C ₁₅ H ₂₁ O ₄ ⁻	0.8	3.2	9.25
	249.1501	C ₁₅ H ₂₁ O ₄ ⁻	1.0	4.0	10.14
	255.1611	C ₁₄ H ₂₃ O ₄ ⁻	1.5	5.9	9.88
	255.1622	C ₁₄ H ₂₃ O ₄ ⁻	2.6	10.2	8.99
	267.1602	C ₁₅ H ₂₃ O ₄ ⁻	0.6	2.2	8.88
	267.1606	C ₁₅ H ₂₃ O ₄ ⁻	1.0	3.7	9.01
	267.1611	C ₁₅ H ₂₃ O ₄ ⁻	1.5	5.6	9.28
	267.1601	C ₁₅ H ₂₃ O ₄ ⁻	0.5	1.9	9.70
	269.1392	C ₁₄ H ₂₁ O ₅ ⁻	0.3	1.1	7.71
	283.1561	C ₁₅ H ₂₃ O ₅ ⁻	1.6	5.7	7.35
	313.2018	C ₁₇ H ₂₉ O ₅ ⁻	0.3	1.0	9.20
	H ₂ O ₂ + NO	223.1337	C ₁₃ H ₁₉ O ₃ ⁻	0.3	1.3
239.1649		C ₁₄ H ₂₃ O ₃ ⁻	0.2	0.8	10.49
265.1442		C ₁₅ H ₂₁ O ₄ ⁻	0.2	0.8	8.93
269.1401		C ₁₄ H ₂₁ O ₅ ⁻	1.2	4.5	7.72
316.1396		C ₁₄ H ₂₂ NO ₇ ⁻	0.0	0.0	9.88
329.1972		C ₁₇ H ₂₉ O ₆ ⁻	0.8	2.4	9.35
372.1664		C ₁₇ H ₂₆ NO ₈ ⁻	0.6	1.6	10.58
374.1829		C ₁₇ H ₂₈ NO ₈ ⁻	1.4	3.7	9.14
374.1829		C ₁₇ H ₂₈ NO ₈ ⁻	1.4	3.7	9.35
390.1775		C ₁₇ H ₂₈ NO ₉ ⁻	1.1	2.8	9.46
HONO	223.1334	C ₁₃ H ₁₉ O ₃ ⁻	-0.1	-0.4	8.92
	241.1453	C ₁₃ H ₂₁ O ₄ ⁻	1.3	5.4	7.55
	253.1431	C ₁₄ H ₂₁ O ₄ ⁻	-0.9	-3.6	8.02
	269.1394	C ₁₄ H ₂₁ O ₅ ⁻	0.5	1.9	7.18
	269.1408	C ₁₄ H ₂₁ O ₅ ⁻	1.9	7.1	7.71
	342.1930	C ₁₇ H ₂₈ NO ₆ ⁻	1.3	3.8	9.65
	344.1348	C ₁₅ H ₂₂ NO ₈ ⁻	0.3	0.9	8.25
	346.1502	C ₁₅ H ₂₄ NO ₈ ⁻	0.2	0.6	8.34
	360.1674	C ₁₆ H ₂₆ NO ₈ ⁻	1.6	4.4	8.89
	372.1667	C ₁₇ H ₂₆ NO ₈ ⁻	-0.6	-1.6	10.61
	374.1809	C ₁₇ H ₂₈ NO ₈ ⁻	-0.6	-1.6	8.89
	374.1816	C ₁₇ H ₂₈ NO ₈ ⁻	0.1	0.3	9.13
	374.1808	C ₁₇ H ₂₈ NO ₈ ⁻	-0.7	-1.9	9.35
	390.1773	C ₁₇ H ₂₈ NO ₉ ⁻	0.9	2.3	8.49
	390.1778	C ₁₇ H ₂₈ NO ₉ ⁻	1.4	3.6	9.21
435.1619	C ₁₇ H ₂₇ N ₂ O ₁₁ ⁻	0.4	0.9	9.56	

Figure 7. 1. Time-dependent growth curves for α -pinene photooxidation under different NO_x conditions.

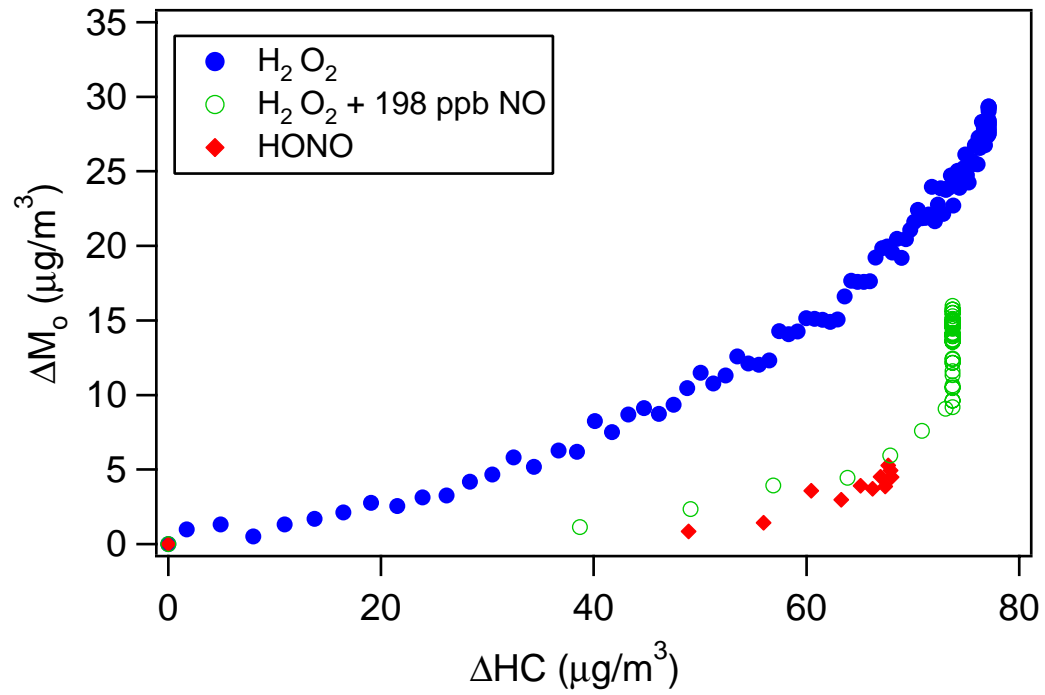


Figure 7. 2. Time-dependent growth curves for longifolene photooxidation under high- and low- NO_x conditions. The mixing ratios in the legend refer to the amount of longifolene reacted in each experiment.

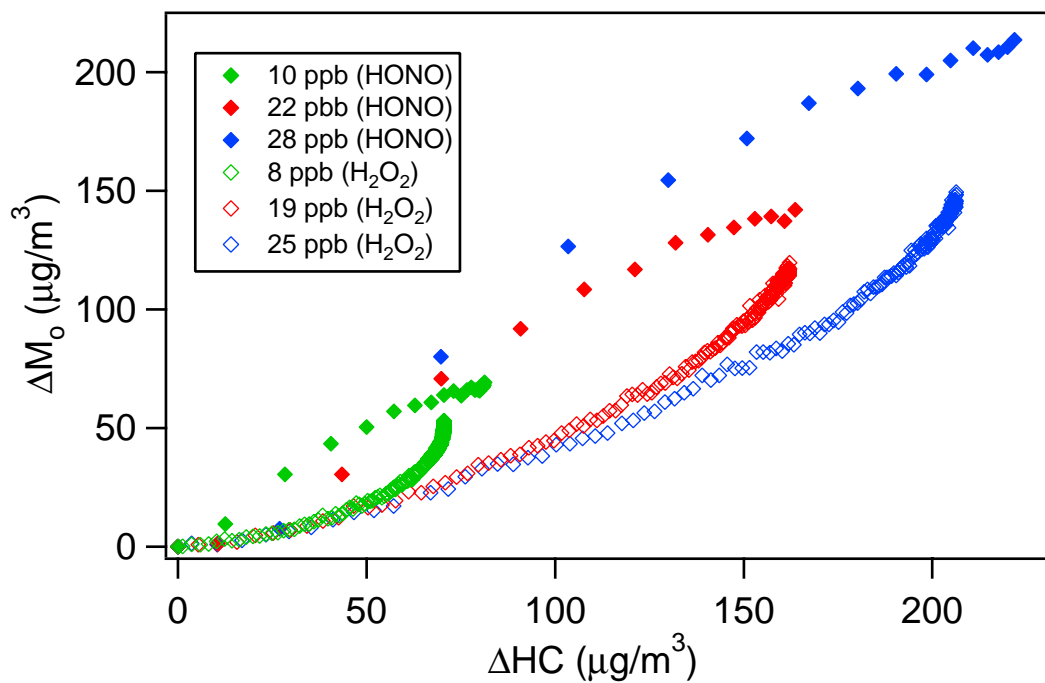


Figure 7. 3. Time-dependent growth curves for longifolene photooxidation with H_2O_2 as an OH precursor. Aerosol growth in the presence of ~ 300 ppb NO (Experiment 7 in Table 7.3) exceeds that without NO.

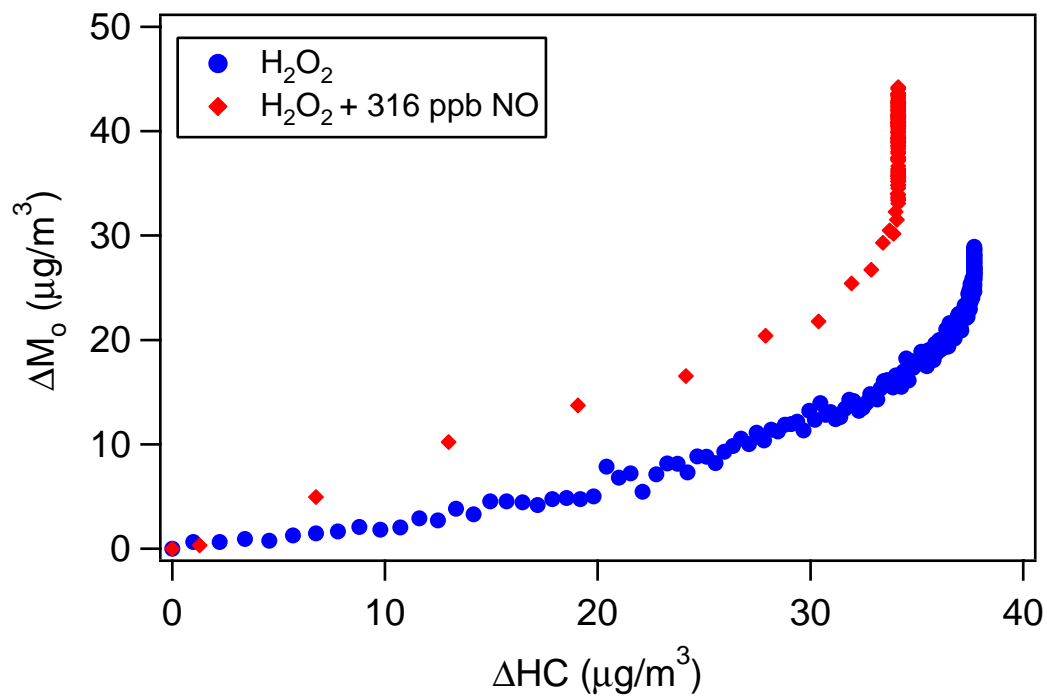


Figure 7. 4. SOA growth as a function of initial NO_x concentrations, for a fixed longifolene concentration (~ 4.3 ppb). Results shown are from Table 7.3.

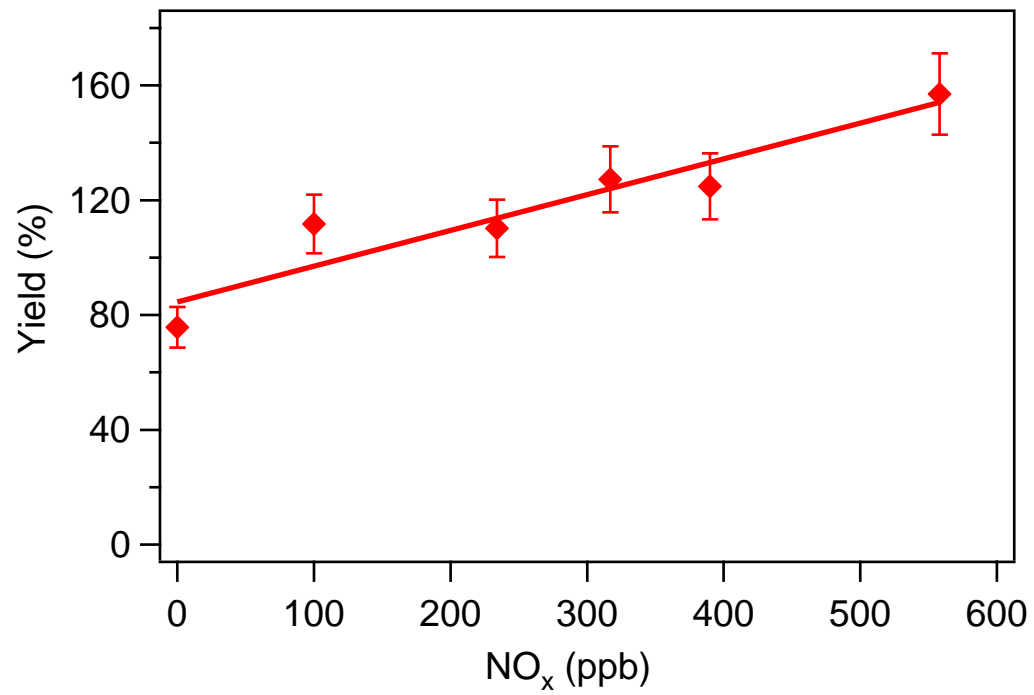


Figure 7. 5. SOA growth as a function of initial NO_x concentration, at a fixed initial aromadendrene concentration (~ 5 ppb). Results shown are from Table 7.4.

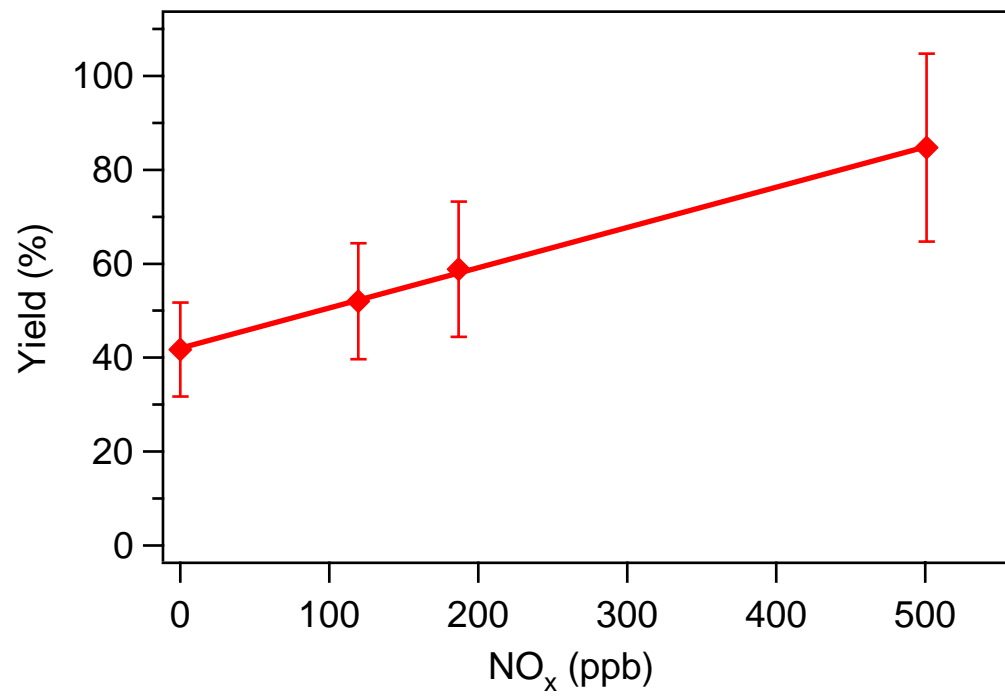


Figure 7. 6. AMS high-NO_x spectra signal versus low-NO_x spectra signal for α -pinene photooxidation. Each mass fragment is normalized by the total signal. The solid black line is the one-to-one line. The spectra are taken when all hydrocarbon has been consumed.

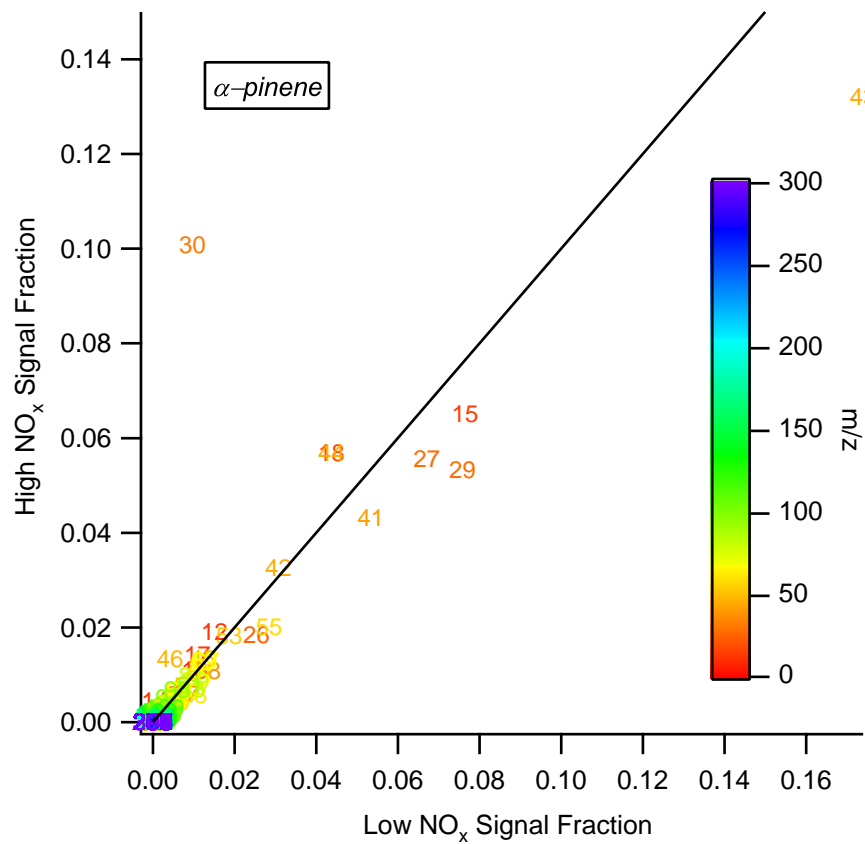


Figure 7. 7. AMS high-NO_x spectra signal versus low-NO_x spectra signal for longifolene photooxidation. Each mass fragment is normalized by the total signal. The solid black line is the 1:1 line. The spectra are taken when all hydrocarbon has been consumed.

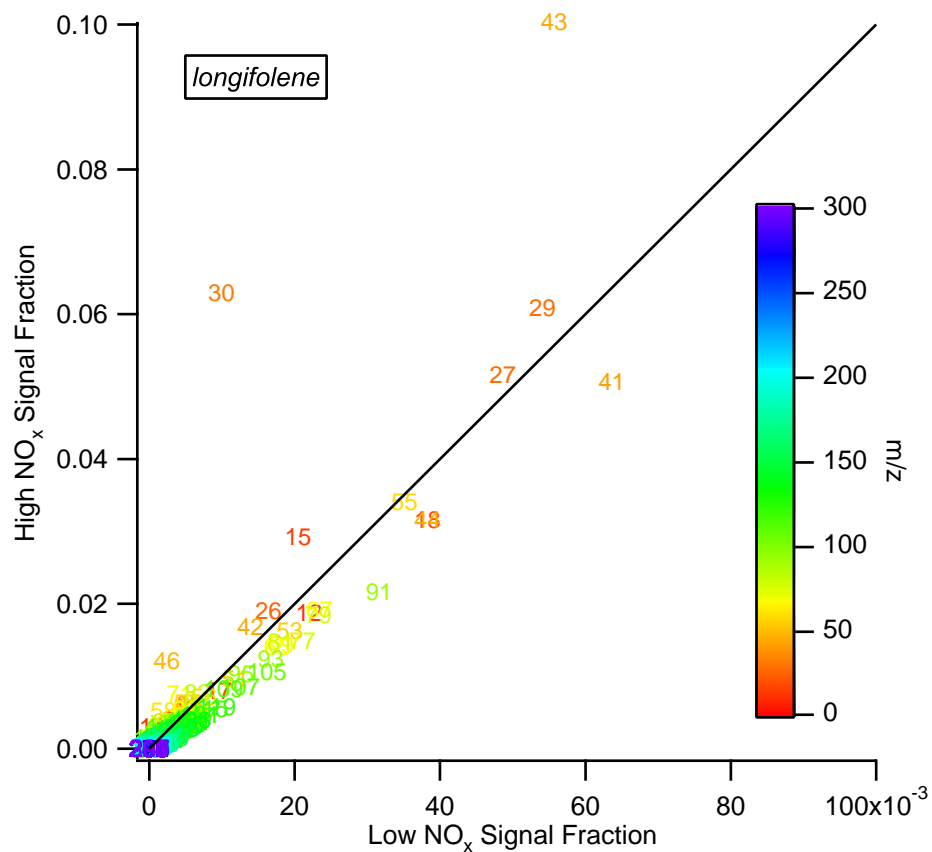


Figure 7. 8. Ratio of the sum of masses at m/z 30 and 46 to total organic mass as a function of organic mass as measured by the AMS for α -pinene photooxidation. The higher ratio for high- NO_x experiments suggests the formation of nitrate species.

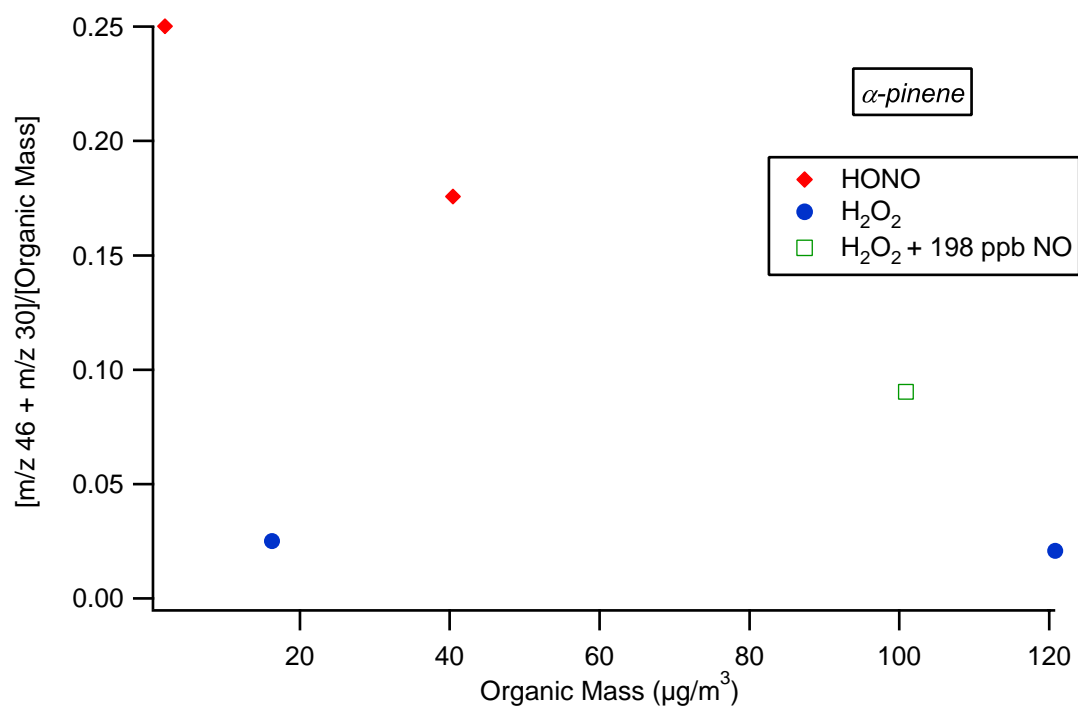


Figure 7. 9. Ratio of the sum of masses at m/z 30 and 46 to total organic mass as a function of organic mass as measured by the AMS for longifolene photooxidation. The higher ratio for high- NO_x experiments suggests the formation of nitrate species.

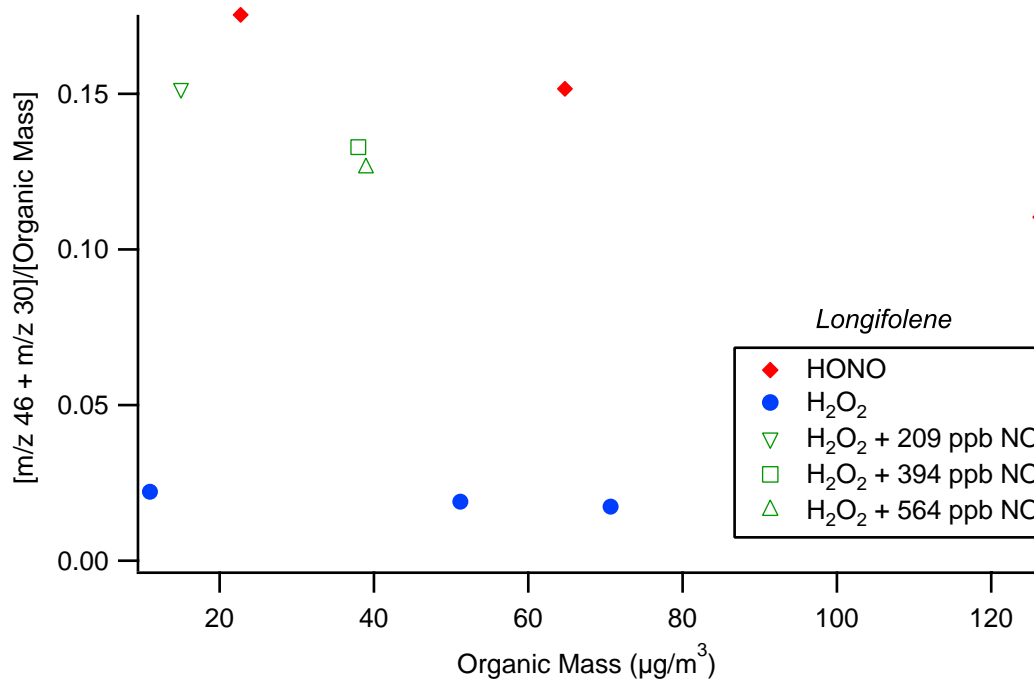


Figure 7. 10. Changes in AMS spectrum over the course of longifolene photooxidation under high- NO_x conditions. Top panel: Fractional contribution of each mass fragment to the total organic and nitrate signal during the growth phase of the experiment. Bottom panel: Percentage change of each mass fragment from the growth phase to the point at which all of the hydrocarbon is consumed.

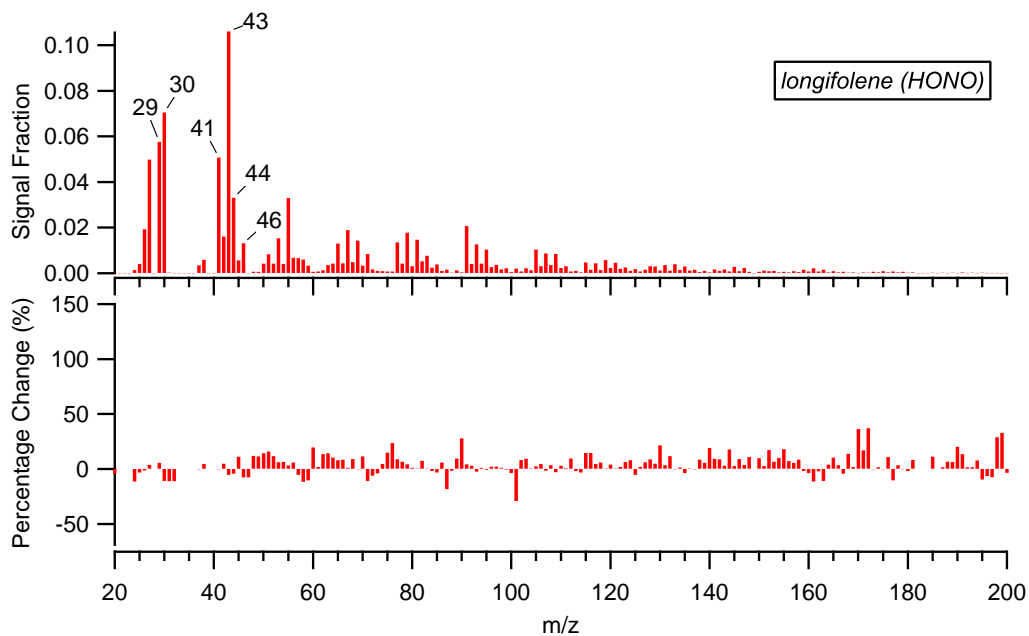


Figure 7. 11. Changes in AMS spectrum over the course of longifolene photooxidation under low-NO_x conditions. Top panel: Fractional contribution of each mass fragment to the total organic and nitrate signal during the growth phase of the experiment. Bottom panel: Percentage change of each mass fragment from the growth phase to the point at which all of the hydrocarbon is consumed.

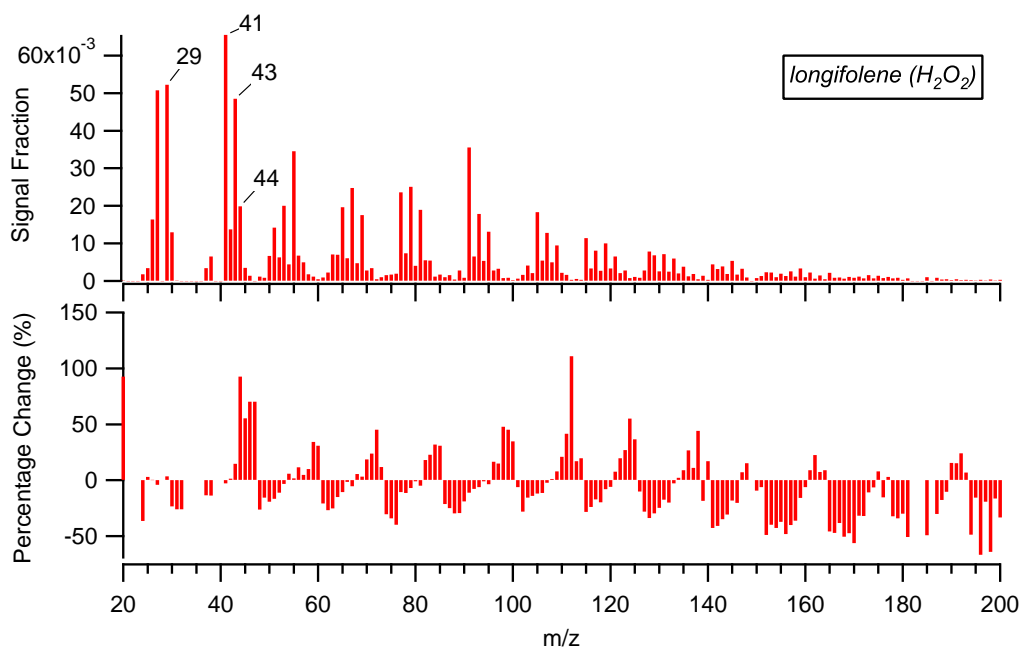


Figure 7. 12. UPLC/ESI-TOFMS extracted ion chromatograms (EICs) ($= m/z$ 346 + 374 + 390) for longifolene photooxidation experiments. The even $[M - H]^-$ ions listed above the chromatographic peaks correspond to organic nitrates detected in longifolene SOA. No organic nitrates are detected in the H_2O_2 experiment. The HONO experiment has the widest array of organic nitrates detected (as shown in Table 7.7), as well as the largest chromatographic peaks; m/z 372 is the only exception, and is most abundant in the " $H_2O_2 + NO$ " experiment. These EICs are directly comparable as the volume of chamber air sampled is approximately the same ($2 m^3$).

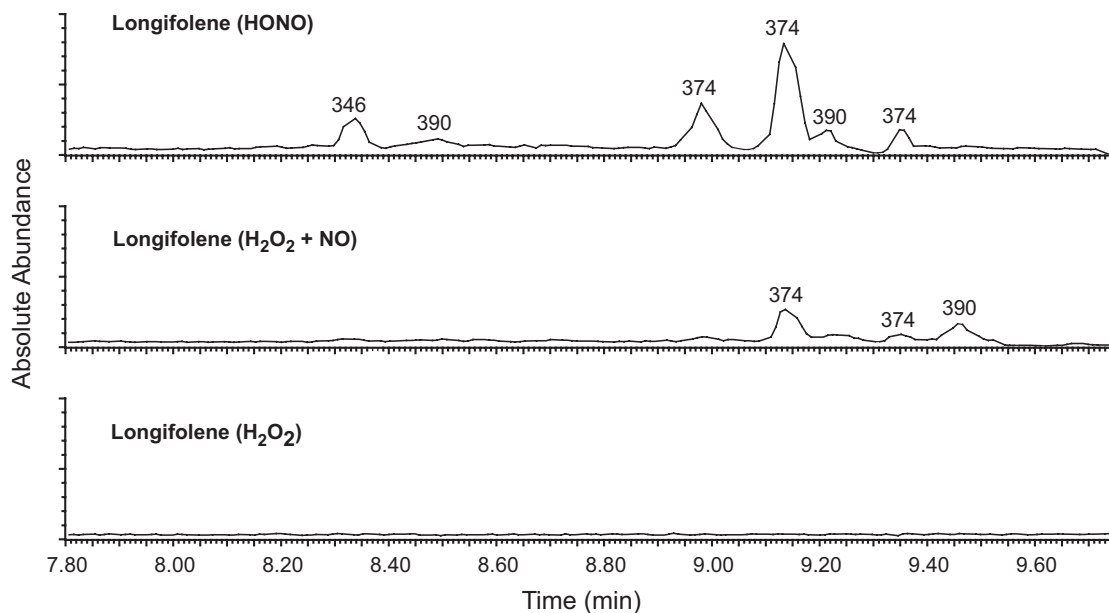


Figure 7. 13. General schematic of gas-phase peroxy radical chemistry in SOA formation.

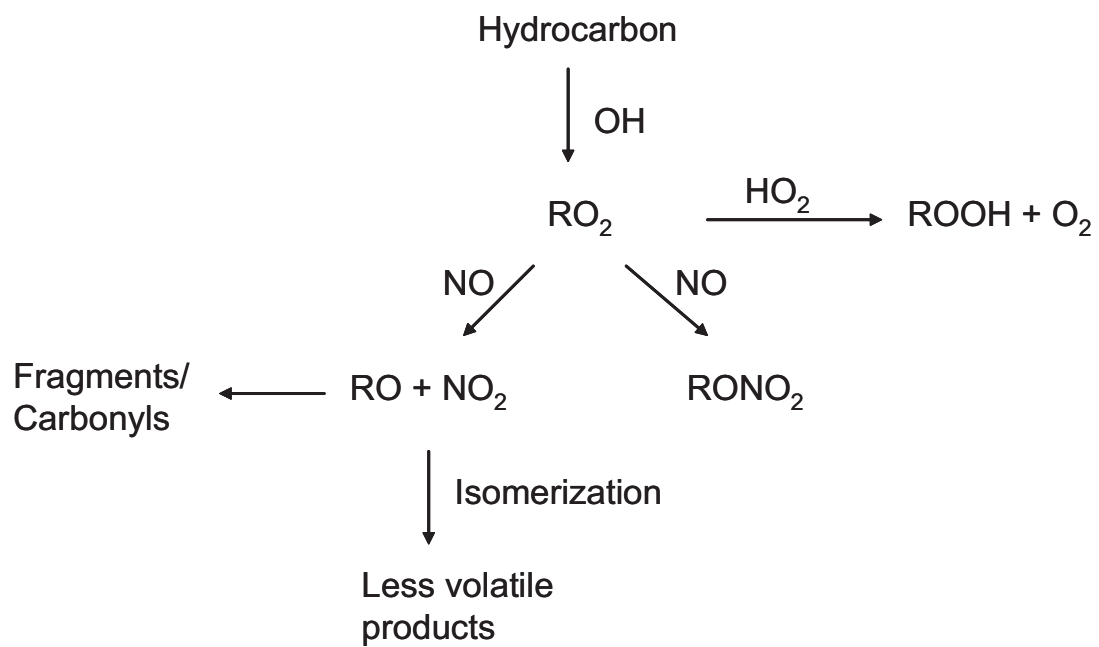
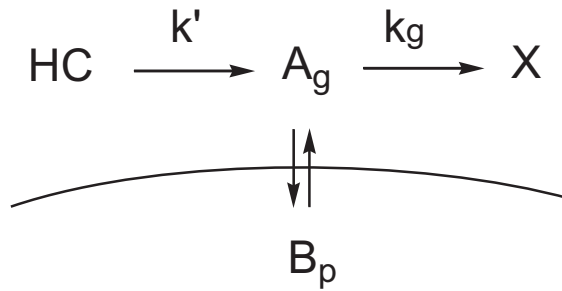


Figure 7. 14. A kinetic scheme depicting the competition between gas-particle partitioning and irreversible loss of the gas-phase semivolatiles. X represents the product of generic loss of semivolatile species A_g by chemical reaction, and/or loss to chamber walls. k' is the pseudo-first-order rate constant ($k' = k_{OH}[OH]$) for photooxidation of the parent hydrocarbon; k_g is the first-order rate constant of loss of semivolatiles.



Chapter 8

Secondary Organic Aerosol Formation from *m*-Xylene, Toluene, and Benzene*

*This chapter is reproduced by permission from “Secondary organic aerosol formation from *m*-xylene, toluene, and benzene” by N. L. Ng, J. H. Kroll, A. W. H. Chan, P. S. Chhabra, R. C. Flagan, J. H. Seinfeld, *Atmospheric Chemistry and Physics Discussion*, 7, 4085-4126, 2007. © 2007 Author(s). This work is licensed under a Creative Commons License.

8.1 Abstract

Secondary organic aerosol (SOA) formation from the photooxidation of *m*-xylene, toluene, and benzene is investigated in the Caltech environmental chambers. Experiments are performed under two limiting NO_x conditions; under high-NO_x conditions the peroxy radicals (RO₂) react only with NO, while under low-NO_x conditions they react only with HO₂. For all three aromatics studied (*m*-xylene, toluene, and benzene), the SOA yields (defined as the ratio of the mass of organic aerosol formed to the mass of parent hydrocarbon reacted) under low-NO_x conditions substantially exceed those under high-NO_x conditions, suggesting the importance of peroxy radical chemistry in SOA formation. Under low-NO_x conditions, the SOA yields for *m*-xylene, toluene, and benzene are constant (36%, 30%, and 37%, respectively), indicating that the SOA formed is essentially nonvolatile. Under high-NO_x conditions, aerosol growth occurs essentially immediately, even when NO concentration is high. The SOA yield curves exhibit behavior similar to that observed by Odum et al. (1996, 1997ab), although the values are somewhat higher than in the earlier study. The yields measured under high-NO_x conditions are higher than previous measurements, suggesting a “rate effect” in SOA formation, in which SOA yields are higher when the oxidation rate is faster. Experiments carried out in the presence of acidic seed aerosol reveal no change of SOA yields from the aromatics as compared with those using neutral seed aerosol.

8.2 Introduction

Aromatic hydrocarbons contribute an important fraction (~20–30%) of total volatile organic compounds in the urban atmosphere (Calvert et al., 2002). Atmospheric oxidation of aromatic hydrocarbons leads to the production of ozone as well as low-

volatility species which then partition into the condensed phase, forming secondary organic aerosol (SOA).

The anthropogenic contribution to global SOA formation is currently estimated to be small, roughly about 10% (Tsigaridis and Kanakidou, 2003). Ambient measurements suggest that SOA formation in the atmosphere is higher than that predicted by current models (Heald et al., 2005, 2006; de Gouw et al., 2005; Volkamer et al., 2006). In addition, it has been suggested that SOA formation from anthropogenic sources is substantially higher than currently thought (de Gouw et al., 2005; Volkamer et al., 2006).

Gas-phase chemistry of aromatic hydrocarbons is dominated by reaction with the OH radical (Calvert et al., 2002). Despite considerable study of the oxidation chemistry of aromatic hydrocarbons, the basic underlying mechanisms of SOA formation and growth from aromatic precursors remain poorly understood. There have been few studies on the molecular composition of SOA from aromatic hydrocarbons (Forstner et al., 1997; Jang and Kamens, 2001; Kleindienst et al., 2004). The carbon balance is poorly constrained; generally, only about 50% of the reacted carbon has been identified as products (Calvert et al., 2002).

SOA formation from individual precursors is typically studied in laboratory chamber experiments. Aerosol yields from the photooxidation of aromatic hydrocarbons have been shown to be highly sensitive to the NO_x level (Hurley et al., 2001; Johnson et al., 2004, 2005; Song et al., 2005); generally, a higher SOA yield is observed under low-NO_x conditions. This general dependence of SOA formation on the NO_x level has been proposed to be the result of differences in concentrations of different oxidants (OH, O₃, and NO₃) (Hurley et al., 2001), or in changes in peroxy radical chemistry (Hatakeyama et

al., 1991; Johnson et al., 2004, 2005; Presto et al., 2005; Kroll et al., 2006). In addition, particle-phase reactions have been found to be important processes in SOA formation (Kalberer et al., 2004; Gao et al., 2004ab; Tolocka et al., 2004), and the presence of sulfuric acid seed has been shown to lead to increased SOA yields in a number of systems (Jang et al., 2002; Iinuma et al., 2004; Gao et al., 2004ab; Edney et al., 2005). Odum et al. (1996, 1997ab) performed an extensive study on aromatic SOA formation. In light of the recent findings on the NO_x dependence and effect of seed aerosol acidity on SOA yields, it is important that SOA formation from aromatics be restudied to establish fully the NO_x dependence and effect of particle acidity on SOA formation.

Most chamber experiments of SOA formation by aromatics involve the irradiation of aromatic/ NO_x mixtures (Izumi and Fukuyama, 1990; Odum et al., 1996, 1997ab; Hurley et al., 2001; Johnson et al., 2004; Song et al., 2005). In these classical photooxidation experiments, the NO_x level in the chamber constantly changes, making it difficult to isolate the effect of NO_x on SOA formation. For example, the decreasing NO concentration over the course of the experiment may lead to a switch from “high- NO_x ” conditions to “low- NO_x ” conditions for the peroxy radical chemistry (Johnson et al., 2004). Another potential complication in interpreting SOA data is that a delay in aerosol formation from the onset of photooxidation has been frequently observed in aromatic systems; in particular, aerosol does not form until the concentration of NO approaches zero. When extrapolating to urban areas where the NO_x level is usually high, this would suggest that aromatics (and other hydrocarbons) do not produce SOA in the atmosphere. The observation that SOA does not form until [NO] approaches zero is not universal, however; in a study of toluene photooxidation by Stroud et al. (2004), aerosol growth is

observed even at NO concentrations of 1–3 ppm. Thus the NO_x dependence of SOA yields, which is a crucial parameter for atmospheric modeling, is very poorly understood.

In this work, SOA formation from the photooxidation of *m*-xylene, toluene, and benzene is investigated. A main goal of this study is to establish the NO_x dependence of SOA formation for these aromatic hydrocarbons. In the experiments, SOA formation under two NO_x conditions is studied: (1) high-NO_x experiments in which HONO is used as the OH precursor and the initial NO_x is ~1 ppm; and (2) low-NO_x experiments in which H₂O₂ is used as the OH precursor and the initial NO_x is < 1 ppb. By performing experiments at these extreme NO_x limits, the oxidation conditions (initiating oxidant and fate of peroxy radicals) can be maintained relatively constant over the course of the experiment, allowing for the evaluation of the effect of NO_x level on SOA formation. Additionally, the effect of seed aerosol acidity on SOA formation is studied under both high- and low-NO_x conditions. The SOA yield parameters obtained at the two NO_x limits allow one to parameterize the NO_x dependence of SOA formation for use in atmospheric models (Presto et al., 2006).

8.3 Experimental

Experiments are performed in Caltech's indoor, dual 28 m³ Teflon environmental chambers. Details of the facilities have been given elsewhere (Cocker et al., 2001; Keywood et al., 2004). Before each experiment, the chambers are flushed continuously with dry purified air for ~24 h. Each chamber has a dedicated Differential Mobility Analyzer (DMA, TSI model 3081) coupled with a condensation nucleus counter (TSI model 3760) for measuring aerosol size distribution, number concentration, and volume concentration. All aerosol growth data are corrected for wall loss, in which size-

dependent coefficients determined from inert particle wall loss experiments are applied to the aerosol volume data (Keywood et al., 2004). Temperature, relative humidity (RH), O₃, NO, and NO_x are continuously monitored. Half of the available black lights are used in the experiments. The initial temperature of the experiment is 20°C; over the course of an experiment, heating from the lights leads to a temperature increase of ~5°C inside the chambers.

Seed particles are introduced into the chamber to act as a substrate onto which the gas-phase products may condense. In an earlier work, we have shown that without seed particles, there is an “induction period” in which hydrocarbon is reacted but no aerosol is formed, which has the effect of biasing SOA yield measurements low (Kroll et al., 2007). Therefore, for all experiments in this study seed particles are used to eliminate this effect. Seed particles are generated by atomizing an aqueous solution with a constant-rate atomizer. The nonacid seed consists of 0.015 M (NH₄)₂SO₄, while the acidic seed contains a mixture of 0.015 M (NH₄)₂SO₄ and 0.015 M H₂SO₄. Since all experiments are performed at RH~5%, which is lower than the crystallization RH (35%) of ammonium sulfate, the nonacid seed is likely a solid (Seinfeld and Pandis, 2006). The initial particle number concentration is about 30,000 particles cm⁻³, with a geometric mean diameter of about 50 nm. Initial aerosol seed volume is about 15 μm³ cm⁻³. After introduction of the seed aerosol, a known volume of the parent hydrocarbon is injected into a glass bulb, and introduced into the chambers by an air stream. The concentration (mixing ratio) of the parent hydrocarbon is monitored with a Hewlett Packard gas chromatograph (model 5890) with flame ionization detection (GC-FID).

In most of the high-NO_x experiments nitrous acid (HONO) serves as the OH precursor. It is introduced into the chamber after injection of the seed aerosol and parent hydrocarbon. HONO is prepared by dropwise addition of 15 mL of 1% NaNO₂ into 30 mL of 10% H₂SO₄ in a glass bulb. The bulb is then attached to the chamber and a stream of dry air is passed through the bulb into the chamber. NO and NO₂, formed as side products in the preparation of HONO, are also introduced into the chamber, and are measured by a commercial NO_x monitor (Horiba APNA-360, Irvine, CA). Additional NO from a 500 ppm gas cylinder (Scott Marrin, Inc.) is introduced into the chamber after the addition of HONO to achieve a total NO_x level in the chamber of about 1 ppm (detection limit of the NO_x monitor). In some high-NO_x experiments, only NO and NO₂ (from gas cylinders) are added to the chamber. To differentiate these experiments from the high-NO_x experiments in which HONO is used as the OH precursor, we refer to these experiments as classical photooxidation experiments. The majority of the high-NO_x experiments in this study are performed with HONO; only a few classical photooxidation experiments are performed for comparison purposes.

For low-NO_x experiments, H₂O₂ is used as the OH precursor. The background NO_x level in the chamber during the experiment is < 1 ppb. H₂O₂ is introduced into the chamber (prior to introduction of seed particles and parent hydrocarbon) by bubbling air through a 50% H₂O₂ solution for 2.5 h at 5 L/min. The air stream then passes through a particle filter to remove any droplets. The concentration of H₂O₂ in the chamber is not measured; based on the rate of hydrocarbon decay we estimate [H₂O₂] to be ~3–5 ppm (Kroll et al., 2006).

Once the seed, parent hydrocarbon, and NO_x concentrations stabilize, reaction is initiated by irradiating the chamber with blacklights. Output from the lights is between 300 and 400 nm, with a maximum at 354 nm. At these wavelengths HONO efficiently photolyzes to OH and NO. By contrast H₂O₂ absorbs only weakly in this wavelength range, requiring the use of ppm concentrations of H₂O₂ to achieve reasonable levels of OH.

The parent aromatics studied (shown in Table 8.1) and their stated purities are as follows: *m*-xylene (Aldrich, anhydrous, 99+%), toluene (Aldrich, anhydrous, 99.8%), and benzene (Aldrich, anhydrous, 99.8%). Experimental conditions and results for high-NO_x and low-NO_x experiments are given in Tables 8.2 and 8.3, while those for studying the effect of seed acidity on SOA growth are given in Table 8.4. In calculating SOA yield (defined as the ratio of the mass of organic aerosol formed to the mass of parent hydrocarbon reacted), knowledge of the SOA density is required. By comparing volume distributions from the DMA and mass distributions from an Aerodyne quadrupole Aerosol Mass Spectrometer (AMS), the effective densities for the SOA formed can be estimated (Bahreini et al., 2005). The estimated densities of the SOA formed from different systems are given in Table 8.5.

8.4 Results

8.4.1 High-NO_x conditions

Figure 8.1 shows a typical reaction profile under high-NO_x conditions in which HONO is used as the OH precursor. In this experiment, 89 ppb of *m*-xylene is reacted, and initial NO and NO₂ concentrations are 470 ppb and 473 ppb, respectively. The efficient photolysis of HONO generates high concentrations of OH ($\sim 3 \times 10^7$ molecules

cm⁻³ initially), leading to a rapid hydrocarbon decay. This decay slows down after ~1 h, suggesting that the HONO is consumed and OH radicals are instead generated through recycling via NO_x/HO_x chemistry. Aerosol growth occurs essentially immediately, even when [NO] is high (100's of ppb). With the high NO concentration, formation of ozone (and hence NO₃ radicals) is suppressed.

Concentration (mixing ratio) profiles from two classical photooxidation experiments with different initial NO_x concentrations are shown in Fig. 8.2. Figure 8.2 (a) shows the reaction profile from the photooxidation of 101.6 ppb *m*-xylene, with initial NO and NO₂ concentrations of 97 ppb and 26 ppb, respectively. The hydroxyl radical source in classical photooxidation experiments is likely from the photolysis of HONO, which is formed from the heterogeneous reaction of NO₂ on the chamber wall. The *m*-xylene-OH reaction leads to formation of RO₂ radicals, which react with NO rapidly, converting NO to NO₂. Ozone is formed from the photolysis of NO₂, with its concentration increasing rapidly when [NO] falls below ~50 ppb. Only when the NO concentration approaches zero does aerosol growth begin, consistent with other classical photooxidation experiments (Izumi and Fukuyama, 1990; Hurley et al., 2001; Johnson et al., 2004; Martin-Reviejo and Wirtz, 2005; Song et al., 2005). The difference between high-NO_x experiments and classical photooxidation experiments will be discussed in Section 8.5.2. Figure 8.2 (b) shows the reaction profile for the photooxidation of 94.8 ppb *m*-xylene, with initial NO and NO₂ concentrations of 878 ppb and 65 ppb, respectively. The NO concentration decreases over the course of the experiment, but does not fall below 100 ppb, even after 20 h. A negligible amount of ozone is formed during the experiment, and no SOA is formed.

For *m*-xylene and toluene, a series of high-NO_x experiments (HONO experiments) with varying initial hydrocarbon concentrations are carried out. The time-dependent “growth curves” (organic aerosol ΔM_o as a function of hydrocarbon reacted ΔHC) over the course of the experiment, for four *m*-xylene experiments, with initial hydrocarbon concentrations ranging from 42 to 172 ppb, are shown in Fig. 8.3. In these experiments, 67–79% of the initial *m*-xylene is consumed. Most of the parent hydrocarbon is consumed in the first hour and the maximum aerosol yield is reached. After that hydrocarbon continues to decay slowly and there is little or no SOA growth, as a result the aerosol yield decreases. Only SOA growth data up to the maximum aerosol yield are shown.

The time-dependent growth curves for four toluene experiments are shown in Fig. 8.4. The initial toluene concentration ranges from 88 to 270 ppb. Since the toluene-OH reaction rate constant is ~4 times lower than that of *m*-xylene-OH, more initial toluene is needed relative to *m*-xylene; only about 30–37% of the initial toluene injected is consumed at the point of maximum aerosol yield. Photooxidation of toluene under high-NO_x conditions results in slightly more SOA growth than for *m*-xylene.

Because benzene reacts slowly with OH radicals ($k = 1.22 \times 10^{-12} \text{ cm}^3 \text{ molecule}^{-1} \text{ s}^{-1}$, Calvert et al., 2002), it is not feasible to carry out photooxidation experiments over a range of initial benzene concentrations unless high levels (ppm) of benzene are used. Thus only a single benzene photooxidation experiment at high NO_x was carried out; at an initial benzene concentration of 337 ppb, only 12% is reacted at the point of maximum aerosol yield. The time-dependent growth curve from benzene under high-NO_x conditions (as well as under low-NO_x conditions) is shown in Fig. 8.5.

8.4.2 Low-NO_x conditions

Under low-NO_x conditions, aerosol growth is observed immediately after initiation of irradiation. The parent hydrocarbon decays at a much slower rate than under high-NO_x conditions, due to the slow production of OH radicals by H₂O₂ photolysis and lack of OH regeneration by NO_x/HO_x cycling. As OH radicals are continually produced, the OH concentration is constant throughout the experiment ($\sim 3 \times 10^6$ molecules cm⁻³). Ozone formation of ~ 10 – 15 ppb is observed, possibly owing to residual material released from the chamber walls.

Time-dependent growth curves for four *m*-xylene low-NO_x experiments are shown in Fig. 8.6, with initial *m*-xylene concentrations ranging from 9 to 37 ppb. About 83–89% of the initial hydrocarbon injected is consumed at the point at which the SOA yield reaches its maximum. From Fig. 8.6 it is clear that the SOA yield from *m*-xylene photooxidation is constant under low-NO_x conditions, at 36%. Since the *m*-xylene SOA yield is much higher under low-NO_x conditions, a smaller amount of initial parent hydrocarbon is needed to produce the same amount of SOA than under high-NO_x conditions. Comparable time-dependent growth curves for four toluene low-NO_x experiments are shown in Fig. 8.7. The initial toluene concentration ranges from 21 to 140 ppb. With the slower reactivity of toluene relative to *m*-xylene, only about 45–48% of the initial toluene is consumed. As with *m*-xylene, the aerosol yield (30%) is substantially higher than under high-NO_x conditions.

The time-dependent growth curve for benzene photooxidation is shown in Fig. 8.5. Similar to *m*-xylene and toluene, benzene photooxidation under low-NO_x conditions results in a constant SOA yield (37%).

8.4.3 SOA yield parameters

SOA yield has traditionally been described by a semi-empirical model based on absorptive gas-particle partitioning of two semivolatile products (Odum et al., 1996, 1997ab):

$$Y = \Delta M_o \left[\frac{\alpha_1 K_{om,1}}{1 + K_{om,1} M_o} + \frac{\alpha_2 K_{om,2}}{1 + K_{om,2} M_o} \right] \quad (8.1)$$

in which Y is the aerosol yield, ΔM_o is the organic aerosol mass produced, M_o is the organic aerosol mass present (equal to ΔM_o in chamber experiments with no absorbing organic mass present initially), α_i is the mass-based gas-phase stoichiometric fraction for semivolatile species i , and $K_{om,i}$ is the gas-particle partitioning coefficient for species i . With this two-product model, Eq. (1) can be fit to experimental yield data to determine values for α_i and $K_{om,i}$, and the resulting plot (Y versus M_o) is generally referred to as a “yield curve”.

For *m*-xylene and toluene, the final SOA yield for each high-NO_x (HONO) experiment is calculated, and the data are fitted to Eq. (1) to obtain the SOA yield parameters. The high-NO_x yield curves for *m*-xylene and toluene are shown in Fig. 8.8. For all three aromatics (*m*-xylene, toluene, and benzene), the low-NO_x experiments result in a constant aerosol yield (the slope of the “growth curve”), implying the SOA formed can be represented by a single product with very low volatility. Under these conditions the yield curve is simply a horizontal line, and the constant yield corresponds to α_1 in Eq. (1). SOA growth parameters for the three compounds under high-NO_x and low-NO_x conditions are summarized in Table 8.6.

8.4.4 Acid/nonacid seed experiments

Several *m*-xylene and toluene photooxidation experiments are performed in the presence of acid seed to study the effect of seed acidity on SOA growth. The nonacid seed consists of 0.015 M (NH₄)₂SO₄ while the acid seed contains 0.015 M (NH₄)₂SO₄ and 0.015 M H₂SO₄. The nonacid seed is solid since the experiments are performed under dry conditions (RH~5%). The pH of the acid seed is calculated with two aerosol thermodynamic models, the Aerosol Inorganic Model II (AIM) and ISORROPIA (<http://mae.ucdavis.edu/~sclegg/aim.html>; <http://nenes.eas.gatech.edu/ISORROPIA/>). The lowest RH specified in AIM is 10%, therefore this value is used as the input rather than the actual RH at which the experiments were performed (~5%). The pH calculated by AIM is -1.7. For ISORRPIA, the “reverse” model (assume aerosol-phase concentrations are known) gives a pH of 1.5, while the “forward” model (assume total (i.e. gas + aerosol) concentrations are known) gives a pH of 1.7. The large difference in the pH values calculated by the two models is likely a result of the uncertainty of the calculation at the high ionic strength corresponding to low RH.

Growth curves for toluene photooxidation under acidic and nonacid conditions are shown in Fig. 8.9. Regardless of the NO_x level, the time-dependent growth curves from the acid and nonacid experiments are essentially indistinguishable. Therefore, there is no evidence that the presence of acidic seed enhances SOA growth in the photooxidation of toluene; similar results are observed for *m*-xylene.

8.5 Discussion

8.5.1 Effect of NO_x on SOA yields

Experiments have been performed under two limiting NO_x conditions: (1) high-NO_x experiments in which HONO is used as the OH precursor; and (2) low-NO_x experiments in which H₂O₂ is used as the OH precursor. For all hydrocarbons, considerably more SOA is formed under low-NO_x than high-NO_x conditions (Fig. 8.3–7). Under high-NO_x conditions, the SOA yields from *m*-xylene and toluene photooxidation are about 10%; they are 36% and 30%, respectively, under low-NO_x conditions. Similar NO_x dependences have been observed in other SOA-forming systems (Hatakeyama et al., 1991; Zhang et al., 1992; Hurley et al., 2001; Johnson et al., 2004; Song et al., 2005; Presto et al., 2005; Kroll et al., 2006). Since O₃ and NO₃ are not formed appreciably under either set of conditions, oxidation is dominated by OH radicals for all experiments, so this NO_x effect cannot be a result of differences in relative oxidant levels (Hurley et al., 2001). Instead the NO_x level likely governs the fate of the organic peroxy radicals formed subsequent to the hydrocarbon-OH reaction, which in turn controls the volatility of molecular products and hence the amount of SOA formed.

Shown in Fig. 8.10 is the simplified mechanism of the initial steps of toluene-OH reaction, leading to the formation of condensable products. One mechanism by which NO_x levels may affect the products formed in the oxidation of aromatic hydrocarbons is by reaction with the aromatic-OH adduct. Under atmospheric conditions, such radicals react with O₂, but under very high levels of NO_x (as is often the case in chambers), the adduct + NO₂ reaction increases in importance, leading to nitrogen-containing ring-retaining products such as nitrobenzene and nitrotoluene (Atkinson et al., 1989; Atkinson

and Aschmann, 1994). In the current work, photooxidation of *m*-xylene and toluene is carried out in the presence of ~500 ppb each of NO and NO₂; while for photooxidation of benzene the initial NO₂ concentration is <100 ppb. At these NO_x levels, the reaction of the aromatic-OH adduct with NO₂ is not expected to be significant, so such reactions cannot be responsible for the observed effect of NO_x on SOA yield (Volkamer et al., 2002; Koch et al., 2006).

Reaction of the aromatic-OH adduct with O₂ results in the formation of peroxy radicals. Theoretical studies have shown that the peroxy radicals preferentially cyclize to form bicyclic radicals, which then react with O₂ to form bicyclic peroxy radicals (Andino et al., 1996; Lay et al., 1996; Suh et al., 2003; Fan et al., 2006). As is typical for RO₂ radicals, the fate of the bicyclic peroxy radicals depends mainly on the relative concentrations of NO, HO₂, and RO₂. At the two limiting NO_x conditions of this study, the peroxy radical chemistry is straightforward; under high-NO_x conditions, RO₂ reacts virtually entirely with NO, as NO concentration is high throughout the entire experiment, while under low-NO_x conditions, RO₂ reacts predominantly with HO₂. Based on the Master Chemical Mechanism version 3.1 (MCM v 3.1, <http://www.chem.leeds.ac.uk/Atmospheric/MCM/mcmproj.html>), a simple kinetic simulation shows that under low-NO_x conditions, the RO₂ + RO₂ reaction accounts for less than 1% of the RO₂ reacted because of the relative reaction rate constants ($k_{\text{RO}_2+\text{RO}_2} = 8.8 \times 10^{-13} \text{ cm}^3 \text{ molecule}^{-1} \text{ s}^{-1}$, $k_{\text{RO}_2+\text{HO}_2} = 2.3 \times 10^{-11} \text{ cm}^3 \text{ molecule}^{-1} \text{ s}^{-1}$) as well as the high HO₂ concentration. Thus the larger SOA yields obtained under low-NO_x conditions imply that the products formed via the RO₂ + HO₂ partition much more readily into the aerosol phase than those formed via the RO₂ + NO reaction. This conclusion is the same

as that reached by previous studies (Hatakeyama et al., 1991; Johnson et al., 2004, 2005; Presto et al., 2005; Kroll et al., 2006). That SOA yields are constant under low-NO_x conditions implies that the SOA formed by this channel is essentially nonvolatile.

In the classical photooxidation experiments carried out in this study and by other researchers (Izumi and Fukuyama, 1990; Hurley et al., 2001; Johnson et al., 2004; Martin-Reviejo and Wirtz, 2005; Song et al., 2005), an “induction period”, a delay between the onset of oxidation and SOA formation, was observed. This too is a likely result of the role of NO_x in peroxy radical chemistry, and hence in product volatility and SOA formation. As illustrated in Fig. 8.2 (a), only when [NO] approaches zero does aerosol growth commence. As [NO] approaches zero (from the RO₂+NO and HO₂+NO reactions), the RO₂ + HO₂ reaction starts to compete with the RO₂ + NO reaction. The fraction of RO₂ which reacts with HO₂, $k_{\text{RO}_2+\text{HO}_2} [\text{HO}_2] / (k_{\text{RO}_2+\text{NO}} [\text{NO}] + k_{\text{RO}_2+\text{HO}_2} [\text{HO}_2])$, can be calculated based on the rate reaction rate constants ($k_{\text{RO}_2+\text{HO}_2} = 2.3 \times 10^{-11} \text{ cm}^3 \text{ molecule}^{-1} \text{ s}^{-1}$; $k_{\text{RO}_2+\text{NO}} = 8.5 \times 10^{-12} \text{ cm}^3 \text{ molecule}^{-1} \text{ s}^{-1}$) (MCM v 3.1). For instance, at ~1 ppb of NO, it only requires 42 ppt of HO₂ for 10% of the RO₂ to react via RO₂ + HO₂. Thus it is likely that initial SOA formation results from the RO₂ + HO₂ reaction, consistent with the simulations of SOA formation from classical photooxidation experiments of toluene (Johnson et al., 2004). To further study the role of peroxy radical chemistry in the “induction period”, in one of the experiments additional NO was injected after its initial consumption. SOA growth slows down immediately. This provides strong evidence that the presence of NO suppresses the formation of nonvolatile hydroperoxides (and hence further particle-phase reactions of hydroperoxides) from the RO₂ + HO₂ reaction and results in a lower SOA yield (Johnson et al., 2004, 2005).

The time-dependent growth curves for benzene photooxidation under high- and low- NO_x conditions exhibit the same trend as that of *m*-xylene and toluene, in which more SOA is formed under low- NO_x conditions. Martin-Reviejo and Wirtz (2005) studied the formation of SOA from benzene photooxidation under different NO_x conditions. However, as the NO_x dependence of SOA formation was not systematically studied, it is difficult to draw a definite conclusion on the effect of NO_x on SOA yields from their data. Additionally, the experimental conditions are somewhat different; in particular, the experiments in that study were performed in the absence of seed aerosol while in the current work ammonium sulfate seed aerosol is employed. Kroll et al. (2007) find that SOA yields from the photooxidation of aromatic hydrocarbons are lower when inorganic seed particles are not present initially. The absence of seed particles results in a period in which the hydrocarbon is reacted but no aerosol is formed. The length of the “seed induction period” (and hence the amount of hydrocarbon reacted in this period, ΔHC) is likely to be affected by the NO_x levels. Thus the aerosol yields ($\Delta M_o/\Delta\text{HC}$) obtained by Martin-Reviejo and Wirtz (2005) under different NO_x conditions may be affected by this “seed induction period” and cannot be directly compared.

8.5.2 Effect of oxidation rate

In contrast to the classical photooxidation experiments, under high- NO_x conditions, SOA formation is observed even when $[\text{NO}]$ is several hundreds of ppb (Fig. 8.1), suggesting that $\text{RO}_2 + \text{NO}$ reactions can indeed form condensable products. This can be seen directly by comparing Fig. 8.1 (HONO) with Fig. 8.2 (b) (classical). In both cases, the initial *m*-xylene concentration and NO_x concentration are about 100 ppb and 1 ppm, respectively. However, while SOA is formed immediately after photooxidation

commences in the HONO experiment, no SOA growth is observed in the classical photooxidation experiment. HONO photolysis is an efficient source of OH in the wavelength range of our blacklights; thus there is a surge of OH once the lights are turned on, resulting in a rapid rate of *m*-xylene oxidation. In the classical photooxidation experiment, OH is generated mainly from recycling through NO_x and HO_x cycles, and OH concentrations are generally far lower than in the HONO experiments. The large difference between these two cases suggests that SOA yields are dependent on the oxidation rate, with faster oxidation rates resulting in higher SOA yields.

This “rate effect” could arise as a result of loss of semivolatiles through processes other than the simple formation and partitioning of semivolatile organics. The loss of semivolatiles has been proposed as one of the mechanisms for higher SOA yields observed from aromatic photooxidation in the presence of seed aerosols as compared to nucleation experiments (Kroll et al., 2007). In the mechanism shown in Fig. 8.10, X represents the generic non particle-phase product of all gas-phase loss processes. Possibilities include loss of organic species to the chamber walls, photolysis, and further reactions to form volatile products. With a rapid oxidation rate, the gas-phase concentration of semivolatiles increases quickly, and the high concentrations of semivolatiles ensure that aerosol growth ensues even in the presence of semivolatile loss processes (i.e. paths not forming SOA). On the other hand, the slower formation of semivolatiles in the presence of semivolatile sinks leads to less SOA growth. If the dominant loss of semivolatiles is deposition to the chamber walls, then conditions in which the effect of wall loss is minimized (i.e., when the reaction is fastest) are expected to be most representative of atmospheric SOA formation.

The observed formation of SOA under high-NO_x conditions is consistent with the study by Stroud et al. (2004), in which the photooxidation of toluene resulted in SOA growth despite the high NO concentration throughout the experiment. According to the simulations by Johnson et al. (2004), the ppm level of NO_x employed by Stroud et al. (2004) should entirely suppress SOA formation. The rate effect could resolve this discrepancy: the use of isopropyl nitrite as an OH source in the study by Stroud et al. (2004) facilitates a rapid oxidation rate of toluene, leading to SOA formation despite the presence of high levels of NO. This suggests a missing sink of semivolatiles (possibly wall loss) in the detailed simulations of Johnson et al. (2004).

The rate effect also can explain higher SOA yields in the high-NO_x experiments (HONO) compared to the classical photooxidation experiments (Odum et al., 1996) (Fig. 8.11). Several classical photooxidation experiments with similar NO_x levels as in Odum et al. (1996) were performed in the present study, with SOA yields comparable to those of Odum et al. (1996). The yield curve from Odum et al. (1996) has been adjusted based on the temperature (25°C) and SOA density (1.48 g cm⁻³) obtained in this study. The NO_x concentrations (several hundreds of ppb) used by Odum et al. (1996) are lower than those in the current experiments (~1 ppm). The higher SOA yields obtained here suggest that the enhancement in SOA yield from a faster oxidation rate is greater than the suppression in SOA yield at a higher NO_x concentration. This competition between the NO_x effect and the rate effect may also explain the observed maximum in SOA yields as a function of NO_x from isoprene photooxidation (Kroll et al., 2006).

The pair of experiments (Fig. 8.1 and Fig. 8.2 (b)) also provides insight into the extent to which the hydrocarbon/NO_x (HC/NO_x) ratio characterizes the NO_x level in

chamber experiments. Song et al. (2005), for example, report a series of classical photooxidation experiments to study the effect of HC/NO_x ratio on SOA formation from *m*-xylene. It was found that aerosol yields increase with increasing HC/NO_x ratio (i.e. more aerosol growth at lower NO_x levels), which is consistent with the present study. However, the experiments in Fig. 8.1 and 8.2 (b) have essentially similar HC/NO_x ratios but exhibit very different SOA growth. Therefore, while the HC/NO_x ratio may be a useful metric for photochemistry for experiments with similar oxidation conditions, it is less useful when comparing systems with very different oxidative conditions, as both oxidation rate and fate of peroxy radicals may differ. Given the importance of the peroxy radical in SOA formation, the NO/HO₂ ratio would be the more appropriate measure of different NO_x levels (Kroll et al., 2006), although continuous measurement of HO₂ is not currently feasible.

8.5.3 General mechanism of SOA formation

Despite uncertainties in the detailed chemical mechanism of aromatic photooxidation beyond the initial peroxy radical chemistry, we can gain insights into the general SOA formation mechanism and growth kinetics from the shapes of the growth curves under both high-NO_x and low-NO_x conditions (Fig. 8.3–7). Such curves allow for the identification of the rate-determining steps in SOA formation (Ng et al., 2006). In cases where the initial oxidation step determines the rate of SOA formation (condensable products are first-generation, or are formed extremely rapidly after the initial oxidation), SOA is formed at the same rate of hydrocarbon oxidation, and aerosol growth ceases once the parent hydrocarbon is consumed. In this case, time-dependent growth-curves from experiments with different initial hydrocarbon concentrations would overlap, as is

the case for α -pinene ozonolysis (Ng et al., 2006). On the other hand, when there are further rate-limiting steps to the formation of condensable products, there is a time lag between hydrocarbon oxidation and SOA formation and the growth curve exhibits a vertical section at the end, as is the case for the ozonolysis and photooxidation of compounds with multiple double bonds (Ng et al., 2006).

Figures 8.3–7 show the time-dependent growth curves for *m*-xylene, toluene, and benzene photooxidation under high-NO_x and low-NO_x conditions. In all cases, SOA growth is observed immediately after photooxidation commences, resulting in a smooth growth curve from the onset of oxidation. Some hydrocarbon remains unreacted by the end of these experiments. In experiments in which all the hydrocarbon is reacted (not shown), no vertical section in the growth curve is observed, indicating there is no further SOA formation after the complete consumption of the parent hydrocarbon. This indicates that the first oxidation step (oxidation of the parent hydrocarbon) governs the rate of SOA formation.

However, unlike with α -pinene ozonolysis (Ng et al., 2006), the time-dependent growth curves from experiments with different initial aromatic hydrocarbon concentrations do not overlap, and aerosol growth is not the same for a given amount of hydrocarbon reacted (ΔHC). Instead, SOA growth at a given value of ΔHC depends on the initial hydrocarbon concentration (HC_0): experiments with higher HC_0 reach a given ΔHC in a shorter time than those with smaller HC_0 . At smaller HC_0 , during the longer time required to reach ΔHC , the first generation products have more time to be converted to SOA. Therefore, the divergence in growth curves at different initial hydrocarbon concentrations indicates that even though the first step is the rate-limiting in SOA

formation, subsequent oxidation steps also occur prior to SOA formation. While such steps affect the kinetics of SOA formation somewhat (i.e., they are not instantaneous relative to the initial step), the small differences in growth curves at different values of HC_0 indicate they are substantially faster than the initial oxidation step. The degree of divergence in growth curves is not as pronounced for low- NO_x experiments, suggesting that this difference in rates is greater under low- NO_x than high- NO_x conditions. The formation of SOA by multiple oxidation steps, in which the later steps are substantially faster than the initial oxidation, is consistent with available kinetic data and current understanding of the photooxidation of aromatic hydrocarbons. In general, first-generation products of aromatic photooxidation react about an order of magnitude faster with OH than do their parent hydrocarbons (Calvert et al., 2002). For example, whereas the benzene-OH rate constant is $1.22 \times 10^{-12} \text{ cm}^{-3} \text{ molecule}^{-1} \text{ s}^{-1}$, the rate constant of the reaction of OH with phenol, a major first-generation reaction product, is $2.7 \times 10^{-11} \text{ cm}^{-3} \text{ molecule}^{-1} \text{ s}^{-1}$ (Calvert et al., 2002).

8.5.4 Effect of seed acidity

To our knowledge, there are no published data on the effect of seed aerosol acidity on SOA formed from the photooxidation of aromatic VOCs. As shown in Fig. 8.9, seed particle acidity does not enhance the SOA yield under different NO_x conditions. The composition of the acid and nonacid seed particles, as well as the RH ($\sim 5\%$), are the same as those previously employed in the study of isoprene SOA formation (Surratt et al., 2007); yet, an enhancement in SOA yield is observed for isoprene experiments but not for the aromatics. The chambers are maintained at RH $\sim 5\%$ in this study and so the nonacid seed particles are dry, whereas for acidic seed particles some water might be

present. If aerosol water is essential for the acidity effect, its absence might explain the lack of an observed effect in the current study. The dependence of SOA growth on RH is beyond the scope of this work but warrants future investigation.

8.6 Implication for SOA growth from aromatic hydrocarbons

We report a series of chamber experiments investigating the NO_x dependence and effect of seed aerosol acidity on SOA formation from the photooxidation of aromatic compounds. High- NO_x experiments are performed with HONO as the OH precursor at initial NO_x of ~ 1 ppm. By performing experiments with HONO, SOA is formed under truly high- NO_x conditions, as the NO concentration remains high throughout the entire experiment. In low- NO_x experiments, H_2O_2 is used as the OH precursor and the initial NO_x is < 1 ppb. For each of the aromatic hydrocarbons studied (*m*-xylene, toluene, and benzene), the SOA yields under low- NO_x conditions are significantly larger than those under high- NO_x conditions; this is likely a result of the competition between $\text{RO}_2 + \text{NO}$ and $\text{RO}_2 + \text{HO}_2$ reactions, similar to what has been observed in other studies (Hatakeyama et al., 1991; Johnson et al., 2004, 2005; Presto et al., 2005; Kroll et al., 2006).

In assessing the contribution of aromatic compounds to total ambient SOA, it is important that laboratory conditions are representative of those in the atmosphere. The aromatic SOA yield parameters (α_i and $K_{\text{om},i}$) currently employed in atmospheric models are those obtained by Odum et al. (1996, 1997ab) almost a decade ago by irradiation of hydrocarbon/ NO_x mixtures. With the profound dependence of NO_x on SOA formation, it is necessary that the effect of NO_x on SOA yields be included in atmospheric models. For instance, compounds like benzene are mainly emitted in source-rich regions; with its

slow reactivity, however, benzene can be transported to areas with a lower NO_x level before it react substantially, resulting in a higher SOA yield than if it reacted in the immediate vicinity of its sources. By performing experiments at two extreme NO_x conditions, we are able to obtain SOA yield parameters under high- and low- NO_x conditions, allowing for the parameterization of the NO_x dependence for atmospheric models, based upon the reactivity of organic peroxy radicals.

Finally, detailed analysis of the chemical composition of aromatic SOA will assist in unraveling the detailed aromatic SOA formation mechanism under both high and low- NO_x conditions. In a forthcoming publication, the chemical composition of aromatic SOA will be explored. Since a wide array of sulfate esters are observed only when acidified inorganic seed aerosols are employed (Surratt et al., 2007), the chemical composition of the SOA formed in nonacid/acid seed experiments may also provide insights into the lack of a seed acidity effect on SOA yields in the present study.

8.7 Acknowledgements

This research was funded by the U. S. Environmental Protection Agency Science to Achieve Results (STAR) Program grant number RD-83107501-0, managed by EPA's Office of Research and Development (ORD), National Center for Environmental Research (NCER), and by U.S. Department of Energy Biological and Environmental Research Program DE-FG02-05ER63983. The authors would like to thank Athanasios Nenes and Simon Clegg for helpful discussions on the pH calculations.

8.8 References

- Andino, J. M., Smith, J. N., Flagan, R. C., Goddard III, W. A., and Seinfeld, J. H.: Mechanism of atmospheric photooxidation of aromatics: A theoretical study, *J. Phys. Chem.*, 100, 10967-10980, 1996.
- Atkinson, R., Aschmann, S. M., Arey, J., and Carter, W. P. L.: Formation of ring-retaining products from the OH radical-initiated reactions of benzene and toluene, *Int. J. Chem. Kinet.*, 21, 801-827, 1989.
- Atkinson R, and Aschmann, S. M.: Products of the gas-phase reactions of aromatic hydrocarbons: effect of NO₂ concentration, *Int. J. Chem. Kinet.*, 26, 929-944, 1994.
- Bahreini, R., Keywood, M. D., Ng, N. L., Varutbangkul, V., Gao, S., Flagan, R. C., Seinfeld, J. H.: Measurements of secondary organic aerosol (SOA) from oxidation of cycloalkenes, terpenes, and m-xylene using an Aerodyne aerosol mass spectrometer, *Environ. Sci. Technol.*, 39, 5674-5688, 2005.
- Calvert, J. G., Atkinson, R., Becker, K. H., Kamens, R. M., Seinfeld, J. H., Wallington, T. J., and Yarwood, G.: *The Mechanisms of Atmospheric Oxidation of Aromatic Hydrocarbons*, Oxford University Press, New York, 2002.
- Cocker III, D. R., Flagan, R. C., Seinfeld, J. H.: State-of-the-art chamber facility for studying atmospheric aerosol chemistry, *Environ. Sci. Technol.*, 35, 2594-2601. 2001.
- de Gouw, J. A., Middlebrook, A. M., Warneke, C., Goldan, P. D., Kuster, W. C., Roberts, J. M., Fehsenfeld, F. C., Worsnop, D. R., Canagaratna, M. R., Pszenny, A. A. P., Keene, W. C., Marchewka, M., Bertman, S. B., and Bates, T. S.: Budget of organic

- carbon in a polluted atmosphere: Results from the New England Air Quality Study in 2002, *J. Geophys. Res.*, 110, D16305, doi: 10.1029/2004JD005623, 2005.
- Edney, E. O., Kleindienst, T. E., Jaoui, M., Lewandowski, M., Offenberg, J. H., Wang, W., Claeys, M.: Formation of 2-methyl tetrols and 2-methylglyceric acid in secondary organic aerosol from laboratory irradiated isoprene/NO_x/SO₂/air mixtures and their detection in ambient PM_{2.5} samples collected in the eastern United States, *Atmos. Environ.*, 39, 5281-5289, 2005.
- Fan, J. and Zhang, R.: Atmospheric oxidation mechanism of *p*-xylene: A density function theory study, *J. Phys. Chem. A*, 110, 7728-7737, 2006.
- Forstner, H. J. L., Flagan, R. C., and Seinfeld, J. H.: Secondary organic aerosol from the photooxidation of aromatic hydrocarbons: Molecular composition, *Environ. Sci. Technol.*, 31, 1345-1358, 1997.
- Gao, S., Keywood, M. D., Ng, N. L., Surratt, J. D., Varutbangkul, V., Bahreini, R., Flagan, R. C., and Seinfeld, J. H.: Low-molecule weight and oligomeric components in secondary organic aerosol from the ozonolysis of cycloalkenes and α -pinene, *J. Phys. Chem., A*, 108, 10147-10164, 2004a.
- Gao, S., Ng, N. L., Keywood, M. D., Varutbangkul, V., Bahreini, R., Nenes, A., He, J., Yoo, K. Y., Beauchamp, J. L., Hodyss, R. P., Flagan, R. C., and Seinfeld, J. H.: Particle phase acidity and oligomer formation in secondary organic aerosol, *Environ. Sci. Technol.*, 38, 6582-6589, 2004b.
- Hatakeyama, S., Izumi, K., Fukuyama, T., Akimoto, H., Washida, N.: Reactions of OH with α -pinene and β -pinene in air: Estimates of global CO production from the atmospheric oxidation of terpenes, *J. Geophys. Res.*, 96, D1, 947-958, 1991.

- Heald, C. L., Jacob, D. J., Park, R. J., Russell, L. M., Huebert, B. J., Seinfeld, J. H., Liao, H., and Weber, R. J.: A large organic aerosol source in the free troposphere missing from current models, *Geophys. Res. Lett.*, 32, L18809, doi: 10.1029/2005GL023831, 2005.
- Heald, C. L., Jacob, D.J., Turquety, S., Hudman, R.C., Weber, R. J., Sullivan, A.P., Peltier, R.E., Atlas, E. L., de Gouw, J.A., Warneke, C., Holloway, J. S., Neuman, J. A., F. Flocke, M., and Seinfeld, J. H.: Concentration and sources of organic carbon aerosols in the free troposphere over North America, *J. Geophys. Res.*, 111, D23, D23S47, 10.1029/2006JD007705, 2006.
- Hurley, M. D., Sokolov, O., Wallington, T. J., Takekawa, H., Karasawa, M., Klotz, B., Barnes, I., Becker, K. H.: Organic aerosol formation during the atmospheric degradation of toluene, *Environ. Sci. Technol.*, 35, 1358-1366, 2001.
- Iinuma, Y., Böge, O., Gnauk, T., and Herrmann, H.: Aerosol-chamber study of the pinene/O₃ reaction: Influence of particle acidity on aerosol yields and products, *Atmos. Environ.*, 38, 761-773, 2004.
- Izumi, K. and Fukuyama, T.: Photochemical aerosol formation from aromatic hydrocarbons in the presence of NO_x, *Atmos. Environ.*, 24A, 1433-1441, 1990.
- Jang, M. and Kamens, R. M., Characterization of secondary organic aerosol from the photooxidation of toluene in the presence of NO_x and 1-propene, *Environ. Sci. Technol.*, 35, 3626-3639, 2001.
- Jang, M., Czoschke, N. M., Lee, S., Kamens, R. M.: Heterogeneous atmospheric aerosol production by acid-catalyzed particle-phase reactions, *Science*, 298, 814-817, 2002.

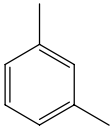
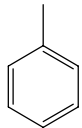
- Johnson, D., Jenkin, M. E., Wirtz, K., Martín-Reviejo, M.: Simulating the formation of secondary organic aerosol from the photooxidation of toluene, *Environ. Chem.*, 1, 150-165, 2004.
- Johnson, D., Jenkin, M. E., Wirtz, K., Martín-Reviejo, M. Simulating the formation of secondary organic aerosol from the photooxidation of aromatic hydrocarbons, *Environ. Chem.*, 2, 35-48, 2005.
- Kalberer, M., Paulsen, S., Sax, M., Steinbacher, M., Dommen, J., Prevot, A. S. H., Fisseha, R., Weingartner, E., Frankevich, V., Zenobi, R., and Baltensperger, U.: Identification of polymers as major components of atmospheric organic aerosols, *Science*, 303, 1659-1662, 2004.
- Keywood, M. D., Varutbangkul, V., Bahreini, R., Flagan, R. C., Seinfeld, J. H.: Secondary organic aerosol formation from the ozonolysis of cycloalkenes and related compounds, *Environ. Sci. Technol.*, 38, 4157-4164, 2004.
- Kleindienst, T. E., Conner, T. S., McIver, C. D., and Edney, E. O.: Determination of secondary organic aerosol products from the photooxidation of toluene and their implications in ambient PM_{2.5}, *J. Atmos. Chem.*, 47, 79-100, 2004.
- Koch, R., Knispel, R., Elend, M., Siese, M., and Zetzsch, C.: Consecutive reactions of aromatic-OH adducts with NO, NO₂, and O₂: Benzene, toluene, *m*- and *p*-xylene, hexamethylbenzene, phenol, *m*-cresol, and aniline, *Atmos. Chem. Phys. Discuss.*, 6, 7623-7656, 2006.
- Kroll, J. H., Ng, N. L., Murphy, S. M., Flagan, R. C., and Seinfeld, J. H.: Secondary organic aerosol formation from isoprene photooxidation, *Environ. Sci. Technol.*, 40, 1869-1877, 2006.

- Kroll, J., Chan, A. W. H., Ng, N. L., Flagan, R. C., and Seinfeld, J. H.: Reactions of semivolatile organics and their effects on secondary organic aerosol formation, *Environ. Sci. Technol.*, in press.
- Lay, T. H., Bozzelli, J. W., and Seinfeld, J. H.: Atmospheric photochemical oxidation of benzene: Benzene + OH and the benzene-OH adduct, *J. Phys. Chem.*, 100, 6543-6554, 1996.
- Martin-Reviejo, M., Wirtz, K.: Is benzene a precursor for secondary organic aerosol? *Environ. Sci. Technol.*, 39, 1045-1054, 2005.
- Ng, N. L., Kroll, J. H., Keywood, M. D., Bahreini, R., Varutbangkul, V., Flagan, R. C., Seinfeld, J. H., Lee, A., and Goldstein, A. H.: Contribution of first- versus second-generation products to secondary organic aerosols formed in the oxidation of biogenic hydrocarbons, *Environ. Sci. Technol.*, 40, 2283-2297, 2006.
- Odum, J. R., Hoffmann, T., Bowman, F., Collins, D., R. C. Flagan, R. C., and Seinfeld, J. H.: Gas/particle partitioning and secondary organic aerosol yields, *Environ. Sci. Technol.*, 30, 2580-2585, 1996.
- Odum, J. R., Jungkamp, T. P. W., Griffin, R. J., Flagan, R. C., and Seinfeld, J. H.: The atmospheric aerosol-forming potential of whole gasoline vapor, *Science*, 276, 96-99, 1997a.
- Odum, J. R., Jungkamp, T. P. W., Griffin, R. J., Forstner, H. J. L., Flagan, R. C., and Seinfeld, J. H.: Aromatics, reformulated gasoline and atmospheric organic aerosol formation, *Environ. Sci. Technol.*, 31, 1890-1897, 1997b.

- Presto, A. A., Huff Hartz, K. E., Donahue, N. M.: Secondary organic aerosol production from ozonolysis: 2. Effect of NO_x concentration, *Environ. Sci. Technol.*, 39, 7046-7054, 2005.
- Presto, A. A., Donahue, N. M.: Investigation of α -pinene + ozone secondary organic aerosol formation at low total aerosol mass, *Environ. Sci. Technol.*, 40, 3536-3543, 2006.
- Seinfeld, J. H. and Pandis, S. N.: *Atmospheric Chemistry and Physics: From Air Pollution to Climate Change*, Wiley, New Jersey, 2006.
- Song, C., Na, K., Cocker III, D. R.: Impact of the hydrocarbon to NO_x ratio on secondary organic aerosol formation, *Environ. Sci. Technol.*, 39, 3143-3149, 2005.
- Stroud, C. A., Makar, P. A., Michelangeli, D. V., Mozurkewich, M., Hastie, D. R., Barbu, A., and Humble, J.: Simulating organic aerosol formation during photooxidation of toluene/NO_x mixtures: Comparing the equilibrium and kinetic assumption. *Environ. Sci. Technol.*, 38, 1471-1479, 2004.
- Suh, I., Zhang, R., Molina, L. T., and Molina, M. J.: Oxidation mechanism of aromatic peroxy and bicyclic radicals from OH-toluene reactions, *J. Am. Chem. Soc.*, 125, 12655-12665, 2003.
- Surratt, J. D., Kroll, J. H., Kleindienst, T. E., Edney, E. O., Claeys, M., Sorooshian, A., Ng, N. L., Offenberg, J. H., Lewandowski, M., Jaoui, M., Flagan, R. C., and Seinfeld, J. H.: Evidence for organosulfates in secondary organic aerosol, *Environ. Sci. Technol.*, in press.

- Tolocka, M. P., Jang, M., Ginter, J. M., Cox, F. J., Kamens, R. M., and Johnston M. V.: Formation of oligomers in secondary organic aerosol, *Environ. Sci. Technol.*, 38, 1428-1434, 2004.
- Tsigaridis, K. and Kanakidou, M.: Global modelling of secondary organic aerosols in the troposphere: A sensitivity study, *Atmos. Chem. Phys.*, 3, 1849-1869, 2003.
- Volkamer, R., Klotz, B., Barnes, I., Imamura, T., Wirtz, K., Washida, N., Becker, K. H., and Platt, U.: OH-initiated oxidation of benzene, Part I, phenol formation under atmospheric conditions, *Phys. Chem. Chem. Phys.*, 4, 1589-1610, 2002.
- Volkamer, R., Jimenez, J. L., San Martini, F., Dzepina, K., Zhang, Q., Salcedo, D., Molina, L. T., Worsnop, D. R., Molina, M. J.: Secondary organic aerosol formation from anthropogenic air pollution: Rapid and higher than expected, *Geophys. Res. Lett.*, 33, L17811, doi:10.1029/2006GL026899, 2006.
- Zhang, S., Shaw, M., Seinfeld, J. H., and Flagan, R. C.: Photochemical aerosol formation from α -pinene and β -pinene, *J. Geophys. Res.*, 97, 20717-20729, 1992.

Table 8. 1. Aromatic hydrocarbons studied

Parent Hydrocarbon	Structure	Formula (MW)	k_{OH}^a ($\text{cm}^3 \text{ molec}^{-1} \text{ s}^{-1}$)
<i>m</i> -xylene		C_8H_{10} (106)	2.31×10^{-11}
toluene		C_7H_8 (92)	5.63×10^{-12}
benzene		C_6H_6 (78)	1.22×10^{-12}

a: Rate constants were obtained from Calvert et al. (2002)

Table 8. 2. Initial conditions and data for high-NO_x (HONO) experiments

Expt. No.	Parent Hydrocarbon	T (K)	RH (%)	NO (ppb)	NO ₂ (ppb)	Seed	ΔHC (ppb)	ΔM ₀ (μg/m ³) ^a	SOA Yield (%) ^a
1	<i>m</i> -xylene	297	5.5	470	473	(NH ₄) ₂ SO ₄	70.9	18.2 ± 1.8	5.9 ± 0.4
2	<i>m</i> -xylene	298	5.7	451	494	(NH ₄) ₂ SO ₄	28.1	4.3 ± 1.2	3.5 ± 0.7
3	<i>m</i> -xylene	298	5.9	432	511	(NH ₄) ₂ SO ₄	132.5	46.4 ± 3.7	8.0 ± 0.3
4	<i>m</i> -xylene	297	5.1	431	514	(NH ₄) ₂ SO ₄	106.1	36.7 ± 2.8	8.0 ± 0.2
5	toluene	298	3.8	421	524	(NH ₄) ₂ SO ₄	30.1	9.1 ± 1.3	8.0 ± 0.7
6	toluene	298	4.3	414	532	(NH ₄) ₂ SO ₄	56.7	23.8 ± 2.2	11.1 ± 0.4
7	toluene	298	4.9	388	559	(NH ₄) ₂ SO ₄	80.2	38.7 ± 3.3	12.8 ± 0.4
8	toluene	298	4.4	373	568	(NH ₄) ₂ SO ₄	50.7	20.9 ± 1.9	10.9 ± 0.5
9	benzene	297	5.2	83	86	(NH ₄) ₂ SO ₄	39.4	35.4 ± 2.7 ^b	28.1 ± 0.9

a: Stated uncertainties (1σ) are from scatter in particle volume measurements

b: Assuming an SOA density of 1.4 g cm⁻³

Table 8. 3. Initial conditions and data for low-NO_x (H₂O₂) experiments

Expt. No.	Parent Hydrocarbon	T (K)	RH (%)	Seed	ΔHC (ppb)	ΔM ₀ (μg/m ³) ^a	SOA Yield (%) ^a
1	<i>m</i> -xylene	298	5.1	(NH ₄) ₂ SO ₄	32.5	53.0 ± 4.2	37.7 ± 0.8
2	<i>m</i> -xylene	298	5.2	(NH ₄) ₂ SO ₄	16.1	24.6 ± 2.2	35.2 ± 1.8
3	<i>m</i> -xylene	298	5.1	(NH ₄) ₂ SO ₄	8.0	12.8 ± 1.7	36.7 ± 2.6
4	<i>m</i> -xylene	297	6.2	(NH ₄) ₂ SO ₄	26.1	40.5 ± 3.4	35.7 ± 1.0
5	toluene	297	6.8	(NH ₄) ₂ SO ₄	32.1	37.4 ± 2.8	30.8 ± 1.7
6	toluene	297	6.2	(NH ₄) ₂ SO ₄	63.9	73.1 ± 5.6	30.2 ± 0.7
7	toluene	298	5.2	(NH ₄) ₂ SO ₄	10.0	11.5 ± 1.6	30.4 ± 4.1
8	toluene	298	5.9	(NH ₄) ₂ SO ₄	23.8	26.7 ± 2.5	29.8 ± 1.6
9	benzene	298	6.6	(NH ₄) ₂ SO ₄	64.7	76.4 ± 5.8 ^b	36.9 ± 0.9

a: Stated uncertainties (1σ) are from scatter in particle volume measurements

b: Assuming an SOA density of 1.4 g cm⁻³

Table 8. 4. Initial conditions and data for acid/nonacid experiments

Expt. No.	Parent Hydrocarbon	T (K)	RH (%)	NO _x Condition ^a	Seed	ΔHC (ppb)	ΔM ₀ (μg/m ³) ^b	SOA Yield (%) ^b
1	<i>m</i> -xylene	297	4.3	Low NO _x	(NH ₄) ₂ SO ₄	60.2	101.3 ± 7.8	38.6 ± 0.5
2	<i>m</i> -xylene	297	4.5	Low NO _x	(NH ₄) ₂ SO ₄ + H ₂ SO ₄	58.8	103.5 ± 8.0	40.4 ± 0.6
3	<i>m</i> -xylene	297	5.0	High NO _x	(NH ₄) ₂ SO ₄	68.9	78.9 ± 5.6 ^c	26.3 ± 0.5
4	<i>m</i> -xylene	298	4.2	High NO _x	(NH ₄) ₂ SO ₄ + H ₂ SO ₄	68.5	78.3 ± 5.4 ^c	26.3 ± 0.4
5	toluene	298	5.9	Low NO _x	(NH ₄) ₂ SO ₄	37.9	41.0 ± 3.0	28.7 ± 0.6
6	toluene	299	4.6	Low NO _x	(NH ₄) ₂ SO ₄ + H ₂ SO ₄	38.9	43.2 ± 3.2	29.5 ± 0.7
7	toluene	296	4.9	High NO _x	(NH ₄) ₂ SO ₄	60.0	43.8 ± 3.6 ^c	19.3 ± 0.4
8	toluene	298	4.9	High NO _x	(NH ₄) ₂ SO ₄ + H ₂ SO ₄	58.2	38.3 ± 3.2 ^c	17.4 ± 0.5

a: low NO_x (H₂O₂ only); high NO_x (H₂O₂ + about 100 ppb NO added)

b: Stated uncertainties (1σ) are from scatter in particle volume measurements

c: Assuming SOA densities are the same as those determined for HONO experiments (see Table 8.5)

Table 8. 5. Estimated effective SOA densities

Parent Hydrocarbon	NO_x Condition	Effective Density (g cm⁻³)^a
m-xylene	Low NO _x	1.33 ± 0.10
m-xylene	High NO _x	1.48 ± 0.10
toluene	Low NO _x	1.45 ± 0.10
toluene	High NO _x	1.24 ± 0.10

a: Stated uncertainties (1σ) are from repeated measurements of ammonium sulfate seed densities

Table 8. 6. Aerosol yield parameters

Parent Hydrocarbon	NO_x Condition	α_1	$K_{om,1}$ (m³ ug⁻¹)	α_2	$K_{om,2}$ (m³ ug⁻¹)
<i>m</i> -xylene	Low NO _x	0.30	N/A	N/A	N/A
<i>m</i> -xylene	High NO _x	0.031	0.761	0.090	0.029
toluene	Low NO _x	0.36	N/A	N/A	N/A
toluene	High NO _x	0.058	0.430	0.113	0.047
benzene	Low NO _x	0.37	N/A	N/A	N/A
benzene	High NO _x	0.072	3.315	0.888	0.009

N/A: Not applicable

Figure 8. 1. Typical reaction profile of a high-NO_x experiment in which HONO is used as the OH precursor (initial conditions: 89.3 ppb of *m*-xylene, 470 ppb NO, and 473 ppb NO₂).

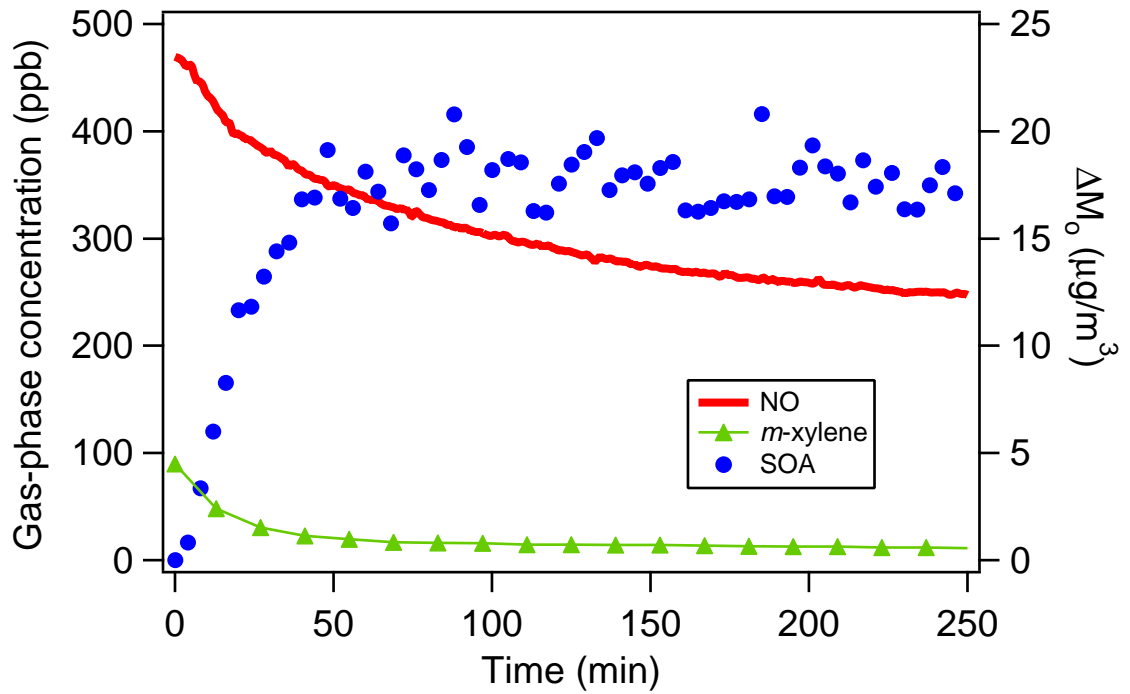
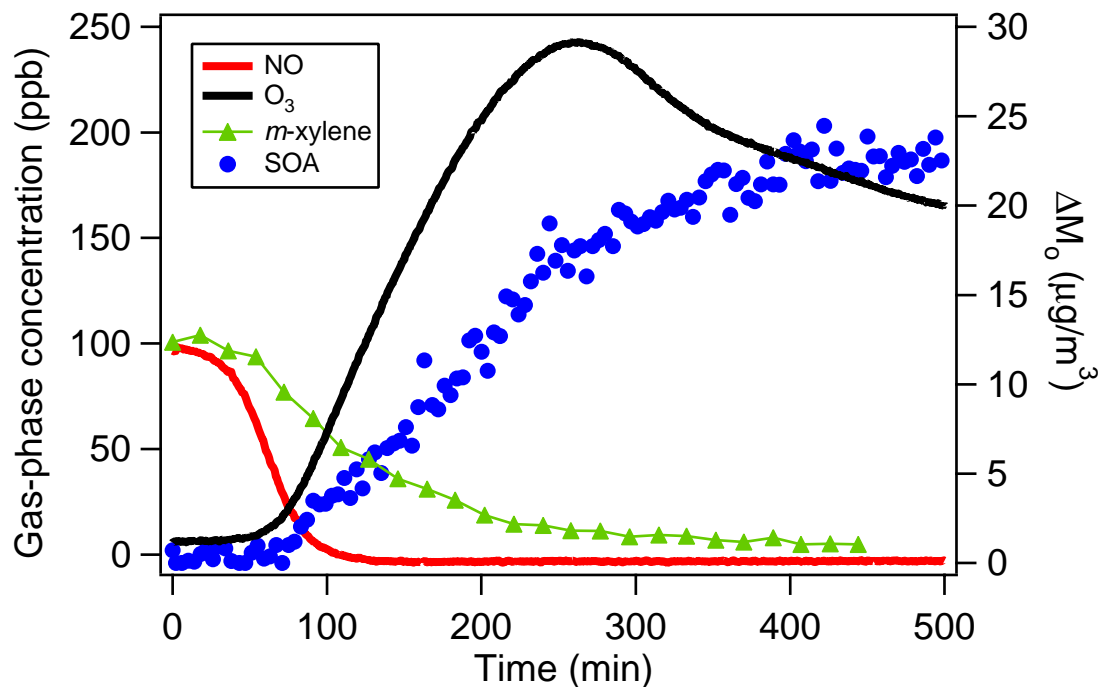


Figure 8. 2 (a). Reaction profile of a typical classical photooxidation experiment (initial conditions: 101.6 ppb *m*-xylene, 97 ppb NO, and 26 ppb NO₂). (b) Reaction profile of a classical photooxidation experiment in the presence of ~1 ppm NO_x (initial conditions: 94.8 ppb *m*-xylene, 878 ppb NO, and 65 ppb NO₂). A negligible amount of ozone is formed during the experiment, and no SOA is formed.

(a)



(b)

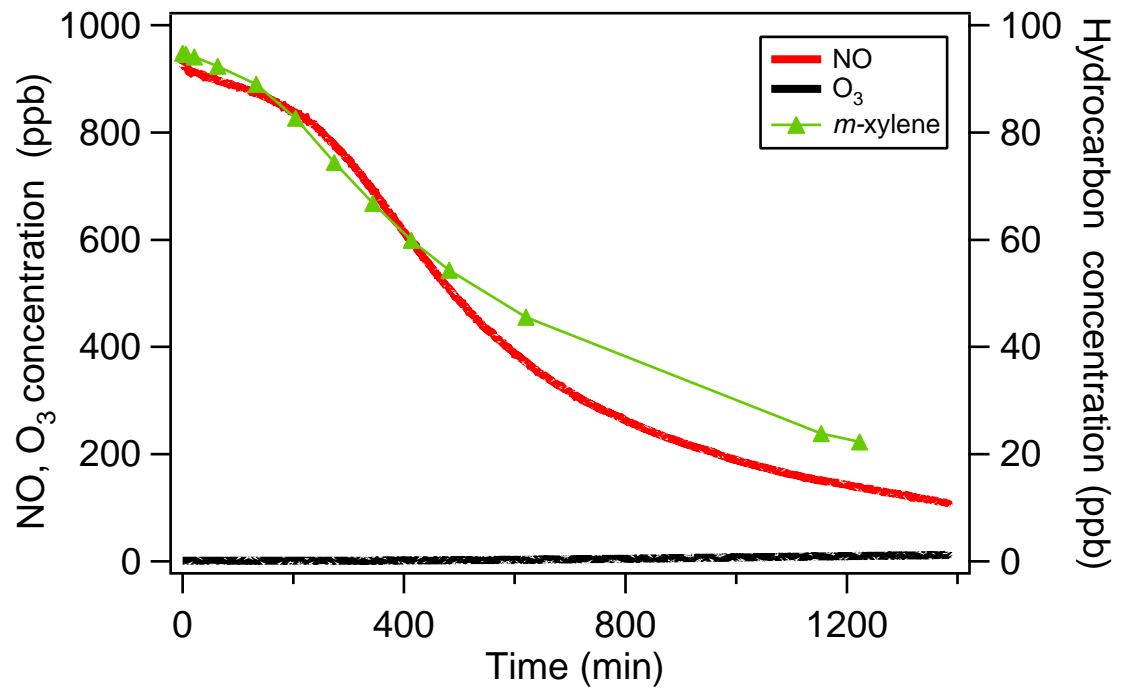


Figure 8. 3. Time-dependent growth curves for *m*-xylene photooxidation under high-NO_x conditions. The concentrations in the legend refer to the amount of *m*-xylene reacted in each experiment.

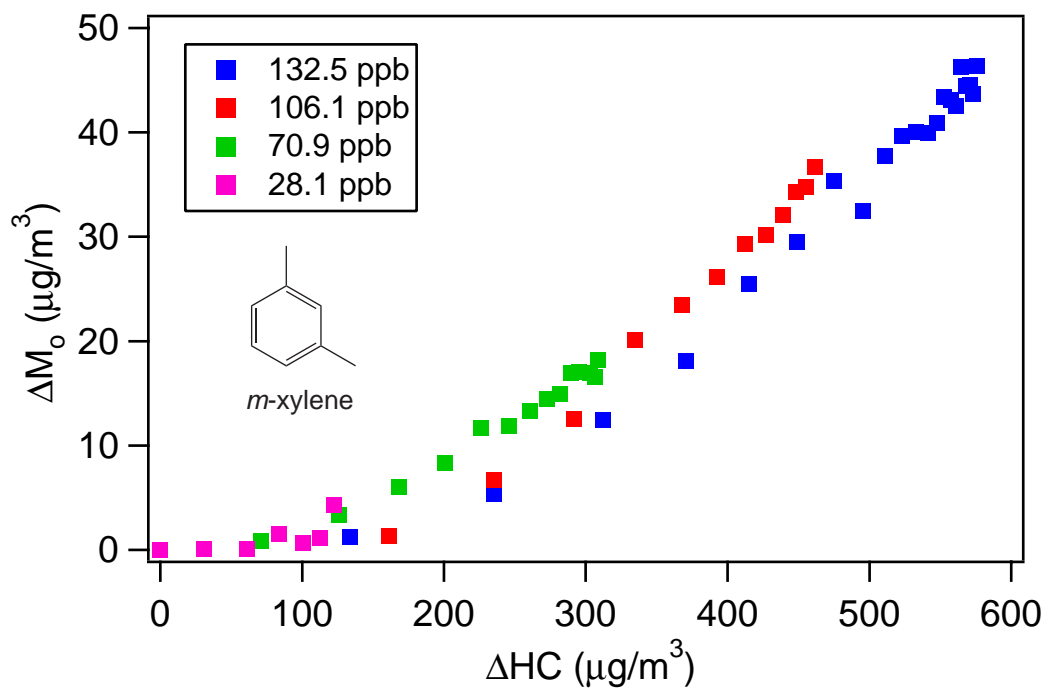


Figure 8. 4. Time-dependent growth curves for toluene photooxidation under high-NO_x conditions. The concentrations in the legend refer to the amount of toluene reacted in each experiment.

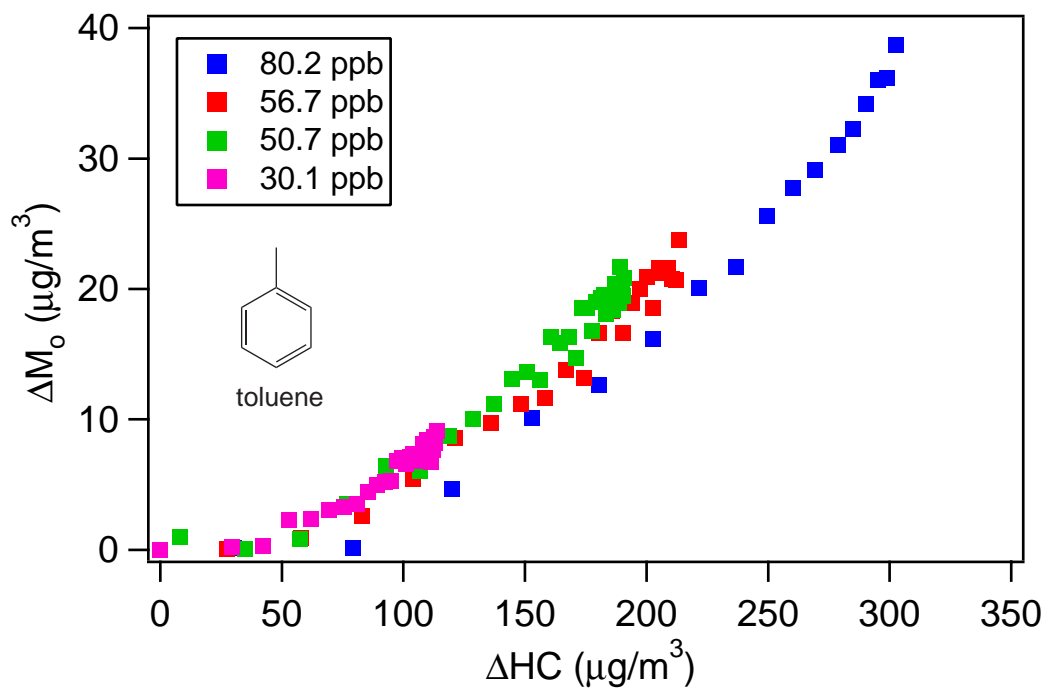


Figure 8. 5. Time-dependent growth curves for benzene photooxidation under high- and low- NO_x conditions. Under high- NO_x conditions, the initial benzene concentration is 337 ppb (12% reacted). Under low- NO_x conditions, the initial benzene concentration is 395 ppb (16% reacted) and the system has a constant yield of 37%.

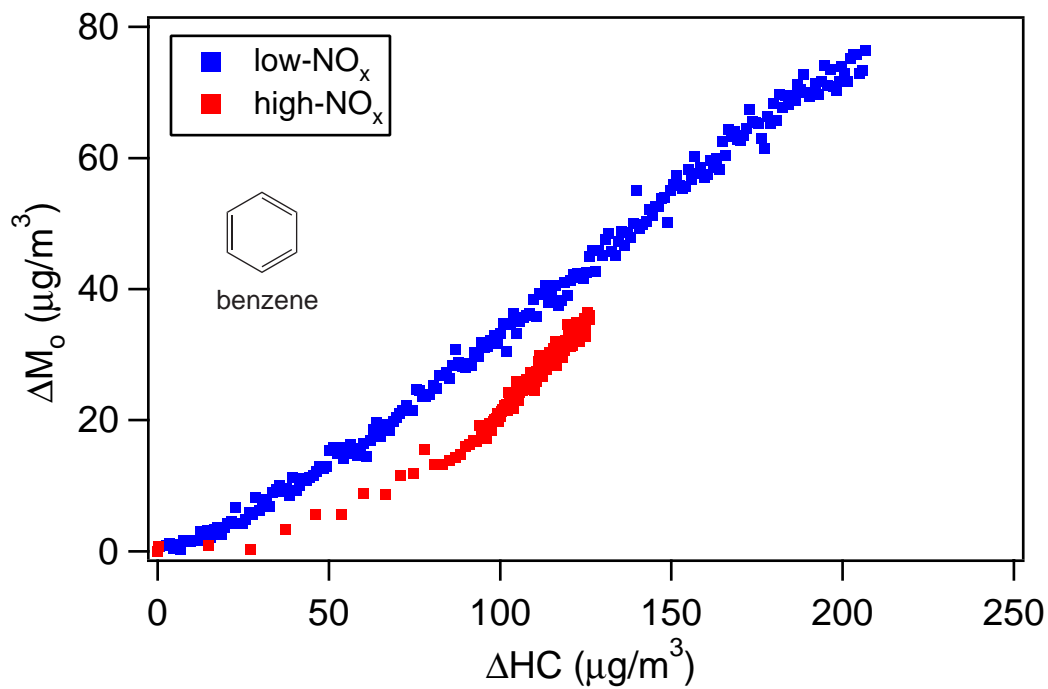


Figure 8. 6. Time-dependent growth curves for *m*-xylene photooxidation under low-NO_x conditions. The concentrations in the legend refer to the amount of *m*-xylene reacted in each experiment. The system exhibits a constant yield of 36%.

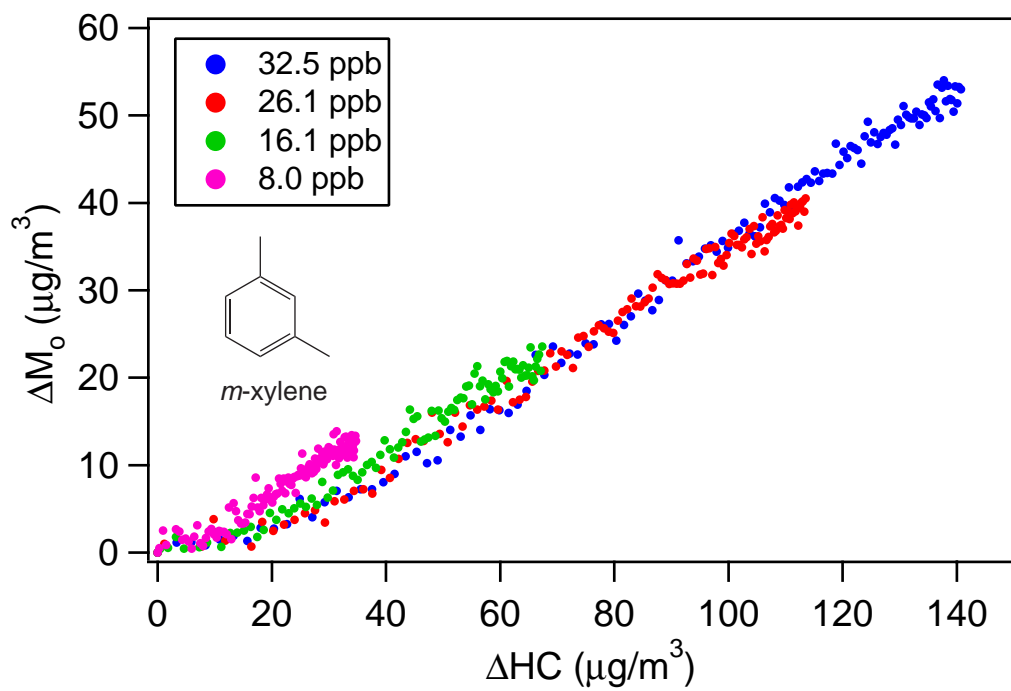


Figure 8. 7. Time-dependent growth curves for toluene photooxidation under low-NO_x conditions. The concentrations in the legend refer to the amount of toluene reacted in each experiment. The system exhibits a constant yield of 30%.

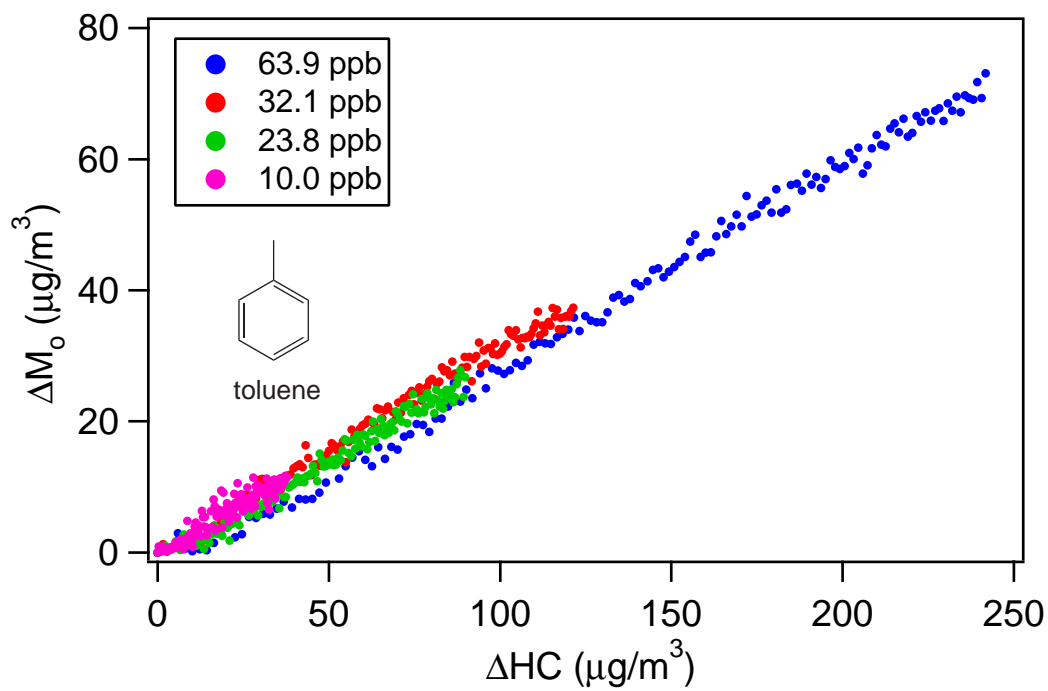


Figure 8. 8. Yield curves for toluene and *m*-xylene under high-NO_x conditions. The parameters for fitting the yield curves are, toluene: $\alpha_1 = 0.058$, $K_{om,1} = 0.430$, $\alpha_2 = 0.113$, and $K_{om,2} = 0.047$; *m*-xylene: $\alpha_1 = 0.031$, $K_{om,1} = 0.761$, $\alpha_2 = 0.090$, and $K_{om,2} = 0.029$.

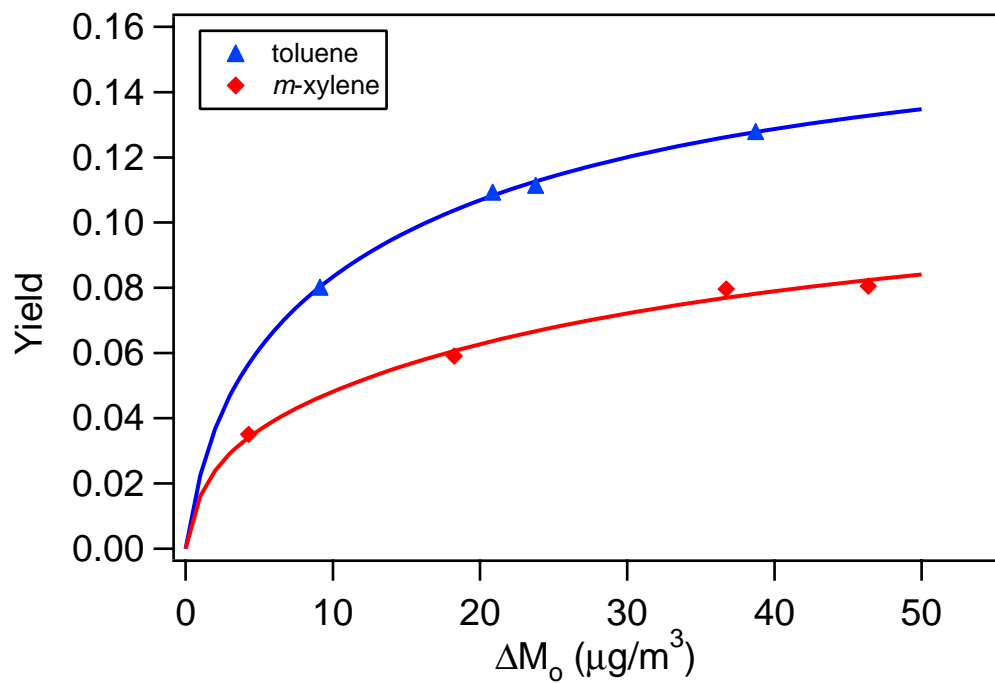


Figure 8. 9. Time-dependent growth curves for toluene photooxidation in the presence of neutral seed versus acidic seed.

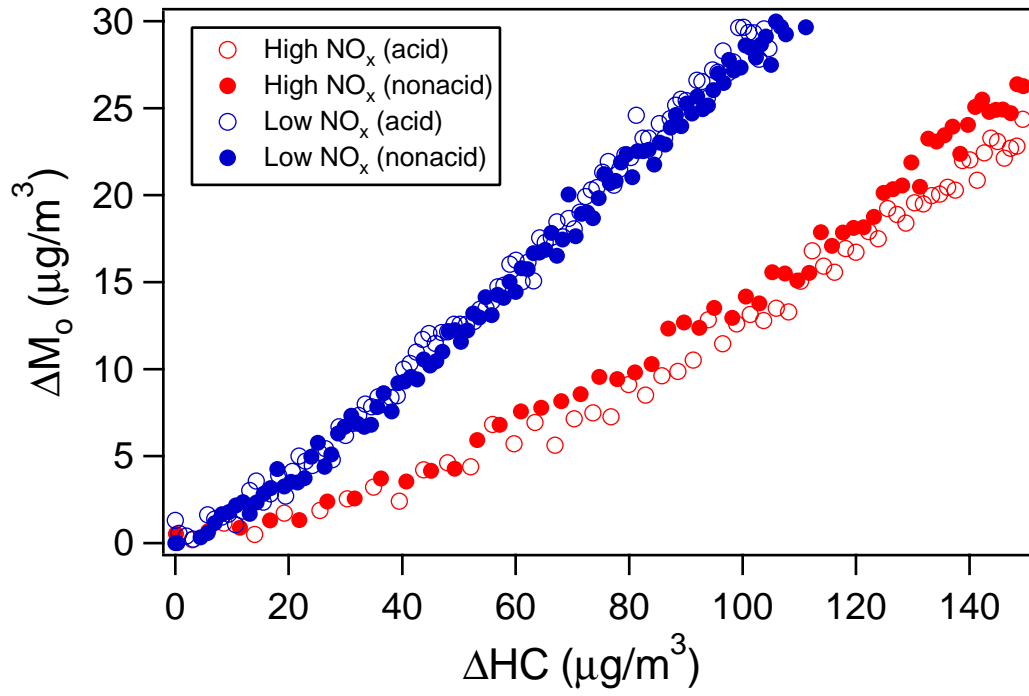


Figure 8. 10. A simplified SOA formation mechanism for toluene photooxidation. X represents the generic non particle-phase product from all gas-phase loss processes.

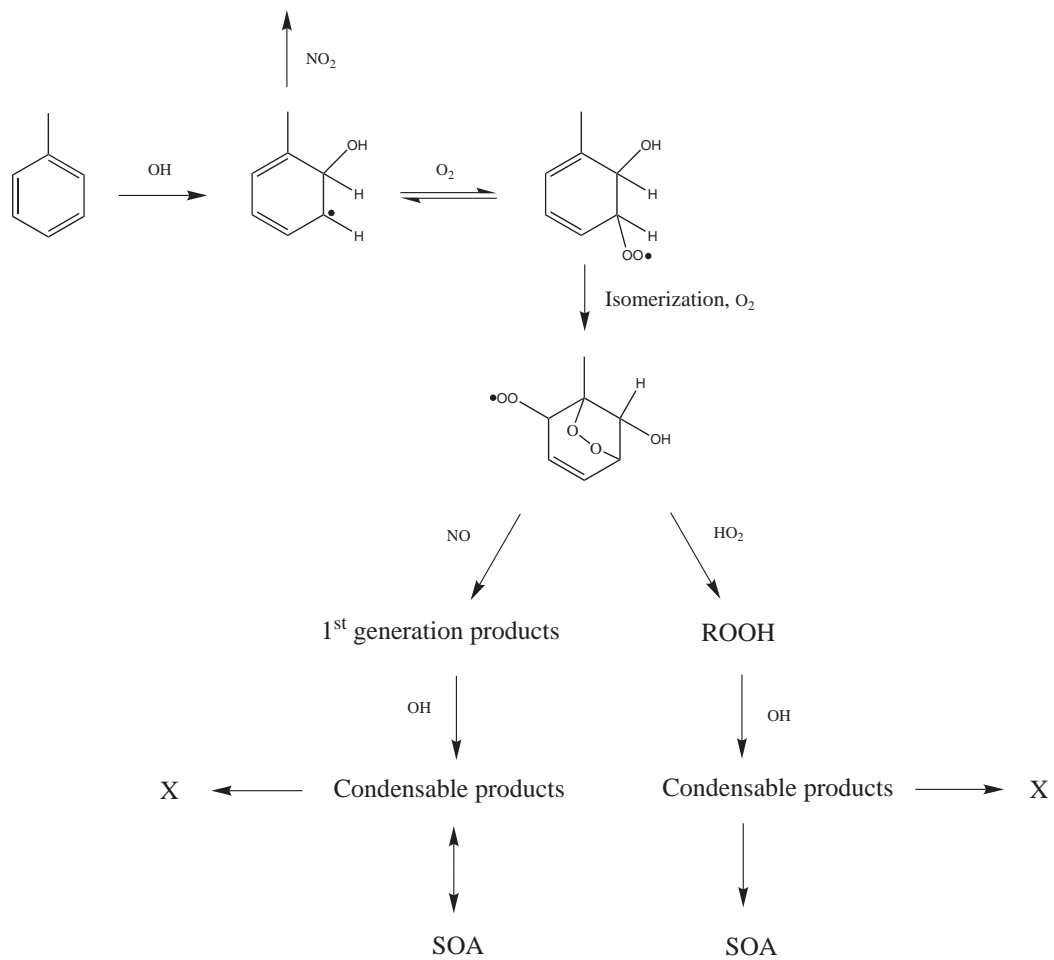
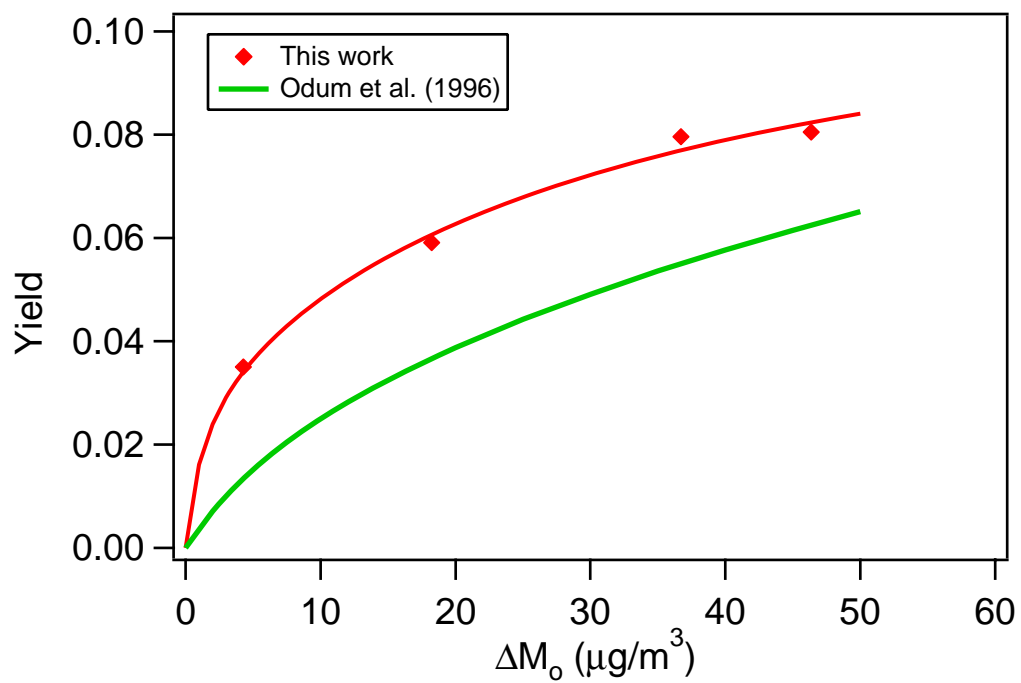


Figure 8. 11. Comparison of *m*-xylene high-NO_x yield curve obtained in the current work to that from Odum et al. (1996). The yield curve from Odum et al. (1996) has been corrected for the temperature (25°C) of this study and density (1.48 g cm⁻³) of the SOA.



Chapter 9

Conclusions

Conclusions

Laboratory chamber studies provide the basis for evaluating SOA formation mechanism and chamber data are the foundation for predicting SOA formation. This thesis presents chamber study results on aerosol formation from a wide range of parent organic compounds under a variety of experimental conditions.

Over the last two decades, yield curves have been widely used to represent the aerosol-forming potential of different hydrocarbon precursors, providing the important yield parameters for use in atmospheric models. In chapter 2 it is shown that this two-product model can be extended to infer the general mechanisms of SOA formation, by plotting aerosol mass formed versus the amount of hydrocarbon reacted and we refer to this as the “growth curve”. In studying aerosol formation from ozonolysis and photooxidation of a series of biogenics hydrocarbons, it is found that for compounds with only one double bond, the first oxidation step is rate-limiting and aerosols are formed mainly from low volatility first-generation oxidation products; whereas for compounds with more than one double bond, the second oxidation step may also be rate-limiting and second-generation products contribute substantially to SOA growth. This behavior is characterized by a vertical section in the growth curve, in which continued aerosol growth is observed even after all the parent hydrocarbon is consumed. The growth curve approach has been shown to be useful in interpreting SOA growth mechanism in different systems (chapters 7 and 8).

The effect of seed particle acidity on SOA yield and composition is demonstrated in chapter 3. The ubiquitous presence of oligomers in SOA suggests that in addition to gas-phase reactions and gas-particle partitioning, particle-phase reactions are important

processes in the formation of secondary organic aerosol. As seed particle acidity increases, oligomers are formed more abundantly and the aerosol yield increases; for α -pinene mixing ratios ranging from ~10-140 ppb, aerosol yield increases by 10-40% in the presence of acidic seed particles.

Chapters 4 and 5 demonstrate the aerosol-formation potential of glyoxal and isoprene, compounds previously not thought to be aerosol precursors because of volatility considerations. Glyoxal is observed to partition into the aerosol phase much more efficiently than its Henry's Law constant would predict, possibly due to the presence of particle-phase reactions. The reactive uptake of glyoxal indicates that small molecules with vapor pressures far too high to qualify as semivolatile can produce SOA via reactive absorption. Given the large emissions of isoprene, the discovery of the aerosol-forming potential from isoprene photooxidation has significant impacts on predicting SOA formation from biogenic hydrocarbons. SOA yield is found to increase substantially as the NO_x level decreases (chapter 6). The proposed mechanism for this effect is the competitive chemistry of peroxy radicals between NO and HO_2 , with the HO_2 reaction route producing products of lower volatility and hence a higher SOA yield

Given the importance of NO_x dependence on SOA formation, this effect is examined in detail for other biogenic hydrocarbons in chapter 7. The NO_x dependence of α -pinene photooxidation follows the same trend as that of isoprene, in which SOA yield decreases as NO_x levels increases. The NO_x dependence of SOA yield for the sesquiterpenes, longifolene and aromadendrene, however, differs from that determined for isoprene and α -pinene; the aerosol yield under high- NO_x conditions substantially exceeds that under low- NO_x conditions. The reversal of the NO_x dependence of SOA

formation for the sesquiterpenes is consistent with formation of relatively nonvolatile organic nitrates, and/or the isomerization of large alkoxy radicals that leads to less volatile products. Analysis of the aerosol chemical composition confirms the presence of organic nitrates under high-NO_x conditions. Consequently the formation of SOA from certain biogenic hydrocarbons such as sesquiterpenes may be more efficient in polluted air.

The SOA formation from aromatic hydrocarbons is presented in chapter 8. The photooxidation of *m*-xylene, toluene, and benzene follows the same NO_x dependence as smaller biogenic hydrocarbons, such as isoprene and α -pinene, in which aerosols yields under low-NO_x conditions substantially exceed those under high-NO_x conditions, suggesting the importance of peroxy radical chemistry in SOA formation. The SOA yield parameters obtained under high- and low-NO_x conditions allow one to parameterize the NO_x dependence for atmospheric models. In contrast to the α -pinene ozonolysis system (chapter 3), experiments carried out in the presence of acidic seed aerosol reveal no change of SOA yields from the aromatics as compared with those using neutral seed aerosol.

With the above findings concerning the ubiquitous existence of particle-phase reactions, the SOA-forming potential of volatile compounds, as well as the profound dependence of NO_x on SOA formation, it is necessary to revise the modeling basis to incorporate these new understandings on SOA formation. In light of the aerosol formation from isoprene photooxidation, it is important to evaluate the SOA-forming potential of unstudied classes of VOCs, including ones previously thought not to be able to produce SOA because of volatility considerations. Classes of VOCs already known to

form SOA should also be restudied to establish fully the NO_x dependence of SOA formation and to determine the role of particle-phase reactions, including the effect of particle-phase acidity.

Appendix A

Reactions of Semivolatile Organics and Their Effects on Secondary Organic Aerosol Formation*

* This chapter is reproduced by permission from “Reactions of Semivolatile Organics and Their Effects on Secondary Organic Aerosol Formation” by J. H. Kroll, A. W. H. Chan, N. L. Ng, R. C. Flagan, J. H. Seinfeld, *Environmental Science and Technology*, doi: 10.1021/es062059x, 2007. Copyright 2005. American Chemical Society.

Reactions of Semivolatile Organics and Their Effects on Secondary Organic Aerosol Formation

JESSE H. KROLL,[†] ARTHUR W. H. CHAN, NGA L. NG, RICHARD C. FLAGAN, AND JOHN H. SEINFELD*

Departments of Environmental Science and Engineering and Chemical Engineering, California Institute of Technology, Pasadena, California 91125

Secondary organic aerosol (SOA) constitutes a significant fraction of total atmospheric particulate loading, but there is evidence that SOA yields based on laboratory studies may underestimate atmospheric SOA. Here we present chamber data on SOA growth from the photooxidation of aromatic hydrocarbons, finding that SOA yields are systematically lower when inorganic seed particles are not initially present. This indicates that concentrations of semivolatile oxidation products are influenced by processes beyond gas-particle partitioning, such as chemical reactions and/or loss to chamber walls. Predictions of a kinetic model in which semivolatile compounds may undergo reactions in both the gas and particle phases in addition to partitioning are qualitatively consistent with the observed seed effect, as well as with a number of other recently observed features of SOA formation chemistry. The behavior arises from a kinetic competition between uptake to the particle phase and reactive loss of the semivolatile product. It is shown that when hydrocarbons react in the absence of preexisting organic aerosol, such loss processes may lead to measured SOA yields lower than would occur under atmospheric conditions. These results underscore the need to conduct studies of SOA formation in the presence of atmospherically relevant aerosol loadings.

Introduction

Secondary organic aerosol (SOA), formed in the atmospheric oxidation of gas-phase organic compounds and subsequent gas-particle partitioning of lower-volatility reaction products, is known to be a major contributor to the total tropospheric particulate burden (1). As a result, our need for an accurate understanding of atmospheric aerosols and their effects requires that models of atmospheric chemistry include processes governing the formation and fate of SOA. Because the chemistry of SOA formation is so complex and uncertain, most descriptions of SOA formation (e.g., 2–4) are semiempirical, constrained by environmental chamber studies of SOA formation and growth.

The primary framework for including SOA formation in atmospheric chemistry models, and relating the amount of aerosol generated in chambers with that in the troposphere, is the treatment of condensable species in SOA as semivolatile

organics, present in appreciable amounts in both the gas and particle phases. Work by Pankow (5, 6) and Odum et al. (7) demonstrated that SOA yield Y (defined as $\Delta M/\Delta HC$, the amount of aerosol formed per hydrocarbon reacted) can be expressed in terms of the gas-particle partitioning of a collection of i semivolatile species:

$$Y = \frac{\Delta M}{\Delta HC} = M \sum_i \frac{\alpha_i K_{p,i}}{1 + MK_{p,i}} \quad (1)$$

in which α_i and $K_{p,i}$ are the stoichiometric coefficient and gas-particle partitioning coefficient of species i , respectively, and M is the mass concentration of absorbing (typically organic) aerosol present. Therefore SOA formation is a function of not only the amount and volatility of the semivolatile compounds, but also the aerosol mass into which they can partition. This non-stoichiometric nature of aerosol yields is a known feature of SOA formation, and aerosol growth data have been shown to be well-represented by eq 1 (typically as “yield curves”, plots of Y vs M) (7, 8). This expression is also used to describe SOA formation in the atmosphere: α 's and K_p 's for a given hydrocarbon are those determined in chamber studies, and M is the ambient atmospheric organic aerosol mass loading, typically 1–20 $\mu\text{g}/\text{m}^3$. However, recent work suggests that this semiempirical approach, in which SOA formation is estimated based on experimentally determined aerosol yields, generally predicts SOA levels that are substantially lower (often by an order of magnitude or more) than measured values (2–4). Such discrepancies suggest that the reaction conditions of environmental chambers may lead to less SOA growth than occurs in the atmosphere, though unidentified SOA precursors may also play a role.

In this work we examine a chemical system for which SOA yields are dependent on the timing of the onset of gas-particle partitioning. Specifically it is shown that in the photooxidation of aromatic compounds, aerosol growth begins sooner, and hence aerosol yields are higher, in the presence of seed particles. Such an effect indicates that processes governing the amount of SOA formed are more complex than the simple formation and condensation of semivolatile compounds. Additional reactions of semivolatile organics may occur in both the gas and particle phases, changing the concentration and/or volatility of the organics. We examine the kinetics and partitioning of a model semivolatile compound which may undergo reactions in the gas and particle phases, in order to better understand the effect of such reactions on SOA growth. It is also shown that in the absence of initial absorbing aerosol mass, SOA yields as measured in chambers may be significantly lower than those in the real atmosphere.

Experimental Section

SOA formation from the photooxidation of aromatic hydrocarbons was measured using experimental protocols described previously in detail (9–11). Briefly, ~ 3 ppm H_2O_2 (the OH precursor) and the aromatic (71–72 ppb *m*-xylene or 87–91 ppb toluene, Aldrich) are added to a 28 m^3 Teflon chamber; for some experiments NO and/or ammonium sulfate seed are also added. For “ NO_x ” experiments, initial NO and NO_2 levels are 85 ± 4 ppb and 6 ± 4 ppb, respectively (otherwise NO_x levels are < 1 ppb), and for “seeded” experiments, seed number concentrations are $21\,000 \pm 4000$ particles/ cm^3 (otherwise concentrations are $< 5/\text{cm}^3$). Reaction begins when the blacklights surrounding the chamber

* Corresponding author phone: (626) 395-4635; fax: (626) 796-2591; e-mail: seinfeld@caltech.edu.

[†] Current address: Aerodyne Research, Inc., 45 Manning Road, Billerica MA 01821.

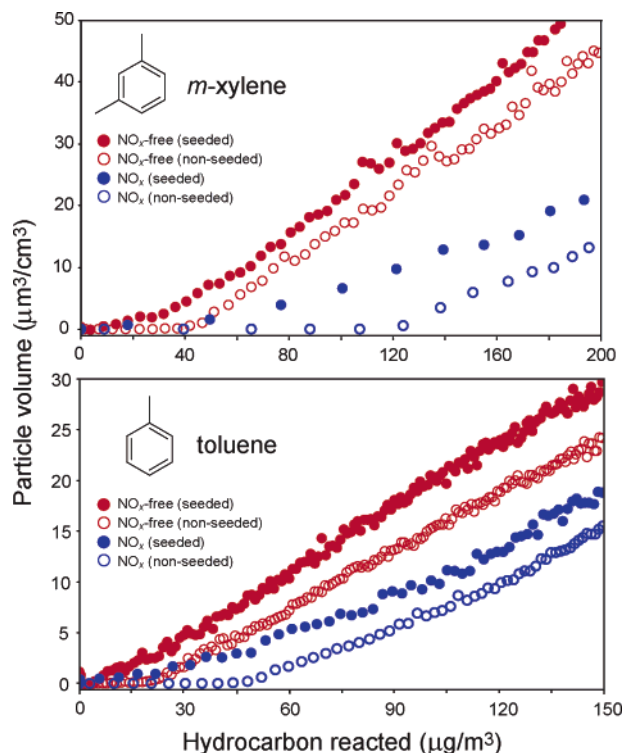


FIGURE 1. “Growth curves” for photooxidation of *m*-xylene and toluene. Each curve represents a single experiment; individual points are in 4 min increments. Color denotes NO_x condition (red, NO_x -free; blue, ~ 90 ppb NO_x initially present) and symbol denotes seed (filled circles, ammonium sulfate seed present; open circles, no seed present). In all nonseeded experiments there is a substantial induction period, leading to lower SOA yields.

are turned on; hydrocarbon concentration is monitored by gas chromatography–flame ionization detection, and aerosol volume is monitored by a differential mobility analyzer. Particle volume is corrected for losses of particles to the walls (10). Temperature and relative humidity are the same in all experiments (initial values of 23–25 °C and 4–7%, respectively). A total of eight experiments, systematically varying aromatic hydrocarbon (toluene vs *m*-xylene), ammonium sulfate seed (“seeded” vs “nonseeded”), and NO_x level (“ NO_x ” vs “ NO_x -free”), were conducted.

Results and Discussion

Shown in Figure 1 is SOA growth from the four pairs of seeded/nonseeded experiments. Data are presented as “growth curves”, plots of aerosol growth vs hydrocarbon reacted. As hydrocarbon measurements are made with much lower frequency than those of particle volume, the HC values shown are obtained by interpolation of GC measurements, fitting the data to a double-exponential decay (which reproduces measured hydrocarbon concentrations well, $R^2 > 0.95$). Only the growth near the beginning of the experiments (including the atmospherically relevant range of M) is shown; beyond this, the shapes of the curves do not change substantially, remaining slightly curved until all hydrocarbon is consumed ($\Delta\text{HC} = \text{HC}(0)$). Aerosol yields are generally higher than previously reported for aromatic photooxidation (12), likely a result of the lower NO_x levels employed in this work (13, 14).

We focus on the systematic differences between aerosol growth in the seeded and nonseeded cases; the effects of the other parameters varied (such as NO_x level) are beyond the scope of this work and are discussed elsewhere (15). The presence of seed is expected to have a negligible effect on hydrocarbon oxidation, and indeed the observed decays of

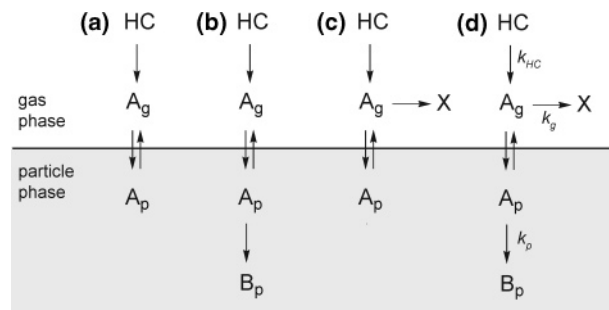


FIGURE 2. Mechanisms for SOA formation from a single semivolatile species A: (a) simple gas–particle partitioning, the standard model for SOA growth; (b) gas–particle partitioning followed by irreversible reaction to form nonvolatile product B_p ; (c) competition between gas–particle partitioning and irreversible loss of the gas-phase semivolatile compound; (d) both gas- and particle-phase reactions in addition to partitioning.

the hydrocarbon (from reaction with OH) are the same in seeded and nonseeded experiments. However, in all cases the aerosol growth exhibits a marked dependence on whether seed particles are present. In all seeded experiments, SOA growth is observed to begin essentially immediately, whereas in all nonseeded experiments, there is a substantial “induction period”, a period of time during which the parent hydrocarbon reacts away but no aerosol is formed. The amount of hydrocarbon reacted during this period in the nonseeded cases ranges from 20 $\mu\text{g}/\text{m}^3$ (~ 5 ppb) for the toluene/ NO_x -free experiment to 120 $\mu\text{g}/\text{m}^3$ (~ 27 ppb) for the *m*-xylene/ NO_x experiment. Once SOA growth begins, its rate is the same as in the seeded experiments, leading to roughly fixed differences in ΔM at a given value of ΔHC , and hence differences in SOA yields. Such differences persist throughout the experiments, but are most pronounced at lower (atmospherically relevant) aerosol loadings: for example, in the *m*-xylene/ NO_x experiments, at $M = 5 \mu\text{g}/\text{m}^3$ SOA yield in the seeded case is almost twice that of the nonseeded case (assuming densities are similar). We note that such a difference between yields in seeded and nonseeded experiments was not observed in an earlier study of high- NO_x photooxidation of *m*-xylene from our laboratory (16); in that study there were few data at low ($< 25 \mu\text{g}/\text{m}^3$) aerosol loadings, the condition at which this effect is most pronounced, as well as higher scatter in the yield results than we currently observe (10), and possibly differing chemistry due to higher NO_x levels.

The observed effect of seed on SOA growth implies differences in effective gas-particle partitioning coefficients (17): partitioning into the particle phase is stronger in the seeded experiments than in the nonseeded ones. This difference cannot be explained by the simple model of SOA formation described in the Introduction (and shown in Figure 2a): the semivolatile species initially formed are the same regardless of the presence of seed, and the solid seed particles cannot promote absorptive partitioning. Instead, the distribution of reaction products must be affected by additional processes, leading to enhancements in lower-volatility compounds in the presence of seed particles, and/or decreases in their absence.

The former possibility is consistent with recent work suggesting that particle-phase reactions, forming high-MW, low-volatility products, are important processes in SOA formation. The formation of such compounds, including oligomers (18–24) and organosulfates (25–27), is accompanied by the depletion of the semivolatile reactants in the particle phase; the resulting shift in the gas-particle equilibrium leads to more SOA formation than would be inferred on the basis of physical partitioning alone (14, 28). Many

such products are thermally stable (e.g., 18, 24–27), suggesting they are relatively long-lived, and cannot quickly revert to reactants. While the reversibility of SOA formation over long time scales is highly uncertain (experimental studies are largely lacking at present), the formation of high-MW species may be approximated as an irreversible step, so long as decomposition occurs on time scales longer than the time scales studied. Oxidation of aerosol components (“photochemical aging”) is another mechanism by which lower-volatility compounds may be irreversibly formed. The irreversible formation of nonvolatile species in SOA suggests the reaction scheme shown in Figure 2b, in which the semivolatile species (A_p) reacts further in the condensed phase to form a purely particle-phase species (B_p). The promotion of such reactions by ammonium sulfate particles may account for the differences in SOA growth illustrated in Figure 1.

Alternately, such differences could result from reactions of semivolatile species forming products other than SOA. Such processes serve to lower the concentration of the gas-phase species, thereby reducing the amount that partitions into the aerosol phase. Shown in Figure 2c is such a mechanism, in which the gas-phase semivolatile organic (A_g) reacts to form X, a generic non-particle-phase product. This may be a volatile species present only in the gas phase, formed by bond-breaking oxidation or photolysis reactions; or it may represent organics lost to the chamber walls. Such losses of semivolatile species have received little study in terms of their role in SOA formation, but certainly occur in many cases. For example, it has been shown that photolysis of organic aerosol components forms relatively volatile organics (29–31), which lead to reductions in SOA mass. Similarly, glyoxal, formed in the oxidation of aromatics, is known to efficiently partition into the particle phase (25, 32, 33), but it is also known to react with OH, photolyze, and be taken up onto surfaces; all these processes are expected to compete with gas-particle partitioning and hence reduce SOA growth.

Thus additional reactions of semivolatile organics, such as those shown in Figure 2b and c, may qualitatively explain differences in SOA yields between seeded and nonseeded photooxidation experiments (Figure 1). However, neither scheme represents a reasonable mechanism by which all semivolatile compounds will react: in one case (Figure 2b) all the organic is incorporated into the gas phase, so growth does not depend on gas-particle partitioning, and in the other (Figure 2c), at long reaction times no SOA is formed at all. Instead, most SOA-forming reactions involve a spectrum of semivolatile products, which likely exhibit varying chemistries, including reactions in both phases. The generalized mechanism shown in Figure 2d, in which the semivolatile species A can react by both pathways in Figure 2b and c, serves as a useful model system for investigating the role of the reactions of semivolatile organics in SOA growth, and may even roughly approximate the behavior of a more complex mixture. In this scheme, SOA yields are dependent not only on the volatility of the product A, but also on the rates of these additional reactions. In the following sections, we illustrate the possible role of such chemistry on aerosol growth. The dependence of SOA growth on the presence of seed particles is predicted, due largely to the delayed onset of gas-particle partitioning in the nonseeded case.

Model Description. The mechanism shown in Figure 2d is considered for only a single semivolatile species; we emphasize this is not intended to be a detailed mechanism of SOA formation, but rather a model system for studying the role of additional chemical reactions on gas-particle partitioning. All steps in the mechanism are represented as unimolecular processes, with rate constants k_{HC} , k_g , and k_p for the reactions $HC \rightarrow A_g$, $A_g \rightarrow X$, and $A_p \rightarrow B_p$, respectively. For simplicity, specific reaction conditions such as oxidant level are omitted, and all reactions are assumed to be

irreversible over the time scale of the simulation; the effects of specific reaction conditions and reversible processes are beyond the scope of this work, but are worth further study. Gas-particle partitioning is treated as in Bowman et al. (34), with the net rate of uptake of a species by physical partitioning given by J , its flux to the particle surface:

$$J = \frac{N_p 2\pi D_p \lambda \bar{c} ([A_g] - [A_g]_{eq})}{1 + \frac{8\lambda}{\alpha_c D_p}} \quad (2)$$

in which N_p is the particle number density, D_p is the diameter of the particle, λ is the mean free path of air (65 nm), \bar{c} is the mean molecular speed of the species, α_c is the accommodation coefficient, and $[A_g]$ and $[A_g]_{eq}$ are the mass concentrations of the bulk and near-surface (equilibrium) gas-phase species, respectively. $[A_g]_{eq}$ is calculated by absorptive partitioning (5):

$$[A_g]_{eq} = \frac{[A_p]}{K_p M} = \frac{[A_p]}{K_p ([A_p] + [B_p] + M(0))} \quad (3)$$

in which $M(0)$ is mass concentration of preexisting organic aerosol. For simulations of reactions carried out in the absence of organic aerosol (i.e., chamber experiments), initial absorbing aerosol mass loading $M(0)$ is set to a very small but nonzero value (0.1 ng/m^3). The kinetics of gas-particle partitioning (eq 2) require values for D_p and N_p ; to simplify the modeling, three assumptions are made: (1) particle number concentration is fixed at $2 \times 10^4/\text{cm}^3$, (2) the aerosol population is monodisperse, and (3) the organic aerosol has unit density. Relaxation of any of these assumptions is expected to have a minimal effect on model results.

For the simulations discussed here, the parent hydrocarbon reacts with rate $k_{HC} = 0.015 \text{ min}^{-1}$, forming A with a stoichiometric yield of 0.2, reasonable values for an SOA-forming reaction. Rates of the reactions of species A are chosen to be comparable to hydrocarbon oxidation, with $k_p = k_{HC}$ and $k_g = 0.3 k_{HC}$; if the reactions were substantially slower, their effects would not be observed on the time scale of chamber experiments. The semivolatile compound A is assigned a K_p of $0.1 \mu\text{g}^{-1} \text{ m}^3$ (for a saturation vapor pressure of $10 \mu\text{g/m}^3$), \bar{c} of 200 m/s (corresponding to a MW of $\sim 150 \text{ g/mol}$), and α_c of 0.02 (as determined for glyoxal (34)). For most simulations, only the initial conditions ($HC(0)$, $M(0)$, and seed volume) are varied.

Model Predictions. Figure 3a shows concentrations as a function of time after reaction initiation, for conditions typical of “seeded” chamber experiments: initial hydrocarbon concentration is relatively high ($HC(0) = 91 \mu\text{g/m}^3$), and the preexisting aerosol seed is ammonium sulfate ($20 \mu\text{g/m}^3$), with negligible initial organic mass ($M(0) = 0.1 \text{ ng/m}^3$).

Following reaction initiation, there is an induction period, a result of the absence of absorbing aerosol into which the semivolatile organic may partition. Thus the semivolatile species increases in concentration in the gas phase, during which time some fraction reacts away to form X. Only when A_g approaches its saturation vapor pressure does partitioning begin and SOA mass is formed. After $\sim 12 \text{ h}$ all the hydrocarbon is reacted away, A has fully reacted to form X or B_p , and aerosol formation is completed, with $\Delta M = 10 \mu\text{g/m}^3$. Thus the SOA mass yield is 11% at an organic aerosol loading of $10 \mu\text{g/m}^3$.

SOA yields over a range of aerosol mass loadings are generally determined by varying the amount of hydrocarbon reacted, which leads to differences in M . Calculated yields over a range of M 's are presented in Figure 4 (curve a). The curve of yield vs M (over the atmospherically relevant range of M 's) has the qualitative shape of a typical “yield curve”,

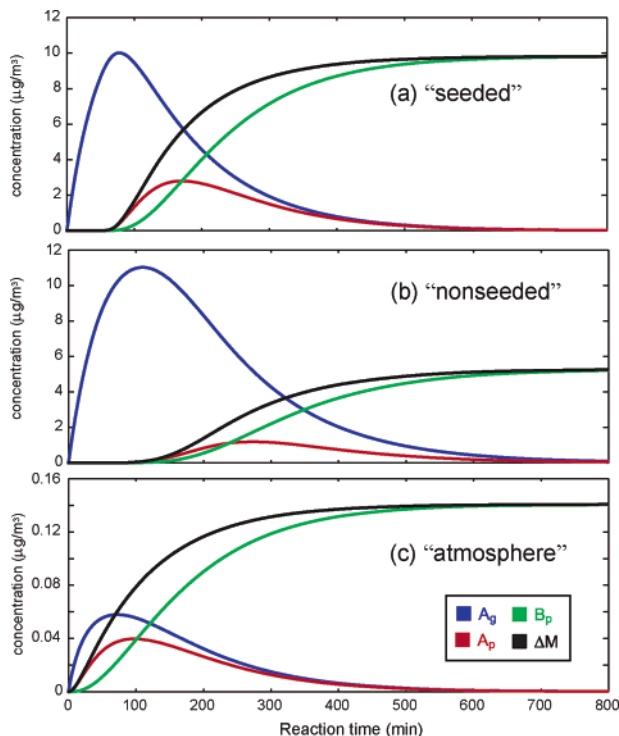


FIGURE 3. Predictions from the mechanism in Figure 2d, showing the time-dependent mass concentrations of key species. In all cases $\alpha = 0.2$, $K_p = 0.1 \text{ m}^3 \mu\text{g}^{-1}$, $k_{HC} = k_p = 0.015 \text{ min}^{-1}$, and $k_g = 0.0045 \text{ min}^{-1}$. (a) Initial concentrations typical of chamber conditions: $\text{HC}(0) = 92 \mu\text{g}/\text{m}^3$, $M(0) = 0.1 \text{ ng}/\text{m}^3$, and $20 \mu\text{g}/\text{m}^3$ ammonium sulfate seed. (b) Same as a but with no ammonium sulfate seed. (c) Initial concentrations more typical of atmospheric conditions: $\text{HC}(0) = 1 \mu\text{g}/\text{m}^3$ and $M(0) = 10 \mu\text{g}/\text{m}^3$.

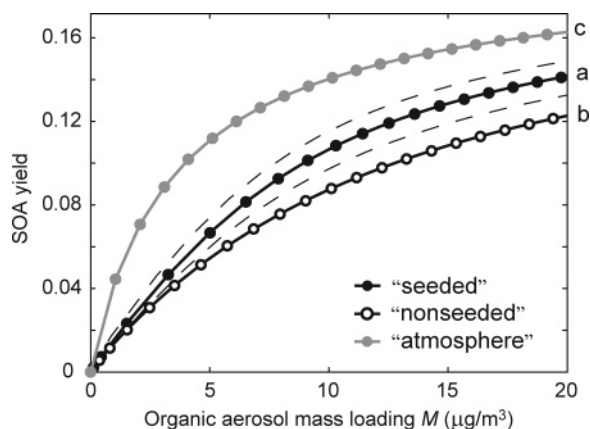


FIGURE 4. Yield curves predicted from the kinetic model. Curves a and b: “seeded” and “nonseeded” cases, in which model parameters are the same as those in Figure 3a and b. M is varied by changing $\text{HC}(0)$, as is typically done in chamber studies (increments of $5 \mu\text{g}/\text{m}^3$). Dashed lines are the same as curve a but with k_p increased by 50% (upper curve) or k_g increased by 25% (lower curve). Curve c: “atmosphere” case, as in Figure 3c. M is varied by changes to $M(0)$ (in increments of $1 \mu\text{g}/\text{m}^3$); $\text{HC}(0)$ is held at $1 \mu\text{g}/\text{m}^3$.

consistent with the simple partitioning of a single semivolatile compound (Figure 2a). Thus SOA growth is governed by semivolatile partitioning, even though nonvolatile species are also formed. This yield curve (and the others in Figure 4) may be fit to the single-product partitioning expression (eq 1), to obtain effective partitioning parameters; however, these do not match those used in the model, as SOA growth is also strongly influenced by reaction rates (k_{HC} , k_p and k_g).

The effects on SOA yields of the values of these reaction rates are illustrated by the dashed curves in Figure 4. The upper curve is the case in which k_p , the particle-phase reaction rate constant, is increased by 50%; this is consistent with laboratory measurements of enhanced SOA yields in the presence of acidic seed particles, presumably by acid-catalyzed reactions (19, 21, 23, 28). The lower curve shows the effect of increasing k_g , the rate constant for reaction in the gas phase, by 25%, leading to decreased aerosol yields. This is consistent with laboratory evidence that photolysis of semivolatile compounds leads to the formation of relatively volatile products (29–31). In the case where such gas-phase reactions dominate ($k_g > k_p$) and the condensable product is reasonably nonvolatile (high K_p), SOA mass can actually decrease via this volatilization mechanism; such behavior has been observed recently in SOA formation from isoprene oxidation under NO_x -free conditions (11). These gas-phase reactions reduce SOA growth by reducing the concentration of the semivolatile species in the gas phase; similarly, an increase in the rate of formation of the semivolatile species, which increases its gas-phase concentration, will increase the SOA yield. The role of hydrocarbon oxidation rate on SOA formation from aromatic photooxidation is discussed in a separate study (15).

Shown in Figure 3b is the reaction profile for the “nonseeded” case, with conditions the same as those in Figure 3a, only without any ammonium sulfate seed present. Nucleation dynamics are not explicitly included in this model, as very small particles ($D_p < 5 \text{ nm}$), composed of the trace preexisting organic mass ($0.1 \text{ ng}/\text{m}^3$), are assumed to be present. The hydrocarbon oxidation (and hence formation of the semivolatile species) is the same as in the “seeded” case, but because of the much lower particle surface area, there is a mass transfer limitation to gas–particle partitioning. Thus A accumulates in the gas phase, even exceeding its saturation vapor pressure, and partitioning (SOA formation) does not occur until later in the reaction. Such an increase in induction period was predicted by Bowman et al. (34), but in that work the semivolatile organic underwent partitioning only (as in Figure 2a), so only the rate of SOA growth was affected. However, in the present case, the reaction $A_g \rightarrow X$ competes with partitioning, so that longer induction periods lead to more depletion of the semivolatile compound, and less SOA is formed.

As shown in Figure 4 (curve b), yields in the nonseeded case are consistently lower than those in the seeded case, over a range of values of M . Thus this mechanism is qualitatively consistent with the seed effect observed in aromatic photooxidation (Figure 1). Fitting the SOA growth data to this kinetic model is beyond the scope of this work, but simple comparisons are possible; for example, the fact that in the seeded case no induction period is observed even though one is predicted suggests that aromatic oxidation products are less volatile (higher K_p) than simulated in the model. The modeled differences between the seeded and nonseeded cases in Figure 4 are relatively modest, but would be larger under conditions of greater aerosol formation (higher K_p , higher k_p , etc.), or a longer induction period (higher saturation ratio S prior to aerosol growth).

Therefore reactions of semivolatile compounds may have a large influence on SOA yields, and their importance is governed in part by the timing of the onset of gas–particle partitioning. In the seeded case (Figure 3a) this induction period is a result of the initial lack of organic aerosol mass into which the semivolatile organics may partition; in the unseeded case (Figure 3b) it is longer due to the mass-transfer limitation arising from the initially small aerosol surface area. However, in the atmosphere, organic aerosol is generally present, so such effects are not expected. Shown in Figure 3c is a simulation using more realistic tropospheric condi-

tions: a small amount of hydrocarbon ($\text{HC}(0) = 1 \mu\text{g}/\text{m}^3$) reacted in the presence of background organic aerosol ($M(0) = 10 \mu\text{g}/\text{m}^3$). These initial conditions are different from those of chamber experiments (Figure 3a and b), in which large amounts of hydrocarbon are reacted with no organic aerosol present; however all other parameters are left unchanged. Because absorbing aerosol is already present, there is no induction period and gas–particle partitioning of the semivolatile species begins immediately. As a result, a smaller fraction of A reacts to form X in the early stages of the reaction. Final aerosol growth (ΔM) is $0.14 \mu\text{g}/\text{m}^3$, for an SOA yield of 14% at an organic mass loading of $10.1 \mu\text{g}/\text{m}^3$; this yield is significantly higher than that of the “seeded” case (Figure 3a) at nearly the same value of M .

Aerosol yields over a range of organic aerosol loadings are shown in Figure 4, curve c. Unlike for chamber studies (curves a and b), M is varied by changing not $\text{HC}(0)$ (which is fixed at $1 \mu\text{g}/\text{m}^3$) but instead the preexisting organic aerosol loading $M(0)$. Over the range of M 's shown, SOA yields in the atmospheric case are significantly higher than those in the chamber case, owing to differences in initial partitioning conditions. Such differences in yields are significant (at $M = 5 \mu\text{g}/\text{m}^3$, yield in the “atmosphere” case is about twice that in the “unseeded” case), and are comparable to those from changing reaction conditions (dashed curves).

Implications. We have presented experimental data showing that SOA yields from the photooxidation of aromatic hydrocarbons are enhanced when ammonium sulfate is present. Such an effect is inconsistent with a mechanism of SOA formation that involves only the formation and partitioning of semivolatile species (Figure 2a). Instead, there must be additional processes (chemical reactions and/or surface losses) that affect the concentrations of semivolatile organics; the effect on SOA yields of such reactions, particularly those occurring in the gas phase, have so far received little attention. We propose as a model system the mechanism shown in Figure 2d, in which a semivolatile species may undergo reactions in both the gas phase (reducing its concentration and hence reducing SOA formation) and the particle phase (promoting SOA formation). The seed effect arises from loss of the semivolatile compound during the induction period, which is longer in the nonseeded experiment as a result of mass-transfer limitations. The additional reactions of semivolatile species may also account for a number of other recent experimental observations, such as nonvolatile species in SOA, increased SOA yields with acidic seed, and photochemical loss of SOA mass. An important implication of these reactions is that SOA yields may be quite dependent on detailed reaction conditions. In particular, in laboratory studies of SOA formation, an induction period prior to gas–particle partitioning, during which time gas-phase semivolatile species may be depleted by chemical reaction or wall loss, may lead to lower SOA formation than occurs under atmospheric conditions. Such an effect may contribute to the discrepancies between modeled and measured SOA in the atmosphere (2–4).

Our results suggest that chamber experiments need to be carried out as much as possible under atmospherically realistic conditions, in terms of not only chemistry (oxidant levels, NO_x levels, etc.) but also partitioning (preexisting aerosol). The aromatic photooxidation results presented here indicate that the presence of inorganic seed aerosol can be important for initiating gas–particle partitioning, as lack of aerosol surface area may inhibit uptake of organics; our modeling results suggest the presence of organic aerosol, which allows for immediate absorptive partitioning of organics, may be important as well. Running experiments under conditions similar to those of Figure 3c is infeasible, but the presence of even a small amount of organic seed aerosol (a few $\mu\text{g}/\text{m}^3$) would eliminate the induction period,

substantially reducing differences between “chamber” and “atmospheric” conditions. The loading of preexisting organic seed is a parameter that has not been explored in chamber experiments of SOA formation thus far, and certainly warrants future study.

The effect of preexisting organic aerosol is expected to be most important for reactions that form semivolatile compounds with relatively high vapor pressures (low K_p 's), and hence which exhibit significant induction times. For reactions involving relatively low-volatility condensable compounds (high K_p 's), SOA growth begins very early in the reaction. For these reactions, such as α -pinene ozonolysis (36, 37), the induction period is negligible, and gas–particle partitioning occurs throughout the experiment at atmospherically relevant levels.

The induction periods described here are a result of the buildup of semivolatile products in the gas-phase prior to gas–particle partitioning; induction periods may arise from other effects as well. Examples include photooxidation reactions carried out under high- NO_x conditions, in which SOA formation does not begin until $[\text{NO}]$ falls to ppb levels (e.g., 11, 14), and reactions involving multiple rate-limiting steps to SOA formation (34, 36). In both cases the delay is in the formation of the semivolatile species rather than in gas–particle partitioning, so may occur under atmospheric conditions. The sources of (and relationships between) different induction periods need to be understood in order for chamber yield measurements to accurately represent atmospheric conditions.

We emphasize that the mechanism shown in Figure 2d, while likely to be valid for some semivolatile organics, is not intended as a general scheme describing the chemistry of all condensable compounds. Most SOA-forming reactions involve a large number of semivolatiles, which may react via any number of mechanisms, including those shown in Figure 2. This mechanism is instead used as a model system illustrating the potential influence of reactions of semivolatile species on SOA formation, and the resulting dependence of SOA yields on reaction and partitioning conditions. Such reactions are often not treated explicitly in models of SOA formation, but certainly occur for a wide range of compounds: most organics are susceptible to reaction with OH, and loss to chamber walls is a potential sink for species that are efficiently taken up to the aerosol phase. If these processes are fast on the time scale of chamber experiments, they may have a substantial impact on SOA growth, and on the relationship between chamber studies and real atmospheric conditions. Only by explicitly including such reactions in models of SOA formation, or by making SOA yield measurements under oxidative and partitioning conditions relevant to the atmosphere, can such effects be taken fully into account.

Acknowledgments

This research was funded by the U.S. Environmental Protection Agency Science to Achieve Results (STAR) Program grant RD-83107501-0, managed by EPA's Office of Research and Development (ORD), National Center for Environmental Research (NCER), and by U.S. Department of Energy Biological and Environmental Research Program DE-FG02-05ER63983; this work has not been subjected to the EPA's required peer and policy review and therefore does not necessarily reflect the views of the Agency and no official endorsement should be inferred.

Literature Cited

- 1) Kanakidou, M.; Seinfeld, J. H., Pandis, S. N.; Barnes, I.; Dentener, F. J.; Facchini, M. C.; Van Dingenen, R.; Ervens, B.; Nenes, A.; Nielsen, C. J. Organic aerosol and global climate modelling: a review. *Atmos. Chem. Phys.* **2005**, *5*, 1053–1123.

- (2) De Gouw, J. A.; Middlebrook, A. M.; Warneke, C.; Goldan, P. D.; Kuster, W. C.; Roberts, J. M.; Fehsenfeld, F. C.; Worsnop, D. R.; Canagaratna, M. R.; Pszenny, A. A. P. Budget of organic carbon in a polluted atmosphere: Results from the New England Air Quality Study in 2002. *J. Geophys. Res.* **2005**, *110*, D16305, doi:10.1029/2004JD005623.
- (3) Heald, C. L.; Jacob, D. J.; Park, R. J.; Russell, L. M.; Huebert, B. J.; Seinfeld, J. H.; Liao, H.; Weber, R. J. A large organic aerosol source in the free troposphere missing from current models. *Geophys. Res. Lett.* **2005**, *32*, L18809, doi:10.1029/2005GL023831.
- (4) Volkamer R.; Jimenez, J. L.; San Martini, F.; Szepina, K.; Zhang, Q.; Salcedo, D.; Molina, L. T.; Worsnop, D. R.; Molina, M. J. Secondary organic aerosol formation from anthropogenic air pollution: rapid and higher than expected. *Geophys. Res. Lett.* **2006**, *33*, L17811, doi:10.1029/206GL026899.
- (5) Pankow, J. F. An absorption model of gas/particle partitioning of organic compounds in the atmosphere. *Atmos. Environ.* **1994**, *28A*, 185–188.
- (6) Pankow, J. F. An absorption model of the gas/aerosol partitioning involved in the formation of secondary organic aerosol. *Atmos. Environ.* **1994**, *28A*, 189–193.
- (7) Odum J. R.; Hoffmann, T.; Bowman, F.; Collins, D.; Flagan, R. C.; Seinfeld, J. H. Gas/particle partitioning and secondary organic aerosol yields. *Environ. Sci. Technol.* **1996**, *30*, 2580–2585.
- (8) Seinfeld, J. H.; Pankow, J. F. Organic atmospheric particulate matter. *Annu. Rev. Phys. Chem.* **2003**, *54*, 121–140.
- (9) Cocker, D. R., III; Flagan, R. C.; Seinfeld, J. H. State-of-the-art chamber facility for studying atmospheric aerosol chemistry. *Environ. Sci. Technol.* **2001**, *35*, 2594–2601.
- (10) Keywood, M. D.; Varutbangkul, V.; Bahreini, R.; Flagan, R. C.; Seinfeld, J. H. Secondary organic aerosol formation from the ozonolysis of cycloalkenes and related compounds. *Environ. Sci. Technol.* **2004**, *38*, 4157–4164.
- (11) Kroll, J. H.; Ng, N. L.; Murphy, S. M.; Flagan, R. C.; Seinfeld, J. H. Secondary organic aerosol formation from isoprene photooxidation. *Environ. Sci. Technol.* **2006**, *40*, 1869–1877.
- (12) Odum, J. R.; Jungkamp, T. P. W.; Griffin, R. J.; Forstner, H. J. L.; Flagan, R. C.; Seinfeld, J. H. Aromatics, reformulated gasoline, and atmospheric organic aerosol formation. *Environ. Sci. Technol.* **1997**, *31*, 1890–1897.
- (13) Song, C.; Na, K. Cocker, D. R., III. Impact of the hydrocarbon to NO_x ratio on secondary organic aerosol formation. *Environ. Sci. Technol.* **2005**, *39*, 3143–3149.
- (14) Johnson, D.; Jenkin, M. E.; Wirtz, K.; Martín-Reviejo, M. Simulating the formation of secondary organic aerosol from the photooxidation of toluene. *Environ. Chem.* **2004**, *1*, 150–165.
- (15) Ng, N. L.; Kroll, J. H.; Chan, A. W. H.; Chhabra, P.; Flagan, R. C.; Seinfeld, J. H. Secondary organic aerosol formation from m-xylene, toluene, and benzene. *Atmos. Chem. Phys. Discuss.* **2007**, *7*, 4085–4126.
- (16) Cocker, D. R., III; Mader B. T.; Kalberer, M.; Flagan, R. C.; Seinfeld, J. H. The effect of water on gas–particle partitioning of secondary organic aerosol: II. m-xylene and 1,3,5-trimethylbenzene photooxidation systems. *Atmos. Environ.* **2001**, *35*, 6073–6085.
- (17) Kroll, J. H.; Seinfeld, J. H. Representation of secondary organic aerosol (SOA) laboratory chamber data or the interpretation of mechanisms of particle growth. *Environ. Sci. Technol.* **2005**, *39*, 4159–4165.
- (18) Tobias, H. J.; Ziemann, P. J. Thermal desorption mass spectrometric analysis of organic aerosol formed from reactions of 1-tetradecene and O₃ in the presence of alcohols and carboxylic acids. *Environ. Sci. Technol.* **2000**, *34*, 2105–2115.
- (19) Tolocka, M. P.; Jang, M.; Ginter, J. M.; Cox, F. J.; Kamens, R. M.; Johnston, M. V. Formation of oligomers in secondary organic aerosol. *Environ. Sci. Technol.* **2004**, *38*, 1428–1434.
- (20) Kalberer, M.; Paulsen, D.; Sax, M.; Steinbacher, M.; Dommen, J.; Prevot, A. S. H.; Fisseha, R.; Weingartner, E.; Frankevich, V.; Zenobi, R.; Baltensperger, U. Identification of polymers as major components of atmospheric organic aerosols. *Science* **2004**, *303*, 1659–1662.
- (21) Iinuma, Y.; Böge, O.; Gnauk, T.; Herrmann, H. Aerosol-chamber study of the α -pinene/O₃ reaction: influence of particle acidity on aerosol yields and products. *Atmos. Environ.* **2004**, *38*, 761–773.
- (22) Gao, S.; Ng, N. L.; Keywood, M.; Varutbangkul, V.; Bahreine, R.; Nenes, A.; He, J.; Yoo, K. Y.; Beauchamp, J. L.; Hodyss, R. P.; Flagan, R. C.; Seinfeld, J. H. Particle phase acidity and oligomer formation in secondary organic aerosol. *Environ. Sci. Technol.* **2004**, *38*, 6582–6589.
- (23) Gao, S.; Keywood, M.; Ng, N. L.; Surratt, J.; Varutbangkul, V.; Bahreini, R.; Flagan, R. C.; Seinfeld, J. H. Low-molecular weight and oligomeric components in secondary organic aerosol from the ozonolysis of cycloalkenes and α -pinene. *J. Phys. Chem. A* **2004**, *108*, 10147–10164.
- (24) Surratt, J. D.; Murphy, S. M.; Kroll, J. H.; Ng, N. L.; Hildebrandt, L.; Sorooshian, A.; Szmigielski, R.; Vermeylen, R.; Maenhaut, W.; Claeys, M.; Flagan, R. C.; Seinfeld, J. H. Chemical composition of secondary organic aerosol formed in the photooxidation of isoprene. *J. Phys. Chem. A* **2006**, *110*, 9665–9690.
- (25) Liggio, J.; Li, S.-M.; McLaren, R. Heterogeneous reactions of glyoxal on particulate matter: Identification of acetals and sulfate esters. *Environ. Sci. Technol.* **2005**, *39*, 1532–1541.
- (26) Liggio, J.; Li, S.-M. Organosulfate formation during the uptake of pinonaldehyde on acidic sulfate aerosols. *Geophys. Res. Lett.* **2006**, *33*, L13808, doi:10.1029/2006GL026079.
- (27) Surratt, J. D.; Kroll, J. H.; Kleindienst, T. E.; Edney, E. O.; Claeys, M.; Sorooshian, A.; Ng, N. L.; Offenberg, J. H.; Lewandowski, M.; Jaoui, M.; Flagan, R. C.; Seinfeld, J. H. Evidence for organosulfates in secondary organic aerosol. *Environ. Sci. Technol.* **2007**, *41* (2), 517–527.
- (28) Jang, M.; Czoschke, N. M.; Lee, S.; Kamens, R. M. Heterogeneous atmospheric aerosol production by acid-catalyzed particle-phase reactions. *Science* **2002**, *298*, 814–817.
- (29) Presto, A. A.; Huff Hartz, K. E.; Donahue, N. M. Secondary organic aerosol production from terpene ozonolysis. 1. Effect of UV radiation. *Environ. Sci. Technol.* **2005**, *39*, 7036–7045.
- (30) Gomez, A. L.; Park, J.; Walser, M. L.; Lin, A.; Nizkorodov, S. A. UV photodissociation spectroscopy of oxidized undecylenic acid films. *J. Phys. Chem. A* **2006**, *110*, 3854–3592.
- (31) Park, J.; Gomez, A. L.; Walser, M. L.; Lin, A.; Nizkorodov, S. A. Ozonolysis and photolysis of alkene-terminated self-assembled monolayers on quartz nanoparticles: implications for photochemical aging of organic aerosol particles. *Phys. Chem. Chem. Phys.* **2006**, *8*, 2506–2512.
- (32) Hastings, W. P.; Koehler, C. A.; Bailey, E. L.; De Haan, D. O. Secondary organic aerosol formation by glyoxal hydration and oligomer formation: Humidity effects and equilibrium shifts during analysis. *Environ. Sci. Technol.* **2005**, *39*, 8728–8735.
- (33) Kroll, J. H.; Ng, N. L.; Murphy, S. M.; Varutbangkul, V.; Flagan, R. C.; Seinfeld, J. H. Chamber studies of secondary organic aerosol growth by reactive uptake of simple carbonyl compounds. *J. Geophys. Res.* **2005**, *110*, D23207, doi:10.1029/2005JD006004.
- (34) Bowman, F. M.; Odum, J. R.; Seinfeld, J. H.; Pandis, S. N. Mathematical model for gas-particle partitioning of secondary organic aerosols. *Atmos. Environ.* **1997**, *31*, 3921–3931.
- (35) Schweitzer, F.; Magi, L.; Mirabel, P.; George, C. Uptake rate measurements of methanesulfonic acid and glyoxal by aqueous droplets. *J. Phys. Chem. A* **1998**, *102*, 593–600.
- (36) Ng, N. L.; Kroll, J. H.; Keywood, M. D.; Bahreine, R.; Varutbangkul, V.; Flagan, R. C.; Seinfeld, J. H.; Lee, A.; Goldstein, A. H. Contribution of first- versus second-generation products to secondary organic aerosols formed in the oxidation of biogenic hydrocarbons. *Environ. Sci. Technol.* **2006**, *40*, 2283–2297.
- (37) Presto, A. A.; Donahue, N. M. Investigation of α -pinene + ozone secondary organic aerosol formation at low total aerosol mass. *Environ. Sci. Technol.* **2006**, *40*, 3536–3543.

Received for review August 28, 2006. Revised manuscript received November 21, 2006. Accepted February 28, 2007.

ES062059X

Appendix B

Low-Molecular-Weight and Oligomeric Components in Secondary Organic Aerosol from the Ozonolysis of Cycloalkenes and α -Pinene*

* This chapter is reproduced by permission from “Low-Molecular-Weight and Oligomeric Components in Secondary Organic Aerosol from the Ozonolysis of Cycloalkenes and α -Pinene” by S. Gao, M. Keywood, N. L. Ng, J. Surratt, V. Varutbangkul, R. Bahreini, R. C. Flagan, J. H. Seinfeld, *Journal of Physical Chemistry A*, 108 (46): 10147-10164, 2004. Copyright 2004, American Chemical Society.

Low-Molecular-Weight and Oligomeric Components in Secondary Organic Aerosol from the Ozonolysis of Cycloalkenes and α -Pinene

Song Gao, Melita Keywood, Nga L. Ng, Jason Surratt, Varuntida Varutbangkul, Roy Bahreini, Richard C. Flagan, and John H. Seinfeld*

Departments of Environmental Science and Engineering and Chemical Engineering, California Institute of Technology, Pasadena, California 91125

Received: June 11, 2004; In Final Form: August 30, 2004

The composition of secondary organic aerosol (SOA) from the ozonolysis of C₅–C₈ cycloalkenes and α -pinene, as well as the effects of hydrocarbon precursor structure and particle-phase acidity on SOA formation, have been investigated by a series of controlled laboratory chamber experiments. A liquid chromatography–mass spectrometer and an ion trap mass spectrometer are used concurrently to identify and to quantify SOA components with molecular weights up to 1600 Da. Diacids, carbonyl-containing acids, diacid alkyl esters, and hydroxy diacids are the four major classes of low-molecular-weight (MW < 250 Da) components in the SOA; together they comprise 42–83% of the total SOA mass, assuming an aerosol density of 1.4 g/cm³. In addition, oligomers (MW > 250 Da) are found to be present in all SOA. Using surrogate standards, it is estimated that the mass fraction of oligomers in the total SOA is at least 10% for the cycloalkene systems (with six or more carbons) and well over 50% for the α -pinene system. Higher seed particle acidity is found to lead to more rapid oligomer formation and, ultimately, to higher SOA yields. Because oligomers are observed to form even in the absence of seed particles, organic acids produced from hydrocarbon oxidation itself may readily promote acid catalysis and oligomer formation. The distinct effects of carbon numbers, substituent groups, and isomeric structures of the precursor hydrocarbons on the composition and yield of SOA formed are also discussed.

Introduction

Secondary organic aerosol (SOA) is formed when the atmospheric oxidation of organic species leads to compounds of increased polarity and decreased vapor pressure that condense into the particulate phase.¹ Predicting the amount of SOA that results from atmospheric oxidation of particular organic molecules has proven challenging because (1) oxidation pathways for the relatively larger parent organics that lead to SOA are not well established, and (2) current analytical techniques, especially when a single method is used, commonly fail to identify many SOA components. Traditional techniques such as gas chromatography–mass spectrometry (GC–MS) can typically resolve only about 10% (by mass) of total atmospheric aerosol organics.^{2–4}

Recent work has made substantial progress in achieving a better mass closure of SOA, for example, by using GC–MS with a double derivatization technique.^{5,6} However, the tedious derivatization procedures risk sample contamination and/or loss, and they are compound-specific only. Intrinsically, a substantial fraction of SOA components, such as the least volatile and very polar, may readily evade detection by GC–MS, either by never eluting off the column or decomposing during the analysis.⁷ Therefore, an analytical method that can preserve molecular integrity and capture the main feature of SOA composition, especially the very polar and less volatile species, is desirable.

Another major issue is to understand the relationship between the structures of the parent molecule and the amount and composition of SOA subsequently formed. Although previous

studies have identified a number of SOA components with various functional groups, polarities, and volatilities, it is generally unclear how factors such as carbon number, presence or absence of double bonds, and presence or absence of alkyl substituent groups affect both resultant SOA amount and composition. Of course, answers to these questions lie in understanding the mechanisms of gas-phase oxidation of the parent hydrocarbons. As we noted above, these oxidation mechanisms tend to be complex. One approach is to use measured SOA yields and compositions as a means to infer the mechanisms that lead to SOA formation. By selecting precursor hydrocarbons that vary structurally in a determined manner, it is possible to infer how structural differences in parent hydrocarbons translate into differences in the SOA formation pathways. It is this approach that we follow in the present work.

The traditional view of SOA formation is that gas-phase oxidation of the parent hydrocarbons leads to multifunctional, low-volatility products that partition themselves between the gas and aerosol phases.¹ The partitioning is strongly affected by temperature and, to a somewhat lesser extent, by the phase state of the aerosol. Because of the lack of direct information to the contrary, it had been assumed that, once in the aerosol phase, the oxidation products did not react further and that the amount of SOA formed depended entirely on the gas-particle partitioning.

Recent discoveries show that once the gas-phase polar oxidation products condense into the aerosol phase particle-phase reactions may take place. First, it was demonstrated that acid-catalyzed heterogeneous reactions can occur,^{8,9} and second, the presence of oligomers in the aerosol phase was shown.^{10–13}

* Corresponding author. Email: seinfeld@caltech.edu.

A consequence of heterogeneous chemistry and oligomer formation is that species that partition between the gas and aerosol phases are converted to larger compounds of extremely low volatility, thereby locking these compounds into the aerosol phase and increasing the SOA yield over that in the absence of heterogeneous chemistry.

Consequently, fundamental questions arise: Are acids required for heterogeneous reactions and the associated increased SOA yields? If so, what types of acids? Are heterogeneous reactions directly responsible for the formation of oligomers? Are oligomers ubiquitous in atmospheric organic aerosols?

The major classes of parent hydrocarbons responsible for SOA formation are alkenes and aromatics. Whereas atmospheric aromatics are almost entirely anthropogenic in origin, alkenes arise from both anthropogenic and biogenic sources. On a global basis, it is estimated that the predominance of SOA results from biogenic terpenes.¹⁴ The oxidation of alkenes (including terpenes) includes reactions with O₃, OH, and NO₃. For a number of these alkenes, reaction with O₃ is a dominant path. From a mechanistic point of view, gas-phase O₃ oxidation should be less complex to unravel than photooxidation in the presence of NO_x. With the goal of understanding the effects of hydrocarbon structure and particle-phase acidity on SOA formation, we report here on a series of controlled experiments carried out in Caltech's dual laboratory chambers. We focus on the cycloalkenes with carbon number 5 and greater; these compounds are known to form SOA and, through choice of compounds, key structural factors such as the locations of double bonds and of alkyl substituent groups can be varied to determine the effects of these factors on SOA formation.

Seven cycloalkenes with 5 to 8 carbon numbers, serving as model compounds for many atmospheric hydrocarbons bearing similar molecular skeletons, were reacted with ozone under dark conditions. We employ liquid chromatography–mass spectrometry (LC–MS) in tandem with ion trap mass spectrometry (ITMS) to analyze the molecular composition of SOA formed and to explore the relationship between the SOA composition and hydrocarbon precursor structure. The overall yields of SOA formed in these systems and their relationships with precursor structures are discussed elsewhere.¹⁵ In addition, α -pinene, one of the most common biogenic hydrocarbons, was reacted with ozone under a set of controlled conditions to study the explicit effect of aerosol acidity on the amounts and composition of SOA formed and to explore the possible ubiquity of oligomers in atmospheric aerosols.

Experimental Section

All experiments were carried out under dark conditions in Caltech's dual 28-m³ Teflon chambers. Salt solutions were first nebulized into the precleaned chamber to form seed aerosols. For cycloalkene ozonolysis, dry (NH₄)₂SO₄ seed particles were generated from a 0.03 M salt solution. For α -pinene ozonolysis, wet MgSO₄ and (NH₄)₂SO₄ seed particles, and the corresponding particles from acidified solutions, were generated in most cases. A few dry seed particle experiments were also carried out for comparison purposes as well as a few experiments in the absence of any seed particles. The MgSO₄ and (NH₄)₂SO₄ solutions were 0.03 M each, with their acidified counterparts containing 0.03 M salt and 0.05 M H₂SO₄. Cyclohexane was then injected into the chamber to act as a hydroxyl radical scavenger, followed by hydrocarbon and ozone injections. The relative humidity was maintained at about 5% (dry chamber) for the cycloalkene experiments and 55% (humid chamber) for the α -pinene experiments. The temperature was always maintained at about

20 °C. Aerosol number concentration, size distribution, hygroscopic growth, and hydrocarbon mixing ratio were continuously measured. Particle loss to the chamber wall was accounted for in the analysis of the SOA yield data. More details on these individual measurements and chamber characteristics can be found in Keywood et al.¹⁵

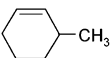
A series of cycloalkene ozonolysis experiments were carried out with the cycloalkene mixing ratio ranging from about 50 to 300 ppb and the ozone mixing ratio three times that of cycloalkene to ensure adequate oxidation. Detailed experimental conditions are given in Keywood et al.¹⁵ In each experiment, teflo membrane filter samples (PALL Life Sciences, 47-mm diameter, 1.0- μ m pore size) were collected at similar elapsed time (\sim 4–5 h) from the onset of ozone injection and for a duration of about 2–4 h, depending on the amount of SOA generated. During filter sampling, the parent hydrocarbons had already been completely consumed and the aerosol volume had reached its maximum value. In the case of α -pinene ozonolysis, we carried out seven pairs of “nonacid” and “acid” experiments, differing only by the absence or presence of externally added H₂SO₄ in the seed particles, in the two chambers in parallel, with all other conditions held identical. In each pair, filter samples were collected at nearly the same elapsed times (\sim 5–7 h) from the onset of ozone injection and for nearly the same duration (\sim 1–2 h). The α -pinene mixing ratios ranged from 12 to 135 ppb (Figure 9), whereas the ozone mixing ratio was two times that of α -pinene. In all experiments, the number concentration of the initial seed particles was about 20 000 cm⁻³ and the size distribution had a mean diameter of 80–100 nm.

Each filter was extracted in 5 mL of HPLC-grade methanol by sonication. The extract solution was then blown dry under a gentle stream of N₂ and reconstituted by 1 mL of 0.1% acetic acid in water solution with 50% methanol. A portion of this filter extract was analyzed by a Hewlett-Packard 1100 series LC–MS system mainly to identify and quantify low-molecular-weight species (roughly, MW < 250). The electrospray ionization (ESI) mode of the quadrupole MS was optimized so that carboxyl-containing species had the highest sensitivities. A Nova-Pak C₁₈ column (300 \times 3.9 mm, Waters) was used. The eluents were 0.1% acetic acid in water solution (A) and methanol (B), with B programmed from 25 to 60% in 15 min. Another portion of the filter extract was analyzed by a Finnigan LCQ ion trap mass spectrometer (ITMS) to identify species with molecular weights up to 1600 Da and to capture the overall feature of SOA composition, including high-molecular-weight species. Both negative and positive (Na⁺ added) ion modes of the ITMS were carried out so that compounds of different acidity and polarity could be detected. In addition, specific ions of interest were isolated from the rest of the sample matrix in the ITMS and were further fragmented to produce tandem MS, aiding structure elucidation.

Results and Discussion

1. Low-Molecular-Weight (low-MW) Components of SOA from Cycloalkene Ozonolysis. Seven cycloalkenes (Table 1), cyclopentene, cyclohexene, cycloheptene, cyclooctene, 1-methylcyclopentene, 1-methylcyclohexene, and 3-methylcyclohexene, at initial mixing ratios from 25 to 300 ppb, were reacted with ozone in the laboratory chambers described above. Because the low-MW species (MW < 250) in SOA from α -pinene ozonolysis have previously received rather extensive attention in the literature,^{16–18} discussion of those species in this system is not reiterated. In addition, because of the similarity of the SOA products of cyclooctene to those of the nonmethylated

TABLE 1: Molecular Structures of Precursor Hydrocarbons Investigated in This Study

Precursor Hydrocarbon	Molecular Structure	Precursor Hydrocarbon	Molecular Structure
Cyclopentene		1-methyl cyclopentene	
Cyclohexene		1-methyl cyclohexene	
Cycloheptene		3-methyl cyclohexene	
Cyclooctene		α -pinene	

C₅, C₆, and C₇ cycloalkenes, we will not discuss the cyclooctene system in detail here.

Figure 1 shows the total ion chromatograms (TIC) of SOA filter extracts from cyclopentene, cyclohexene, cycloheptene, and cyclooctene. After blank correction, each chromatographic peak represents at least one SOA species. Because of the large number of SOA components, however, some peaks are convoluted in the TIC to various extents. To deconvolute these peaks (thus identify components) and to accurately quantify each species, extracted ion chromatograms (EIC) can be generated from the TIC for individual ions based on their mass-to-charge ratios (m/z), as can be seen in Figure 2, where the TIC and EIC of the extract of SOA from cycloheptene ozonolysis are shown. For illustration, only the ions with m/z of 145, 185, and 243 are shown here, although 20 species in total are identified in this system. Positive identification is based on the matching of (1) retention time and (2) m/z of standard compounds with chromatographic peaks. Under optimal electrospray ionization conditions, all 30 standard compounds are detected in the form of their molecular ions $[M - 1]^-$ and display no or minimal fragmentation. Table 1S (Supporting Information) lists the standard compounds calibrated, the m/z of each molecular ion, and the average and standard deviation of the corresponding retention time from at least three sets of calibrations on different days. The reproducibility of retention times is mostly within 0.05 min and never exceeds 0.1 min. Most species, therefore, can be chromatographically separated cleanly, and in the cases where there is an overlap of retention times, the m/z often allows definitive identification, such as malonic acid, 2-oxoglutaric acid, and 2-ketogulonic acid. The standard compounds represent a wide range of polarity and carbon numbers, from which a set of rules-of-thumb are deduced with regard to their retention times. For example, for homologous compounds, the retention time becomes longer as the carbon number increases. For the same carbon number, the elution sequence from earliest to latest is carbonyl diacid, hydroxy diacid, carbonyl monoacid, and diacid. C₆ and C₇ diacids commonly elute about 1 min earlier than their methyl ester isomers, which, in turn, elute about 1 min earlier than their ethyl ester isomers, whereas for C₅ diacid, this interval decreases to 0.8 min. On the basis of these rules and some extrapolation, we are able to assign identities to many species with no standards matching their retention times. Some isomers can be separated by their different retention times, such as 2-oxoadipic acid and pimelic acid. However, some isomers elute at nearly the same retention time; in some cases, one of the isomers does not have the standard available. In such cases,

we rely on known reaction mechanisms, albeit speculative, to assign an isomeric structure to represent these isomeric components. For example, in the SOA from cyclohexene ozonolysis, a peak eluting closely (~ 0.5 min) after 5-oxohexanoic acid (for which the standard is available) and having the same MW is identified as 6-oxohexanoic acid (for which a standard is not available). For nonmethylated cycloalkenes, reaction mechanisms point to the formation of ozonolysis products with carbonyl and carboxyl groups at the end, rather than in the middle, of the carbon chain.^{6,16} Although it is crucial to know exact structures of isomeric species to deduce reaction pathways, these isomers, with major functional groups being the same, are expected to play more or less identical roles in aerosol and cloud-related processes.

The mass concentration of each identified low-MW component in SOA was quantified with the corresponding standard's calibration curve. If a standard is not available, then a surrogate standard is chosen that has both similar MW and major functional groups. The identified and quantified low-MW species in a typical SOA in the six hydrocarbon systems are listed in Tables 2–7. The mass yield of a SOA component is defined as its mass quantified relative to the mass of the consumed hydrocarbon. On the basis of the major functional groups in the molecules, these species are grouped into four classes of compounds, that is, diacid, diacid alkyl ester, hydroxy diacid, and carbonyl-containing acid. The molecular structures and molecular weights of all these species are listed in Table 2S (Supporting Information), and are also grouped into these four classes of compounds. Kalberer et al.⁶ also studied the composition of SOA from cyclohexene ozonolysis under somewhat similar conditions using a well-developed GC–MS speciation technique. Among the most abundant SOA components, seven species were identified and quantified in both Kalberer et al.⁶ and this work. The molar yields (%) for adipic acid, glutaric acid, succinic acid, hydroxyadipic acid, hydroxyglutaric acid, 6-oxohexanoic acid, and 5-oxopentanoic acid were 0.74, 0.69, 0.14, 0.97, 1.99, 0.39, and 0.39%, respectively, in Kalberer et al.⁶ and were 0.89, 0.64, 0.05, 0.04, 0.16, 0.12, and 0.32%, respectively, in this work. Except for the two hydroxyl diacids, which have large uncertainties (to be discussed later), the two sets of measurements agree reasonably well.

In the cyclopentene, cyclohexene, 1-methylcyclopentene, and 3-methylcyclohexene systems, a small amount of C_{*n*+1} diacid was identified in the SOA from the ozonolysis of C_{*n*} (*n* being the total carbon number) hydrocarbon precursor. In addition, C_{*n*+2} diacid was identified in cyclopentene, cyclohexene, and 1-methylcyclopentene systems at lower abundance than the C_{*n*+1} diacid, and a minimal amount of C_{*n*+3} diacid was identified in SOA from 1-methylcyclopentene ozonolysis. Previous studies^{19,20} have shown that various carbonyls are gas-phase products from alkene and cycloalkene ozonolysis; for example, from cyclopentene ozonolysis, glyoxal (C₂), propanal, and butanal were produced with yields of 0.15, 0.04, and 0.12, respectively. From cyclohexene ozonolysis, pentanal, butanal, and formaldehyde were produced with yields of 0.16, 0.03, and 0.02, respectively. In addition, formaldehyde, acetaldehyde, and propanal were produced from ozonolysis of C₅ to C₇ linear alkenes with yields from 0.02 to 0.05.^{19,20} From C_{*n*} cycloalkene, ozonolysis would initially lead to an excited Criegee intermediate (C_{*n*}). With the presence of small carbonyls in the reaction system, both the excited and stabilized Criegee intermediate can react with these carbonyls to form secondary ozonides, which may further rearrange or decompose to form the C_{*n*+1}, C_{*n*+2}, and C_{*n*+3} diacids observed.

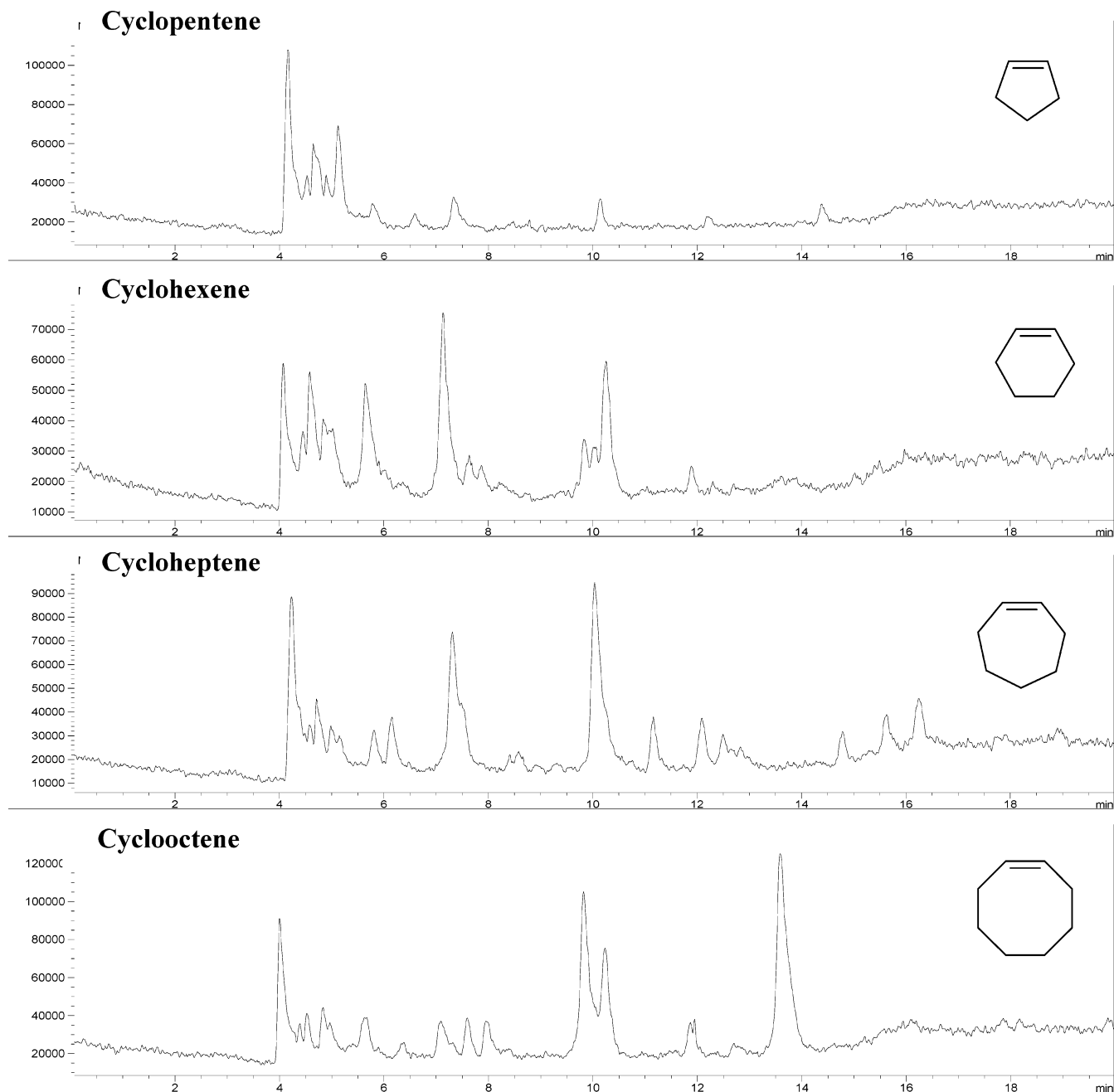
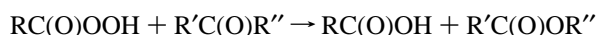


Figure 1. Typical total ion chromatograms of SOA from the ozonolysis of cycloalkenes.

Diacid methyl and ethyl esters were also identified in SOA from the ozonolysis of all six cycloalkenes. Standard runs have confirmed that these compounds do not result from the methanol extraction procedures. There are at least two possible reaction pathways involved. One is similar to the formation of C_{n+1} , C_{n+2} , C_{n+3} diacids, where Criegee intermediates can react with small carbonyls to form secondary ozonides. However, rearrangement or decomposition of ozonides may lead to the formation of esters, rather than diacids. Another possibility arises from the recent discovery²¹ that a C_5 peracid ($RC(O)OOH$) is a gas-phase product from cyclohexene ozonolysis. The well-known Baeyer–Villiger reaction between a peracid and a carbonyl²² would lead to the formation of an ester



Following this reaction, some carbonyl products discussed earlier may lead to the formation of methyl and ethyl esters. However,

whether and in what phase this reaction takes place requires further study.

We next discuss the relative abundance of identified SOA components in the six cycloalkene ozonolysis systems. Table 8 shows the mass percentage of each class of compounds in the total identified low-MW SOA species for the six systems. Rather constant percentages are observed from system to system: on average, diacids comprise $69 \pm 7\%$, hydroxy diacids comprise $8 \pm 4\%$, carbonyl-containing acids comprise $15 \pm 3\%$, and diacid alkyl esters comprise $11 \pm 7\%$ of the total identified low-MW species. C_n or C_{n-1} diacid is consistently the most abundant species, followed by either other diacids, or hydroxy C_n diacids, or C_n esters. Together, C_n , C_{n-1} , and C_{n+1} diacids comprise $62 \pm 9\%$ of the total identified low-MW species. This implies that there are stable, dominant reaction pathways of cycloalkene ozonolysis leading to the formation of these diacids, as speculated by earlier work.^{6,23}

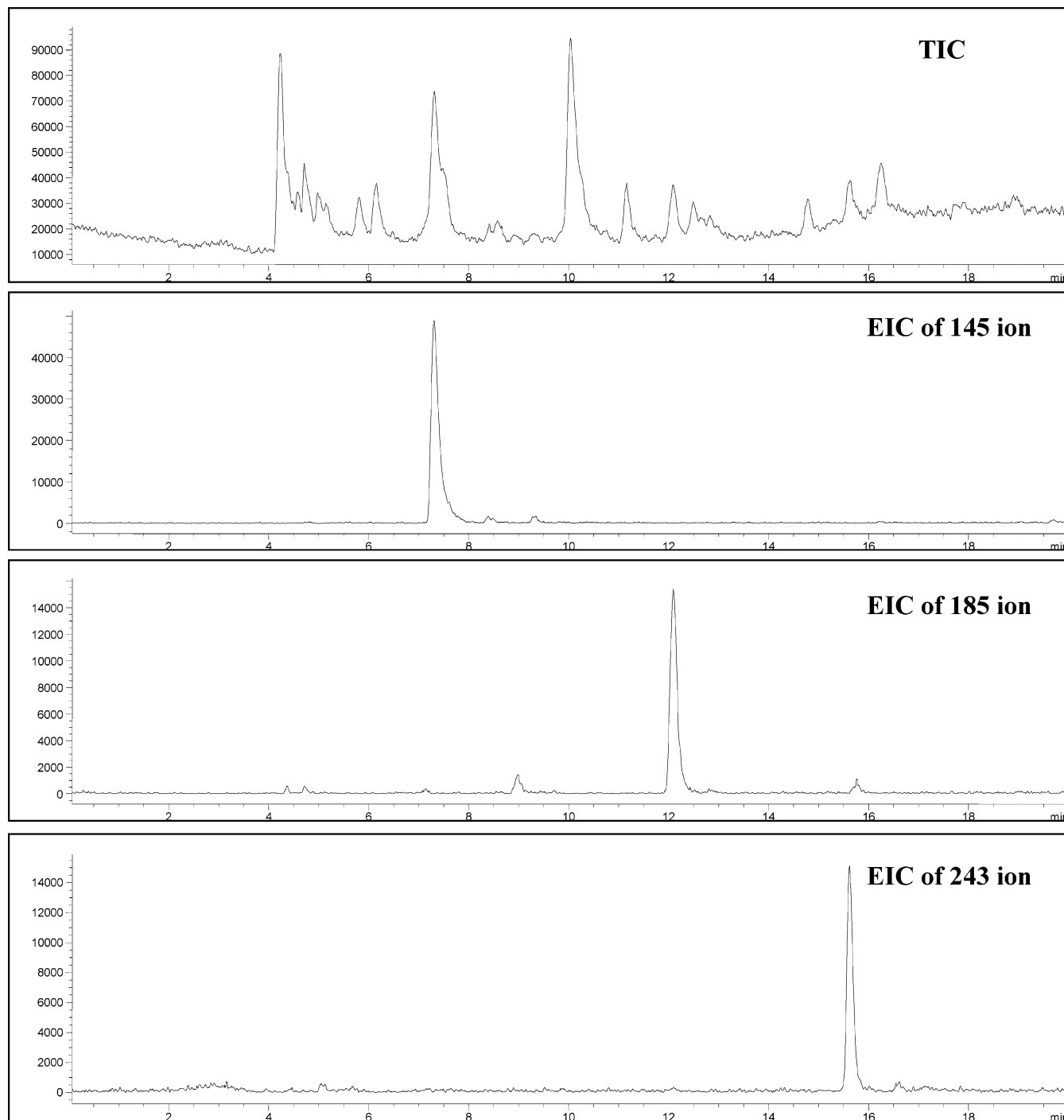


Figure 2. Total ion chromatograms (TIC) and extracted ion chromatograms (EIC) of 145, 185, and 243 ions of SOA from cycloheptene ozonolysis.

In comparison, the mass percentage of each class of compounds in the total SOA derived from the aerosol size distribution measurements, assuming an aerosol density of 1.4 g/cm^3 , varies greater from one cycloalkene system to another, as can be seen from the first four rows of Table 9. This variation is probably, in part, a result of the very different fractions of total identified low-MW species in the total SOA mass from system to system, as seen in the 5th row of Table 9. The use of 1.4 g/cm^3 (estimated for SOA from cyclohexene ozonolysis by Kalberer et al.⁶) as the density for the SOA in all six systems may be an important reason for this variation. Densities of some identified low-MW species are unknown, making it difficult to compute the overall aerosol density. Indeed, the exact density of SOA remains unknown and, as we discuss later, could very well be larger than that assumed. However, with regard to a

more accurate SOA mass closure, one correction we can do is to recover the mass of oxalic acid in all SOA. Oxalic acid was identified at substantial amount in the cyclohexene system;⁶ mechanistically, it is a degradation or final oxidation product of all cycloalkene ozonolyses. However, oxalic acid eluted off the LC column too quickly to be detected. Because oxalic acid was found by Kalberer et al.⁶ to have roughly the same abundance as adipic acid or glutaric acid in the SOA from cyclohexene ozonolysis, we used the amount of the most abundant diacid identified (C_n or C_{n-1}) to estimate the amount of oxalic acid in all SOAs. With this correction, the fractions of total identified low-MW SOA species range from 42 to 83%, as shown in the 6th row of Table 9.

One primary reason that Kalberer et al.⁶ achieved a mass closure of SOA products from cyclohexene ozonolysis close to

TABLE 2: Low-MW Components in SOA from Cyclopentene Ozonolysis^a

class of SOA components	identified low-MW species in SOA	surrogate standard for quantification ^b	mass yield (%) ^c
diacid	pimelic acid		0.19
	adipic acid		0.27
	glutaric acid		0.40
	succinic acid		2.72
diacid alkyl ester	adipic acid monomethyl ester		0.01
	glutaric acid monomethyl ester		0.02
	succinic acid monomethyl ester		0.09
	malonic acid monoethyl ester	succinic acid monomethyl ester	0.22
hydroxy diacid	2-hydroxyglutaric acid	2-hydroxy-2-methylsuccinic acid	0.57
	2-hydroxysuccinic acid	succinic acid	0.10
carbonyl-containing acid	4,5-dioxopentanoic acid	2-oxoglutaric acid	0.04
	5-oxopentanoic acid	4-oxopentanoic acid	0.01
sum of identified low-MW species ^d			4.64
total SOA mass derived from DMA ^e			6.04

^a 224 ppb of cyclopentene was consumed in this experiment. The filter was collected ~ 5 h from the onset of ozonolysis for a duration of ~ 4 h. ^b A blank cell indicates a standard was available for quantification. ^c To examine the variation of these yields, we analyzed SOA samples from three cyclopentene ozonolysis experiments, and the variation of these yields is on average within $\pm 25\%$, caused by analysis uncertainties and slightly different sampling times and duration. For the mass yields of other cycloalkene systems, we estimate the variation to be roughly $\pm 25\%$ as well. ^d The sum of identified low-MW species accounts for 77% of the total SOA mass derived from the DMA measurements. ^e A differential mobility analyzer (DMA) was used to measure the aerosol size distribution. The mass yield of the total SOA reported here, derived from the DMA measurement with the assumption of an aerosol density of 1.4 g/cm^3 , has not been corrected for particle loss to the chamber wall; therefore, it is somewhat lower than the actual total SOA mass yield. Both the “sum of identified low-MW species” and the “total SOA mass derived from DMA” here refer to their yields (in percentage, relative to the mass of the consumed hydrocarbon) as defined in text similarly for individual SOA components.

TABLE 3: Low-MW Components in SOA from Cyclohexene Ozonolysis^a

class of SOA components	identified low-MW species in SOA	surrogate standard for quantification ^b	mass yield (%)
diacid	suberic acid		0.03
	pimelic acid		0.90
	adipic acid		1.59
	glutaric acid		1.03
	succinic acid		0.08
diacid alkyl ester	glutaric acid monomethyl ester		0.05
	2-hydroxysuccinic acid monoethyl ester	succinic acid monoethyl ester	0.03
hydroxy diacid	2-hydroxypimelic acid	pimelic acid	0.01
	2-hydroxyadipic acid	3-hydroxy-3-methylglutaric acid	0.08
	2,5-dihydroxyadipic acid	3-hydroxy-3-methylglutaric acid	0.02
	2-hydroxyglutaric acid	2-hydroxy-2-methylsuccinic acid	0.28
	2-hydroxysuccinic acid	succinic acid	0.03
carbonyl-containing acid	2-oxoadipic acid		0.02
	5-oxohexanoic acid		0.02
	6-oxohexanoic acid	5-oxohexanoic acid	0.16
	4,5-dioxopentanoic acid	5-oxohexanoic acid	0.02
	4-oxopentanoic acid		0.09
	5-oxopentanoic acid	4-oxopentanoic acid	0.37
sum of identified low-MW species ^c			4.80
total SOA mass derived from DMA ^d			15.37

^a 313 ppb of cyclohexene was consumed in this experiment. The filter was collected ~ 4.5 h from the onset of ozonolysis for a duration of ~ 2 h. ^b A blank cell indicates a standard was available for quantification. ^c The sum of identified low-MW species accounts for 31% of the total SOA mass derived from the DMA measurements. ^d The mass yield of the total SOA reported here, derived from the DMA measurement with the assumption of an aerosol density of 1.4 g/cm^3 , has not been corrected for particle loss to the chamber wall; therefore, it is somewhat lower than the actual total SOA mass yield. Both the “sum of identified low-MW species” and the “total SOA mass derived from DMA” here refer to their yields (in percentage, relative to the mass of the consumed hydrocarbon) as defined in text similarly for individual SOA components.

100% is that they identified substantial amounts of hydroxy diacids, even more abundant than diacids. In contrast, in all six SOA systems we studied, hydroxy diacids are far less abundant than diacids. CO was used as the OH scavenger in Kalberer et al.,⁶ whereas cyclohexane was used in this study. As discussed by Keywood et al.,²⁴ different OH scavengers can affect the SOA formation because of different amounts of HO₂ versus RO₂ in the reaction system. In addition, sampling artifacts, such

as the use of different filters, presence or absence of denuders and interference during sample preparation, may also have played a role in causing this discrepancy.

At least three categories of compounds are likely to account for the SOA species not identified. Because of their relatively high volatility, less oxidized species such as carbonyls, which could not be identified by the LC-MS method, are expected to comprise only a small fraction of SOA mass in the systems

TABLE 4: Low-MW Components in SOA from Cycloheptene Ozonolysis^a

class of SOA components	identified low-MW species in SOA	surrogate standard for quantification ^b	mass yield (%)
diacid	pimelic acid		1.66
	adipic acid		1.85
	glutaric acid		0.48
	succinic acid		0.02
	malonic acid		0.02
diacid alkyl ester	pimelic acid monomethyl ester	suberic acid	0.20
	adipic acid monomethyl ester		0.28
	glutaric acid monoethyl ester	adipic acid monomethyl ester	0.01
	glutaric acid monomethyl ester		0.04
	succinic acid monoethyl ester		0.06
	malonic acid monoethyl ester	succinic acid monomethyl ester	0.10
hydroxy diacid	2-hydroxypimelic acid	2-hydroxy-2-isopropylsuccinic acid	0.51
	2-hydroxyadipic acid	3-hydroxy-3-methylglutaric acid	0.04
	2-hydroxyglutaric acid	2-hydroxy-2-methylsuccinic acid	0.08
	2,6-dihydroxypimelic acid	2-hydroxy-2-isopropylsuccinic acid	0.03
carbonyl-containing acid	5,6-dioxohexanoic acid	5-oxohexanoic acid	0.02
	8-oxooctanoic acid ^c	7-oxooctanoic acid	0.06
	7-oxoheptanoic acid ^c	6-oxoheptanoic acid	0.26
	6-oxohexanoic acid ^c	5-oxohexanoic acid	0.36
	5-oxopentanoic acid	4-oxopentanoic acid	0.02
sum of identified low-MW species ^d			6.11
total SOA mass derived from DMA ^e			18.21

^a 184 ppb of cycloheptene was consumed in this experiment. The filter was collected ~ 5 h from the onset of ozonolysis for a duration of ~ 2 h. ^b A blank cell indicates a standard was available for quantification. ^c Isomers are present in this SOA based on extracted ion chromatograms, and are quantified together here by the corresponding surrogate standard. ^d The sum of identified low-MW species accounts for 34% of the total SOA mass derived from the DMA measurements. ^e The mass yield of the total SOA reported here, derived from the DMA measurement with the assumption of an aerosol density of 1.4 g/cm^3 , has not been corrected for particle loss to the chamber wall; therefore, it is somewhat lower than the actual total SOA mass yield. Both the "sum of identified low-MW species" and the "total SOA mass derived from DMA" here refer to their yields (in percentage, relative to the mass of the consumed hydrocarbon) as defined in text similarly for individual SOA components.

TABLE 5: Low-MW Components in SOA from 1-Methylcyclopentene Ozonolysis^a

class of SOA component	identified low-MW species in SOA	surrogate standard for quantification ^b	mass yield (%)
diacid	azelaic acid		0.01
	suberic acid		0.16
	pimelic acid		0.55
	adipic acid		0.31
	glutaric acid		1.05
	succinic acid		0.25
	malonic acid		0.05
diacid alkyl ester	pimelic acid monomethyl ester	adipic acid monomethyl ester	0.02
	adipic acid monomethyl ester		0.01
	glutaric acid monomethyl ester		0.19
	succinic acid monoethyl ester		0.06
	malonic acid monoethyl ester	succinic acid monomethyl ester	0.53
	2-hydroxysuccinic acid monoethyl ester	succinic acid monoethyl ester	0.05
hydroxy diacid	2-hydroxypimelic acid	2-hydroxy-2-isopropylsuccinic acid	0.08
	2-hydroxyadipic acid	3-hydroxy-3-methylglutaric acid	0.01
	3-hydroxyadipic acid	3-hydroxy-3-methylglutaric acid	0.01
	2-hydroxyglutaric acid	2-hydroxy-2-methylsuccinic acid	0.05
	2-hydroxysuccinic acid	succinic acid	0.08
carbonyl-containing acid	5,6-dioxohexanoic acid	5-oxohexanoic acid	0.04
	5-oxohexanoic acid		0.09
	4-oxopentanoic acid		0.19
	5-oxo-6-hydroxyhexanoic acid	3-hydroxy-3-methylglutaric acid	0.17
	5-oxo-4,6-dihydroxyhexanoic acid	2-ketogulonic acid	0.03
sum of identified low-MW species ^c			3.96
total SOA mass derived from DMA ^d			8.85

^a 193 ppb of 1-methylcyclopentene was consumed in this experiment. The filter was collected ~ 4.5 h from the onset of ozonolysis for a duration of ~ 3 h. ^b A blank cell indicates that a standard was available for quantification. ^c The sum of identified low-MW species accounts for 45% of the total SOA mass derived from the DMA measurements. ^d The mass yield of the total SOA reported here, derived from the DMA measurement with the assumption of an aerosol density of 1.4 g/cm^3 , has not been corrected for particle loss to the chamber wall; therefore, it is somewhat lower than the actual total SOA mass yield. Both the "sum of identified low-MW species" and the "total SOA mass derived from DMA" here refer to their yields (in percentage, relative to the mass of the consumed hydrocarbon) as defined in text similarly for individual SOA components.

TABLE 6: Low-MW Components in SOA from 1-Methylcyclohexene Ozonolysis^a

class of SOA components	identified low-MW species in SOA	surrogate standard for quantification ^b	mass yield (%)
diacid	pimelic acid		0.35
	adipic acid		3.38
	glutaric acid		0.36
	succinic acid		0.04
	malonic acid		0.04
diacid alkyl ester	pimelic acid monomethyl ester	suberic acid	0.03
	adipic acid monomethyl ester		0.47
	glutaric acid monomethyl ester		0.08
	malonic acid monoethyl ester	succinic acid monomethyl ester	0.16
hydroxy diacid	2-hydroxypimelic acid	2-hydroxy-2-isopropylsuccinic acid	0.03
	2-hydroxyadipic acid	3-hydroxy-3-methylglutaric acid	0.02
	2-hydroxyglutaric acid	2-hydroxy-2-methylsuccinic acid	0.03
	2,3,4,5,6-pentahydroxypimelic acid ^c	2-ketogulonic acid	0.07
carbonyl-containing acid	6,7-dioxoheptanoic acid ^d	4-oxopimelic acid	0.42
	6-oxoheptanoic acid		0.10
	5-oxohexanoic acid		0.15
	4-oxopentanoic acid		0.04
	6-oxo-7-hydroxyheptanoic acid	4-oxopimelic acid	0.46
	sum of identified low-MW species ^e		6.22
	total SOA mass derived from DMA ^f		14.15

^a 157 ppb of 1-methylcyclohexene was consumed in this experiment. The filter was collected ~6 h from the onset of ozonolysis for a duration of ~3.5 h. ^b A blank cell indicates that a standard was available for quantification. ^c This structure is tentatively identified based on the chromatographic retention time and molecular weight. Other isomeric structures may also be present in this SOA. ^d Isomers are present in this SOA based on the extracted ion chromatograms, and are quantified together here by the corresponding surrogate standard. ^e The sum of identified low-MW species accounts for 44% of the total SOA mass derived from the DMA measurements. ^f The mass yield of the total SOA reported here, derived from the DMA measurement with the assumption of an aerosol density of 1.4 g/cm³, has not been corrected for particle loss to the chamber wall; therefore, it is somewhat lower than the actual total SOA mass yield. Both the “sum of identified low-MW species” and the “total SOA mass derived from DMA” here refer to their yields (in percentage, relative to the mass of the consumed hydrocarbon) as defined in text similarly for individual SOA components.

studied here. Indeed, dialdehydes were found to comprise about 5% of the total mass of SOA from cyclohexene ozonolysis by Kalberer et al.⁶ However, highly oxidized species, such as multihydroxy diacids or multioxo acids, may also evade LC–MS detection because they would elute off the column with little or no retention. The mass fractions of such species in the SOA remain unknown at this time. In addition, species eluting late from the LC column were found in all SOAs, all with relatively high molecular weights. Figure 3 shows the detection of species with m/z of 243, 259, and 291 (i.e., the corresponding negative ions) in the SOA from the ozonolysis of cycloheptene, 1-methylcyclohexene and 1-methylcyclopentene, respectively. Judged from peak areas, they may comprise a substantial portion of the total SOA mass, yet their identities cannot be revealed by LC–MS alone. We next discuss the use of ion trap MS to analyze higher-MW species in SOA.

2. Oligomeric Components of SOA. 2.1. Identification and Structure Elucidation of Oligomers in SOA. The ESI source in the ion trap MS (ITMS) preserves the molecular integrity of analytes by soft ionization. Some acidic species, readily surrendering a proton, are detected in the form of their molecular ions $[M - 1]^-$ in the negative ion mode. For example, Figure 4 shows the ion trap mass spectrum of a SOA sample from cycloheptene ozonolysis. The 131, 145, and 159 ions correspond to glutaric acid, adipic acid, and pimelic acid, respectively, which were also identified by the LC–MS. However, higher-MW species, such as those with m/z of 259, 329, 373, 417, 461, and 505, are also present in this sample, at intensities comparable to or even higher than the low-MW species. Figure 5 shows the ion trap mass spectrum of a SOA sample from 1-methylcyclopentene ozonolysis. Higher-MW species, such as those with m/z of 245, 261, 299, 381, and 403, are present at intensities comparable to low-MW species. Figure 6a shows

the ion trap mass spectrum of a SOA sample from α -pinene ozonolysis with preexisting MgSO₄ seed particles. The low-MW species with m/z 171, 185, and 199 correspond to norpinic acid, *cis*-pinic acid, and OH-pinonic acid, which have previously been identified as major SOA components^{16,18} and are also identified by the LC–MS method in this work. Again, higher-MW species, such as those with m/z of 329, 343, 357, 371, and 385, are also present in this SOA. Their presence is confirmed by the corresponding detection of ions with m/z of 353, 367, 381, 395, and 409 (Na⁺ adducts of neutral molecules) in the positive ion mode of the ITMS, as shown in Figure 6b. Because a broad range of compounds can be detected as their Na⁺ adducts in this mode, the overall composition of SOA can be better captured by the positive ion mode mass spectrum. Figure 6b illustrates that in the SOA formed on the nearly neutral MgSO₄ seed, species with MW from 250 to 450 are the most abundant species, followed by some even larger species (MW > 450). These species are separated regularly by mass units such as 14, 16, 18, and 30, which is characteristic of a copolymer system,²⁵ indicating the difference in CH₂, O, H₂O groups, or a combination of them, among monomers and oligomers. Strikingly, low-MW species (MW < 250) likely comprise only a very minor fraction of the total SOA mass, assuming they have similar response factors to oligomers on the MS detector.

That the higher-MW species (MW > 250) shown in Figures 4–6 are indeed oligomers is confirmed from the tandem MS of these ions. In the ITMS, specific ions can be isolated and stored and further fragmented by collision-induced dissociation to produce the so-called tandem MS. For example, Figure 7 shows the MS/MS (negative ion mode) of the 373 ion in SOA from the ozonolysis of cycloheptene. The molecular structure shown alongside the MS/MS explains the major fragment. The corresponding monomers are 1,4-butanediol and 4-oxobutanoic

TABLE 7: Low-MW Components in SOA from 3-Methylcyclohexene Ozonolysis^a

class of SOA components	identified low-MW species in SOA	surrogate standard for quantification ^b	mass yield (%)
diacid	suberic acid ^c		0.05
	pimelic acid		0.36
	2-methyladipic acid	pimelic acid	1.82
	adipic acid		0.35
	2-methylglutaric acid	adipic acid	0.80
	glutaric acid		0.45
	succinic acid		0.07
diacid alkyl ester	pimelic acid monomethyl ester	suberic acid	0.11
	adipic acid monomethyl ester		0.08
	glutaric acid monomethyl ester		0.03
	succinic acid monoethyl ester		0.05
	succinic acid monomethyl ester		0.08
	malonic acid monoethyl ester	succinic acid monomethyl ester	0.24
hydroxy diacid	2-hydroxypimelic acid	2-hydroxy-2-isopropylsuccinic acid	0.19
	2-hydroxy-2-methyladipic acid	2-hydroxy-2-isopropylsuccinic acid	0.12
	2-hydroxy-2-methylglutaric acid ^d	3-hydroxy-3-methylglutaric acid	0.06
	2-hydroxyglutaric acid ^e	2-hydroxy-2-methylsuccinic acid	0.02
	2,6-dihydroxypimelic acid	2-hydroxy-2-isopropylsuccinic acid	0.02
carbonyl-containing acid	4,5-dioxo-2-methylpentanoic acid	5-oxohexanoic acid	0.02
	6-oxo-2-methylhexanoic acid ^f	6-oxoheptanoic acid	0.40
	5-oxohexanoic acid		0.26
	6-oxohexanoic acid ^f	5-oxohexanoic acid	0.22
	4-oxopentanoic acid		0.05
	sum of identified low-MW species ^g		5.84
	total SOA mass derived from DMA ^h		8.67

^a 307 ppb of 3-methylcyclohexene was consumed in this experiment. The filter was collected \sim 4.5 h from the onset of ozonolysis for a duration of \sim 2 h. ^b A blank cell indicates that a standard was available for quantification. ^c A likely isomer, also present in this SOA, is 2-methylpimelic acid. ^d A likely isomer, also present in this SOA, is 2-hydroxyadipic acid. ^e A likely isomer, also present in this SOA, is 2-hydroxy-2-methylsuccinic acid. ^f Isomers are present in this SOA based on the extracted ion chromatograms, and are quantified together here by the corresponding surrogate standard. ^g The sum of identified low-MW species accounts for 67% of the total SOA mass derived from the DMA measurements. ^h The mass yield of the total SOA reported here, derived from the DMA measurement with the assumption of an aerosol density of 1.4 g/cm³, has not been corrected for particle loss to the chamber wall; therefore, it is somewhat lower than the actual total SOA mass yield. Both the “sum of identified low-MW species” and the “total SOA mass derived from DMA” here refer to their yields (in percentage, relative to the mass of the consumed hydrocarbon) as defined in text similarly for individual SOA components.

TABLE 8: Mass Percentage of Each Class of Compounds in the Total Identified Low-MW SOA Species in Six Ozonolysis Systems

class of compounds	cyclopentene	cyclohexene	1-methyl-cyclopentene	1-methyl-cyclohexene	3-methyl-cyclohexene	cycloheptene	average	standard deviation
diacid	77%	75%	60%	67%	67%	66%	69%	7%
hydroxy diacid	14%	9%	5%	2%	7%	11%	8%	4%
carbonyl-containing acid	1%	14%	13%	19%	16%	12%	15%	3%
diacid alkyl ester	7%	2%	22%	12%	10%	11%	11%	7%
sum							102%	

acid, both first-generation oxidation products. Overall, our MS/MS results confirm that oligomers originate from low-MW SOA species in all of the systems that were studied. For the α -pinene ozonolysis system, with the monomers having MW centered about 180 Da,¹⁸ the small oligomers (MW from 250 to 450) are probably dimers, whereas larger oligomers (MW from 450 to 950) are likely trimers, tetramers, and pentamers. On the basis of the structures of oligomers and corresponding monomers, we propose three possible oligomerization reactions in the aerosol phase: aldol reaction, gem-diol reaction, and acid dehydration. All three reactions require acid or base catalysis.²² We note that, because many of the low-MW SOA species have functional groups in branched positions, the oligomers eventually formed may contain both straight-chain and cross-linked sections.

To test whether oligomers may have formed during the electrospray process, we analyzed individual monomers and cocktails of monomers by the ITMS with the same procedures as those for the SOA samples. These monomers include C₆–

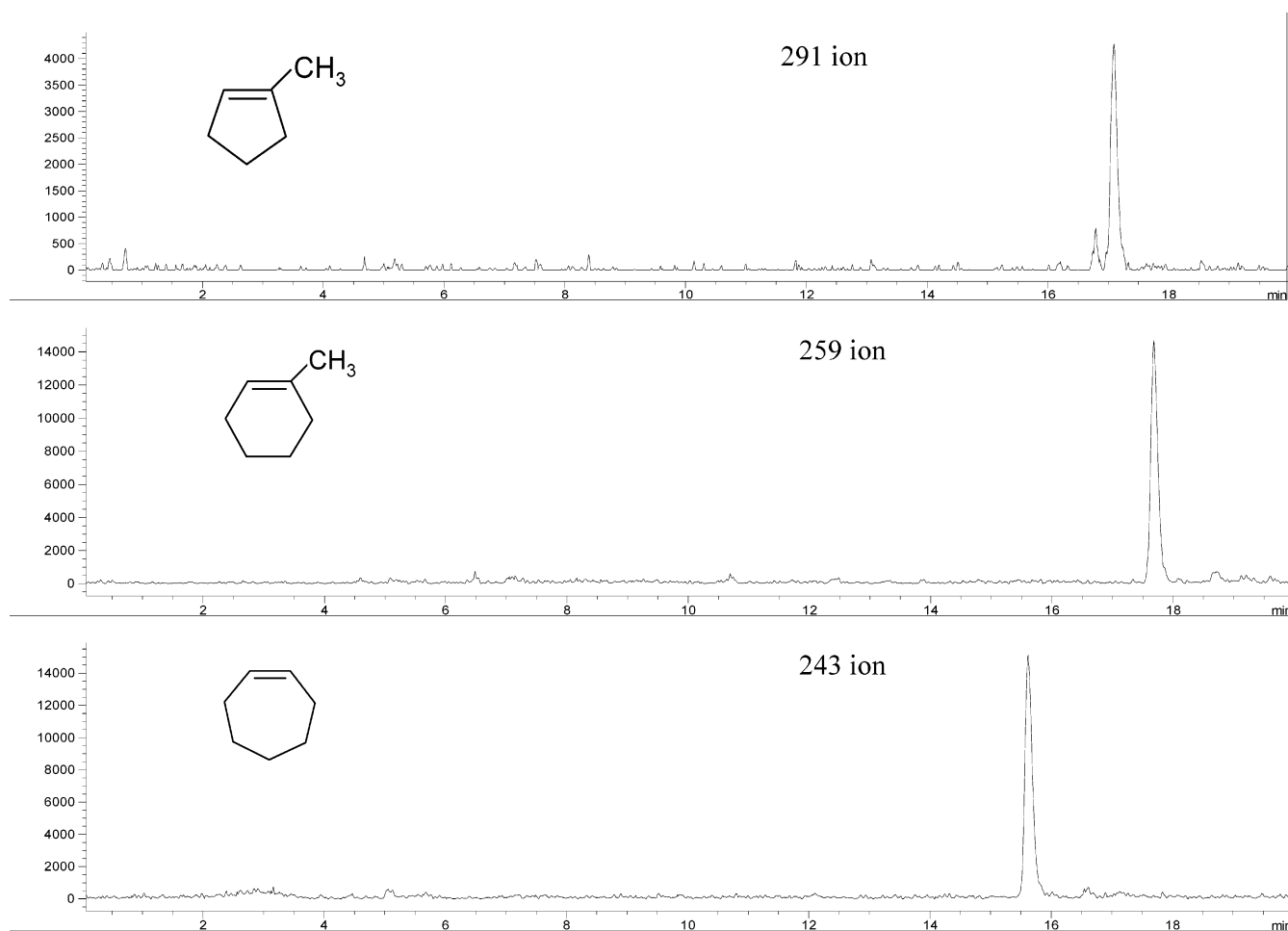
C₈ carbonyl acids, pinonic acid and pinic acid. Only minimal amounts of ions with m/z from 250 to 450 were detected under the negative ion mode. Single ion isolation and MS/MS fragmentation indicated they were unstable “adduct” ions, possibly formed during electrospray. Under the positive ion mode, some dimers were present but an overall polymeric signature (up to pentamers) was lacking in these standard mixtures. In addition, the detection of some high-MW species by the LC–MS (e.g., Figure 3), such as the 243 and 259 ions in the cycloheptene ozonolysis system (Figure 4) and the 357 ion in the α -pinene ozonolysis system (Figure 6a), also verifies the presence of oligomers in the SOA. Finally, to test whether oligomers may have formed from the oxidation of background hydrocarbons, we injected seed particles into the clean chamber both in the absence and presence of ozone. No oligomers were present in aerosol samples that were collected.

In summary, oligomers with MW from 250 to 1600 are present in all SOA samples from α -pinene ozonolysis, regardless of initial seed acidity or water content. Oligomers with MW

TABLE 9: Fraction of Each Class of Compounds in the Total SOA Mass Derived from the DMA Measurements (First Four Rows)^a

class of compounds	cyclopentene	cyclohexene	1-methyl-cyclopentene	1-methyl-cyclohexene	3-methyl-cyclohexene	cycloheptene	average	standard deviation
diacid	59%	24%	27%	29%	45%	22%	34%	15%
hydroxy diacid	11%	3%	2%	1%	5%	4%	4%	4%
carbonyl-containing acid	1%	4%	6%	8%	11%	4%	6%	4%
diacid alkyl ester	6%	1%	10%	5%	7%	4%	5%	3%
% of identified low-MW species in the total SOA (no oxalic acid)	77%	31%	45%	44%	67%	34%		
% of identified low-MW species in the total SOA (including oxalic acid)	83%	42%	57%	68%	81%	44%		
% of total identified low-MW and oligomeric species in the total SOA	89%	45%	67%	79%	90%	53%		

^a Fractions of identified low-MW species (no oxalic acid) in the total SOA mass (5th row). Fractions of the identified low-MW species (including the estimated oxalic acid) in the total SOA mass (6th row). Fractions of the total identified species, both low-MW and oligomeric, in the total SOA mass (7th row).

**Figure 3.** Late-eluting chromatographic peaks in SOA from cycloalkene ozonolysis.

from 200 to 700 are present in all SOA samples from the ozonolysis of cyclohexene, 1-methylcyclopentene, cycloheptene, 1-methylcyclohexene, and cyclooctene. Oligomers are present in SOA from cyclopentene ozonolysis in only minimal amounts, judged from the ion trap mass spectra. Taken with the fact that 83% of the total mass of this SOA is low-MW species (Table 9), it is likely that oligomer formation is not favored with hydrocarbons with fewer than six carbon atoms. This is not unreasonable because, even after dimerization, most species have relatively small MW (below 250), probably rendering them still too volatile to stay in the aerosol phase.

2.2. Effect of Particle-Phase Acidity on Oligomer Formation in SOA. Even though oligomers are universally present in the SOA that we studied, an important question arises, how does seed particle acidity affect oligomer formation in SOA? The ozonolysis of α -pinene (mixing ratio from 12 to 135 ppb) was chosen to address this question. We use two nonacid seeds, containing either MgSO_4 or $(\text{NH}_4)_2\text{SO}_4$, and two acid seeds, containing either $[\text{MgSO}_4 + \text{H}_2\text{SO}_4]$ or $[(\text{NH}_4)_2\text{SO}_4 + \text{H}_2\text{SO}_4]$. Thermodynamic calculations show that the four seed aerosols, once stabilized at the ambient RH in the chamber, span a spectrum of pH values. For example, at $\text{RH} = 55\%$, the pH

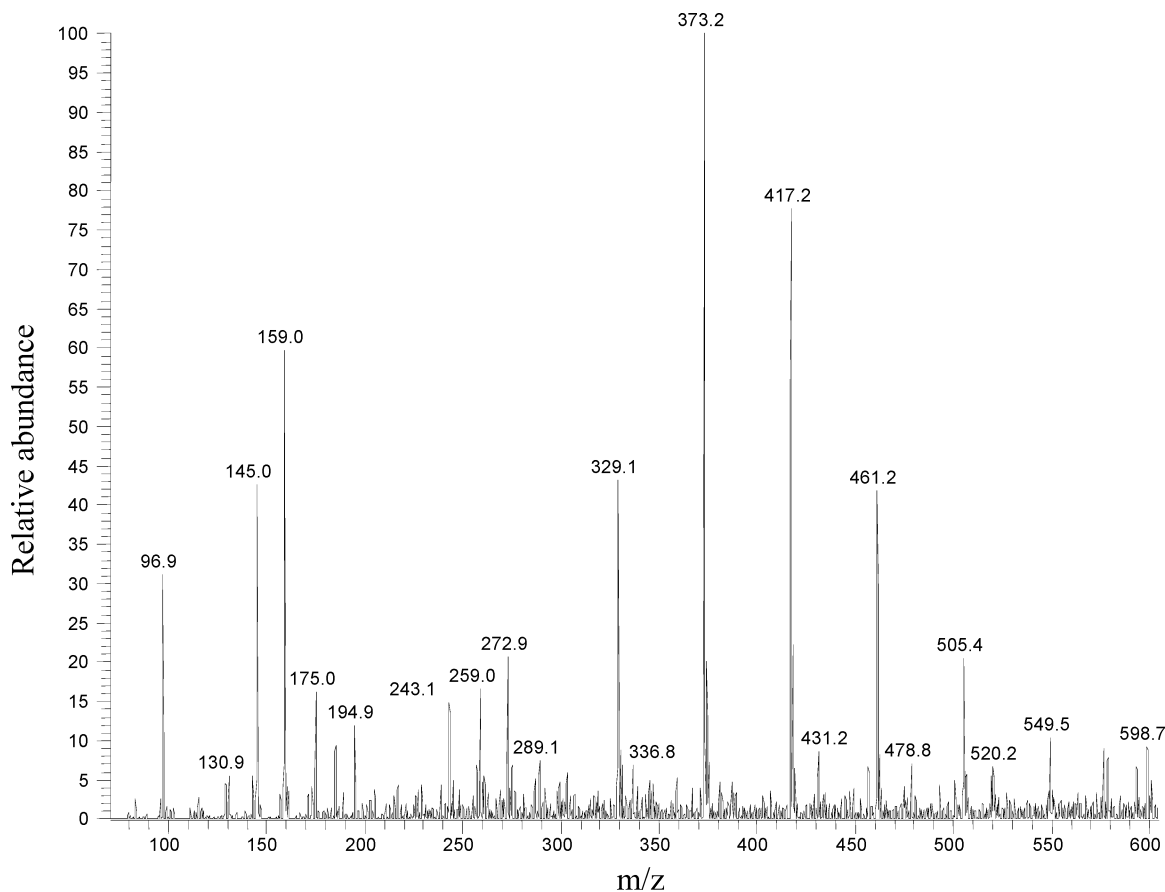


Figure 4. Ion trap mass spectrum (negative ion mode) of SOA from cycloheptene ozonolysis. The background ion intensities are almost always lower than 5% of the maximum ion intensity ($m/z = 373.2$ at 100% intensity).

values for the $[\text{MgSO}_4\text{-only}]$ seed and the $[\text{MgSO}_4 + \text{H}_2\text{SO}_4]$ seed are about 6.5 and -0.3 , respectively. The pH values for the $[(\text{NH}_4)_2\text{SO}_4\text{-only}]$ seed and the $[(\text{NH}_4)_2\text{SO}_4 + \text{H}_2\text{SO}_4]$ seed are about 4.6 and 2.4, respectively. The acidity increase from the nonacid to the acid seed for MgSO_4 exceeds that in the $(\text{NH}_4)_2\text{SO}_4$ case by about 4.6 pH units.

Figure 8a shows the ion trap mass spectrum (positive ion mode) of the SOA from the ozonolysis of 120 ppb α -pinene in the presence of MgSO_4 -only seed. When the seed becomes much more acidic ($\text{MgSO}_4\text{-H}_2\text{SO}_4$), as shown in Figure 8b, the resultant SOA comprises many more large oligomers (MW from 450 to 950), most of which have higher ion intensities; thus, mass concentrations of these species exceed, by at least a factor of 2, those in the SOA formed on MgSO_4 -only seed. Some even larger oligomers (MW from 950 to 1600) are detected (with signal-to-noise ratios larger than 3) in the SOA formed on the acidic seed. However, the mass distribution of small oligomers (MW from 250 to 450) remains roughly in the same pattern, with ion intensities changing only modestly. A similar difference in SOA composition between nonacid and acid MgSO_4 seeds is observed in all of the other six pairs of experiments on the α -pinene system, with large oligomers increasing in abundance by 2–4 times in the acid cases. In comparison, the composition difference between SOA formed on the $(\text{NH}_4)_2\text{SO}_4$ -only seed and the $(\text{NH}_4)_2\text{SO}_4\text{-H}_2\text{SO}_4$ seed is less pronounced than on the corresponding MgSO_4 seeds. There is only a moderate increase in the types and amounts of small oligomers in the SOA formed on the more acidic seed and essentially no change in the mass distribution of the large oligomers.

Kinetically, as the acidity of the seed particles increases, acid-catalyzed reactions and oligomer formation accelerate and larger

oligomers form within the same experimental time frame than those that form on less acidic seed. The slight decrease in the ion intensities of some small oligomers in the more acidic case (e.g., see 381 and 395 ions in Figure 8a and b) actually may reflect their transformation into larger oligomers.

Oligomerization can be expected to shift the gas-to-particle equilibrium of some condensing low-MW species to the particle phase, eventually increasing the SOA yield over that in the absence of heterogeneous reactions. Indeed, this is confirmed by the overall SOA yield difference between systems containing nonacid and acid seeds. The absolute SOA yield is defined as the mass of SOA produced relative to the mass of hydrocarbon consumed. Figure 9 shows the absolute SOA yield versus the α -pinene mixing ratio, for seven pairs of experiments in the presence of acid versus nonacid seed particles as well as for two experiments in the absence of seed particles. Consistently, the SOA formed on the more acidic $\text{MgSO}_4\text{-H}_2\text{SO}_4$ seed has a higher yield than that formed on the MgSO_4 -only seed. Overall, within the range of α -pinene mixing ratios studied, the SOA yield increases by 10–40% on the acidic seed over the nearly neutral seed. Concurrent hygroscopicity measurements show that these SOA, at the time of filter collection, have approximately 10–20% water content; thus, the increased types and amounts of oligomers formed on the more acidic seed appear to be the primary cause for the increased SOA yield. In comparison, the SOA yield increases by only about 5% on the $(\text{NH}_4)_2\text{SO}_4\text{-H}_2\text{SO}_4$ seed over the $(\text{NH}_4)_2\text{SO}_4$ -only seed at similar α -pinene mixing ratios. This smaller yield increase, consistent with the smaller composition change, is likely a result of the smaller acidity difference between the nonacid and acid seeds of $(\text{NH}_4)_2\text{SO}_4$, as compared with MgSO_4 . In all, the above

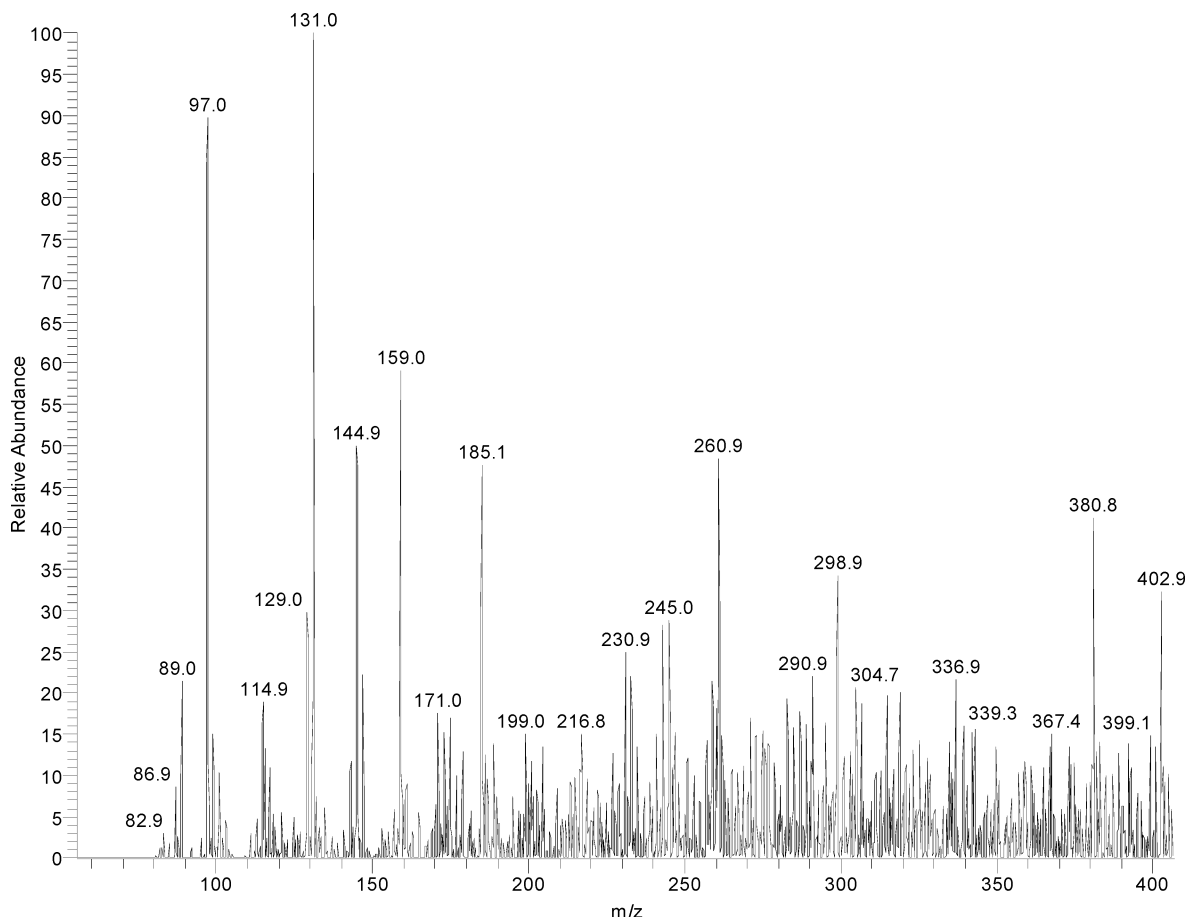


Figure 5. Ion trap mass spectrum (negative ion mode) of SOA from 1-methylcyclopentene ozonolysis. The background ion intensities are almost always lower than 9% of the maximum ion intensity ($m/z = 131.0$ at 100% intensity).

differences in the composition and amounts of SOA formed between these two sets of seed particles clearly demonstrate the direct impact of seed particle acidity.

Importantly, in the α -pinene ozonolysis system, similar types of oligomers are present in SOA both in the presence and absence of preexisting particles. This suggests that organic acids produced from the gas-phase hydrocarbon oxidation itself may actually provide the necessary acidity for catalytic reactions. Interestingly, the yields of SOA in the absence of seed particles appear to be lower than those in the presence of acid seeds but higher than those in the presence of nonacid seeds (Figure 9). Although the former is probably due to the higher acidity of the acid seeds and the subsequent SOA as compared with that of the nucleated SOA, the cause for the latter is less clear. One possible explanation is that the organic acids produced from α -pinene ozonolysis are “diluted” by the preexisting, neutral particles as compared with the freshly nucleated ones, resulting in slower catalytic reactions and ultimately lower SOA yields. On the basis of these observations, we speculate that oligomers are widely present in atmospheric secondary organic aerosols.

2.3. Assessing Relative Abundance of Oligomers in SOA. It is difficult to quantify individual oligomeric species identified by the ion trap MS because no standard is available at present and the exact structures of these high-MW species are not known. However, as illustrated by Figure 3, some oligomeric species are also identified by the LC-MS, equipped with ESI. Because the retention times of these oligomers are known from the LC-MS data, a surrogate compound with a similar retention time as well as presumed functional groups can be chosen to roughly quantify a detected oligomeric species. For example, a C_{m+n} diacid is chosen as the surrogate for a dimer formed via

acid dehydration of C_m and C_n diacids, and a C_{m+n} carbonyl acid is chosen as the surrogate for a dimer formed via aldol reaction of a C_m dialdehyde and a C_n carbonyl acid. All of the major high-MW species detected by LC-MS are then quantified using their surrogates' calibration factors, assuming their response factors on the MS are the same. Quantified oligomers are then added with the identified low-MW species, and the mass fractions of the total identified SOA species are listed in the 7th row in Table 9. Oligomers that were quantified this way account for another 3–11% of the total SOA mass, bringing the mass closure of analytical speciation to 45–90%, or 71% averaged for all six cycloalkene ozonolysis systems. Because only a fraction of oligomers were quantified by the LC-MS, oligomers in total are estimated to comprise at least 10% of the total mass of SOA from cycloalkene (carbon number > 5) ozonolysis in general. In the case of α -pinene ozonolysis, the ITMS data suggest that the majority of SOA mass is composed of oligomeric species.

Indeed, in light of the substantial presence of oligomers in SOA, the common approach to calculating SOA mass closure is thrown into question. Because oligomers may have somewhat higher densities than low-MW species, the overall aerosol density may actually exceed the commonly assumed 1.4 g/cm^3 . A higher density would lead to lower mass closures achieved in this work and most previous work. In addition, because oligomers may decompose in the GC injector or column, reverting back to initial monomers, common GC-MS based speciation may overestimate the mass of low-MW species while underestimate the mass of oligomeric species.

3. Relationship between Hydrocarbon Precursor Structure and SOA Composition and Yield. Investigating the relation-

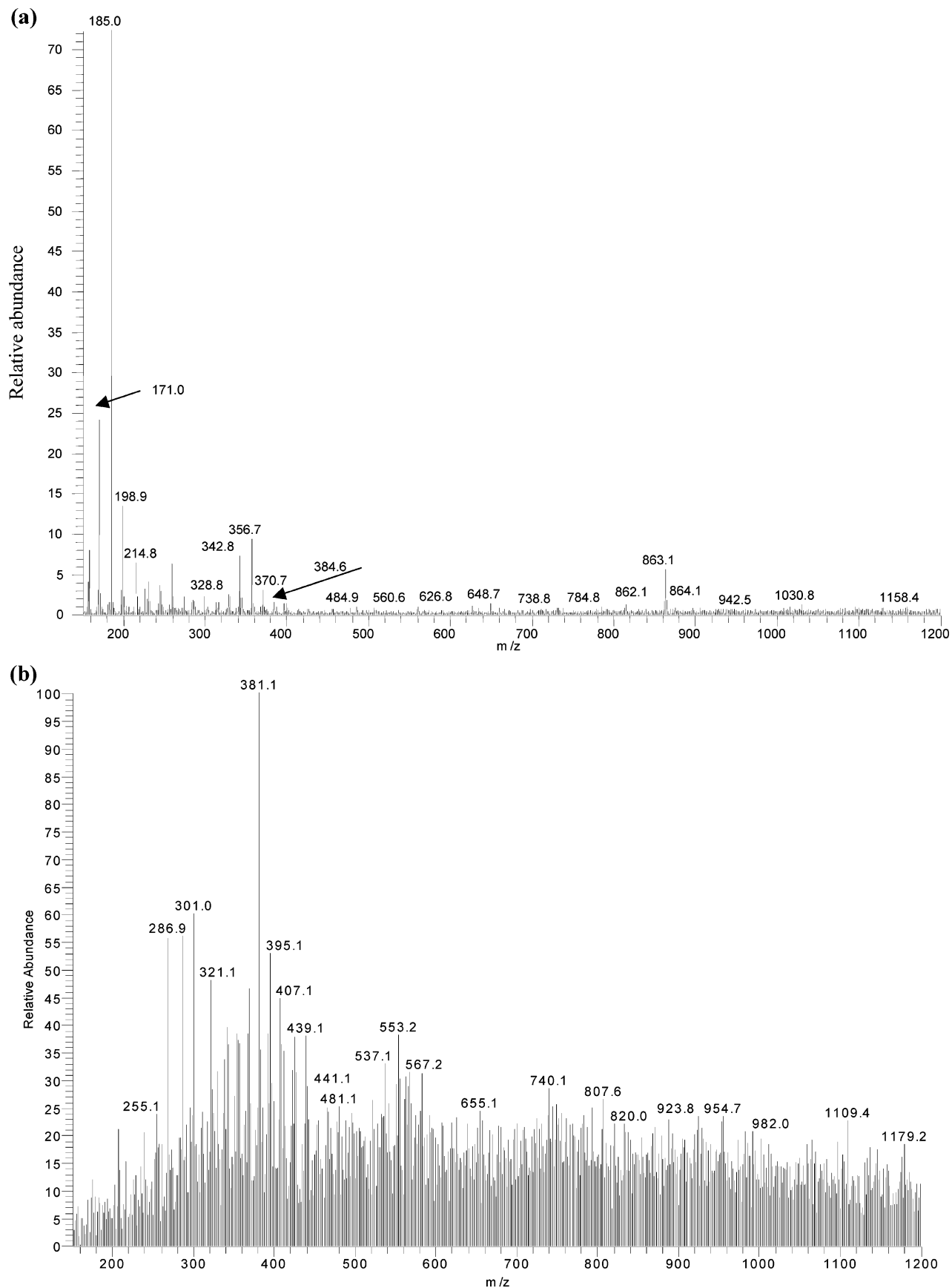


Figure 6. (a) Ion trap mass spectrum (negative ion mode) of SOA from α -pinene ozonolysis with preexisting MgSO_4 seed particles. The background ion intensities are almost always lower than 1% of the maximum ion intensity ($m/z = 185.0$ at 100% intensity). The 863.1 ion is from the instrument background. (b) Ion trap mass spectrum (positive ion mode) of the same SOA as in (a). The background ion intensities are almost always lower than 6% of the maximum ion intensity ($m/z = 381.1$ at 100% intensity).

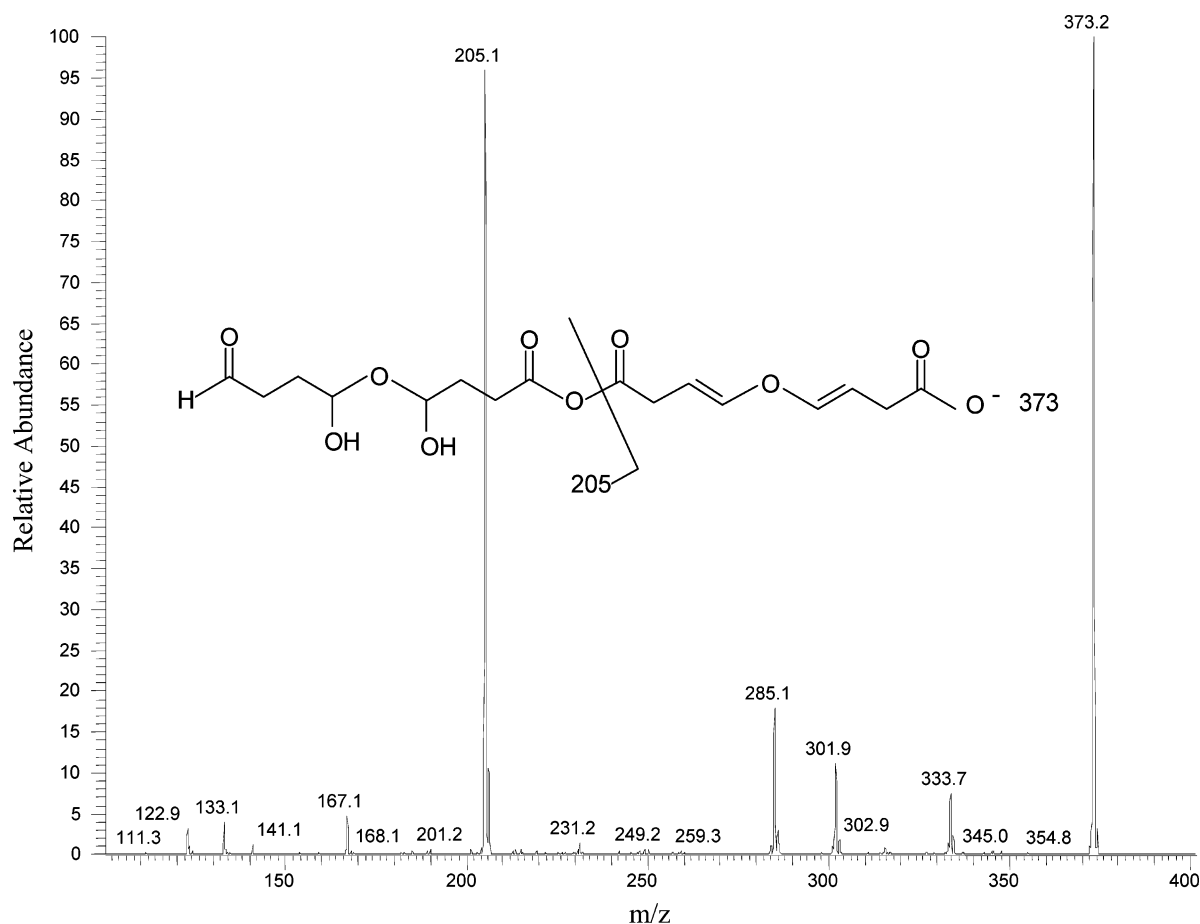


Figure 7. MS/MS (negative ion mode) of 373 ion in the SOA from cycloheptene ozonolysis, as shown in Figure 4. It is likely formed through gem-diol reaction and acid dehydration of monomers including 1,4-butanediol and 4-oxobutanoic acid.

ship between parent cycloalkene structure and its SOA composition is a complex issue because (1) the gas-phase chemistry of cycloalkene ozonolysis is not yet fully understood; (2) the heterogeneous reactions involved are even less well understood, and oligomers that form via these reactions appear to comprise a substantial fraction of the final SOA mass; and (3) even though major gas-phase reactions are probably completed within the first 3 h from the onset of ozonolysis, as indicated by the observed disappearance of the cycloalkenes, oligomerization may take place well beyond the time when the parent hydrocarbon has been consumed. For this reason, bulk filter measurements at a certain time during SOA evolution may not be entirely comparable among systems from different parent hydrocarbons. Keeping this kinetic factor in mind, it is still possible to glean important trends from the bulk, average composition measurements, which were taken at similar elapsed times for similar durations.

3.1. Carbon Number in Homologous Cycloalkenes. Cyclopentene, cyclohexene, and cycloheptene are homologous compounds. As discussed earlier, within the total identified SOA low-MW species, diacids comprise rather constant mass fractions from system to system, as do hydroxy diacids (Table 8). These two categories of species are likely the low-MW species with the lowest volatility. Although these constant fractions are of interest themselves, this also indicates that low-MW species alone cannot explain the increasing overall SOA yield from C_5 to C_7 .¹⁵ However, the 6th row in Table 9 shows that the total identified low-MW species comprises 83% of the total SOA mass in the C_5 system, whereas this fraction decreases dramatically to 42 and 44% for C_6 and C_7 systems, respectively. Incomplete speciation or experimental uncertainties cannot

explain such a large difference. Because the four classes of compounds that were identified should represent the major low-MW species, the fraction of oligomers, which we assume are the main unidentified species by LC-MS, is therefore probably considerably higher in the SOA from the C_6 and C_7 than the C_5 cycloalkene. Indeed, as noted earlier, the ion trap MS data show minimal amounts of oligomers in the cyclopentene system. The oligomers that were quantified by LC-MS comprise about 6, 3, and 9% of the total SOA mass for the C_5 , C_6 , and C_7 systems, respectively. While an increasing fraction of oligomers in the SOA with increasing carbon number is suggested by the data (considering the quantification was not complete for especially the larger systems), theoretical considerations strongly support this trend simply because increasingly larger monomers would form in these systems from C_5 to C_7 , further leading to increasingly less volatile and eventually more abundant oligomers in the SOA. Consequently, it is likely that the density of SOA also increases as the carbon number increases, further increasing the overall yield of SOA, as observed.

3.2. Methyl-Substitution Effect. 1-methylcyclopentene and cyclohexene ($n = 6$) have the same MW, as do 1-methylcyclohexene and cycloheptene ($n = 7$). The total identified low-MW species in the SOA is 15% more for 1-methylcyclopentene than cyclohexene and 24% more for 1-methylcyclohexene than cycloheptene, as shown in Table 9. Although this may indicate that there are relatively more low-MW species than oligomers in the methyl-substituted systems, the overall SOA yield does not depend solely on the relative amounts of low-MW species and oligomers; instead, it depends on the absolute amount of all species eventually present in the SOA. Known gas-phase reactions²³ suggest that the initial steps of oxidation of 1-meth-

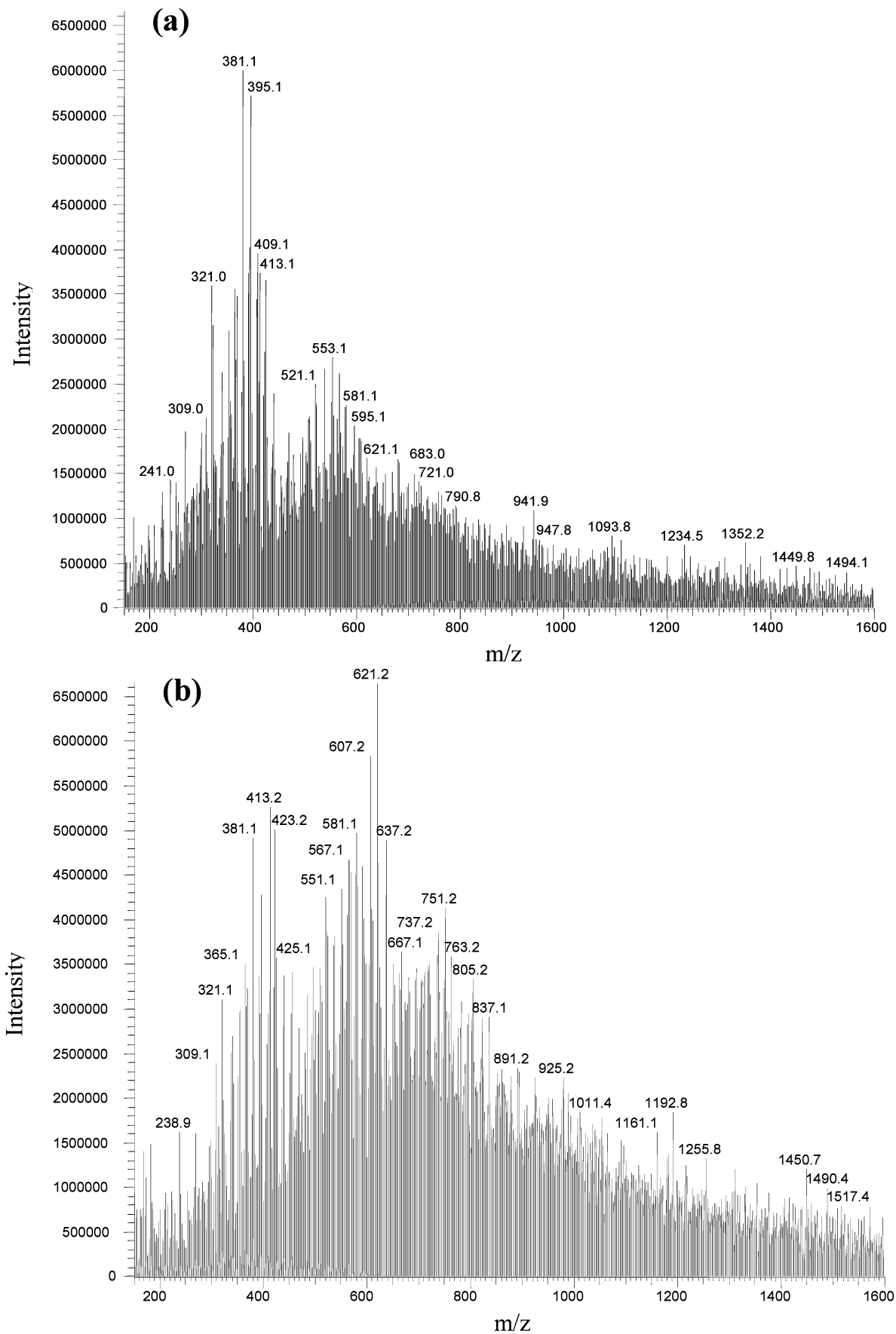


Figure 8. (a) Ion trap mass spectrum (positive ion mode) of the SOA from the ozonolysis of 120 ppb α -pinene on $MgSO_4$ -only seed (b) Ion trap mass spectrum (positive ion mode) of the SOA from the ozonolysis of 120 ppb α -pinene on $MgSO_4-H_2SO_4$ seed. The background ion intensities are almost always lower than 400 000 in both a and b.

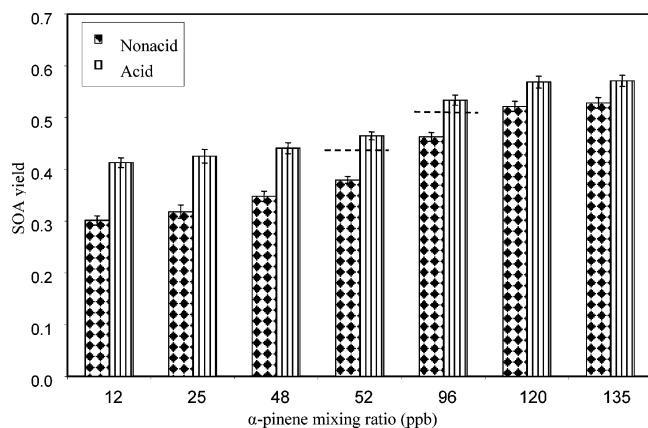


Figure 9. Absolute yields of SOA formed on nonacid (dotted bars) and acid (lined bars) MgSO_4 seed particles at seven initial α -pinene mixing ratios. The relative yield difference (after normalization to the SOA yield in the nonacid case) increases linearly with decreasing mixing ratio of initial α -pinene, possibly because of the relatively increasing amount of H_2SO_4 in the particles. This applies that in the atmosphere, where α -pinene and other hydrocarbons are usually present at mixing ratios no higher than the lower-end values in this Figure, the effect of particle acidity on SOA yield can be quite substantial. In addition, at 52 and 96 ppb, the absolute yields of SOA in the absence of any seed particles are 0.43 and 0.51, respectively, as roughly shown by the two dashed, horizontal lines. The error bars of the two no-seed SOA yields are similar to those of the with-seed SOA yields at corresponding mixing ratios.

lucyclohexene would mainly lead to 6-oxoheptanoic acid (a C_7 carbonyl acid) and no C_7 diacid at all. However, from cycloheptene, initial steps can lead to both C_7 carbonyl acid and C_7 diacid. Consequently, the more abundant 6-oxoheptanoic acid in the 1-methylcyclohexene system can lead to the formation of C_{14} and even larger oligomers via aldol reaction or gem-diol reaction. In comparison, lesser amounts of C_7 carbonyl acids are available in the cycloheptene system to form C_{14} oligomers, which should have the lowest volatility of all possible dimers (C_{14} , C_{13} , C_{12} , etc.). By shifting gas-to-particle equilibrium, this can eventually transfer more volatile carbonyl species into the aerosol phase in the 1-methylcyclohexene system and eventually increase the overall SOA yield, as observed by Keywood et al.¹⁵ Similar explanations should apply to other isomeric pairs of cycloalkene precursors with even higher carbon numbers.

3.3. Isomeric Effect. 3-methylcyclohexene differs from 1-methylcyclohexene in the position of the methyl substituent group on the ring. Together with cycloheptene, these three compounds comprise a set of isomers that display fascinating patterns of SOA composition and yield. Within the low-MW SOA species, carbonyl acids have the highest mass fraction in the 1-methylcyclohexene system (19%) and the lowest in the cycloheptene system (12%), consistent with the discussion in section 3.2. Interestingly, almost the same compounds with fewer than six carbon numbers are identified in all three systems, implying that only the initial oxidation pathways differ substantially. After some steps of oxidation, the differences due to the 1-methyl and 3-methyl substitution versus nonsubstitution diminish, probably because these carbons have been effectively oxidized “off” the main carbon chain, as suggested by known mechanisms.²³ This is further supported by the somewhat different extracted ion chromatograms (EIC) of the 143 (C_7 carbonyl acid) and 129 (C_6 carbonyl acid) ions but the very similar EICs of the 115 (C_5 carbonyl acid) ion in SOA of these three systems. However, strikingly, the overall SOA yield is highest for 1-methylcyclohexene and lowest for 3-methylcyclohexene, differing to a substantial extent.¹⁵

TABLE 10: Structures Illustrating the Numbers of Available α -C and α -H for Aldol Reactions in Some Initial Oxidation Products in 1-Methylcyclohexene, Cycloheptene, and 3-Methylcyclohexene Ozonolysis Systems

Hydrocarbon precursor			
C_7 dicarbonyl			
Available α -C(*) number	2	1	1
Available α -H number	5	2	1
C_7 carbonyl acid			
Available α -C(*) number	2	1	1
Available α -H number	5	2	1

A look at selected high-MW species that were detected by the LC-MS reveals contrasting composition patterns. For example, as shown in Figure 10, the species detected by m/z of 289 show different extracted ion chromatograms with the three C_7 isomeric cycloalkene systems. At least six major peaks are detected in the SOA from 1-methylcyclohexene, corresponding most likely to oligomeric SOA components. In comparison, the SOA from cycloheptene ozonolysis exhibits only three major peaks, all of which are detected in the 1-methylcyclohexene case with very similar retention times (differing by less than 0.1 min), indicating that they are the same or isomeric species. In sharp contrast, the SOA from 3-methylcyclohexene ozonolysis exhibits only two major peaks, with different retention times from the other two isomeric systems. Assuming a similar response factor for all of these species, the abundance of 289 ion decreases from 1-methylcyclohexene to cycloheptene to 3-methylcyclohexene substantially, indicating decreasing amounts of oligomers are formed in this sequence. Some other high-MW species exhibit similar patterns. Mechanistic considerations provide a consistent explanation for these observed differences. The m/z of 289 likely corresponds to a dimer of a C_7 carbonyl acid (MW = 144) and a C_7 dicarbonyl (MW = 128) formed via aldol reaction, which requires the enolization of a carbonyl (involving its neighboring α -C and α -H). As depicted in Table 10, the mechanistic possibilities of enolization in these three systems differ substantially. Consider the carbonyl group depicted on the right side in the C_7 dicarbonyl and C_7 carbonyl acid, both initial oxidation products. This carbonyl has either a methyl group attached to it, in the 1-methylcyclohexene system, or a methyl group attached to its α -carbon, in the 3-methylcyclohexene system, or no methyl substitution, in the cycloheptene system. As explained earlier, larger amounts of C_7 dicarbonyl and carbonyl acid are expected to form in the system of 1-methylcyclohexene than cycloheptene and 3-methylcyclohexene. In addition, with both the dicarbonyl and carbonyl acid, there are two α -carbons and five α -hydrogens available for enolization in the 1-methylcyclohexene system. In comparison, available α -C and α -H numbers decrease to one and two, respectively, in the cycloheptene system, and one and one, respectively, in the 3-methylcyclohexene system. As a result, enolization becomes increasingly difficult moving from 1-methylcyclohexene to cycloheptene to 3-methylcyclohexene, as does the subsequent dimerization. Either slower reactions or fewer dimerization possibilities ultimately lead to increasingly

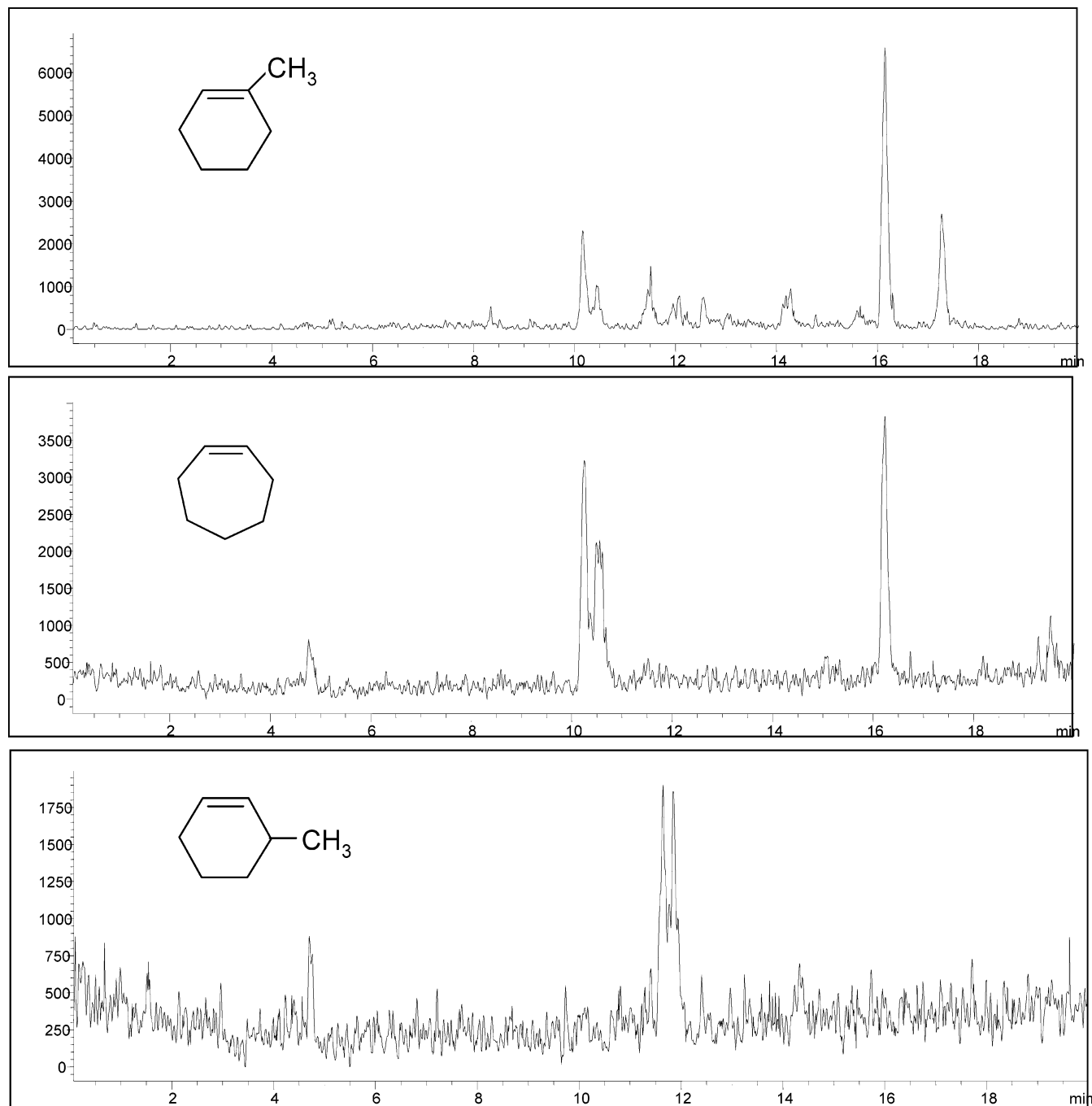


Figure 10. Extracted ion chromatograms of 289 ion in SOA from the ozonolysis of 1-methylcyclohexene, cycloheptene, and 3-methylcyclohexene.

smaller amounts of oligomers formed in the SOA and, therefore, smaller overall SOA yield.

Conclusions

The composition of SOA from cycloalkene (C_5 – C_8) and α -pinene ozonolysis is investigated by the concurrent use of a LC–MS and an ion trap MS, both equipped with ESI. A large variety of polar, low-volatility species are identified and quantified. Four classes of compounds, diacids, carbonyl-containing acids, diacid alkyl esters, and hydroxy diacids, comprise relatively constant mass fractions of the total identified low-MW species ($MW < 250$) in SOA in all six cycloalkene systems; on average, these fractions are 69, 15, 11, and 8%, respectively. In particular, C_n , C_{n-1} , and C_{n+1} diacids comprise, on average, 62% of the total identified low-MW species. With

an estimate for oxalic acid and assuming an SOA density of 1.4 g/cm^3 , identified low-MW species comprise 42 to 83% of the total SOA mass in the six cycloalkene systems that were quantified.

Oligomeric species ($MW > 250$) are ubiquitous in the SOA from all parent cycloalkenes (although those from cyclopentene are at minimal amounts). Using surrogate standards, it is estimated that oligomers comprise at least 10% of the total mass of SOA from cycloalkene ozonolysis. The mass fraction of oligomers may well exceed 50% in the SOA from α -pinene ozonolysis. Two issues need to be understood more fully before SOA mass closure can be more accurately assessed: how to quantify the mass of oligomers, and what is the actual density of the SOA. Mass closures may have been overestimated due to the density values used (e.g., 1.4 g/cm^3 or less calculated on the basis of low-MW components alone).

The acidity of the seed particles upon which SOA components condense has an explicit effect on oligomer formation. Higher acidity appears to lead to more rapid formation of oligomers, ultimately resulting in higher SOA yields than in systems with more neutral seed particles. Although acidity is required to facilitate the three heterogeneous reactions proposed, organic acids produced from gas-phase oxidations may readily promote oligomer formation, as suggested by the formation of similar oligomers in SOA both in the presence and absence of seed particles.

Systematic relationships between hydrocarbon precursor structure and the composition and yield of resultant SOA were discussed. Carbon numbers, substituent groups, and isomeric structures all have distinct effects on the SOA formed, either by different gas-phase reaction pathways or by different oligomer formation processes or both. Work remains to describe quantitatively these complex and coupled effects.

Acknowledgment. This work was supported by U.S. Department of Energy Biological and Environmental Research Program DE-FG03-01ER63099, Electric Power Research Institute, and U.S. Environmental Protection Agency RD-83107501-0. We thank Jiwen He, Kee-Yoon Yoo, and Athanasios Nenes for assistance with calculating pH values of seed aerosols used in the α -pinene ozonolysis experiments. J. L. Beauchamp and R. Hodyss are acknowledged for their help with the use of ion trap mass spectrometry.

Supporting Information Available: A table of standard compounds calibrated, m/z of molecular ions $[M - 1]^-$, and average and standard deviation of retention times and a table of molecular structures and molecular weights of identified low-MW components in SOA from the ozonolysis of cycloalkenes. This material is available free of charge via the Internet at <http://pubs.acs.org>.

References and Notes

(1) Seinfeld, J. H.; Pankow, J. F. *Annu. Rev. Phys. Chem.* **2003**, *54*, 121.

- (2) Rogge, W.; Mazurek, M. A.; Hildemann, L. M.; Cass, G. R.; Simoneit, B. R. T. *Atmos. Environ.* **1993**, *27A*, 1309.
- (3) Saxena, P.; Hildemann, L. J. *Atmos. Chem.* **1996**, *24*, 57.
- (4) Jacobson, M. C.; Hansson, H. C.; Noone, K. J.; Charlson, R. J. *Rev. Geophys.* **2000**, *38*, 267.
- (5) Yu, J.; Flagan, R. C.; Seinfeld, J. H. *Environ. Sci. Technol.* **1998**, *32*, 2357.
- (6) Kalberer, M.; Yu, J.; Cocker, D. R.; Flagan, R. C.; Seinfeld, J. H. *Environ. Sci. Technol.* **2000**, *34*, 4894.
- (7) Tobias, H. J.; Ziemann, P. J. *Anal. Chem.* **1999**, *71*, 3428.
- (8) Jang, M.; Czoschke, N. M.; Lee, S.; Kamens, R. M. *Science* **2002**, *298*, 814.
- (9) Czoschke, N. M.; Jang, M.; Kamens, R. M. *Atmos. Environ.* **2003**, *37*, 4287.
- (10) Limbeck, A.; Kulmala, M.; Puxbaum, H. *Geophys. Res. Lett.* **2003**, *30*, 1996, doi: 10.1029/2003GL017738.
- (11) Iinuma, Y.; Böge, O.; Gnauk, T.; Herrmann, H. *Atmos. Environ.* **2004**, *38*, 761.
- (12) Tolocka, M. P.; Jang, M.; Ginter, J. M.; Cox, F. J.; Kamens, R. M.; Johnston, M. V. *Environ. Sci. Technol.* **2004**, *38*, 1428.
- (13) Kalberer, M.; Paulsen, D.; Sax, M.; Steinbacher, M.; Dommen, J.; Prevot, A. S. H.; Fisseha, R.; Weingartner, E.; Frankevich, V.; Zenobi, R.; Baltensperger, U. *Science* **2004**, *303*, 1659.
- (14) Chung, S. H.; Seinfeld, J. H. *J. Geophys. Res.* **2002**, *107*, 4407, doi: 10.1029/2001JD001397.
- (15) Keywood, M. D.; Varutbangkul, V.; Bahreini, R.; Flagan, R. C.; Seinfeld, J. H. *Environ. Sci. Technol.* **2004**, *38*, 4157.
- (16) Yu, J.; Cocker, D. R., III; Griffin, R. J.; Flagan, R. C.; Seinfeld, J. H. *J. Atmos. Chem.* **1999**, *34*, 207.
- (17) Koch, S.; Winterhalter, R.; Uherek, E.; Koloff, A.; Neeb, P.; Moortgat, G. K. *Atmos. Environ.* **2000**, *34*, 4031.
- (18) Winterhalter, R.; Dingenen, R. V.; Larsen, B. R.; Jensen, N. R.; Hjorth, J. *Atmos. Chem. Phys. Discuss.* **2003**, *3*, 1.
- (19) Grosjean, E.; Grosjean, D. *Environ. Sci. Technol.* **1996**, *30*, 1321.
- (20) Grosjean, E.; Grosjean, D.; Seinfeld, J. H. *Environ. Sci. Technol.* **1996**, *30*, 1038.
- (21) Aschmann, S. M.; Tuazon, E. C.; Arey, J.; Atkinson, R. *J. Phys. Chem. A* **2003**, *107*, 2247.
- (22) Streitwieser, A., Jr.; Heathcock, C. H. *Introduction to Organic Chemistry*, 3rd ed.; Macmillan Publishing Company: New York, 1985.
- (23) Calvert, J. G.; Atkinson, R.; Kerr, J. A.; Madronich, S.; Moortgat, G. K.; Wallington, T. J.; Yarwood, G. *The Mechanism of Atmospheric Oxidation of the Alkenes*; Oxford University Press: New York, 2000.
- (24) Keywood, M. D.; Kroll, J. H.; Varutbangkul, V.; Bahreini, R.; Flagan, R. C.; Seinfeld, J. H. *Environ. Sci. Technol.* **2004**, *38*, 3343.
- (25) Zoller, D. L.; Johnston, M. V. *Macromolecules* **2000**, *33*, 1664.

Appendix C

Chemical Composition of Secondary Organic Aerosol Formed from the Photooxidation of Isoprene*

* This chapter is reproduced by permission from “Chemical Composition of Secondary Organic Aerosol Formed from the Photooxidation of Isoprene” by J. D. Surratt, S. M. Murphy, J. H. Kroll, N. L. Ng, L. Hildebrandt, A. Sorooshian, R. Szmigielski, R. Vermeylen, W. Maenhaut, M. Claeys, R. C. Flagan, J. H. Seinfeld, *Journal of Physical Chemistry A*, 110: 9665-9690, 2006. Copyright 2006, American Chemical Society.

Chemical Composition of Secondary Organic Aerosol Formed from the Photooxidation of Isoprene

Jason D. Surratt,[†] Shane M. Murphy,[‡] Jesse H. Kroll,[§] Nga L. Ng,[‡] Lea Hildebrandt,[‡] Armin Sorooshian,[‡] Rafal Szmigielski,^{||} Reinhilde Vermeylen,^{||} Willy Maenhaut,[⊥] Magda Claeys,^{||} Richard C. Flagan,[§] and John H. Seinfeld^{*,§}

Department of Chemistry, California Institute of Technology, Pasadena, California 91125, Department of Chemical Engineering, California Institute of Technology, Pasadena, California 91125, Departments of Environmental Science and Engineering and Chemical Engineering, California Institute of Technology, Pasadena, California 91125, Department of Pharmaceutical Sciences, University of Antwerp (Campus Drie Eiken), Universiteitsplein 1, BE-2610 Antwerp, Belgium, and Department of Analytical Chemistry, Institute for Nuclear Sciences, Ghent University, Proeftuinstraat 86, BE-9000 Gent, Belgium

Received: March 20, 2006; In Final Form: June 15, 2006

Recent work in our laboratory has shown that the photooxidation of isoprene (2-methyl-1,3-butadiene, C₅H₈) leads to the formation of secondary organic aerosol (SOA). In the current study, the chemical composition of SOA from the photooxidation of isoprene over the full range of NO_x conditions is investigated through a series of controlled laboratory chamber experiments. SOA composition is studied using a wide range of experimental techniques: electrospray ionization–mass spectrometry, matrix-assisted laser desorption ionization–mass spectrometry, high-resolution mass spectrometry, online aerosol mass spectrometry, gas chromatography/mass spectrometry, and an iodometric-spectroscopic method. Oligomerization was observed to be an important SOA formation pathway in all cases; however, the nature of the oligomers depends strongly on the NO_x level, with acidic products formed under high-NO_x conditions only. We present, to our knowledge, the first evidence of particle-phase esterification reactions in SOA, where the further oxidation of the isoprene oxidation product methacrolein under high-NO_x conditions produces polyesters involving 2-methylglyceric acid as a key monomeric unit. These oligomers comprise ~22–34% of the high-NO_x SOA mass. Under low-NO_x conditions, organic peroxides contribute significantly to the low-NO_x SOA mass (~61% when SOA forms by nucleation and ~25–30% in the presence of seed particles). The contribution of organic peroxides in the SOA decreases with time, indicating photochemical aging. Hemiacetal dimers are found to form from C₅ alkene triols and 2-methyltetrols under low-NO_x conditions; these compounds are also found in aerosol collected from the Amazonian rainforest, demonstrating the atmospheric relevance of these low-NO_x chamber experiments.

1. Introduction

Secondary organic aerosol (SOA) is formed in the troposphere from the oxidation of volatile organic compounds (VOCs), where the resultant low-vapor-pressure oxidation products partition between the gas and aerosol phases. Recent laboratory experiments have established that SOA formation can also result from the heterogeneous reactions between particle-associated substances and relatively volatile species resulting in the formation of high-molecular-weight (MW) products via oligomerization (polymerization).^{1–5} Until recently, the formation of SOA from the photooxidation of isoprene, the atmosphere's most abundant nonmethane hydrocarbon, was considered insignificant.^{6,7} This was largely due to the known volatility of first-generation gas-phase oxidation products, such as meth-

acrolein (MACR), methyl vinyl ketone (MVK), and formaldehyde, from isoprene oxidation in the presence of NO_x, and a previous chamber study that concluded that isoprene oxidation does not lead to SOA formation.⁸ Recent field observations of certain organic aerosol compounds, diastereoisomeric 2-methyltetrols (2-methylerythritol and 2-methylthreitol), and 2-methylglyceric acid, attributable to isoprene oxidation, and the experimental observation that isoprene under highly acidic conditions can lead to the formation of polymeric, humic-like substances through heterogeneous reactions, re-opened the issue of SOA formation from isoprene.^{7,9–13} After their ambient identification, Edney et al.¹⁴ and Böge et al.¹⁵ detected 2-methyltetrols in SOA formed from laboratory chamber studies of isoprene.

Recent work in our laboratory has shown that SOA formation from isoprene oxidation can be significant.^{16,17} Extensive experiments were carried out under both low- and high-NO_x conditions using either nitrous acid (HONO) or hydrogen peroxide (H₂O₂) as the OH radical source. Photooxidation experiments were also conducted using isoprene first-generation gas-phase oxidation products as the VOC precursor. Although no aerosol growth was observed from MVK oxidation, SOA

* To whom correspondence should be addressed. Phone: (626) 395-4635. Fax: (626) 796-2591. E-mail seinfeld@caltech.edu.

[†] Department of Chemistry, California Institute of Technology.

[‡] Department of Chemical Engineering, California Institute of Technology.

[§] Departments of Environmental Science and Engineering and Chemical Engineering, California Institute of Technology.

^{||} University of Antwerp.

[⊥] Ghent University.

formation was observed from MACR at high-NO_x conditions. High-molecular-weight (MW) species were observed to form from isoprene oxidation under both low- and high-NO_x conditions.¹⁷ Moreover, SOA yields were observed to exhibit a dependence on the NO_x level. This dependence appears to be attributed to differences in organic peroxy radical (RO₂) chemistry. At high [NO] (i.e., high-NO_x conditions), RO₂ radicals react mainly with NO to produce small alkoxy radicals (RO) that likely fragment into smaller organics, which are expected to be too volatile to partition appreciably to the aerosol phase, or form organic nitrate species (RONO₂). In the absence of NO_x (i.e., low-NO_x conditions), RO₂ radicals instead react with HO₂ radicals (present in the chamber experiments in large quantities from the OH + H₂O₂ reaction) to form organic hydroperoxides, which have been experimentally shown to be important SOA components from other VOC precursors.^{18,19} Hydroperoxides have been suggested to be involved in polymerization in the aerosol phase via reactions with aldehydes to form peroxyhemiacetals.^{18,19}

Although it is now established that OH-initiated oxidation of isoprene leads to SOA, a detailed understanding of the chemical reaction pathways leading to the production of isoprene SOA is lacking. Results from chamber studies have elucidated the importance of the further oxidation of MACR as a primary route for SOA formation from isoprene under high-NO_x conditions. Known RO₂ chemistry at low-NO_x conditions leads to the initial gas-phase oxidation products, likely hydroxyhydroperoxides, of isoprene, which upon further oxidation leads to SOA production. Nonetheless, detailed evaluation of the mechanism of SOA formation from the oxidation of isoprene has not yet been carried out.

In the present work, a suite of offline analytical techniques is used in conjunction with online aerosol mass spectrometry to investigate the detailed chemical composition of SOA from isoprene oxidation. SOA is produced from the photooxidation of isoprene under varying NO_x conditions and is collected onto filters for offline chemical analyses. Offline mass spectrometry (MS) techniques are used to detect organic species from aerosol filter samples, including oligomeric components of isoprene SOA (as detected in prior studies only by online time-of-flight aerosol mass spectrometry (TOF-AMS) measurements). Tandem MS and gas chromatography (GC)/MS derivatization techniques are employed to structurally elucidate oligomeric components. Organic peroxides are detected and quantified from low-NO_x isoprene SOA using a conventional iodometric-spectroscopic method. Tracer compounds for isoprene oxidation in the ambient atmosphere, as found in the Amazonian rainforest, are detected here for the first time in the low-NO_x chamber experiments. The low-NO_x conditions are most relevant to understanding SOA formation in highly vegetated, remote regions.⁷ In some cases, such as the southeastern U.S., where atmospheric transport of pollutants from urban areas can influence SOA formation,²⁰ conditions closer to those of the high-NO_x experiments may be applicable.

2. Experimental Section

2.1. Chamber Experiments. Experiments were carried out in Caltech's dual indoor 28 m³ Teflon smog chambers.^{21,22} Experimental protocols are similar to those described previously,^{16,17} so they will be described only briefly here. Most experiments were carried out with hydrogen peroxide (H₂O₂) as the hydroxyl radical (OH) precursor; in some cases, HONO was used instead to demonstrate that the particular OH source has no effect on the outcome of the experiments. For some

experiments, ammonium sulfate seed particles were introduced into the chamber (at volume concentrations of 20–30 μm³/cm³) by atomization of a 0.015 M ammonium sulfate solution. A known concentration of isoprene (or any other precursor, such as MACR) was then introduced by sending air over a measured volume of the pure compound (Aldrich, 99.8%) into the chamber. For H₂O₂/high-NO_x experiments, NO was also introduced into the chamber from a gas mixture (500 ppm gas cylinder in N₂, Scott Specialty Gases). In low-NO_x experiments, NO was not added and NO_x concentrations were <1 ppb. When the isoprene (monitored by gas chromatography–flame ionization detection (GC-FID)), NO_x, and seed concentrations became constant inside the chamber, irradiation by UV lights (centered at 354 nm) was started, initiating the reaction.

SOA volume growth (μm³/cm³) was monitored with a differential mobility analyzer (DMA). For quantification of SOA products collected on filter samples, the DMA volumes were used for each experiment to determine the total SOA mass collected. Filter sampling commenced when the particle growth had terminated, that is, when the aerosol volume had reached its maximum value. Depending on the total volume concentration of aerosol in the chamber, the filter sampling time was 2–4 h, which typically resulted in 3–7 m³ of total chamber air sampled.

2.2. Filter Extractions. Collected Teflon filters (PALL Life Sciences, 47-mm diameter, 1.0-μm pore size, teflo membrane) were extracted in 5 mL of HPLC-grade methanol by 40 min of sonication. The filters were then removed from the methanol sample extracts and archived at –20 °C. Each extract was blown dry under a gentle N₂ stream (without added heat) and then reconstituted with 1 mL of a 50:50 (v/v) solvent mixture of HPLC-grade methanol and 0.1% aqueous acetic acid solution. The reconstituted extracts were then stored at –20 °C until analysis was performed. In most cases, filter extracts were chemically analyzed within 1–2 days after filter extraction. Lab control filters were extracted and treated in the same manner as the samples. Aliquots of each of these filter extracts were analyzed by the four mass spectrometry techniques to follow.

To ensure that H₂O₂ was not condensing onto filter media and introducing artifacts in the chemical analyses, we collected several blank filters under dark conditions from the chamber containing typical experimental well-mixed concentrations of isoprene, NO, and ammonium sulfate seed aerosol, sampled for the same duration (~2–4 h) as a sample filter. No significant chemical artifacts or contaminants were observed in the analytical techniques from these blank filters, consistent with the lack of observed aerosol growth under dark conditions.

2.3. Liquid Chromatography/Electrospray Ionization–Mass Spectrometry (LC/ESI-MS). A Hewlett-Packard 1100 Series HPLC instrument, coupled with a single quadrupole mass analyzer and equipped with an electrospray ionization (ESI) source, was used to identify and quantify relatively polar, acidic SOA components. Data were collected in both positive (+) and negative (–) ionization modes; the quantitative analysis presented here is limited to the negative ionization mode. An Agilent Eclipse C₁₈ column (3.0 × 250 mm) was used to separate the organic species before detection. The eluents used were 0.1% aqueous acetic acid (A) and methanol (B). In the 40-min gradient elution program used, the concentration of eluent B increased from 5% to 90% in 35 min, and then decreased to 5% in 5 min. The total flow rate of the eluent used in the LC/MS analysis was 0.8 mL min^{–1}. Optimum electrospray conditions were found using a 60 psig nebulizing pressure, 3.5 kV capillary voltage, 13 L min^{–1} drying gas

flowrate, and a 330 °C drying gas temperature. During the full scan mode of analysis, the cone voltage was set at 60 V, avoiding fragmentation of most species and allowing their detection as deprotonated molecules ($[M - H]^-$). During the upfront collision-induced dissociation (CID) mode of analysis, the cone voltage was set to 110 V, resulting in partial fragmentation of the $[M - H]^-$ ions. By comparing these two sets of MS data (upfront CID mode to the full scan mode of analysis) and by examining the fragmentation patterns of the species, some structural information on the analyzed species was obtained. This was particularly useful in confirming results from other MS/MS techniques used and for the identification of oligomeric components.

Using a set of six acidic species (*meso*-erythritol, citramalic acid, 2-hydroxy-3-methylbutyric acid, pimelic acid, pinic acid, and suberic acid monomethyl ester) as surrogate standards, this method was also used to quantify the amount of polar acidic species. Filter extraction efficiency was established by standard additions of these surrogate standards to blank filters. On average, the extraction efficiency for each standard was ~60% with an estimated error bar of ca. $\pm 15\%$ over the concentration range used to generate the LC/MS calibration curves. This average extraction efficiency was included in the calculations to quantify identified isoprene SOA products.

As we will note shortly, to investigate the probable importance of a C₄ hydroxy dialdehyde species formed under high-NO_x conditions, we derivatized selected sample extracts using Girard Reagent P (1-(carboxymethyl)pyridinium chloride hydrazide, MW = 187) to increase sensitivity for aldehydic species in the (+)LC/MS mode. Girard Reagent P (GirP) reacts with aldehydes and ketones to form water-soluble hydrazones with a permanently charged pyridine moiety, and water is eliminated in this reaction.²³ The organic unit that adds to aldehydes and ketones has a mass of 152 Da. A series of aldehyde standards, glyoxal (MW = 58), succinic semialdehyde (MW = 102), and glutaraldehyde (MW = 100), were derivatized using the GirP and analyzed with (+)LC/MS. These small polar aldehyde standards typically go undetected using (+)ESI techniques such as in LC/MS; however, upon derivatization they were detected as the singly charged $[M - H_2O + 152(\text{GirP})]^+$ ions (glyoxal was also detected as doubly charged $[M - 2H_2O + 152(\text{GirP})]^{2+}$ ion), where M is the MW of the aldehyde species. These compounds eluted between 1 and 2 min from the LC column, including a derivatized compound corresponding to the proposed C₄ hydroxy dialdehyde species (MW = 102 and $[M - H_2O + 152(\text{GirP})]^+ = 236$).

2.4. ESI-Ion Trap Mass Spectrometry (ESI-ITMS). Aliquots of the filter extracts were also analyzed by a ThermoElectron LCQ ion trap mass spectrometer equipped with an ESI source, via direct infusion. This instrument does not provide chromatographic separation, precluding quantification. Instead, the instrument was used for the qualitative detection of product species. In addition, specific ions of interest were isolated from the rest of the sample ion matrix and further fragmented to produce product ion mass spectra, aiding in structural elucidation.

Data were collected in both positive and negative ionization modes. Because the same species were detected in both modes ($[M - H]^-$ and $[M + Na]^+$ ions), we only present here the data collected under negative ionization; the data collected under positive ionization serve as confirmation of the negative ionization data.

2.5. Matrix-Assisted Laser Desorption Ionization-Time-of-Flight Mass Spectrometer (MALDI-TOFMS). Another

aliquot of the filter extract was analyzed on an Applied Biosystems Voyager-DE Pro MALDI-TOFMS instrument. After 6 μL of each extract had been dried on the steel target plate, the plate was gently brushed with graphite particles, which served as the matrix. The samples were analyzed in the linear mode, in both positive and negative ionization modes. 400–500 laser shots were summed to obtain a representative mass spectrum of each sample. This method was mainly used to assess the molecular weight (MW) range of the aerosol, to detect oligomeric signatures, and to confirm the MWs of species identified by the ESI techniques.

2.6. High-Resolution ESI-MS. Extracts were also analyzed by a Waters LCT Premier Electrospray time-of-flight mass spectrometer with W geometry in the Department of Chemistry at the University of California, Irvine, operated in the negative ionization mode. Samples were analyzed by flow injection. The calibration was carried out using sodium formate clusters with co-injection of fmoc-amino acids of appropriate mass spiked into the analytical sample for lock-mass corrections to obtain accurate mass for the oligomeric ions with m/z 266, 323, 365, 368, 467, and 470. These ions were only detected in the high-NO_x experiments, and elemental compositions were determined with reasonable accuracy (within ± 5 ppm) and were consistent with other analytical observations (such as ESI-MS/MS and GC/MS derivatization data).

2.7. Aerodyne Time-of-Flight Aerosol Mass Spectrometer (TOF-AMS). During most chamber experiments, real-time particle mass spectra were collected continuously by an Aerodyne Time-of-Flight Aerosol Mass Spectrometer (TOF-AMS), and averaged spectra were saved every 5 min. The design and capabilities of the TOF-AMS instrument are described in detail elsewhere.²⁴ Briefly, chamber air enters the instrument through a 100- μm critical orifice at a flowrate of 1.4 cm³/s. Particles with vacuum aerodynamic diameters between 50 and 800 nm are efficiently focused by an aerodynamic lens, passed through a chopper, and then impacted onto a tungsten vaporizer. The chopper can be operated in three modes: (1) completely blocking the beam to gather background mass spectra; (2) out of the beam's path to collect ensemble average mass spectra over all particles sizes; and (3) chopping the beam to create size-resolved mass spectra. The vaporizer is typically run at ~550 °C to ensure complete volatilization of the SOA and the inorganic seed; during several runs the vaporizer temperature was lowered to ~160 °C to reduce thermally induced fragmentation of oligomers. Once vaporized, molecules undergo electron ionization at 70 eV and are orthogonally pulsed every 19 μs into the time-of-flight mass analyzer.

2.8. Gas Chromatography/Mass Spectrometry (GC/MS). Extracts of selected filters were analyzed for polar organic compounds by GC/MS using a method that was adapted from that reported by Pashynska et al.²⁵ The sample workup consisted of extraction of all or half of the filter with methanol under ultrasonic agitation and derivatization of carboxyl and hydroxyl functions into trimethylsilyl (TMS) derivatives. The extract was divided into two parts; one part was trimethylsilylated while the other part was stored in a refrigerator at 4 °C for eventual further analysis. GC/MS analyses were performed with a system comprising a TRACE GC2000 gas chromatograph, which was coupled to a Polaris Q ion trap mass spectrometer equipped with an external ionization source (ThermoElectron, San Jose, CA). A Heliflex AT-5MS fused-silica capillary column (5% phenyl, 95% methylpolysiloxane, 0.25 μm film thickness, 30 m \times 0.25 mm i.d.) preceded by a deactivated fused-silica precolumn (2 m \times 0.25 mm i.d.) (Alltech, Deerfield, IL) was

used to separate the derivatized extracts. Helium was used as carrier gas at a flow rate of 1.2 mL min⁻¹. The temperature program was as follows: isothermal hold at 50 °C for 5 min, temperature ramp of 3 °C min⁻¹ up to 200 °C, isothermal hold at 200 °C for 2 min, temperature ramp of 30 °C min⁻¹ up to 310 °C; and isothermal hold at 310 °C for 2 min. The analyses were performed in the full scan mode (mass range: *m/z* 50–800), and were first carried out in the electron ionization (EI) mode and subsequently in the chemical ionization (CI) mode. The ion source was operated at an electron energy of 70 eV and temperatures of 200 °C and 140 °C in the EI and CI modes, respectively. The temperatures of the GC injector and the GC/MS transfer line were 250 °C and 280 °C, respectively. For chemical ionization, methane was introduced as reagent gas at a flow rate of 1.8 mL min⁻¹. We present here mainly the data collected in the EI mode; the data collected in the CI mode are used if insufficient MW information is obtained in the EI mode.

Selected extracts were also subjected to a hydrolysis/ethylation and/or a methoximation procedure prior to trimethylsilylation. The purpose of the hydrolysis/ethylation procedure was to confirm the presence of ester linkages, while that of the methoximation procedure was to evaluate the presence of aldehyde/keto groups, in oligomeric SOA. The hydrolysis/ethylation procedure involved reaction of the extract residues with 40 μ L of analytical-grade ethanol and 8 μ L of trimethylchlorosilane (Supelco, Bellefonte, PA) for 1 h at 60 °C. Details about the methoximation procedure can be found in Wang et al.¹²

2.9. Gas Chromatography–Flame Ionization Detection (GC-FID). Quantitative determination of the 2-methyltetrols (i.e., 2-methylthreitol and 2-methylerythritol), the C₅ alkene triols [i.e., 2-methyl-1,3,4-trihydroxy-1-butene (cis and trans) and 3-methyl-2,3,4-trihydroxy-1-butene], and 2-methylglyceric acid, in selected filters, was performed by GC-FID with a GC 8000 Top instrument (Carlo Erba, Milan, Italy). The sample workup was the same as that for GC/MS analysis except that filter parts were spiked with a known amount of erythritol (Sigma, St. Louis, MO) as an internal recovery standard; it was assumed that the GC-FID responses of the trimethylsilyl derivatives of the analytes and the internal recovery standard were similar. The GC column and conditions were comparable with those used for GC/MS; the column was a CP-Sil 8 CB capillary column (5% diphenyl, 95% methylpolysiloxane, 0.25 μ m film thickness, 30 m \times 0.25 mm i.d.) (Chrompack, Middelburg, The Netherlands) and the temperature program was as follows: isothermal hold at 45 °C for 3 min, temperature ramp of 20 °C min⁻¹ up to 100 °C, isothermal hold at 100 °C for 10 min, temperature ramp of 5 °C min⁻¹ up to 315 °C, and isothermal hold at 315 °C for 20 min. Measurement of the 2-methyltetrols in the low-NO_x SOA samples was performed after the unstable products tentatively characterized as 2-methyltetrol performate derivatives had decayed to 2-methyltetrols, that is, after leaving the reaction mixture for 2 days at room temperature.

2.10. Total Aerosol Peroxide Analysis. The total amount of peroxides in the low-NO_x isoprene SOA was quantified using an iodometric-spectrophotometric method adapted from that used by Docherty et al.¹⁸ to analyze peroxides formed by α -pinene-ozonolysis. The method employed here differed only in the choice of extraction solvent: we used a 50:50 (v/v) mixture of methanol and ethyl acetate, rather than pure ethyl acetate. Calibration and measurements were performed at 470 nm on a Hewlett-Packard 8452A diode array spectrophotometer. A standard calibration curve was obtained from a series of

benzoyl peroxide solutions. Benzoyl peroxide was the standard used for quantification of organic peroxides formed from low-NO_x experiments, because its MW is close to the average MW determined from the mass spectrometry techniques, in particular the MALDI-TOFMS measurements. The molar absorptivity determined from the standard curve was \sim 852, in excellent agreement with that determined by Docherty et al. and with the value of 845 determined with the original method development paper.^{18,26} As a confirmation that the technique was reproducible, we extracted and analyzed in the same fashion, three α -pinene-ozonolysis filters collected from our laboratory chambers. We measured \sim 49% of the SOA mass, produced from α -pinene ozonolysis, to be organic peroxides, in excellent agreement to that of Docherty et al.'s measurement of \sim 47% for the same system. A few high-NO_x isoprene filter samples were also analyzed by this method, but resulted in the detection of no organic peroxides (below detection limits of this technique).

2.11. Particle-Into-Liquid Sampler Coupled to Ion Chromatography (PILS/IC). The PILS/IC (particle-into-liquid sampler coupled to ion chromatography) is a quantitative technique for measuring water-soluble ions in aerosol particles. The PILS developed and used in this study²⁷ is based on the prototype design²⁸ with key modifications, including integration of a liquid sample fraction collector and real-time control of the steam injection tip temperature. Chamber air is sampled through a 1- μ m cut-size impactor and a set of three denuders (URG and Sunset Laboratories) to remove inorganic and organic gases that may bias aerosol measurements. Sample air mixes with steam in a condensation chamber where rapid adiabatic mixing produces a high water supersaturation. Droplets grow sufficiently large to be collected by inertial impaction before being delivered to vials held on a rotating carousel. The contents of the vials are subsequently analyzed off-line using a dual IC system (ICS-2000 with 25 μ L sample loop, Dionex Inc.) for simultaneous anion and cation analysis. The background levels of individual species (Na⁺, NH₄⁺, K⁺, Mg²⁺, Ca²⁺, SO₄²⁻, Cl⁻, NO₂⁻, NO₃⁻, oxalate, acetate, formate, methacrylate, pyruvate) concentrations for analyzed filter samples, presented as the average concentration plus three times the standard deviation (σ), are less than 0.28 μ g m⁻³.

3. Results

As noted, experiments were conducted at high- and low-NO_x conditions. High-NO_x conditions were achieved through the addition of substantial NO_x (\sim 800 to 900 ppb NO_x) to the reaction chamber, leading to isoprene/NO_x molar ratios of \sim 0.56 to 0.63. Under low-NO_x conditions no NO_x is added to the chamber, where NO_x mixing ratios of $<$ 1 ppb (small amounts of NO_x likely desorb from chamber walls) were observed. The low-NO_x condition simulates a remote (NO_x-free) atmosphere; for example, at typical isoprene and NO_x mixing ratios observed in the Amazonian rainforest (\sim 4 to 10 ppb and 0.02 to 0.08 ppb, respectively),^{7,29} the isoprene/NO_x ratios that result are \sim 50 to 500, comparable to the isoprene/NO_x ratio of the present experiments (\sim 500).

3.1. High-NO_x Condition. Table 1 lists nine high-NO_x chamber experiments that were conducted to generate SOA for aerosol filter sampling. All experiments were conducted with 500 ppb of isoprene or MACR in order to produce sufficient aerosol mass for all offline analytical measurements. In most of the experiments conducted, H₂O₂ served as the OH radical precursor; in this manner, initial oxidation of isoprene is dominated by OH. It is estimated that \sim 3–5 ppm of H₂O₂ was

TABLE 1: High-NO_x Chamber Experiments Conducted

expt no.	VOC ^a	OH precursor ^b	seeded/ ^c nucleation	initial [NO] ppb	initial [NO ₂] ppb	initial [NO _x] ppb	[O ₃] ^d ppb	T, °C ^d	total SOA mass concentration ^{d,e,f} μg/m ³
1	isoprene	H ₂ O ₂	nucleation	827	34	860	498	28.5	74
2	isoprene	H ₂ O ₂	dry AS	759	112	869	525	28.3	73
3	MACR	H ₂ O ₂	dry AS	791	60	850	540	25.2	181
4	MACR	H ₂ O ₂	nucleation	898	30	926	519	25.0	197
5	isoprene	H ₂ O ₂	nucleation	805	87	891	294	24.3	104
6	isoprene	H ₂ O ₂	AAS	825	80	904	450	24.6	111
7 ^g	isoprene	HONO	dry AS	50	333	382	132	20.1	68
8 ^g	isoprene	HONO	nucleation	89	279	366	134	21.4	73
9	isoprene	H ₂ O ₂	dry AS	891	74	963	325	24.9	95

^a All VOC gas phase mixing ratios were 500 ppb. MACR = methacrolein. ^b H₂O₂ and HONO are not measured directly, but from isoprene decay during irradiation we estimate ~3 ppm of H₂O₂, and [HONO] is unlikely greater than measured [NO₂]. ^c AS = ammonium sulfate seed, AAS = acidic ammonium sulfate seed. ^d Averaged over the course of the filter sampling. ^e Subtraction of seed aerosol taken into account when necessary. SOA volume derived from DMA wall loss uncorrected measurements for use in mass closure from filter sample analyses. ^f Assuming a SOA density of 1.35 g/cm³. This value is derived from comparison of DMA aerosol mass measurements. ^g 10% of light bank used and hence lower temperature observed. Also lower amounts of initial NO due to HONO as precursor.

used in each of these experiments based upon isoprene decay during irradiation.¹⁷ All of these experiments were conducted at low relative humidity ($RH < 5\%$) in order to limit the uptake of H₂O₂ into the particle phase. In the high-NO_x experiments using H₂O₂ as an OH source, ~800 to 900 ppb of NO was injected into the chamber. With the HONO source, lower initial NO concentrations were achieved, because the source of NO was HONO photolysis and a NO_x side-product from the HONO synthesis. Nucleation (seed-free) and ammonium sulfate seeded experiments were also conducted to examine if the presence of seed aerosol has an effect on the chemistry observed. In Experiment 6, acidified ammonium sulfate seed (0.015 M (NH₄)₂SO₄ + 0.015 M H₂SO₄) was used to investigate the possible effect of acid catalysis on oligomerization reactions, which has previously been observed to occur for other VOC precursors, such as α -pinene and 1,3,5-trimethylbenzene.^{1,3-5,30} No discernible increase in SOA mass is observed for this acid-seeded experiment (Experiment 6) when comparing to its corresponding dry-seeded and nucleation (seed-free) experiments (Experiments 5 and 9).

To illustrate the overall chemical composition typically observed under high-NO_x conditions, shown in Figure 1a is a first-order (-)ESI-IT mass spectrum obtained via direct infusion analysis of an isoprene SOA sample collected from Experiment 1. Prior work in our laboratory has shown that most organics detected in the negative ion mode occur as the deprotonated molecules ($[M - H]^-$ ions),^{2,3,20} making (-)ESI sensitive for the detection of polar acidic species. As can be seen in Figure 1a, many such species are detected. Observable 102 Da differences between many of the $[M - H]^-$ ions and the detection of high-MW species (up to MW ~470) indicate the presence of oligomeric species with more than the five carbons of the parent isoprene. Organic nitrate species are detected in this spectrum as even-mass $[M - H]^-$ ions (m/z 266, 368, and 470).

Figure 1b shows, by comparison, a first-order (-)ESI-IT spectrum, also obtained via direct infusion analysis, for a MACR high-NO_x sample (Experiment 3). Many of the ions detected correspond exactly to those observed from isoprene oxidation (Figure 1a). It should be noted that when the MACR, H₂O₂, and dry ammonium sulfate seed aerosol are well-mixed in the chamber under dark conditions, no aerosol growth is observed, confirming that photooxidation is required to produce SOA. The SOA components formed in this MACR experiment (as shown in Figure 1b) extend out to higher MWs than those of isoprene, which is likely a result of the amount of MACR precursor

available in this experiment and also owing to the removal of one oxidation step (the oxidation of isoprene).

The SOA products detected in Figure 1a and b are confirmed by additional mass spectrometry techniques. Figure 2 shows a mass spectrum collected using the MALDI-TOFMS instrument in the positive ion mode for a high-NO_x, seeded isoprene photooxidation experiment (Experiment 9). SOA components observed here are detected mainly as the sodiated molecules ($[M + Na]^+$ ions), which is consistent with our experiences in analyzing polymeric standards, such as aqueous glyoxal, with a graphite matrix. In Figure 2, only species that correspond to ions detected in the (-)ESI-IT spectra are highlighted. For example, for the $[M - H]^-$ ion series detected in (-)ESI-IT spectra at m/z 161, 263, 365, and 467, a corresponding $[M + Na]^+$ ion series is detected at m/z 185, 287, 389, and 491, respectively, using MALDI-TOFMS. It should be noted that the (+)ESI-IT spectra also detected the same ions ($[M + Na]^+$) as those of the MALDI technique, confirming that the species observed in Figures 1 and 2 are not a result of ionization artifacts specific to individual techniques.

The LC/MS results obtained in the negative ionization mode are used to quantify the SOA components common to all high-NO_x isoprene SOA (as detected in Figures 1 and 2). Figure 3a and b show total ion chromatograms (TICs) for an isoprene photooxidation experiment (Experiment 1) and a MACR photooxidation experiment (Experiment 4), respectively, both carried out at high NO_x in the absence of seed aerosol. These TICs show that many of the SOA products formed in each system are the same because the retention times (RTs) are comparable and the m/z values of the molecular ion species ($[M - H]^-$) associated with each chromatographic peak are the same. Shown in Figure 3c-e are extracted ion chromatograms (EICs) for three organic nitrate species ($[M - H]^-$ at m/z 266, 368, and 470) common to both isoprene and MACR high-NO_x photooxidation experiments. For each chamber experiment, EICs were used instead of TICs for the quantification of each $[M - H]^-$ ion detected in order to deconvolute any coeluting species. Figure 4a shows a mass spectrum recorded for the largest chromatographic peak ($RT = 15.7$ min) from the EIC of m/z 368 (Figure 3d). The m/z 759 ion that is also detected in this mass spectrum is a cluster ion corresponding to $[2M + Na - 2H]^-$; such cluster ions are commonly observed in (-)LC/ESI-MS conditions. In Figure 4b is a resultant upfront CID mass spectrum taken for this same chromatographic peak, showing many product ions from the dissociation of m/z 368. The product ion m/z 305 corresponds to a neutral loss of 63 Da, which is

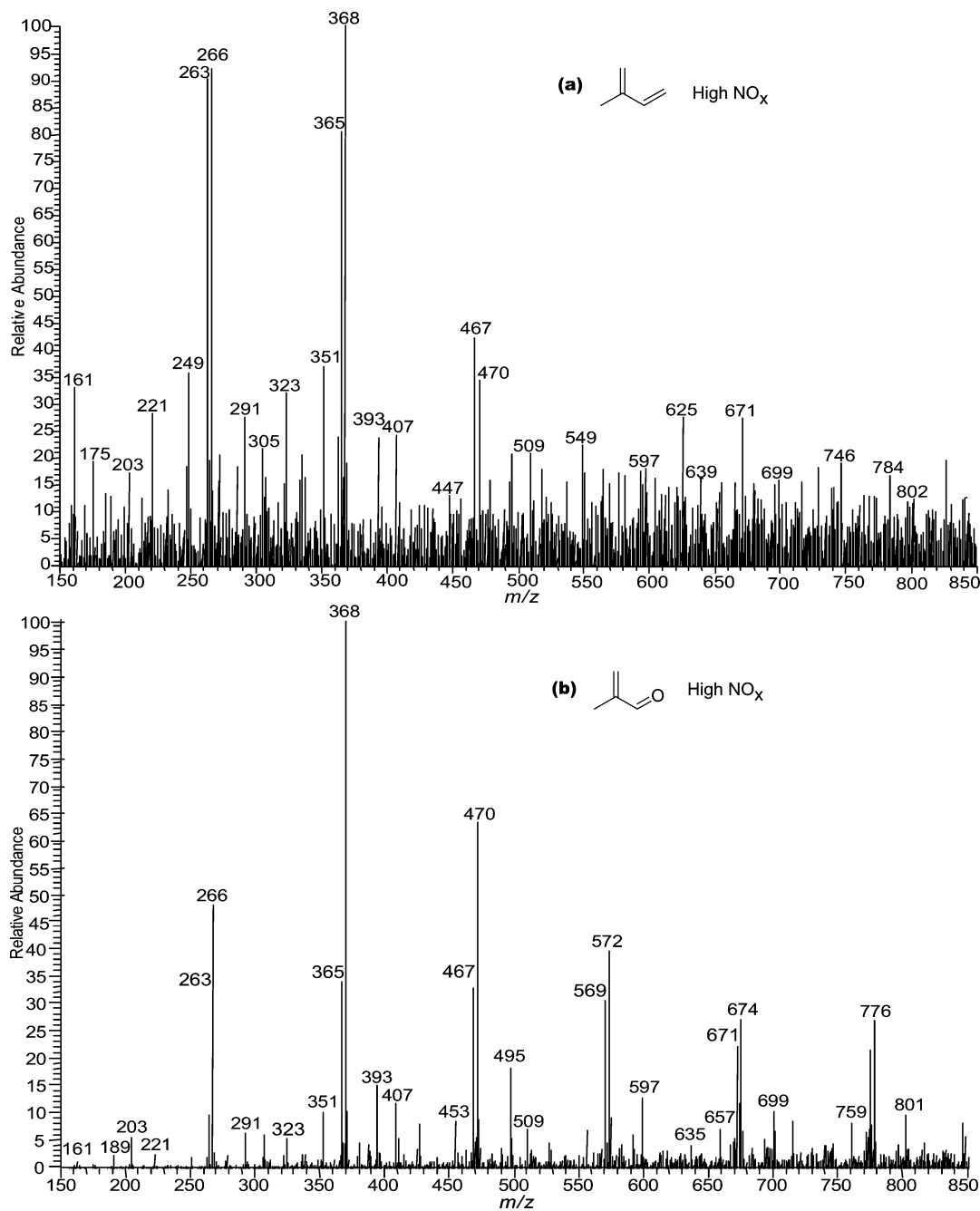


Figure 1. ESI-ITMS negative mode spectra collected via direct infusion analyses. (a) MS scan of a filter extract obtained from a 500 ppb isoprene, high- NO_x , seeded experiment. (b) MS scan of a filter extract obtained from a 500 ppb MACR, high- NO_x , seeded experiment. These mass spectra show that MACR oxidation produces many of the same SOA products as that of isoprene oxidation under high- NO_x conditions. Common 102 Da differences between ions in both spectra are observed indicating the presence of oligomers.

likely nitric acid (HNO_3). Another product ion m/z 291 corresponds to neutral loss of 77 Da, likely from the combined losses of a methyl (CH_3) radical and a nitrate (NO_3) radical (or CH_3ONO_2). The neutral loss of 102 Da results in the product ion m/z 266; these types of product ions are used to aid in the structural elucidation of SOA components and will be discussed subsequently. Owing to the lack of available authentic oligomeric standards, quantification was carried out by using a series of calibration curves generated from surrogate standards (listed in the Experimental Section) covering the wide range of RT s for all detected species. Each surrogate standard contained a carboxylic acid group, the likely site of ionization for detected SOA components, except for the *meso*-erythritol standard. Because of the initial high percentage of aqueous buffer present in the LC/MS gradient, we were able to detect small polar

organics, such as 2-methylglyceric acid. To quantify this compound, the polyol *meso*-erythritol, detected as the $[M - \text{H} + \text{acetic acid}]^-$ ion, was used. Unlike *meso*-erythritol, 2-methyltetrols (and other polyols) were not detected using the $(-)$ -LC/MS technique. All surrogate standards were within ca. ± 1.5 min of the RT s of the detected SOA components. Table 2 shows the LC/MS quantification results for high- NO_x SOA. Four types of oligomers are quantified here. For ease of comparison, experiments corresponding to the same VOC and OH precursor type are grouped together under the same column heading.

SOA components observed thus far are not artifacts formed on filters and are observed over varying isoprene concentrations, as confirmed by online particle mass spectrometry, Figure 5 shows mass spectra collected from three high- NO_x chamber experiments using the Aerodyne TOF-AMS instrument. In these

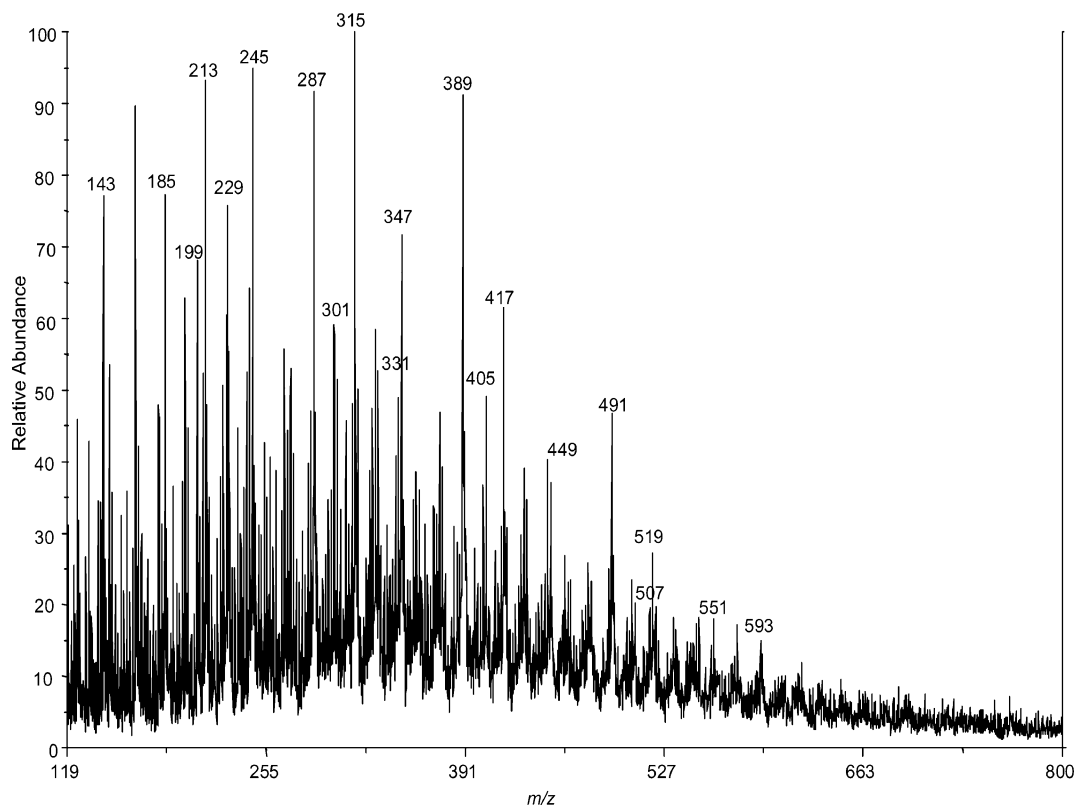


Figure 2. MALDI positive mode spectrum obtained with a graphite matrix for a 500 ppb isoprene, high-NO_x, dry seeded experiment (Experiment 9). Highlighted Na⁺ adduct ions confirm the existence of the species detected by ESI.

experiments, the TOF-AMS instrument was operated at ~ 160 °C to lessen the degree of thermal fragmentation of the high-MW SOA components. Figure 5a shows a TOF-AMS spectrum collected for a 50 ppb isoprene, high-NO_x nucleation experiment (not included in Table 1 because of insufficient aerosol mass for offline chemical analysis techniques). Even at these isoprene concentrations, high-MW species are detected in the SOA produced. Differences of 102 Da are noted in this spectrum, again indicating the presence of oligomers. The oligomers present here confirm the species detected by the (-)ESI and (+)MALDI techniques (Figures 1 and 2, respectively), where the observed TOF-AMS ions result from a loss of a hydroxyl (OH) radical from the molecular ion (i.e., α -cleavage of a hydroxyl radical from a carboxylic acid group). ESI detects these oligomers as the $[M - H]^-$ ion and MALDI as the $[M + Na]^+$ ion, so ions measured in the TOF-AMS instrument are lower by 16 and 40 units, respectively. For example, ions of m/z 145, 187, 247, and 289 measured by the TOF-AMS instrument (Figure 5), correspond to m/z 161, 203, 263, and 305, respectively, using (-)ESI (Figure 1). Four different series of oligomers are highlighted in this spectrum, where ions of the same oligomeric series are indicated in a common color. Figure 5b corresponds to a MACR high-NO_x, dry seeded experiment, in which a filter sample was collected (Experiment 3), showing the same oligomeric signature to that of the low concentration (50 ppb) isoprene experiment. Figure 5c corresponds to an isoprene high-NO_x, HONO experiment (Experiment 8). Again, many ions at the same m/z values are detected, as those of Figures 5a and 5b, suggesting the chemical components of the SOA are the same in these samples. Though probably present, oligomeric compounds formed under conditions similar to those of Figure 5c were not detected in the original study of SOA formation from this laboratory¹⁶ because a less-sensitive quadrupole AMS was used; such high-MW species were reported

in a subsequent study using the TOF-AMS.¹⁷ These online chemical results confirm that the 102 Da differences observed in the offline analytical techniques (ESI and MALDI) are not a result of sample workup or ionization artifacts. Also, these online chemical results suggest that seeded versus nucleation experiments do not lead to significant differences in the chemistry observed, in agreement with the ESI analyses. The OH precursor (HONO or H₂O₂) also does not have a substantial effect on the chemistry observed (i.e., similar products formed, however, abundances may vary), an observation that is also consistent with the offline mass spectrometry analyses.

PILS/IC measurements were carried out for Experiments 1 (nucleation) and 2 (dry seeded). In both experiments, the acetate anion was the most abundant organic anion detected ($14.72 \mu\text{g}/\text{m}^3$ in Experiment 1 and $23.47 \mu\text{g}/\text{m}^3$ in Experiment 2) followed by the formate anion ($1.18 \mu\text{g}/\text{m}^3$ in Experiment 1 and $2.90 \mu\text{g}/\text{m}^3$ in Experiment 2). It should be noted that these two ions elute off the IC column immediately after sample injection, and there is a possibility that other early-eluting monocarboxylic acid species coeluted with these two species leading to an overestimate of their mass. In addition, the extent to which the acetate and formate levels quantified here represent decay products from oligomers detected in the particle phase is uncertain. It is likely that a significant fraction of this mass results from the decomposition of oligomers at the sample collection conditions (high water concentrations and temperatures) in the PILS instrument and possibly by the use of potassium hydroxide (KOH) as the eluent for anion analyses in the IC instrument.

GC/MS with TMS derivatization (restricted to carboxyl and hydroxyl groups) was employed to determine the functional groups present within SOA components formed under high-NO_x conditions. Figure 6a shows a GC/MS TIC of a high-NO_x isoprene nucleation experiment (Experiment 5). 2-methylglyceric

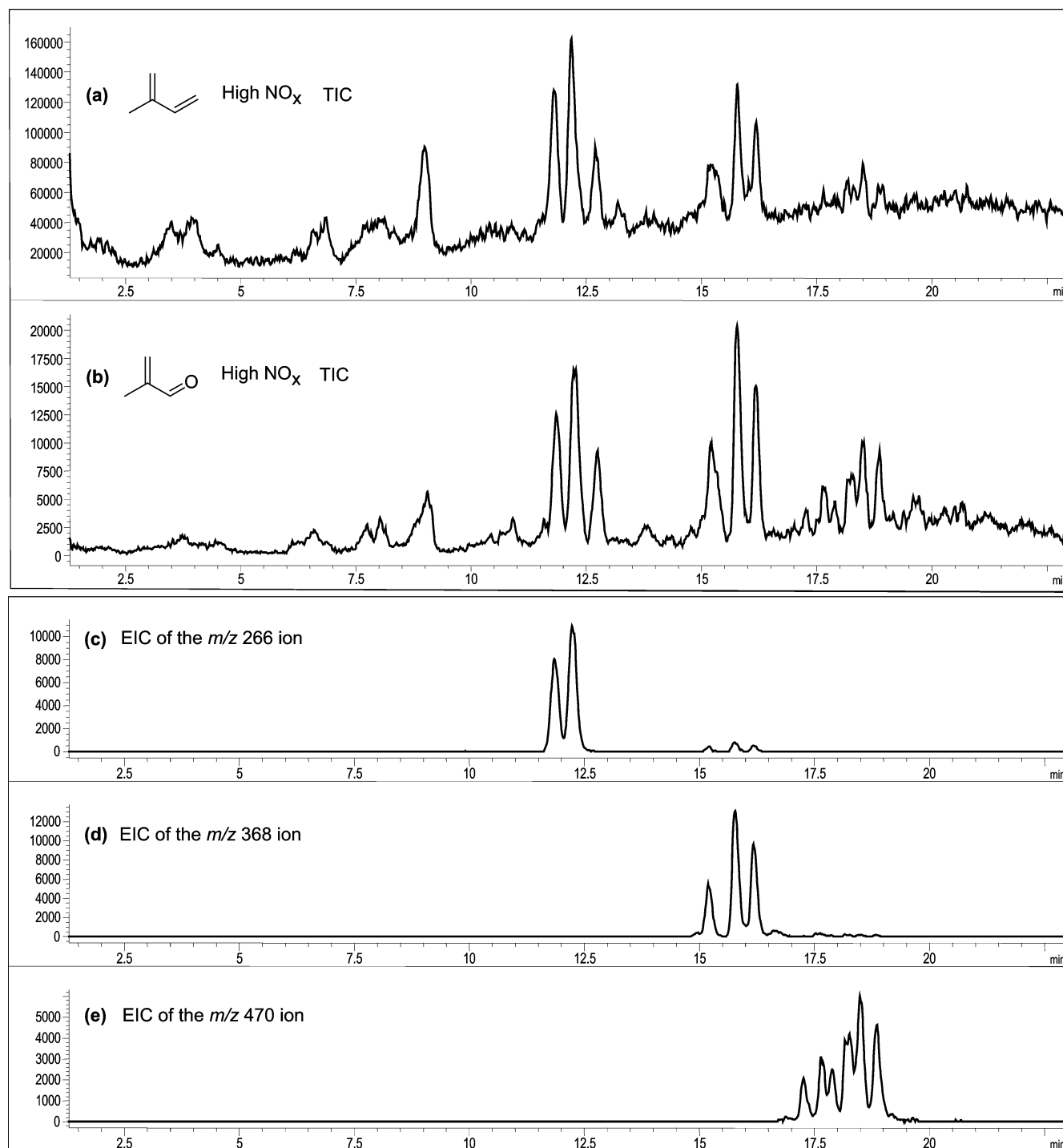


Figure 3. (a) LC/MS TIC of a filter extract from a 500 ppb isoprene, high- NO_x , nucleation experiment. (b) LC/MS TIC of a filter extract from a 500 ppb MACR, high- NO_x , nucleation experiment. The similar retention times and mass spectra associated with each chromatographic peak in these two TICs indicate that MACR is an important SOA precursor from isoprene oxidation under high- NO_x conditions. c–e are LC/MS EICs of organic nitrate species common to both MACR and isoprene high- NO_x samples. These organic nitrate ions are a part of the same oligomeric series confirmed by MS/MS analyses.

acid (2-MG), detected previously in ambient and laboratory filter samples,^{10,11,13,14} was found to elute from the GC column at 29.08 min. The corresponding EI mass spectrum for this peak is shown in Figure 6b. The chemical structure of trimethylsilylated 2-MG, along with its respective MS fragmentation, is also shown in this mass spectrum. Using GC-FID to quantify the amount of 2-MG present in this same sample, it was found that $3.8 \mu\text{g}/\text{m}^3$ was formed, which accounted for $\sim 3.7\%$ of the SOA mass. This was consistent with LC/MS measurements of 2-MG from other high- NO_x isoprene nucleation experiments

(such as 2.7% of the SOA mass for Experiment 1). A *di*-ester peak was observed to elute from the GC column at 51.59 min. The corresponding EI mass spectrum for this chromatographic peak is shown in Figure 6c along with its proposed chemical structure and MS fragmentation pattern.

3.2. Low- NO_x Condition. Table 3 lists nine low- NO_x chamber experiments. All experiments were conducted with H_2O_2 as the OH radical precursor with no added NO_x . Ozone formation is attributed mainly to residual NO_x emitted by the chamber walls; these O_3 concentrations observed likely have a

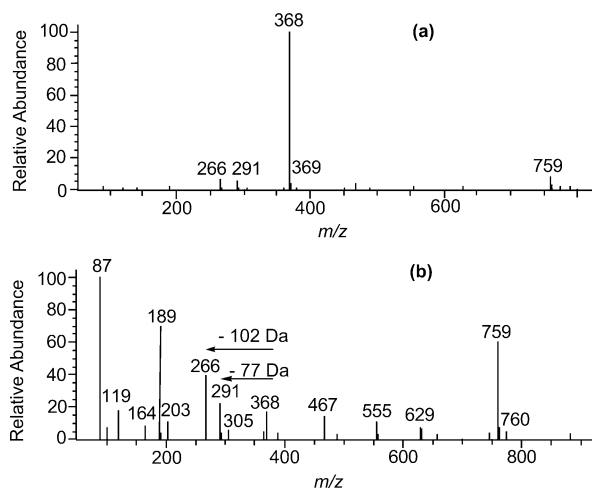


Figure 4. (a) Mass spectrum for the largest chromatographic peak ($RT = 15.7$ min) from Figure 3d (EIC of m/z 368 ion). (b) Upfront CID mass spectrum for the same chromatographic peak in Figure 3d (EIC of m/z 368 ion). The neutral losses observed in the upfront CID mass spectrum are associated with a trimeric organic nitrate species. This fragmentation pattern of m/z 368 is consistent with ion trap MS/MS results. The product ion m/z 266 corresponds to a neutral loss of 102 Da (common to all MS techniques), the product ion m/z 291 corresponds to a neutral loss of 77 Da (likely CH_3 radical and NO_3 radical, $\text{CH}_3\text{-NO}_3$), the product ion m/z 305 corresponds to a neutral loss of 63 Da (likely HNO_3), the product ion m/z 203 corresponds to a neutral loss of 165 Da, and the product ion m/z 164 corresponds to a neutral loss of 204 Da (two losses of common monomer).

negligible effect on the gas-phase chemistry because of the slow reactivity of O_3 toward isoprene. Experiments were conducted with 50% of the light banks in the chamber except for Experiments 10 and 11, in which 100% of the light banks were used and resulted in the higher temperatures observed. All experiments were conducted with 500 ppb of isoprene except for Experiment 17, in which 100 ppb of isoprene was used. As in the high- NO_x experiments, these experiments were conducted at low relative humidity ($RH < 9\%$) in order to limit the uptake of H_2O_2 into the particle phase. Nucleation (seed-free) and seeded (ammonium sulfate and acidified ammonium sulfate) experiments were conducted in order to examine if the presence of seed aerosol has an effect on the chemistry observed. Assuming a density of ~ 1.25 g/cm³ (derived from the comparison of DMA aerosol volume and TOF-AMS aerosol mass measurements), acid seeded (0.015 M $(\text{NH}_4)_2\text{SO}_4 + 0.015$ M H_2SO_4) experiments formed the largest amounts of SOA mass (~ 259 $\mu\text{g}/\text{m}^3$ for Experiment 14) compared to the corresponding nucleation (~ 72.5 $\mu\text{g}/\text{m}^3$ for Experiment 12) and ammonium sulfate seeded experiments (~ 72.8 $\mu\text{g}/\text{m}^3$ for Experiment 15). Lower mixing ratios of isoprene (Experiment 17) in the presence of acid seed also resulted in larger amounts of SOA when compared to the nucleation and ammonium sulfate seeded experiments.

No particle-phase organics were detected using (–) and (+)-ESI techniques. Analysis of filter sample extracts using these techniques were nearly identical to the blank and control filters. This shows that SOA components at low- NO_x conditions are not acidic in nature like those of the high- NO_x SOA. Because of the expected presence of hydroperoxides and polyols, other analytical techniques, such as the iodometric-spectrophotometric method and GC/MS with TMS derivatization, were employed to understand the chemical nature of low- NO_x SOA. The peroxide aerosol mass concentration was measured for all experiments except for Experiments 12, 13, and 16. The

iodometric-spectrophotometric method measures the total peroxide content (sum of ROOH, ROOR, and H_2O_2) of the aerosol, but because no peroxides were measured from filters collected from air mixtures containing isoprene, H_2O_2 , and seed aerosol, it is assumed that the peroxides measured are organic peroxides. The nucleation experiments (Experiments 10 and 18a) had the highest contribution of peroxides ($\sim 61\%$ on average) to the SOA mass observed. Dry ammonium sulfate (Experiments 11 and 15) and acidified ammonium sulfate seeded experiments (Experiments 14 and 17) led to comparable contributions of organic peroxides to the overall SOA mass (~ 25 and 30%, respectively). Quality control tests were conducted by the addition of ammonium sulfate to standard solutions of benzoyl peroxide to test if the seed had an effect on the UV–vis measurement of total peroxides. The amount of ammonium sulfate added to the benzoyl peroxide standards was determined by the ratio of SOA volume growth to the typical ammonium sulfate seed volume employed ($\sim 3:1$) as determined from the DMA. Little difference was observed ($\sim 0.6\%$), showing that ammonium sulfate seed has a negligible effect on the measurement of peroxide content from seeded experiments. As observed previously,¹⁷ the SOA mass was found to decrease rapidly in nucleation experiments after reaching peak growth, and as a result, the peroxide content of the SOA was measured at different times in Experiment 18. The iodometric-spectrophotometric measurement made at the peak growth in the aerosol volume, as determined from the DMA, for Experiment 18, showed that the peroxides accounted for $\sim 59\%$ of the total SOA mass. Twelve hours later, once the aerosol volume decay reached its constant value, the peroxide contribution to the SOA mass was found to have dropped to 26%.

Figure 7 shows a (+)MALDI mass spectrum for a low- NO_x acid-seed experiment (Experiment 14). The m/z range (49–620) of ion species observed was not significantly different from (+)-MALDI results obtained for nonacid-seeded experiments. The abundances of these ions were higher for the acid experiments, but quantification of these species is not possible because of uncertainties in the ionization efficiencies. In the absence of seed MALDI signal was low or nonexistent, likely due to very low ionization efficiencies in the absence of a sulfate matrix. Quantification is also difficult with MALDI because of inconsistencies and inhomogeneities of sample preparation and lack of understanding of sample matrix effects.³¹ It is clear, however, that oligomerization occurs in low- NO_x SOA. Common 14, 16, and 18 Da differences are observed between many peaks throughout this spectrum. Structural elucidation of these peaks in Figure 7 was not possible using the (+)MALDI technique owing to the inability of performing MS/MS experiments on selected ions from the sample matrix.

Figure 8 shows two TOF-AMS mass spectra for a 500 ppb, low- NO_x nucleation experiment (Experiment 12) in the m/z range of 200–450. These mass spectra also indicate the existence of oligomeric components for low- NO_x SOA. The mass spectrum in Figure 8a was collected at a low vaporizer temperature (~ 150 °C) while that in Figure 8b was collected at a higher temperature (~ 600 °C). The presence of more higher-mass peaks at high vaporizer temperatures (Figure 8b) may indicate that the low- NO_x oligomers are heterogeneous, with some series of oligomers being easily volatilized below 200 °C while others are not volatile at these temperatures.

The chemical composition of the SOA formed under low- NO_x conditions was found to change over the course of the experiment. The evolution of selected ions and of the total organic mass measured by the TOF-AMS instrument is shown

TABLE 2: Quantified SOA Products (in ng/m³) from High-NO_x Chamber Experiments

	$[M - H]^-$ ion	surrogate standard used for quantification ^a	isoprene/high NO _x /H ₂ O ₂				MACR/high NO _x /H ₂ O ₂		isoprene/HONO	
			expt 1	expt 2	expt 6	expt 9	expt 3	expt 4	expt 7	expt 8
<i>mono</i> -nitrate oligomers	266	pimelic acid	1970	4170	3890	3910	9360	3860	1470	830
	368	pinic acid	1350	2450	3700	4440	20600	10100	830	750
	470	pinic acid	2330	2930	2300	2640	28900	16700		210
	572	pinic acid	^b				2960	6810		
	674	suberic acid monomethyl ester					670	710		
	776	suberic acid monomethyl ester					220	450		
	878	suberic acid monomethyl ester						210		
total mass from <i>mono</i> -nitrate oligomers (μg/m ³)			5.65	9.55	9.89	11.0	62.7	38.8	2.30	1.79
% contribution to the total SOA mass			8	13	9	12	35	20	3	2
2-MG ^c oligomers	119	<i>meso</i> -erythritol	2050	3170	9680	4500	1240	460	4170	11600
	221	citramalic acid	1170	2590	2330	2110	3840	1720	550	1000
	323	2-hydroxy-3-methylbutyric acid	630	970	430	470	2740	1320	70	160
	425	pimelic acid		280	290	260	1650	680		130
	527	pimelic acid					720	480		
total mass from 2-MG oligomers (μg/m ³)			3.85	7.01	12.7	7.34	10.2	4.66	4.79	12.9
% contribution to the total SOA mass			5	10	11	8	6	2	7	18
<i>mono</i> -acetate oligomers	161	citramalic acid		40	100		90		110	70
	263	2-hydroxy-3-methylbutyric acid	680	1720	600	670	4070	1300	360	160
	365	pimelic acid	770	1890	820	1240	4830	1760	250	290
	467	pinic acid	340	450	180	420	3750	1310		130
	569	pinic acid		790			8600	2960		
	671	suberic acid monomethyl ester					450	360		
total mass from <i>mono</i> -acetate oligomers (μg/m ³)			1.79	4.89	1.70	2.33	21.8	7.69	0.72	0.65
% contribution to the total SOA mass			2	7	2	2	12	4	1	1
<i>mono</i> -formate oligomers	147	<i>meso</i> -erythritol	200	380	11300		200			1370
	249	2-hydroxy-3-methylbutyric acid	460	1340		40	1970	810	60	
	351	2-hydroxy-3-methylbutyric acid	370	1000		60	2880	1390	30	
	453	pimelic acid	290	380			1800	710		
total mass from <i>mono</i> -formate oligomers (μg/m ³)			1.32	3.10	11.3	0.10	6.85	2.91	0.09	1.37
% contribution to the total SOA mass			2	4	10	0.1	4	1	0.1	2
total mass identified (g/m ³)			12.6	24.6	35.6	20.8	102	54.1	7.90	16.7
% of SOA identified			17	34	32	22	56	27	12	23

^a Surrogate standards used covered the range of retention times for detected $[M - H]^-$ ions. All standards used were within ± 1.5 minutes of retention times for sample $[M - H]^-$ ions. ^b A blank cell indicates that the corresponding species was below the detection limit. ^c 2-MG = 2-methylglyceric acid.

in Figure 9. All ion signal intensities shown here are divided by the signal intensity of sulfate to correct for loss of particle mass to the chamber walls. Figure 9a shows the evolution of two prominent high-mass fragment ions m/z 247 and 327. These high-mass fragment ions increase in abundance with time, with the increase in m/z 327 being more significant. This increase is observed for all high-mass ($m/z > 200$) fragment ions. Figure 9b shows the change in the intensity of the fragment ion m/z 91, which is proposed to serve as a tracer ion for peroxides formed under low-NO_x conditions, where the proposed formula for this fragment ion is C₃H₇O₃, and the structure for one of its isomers is shown in Figure 9b. This peroxide tracer ion reaches its maximum signal after 7 h have elapsed in the experiment. Over the next 6 h, this ion decreases to a lower constant value; such a loss cannot be attributed to wall loss processes because the m/z 91 signal has already been normalized to the sulfate signal. Figure 9c shows the time evolution of the organic mass from Experiment 13. The organic mass also decreases slightly after reaching its peak value; however, the decrease observed for the organic mass is much lower than that of the peroxide tracer ion (m/z 91).

PILS/IC data were collected for some low-NO_x experiments. Aerosol mass concentrations of acetate were much lower than those in the high-NO_x case. For example, for Experiment 12, the acetate anion accounted for only 1.67 μg/m³, ~14–22 times lower than that of high-NO_x levels. Formate anion was detected

at comparable mass concentrations to that of the high-NO_x experiments (~1.51 μg/m³). Again, it should be noted that these two ions elute off the IC column immediately after sample injection and there is a possibility that other early-eluting monocarboxylic acid species coeluted with these two species, leading to an overestimate of their mass. No other organic anions were detected at significant levels from these low-NO_x experiments.

Figure 10a shows a GC/MS TIC of a low-NO_x, dry ammonium sulfate seeded experiment (Experiment 13). The chromatographic peaks at $RT = 31.21$, 32.25, and 32.61 min correspond to isomeric C₅ alkene triol species (*cis*-2-methyl-1,3,4-trihydroxy-1-butene, 3-methyl-2,3,4-trihydroxy-1-butene, *trans*-2-methyl-1,3,4-trihydroxy-1-butene, respectively), which have been measured previously in ambient aerosol from the Amazonian rainforest and Finnish boreal forests.^{11,12} This is the first detection of these species in a controlled laboratory chamber experiment. The chromatographic peaks at RT s 38.22 and 38.97 min correspond to the 2-methyltetrols (2-methylthreitol and 2-methylerythritol, respectively), which also have been detected in ambient aerosol studies,^{7,10,11,13} as well as in one previous photooxidation chamber study.¹⁴ The C₅ alkene triols and 2-methyltetrols have received much attention in prior studies; the corresponding mass spectra for their respective chromatographic peaks can be found in Figure 1S (Supporting Information). GC-FID measurements were made to quantify the

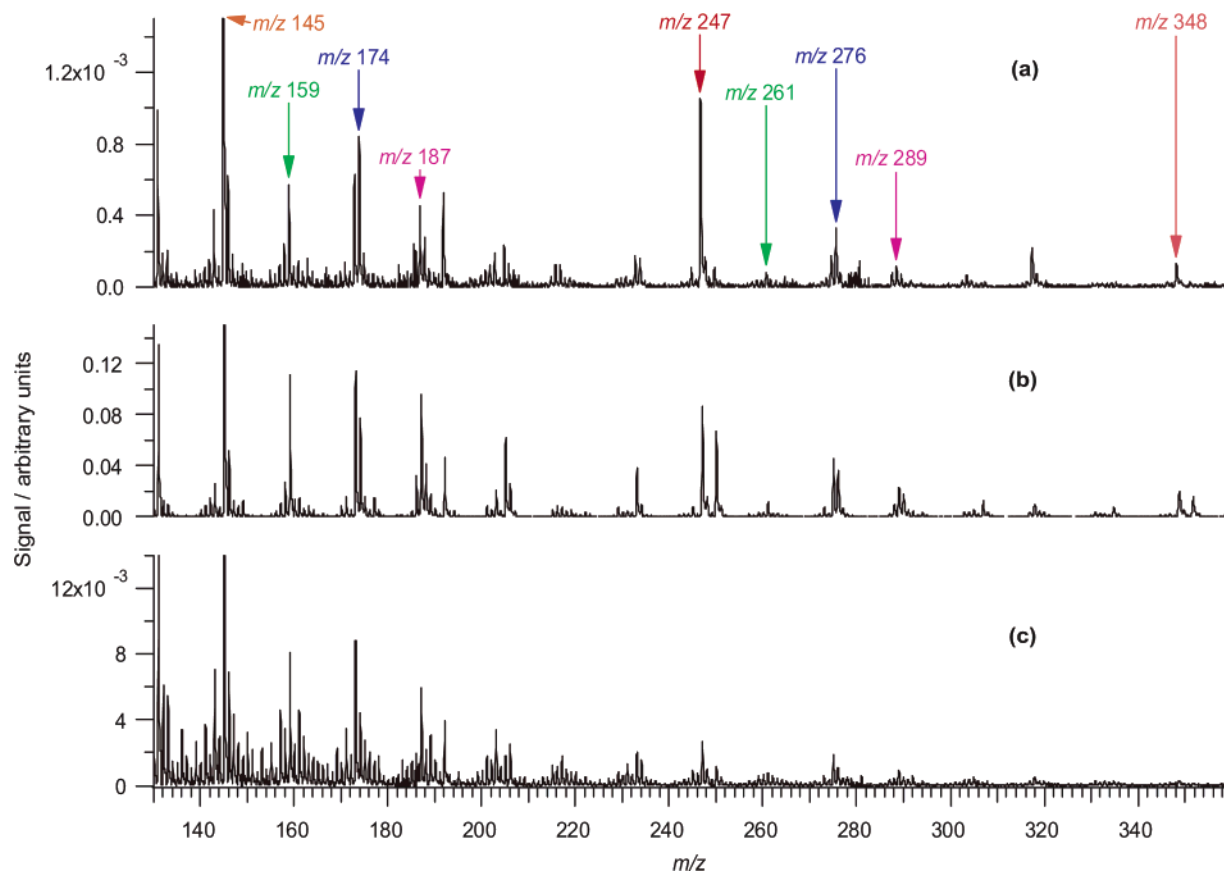


Figure 5. TOF-AMS spectra collected at low vaporizer temperatures for the following high- NO_x chamber experiments: (a) 50 ppb isoprene, 250 ppb NO_x , H_2O_2 as the OH precursor, no seed; (b) 500 ppb MACR, 800 ppb NO_x , H_2O_2 as the OH precursor, with seed; and (c) 500 ppb isoprene, HONO as the OH precursor, no seed. These spectra indicate that the OH precursor does not have a substantial effect on the chemistry observed, that MACR is an important SOA precursor from isoprene oxidation, and that the 102 Da differences observed in the offline mass spectrometry data are not a result of sample workup or ionization artifacts.

2-methyltetrols and C_5 alkene triols for a low- NO_x dry seeded experiment (Experiment 13—peaks in Figure 10a) and a low- NO_x acid seeded experiment (Experiment 14). It was found that the 2-methyltetrols and C_5 alkene triols accounted for 3.91% and 0.60% of the SOA mass, respectively, for the dry seeded experiment (Experiment 13), and decreased to 0.46% and 0.06% of the SOA mass, respectively, for the acid seeded experiment (Experiment 14). The inset shown in Figure 10a is the m/z 219 EIC for six isomeric dimers (MW = 254) eluting between 58.8 and 59.2 min. The corresponding averaged EI mass spectrum for these chromatographic peaks is shown in Figure 10b. The general chemical structure of the trimethylsilylated dimer, along with its respective MS fragmentation, is also shown in this mass spectrum. The fragmentation pattern shown here indicates that the dimer forms by the reaction of a C_5 alkene triol (indicated by the m/z 335 fragment ion) with a 2-methyltetrol (indicated by the m/z 219 fragment ion) to form the hemiacetal dimer shown. To confirm the MW of the isomeric hemiacetal dimers eluting between 58.8 and 59.2 min, an averaged CI(CH_4) mass spectrum was also collected and is shown in Figure 10c. The MW of the trimethylsilylated dimer (derivatized MW = 686) is confirmed by the $[M + \text{H} - \text{CH}_4]^+$ ion at m/z 671. The SOA products that elute at 34.91 and 35.47 min were tentatively characterized as diastereoisomeric 2-methyltetrol performate derivatives, which are unstable and upon reaction in the trimethylsilylation reagent mixture are converted into 2-methyltetrols. Their corresponding EI mass spectra can also be found in Figure 1S (Supporting Information). It should be noted that the peaks labeled *1, *2, and *3 in the GC/MS TIC (Figure

10a) were also present in the laboratory controls and were identified as palmitic acid, stearic acid, and palmitoyl monoglyceride, respectively. Table 4 summarizes all low- NO_x SOA components elucidated by GC/MS.

4. Discussion

4.1. Gas-Phase Chemistry. Gas-phase oxidation of isoprene is dominated by the reaction with OH.^{16,17} Under high- NO_x conditions, O_3 and NO_3 radicals play only a minor role in the initial oxidation of isoprene because they form only once $[\text{NO}]$ approaches zero, by which time most of the isoprene is consumed. Under low- NO_x conditions, O_3 and NO_3 radicals also contribute negligibly to isoprene oxidation. Figure 11 shows the initial gas-phase reactions that occur under both low- and high- NO_x conditions. In both cases, the initial oxidation of isoprene occurs by reaction with OH, followed by the immediate addition of O_2 to form eight possible isomeric isoprene hydroperoxy (RO_2) radicals (for simplicity, only three are shown).

Under high- NO_x conditions, the isoprene hydroperoxy radicals react predominantly with NO ; however, they may also react with NO_2 to form peroxy nitrates (ROONO_2 , not shown in Figure 11), but these are likely unimportant to the formation of isoprene SOA because of their thermal instability. $\text{RO}_2 + \text{NO}$ reactions result in the formation of either hydroxynitrates or hydroxyalkoxy (RO) radicals. Our observations of organic nitrates in high- NO_x SOA as observed in Figure 1 ($[M - \text{H}]^-$ ions with even m/z values) indicate that these hydroxynitrates

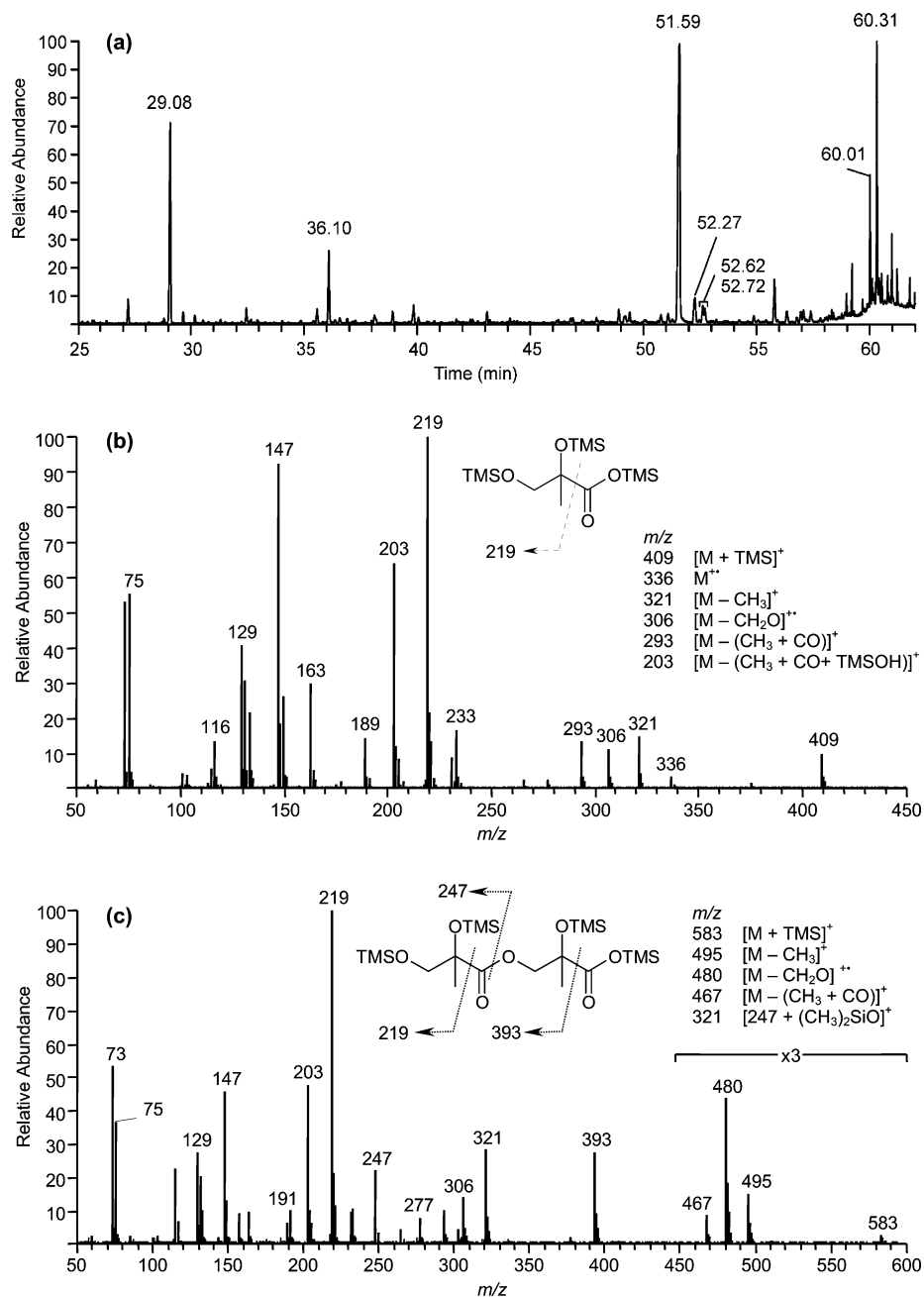


Figure 6. (a) TIC of a high-NO_x isoprene nucleation experiment (Experiment 5) collected using GC/MS in the EI mode. (b) EI mass spectrum for the 2-MG residue (*RT* = 29.08 min). (c) EI mass spectrum for a linear dimer made up of two 2-MG residues (*RT* = 51.59 min). These two mass spectra confirm that 2-MG is present in high-NO_x SOA and that it is involved in particle-phase esterification reactions resulting in polyesters (as shown by the dimer structure above).

are likely SOA precursors. Two of the hydroxyalkoxy radicals decompose into MVK and MACR, where their yields are 32–44% and 22–28%, respectively.^{32–35} The remaining hydroxyalkoxy radical forms a 1,4-hydroxycarbonyl, which may isomerize and dehydrate to form 3-methylfuran.³⁶ SOA formation has been observed from the photooxidation of MACR and 3-methylfuran, indicating that these are SOA precursors (indicated by black boxes in Figure 11).¹⁷ However, 3-methylfuran is not expected to contribute greatly to the SOA formed by isoprene oxidation because of its low gas-phase product yield (<2–5%).^{33–35} The higher gas-phase product yields observed for MACR suggest that it is the most important SOA precursor from isoprene oxidation under high-NO_x conditions; this is consistent with the similarities of the chemical products observed in isoprene and MACR SOA (Figure 1 and Table 2). Even though

MVK typically has the highest gas-phase product yield observed, it is not a contributor to SOA formation under high-NO_x conditions because negligible amounts of aerosol were produced from the high-NO_x photooxidation of 500 ppb MVK. Other products of isoprene oxidation under high-NO_x conditions (not shown in Figure 11) include C₅ hydroxycarbonyls, C₄ hydroxycarbonyls, and C₅ carbonyls; these may contribute to SOA formation, but experimental evidence is currently lacking.

Under low-NO_x conditions, the isoprene hydroxyperoxy radicals react predominantly with HO₂. These reactions result in the formation of hydroxy hydroperoxides, which are highlighted in dotted boxes to indicate that these species are possible SOA precursors. Under similar reaction conditions, Miyoshi et al.³² observed by IR spectroscopy that hydroperoxides are major gas-phase products from isoprene oxidation under NO_x-

TABLE 3: Low-NO_x Chamber Experiments Conducted

expt no. ^{a,b}	seeded ^c / nucleation	[O ₃] ^d ppb	T, °C ^d	total SOA mass concentration ^{d,e,f} μg/m ³	peroxide aerosol mass concentration μg/m ³	% contribution of peroxides to the SOA mass concentration observed
10 ^g	nucleation	32	29.1	186	116	62
11 ^g	dry AS	36	28.7	282	97	34
12	nucleation	b.d.l.	23.7	73	^h	^h
13	dry AS	12	24.1	69	^h	^h
14	AAS	b.d.l.	23.8	259	67	26
15	dry AS	11	23.9	73	19	25
16 ⁱ	dry AS	2	25.6	24	^h	^h
17	AAS	b.d.l.	23.6	93	23	24
18a	nucleation	7	26.2	55	32	59
18b ^j	nucleation	37	27.0	22	6	26

^a All VOC gas-phase mixing ratios were 500 ppb, except for Experiment 17 (100 ppb). ^b H₂O₂ was the OH precursor used for each low NO_x isoprene experiment. H₂O₂ is not measured directly, but from isoprene decay during irradiation we estimate ~3 ppm of H₂O₂. ^c AS = ammonium sulfate seed, AAS = acidic ammonium sulfate seed. ^d Averaged over the course of filter sampling. ^e Subtraction of seed aerosol taken into account when necessary. SOA volume derived from DMA wall loss uncorrected measurements for use in mass closure from filter sample analyses. ^f Assuming a SOA density of 1.25 g/cm³. This value is derived from comparison of DMA aerosol volume and AMS aerosol mass measurements. ^g 100% of light bank used and hence higher temperatures in chamber observed during sampling. ^h No peroxide measurement made for this sample. ⁱ Half of the typical [H₂O₂] used ~1.5 ppm. ^j Late sampling, after peak growth, during the rapid decay of the aerosol mass/volume typical of low NO_x experiments.

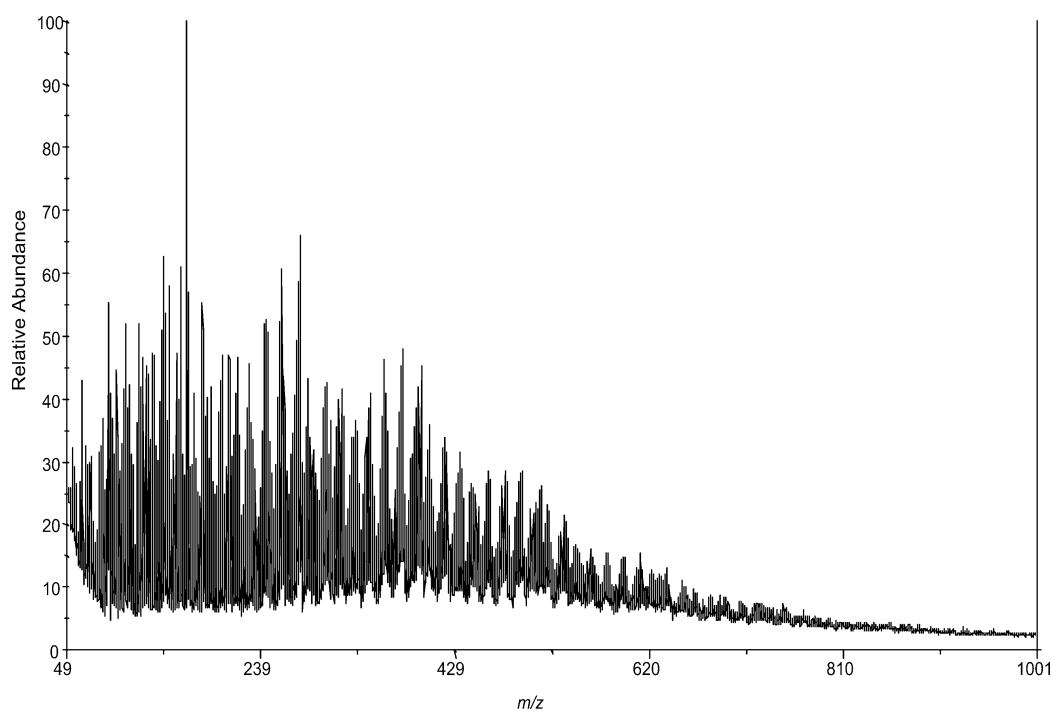


Figure 7. MALDI positive mode spectrum obtained with a graphite matrix for a 500 ppb isoprene, low-NO_x, acid seeded experiment (Experiment 14). High-molecular mass species formed up to ~620 Da.

free conditions. Aerosol formation was also observed; however, the composition of the resultant aerosol was not investigated.

In contrast to Kroll et al.,¹⁶ under the present conditions there may be some contribution (~10–30%) of RO₂ + RO₂ reactions under low-NO_x conditions owing to the higher [isoprene]/[H₂O₂] ratios used in the current study.³² For simplicity, only the RO₂ + RO₂ reactions that lead to hydroxyalkoxy radicals are shown in Figure 11. As in the high-NO_x case, these hydroxyalkoxy radicals will likely form MVK, MACR, and hydroxycarbonyls. The RO₂ + RO₂ reactions not shown can lead to the formation of diols and other isomeric hydroxycarbonyls. As will be discussed subsequently, the diols that result from RO₂ + RO₂ reactions (not shown) may form SOA as well.¹⁵

4.2. High-NO_x SOA. **4.2.1. Importance of MACR Oxidation.** MACR oxidation under high-NO_x conditions produces significant amounts of SOA (Experiments 3 and 4). When comparing the SOA products from isoprene and MACR oxidation at high-NO_x conditions, many of the same products are observed (Figure 1). Tandem MS data obtained for selected ions common to both isoprene and MACR samples, like the *m/z* 368 ion shown in Figure 4, produced similar product ion spectra, further indicating that these species are indeed the same. This observation is consistent with our previous proton-transfer reaction-mass spectrometry (PTR-MS) studies of isoprene oxidation, which demonstrate a strong correlation between the amount of SOA formed and the MACR reacted in the gas phase.^{37,38} In these studies, aerosol growth continued well after isoprene was fully consumed, indicating the likely importance of second- (or later-)

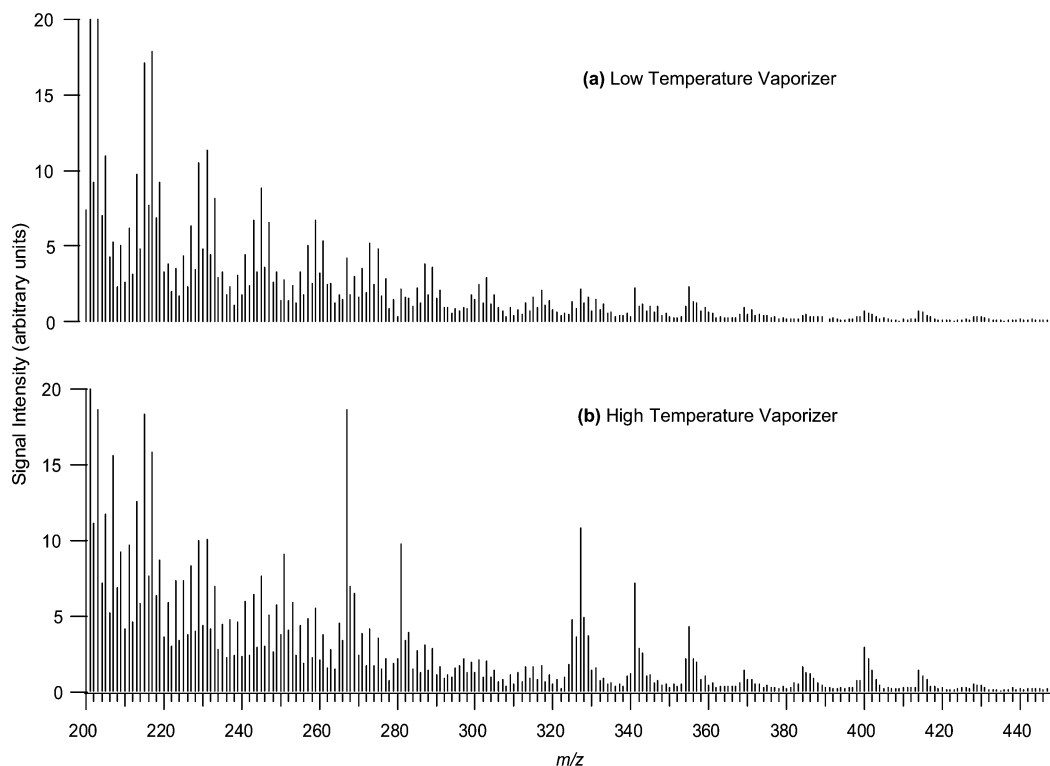


Figure 8. TOF-AMS spectra for a 500 ppb isoprene low- NO_x experiment (Experiment 12). (a) Mass spectrum obtained with a low temperature vaporizer ($\sim 150^\circ\text{C}$). (b) Mass spectrum obtained with a high temperature vaporizer ($\sim 600^\circ\text{C}$). The spectrum is richer at higher m/z , indicating that the high- MW oligomers that are not easily volatilized at $<200^\circ\text{C}$.

generation gas-phase products and/or heterogeneous (particle-phase) reactions. It should be noted that when the MACR, H_2O_2 , and dry ammonium sulfate seed aerosol are well mixed in the chamber before irradiation begins, no aerosol growth is observed. This rules out the possibility of reactive uptake of MACR into the particle phase; instead the oxidation of MACR is a necessary step in SOA formation from the photooxidation of isoprene.

4.2.2. Oligomers. Oligomerization occurs in SOA formed under high- NO_x conditions, where both offline and online mass spectrometry techniques (Figures 1, 2, and 5) measure species with much higher MWs than those of the parent isoprene, with characteristic 102 Da differences. Tandem MS techniques, such as upfront CID on the LC/MS instrument, confirm that oligomers are indeed formed from a common 102 Da monomeric unit. For example, when isolating the m/z 368 ion from the rest of the sample matrix and further fragmenting it to generate a product ion spectrum, two successive neutral losses of 102 Da were observed at m/z 266 and 164 (Figure 4b). Two isomeric compounds with m/z 266 in Figure 3c were found to elute off the LC column at ~ 2.5 – 3 min earlier than the compound with m/z 368 studied here. The fact that the compounds with m/z 266 ions elute off the LC column at earlier RTs, and that m/z 266 is a product ion of m/z 368, strongly suggests that these two ions are characteristic of the same oligomeric series. The compounds characterized by m/z 368 and 266 are likely a trimer and dimer, respectively. The other series of oligomers quantified in Table 2 also had 102 Da differences observed and similar LC/MS behaviors, with ions with lower mass eluting from the LC column at earlier RTs.

4.2.3. Organic Nitrates. Organic nitrates, detected as even-mass $[M - \text{H}]^-$ ions in $(-)$ ESI spectra, were measured in all high- NO_x experiments. All organic nitrates detected in high- NO_x SOA samples had similar product ion spectra as m/z 368

(Figure 4b), with neutral losses of 63 (HNO_3), 77 (CH_3 radical + NO_3 radical, possibly CH_3NO_3), and 102 Da, suggesting that all even-mass $[M - \text{H}]^-$ ions are oligomeric organic nitrate species. Unlike the $(-)$ ESI techniques (Figures 1 and 3), the GC/MS technique did not allow for the detection of organic nitrate species, likely a result of their instability at the high temperature of the GC injector and/or derivatization techniques used during sample workup. Organic nitrates were also not clearly detected in the MALDI-TOFMS (Figure 2) and TOF-AMS (Figure 5) instruments. This is likely a result of the harsh ionization techniques employed by these instruments. Even with $(-)$ ESI, these organic nitrates were not completely stable, as shown in Figure 4a for the m/z 368 ion. Organic nitrates found in the high- NO_x SOA likely form from the further oxidation of the hydroxynitrate species found in the gas phase from $\text{RO}_2 + \text{NO}$ reactions.

4.2.4. 2-MG as Monomeric Units. As shown in Table 2, other varieties of oligomers were observed as well. From further use of tandem MS techniques, it was found that one of these series of oligomers likely involved 2-MG (2-methylglyceric acid), a recently discovered SOA tracer compound for isoprene oxidation in the ambient atmosphere,^{10,13,14} as an important monomer. Confirmation of the 2-MG monomer in high- NO_x SOA was provided by GC/MS with TMS derivatization (Figure 6a and b). Because monomeric 2-MG is small and polar, it was not retained effectively by the LC reverse phase column ($RT \approx 1.3$ min) and was detected in its deprotonated form at m/z 119. Figure 12 shows product ion spectra obtained with $(-)$ ESI-ITMS for Experiment 9. In Figure 12a, the m/z 323 ion is isolated in the ion trap from the rest of the ion matrix and is collisionally activated to produce the MS^2 spectrum shown here. The m/z 221 ion is the base peak in this spectrum, and the m/z 119 ion also detected as the result of further fragmentation of the m/z 221 product ion. The fact that the m/z 119 ion was

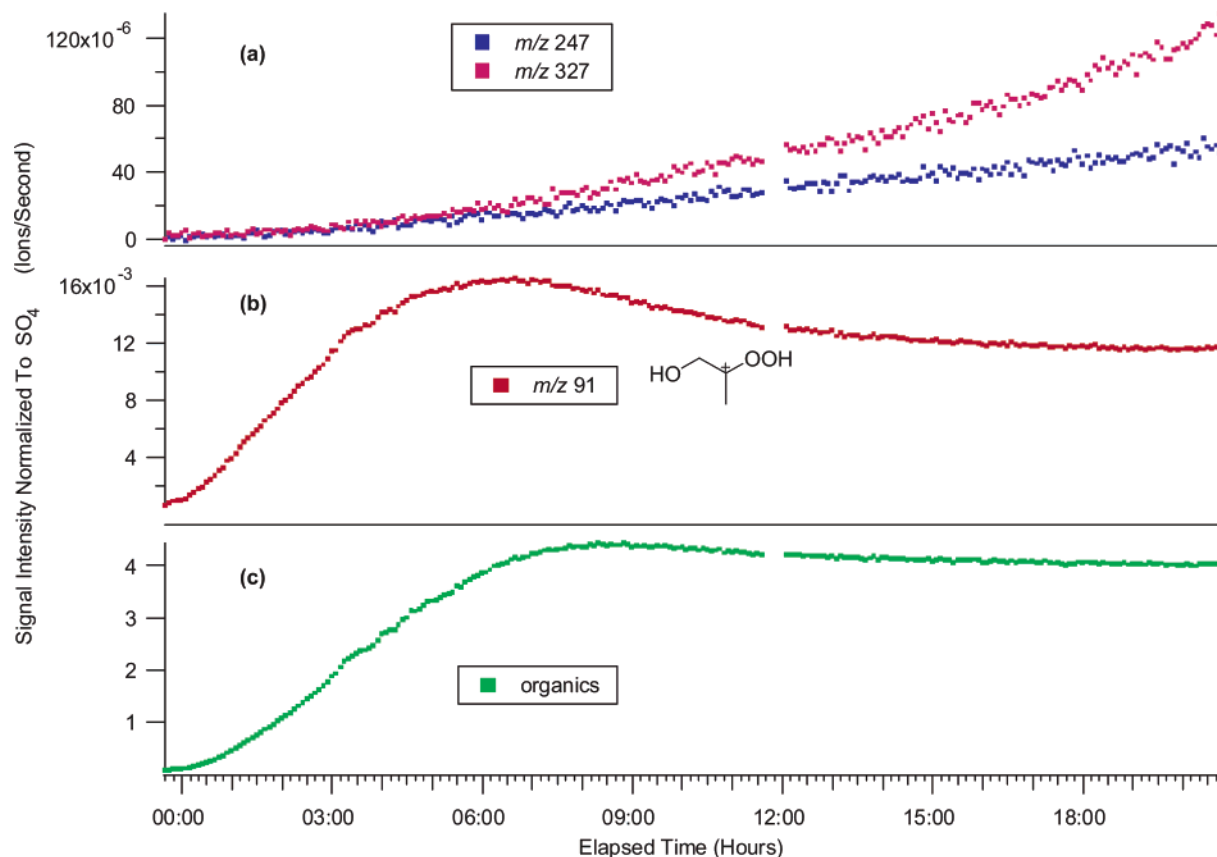


Figure 9. Time evolution plots produced from the TOF-AMS instrument for selected fragment ions and the total organic mass observed from a typical low- NO_x experiment (Experiment 13). All ion signal intensities are divided by the signal intensity of sulfate. Because sulfate concentration is a tracer for wall loss (neither created nor removed during the run), the ratio of ion signal to sulfate signal should give an indication of the behavior without wall loss. (a) Time evolution plot for high-mass fragment ions m/z 247 and 327. (b) Time evolution plot for the proposed peroxide fragment ion m/z 91 ($\text{C}_3\text{H}_7\text{O}_3$), where the structure of one isomer is shown. (c) Time evolution plot for the total organic mass. These plots indicate that the chemical composition changes with experimental time, where the decomposition of organic peroxides correlates to oligomerization within low- NO_x SOA. The missing data points (11:30 to 12:00 hours) in these plots are due to the vaporizer in the TOF-AMS instrument being turned off.

detected as a product ion in the MS^2 and MS^3 spectra shown in Figure 12 strongly suggests that 2-MG is a monomer in this oligomeric series. It is important to note that m/z 119 was also a fragment ion produced in the upfront CID spectrum for the m/z 368 ion in Figure 4b. It was found that m/z 119 was a common product ion to each oligomeric series, suggesting the importance of 2-MG in oligomerization reactions.

4.2.5. Mono-Acetate and Mono-Formate Oligomers. The PILS/IC measurements of high levels of particulate acetate and formate anions in both the seeded (Experiment 1) and nucleation (Experiment 2) experiments, coupled with the high volatilities of their acid forms produced in the gas phase from the oxidation of isoprene, suggests that these compounds resulted from the decomposition of oligomeric SOA. The formation of *mono*-acetate and *mono*-formate oligomers was observed by tandem (-)ESI-MS measurements. Figure 13 shows two product ion spectra for a *mono*-acetate dimer ($[M - \text{H}]^-$ at m/z 161) and *mono*-formate trimer ($[M - \text{H}]^-$ at m/z 249), respectively. The observation of a neutral loss of 42 Da (ketene, $\text{H}_2\text{C}=\text{C}=\text{O}$) and a dominant product ion m/z 59 (acetate anion) in the MS^2 spectrum of the m/z 161 ion (Figure 13a), provides strong evidence for acetylation. In the MS^2 spectrum of the m/z 249 ion (Figure 13b), the major product ion m/z 147 results from the common neutral loss of 102 Da. The product ion m/z 221 results from a neutral loss of 28 Da (CO), a rearrangement reaction that is characteristic of formates. The product ion m/z 119 (deprotonated 2-MG) resulting from the combined neutral losses of 102 and 28 Da is also observed. *Mono*-acetate

oligomers were also detected by the GC/MS TMS derivatization method; the details of these findings will be discussed in a forthcoming GC/MS complementary paper.

4.2.6. Heterogeneous Esterification Reactions. Oligomer species containing the m/z 119, 221, and 323 ions as detected by the (-)ESI techniques were also observed by GC/MS as their respective TMS derivatives as shown Figure 6a. As in previous measurements of 2-MG,¹⁴ the EI mass spectrum shown in Figure 6b confirms the formation of monomeric 2-MG in high- NO_x isoprene SOA. The dimer detected at m/z 221 by (-)ESI techniques (as shown in Figure 12b) involving 2-MG as an important monomer, is detected at 51.59 min in Figure 6a. The chemical structure of this species likely contains one carboxyl and three hydroxyl groups, as shown in Figure 6c. The formation of an ester linkage is also denoted in this structure, which is the expected site of oligomerization. The ions m/z 583 ($[M + \text{TMS}]^+$) and m/z 495 ($[M - \text{CH}_3]^+$) confirm that the MW of this dimer species is 222 (which is also in agreement with the ESI results). The ion m/z 467 ($[M - (\text{CH}_3 + \text{CO})]^+$) is consistent with a terminal trimethylsilylated carboxylic group, while the ion m/z 480 ($[M - \text{CH}_2\text{O}]^+$) is explained by a rearrangement of a trimethylsilyl group and points to a terminal trimethylsilylated hydroxymethyl group. The elemental composition ($\text{C}_8\text{H}_{14}\text{O}_7$) of the structure shown in Figure 6c was also confirmed by high-resolution ESI-TOFMS measurements. These results strongly suggest that particle-phase esterification reactions occurred between 2-MG molecules, where a hydroxyl group of one 2-MG molecule reacted with a

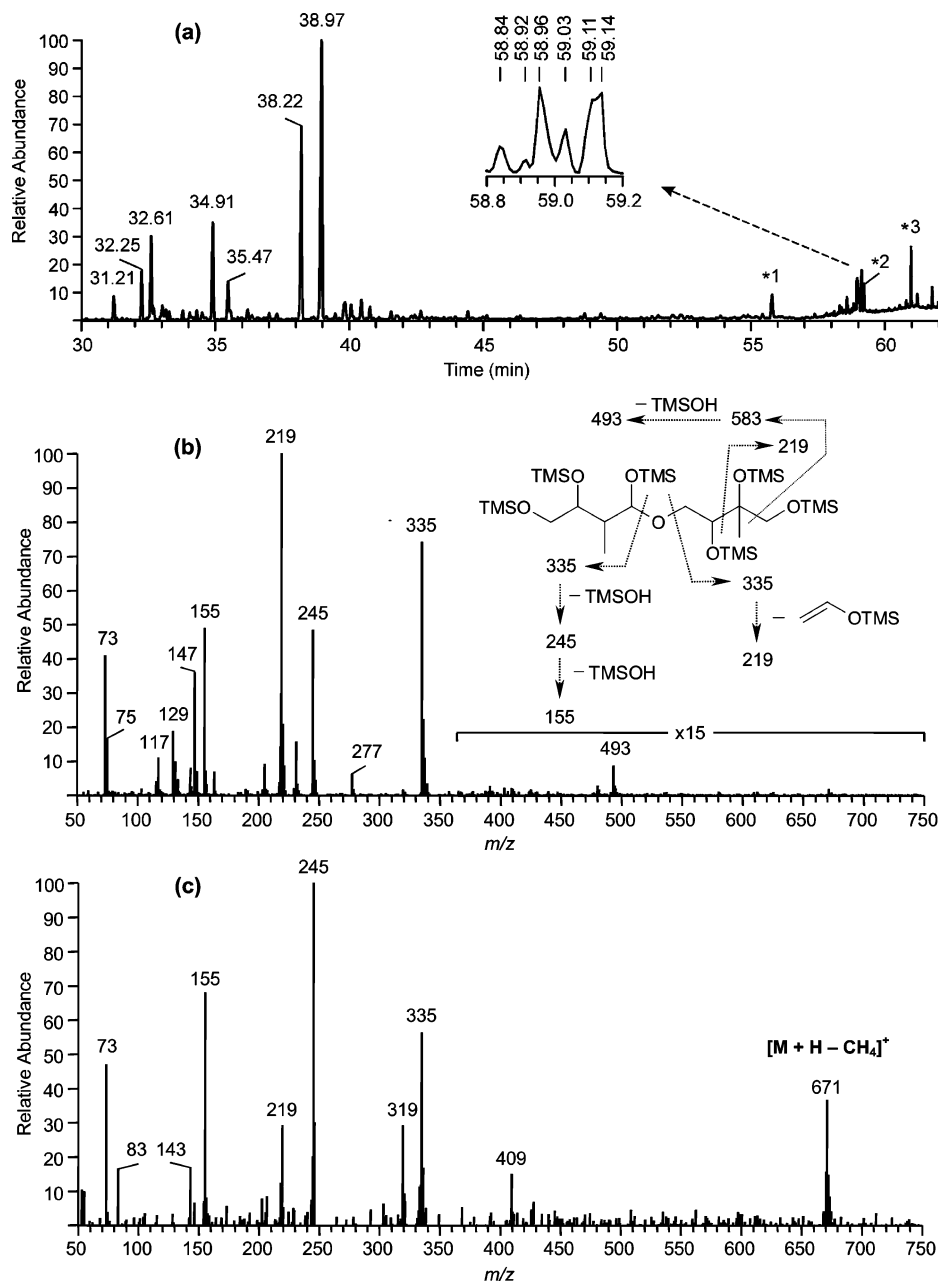
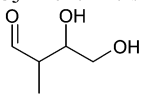
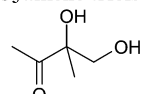
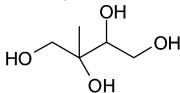
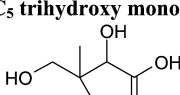
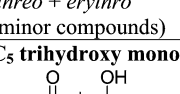
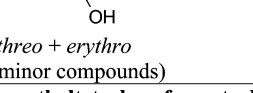
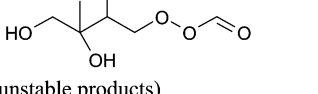


Figure 10. (a) GC/MS TIC of isoprene low- NO_x SOA. The inset shows the m/z 219 EIC for the dimeric products eluting between 58.8 and 59.2 min. Peak identifications: RT s 31.21, 32.25, and 32.61 min: C_5 alkene triols; RT s 34.91 and 35.47 min: unstable products tentatively characterized as 2-methyltetrol performatate derivatives; RT s 38.22 and 38.97 min: 2-methyltetrols (2-methylthreitol and 2-methylerythritol, respectively). The EI spectra for the latter seven compounds are provided in Figure 1S (Supporting Information). The peaks labeled *1, *2, and *3 were also present in the laboratory controls and were identified as palmitic acid, stearic acid, and palmitoyl monoglyceride, respectively. (b) Averaged EI spectrum for the dimeric products eluting between 58.8 and 59.2 min and fragmentation scheme; and (c) averaged $\text{CI}(\text{CH}_4)$ spectrum for the latter products.

carboxylic acid group of another one. The products that result from this reaction would be the ester compound shown in Figure 6c and a water molecule. The neutral loss of 102 Da, likely corresponding to dehydrated 2-MG or a 2-MG residue in the form of a lactone (i.e., 2-hydroxy-2-methylpropiolactone), observed from the ESI-MS/MS techniques can be explained by the charge-directed nucleophilic reaction shown in Figure 14. To our knowledge, this is the first evidence of particle-phase esterification reactions in SOA. It should be noted that the mass spectra, not shown here, for the chromatographic peaks in Figure 6a at 60.01 and 60.31 min, correspond to branched and linear 2-MG acid trimers (corresponding to MW = 324), respectively. A detailed discussion of the EI mass spectral behavior of the TMS derivatives of 2-MG and 2-MG dimer and trimers will be presented in a complimentary GC/MS study.

Figure 15a and b compares the GC/MS EICs, using the m/z 219 ion as the base peak, for a filter sample from Experiment 5 treated with trimethylsilylation only to that of a filter sample (also from Experiment 5) treated by hydrolysis/ethylation + trimethylsilylation, respectively, to show further confirmation of polyesters formed via esterification reactions between 2-MG molecules. When treating SOA from the same chamber experiment with the hydrolysis/ethylation procedure, a noticeable decrease in 2-MG and 2-MG oligomers is observed. For example, the peaks at 29.08, 51.59, and 60.31 min (Figure 15a) observed after trimethylsilylation appear as smaller peaks upon the hydrolysis/ethylation experiment, as shown in the second chromatogram (Figure 15b). This decrease is a result of the formation of ethyl esters of 2-MG and of linear dimer (RT s = 27.42 and 50.48 min, respectively). The mass spectra confirming

TABLE 4: Low-NO_x Isoprene SOA Products Elucidated by GC/MS

Compound / Structure	MW (MW TMS- derivative)	Elemental composition	Detection in Ambient Atmospheres
C₅ alkene triols / ald form 	118 (334)	C ₅ H ₁₀ O ₃	[Wang et al., 2005] ¹² [Kourtchev et al., 2005] ¹¹
C₅ alkene triols / keto form 	118 (334)	C ₅ H ₁₀ O ₃	[Wang et al., 2005] ¹² [Kourtchev et al., 2005] ¹¹
2-methyltetrols  <i>threo + erythro</i>	136 (424)	C ₅ H ₁₂ O ₄	[Claeys et al., 2004] ⁷ [Edney et al., 2005] ¹⁴ [Böge et al., 2006] ¹⁵ [Ion et al., 2005] ¹⁰ [Kourtchev et al., 2005] ¹¹
C₅ trihydroxy monocarboxylic acid  <i>threo + erythro</i> (minor compounds)	150 (438)	C ₅ H ₁₀ O ₅	Not yet detected in ambient aerosol
C₅ trihydroxy monocarboxylic acid  <i>threo + erythro</i> (minor compounds)	150 (438)	C ₅ H ₁₀ O ₅	Not yet detected in ambient aerosol
2-methyltetrol performate derivatives  (unstable products)	180 (396)	C ₆ H ₁₂ O ₆	Not yet detected in ambient aerosol
Dimers (6 isomers)  (minor compounds)	254 (686)	C ₁₀ H ₂₂ O ₇	Detected in ambient aerosol for the first time in this study

the formation of these ethyl ester species are shown in Figure 15c and d, respectively. The m/z 365 and 277 ions in Figure 15c confirm the MW of the ethyl ester of 2-MG to be 148, where its formation is the result of polyesters decomposing into this derivatized monomer. The detection of m/z 539 and 451 in Figure 15d confirm the MW of the ethyl ester of the linear 2-MG dimer, likely a result of the incomplete decomposition of larger polyesters (i.e., trimers, tetramers, pentamers, etc.) in high-NO_x SOA.

Figure 16 shows the overall proposed reaction mechanism for SOA formation from the photooxidation of isoprene under high-NO_x conditions. This figure denotes important initial gas-phase and particle-phase reactions that lead to the observed SOA products. As was discussed earlier, further gas-phase oxidation of MACR is required in order to form SOA from isoprene under high-NO_x conditions. Oligomeric organic nitrates, such as the m/z 368 ion, are comprised of an organic nitrate monomer, which is detected as the deprotonated m/z 164 product ion (Figure 4b); therefore, it is possible that one gas-phase product of MACR oxidation is its hydroxynitrate form, as shown in Figure 16. Through further oxidation of the aldehyde group in this hydroxynitrate species, it is expected that the acid form of

this species results in the particle phase, thus being available for esterification reactions with 2-MG (Reaction 2 in Figure 16). To our knowledge, no organic nitrates have been measured in the gas phase from MACR oxidation (though nitrate formation has been inferred from OH-methacrolein reaction kinetics³⁹); however, the detection of organic nitrates in the particle phase suggests that this is possibly a minor channel for SOA formation. However, the formation of 2-MG from the oxidation of MACR is still uncertain because of the unknown intermediates leading to its formation. Recently, it was proposed that 2-MG forms from the reaction of methacrylic acid or MACR with H₂O₂ in the liquid aerosol phase under acidic conditions.¹³ No aerosol growth was observed for MACR, H₂O₂, and dry ammonium sulfate seed aerosol under dark conditions; however, it is possible that other products such as formic and acetic acid, as well as oxidants formed during isoprene photooxidation, may promote the reactive uptake of MACR into the aerosol phase. Further measurements of MACR oxidation products are needed in order to better understand the formation of 2-MG, which might occur in either the particle or gas phase.

From our detailed analytical measurements discussed above, the importance of 2-MG to particle-phase reactions in high-

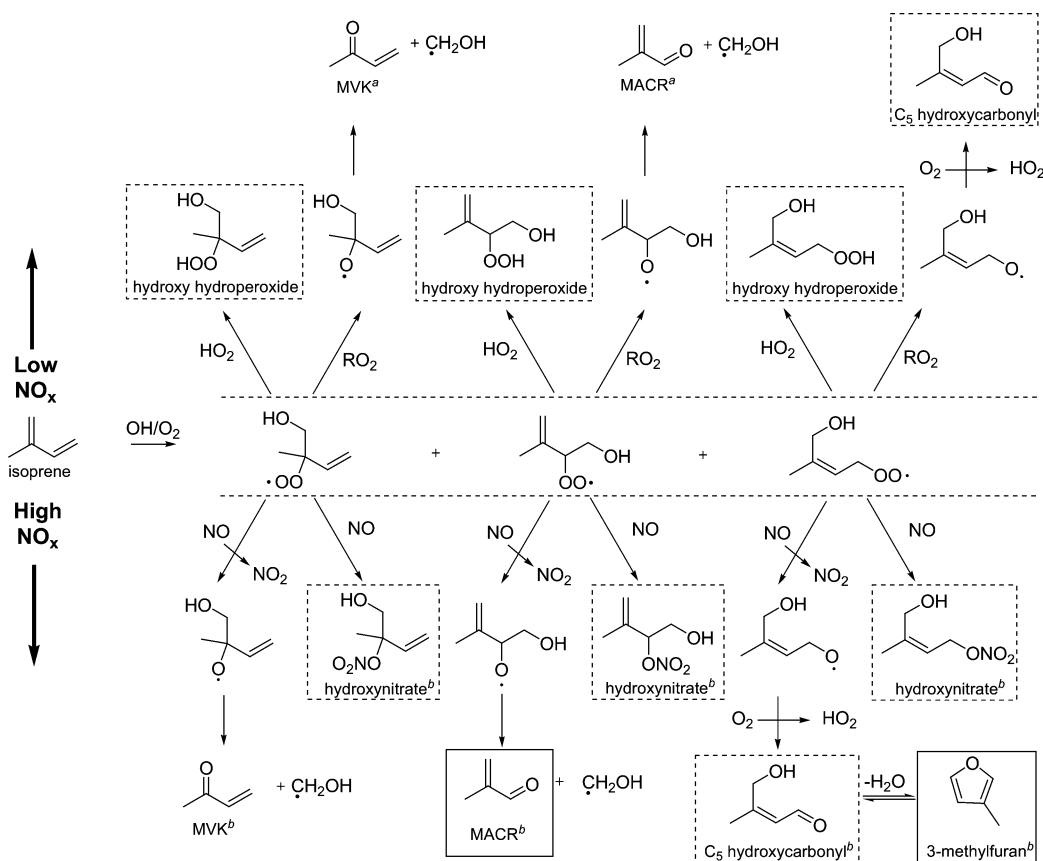


Figure 11. Reaction mechanism of isoprene oxidation under low- and high-NO_x conditions. Dotted boxes indicate possible SOA precursors, whereas black boxes indicate known SOA precursors. For simplicity, only three of the eight initial isoprene hydroxyperoxy (RO₂) radicals are shown. RO₂ + RO₂ reactions leading to diols and other hydroxycarbonyls have been omitted for simplicity. ^aMiyoshi et al.³¹ showed that [isoprene]/[H₂O₂] determines molar yields of MVK, MACR, and formaldehyde under low-NO_x conditions. ^bKroll et al.¹⁶ summarized molar yields of gas-phase products from isoprene oxidation under high-NO_x conditions reported in the literature.

NO_x SOA is now well established. 2-MG monomers can react intermolecularly via esterification to produce 2-MG oligomers (Reaction 1), or react with *mono*-nitrate monomers to produce *mono*-nitrate oligomers (Reaction 2), or react with acetic or formic acid to produce *mono*-acetate and *mono*-formate oligomers, respectively (Reactions 3 and 4). These proposed esterification reactions are equilibrium reactions, and as a result, the addition of an acid or removal of water could promote the formation of these esters. As stated earlier, the high-NO_x experiments were conducted at very low relative humidities ($RH < 5\%$); therefore, this condition could allow for the ester formation we observe. We also observe high concentrations of organic acids (2-methylglyceric, acetic, and formic acid) at high-NO_x conditions, which could provide the acidity needed to drive these reactions. It has been shown⁴⁰ that heterogeneous esterification of polyols by vapor-phase treatment with acetic acid and trifluoroacetic anhydride (used as an alternative to the sulfuric acid catalyst) will occur at room temperature without the use of liquids. Thus, it is reasonable to infer that esterification reactions may occur under the dry, room-temperature conditions of our chamber experiments. It should be noted that there is also evidence from the TOF-AMS that supports this reaction mechanism. The ratio of the TOF-AMS ion signals associated with the 2-MG dimer (m/z 205) to that of the 2-MG monomer (m/z 103) increases during the course of the high-NO_x experiments, therefore providing additional confirmation of our proposed reaction mechanism in Figure 16. These results from the TOF-AMS, however, are not quantitative because of the majority of these molecules being fragmented (thermally or by the electron impact ionization) to smaller ions.

In comparison to MACR oxidation, the further oxidation of MVK likely does not produce SOA under high-NO_x conditions because of its ketone moiety. The lack of an aldehydic hydrogen precludes the formation of acidic products (like that of 2-MG from MACR oxidation), which are necessary components needed for the particle-phase esterification reactions (Figure 16). One of the most abundant gas-phase products produced from MVK oxidation under high-NO_x conditions is methylglyoxal. It was shown in a prior chamber study by Kroll et al.⁴¹ that methylglyoxal does not reactively uptake onto inorganic seed aerosol; therefore, this could explain the lack of SOA growth from the further oxidation of MVK.

For the isoprene/H₂O₂ experiments, except for Experiment 6, the most abundant oligomer series was the *mono*-nitrate oligomers (Table 2). The *mono*-nitrate oligomers accounted for ~8–13% of the SOA mass formed in these experiments. As for the isoprene/H₂O₂ experiments, the *mono*-nitrate oligomers were the most abundant oligomers for the MACR/H₂O₂ experiments (~35% of SOA mass for the seeded experiment versus ~20% for the nucleation experiment). Even though most of the chemical products are the same in the H₂O₂ and HONO experiments, the abundances of these products are different. In contrast to the H₂O₂ experiments, the 2-MG oligomers are the most abundant oligomers for the HONO experiments. These differences could be due to different NO_x levels. SOA mass closure was observed to be the highest for the MACR/H₂O₂/seeded experiment (~57% of SOA identified) and the isoprene/H₂O₂/seeded experiments (22–34% identified). It is important to stress that the organic aerosol mass loadings formed in these isoprene high-NO_x chamber experiments (~50–200 μg m⁻³)

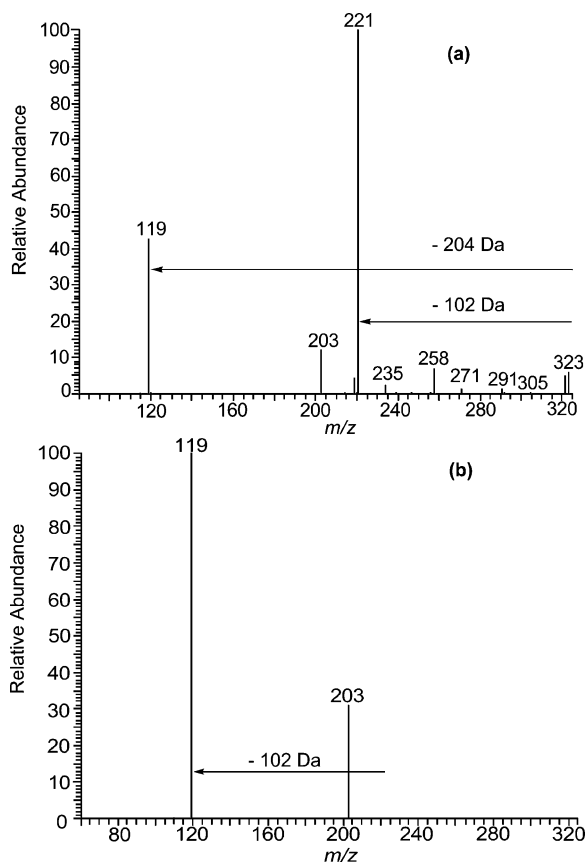


Figure 12. ESI-ITMS negative mode product ion spectra from a high- NO_x isoprene SOA sample (Experiment 9). (a) MS^2 spectrum for an isolated m/z 323 ion. Two neutral losses of 102 Da are observed as shown by the product ions m/z 221 and 119. (b) MS^3 spectrum for an isolated m/z 323 ion generated from the further fragmentation of the dominant daughter ion ($= m/z$ 221) in the MS^2 spectrum. These spectra indicate that 2-MG ($[M - H]^-$ ion $= m/z$ 119) is a monomer for the oligomeric m/z 323 ion.

are much higher than those found in ambient aerosol where isoprene emissions are the highest ($\sim 5 \mu\text{g m}^{-3}$). The amount of organic aerosol mass controls the gas-particle partitioning of semi-volatile species produced from the oxidation of hydrocarbons because more organic aerosol mass allows for more uptake of these species; therefore, the mass closure results presented apply only to the aerosol mass loadings produced in this current study and are not absolute for the isoprene system. The key insight from our analysis is the detection of these various oligomeric products formed from particle-phase esterification reactions.

4.2.7. Additional Routes for SOA Formation. As shown in Table 2, the polyester products from oligomerization of 2-MG and related components account only for a portion (22–34%) of the SOA formed from isoprene oxidation under high- NO_x conditions. This lack of mass closure could result from the LC/MS technique underestimating the amount of polyesters, possibly related to the use of a C_{18} reverse phase column and the unavailability of authentic standards. The C_{18} reverse phase column could have degraded the oligomers into smaller units as they pass through the column, or very large oligomers could have permanently been retained onto the reverse phase material, and hence were not detected. Negative bias associated with filter sampling, such as evaporative losses during sampling or storage, could also be a source of incomplete mass closure. The presence of acetic acid in eluent mixture used for the LC/MS runs could also have caused an underestimation of the oligomers formed

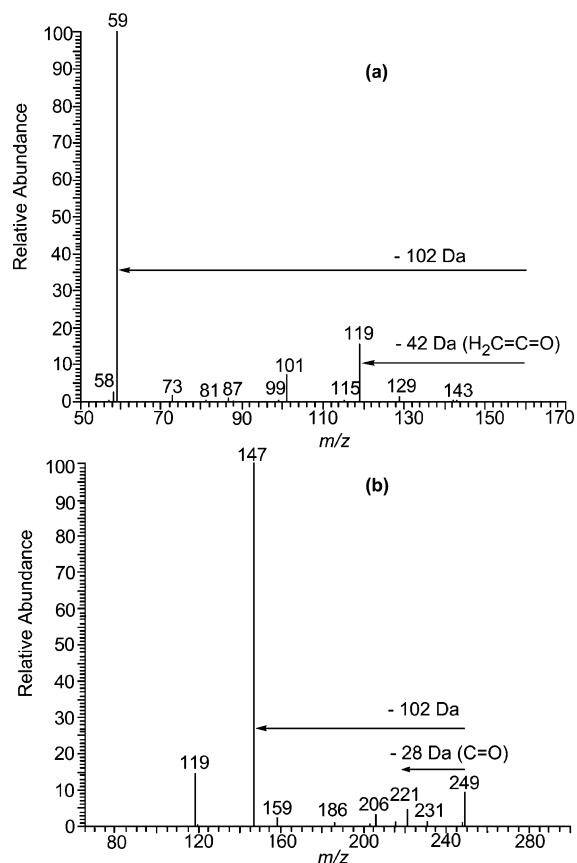


Figure 13. ESI-ITMS negative mode product ion mass spectra providing evidence for *mono*-acetate and *mono*-formate oligomers in high- NO_x SOA. (a) Product ion mass spectrum for a *mono*-acetate dimer (m/z 161). (b) Product ion mass spectrum for a *mono*-formate trimer (m/z 249).

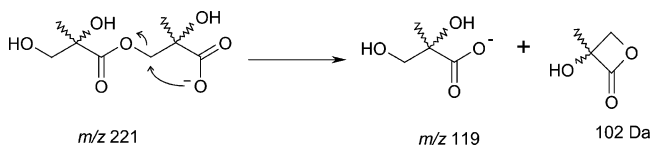


Figure 14. Proposed charge-directed nucleophilic reaction occurring during collisional activation in $(-)$ ESI-ITMS, explaining the observation of 102 Da (2-hydroxy-2 methylpropiolactone) losses from oligomeric high- NO_x SOA.

due to the possibility of acid-catalyzed hydrolysis during ESI, a process that would lead to a decrease in the detection of oligomeric compounds. Besides possible errors associated with quantifying esterification products identified by the LC/MS technique, the possibility still exists that other unidentified second- (or later-) generation gas- or particle-phase products from isoprene oxidation contribute to SOA formation, and as a result, would increase the mass closure significantly.

Glyoxal, a C_2 dialdehyde, has been recently shown to be reactively taken up into particulate matter,^{41,42} however, not at the low RH s employed in this study ($RH < 5\%$). Theoretically, it has been shown that this reactive uptake of glyoxal results from thermodynamically favorable hydration and oligomerization.^{43,44} When first interpreting the MS data from the ESI and MALDI techniques, it was considered that a dialdehyde species possibly corresponded to the 102 Da neutral losses observed from the oligomeric components. Figure 17 shows a proposed gas-phase reaction scheme for the formation of a C_4 hydroxy dialdehyde species ($\text{MW} = 102$) from the further oxidation of MACR. In contrast to glyoxal, dissolution may not be required

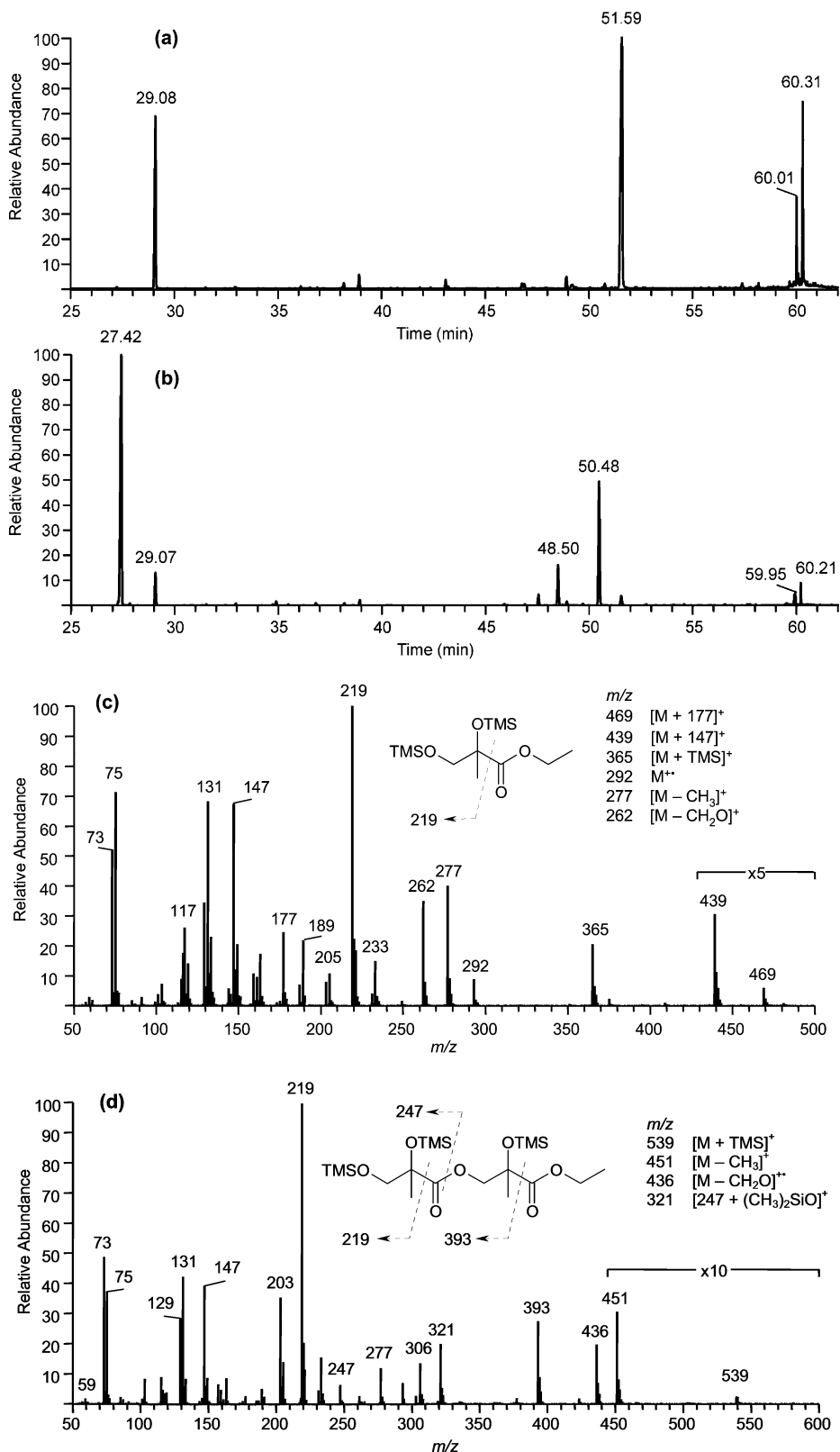


Figure 15. (a) GC/MS EIC ($= m/z$ 219) for high- NO_x isoprene nucleation sample (Experiment 5) treated only with TMS derivatization. (b) GC/MS EIC ($= m/z$ 219) for a duplicate sample of the same experiment (Experiment 5) in part a, but treated this time by hydrolysis/ethylation followed by TMS derivatization. (c) EI mass spectrum for ethyl ester of 2-MG acid detected in part b ($RT = 27.42$ min). (d) EI mass spectrum for ethyl ester of linear 2-MG acid dimer detected in part b ($RT = 50.48$ min). The hydrolysis/ethylation followed by TMS derivatization results presented here confirm the existence of polyesters in high- NO_x SOA.

for this proposed dialdehyde species to form SOA; therefore, other heterogeneous processes may occur. The detailed analysis of the GC/MS derivatization and the ESI tandem MS results, however, provides strong chemical evidence for the formation

of polyesters, where the neutral loss of 102 Da is explained by the dehydrated lactone form of 2-MG (Figure 14). In addition, a GC/MS derivatization analysis made for MACR high- NO_x SOA (Experiment 3) that included a methoximation step prior

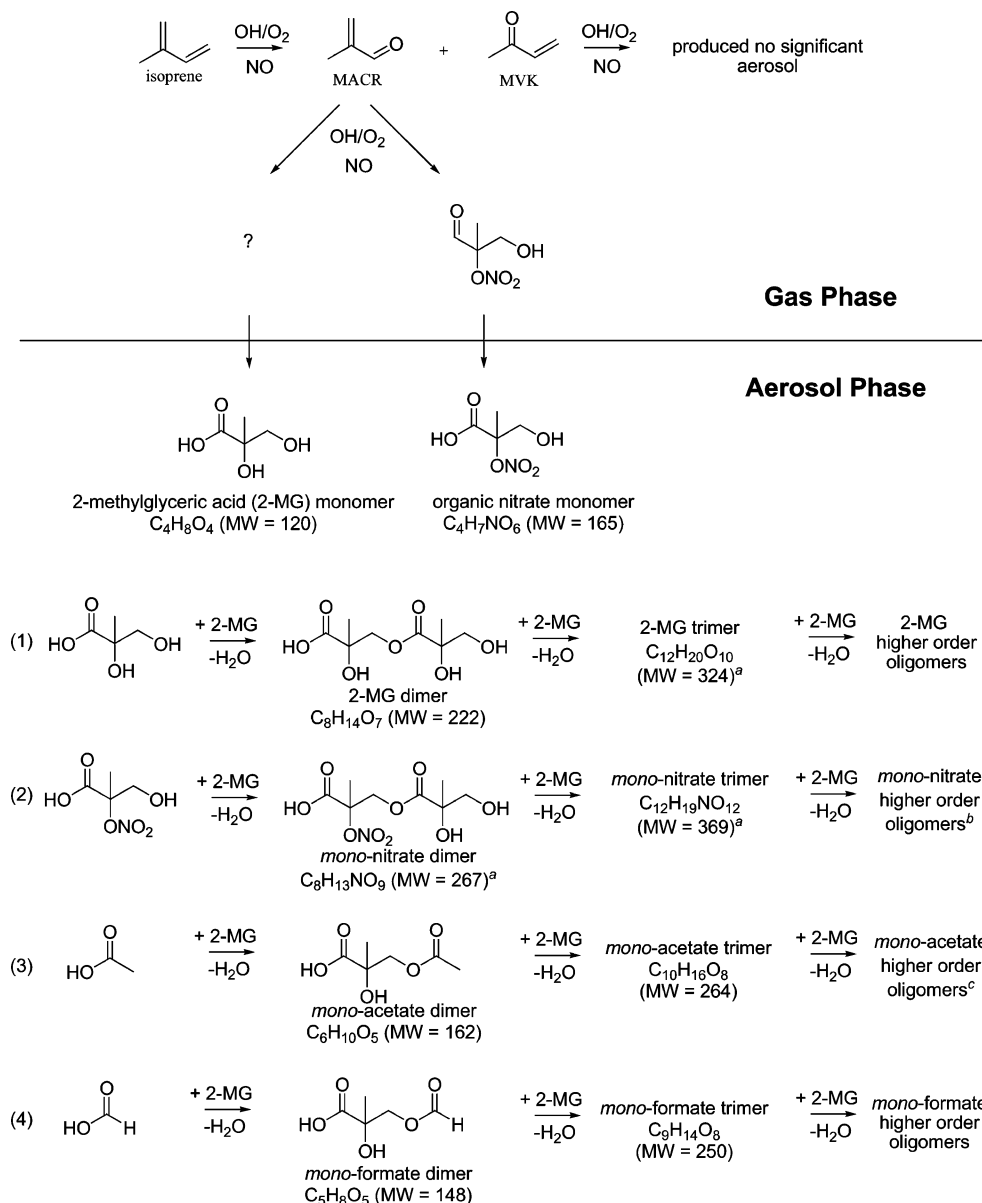


Figure 16. Proposed mechanism for SOA formation from isoprene photooxidation under high- NO_x conditions. Symbol used: ?, further study needed in order to understand the formation (in gas/particle phase) of 2-MG. ^aElemental compositions confirmed by high-resolution ESI-MS. ^bElemental composition of *mono-nitrate* tetramer (MW = 471) confirmed by high-resolution ESI-MS. ^cElemental compositions of *mono-acetate* tetramer and pentamer (MW = 366 and 468, respectively) confirmed by high-resolution ESI-MS.

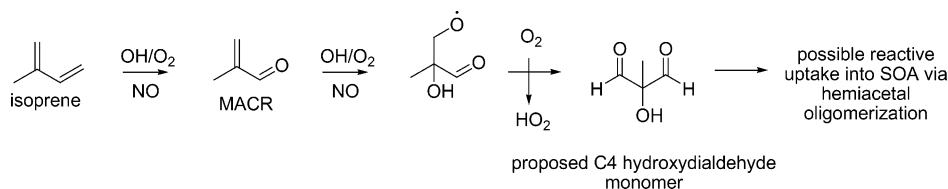


Figure 17. Proposed gas-phase formation mechanism for a C_4 hydroxydialdehyde monomer, possibly accounting for a fraction of the unidentified SOA mass in high- NO_x experiments.

to trimethylsilylation to reveal aldehyde functions in the formed oligomers was negative.

To investigate further the probable importance of a C_4 hydroxy dialdehyde species and its respective hemiacetal oligomers, selected sample extracts were derivatized using Girard Reagent P to increase sensitivity for aldehydic species in the (+)ESI mode. A high- NO_x isoprene and a MACR sample were treated with this derivatizing agent, and as a result, the detection of the m/z 236, 206, and 192 ions resulted for both

samples, which likely corresponds to the detection of the proposed C_4 dialdehyde, glyoxal, and methylglyoxal, respectively. However, the proposed hemiacetal oligomers that would be produced from this C_4 dialdehyde were not detected, consistent with observations made in the methoximation GC/MS experiment. It is possible that the detection of the proposed C_4 dialdehyde resulted from the decomposition of oligomers during the derivatization step of the sample workup procedure (which is equivalent for the detection of glyoxal and methylgly-

lyoxal in the particle phase). As a confirmation that the observed ions were derivatized species of the proposed C₄ dialdehyde, glyoxal, and methylglyoxal, upfront CID LC/MS analysis was used to detect common neutral mass losses and fragment ions associated with derivatized aldehydes and ketones. The common neutral losses and fragment ions associated with the GirP derivatization detected were similar to those found by Lai et al.,²³ providing further evidence of the detection of these small aldehyde species in high-NO_x isoprene and MACR SOA. The detection of these small dicarbonyls provides some evidence that aldehydes may account for a fraction of the unquantified (unidentified) SOA mass (Table 2) produced from isoprene oxidation under high-NO_x conditions. The mechanism (reactive uptake and/or oligomerization) and the degree in which these aldehydes form SOA, however, remains unclear and bears further study.

4.3. Low-NO_x SOA. **4.3.1. Hydroperoxides: Key Component to SOA Formation.** As discussed previously, in the absence of NO_x, the RO₂ radical chemistry is dominated by RO₂ + HO₂ reactions, owing to the large amounts of HO₂ formed from the OH + H₂O₂ reactions.¹⁷ RO₂ + RO₂ reactions are expected to be less substantial (10–30% contribution) because of the high HO₂/RO₂ ratios in these experiments, and as a result, hydroperoxides are expected to be the dominant gas-phase products. Because of their expected low volatilities, hydroperoxide species can partition to the aerosol phase and likely form high-MW species via peroxyhemiacetal formation with aldehydic species.^{18,19} Hydroperoxides resulting from the oxidation of aromatic and biogenic VOCs have been observed and calculated to be important contributors to the overall SOA mass.^{18,45,46} Indeed, as shown in Table 3, organic peroxides (i.e., hydroperoxides or ROOR) are also a significant component (~61% of the SOA mass for nucleation experiments and ~25% and 30% of the SOA mass for dry seeded and acid seeded experiments, respectively) of the low-NO_x isoprene SOA. The large discrepancy in peroxide content observed between nucleation (seed-free) and seeded experiments is currently not understood. As discussed in the results section, there is no evidence of interference from ammonium sulfate on the peroxide content measurement. Owing to the neutral nature of the hydroperoxides (and ROOR) measured by the iodometric-spectrophotometric method, no tandem ESI-MS measurements could be made to structurally elucidate this fraction. Thus, it is difficult to explain the differences in the peroxide content observed between nucleation and seeded experiments. It is possible that in the seeded cases the hydroperoxide species are heterogeneously converted into neutral species other than peroxidic compounds, such as polyols. Further studies should be conducted to investigate the role of inorganic seed on the amount of peroxides formed in the aerosol phase. As noted in the high-NO_x case, the mass closure results presented here apply only to the aerosol mass loadings produced in this current study and cannot be concluded as absolute for the isoprene system at low-NO_x conditions.

4.3.2 Oligomerization. Oligomers were found to form under low-NO_x conditions, as shown in the (+)MALDI (Figure 7), GC/MS with TMS derivatization (Figure 10), and TOF-AMS (Figures 8 and 9) data. In contrast to high-NO_x conditions, no distinct pattern or obvious monomeric unit, like the 102 Da differences observed in the high-NO_x oligomeric SOA (Figures 1, 2, and 5), was observed in the low-NO_x oligomers. The oligomers formed in the low-NO_x case are not acidic in nature like those in the high-NO_x case. Structural elucidation of these oligomers is limited because these neutral products are not

ionizable using ESI-MS. MALDI (Figure 7) was able to provide some indication of the MW ranges of the oligomeric SOA, but structural elucidation was not possible. The large mass contribution of organic peroxides to the low-NO_x SOA (Table 3) provides some insight into the oligomerization reactions occurring. It is possible that some fraction of the oligomeric SOA is formed by peroxyhemiacetals, which result from heterogeneous reactions of hydroperoxides and aldehydes.

Because of the neutral nature of the oligomeric SOA produced under low-NO_x conditions, only the GC/MS derivatization technique provides structural elucidation of the oligomers formed owing to the presence of polyols. Hemiacetal formation reactions between C₅ alkene triols (Table 4) and 2-methyltetrols (Table 4) were found to occur using this technique (Figure 10b). The reaction involves a terminal hydroxyl group of a 2-methyltetrol, which serves as a nucleophile, reacting with the tautomeric keto form of one C₅ alkene triol (Table 4) to form the hemiacetal dimer shown in Figure 10b. As was observed by the GC/MS *m/z* 219 EIC, six isomeric forms of this hemiacetal dimer could be partially resolved. However, further elucidation of higher-order hemiacetal (acetal) oligomers could not be conducted owing to their likely thermal decomposition in the GC injector of the GC/MS instrument, their high MW preventing their elution from the GC column, and lack of ionization when using ESI-MS techniques. As for the confirmation of peroxyhemiacetal oligomers, analytical techniques need to be developed in order to further elucidate the neutral higher-order hemiacetal (acetal) oligomers likely present in low-NO_x SOA.

4.3.3. Acid Catalysis. The SOA mass for the acid seed experiment (Experiment 14) is significantly larger (~3.6 times) than that of the dry seeded/nucleation experiments (Experiments 15/12), in contrast to high-NO_x conditions, in which acid seed had no such observable effect. Note that the SOA mass concentration was virtually identical in experiments using dry (nonacid) seed aerosol and in those in the absence of seed aerosol, where particle formation takes place by nucleation (Experiments 12, 13, and 15). GC-FID measurements made for selected low-NO_x experiments also provide evidence for acid-catalyzed particle-phase reactions. The C₅ alkene triols and 2-methyltetrols decreased in their contributions to the overall SOA mass when acid seed was present. For example, the 2-methyltetrols and C₅ alkene triols contributed ~3.91% and 0.6%, respectively, to the SOA mass for Experiment 13 (nonacid case), whereas in Experiment 14 (acid case), the 2-methyltetrols and C₅ alkene triols were found to decrease to ~0.46% and 0.06%, respectively, of the SOA mass. This result is in contrast to that observed by Edney et al.¹⁴ in which isoprene tracer compounds were observed to increase in concentration, and is possibly due to the differing isoprene/NO_x ratios employed. In conjunction with the above GC-FID results, the fact that C₅ alkene triols and 2-methyltetrols were found to form hemiacetal dimers (and likely higher order oligomers) suggests that the presence of acidified aerosol catalyzes hemiacetal (and likely acetal) oligomer formation under low-NO_x conditions. The same may be the case for peroxyhemiacetal formation reactions.

4.3.4. Formation Mechanism of Low-NO_x SOA products Observed by GC/MS. The detection of organic peroxides in the particle phase (Table 3) by the iodometric-spectrophotometric method provides strong evidence that the hydroperoxides that result from the gas-phase RO₂ + HO₂ reactions are sufficiently polar (nonvolatile) to partition to the aerosol phase, thereby elucidating one major reaction pathway leading to SOA formation under low-NO_x conditions. The detection of 2-methyltetrols,

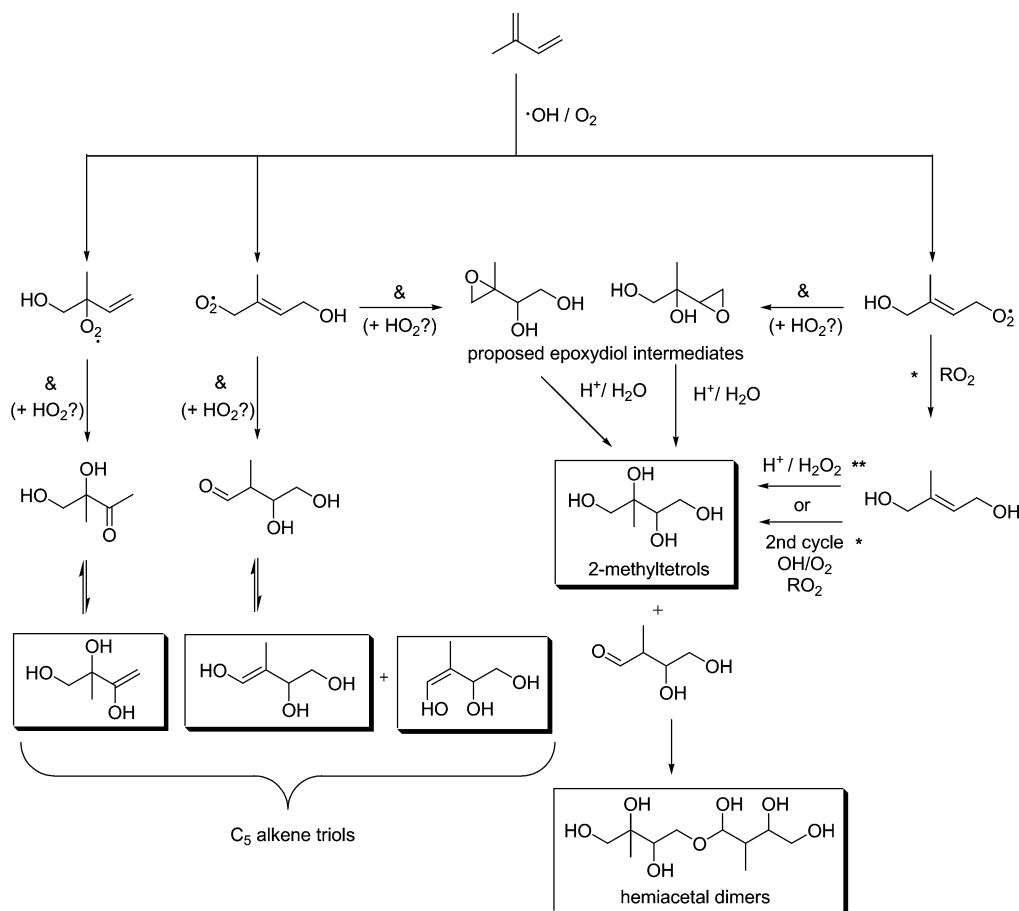


Figure 18. Low-NO_x SOA formation pathways as elucidated by GC/MS. Boxes indicate products detected in low-NO_x SOA. Symbols used: &, further study needed for the formations of the hypothetical carbonyl diol and epoxydiol intermediates which may result from the rearrangements of RO₂ radicals and/or hydroperoxides; *, for details about this pathway leading to 2-methyltetrols and also holding for isomeric products, see reference 7; **, for details about this alternative pathway, see ref 14. 2-methyltetrol performate derivatives (shown in Table 4) were omitted for simplicity; however, these could serve as precursors for 2-methyltetrols if in the presence of acid and water.

C₅ alkene triols, 2-methyltetrol performate derivatives, and hemiacetal dimers (Table 4) suggests that the RO₂ radicals that form from the initial oxidation (OH/O₂) of isoprene follow some other route. The formation of 2-methyltetrols has been explained by self- and cross-reactions of the RO₂ radicals formed from the initial oxidation (OH/O₂) of isoprene, leading to intermediate 1,2-diols, which may undergo a second cycle of oxidation (OH/O₂) reactions followed by self- and cross-reactions of the RO₂ radicals.⁷

The detection of C₅ alkene triols in ambient aerosol may indicate the importance of intermediate epoxydiol derivatives of isoprene, which may also be intermediates in the formation of 2-methyltetrols.^{11,12} Wang et al.¹² hypothesized from MS evidence that these epoxydiol intermediates could be trapped in the aerosol phase and subsequently converted into C₅ alkene triols and 2-methyltetrols through acid-catalyzed reactions. Acid-catalyzed reactions of epoxydiols may be a formation pathway for 2-methyltetrols and C₅ alkene triols, but these monomers may also form from other pathways.

Shown in Figure 18 is a proposed mechanism for the formation of key SOA components from the oxidation of isoprene under low-NO_x conditions. As suggested by Böge et al.,¹⁵ 2-methyltetrols may form by several possible pathways. The formation of the 2-methyltetrols through two cycles of oxidation (OH/O₂) reactions followed by self- and cross-reactions of the RO₂ radicals is only briefly included in this figure. It is possible that epoxydiols may form from rearrangements of hydroxyhydroperoxides or hydroxyperoxy radicals.

Once formed, these epoxydiols could be taken up into the particulate phase, and through hydrolysis form 2-methyltetrols. In addition, an alternative pathway leading to the formation of 2-methyltetrols has been reported in a recent study by Böge et al.¹⁵ That study proposed that intermediates in the formation of 2-methyltetrols (i.e., 2-methyl-3-butene-1,2-diol and 2-methyl-2-vinylloxirane) are converted to 2-methyltetrols through reaction with hydrogen peroxide on acidic particles. The latter pathway is also included in the scheme in Figure 18. Further gas and particle-phase studies are needed in order to fully elucidate the pathways leading to the formation of 2-methyltetrols, the C₅ alkene triols, and related dimeric products.

4.3.5. Evolution of SOA Composition. As in Kroll et al.,¹⁷ a rapid decay of the SOA mass was observed after the initial SOA growth reached its maximum for all low-NO_x nucleation experiments. This loss is not attributable to wall removal processes because the particles shrink in size rather than reduce in number (as measured by the DMA). The loss of SOA mass was observed to stop immediately after chamber lights were turned off, and resume once the lights were turned back on, indicating a photochemical effect.

Indeed, when comparing the peroxide measurements made at (or around) the initial SOA growth maximum to some later experimental time after SOA mass decay, it was found that the organic peroxide content of the aerosol decreased significantly (~59% to 26% of SOA mass, respectively, for Experiment 18). This observation provides strong evidence that organic peroxides decompose in the particle phase due to photolysis

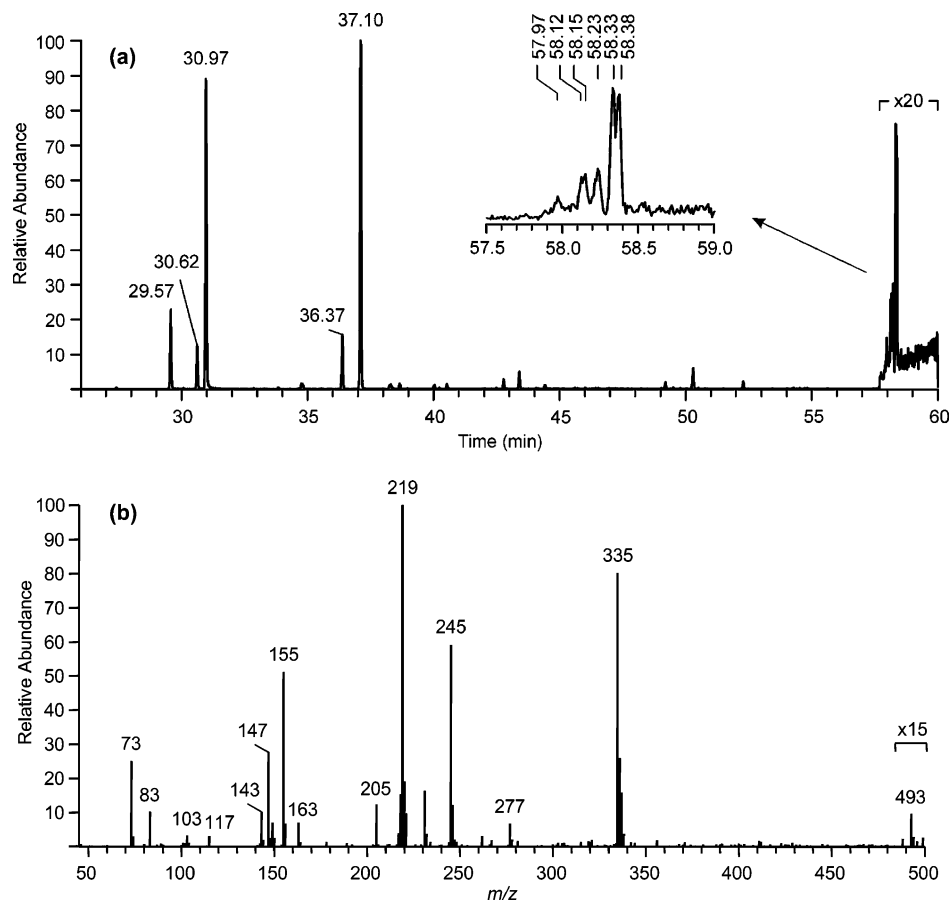


Figure 19. (a) GC/MS EIC using specific ions for the TMS derivatives of 2-methyltetrols (m/z 219), C_5 alkene triols (m/z 231), and hemiacetal dimers (m/z 219 and 335) for a PM_{2.5} aerosol sample collected in Rondônia, Brazil, during the onset of the wet season from 10–12 November 2002 (39 h collection time). The inset shows a detail of the isomeric hemiacetal dimers, formed between 2-methyltetrols and C_5 dihydroxycarbonyls, which elute between 57 and 59 min; (b) averaged EI mass spectrum (only limited mass range m/z 50–500 available) for the TMS derivatives of the isomeric hemiacetal dimers.

and/or subsequent particle-phase reactions, or they are driven out of the particle as a result of gas-phase compounds being reacted away, shifting the equilibrium back to the gas phase. TOF-AMS measurements also confirmed that the peroxide content of low- NO_x SOA decreases with time as shown in Figure 9b. This decrease in peroxide content as a function of time also coincided with high-mass fragment ions ($m/z > 200$) increasing in their abundance (in Figure 9a only m/z 247 and 327 are shown), suggesting the possibility that peroxide decomposition causes oligomerization reactions. These oligomerization reactions likely lead to hemiacetals (as elucidated by GC/MS).

4.3.6. Tracer Compounds for Isoprene Oxidation in the Remote Atmosphere. The low- NO_x chamber experiments conducted in this study confirm that 2-methyltetrols indeed serve as tracer compounds for isoprene oxidation in the ambient atmosphere, especially in remote regions such as the Amazonian rainforest. The detection of C_5 alkene triols and hemiacetal dimers in the present low- NO_x experiments corresponds well to their observation in ambient aerosol collected from the Amazonian rainforest¹² and Finnish boreal forests (note that hemiacetal dimers in aerosol collected from the Finnish boreal forests is not yet confirmed).¹¹ From these field studies, C_5 alkene triols were postulated to form by acid-catalyzed ring-opening reactions of epoxydiol derivatives of isoprene in low RH environments. However, hemiacetal dimers were not recognized in ambient samples; this current study elucidates their formation under low- NO_x conditions. Once it was realized that

hemiacetal dimers form from C_5 alkene triols and 2-methyltetrols, we referred back to data collected from the Amazonian rainforest.⁴⁷ When investigating the GC/MS data carefully, it was found that the hemiacetal dimers were indeed detected, suggesting the atmospheric relevance of these low- NO_x chamber experiments. Shown in Figure 19 is a GC/MS EIC of an Amazonian fine aerosol sample (i.e., PM_{2.5}; particulate matter with an aerodynamic diameter $< 2.5 \mu m$) collected during the wet season (low- NO_x conditions) using multiple ions, that is, m/z 231 (to show the C_5 alkene triols), m/z 219 (to show 2-methyltetrols as well as the dimers), and m/z 335 (characteristic of the dimers). An averaged EI mass spectrum for the hemiacetal dimers is also included in this Figure to further confirm their presence in ambient aerosol.

5. Conclusions

The composition of SOA from the photooxidation of isoprene under both high- and low- NO_x conditions has been thoroughly investigated through a series of controlled laboratory chamber experiments. It is found that the chemical nature of the resultant SOA is significantly different in the two NO_x regimes. Under high- NO_x conditions, the SOA components are acidic and form upon the further oxidation of MACR. SOA components formed under low- NO_x conditions, by contrast, are not acidic, with primary species identified being polyols and organic peroxides. On the basis of SOA growth, acid-catalysis seems to play a larger role under low- NO_x conditions. Organic peroxides (likely

dominated by hydroperoxides) contribute significantly to the low-NO_x SOA mass (~61% for nucleation experiments and ~25% and 30% for dry seeded and acid seeded experiments, respectively). However, differences in the organic peroxide contribution and the rate of loss in SOA mass for nucleation (seed-free) and seeded experiments are not well understood and require further investigation. The chemical composition changes with time in the low-NO_x case, showing evidence of chemical aging.

Oligomerization is an important SOA formation pathway for both low- and high-NO_x conditions because oligomers were observed in both cases. The nature of the oligomers, however, is distinctly different in each NO_x regime. Under high-NO_x conditions, the oligomers have clear monomeric units, with observable 102 Da differences using both online and offline mass spectrometry techniques. Using tandem ESI-MS techniques and GC/MS with trimethylsilylation, it is found that polyesters account for these high-NO_x oligomers, with 2-MG as the key monomeric unit. These polyesters account only for a fraction (~22–34%) of the SOA mass formed from isoprene oxidation. This lack of mass closure could result from an underestimate of the amount of polyesters formed or additional, unidentified MACR or isoprene oxidation products that contribute to the SOA mass. One key unresolved question is the path by which 2-MG is formed, which at present is not understood. Further gas- and particle-phase studies on isoprene oxidation under high-NO_x conditions are needed in order to elucidate the 2-MG formation pathway.

Previously detected tracer compounds for isoprene oxidation in the ambient atmosphere were detected in the low-NO_x experiments. C₅ alkene triols and hemiacetal dimers are reported here for the first time in a controlled laboratory experiment, suggesting that the oxidative conditions used in these experiments are relevant to remote regions. The GC/MS results suggest that hemiacetal dimers formed in these low-NO_x chamber experiments result from the reactions of 2-methyltetrols and C₅ alkene triols (a reaction that is likely relevant to the real atmosphere). Besides the formation of hemiacetal (acetal) oligomers in low-NO_x SOA, it is speculated that peroxyhemiacetal oligomers could also form, because of the large amounts of peroxides measured in the particle phase. The formation of low-NO_x oligomers may correlate to the decomposition of peroxides with experimental time, providing some insight into the mechanism of oligomerization. Additional analytical techniques need to be developed in order to elucidate the neutral/unstable products found in SOA produced from the photooxidation of isoprene.

Acknowledgment. Research at Caltech was funded by the U.S. Environmental Protection Agency to Achieve Results (STAR) Program grant no. RD-83107501-0, managed by EPA's Office of Research and Development (ORD), National Center for Environmental Research (NCER), and by the U.S. Department of Energy, Biological, and Environmental Research Program DE-FG02-05ER63983; this work has not been subjected to the EPA's required peer and policy review and therefore does not necessarily reflect the views of the Agency and no official endorsement should be inferred. Jason Surratt was supported in part by the United States Environmental Protection Agency (EPA) under the Science to Achieve Results (STAR) Graduate Fellowship Program. Research at the Universities of Antwerp and Ghent was supported by the Belgian Federal Science Policy Office through the BIOSOL project (contract SD/AT/02A) and a visiting postdoctoral fellowship to Rafal Szmigielski, and by the Research Foundation –

Flanders (FWO). We would like to thank John Greaves at the University of California, Irvine for the accurate mass measurements on the ESI-TOF instrument. We would like to also thank Paul Ziemann at the University of California, Riverside for his useful communications regarding peroxide measurements in SOA.

Supporting Information Available: Electron impact (EI) mass spectra for 2-methyltetrols, C₅ alkene triols, and 2-methyltetrol performate derivatives for their respective chromatographic peaks found in Figure 10. This material is available free of charge via the Internet at <http://pubs.acs.org>.

References and Notes

- (1) Inuma, Y.; Böge, O.; Gnauk, T.; Herrmann, H. *Atmos. Environ.* **2004**, *38*, 761.
- (2) Gao, S.; Keywood, M.; Ng, N.; Surratt, J. D.; Varutbangkul, V.; Bahreini, R.; Flagan, R. C.; Seinfeld, J. H. *J. Phys. Chem. A* **2004**, *108*, 10147.
- (3) Gao, S.; Ng, N.; Keywood, M.; Varutbangkul, V.; Bahreini, R.; Nenes, A.; He, J.; Yoo, K.; Beauchamp, J.; Hodyss, R.; Flagan, R.; Seinfeld, J. *Environ. Sci. Technol.* **2004**, *38*, 6582.
- (4) Tolocka, M.; Jang, M.; Ginter, J.; Cox, F.; Kamens, R.; Johnston, M. *Environ. Sci. Technol.* **2004**, *38*, 1428.
- (5) Kalberer, M.; Paulsen, D.; Sax, M.; Steinbacher, M.; Dommen, J.; Prevot, A.; Fisseha, R.; Weingartner, E.; Frankevich, V.; Zenobi, R.; Baltensperger, U. *Science* **2004**, *303*, 1659.
- (6) Kanakidou, M.; Seinfeld, J.; Pandis, S.; Barnes, I.; Dentener, F.; Facchini, M.; Van Dingenen, R.; Ervens, B.; Nenes, A.; Nielsen, C.; Swietlicki, E.; Putaud, J.; Balkanski, Y.; Fuzzi, S.; Horth, J.; Moortgat, G.; Winterhalter, R.; Myhre, C.; Tsigaridis, K.; Vignati, E.; Stephanou, E.; Wilson, J. *Atmos. Chem. Phys.* **2005**, *5*, 1053.
- (7) Claeys, M.; Graham, B.; Vas, G.; Wang, W.; Vermeylen, R.; Pashynska, V.; Cafmeyer, J.; Guyon, P.; Andreae, M. O.; Artaxo, P.; Maenhaut, W. *Science* **2004**, *303*, 1173.
- (8) Pandis, S.; Paulson, S.; Seinfeld, J. H.; Flagan, R. C. *Atmos. Environ.* **1991**, *25*, 997.
- (9) Limbeck, A.; Kulmala, M.; Puxbaum, H. *Geophys. Res. Lett.* **2003**, *30*.
- (10) Ion, A. C.; Vermeylen, R.; Kourtchev, I.; Cafmeyer, J.; Chi, X.; Gelencsér, A.; Maenhaut, W.; Claeys, M. *Atmos. Chem. Phys.* **2005**, *5*, 1805.
- (11) Kourtchev, I.; Ruuskanen, T.; Maenhaut, W.; Kulmala, M.; Claeys, M. *Atmos. Chem. Phys.* **2005**, *5*, 2761.
- (12) Wang, W.; Kourtchev, I.; Graham, B.; Cafmeyer, J.; Maenhaut, W.; Claeys, M. *Rapid Commun. Mass Spectrom.* **2005**, *19*, 1343.
- (13) Claeys, M.; Wang, W.; Ion, A.; Kourtchev, I.; Gelencsér, A.; Maenhaut, W. *Atmos. Environ.* **2004**, *38*, 4093.
- (14) Edney, E. O.; Kleindienst, T. E.; Jaoui, M.; Lewandowski, M.; Offenberg, J. H.; Wang, W.; Claeys, M. *Atmos. Environ.* **2005**, *39*, 5281.
- (15) Böge, O.; Miao, Y.; Plewka, A.; Herrmann, H. *Atmos. Environ.* **2006**, *40*, 2501.
- (16) Kroll, J. H.; Ng, N. L.; Murphy, S. M.; Flagan, R. C.; Seinfeld, J. H. *Geophys. Res. Lett.* **2005**, *32*.
- (17) Kroll, J. H.; Ng, N. L.; Murphy, S. M.; Flagan, R. C.; Seinfeld, J. H. *Environ. Sci. Technol.* **2006**, *40*, 1869.
- (18) Docherty, K.; Wu, W.; Lim, Y.; Ziemann, P. *Environ. Sci. Technol.* **2005**, *39*, 4049.
- (19) Johnson, D.; Jenkin, M. E.; Wirtz, K.; Martin-Reviejo, M. *Environ. Chem.* **2004**, *1*, 150.
- (20) Gao, S.; Surratt, J. D.; Knipping, E. M.; Edgerton, E. S.; Shahgholi, M.; Seinfeld, J. H. *J. Geophys. Res.*, in press, 2006.
- (21) Cocker, D.; Flagan, R. C.; Seinfeld, J. H. *Environ. Sci. Technol.* **2001**, *35*, 2594.
- (22) Keywood, M.; Varutbangkul, V.; Bahreini, R.; Flagan, R.; Seinfeld, J. *Environ. Sci. Technol.* **2004**, *38*, 4157.
- (23) Lai, C.; Tsai, C.; Tsai, F.; Lee, C.; Lin, W. *Rapid Commun. Mass Spectrom.* **2001**, *15*, 2145.
- (24) Drewnick, F.; Hings, S.; DeCarlo, P.; Jayne, J.; Gonin, M.; Fuhrer, K.; Weimer, S.; Jimenez, J.; Demerjian, K.; Borrmann, S.; Worsnop, D. *Aerosol Sci. Technol.* **2005**, *39*, 637.
- (25) Pashynska, V.; Vermeylen, R.; Vas, G.; Maenhaut, W.; Claeys, M. *J. Mass Spectrom.* **2002**, *37*, 1249.
- (26) Banerjee, D.; Budke, C. *Anal. Chem.* **1964**, *36*, 792.
- (27) Sorooshian, A.; Brechtel, F. J.; Ma, Y.; Weber, R. J.; Corless, A.; Flagan, R. C.; Seinfeld, J. H. *Aerosol Sci. Technol.* **2006**, *40*, 396.
- (28) Weber, R.; Orsini, D.; Daun, Y.; Lee, Y.; Klotz, P.; Brechtel, F. *Aerosol Sci. Technol.* **2001**, *35*, 718.

- (29) Seinfeld, J. H.; Pandis, S. N. *Atmospheric Chemistry and Physics: From Air Pollution to Climate Change*; Wiley: New York, 1998.
- (30) Iinuma, Y.; Böge, O.; Miao, Y.; Sierau, B.; Gnauk, T.; Herrmann, H. *Faraday Discuss.* **2005**, *130*, 279.
- (31) Knochenmuss, R.; Zenobi, R. *Chem. Rev.* **2003**, *103*, 441.
- (32) Miyoshi, A.; Hatakeyama, S.; Washida, N. *J. Geophys. Res.* **1994**, *99*, 18779.
- (33) Tuazon, E.; Atkinson, R. *Int. J. Chem. Kinet.* **1990**, *22*, 1221.
- (34) Paulson, S.; Flagan, R. C.; Seinfeld, J. H. *Int. J. Chem. Kinet.* **1992**, *24*, 79.
- (35) Sprengnether, M.; Demerjian, K.; Donahue, N.; Anderson, J. J. *Geophys. Res.* **2002**, *107*.
- (36) Baker, J.; Arey, J.; Atkinson, R. *Environ. Sci. Technol.* **2005**, *39*, 4091.
- (37) Ng, N. L.; Kroll, J. H.; Keywood, M. D.; Bahreini, R.; Varutbangkul, V.; Lee, A.; Goldstein, A. H.; Flagan, R. C.; Seinfeld, J. H. *Environ. Sci. Technol.* **2006**, *40*, 2283.
- (38) Lee, A.; Goldstein, A. H.; Ng, N. L.; Kroll, J. H.; Varutbangkul, V.; Flagan, R. C.; Seinfeld, J. H. *J. Geophys. Res.* **2006**, *111*.
- (39) Chuong, B.; Stevens, P. S. *Int. J. Chem. Kinet.* **2004**, *36*, 12.
- (40) Yuan, H.; Nishiyama, Y.; Kuga, S. *Cellulose* **2005**, *12*, 543.
- (41) Kroll, J. H.; Ng, N. L.; Murphy, S. M.; Varutbangkul, V.; Flagan, R. C.; Seinfeld, J. H. *J. Geophys. Res.* **2005**, *110*.
- (42) Liggio, J.; Li, S.; McLaren, R. *Environ. Sci. Technol.* **2005**, *39*, 1532.
- (43) Barsanti, K.; Pankow, J. *Atmos. Environ.* **2005**, *39*, 6597.
- (44) Tong, C.; Blanco, M.; Goddard, W. A., III; Seinfeld, J. H. *Environ. Sci. Technol.* **2006**, *40*, 2333.
- (45) Johnson, D.; Jenkin, M. E.; Wirtz, K.; Martin-Reviejo, M. *Environ. Chem.* **2005**, *2*, 35.
- (46) Bonn, B.; von Kuhlmann, R.; Lawrence, M. *Geophys. Res. Lett.* **2004**, *31*.
- (47) Decesari, S.; Fuzzi, S.; Facchini, M.; Mircea, M.; Emblico, L.; Cavalli, F.; Maenhaut, W.; Chi, X.; Schkolnik, G.; Falkovich, A.; Rudich, Y.; Claeys, M.; Pashynska, V.; Vas, G.; Kourtchev, I.; Vermeylen, R.; Hoffer, A.; Andreae, M. O.; Tagliavini, E.; Moretti, F.; Artaxo, P. *Atmos. Chem. Phys.* **2006**, *6*, 375.

Appendix D

Evidence for Organosulfates in Secondary Organic Aerosol*

* This chapter is reproduced by permission from “Evidence for Organosulfates in Secondary Organic Aerosol” by J. D. Surratt, J. H. Kroll, T. E. Kleindienst, E. O. Edney, M. Claeys, A. Sorooshian, N. L. Ng, J. H. Offenberg, M. Lewandowski, M. Jaoui, R. C. Flagan, J. H. Seinfeld, *Environmental Science and Technology*, 41: 517-527 2006. Copyright 2006. American Chemical Society.

Evidence for Organosulfates in Secondary Organic Aerosol

JASON D. SURRATT,[†] JESSE H. KROLL,^{‡,*}
 TADEUSZ E. KLEINDIENST,[§]
 EDWARD O. EDNEY,[§] MAGDA CLAEYS,[‡]
 ARMIN SOROOSHIAN,^{||} NGA L. NG,^{||}
 JOHN H. OFFENBERG,[§]
 MICHAEL LEWANDOWSKI,[§]
 MOHAMMED JAOUI,[#]
 RICHARD C. FLAGAN,[‡] AND
 JOHN H. SEINFELD^{*,‡}

Department of Chemistry, California Institute of Technology, Pasadena, California 91125, Departments of Environmental Science and Engineering and Chemical Engineering, California Institute of Technology, Pasadena, California 91125, National Exposure Laboratory, Office of Research and Development, Environmental Protection Agency, Research Triangle Park, North Carolina 27711, Department of Pharmaceutical Sciences, University of Antwerp (Campus Drie Eiken), Universiteitsplein 1, BE-2610 Antwerp, Belgium, Department of Chemical Engineering, California Institute of Technology, Pasadena, California 91125, and Alion Science and Technology, P.O. Box 12313, Research Triangle Park, North Carolina 27709

Recent work has shown that particle-phase reactions contribute to the formation of secondary organic aerosol (SOA), with enhancements of SOA yields in the presence of acidic seed aerosol. In this study, the chemical composition of SOA from the photooxidations of α -pinene and isoprene, in the presence or absence of sulfate seed aerosol, is investigated through a series of controlled chamber experiments in two separate laboratories. By using electrospray ionization–mass spectrometry, sulfate esters in SOA produced in laboratory photooxidation experiments are identified for the first time. Sulfate esters are found to account for a larger fraction of the SOA mass when the acidity of seed aerosol is increased, a result consistent with aerosol acidity increasing SOA formation. Many of the isoprene and α -pinene sulfate esters identified in these chamber experiments are also found in ambient aerosol collected at several locations in the southeastern U.S. It is likely that this pathway is important for other biogenic terpenes, and may be important in the formation of humic-like substances (HULIS) in ambient aerosol.

Introduction

Particle-phase reactions are now understood to play an important role in secondary organic aerosol (SOA) formation

* Corresponding author phone: (626) 395-4635; fax: (626) 796-2591; e-mail: seinfeld@caltech.edu.

[†] Department of Chemistry, California Institute of Technology.

[‡] Departments of Environmental Science and Engineering and Chemical Engineering, California Institute of Technology.

[§] Environmental Protection Agency.

^{||} University of Antwerp.

^{||} Department of Chemical Engineering, California Institute of Technology.

[#] Alion Science and Technology.

^{*} Current address: Aerodyne Research, Inc., 45 Manning Road, Billerica, MA 01281.

(1). Particle-phase oligomerization leads to the formation of high-molecular-weight (MW) species (2–4); suggested oligomerization reactions include the reactive uptake of volatile aldehydes or ketones via peroxyhemiacetal formation (5, 6), hydration, hemiacetal/acetal formation, and aldol condensation (7, 8). Esterification in isoprene photooxidation (9, 10) has also been reported in SOA formation. The role of these reactions remains in some doubt as some of the proposed reactions (e.g., hemiacetal/acetal formation and aldol condensation) are not thermodynamically favorable at ambient conditions (11, 12).

Laboratory chamber studies have demonstrated that the presence of acidic seed aerosol enhances the SOA yields observed from the oxidation of various volatile organic compounds (VOCs), such as α -pinene (2, 3, 13, 14), isoprene (8, 14, 15), and several model cycloalkenes (2) over those with a less acidic seed aerosol. Despite recent advances in understanding particle-phase SOA chemistry, the role of particle-phase acidity in enhancing SOA formation remains essentially unexplained. Recent studies have presented mass spectrometric evidence that the reactive uptake of glyoxal and pinonaldehyde (principal gas-phase oxidation products from aromatics and α -pinene, respectively) on acidic aerosol involves organosulfate formation (sulfate esters or derivatives; for simplicity, we will use hereafter the term sulfate esters to also denote sulfate derivatives; i.e. sulfate derivatives formed from a carbonyl compound) (16–18). In addition, several field studies have reported sulfate ester signatures in aerosol collected on filters using Fourier transform infrared spectroscopy (19, 20) and electrospray ionization (ESI)–mass spectrometry (MS) (21, 22). Nevertheless, the importance of organosulfate formation to SOA remains unclear. Traditional analytical methods, such as gas chromatography/mass spectrometry (GC/MS) with prior derivatization, may not be well suited for identifying organosulfates. It is likely that single derivatization protocols, such as trimethylsilylation, GC injection and column temperatures could cause the degradation or misinterpretation of such species (23). On the other hand, ESI–MS has been shown as an effective method for the detection and quantification of organosulfate species (24, 25).

In the present study ESI–MS is used to detect and structurally elucidate sulfate esters in SOA formed from the photooxidations of isoprene and α -pinene under differing combinations of NO_x levels and seed aerosol acidities. As a result, the formation of sulfate esters may be a major contributor to the observed enhancement in SOA yields in the presence of acidic aerosol.

Experimental Section

Isoprene Chamber Experiments. A summary of experimental conditions for all isoprene photooxidation experiments can be found in Table 1. Isoprene photooxidation experiments were conducted in Caltech's dual indoor 28 m³ Teflon chambers (26, 27) and in EPA's fixed volume 14.5 m³ indoor chamber (15). The temperatures, aerosol size distributions, and relative humidities, as well as the O₃, nitric oxide (NO), NO_x concentrations were continuously measured in both facilities. The isoprene concentrations in both facilities were monitored by GC with flame ionization detection. The Caltech experiments were conducted in the static mode (i.e., batch reactor) whereas the EPA experiments were conducted in the dynamic mode (i.e., continuous stirred tank reactor) with the exception of EPA-326 which was a static mode experiment. Hydroxyl radical (OH) precursors (H₂O₂ or HONO) were employed in the Caltech experiments (28, 29). For all Caltech

TABLE 1. Summary of Experimental Conditions and Sulfate Ester Formation from Isoprene Photooxidation

experiment	inorganic seed aerosol ^a	OH precursor	initial isoprene] (ppb)	initial [NO _x] (ppb)	average T (°C)	[M-H] ⁻ detected sulfate ester ions (m/z)
Caltech low-NO _x	none added	H ₂ O ₂	500	none added	23.7	none detected
Caltech low-NO _x	AS	H ₂ O ₂	500	none added	23.9	215, 333
Caltech low-NO _x	AAS	H ₂ O ₂	500	none added	23.8	153, 155, 169, 215, 333, 451
Caltech high-NO _x	none added	H ₂ O ₂ /NO	500	891	24.3	none detected
Caltech high-NO _x	AS	H ₂ O ₂ /NO	500	963	24.9	199, 215, 244
Caltech high-NO _x	AAS	H ₂ O ₂ /NO	500	904	24.6	139, 153, 155, 197, 199, 215, 244, 260, 301, 346
Caltech high-NO _x	none added	HONO	500	382	20.1	none detected
Caltech high-NO _x	AS	HONO	500	366	21.4	199, 215, 260, 333
EPA-299 stage 1	AS ^b	^c	2500	200	29.0	none detected
EPA-299 stage 2	AAS	^c	2500	200	29.0	153, 155, 167, 169, 181, 197, 199, 215, 244, 260, 333
EPA-299 stage 3	H ₂ SO ₄ only	^c	2500	200	29.0	153, 155, 157, 167, 169, 181, 197, 199, 215, 244, 260, 333
EPA-199 stage 1	60 ppb SO ₂	^c	1598	475	24.6	197, 199, 215, 244, 260, 301, 317, 333
EPA-199 stage 2	200 ppb SO ₂	^c	1598	475	24.6	155, 169, 197, 199, 215, 244, 260, 301, 317, 333, 346

^a AS = 15 mM (NH₄)₂SO₄; AAS = 15 mM (NH₄)₂SO₄ + 15 mM H₂SO₄ for Caltech experiments and 0.31 mM (NH₄)₂SO₄ + 0.612 mM H₂SO₄ for EPA-299 experiments; H₂SO₄ only = 0.92 mM H₂SO₄; EPA-199 had no seed nebulized but instead used the photooxidation of SO₂ to generate sulfuric acid aerosol. ^b Due to the low initial inorganic seed aerosol concentration, this condition is more conducive to nucleation. ^c No OH precursor was used.

TABLE 2. Summary of Experimental Conditions and Sulfate Ester Formation from α -Pinene Photooxidation

experiment	initial [α -pinene] (ppb)	initial [isoprene] (ppb)	initial [toluene] (ppm)	initial [NO _x] (ppb)	SO ₂ (ppb)	average T (°C)	[M-H] ⁻ detected sulfate ester ions (m/z) ^a
EPA-220	220	^b	^b	450	^b	25.5	none detected
EPA-326	186	1108	^b	248	287	20.5	249, 265, 294, 310, 412, 426
EPA-211 stage 1	105	^b	^b	378	^b	24.3	none detected
EPA-211 stage 2	105	^b	1.59	378	^b	24.3	none detected
EPA-211 stage 3	103	820	1.58	378	^b	24.3	none detected
EPA-211 stage 4	117	854	1.57	378	275	24.3	265, 279, 294, 310, 326, 412, 426
EPA-211 stage 5	115	^b	1.59	378	275	24.3	249, 265, 279, 294, 310, 326
EPA-211 stage 6	^b	794	1.56	378	^b	24.3	none detected
EPA-205	106	592	1.45	599	278	24.0	265, 294, 310, 412, 426

^a Isoprene sulfate ester products like those in Table 2 were also detected only when SO₂ and isoprene were copresent. No discernible toluene sulfate ester products were detected. ^b This compound was not present during the experiment.

low-NO_x experiments, only H₂O₂ was added, resulting in NO_x concentrations <1 ppb. Caltech high-NO_x experiments either used H₂O₂ and an initial amount of NO (~800 ppb), or with HONO and NO_x as a side product. In the Caltech experiments, three initial inorganic seed aerosol conditions were used: (1) the absence of aerosol where SOA formation was initiated by nucleation; (2) ammonium sulfate (AS) aerosol; and (3) acidified ammonium sulfate (AAS) aerosol. Concentrations of the aqueous solutions that were introduced into the chambers by atomization are shown in Table 1. The initial seed aerosol concentrations that resulted ranged from ~19–24 $\mu\text{g}/\text{m}^3$. Teflon filters (PALL Life Sciences, 47-mm diameter, 1.0- μm pore size, Teflon filters) were collected for offline chemical analysis from the Caltech experiments at the point at which the aerosol volume reached its maximum value, as determined by the differential mobility analyzer (DMA). All experiments were carried out at relative humidities (RHs) <9%.

In the dynamic experiments in the EPA chamber, reactants such as NO, SO₂, and isoprene were continuously added from high-pressure cylinders to the reaction chamber through a mixing manifold. The steady-state nature of chamber operation allows for filter sampling for extended periods for determining the composition of the resultant SOA. Once steady-state conditions were attained (~24 h), samples for determining the composition of the SOA were collected on glass fiber filters preceded by a carbon strip denuder. Two sets of EPA experiments were conducted. In the first set, the

following aerosol conditions were used: AS, AAS, and sulfuric acid, with each of the aqueous solutions atomized into the chamber by atomization. The initial aerosol concentrations were 0.1, 30.0, and 30.0 $\mu\text{g}/\text{m}^3$, for EPA-299 stage 1, EPA-299 stage 2, and EPA-299 stage 3, respectively. For the second set of EPA experiments, EPA-199 stage 1 and EPA-199 stage 2, acidic aerosol was generated by adding 60 and 200 ppb of SO₂, respectively to the reactant mixture. All EPA experiments were conducted at a relative humidity of ~30%. Results from both EPA experiments (i.e., SOA yields, gas-phase products, trends, etc.) will be discussed in more detail in forthcoming publications; evidence for organosulfates is the focus here.

α -Pinene Chamber Experiments. All α -pinene experiments were conducted in the EPA dynamic chamber (15). Conditions for each experiment are listed in Table 2. The EPA experiments consisted of one α -pinene/NO_x irradiation experiment along with a series of experiments where mixtures of hydrocarbons containing α -pinene were irradiated in the presence of NO_x. For some of these experiments, SO₂ was added to the chamber to generate acidity in the aerosol. The same collection protocol was used here as that employed in the EPA isoprene experiments.

Ambient Aerosol Collection. Ambient aerosol was collected from the Southeastern Aerosol Research and Characterization Study (SEARCH) network and analyzed for sulfate esters. This network comprises of four urban-rural (or urban-suburban) site pairs at locations across the southeast U.S. and was initiated in mid-1998 to carry out systematic

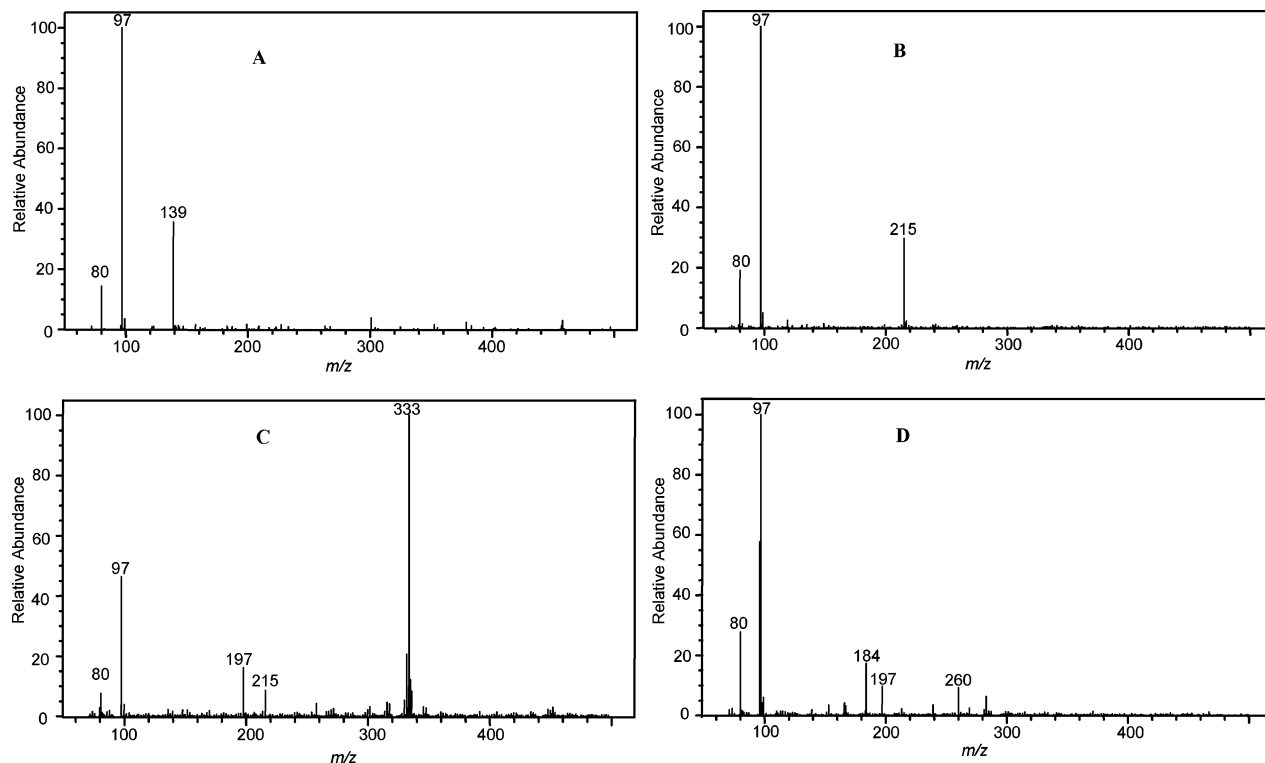


FIGURE 1. (–)LC/ESI–MS upfront CID mass spectra for selected isoprene sulfate ester SOA products shown in Table 2. (A) Product ion mass spectrum for sodium propyl sulfate standard (anionic mass of intact propyl sulfate ester = 139 Da). (B) Product ion mass spectrum for a 2-methyltetrol sulfate ester detected in a Caltech high- NO_x H_2O_2 AS seed photooxidation experiment. (C) Product ion mass spectrum for a hemiacetal dimer sulfate ester detected in a Caltech low- NO_x AAS seed photooxidation experiment. (D) Product ion mass spectrum for a C_5 trihydroxy nitrate sulfate ester detected in EPA-299 stage 2.

measurements of temporal and spatial variability of PM, in particular $\text{PM}_{2.5}$, gases relevant to secondary O_3 formation, and surface meteorology (22). Twenty-four h composite quartz filters were taken on 4 days at four different sites during June 2004: Birmingham, AL (BHM, urban site), Centerville, AL (CTR, rural site outside of BHM), Jefferson Street (JST, near downtown Atlanta, GA), and Pensacola, FL (PS, marine influenced urban site). Details of these sites (terrain, vegetation, transportation, and industrial sources), sample collection and handling procedures, and specific aerosol and gas-phase measurements obtained are given elsewhere (22, 30).

Filter Extraction and Chemical Analyses. Detailed extraction procedures for Teflon and quartz filters are described elsewhere (9, 22). Glass-fiber filters were extracted in the same manner as Teflon filters (9), except resultant extracts were filtered through a PALL Life Sciences Acrodisc CR 25 mm syringe filter (PTFE membrane, 0.2 μm pore size) to remove filter fibers. All sample extracts were analyzed by a Hewlett-Packard 1100 series HPLC instrument, coupled with a quadrupole mass spectrometer, and by direct infusion onto a ThermoElectron LCQ ion trap mass spectrometer (ITMS), both equipped with an ESI source operated in the negative (–) ionization mode. Details of the operating conditions for these instruments are described elsewhere (9). Briefly, all samples were analyzed on the LC/MS instrument in the full scan mode and upfront collision-induced dissociation (CID) mode of analysis. Comparison of the resulting mass spectra produced from these two modes of analyses on the LC/MS instrument allows for some structural information to be obtained on the detected SOA components. Samples were also analyzed on the ThermoElectron LCQ ITMS instrument to confirm these results, and in some cases, provide further structural elucidation. Sulfate standards of sodium propyl sulfate (City Chemical, 98% purity), sodium lauryl sulfate (City Chemical, 98% purity), and 1-butyl-3-methylimidazo-

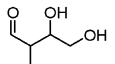
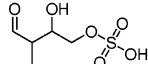
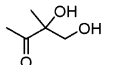
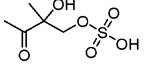
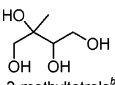
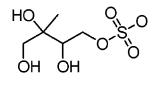
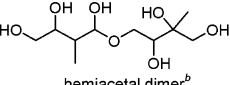
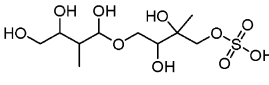
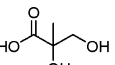
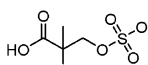
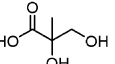
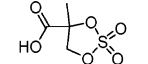
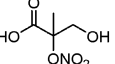
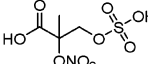
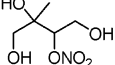
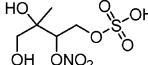
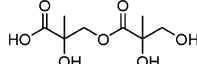
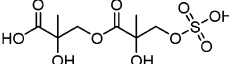
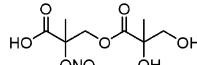
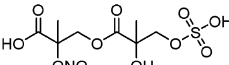
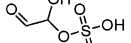
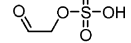
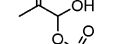
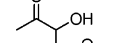
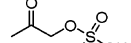
lium 2-(2-methoxyethoxy)ethyl sulfate (Sigma-Aldrich, 95% purity) were analyzed on the LC/MS instrument to determine common product ions associated with sulfate esters. Additional samples were collected with the particle-into-liquid sampler (PILS) with subsequent offline analysis by ion chromatography (IC) (31). The PILS/IC technique allows for the quantitative measurement of water-soluble inorganic ions in aerosol; no IC peaks could be attributed to organosulfates, so for these experiments only inorganic ions are measured.

Results

Sulfate Ester Standards. (–)ESI–MS studies have shown that sulfate esters produce abundant $[\text{M}-\text{H}]^-$ ions, and upon collisional activation of these ions, yield m/z 97 (HSO_4^-) and 80 (SO_3^-) product ions (21, 24, 25). In conjunction with the known isotopic distribution of sulfur, which contains ^{34}S with a natural abundance of 4.2%, these product ions can be used to identify sulfate esters. As confirmation, authentic standards of sodium propyl sulfate (anionic mass = 139 Da), sodium lauryl sulfate (anionic mass = 265 Da), and 1-butyl-3-methylimidazolium 2-(2-methoxyethoxy)ethyl sulfate (anionic mass = 199 Da) were analyzed by the (–)LC/ESI–MS technique in the full scan mode of analysis followed by the upfront CID mode of analysis to generate MS and MS/MS data, respectively. As shown for the sodium propyl sulfate ester standard in Figure 1A, these authentic standards yielded m/z 97 and 80 product ions.

Sulfate Esters from Isoprene Oxidation. Previously characterized (9, 10) isoprene SOA products were observed in these experiments and are shown in Table 3; however, the focus here will be on the identification of sulfate esters. Comparison of (–)ESI–MS data collected from experiments employing no sulfate aerosol to those with sulfate aerosol showed that numerous compounds were detected only when sulfate aerosol was present. To understand the nature of

TABLE 3. Proposed Isoprene Sulfate Ester SOA Products

	previously identified isoprene SOA product ^a	MW	proposed sulfate ester structure ^a	observed [M - H] ⁻ ion (m/z)	major [M - H] ⁻ product ions (m/z)
Low-NO _x	 C ₅ alkene triol / ald form ^b	118		197	97 80
	 C ₅ alkene triol / keto form ^b	118		197	97 80
	 2-methyltetrols ^b	136		215 ^{c,d}	97 80
	 hemiacetal dimer ^b	254		333 ^d	315 (- H ₂ O) ^e 215 (- C ₅ alkene triol) 197 (- 2-methyltetrol) 97 80
High-NO _x	 2-methylglyceric acid (2-MG) ^b	120		199 ^c	119 (- 2-MG) 97 80
	 2-methylglyceric acid (2-MG) ^b	120		181	97 80
	 2-MG acid nitrate ^b	165		244	226 (- H ₂ O) 197 (- HONO) 153 (- [CO ₂ + HONO]) 97
	 C ₅ trihydroxy nitrate ^f	181		260 ^g	197 (- HNO ₃) 183 (- CH ₃ NO ₃) 97 80
	 2-MG dimer ^b	222		301	257 (- CO ₂) 119 97 80
	 2-MG nitrate dimer ^b	267		346	^g
Highest Acidity Conditions	 glyoxal	58		155	^g
	 glycolaldehyde ^h	60		139	^g
	 methacrolein	70		167	^g
	 methylglyoxal ^h	72		169	^g
	 hydroxyacetone ^h	74		153	^g

^a Positional isomers containing nitrate or sulfate groups at other hydroxylated positions are likely. ^b Isoprene SOA products previously identified in prior studies by Surratt et al. (9) and/or Szmigielski et al. (10) and/or Edney et al. (15). ^c Detected in ambient aerosol collected from SEARCH network (summer 2004) for first time. ^d Considered major product due to large MS abundance in chamber studies. ^e Compounds listed in parentheses are neutral losses observed upon (-)ESI-MS/MS. ^f Inferred precursor due to the MS/MS fragmentation of its respective organosulfate product; this parent isoprene product goes undetected by (-)ESI-MS and GC/MS methods. ^g Some evidence for its existence in first-order mass spectra. ^h Detected in ambient aerosol by Matsunaga et al. (32).

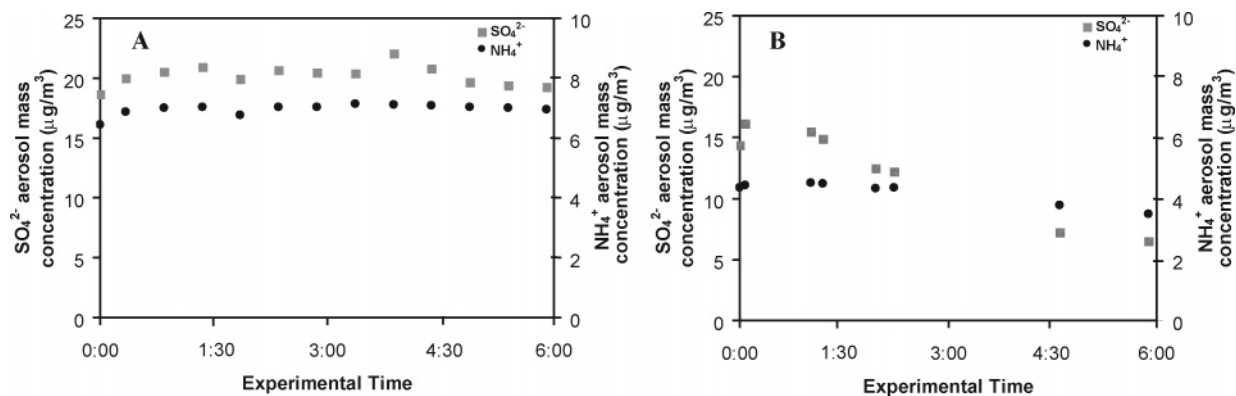


FIGURE 2. Time evolution of the SO_4^{2-} and NH_4^+ aerosol mass concentrations from the PILS/IC analysis. (A) Caltech high- NO_x H_2O_2 isoprene experiment with AS seed aerosol. (B) Caltech low- NO_x isoprene experiment with AAS seed aerosol. A control experiment was conducted in which seed aerosol is atomized from a solution of 0.015 M AS into the Caltech experimental chamber, and no other reactants such as VOCs or NO_x were present. This control experiment produced a similar result to that of Figure 2A (although not evident from the time scale presented, SO_4^{2-} and NH_4^+ decay by ~ 20 and 14%, respectively, over 9 h), indicating that the only loss mechanism for sulfate in this case was wall loss. Of the Caltech isoprene experiments, only the low- NO_x AAS seed aerosol experiment showed a significant decrease in the SO_4^{2-} aerosol mass concentration, indicating that it was likely lost to reaction.

these compounds, tandem MS techniques were employed. Figure 1B–D shows the LC/ESI–MS upfront CID mass spectra collected for large chromatographic peaks common to many of the sulfate aerosol experiments listed in Table 1. The $[\text{M}-\text{H}]^-$ ions associated with these chromatographic peaks include m/z 215, 333, and 260, respectively. As was the case for the sulfate ester standards, the collisional activation of these $[\text{M}-\text{H}]^-$ ions yielded m/z 97 and 80 product ions. In addition, these ions also had an isotopic distribution common to sulfur, and as a result, these compounds were identified as sulfate esters. The other product ions, observed in the spectra shown in Figure 1, provided further information on the chemical structures of the identified sulfate esters. Proposed sulfate ester structures for these ions and all other ions listed in Table 1 are given in Table 3. Many of the sulfate esters shown in Table 3 were formed from previously identified isoprene SOA products, including aldehydes, dicarbonyls, hydroxycarbonyls, alcohols, and acids containing an alcohol moiety (9, 10, 32). Sulfate esters formed from small volatile oxidation products, such as glyoxal, hydroxyacetone, and glycolaldehyde, were only detected in experiments involving the highest aerosol acidity. All sulfate esters listed in Table 3 eluted from the reverse-phase LC column within 3 min, indicating their high water solubility. For example, the m/z 215 sulfate ester had a retention time of ~ 1.4 min, close to that of the inorganic sulfate (first peak to elute). On the other hand, the m/z 260 sulfate ester was found to be slightly less polar with isomers eluting at 2.4, 2.7, and 2.9 min. The presence of a nitrate group was confirmed by its even-mass $[\text{M}-\text{H}]^-$ ion and the observation of a 63 Da (HNO_3) neutral loss shown in Figure 1D. Sulfate ester products given in Table 3 containing nitrate groups were detected only in experiments containing NO_x .

In several previous studies, the presence of acidic sulfate aerosol was found to have a pronounced effect on the quantity of SOA formed by the photooxidation of isoprene (9, 14, 15). In the present study, it appears that sulfate ester formation may be similarly enhanced by the introduction of an acidic sulfate aerosol. In the absence of significant levels of inorganic sulfate, no sulfate esters were detected by LC/ESI–MS in any of the isoprene systems considered here. When experiments were carried out in the presence of AS aerosols, a few sulfate esters were detected, including $[\text{M}-\text{H}]^-$ ions at m/z 199, 215, 244, 260, or 333. Experiments carried out under acidic conditions with AAS aerosol produced a considerably wider array of detectable sulfate ester compounds. In addition, the peak areas of several ions observed in both the AS and AAS experiments were found to be larger in the AAS

experiments. For example, in the low- NO_x experiments, the LC/MS peak area for the m/z 215 sulfate ester was found to double when AAS aerosol was used rather than nonacidic AS aerosol. Although quantitative data could not be obtained for either the sulfate ester concentrations or the effective acidity of the reaction system, these results suggest that sulfate ester formation is enhanced by the presence of an acidic sulfate aerosol, and that this enhanced sulfate ester formation may be contributing to the increased SOA mass detected previously under acidic conditions. Further work is needed in order to accurately quantify these sulfate esters. It was found that (–)LC/ESI–MS calibration curves generated by surrogate standards lacking sulfate groups (such as meso-erythritol) were not suitable for quantifying the identified sulfate esters, resulting from these standards having lower (–)ESI–MS sensitivities. The sulfate ester standards listed in the experimental section were also not suitable for quantification because these compounds had retention times much greater than ± 1 min of the retention times for the isoprene sulfate esters. Also, these standards lack many structural features common to the identified sulfate esters; therefore, synthesis of more representative standards is needed in order to quantify sulfate esters by (–)LC/ESI–MS.

Sulfate ester aerosol was atomized from a standard solution of sodium propyl sulfate and analyzed directly by the PILS/IC technique; no significant levels of inorganic sulfate were detected, suggesting that organosulfates are thermally stable at the operating conditions of this instrument. In addition, no chromatographic peak in the IC data could be attributed to the sulfate ester standard. These results suggest that the PILS/IC technique will observe decreases in inorganic sulfate if sulfate ester formation occurs.

The time evolution of the SO_4^{2-} and NH_4^+ aerosol mass concentrations obtained using the PILS/IC technique for a Caltech low- NO_x isoprene AAS seed aerosol experiment is compared to that of a Caltech high- NO_x AS seed aerosol experiment in Figure 2. As shown in Figure 2A (although not evident from the time scale presented, SO_4^{2-} and NH_4^+ decay by ~ 20 and 14%, respectively, over 9 h), a typical profile for most Caltech isoprene experiments in Table 1, ammonium and sulfate typically decreased slowly with time due to wall-loss processes. However, in the experiment shown in Figure 2B, in which sulfate ester concentrations were exceedingly high, the SO_4^{2-} aerosol mass concentration decreased much faster (i.e., SO_4^{2-} decayed by $\sim 60\%$ over 6 h) than wall loss, suggesting an extra loss process, most likely due to chemical reaction. It should be noted that the initial $\text{NH}_4^+:\text{SO}_4^{2-}$ molar ratio in Figure 2A was not exactly two due to a known source

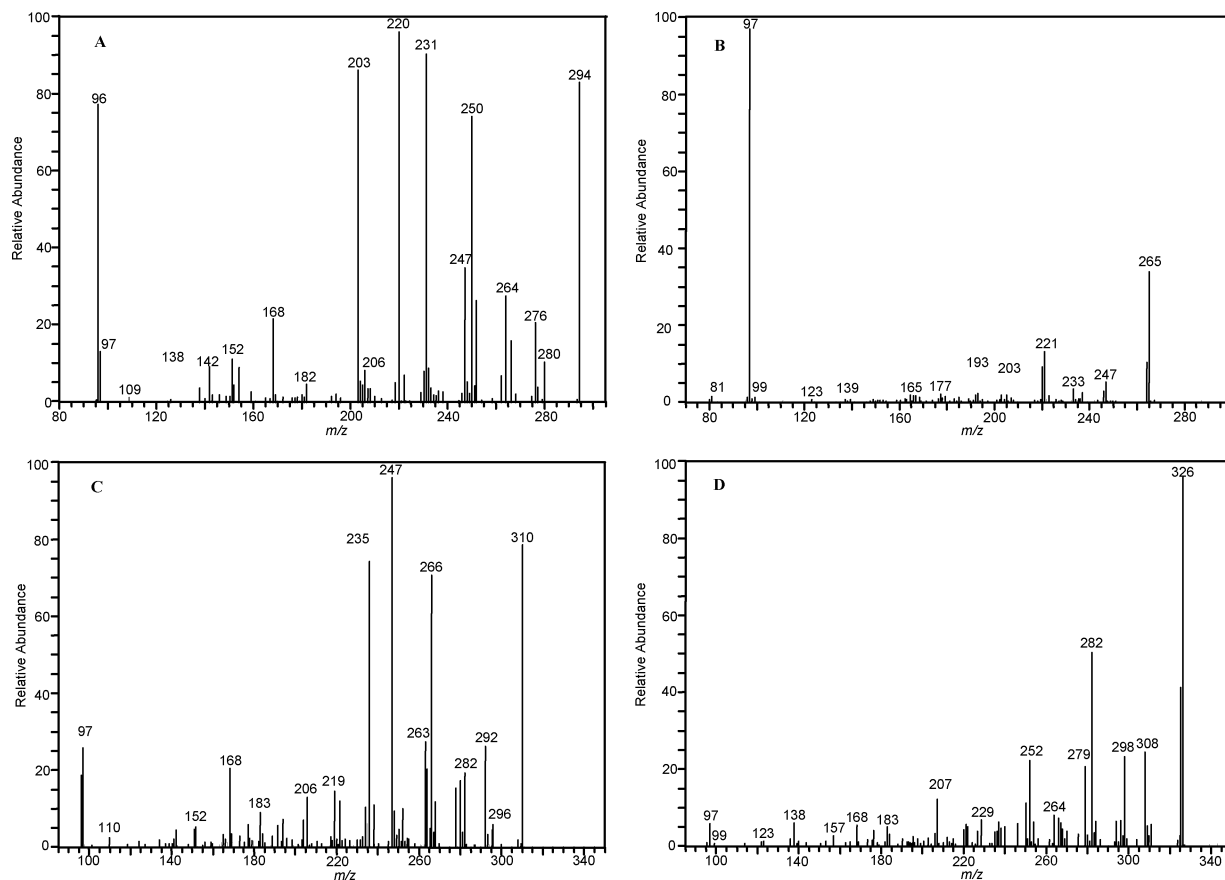


FIGURE 3. (–)ESI–ITMS product ion mass spectra for sulfate esters of α -pinene oxidation products. (A) Product ion mass spectrum for m/z 294 detected in EPA-211 stage 5. (B) Product ion mass spectrum for m/z 265 detected in EPA-211 stage 4. (C) Product ion mass spectrum for m/z 310 detected in EPA-211 stage 5. (D) Product ion mass spectrum for m/z 326 detected in EPA-211 stage 5. These sulfate esters were always present when α -pinene was photooxidized in the presence of SO_2 .

of ammonium volatilization previously characterized (31). The significant decrease in the SO_4^{2-} mass concentration observed for the Caltech low- NO_x AAS seed aerosol experiment is consistent with previously observed increases in SOA yields (9), strongly suggesting that particle-phase sulfate esterification is at least partly responsible for this “acid-effect.” Filter sampling for most Caltech isoprene experiments began ~ 5 – 7 h after the experiment was initiated; sulfate esters are formed by this point in the experiments as shown in Figure 2.

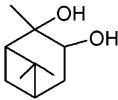
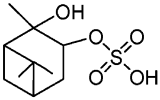
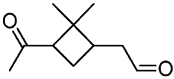
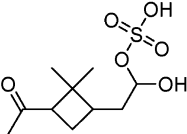
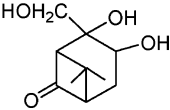
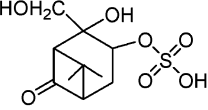
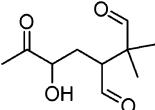
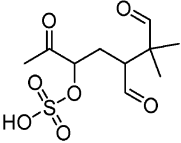
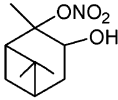
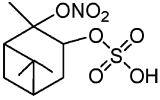
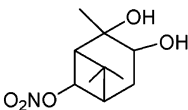
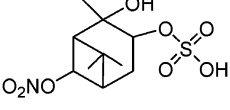
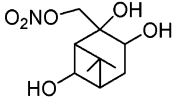
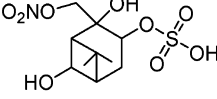
Sulfate Esters from α -Pinene Oxidation. As in the isoprene experiments, α -pinene sulfate esters were found to produce abundant $[\text{M}-\text{H}]^-$ ions, corresponding ^{34}S isotopic ions, m/z 97 and 80 product ions, and were not observed in experiments without SO_2 (Table 2). Isoprene sulfate esters were formed also in experiments involving isoprene and SO_2 photooxidation; for simplicity, these esters are not listed in Table 2. Shown in Figure 3A–D are the (–)ESI–ITMS product ion spectra for representative α -pinene sulfate esters; these include esters containing a $[\text{M}-\text{H}]^-$ ion at m/z 294, 265, 310, and 326, respectively. Analogous to some of the isoprene sulfate esters, the m/z 294, 310, and 326 α -pinene sulfate esters also contain nitrate groups as suggested by their even-mass $[\text{M}-\text{H}]^-$ ions and observed neutral losses of 63 (HNO_3) and/or 47 Da (HONO). The MS/MS spectra of the $[\text{M}-\text{H}]^-$ ions for the four α -pinene sulfate esters yielded m/z 97 product ions. However, the m/z 80 product ion was observed only for the m/z 265 ion due to mass range limits on the mass spectrometer. It should be noted that the MS³ spectra of high-mass product ions shown in Figure 3 (e.g., m/z 250 in Figure 1A) did yield the m/z 97 and m/z 80 product ions,

thus supporting that the $[\text{M}-\text{H}]^-$ ions at m/z 294, 310, and 326 contain a sulfate group. These results were confirmed on the LC/MS instrument operated in the upfront CID mode of analysis.

Sulfate esters from α -pinene were found to elute from the reverse-phase LC column at much later RTs (~ 10 – 26 min) than those formed in isoprene oxidation, indicating differences in water solubility. Identified α -pinene sulfate esters listed in Table 4 were formed from the reactive uptake of previously identified gas-phase oxidation products (33, 34), consistent with previous work (17, 18). Except for pinonaldehyde, no sulfate esters have been identified to form from previously identified α -pinene SOA products; however, further investigation is warranted. For quality control purposes, solid-phase extraction (SPE) was used on duplicate filters collected from selected experiments (EPA-211) to remove excess inorganic sulfate; it was found that the α -pinene sulfate esters were still detected, and in some cases at higher $[\text{M}-\text{H}]^-$ ion abundances, indicating that these sulfate esters are not a result of inorganic sulfate clusters in the mass spectrometer.

Sulfate Esters in Ambient Aerosol. Figures 4A–C compare the LC/MS extracted ion chromatograms (EICs) of m/z 215 obtained from a Caltech low- NO_x isoprene AAS experiment to that of two SEARCH field samples (JST and BHM, respectively). Both the RTs and mass spectra of the chromatographic peaks shown in the EICs of m/z 215 are the same in all samples, strongly suggesting that this isoprene sulfate ester is present in ambient aerosol. In addition, ambient aerosol recently collected at K-puszt, Hungary indicates that the m/z 199 and 260 isoprene sulfate esters

TABLE 4. Proposed α -Pinene Sulfate Ester SOA Products

α -pinene oxidation product ^a	MW	proposed sulfate ester structure ^a	observed [M - H] ⁻ ion (<i>m/z</i>)	major [M - H] ⁻ product ions (<i>m/z</i>)
	170		249	231 (- H ₂ O) ^b 205 97 80
 pinonaldehyde	168 ^c		265 ^{d,e}	247 (- H ₂ O) 221 185 97 (- pinonaldehyde) 80
	200 ^c		279 ^{e,f}	261 (- H ₂ O) 235 199 181 97 80
	200 ^c		279 ^{e,f}	261 (- H ₂ O) 235 199 181 97 80
	215 ^c		294 ^g	247 (- HONO) 231 (- HNO ₃) 220 96 80
	231 ^c		310 ^{g,h}	263 (- HONO) 236 247 (- HNO ₃) 97
	247		326 ^e	308 (- H ₂ O) 282 (- CO ₂) 279 (- HONO) 252 97

^a Positional isomers containing nitrate or sulfate groups at other hydroxylated positions are possible. ^bCompounds listed in parentheses are neutral losses observed upon ESI-MS/MS. ^cPreviously detected α -pinene oxidation product by Aschmann et al. (33, 34). ^dProposed by Liggio et al. (17) to form from pinonaldehyde reactive uptake onto acidic seed particles; however, structure was not confirmed. In the current study, we confirm its structure with (-)ESI-MS. ^eDetected in ambient aerosol collected from SEARCH network June 2004 for first time. ^fESI-MS cannot differentiate between which product is being detected; for completeness both structures are shown here. ^gObserved in an ambient study by Gao et al. (22). ^hNo structural information was provided in the previous study by Gao et al. (22).

are present (M. Claeys, unpublished results); however, these compounds are only weakly detected on some days analyzed from the SEARCH network.

Figure 5A–C compares the LC/MS EICs of *m/z* 294 obtained from two α -pinene experiments (EPA-205 and EPA-326, respectively) and with a SEARCH field sample collected at the BHM field site in June 2004. This figure indicates that the α -pinene *m/z* 294 sulfate ester is a constituent of ambient aerosol, consistent with previous work (22). Other α -pinene sulfate esters identified in this study have been observed in ambient aerosol in the southeastern U.S. (22). It is possible that the *m/z* 294 sulfate ester in the ambient aerosol could also result from the oxidation of other monoterpenes owing

to the lack of detailed connectivity of specific functional groups (e.g., sulfate esters and hydroxyls) provided by ESI-MS/MS methods.

The results above suggest that the chemistry occurring in our laboratory experiments are relevant to the conditions in the southeastern U.S., even though the laboratory aerosol was generated from much higher VOC mixing ratios, lower RHs, and likely higher aerosol acidities observed in the southeastern U.S.

ESI-MS Quality Control Tests. To ensure that the sulfate esters elucidated in this study were formed only during SOA formation and not on the filter or during the ESI process, several quality control tests were conducted. First, a filter

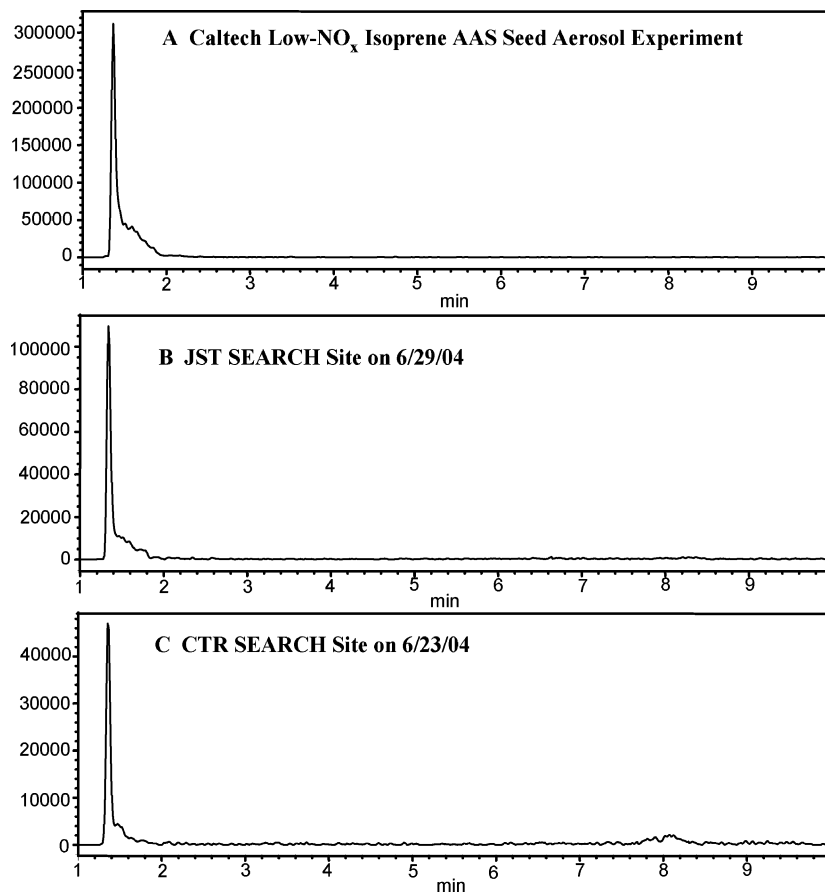


FIGURE 4. (–)LC/ESI–MS extracted ion chromatograms for m/z 215. The retention times of the m/z 215 EICs are the same as well as the mass spectra associated with each chromatographic peak; therefore, the comparison of these EICs suggests that the photooxidation of isoprene in the presence of acid seed produces these sulfate esters observed in the ambient aerosol. In all chamber experiments involving isoprene in the presence of AS seed aerosol, AAS seed aerosol, or SO_2 , the m/z 215 ion was detected.

extract from a Caltech low- NO_x isoprene nucleation (i.e., no inorganic seed aerosol present) experiment was divided into two parts. One part was spiked with a high concentration of $(\text{NH}_4)_2\text{SO}_4$ and the other part was spiked with pure H_2SO_4 . Both of these samples were analyzed by (–)LC/ESI–MS. The sulfate esters listed in Table 1 were not detected in these two test samples, demonstrating that the sulfate esters detected in this study are likely not artifacts formed in the ESI interface. The use of reverse phase chromatography allowed for inorganic sulfate not to be confused with organosulfates, where inorganic sulfate was the very first peak to elute from the column. In the two test samples discussed above, the inorganic sulfate peak was found to have some tailing, which was very similar to the seeded experiments listed in Table 1; however, this tailing seems to have no effect on the formation of sulfate esters.

As a second test, a *meso*-erythritol (a surrogate for the 2-methyltetrols produced from isoprene oxidation) standard was divided into two parts, where one was spiked with $(\text{NH}_4)_2\text{SO}_4$ and the other with pure H_2SO_4 . As for the first quality control test above, these two samples produced no sulfate esters in (–)LC/ESI–MS.

Last, a filter extract from an EPA α -pinene experiment conducted without SO_2 (thus no sulfate aerosol present) was spiked with pure H_2SO_4 . Again, no sulfate esters were detected. These results strongly suggest the organosulfates (sulfate esters) were formed in the aerosol phase and are not an artifact of sampling or measurement.

Discussion

Sulfate Esterification Reaction Mechanism. Reactive uptake of gas-phase alcohols (e.g., methanol and ethanol) and

aldehydes (e.g., formaldehyde) in the upper troposphere and lower stratosphere have been suggested to occur in the presence of sulfate aerosols (35–37), where increased acidity was found to increase their uptake. Some of these studies proposed that the observed uptake of the alcohols and aldehydes likely occurred by sulfate ester formation, although no product studies were conducted. It has also been shown that reactive uptake of butanol and ethanol onto sulfate aerosols occurs at room temperature (38, 39). Esterification was recently shown to occur from the photooxidation of isoprene in the presence of NO_x from condensation reactions of organic acids with alcohols (9, 10). The large amounts of organic acids formed during the photooxidation were proposed to drive these reactions.

Figure 6 shows the general reactions proposed for the formation of sulfate esters from alcohols (2-methyltetrol used as model compound) and sulfate derivatives from carbonyl compounds (pinonaldehyde used as model compound). In the case of sulfate ester formation from alcohols, the proposed reactions likely involve nucleophilic substitution ($\text{S}_\text{N}1$), where the sulfuric acid protonates the alcoholic group, making water the leaving group. The resulting carbocation becomes a nucleophilic site for the unshared pair of electrons on one of the oxygen atoms of the sulfate (40). Due to the low relative humidities of these experiments, this likely shifts the equilibrium in favor of sulfate ester formation. In the case of sulfate ester formation from aldehydes, the proposed reaction likely involves the electron pair of the carbonyl oxygen accepting a proton from sulfuric acid, producing the oxonium ion, and making it more susceptible to nucleophilic attack from an unshared pair of electrons from one of the oxygen atoms on sulfate. It should be stressed that other reaction

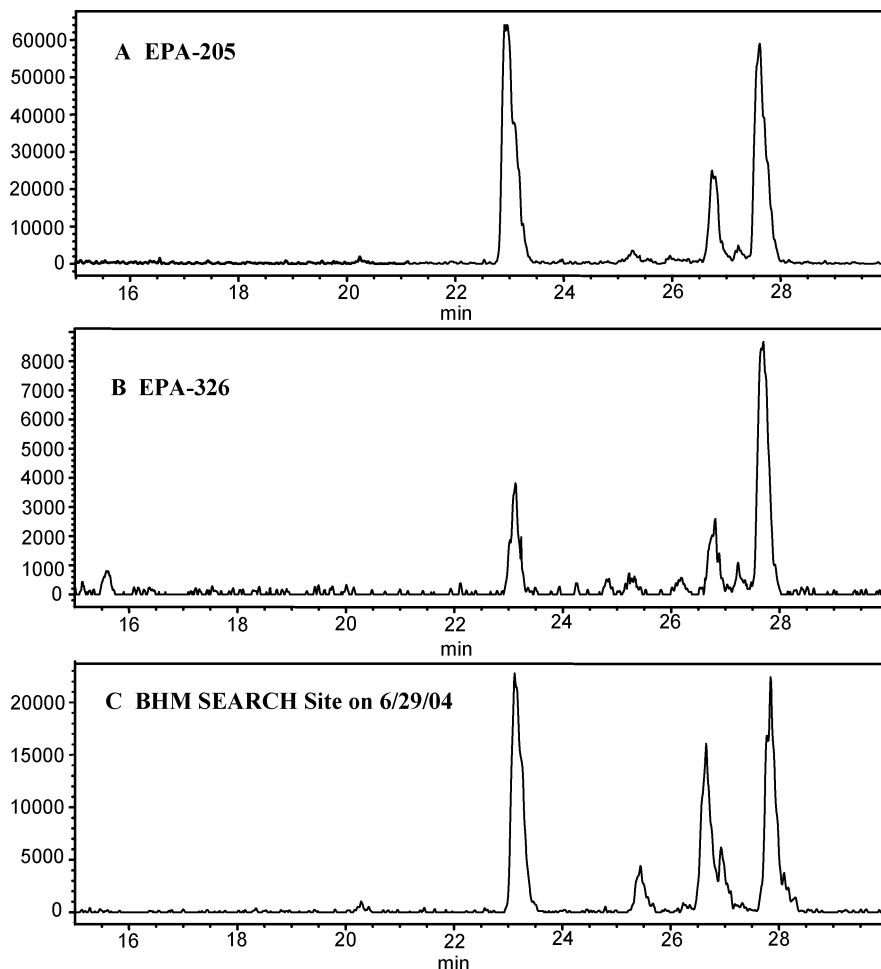


FIGURE 5. (–)LC/ESI–MS extracted ion chromatograms for m/z 294. The retention times of the m/z 294 compounds were the same as well as the mass spectra associated with each chromatographic peak; therefore, the comparison of these EICs suggests that the photooxidation of α -pinene in the presence of NO_x and acid seed produces these sulfate esters in ambient aerosol. No m/z 294 compounds were detected in experiments involving only isoprene and acid seed (or SO_2).

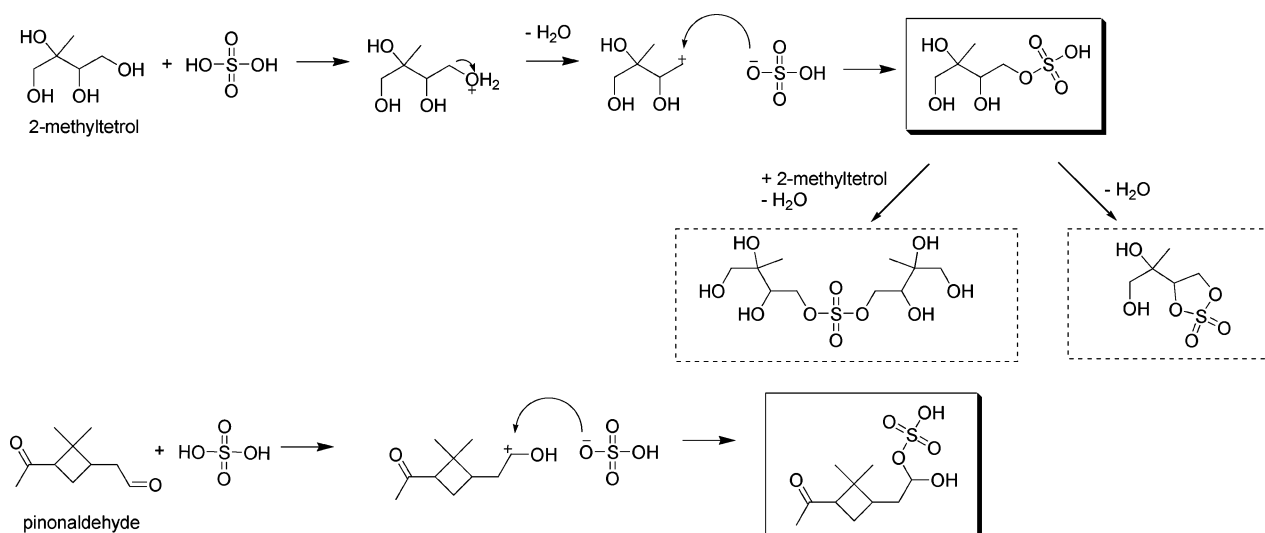


FIGURE 6. Proposed reactions for the formation of sulfate esters from 2-methyltetrol and pinonaldehyde, a representative alcohol and aldehyde generated by the photooxidation of isoprene and α -pinene, respectively. Solid boxes indicate (–)ESI–MS detected species. Dashed boxes indicate other proposed products possibly formed.

mechanisms are also possible, including: electrophilic addition of H_2SO_4 to an aliphatic double bond, addition of SO_3 through some radical process, or by some other unknown mechanism currently not understood. Sulfate diester (ROSO_3R) formation and sulfate ester oligomerization could also take

place in the case of polyols; however, (–)ESI–MS is not sensitive to such neutral species, no such products have yet been identified. In prior work (9) we reported oligomeric signatures (14, 16, 18 Da differences) and compounds with masses up to ~ 620 Da in matrix-assisted laser desorption

ionization (MALDI)–MS data collected for Caltech low-NO_x seeded experiments; AAS seed cases produced the most prominent signals, possibly providing evidence for the sulfate diester or sulfate ester oligomerization reactions.

Isoprene Sulfate Esters and the role of NO_x. Surratt et al. (9) observed a significant increase in the SOA yield in the low-NO_x AAS seed aerosol experiments, whereas very little (if any) increase in the SOA yield was observed in the high-NO_x AAS seed aerosol experiments. This difference likely occurs because of the large abundance of organic acids formed under high-NO_x conditions competing with sulfuric acid (or sulfate) for esterification with alcohols. The low-NO_x SOA was found to comprise largely of neutral polyols (e.g., 2-methyltetrols and hemiacetal dimers in Table 3) and hydroperoxides, which may react readily with sulfuric acid to produce sulfate esters. In previous work (9) we reported detecting no SOA components with (–)LC/ESI–MS for the low-NO_x seeded cases; reanalysis of that data indicates that sulfate esters (*m/z* 215, 333, and 415) were in fact detected, but because they eluted very closely to inorganic sulfate (within 1–1.5 min), they were believed to be an artifact.

Atmospheric Implications. Sulfate esters identified previously in ambient aerosol (21, 22) appear to be secondary in nature, as demonstrated by the present study. Of particular significance is the detection of sulfate esters from isoprene and α -pinene in ambient aerosols, which could be indicators for the acid induced reaction pathway. There is also the possibility that oxidation of other hydrocarbons emitted into the atmosphere in high abundances, including monoterpenes other than α -pinene as well as sesquiterpenes, could lead to the formation of aerosol-bound sulfate esters. These esters could contribute significantly to the HULIS fraction of ambient aerosol due to their high water-solubility, acidity, thermal stability, and high molecular weights, all of which are common properties of HULIS (41). Strong chemical evidence is presented here for the substantial occurrence of sulfate esterification in both laboratory-generated and ambient aerosols. This evidence provides one concrete explanation for the observed increase in SOA yields in response to increasing aerosol acidity. Additional studies are needed to determine the mass fraction of sulfate esters in ambient aerosols and the factors that influence their formation, such as relative humidity, temperature, and initial sulfate aerosol mass concentrations, in order to better understand and model this chemistry.

Acknowledgments

Research at Caltech was funded by the U.S. Environmental Protection Agency Science to Achieve Results (STAR) program grant no. RD-83107501-0, managed by EPA's Office of Research and Development (ORD), National Center for Environmental Research (NCER) and Cooperative Agreement CR-831194001, and by the U.S. Department of Energy, Biological, and Environmental Research Program DE-FG02-05ER63983. This article has been jointly developed and published by EPA and the California Institute of Technology. It was produced under Cooperative Agreement no. CR83194001 and is subject to 40 CFR 30.36. The article has been reviewed by EPA personnel under EPA scientific and technical peer review procedures and approved for joint publication based on its scientific merit, technical accuracy, or contribution to advancing public understanding of environmental protection. However, the Agency's decision to publish the article jointly with Caltech is intended to further the public purpose supported by Cooperative Agreement no. CR83194001 and not to establish an official EPA rule, regulation, guidance, or policy through the publication of this article. Further, EPA does not endorse any products or commercial services mentioned in this publication. J.D.S. was supported in part by the United States Environmental Protection Agency (EPA)

under the Science to Achieve Results (STAR) Graduate Fellowship Program. Research at the University of Antwerp was supported by the Belgian Federal Science Policy Office and the Research Foundation-Flanders (FWO). The Electric Power Research Institute provided support for the SEARCH network. We thank Rafal Szmigielski for his discussions on sulfation reactions.

Literature Cited

- (1) Kanakidou, M.; Seinfeld, J. H.; Pandis, S. N.; Barnes, I.; Dentener, F. J.; Facchini, M. C.; van Dingenen, R.; Ervens, B.; Nenes, A.; Nielsen, C. J.; Swietlicki, E.; Putaud, J. P.; Balkanski, Y.; Fuzzi, S.; Horth, J.; Moortgat, G. K.; Winterhalter, R.; Myhre, C. E. L.; Tsigaridis, K.; Vignati, E.; Stephanou, E. G.; Wilson, J. Organic aerosol and global climate modeling: a review. *Atmos. Chem. Phys.* **2005**, *5*, 1053–1123.
- (2) Gao, S.; Keywood, M.; Ng, N. L.; Surratt, J. D.; Varutbangkul, V.; Bahreini, R.; Flagan, R. C.; Seinfeld, J. H. Low-molecular-weight and oligomeric components in secondary organic aerosol from the ozonolysis of cycloalkenes and α -pinene. *J. Phys. Chem. A* **2004**, *108*, 10147–10164.
- (3) Gao, S.; Ng, N. L.; Keywood, M.; Varutbangkul, V.; Bahreini, R.; Nenes, A.; He, J.; Yoo, K. Y.; Beauchamp, J. L.; Hodyss, R. P.; Flagan, R. C.; Seinfeld, J. H. Particle phase acidity and oligomer formation in secondary organic aerosol. *Environ. Sci. Technol.* **2004**, *38*, 6582–6589.
- (4) Tolocka, M. P.; Jang, M.; Ginter, J. M.; Cox, F. J.; Kamens, R. M.; Johnston, M. V. Formation of oligomers in secondary organic aerosol. *Environ. Sci. Technol.* **2004**, *38*, 1428–1434.
- (5) Tobias, H. J.; Ziemann, P. J. Thermal desorption mass spectrometric analysis of organic aerosol formed from reactions of 1-tetradecene and O₃ in the presence of alcohols and carboxylic acids. *Environ. Sci. Technol.* **2000**, *34*, 2105–2115.
- (6) Docherty, K. S.; Wu, W.; Lim, Y. B.; Ziemann, P. J. Contributions of organic peroxides to secondary aerosol formed from reactions of monoterpenes with O₃. *Environ. Sci. Technol.* **2005**, *39*, 4049–4059.
- (7) Jang, M.; Kamens, R. M. Atmospheric secondary aerosol formation by heterogeneous reactions of aldehydes in the presence of sulfuric acid aerosol catalyst. *Environ. Sci. Technol.* **2001**, *35*, 4758–4766.
- (8) Jang, M.; Czoschke, N. M.; Lee, S.; Kamens, R. M. Heterogeneous atmospheric aerosol production by acid-catalyzed particle-phase reactions. *Science* **2002**, *298*, 814–817.
- (9) Surratt, J. D.; Murphy, S. M.; Kroll, J. H.; Ng, N. L.; Hildebrandt, L.; Sorooshian, A.; Szmigielski, R.; Vermeylen, R.; Maenhaut, W.; Claeys, M.; Flagan, R. C.; Seinfeld, J. H. Chemical composition of secondary organic aerosol formed from the photooxidation of isoprene. *J. Phys. Chem. A* **2006**, *110*, 9665–9690.
- (10) Szmigielski, R.; Surratt, J. D.; Vermeylen, R.; Szmigielska, K.; Kroll, J. H.; Ng, N. L.; Murphy, S. M.; Sorooshian, A.; Seinfeld, J. H.; Claeys, M. Characterization of 2-methylglyceric acid oligomers in secondary organic aerosol formed from the photooxidation of isoprene using trimethylsilylation and gas chromatography / ion trap mass spectrometry. *J. Mass. Spectrom.* **2006**, doi 10.1002/jms.1146.
- (11) Barsanti, K. C.; Pankow, J. F. Thermodynamics of the formation of atmospheric organic particulate matter by accretion reactions—part 1: aldehydes and ketones. *Atmos. Environ.* **2004**, *38*, 4371–4282.
- (12) Barsanti, K. C.; Pankow, J. F. Thermodynamics of the formation of atmospheric organic particulate matter by accretion reactions—part 2: dialdehydes, methylglyoxal, and diketones. *Atmos. Environ.* **2005**, *39*, 6597–6607.
- (13) Iinuma, Y.; Böge, O.; Gnauk, T.; Hermann, H. Aerosol-chamber study of the α -pinene/O₃ reaction: influence of particle acidity on aerosol yields and products. *Atmos. Environ.* **2004**, *38*, 761–773.
- (14) Kleindienst, T. E.; Edney, E. O.; Lewandowski, M.; Offenberg, J. H.; Jaoui, M. Secondary organic carbon and aerosol yields from the irradiations of isoprene and α -pinene in the presence of NO_x and SO₂. *Environ. Sci. Technol.* **2006**, *40*, 3807–3812.
- (15) Edney, E. O.; Kleindienst, T. E.; Jaoui, M.; Lewandowski, M.; Offenberg, J. H.; Wang, W.; Claeys, M. Formation of 2-methyltetrols and 2-methylglyceric acid in secondary organic aerosol from laboratory irradiated isoprene/NO_x/SO₂/air mixtures and their detection in ambient PM_{2.5} samples collected in the eastern United States. *Atmos. Environ.* **2005**, *39*, 5281–5289.

- (16) Liggio, J.; Li, S.; McLaren, R. Heterogeneous reactions of glyoxal on particulate matter: identification of acetals and sulfate esters. *Environ. Sci. Technol.* **2005**, *39*, 1532–1541.
- (17) Liggio, J.; Li, S. Organosulfate formation during the uptake of pinonaldehyde on acidic sulfate aerosols. *Geophys. Res. Lett.* **2006**, *33*, L13808, doi:10.1029/2006GL026079.
- (18) Liggio, J.; Li, S. Reactive uptake of pinonaldehyde on acidic aerosols. *J. Geophys. Res.* **2006**, in press.
- (19) Blando, J. D.; Porcja, R. J.; Li, T.; Bowman, D.; Lioy, P. J.; Turpin, B. J. Secondary formation and the smoky mountain organic aerosol: an examination of aerosol polarity and functional group composition during SEAVS. *Environ. Sci. Technol.* **1998**, *32*, 604–613.
- (20) Maria, S. F.; Russell, L. M.; Turpin, B. J.; Porcja, R. J.; Campos, T. L.; Weber, R. J.; Huebert, B. J. Source signatures of carbon monoxide and organic functional groups in Asian Pacific Regional Characterization Experiment (ACE-Asia) submicron aerosol types. *J. Geophys. Res.* **2003**, *108*, 8637–8650.
- (21) Romero, F.; Oehme, M. Organosulfates—a new component of humic-like substances in atmospheric aerosols? *J. Atmos. Chem.* **2005**, *52*, 283–294.
- (22) Gao, S.; Surratt, J. D.; Knipping, E. M.; Edgerton, E. S.; Shahgholi, M.; Seinfeld, J. H. Characterization of polar organic components in fine aerosols in the southeastern United States: identity, origin, and evolution. *J. Geophys. Res.* **2006**, *111*, D14314, doi:10.1029/2005JD006601.
- (23) Murray, S.; Baillie, T. A. Direct derivatization of sulphate esters for analysis by gas chromatography mass spectrometry. *Biomed. Mass Spectrom.* **1979**, *6*, 81–89.
- (24) Boss, B.; Richling, E.; Herderich, M.; Schreier, P. HPLC-ESI-MS/MS analysis of sulfated flavor compounds in plants. *Phytochemistry* **1999**, *50*, 219–225.
- (25) Metzger, K.; Rehberger, P. A.; Erben, G.; Lehmann, W. D. Identification and quantification of lipid sulfate esters by electrospray ionization MS/MS techniques: cholesterol sulfate. *Anal. Chem.* **1995**, *67*, 4178–4183.
- (26) Cocker, D.; Flagan, R. C.; Seinfeld, J. H. State-of-the-art chamber facility for studying atmospheric aerosol chemistry. *Environ. Sci. Technol.* **2001**, *35*, 2594–2601.
- (27) Keywood, M.; Varutbangkul, V.; Bahreini, R.; Flagan, R. C.; Seinfeld, J. H. Secondary organic aerosol formation from the ozonolysis of cycloalkenes and related compounds. *Environ. Sci. Technol.* **2004**, *38*, 4157–4164.
- (28) Kroll, J. H.; Ng, N. L.; Murphy, S. M.; Flagan, R. C.; Seinfeld, J. H. Secondary organic aerosol formation from isoprene photooxidation under high-NO_x conditions. *Geophys. Res. Lett.* **2005**, *32*, L18808, doi:10.1029/2005GL023637.
- (29) Kroll, J. H.; Ng, N. L.; Murphy, S. M.; Flagan, R. C.; Seinfeld, J. H. Secondary organic aerosol formation from isoprene photooxidation. *Environ. Sci. Technol.* **2006**, *40*, 1869–1877.
- (30) Hansen, D.; Edgerton, E. S.; Hartsell, B. E.; Jansen, J. J.; Kandasamy, N.; Hidy, G. M.; Blanchard, C. L. The southeastern aerosol research and characterization study: Part 1—overview. *J. Air Waste Manage.* **2003**, *53*, 1460–1471.
- (31) Sorooshian, A.; Brechtel, F. J.; Ma, Y.; Weber, R. J.; Corless, A.; Flagan, R. C.; Seinfeld, J. H. Modeling and characterization of a particle-into-liquid sampler (PILS). *Aerosol Sci. Technol.* **2006**, *40*, 396–409.
- (32) Matsunaga, S. N.; Wiedinmyer, C.; Guenther, A. B.; Orlando, J. J.; Karl, T.; Toohey, D. W.; Greenberg, J. P.; Kajii, Y. Isoprene oxidation products are significant atmospheric aerosol components. *Atmos. Chem. Phys. Discuss.* **2005**, *5*, 11143–11156.
- (33) Aschmann, S. M.; Reissell, A.; Atkinson, R.; Arey, J. Products of the gas phase reactions of the OH radical with α - and β -pinene in the presence of NO. *J. Geophys. Res.* **1998**, *103*, 25553–25561.
- (34) Aschmann, S. M.; Atkinson, R.; Arey, J. Products of reaction of OH radicals with α -pinene. *J. Geophys. Res.* **2002**, *107*, 4191–4197.
- (35) Iraci, L. T.; Tolbert, M. A. Heterogeneous interaction of formaldehyde with cold sulfuric acid: Implications for the upper troposphere and lower stratosphere. *J. Geophys. Res.* **1997**, *102*, 16099–16107.
- (36) Kane, S. M.; Leu, M. Uptake of methanol vapor in sulfuric acid solutions. *J. Phys. Chem. A* **2001**, *205*, 1411–1415.
- (37) Michelsen, R. R.; Staton, J. R.; Iraci, L. T. Uptake and dissolution of gaseous ethanol in sulfuric acid. *J. Phys. Chem. A* **2006**, *110*, 6711–6717.
- (38) Hanson, D. R.; Eisele, F. L.; Ball, S. M.; McMurry, P. M. Sizing small sulfuric acid particles with an ultrafine particle condensation nucleus counter. *Aerosol Sci. Technol.* **2002**, *36*, 554–559.
- (39) Joutsensaari, J.; Toivonen, T.; Vaattovaara, P.; Vestnerinen, M.; Vepsäläinen, J.; Laaksonen, A. Time-resolved growth behavior of acid aerosols in ethanol vapor with a tandem-DMA technique. *J. Aerosol Sci.* **2004**, *35*, 851–867.
- (40) Deno, N. C.; Newman, M. S. Mechanism of sulfation of alcohols. *J. Am. Chem. Soc.* **1950**, *72*, 3852–3856.
- (41) Graber, E. R.; Rudich, Y. Atmospheric HULIS: how humic-like are they? A comprehensive and critical review. *Atmos. Chem. Phys.* **2006**, *6*, 729–753.

Received for review August 30, 2006. Revised manuscript received October 18, 2006. Accepted November 3, 2006.

ES062081Q

Appendix E

Characterization of 2-Methylglyceric Acid Oligomers in Secondary Organic Aerosol Formed from the Photooxidation of Isoprene Using Trimethylsilylation and Gas Chromatography/Ion Trap Mass Spectrometry*

* This chapter is reproduced by permission from “Secondary Organic Aerosol Formed from the Photooxidation of Isoprene Using Trimethylsilylation and Gas Chromatography/Ion Trap Mass Spectrometry” by R. Szmigielski, J. D. Surratt, R. Vermeylen, K. Szmigueliska, J. H. Kroll, N. L. Ng, S. M. Murphy, A. Sorooshian, J. H. Seinfeld, M. Claeys, *Journal of Mass Spectrometry*, 42, 101-116, 2007. Copyright 2006, John Wiley & Sons, Ltd.

Characterization of 2-methylglyceric acid oligomers in secondary organic aerosol formed from the photooxidation of isoprene using trimethylsilylation and gas chromatography/ion trap mass spectrometry

Rafal Szmigielski,¹ Jason D. Surratt,² Reinhilde Vermeylen,¹ Katarzyna Szmigielska,¹ Jesse H. Kroll,^{3,4} Nga L. Ng,⁴ Shane M. Murphy,⁴ Armin Sorooshian,⁴ John H. Seinfeld^{3,4} and Magda Claeys^{1*}

¹ Department of Pharmaceutical Sciences, University of Antwerp (Campus Drie Eiken), Universiteitsplein 1, BE-2610 Antwerp, Belgium

² Department of Chemistry, California Institute of Technology, Pasadena, CA 91125, USA

³ Department of Environmental Science and Engineering, California Institute of Technology, Pasadena, CA 91125, USA

⁴ Department of Chemical Engineering, California Institute of Technology, Pasadena, CA 91125, USA

Received 12 July 2006; Accepted 24 October 2006

In the present work, we have characterized in detail the chemical structures of secondary organic aerosol (SOA) components that were generated in a smog chamber and result from the photooxidation of isoprene under high-NO_x conditions typical for a polluted atmosphere. Isoprene high-NO_x SOA contains 2-methylglyceric acid (2-MG) and oligoester derivatives thereof. Trimethylsilylation, in combination with capillary gas chromatography (GC)/ion trap mass spectrometry (MS) and detailed interpretation of the MS data, allowed structural characterization the polar oxygenated compounds present in isoprene SOA up to 2-MG trimers. GC separation was achieved between 2-MG linear and branched dimers or trimers, as well as between the 2-MG linear dimer and isomeric mono-acetate derivatives thereof. The electron ionization (EI) spectra of the trimethylsilyl derivatives contain a wealth of structural information, including information about the molecular weight (MW), oligoester linkages, terminal carboxylic and hydroxymethyl groups, and esterification sites. Only part of this information can be achieved with a soft ionization technique such as electrospray (ESI) in combination with collision-induced dissociation (CID). The methane chemical ionization (CI) data were used to obtain supporting MW information. Interesting EI spectral differences were observed between the trimethylsilyl derivatives of 2-MG linear and branched dimers or trimers and between 2-MG linear dimer mono-acetate isomers. Copyright © 2006 John Wiley & Sons, Ltd.

KEYWORDS: isoprene; 2-methylglyceric acid; oligomers; secondary organic aerosol; trimethylsilylation; gas chromatography/mass spectrometry; oligoesters

INTRODUCTION

Isoprene (2-methyl-1,3-butadiene, C₅H₈) is a volatile organic compound (VOC) that is emitted in large amounts by terrestrial vegetation, estimated at about 500 Tg/year worldwide.¹ In the past, isoprene was assumed not to contribute significantly to secondary organic aerosol (SOA) formation because of the high volatility of its first-generation oxidation products (i.e. methacrolein, methyl vinyl ketone and formaldehyde).² However, during the past 3 years evidence from both field^{3–7} and laboratory^{4,8–13} studies has been obtained that isoprene is photooxidized to polar oxygenated products which are present in the aerosol phase. The aerosol yields from photooxidation of isoprene are rather

low (maximum about 3%),^{11,12} a recent modeling study, however, shows that this aerosol source is quite significant on a global scale.¹⁴ Knowledge of the detailed chemical structures of isoprene oxidation products is required in order to gain insights into the underlying photochemical oxidation mechanisms of isoprene, which so far are only partially understood.

In a recent work,¹⁰ we characterized the chemical structures of SOA components that were produced in a smog chamber from photooxidation of isoprene under both high- and low-NO_x conditions. A combination of several mass spectrometric techniques was used, including electrospray ionization (ESI), matrix-assisted laser desorption ionization (MALDI), aerosol mass spectrometry (MS), and derivatization gas chromatography (GC). It was shown in that study that isoprene high-NO_x SOA contains 2-methylglyceric acid (2-MG), formed by further photooxidation of methacrolein, a

*Correspondence to: Magda Claeys, Department of Pharmaceutical Sciences, University of Antwerp (Campus Drie Eiken), Universiteitsplein 1, BE-2610 Antwerp, Belgium.
E-mail: magda.claeys@ua.ac.be

first-generation oxidation product of isoprene, and oligoester derivatives of 2-MG.

Soft ionization techniques such as ESI and MALDI are widely used currently in the analysis of oligomers and polymers, including oligomeric substances formed by photooxidation of biogenic and anthropogenic hydrocarbons such as isoprene,¹³ α -pinene,^{15–18} cycloalkenes¹⁶ and trimethylbenzene.¹⁹ Combination of these techniques with collision-induced dissociation (CID) and tandem MS techniques generally only partially provide the structural information that is needed for elucidation of unknown multifunctional compounds. In the case of the oligomeric isoprene SOA compounds studied here, partial structural information was obtained by (–/+)-ESI-ion trap MS and by upfront CID mode of analysis on a LC/ESI-MS instrument.¹⁰ The major fragmentation observed for 2-MG oligomers was loss of 102 Da 2-MG residue(s), likely corresponding to 2-hydroxy-2-methylpropiolactone and formed through a nucleophilic reaction directed by the negative charge on the terminal ionized carboxylic acid function. In the present study, we demonstrate that additional structural information can be achieved on oligomeric isoprene SOA compounds by trimethylsilylation in combination with GC/ion trap MS and detailed interpretation of the electron ionization (EI) spectra.

A derivatization protocol based on methylation of carboxylic acid functions prior to trimethylsilylation of neutral hydroxyl groups has been successfully applied in a previous work²⁰ to the analysis of polar oxygenated compounds present in organic aerosol. In the present work, preference was given to a one-step trimethylsilylation procedure that converts neutral and acidic hydroxyl functions to trimethylsilyl (TMS) ether or ester functions and allows the analysis of polar multifunctional compounds in the EI and/or chemical ionization (CI) mode. The EI mass spectra of trimethylsilylated compounds generally contain a wealth of structural information but often provide insufficient molecular weight (MW) information.^{6,20,21} The latter shortcoming can however be overcome by recording spectra in the CI mode. In the EI mode, information can be obtained on functional groups and their locations owing to the fragmentation-directing effect of ionized trimethylsilylated hydroxyl groups. Rearrangement reactions of the trimethylsilyl group may occur, rendering EI mass spectra quite complex and difficult to interpret, but have the merit that they can yield structurally characteristic ions.

The isoprene high-NO_x SOA examined in the present study contains 2-MG, 2-MG dimers, 2-MG dimer monoacetate derivatives, and 2-MG trimers. We will first discuss the EI fragmentation behaviors of the 2-MG monomer and its oligomeric derivatives. In addition, we will examine the fragmentation behaviors of the ethyl ester derivatives that are formed by subjecting isoprene high-NO_x SOA to acidic hydrolysis in ethanol. Part of this work has been briefly presented in our previous study dealing with the overall chemical composition and mechanism of SOA formed from the photooxidation of isoprene under low- and high-NO_x conditions.¹⁰

EXPERIMENTAL

Aerosol samples and workup

SOA was generated from isoprene (500 ppb) in Caltech's indoor 28 m³ Teflon chambers using hydrogen peroxide as the OH radical precursor and 800 ppb NO; the oxidation reaction was initiated by UV irradiation,^{11,12} and the SOA was collected on Teflon filters. Full details about SOA generation from isoprene are given in our previous study.¹⁰ The SOA sample used in the present study was from a high-NO_x isoprene nucleation (seed-free) experiment (Experiment 5). 2-MG and a branched and linear dimer thereof were prepared by reacting methacrylic acid (250 μ l; purity, 99%; Sigma, St. Louis, MI, USA) with hydrogen peroxide (250 μ l; 50% aqueous solution) in the presence of formic acid (125 μ l) for ten days at room temperature, following a procedure adapted from a previously reported one.⁴ The yield of 2-MG, as determined by trimethylsilylation GC with flame ionization detection and using glyceric acid (Sigma) as an internal recovery standard, was 222 mg; the 2-MG linear and branched dimer were produced in small yield (combined yield estimated at about 3.3 mg assuming a similar EI response as 2-MG), and the ratio branched/linear 2-MG dimer was 1:10.

The sample workup of the isoprene SOA sample consisted of extraction of the filter with methanol under ultrasonic agitation and derivatization. The extract was divided into two parts; one part was trimethylsilylated, while the other part was subjected to a hydrolysis/ethylation procedure. For analysis of the methacrylic acid reaction products, 2 μ l of the 30 times diluted reaction mixture (with methanol) was dried and trimethylsilylated. Trimethylsilylation was performed by reacting the extract residue with 40 μ l of a mixture containing 1 ml *N*-methyl-*N*-trimethylsilyltrifluoroacetamide (+1% trimethylchlorosilane) (Pierce, Rockford, IL, USA) and 500 μ l of dry pyridine (Merck) for an hour at 70 °C. The reagent employed for deuterium labeling of the TMS methyl groups, *N,O*-bis(trimethyl-²H₉-silyl)acetamide, was obtained from Cambridge Isotope Laboratories (Andover, MA, USA). The hydrolysis/ethylation procedure involved reaction of the extract residue with 40 μ l of analytical-grade ethanol and 8 μ l of trimethylchlorosilane (Supelco, Bellefonte, PA, USA) for 1 h at 60 °C. Aliquots of 1 μ l were used for GC/MS analysis and were injected in the splitless mode.

GC/ion trap MS

GC/MS analyses were performed with a system comprising a TRACE GC2000 gas chromatograph, which was coupled to a Polaris Q ion trap mass spectrometer equipped with an external ionization source (ThermoElectron, San Jose, CA, USA). A Heliflex AT-5MS fused-silica capillary column (5% phenyl, 95% methylpolysiloxane, 0.25 μ m film thickness, 30 m \times 0.25 mm i.d.) preceded by a deactivated fused-silica precolumn (2 m \times 0.25 mm i.d.) (Alltech, Deerfield, IL, USA) was used to separate the derivatized extracts. Helium was used as the carrier gas at a flow rate of 1.2 ml/min. The temperature program was as follows: isothermal hold at 50 °C for 5 min, temperature ramp of 3 °C/min up to 200 °C, isothermal hold at 200 °C for 2 min, temperature ramp of

30 °C/min up to 310 °C; and isothermal hold at 310 °C for 2 min. The analyses were performed in the full-scan mode (mass range: m/z 50–800), and were first carried out in the EI mode and subsequently in the CI mode. The ion source was operated at an electron energy of 70 eV and temperatures of 200 °C and 140 °C in the EI and CI modes, respectively. The temperatures of the GC injector and the GC/MS transfer line were 250 °C and 280 °C, respectively. For CI, methane was introduced as the reagent gas at a flow rate of 1.8 ml/min. We present here mainly data collected in the EI mode; data collected in the CI mode was used to obtain supporting MW information.

For CID experiments, the ions of interest were activated by applying a percentage of a 5-V supplementary a.c. potential to the end-caps of the ion trap at the resonance frequency of the selected ion [referred to as *collision energy level* (CEL)]. The CEL was 16%, while the excitation time was 15 ms. Helium was introduced as damping and collision gas at a flow rate of 1.1 ml/min. In some cases, MS/MS experiments were performed on several mass-selected precursor ions sequentially during the same chromatographic run. For this purpose, the width of the isolation waveform at which the ion trap separation of the precursor ions turned out to be the best was determined; the optimized value ranged between 3.5 and 5 a.m.u. For each precursor ion, the excitation time was 12 ms.

RESULTS AND DISCUSSION

Figure 1 shows a GC/MS total ion current chromatogram (TIC) obtained for SOA produced from the photooxidation of isoprene under high-NO_x conditions. Compound **1** was identified as the dihydroxymonocarboxylic acid, 2-MG (where 2-methylglyceric acid is its common name), which has retained part of the isoprene skeleton. This compound was reported for the first time in rural PM_{2.5} aerosol collected at K-pusztá, Hungary, during a 2003 summer field campaign,⁴

and has since been reported in several field studies.^{5,7,8} In addition, it was shown in smog chamber studies that 2-MG is formed by photooxidation of isoprene⁸ and, more specifically, by further oxidation of methacrolein, which is a first-generation photooxidation product of isoprene.¹⁰ Compound **2a** was characterized in our previous laboratory study as a linear oligoester dimer of 2-MG (denoted as 2-MG linear dimer), using a combination of several MS techniques, including ESI-MS, MALDI-MS, aerosol-MS, and trimethylsilylation GC/MS.¹⁰ In the present work, we discuss the EI behavior of the TMS derivative of the 2-MG linear dimer in more detail and compare it with that of the branched dimer (**2b**), which is not formed during photooxidation of isoprene under high-NO_x conditions (and therefore is not shown in Fig. 1) but which together with the 2-MG linear dimer is produced as a minor reaction product during the acid-catalyzed oxidation of methacrylic acid with hydrogen peroxide. The 2-MG branched dimer was found to elute at an earlier retention time (RT = 50.37 min) compared to the linear dimer (RT = 51.59 min) (GC/MS TIC not shown). No conclusions can be drawn about the relative amounts of 2-MG and its oligoester derivatives in the samples since it is possible that 2-MG oligoester derivatives are partially degraded owing to hydrolysis during the trimethylsilylation procedure which uses an acidic catalyst (i.e. trimethylchlorosilane). Figure 2 shows the m/z 219 mass chromatogram obtained after subjecting the isoprene high-NO_x SOA extract to acidic hydrolysis in ethanol, an experiment that was performed to obtain evidence for ester linkages in the 2-MG oligomers. Compounds identified are the ethyl ester derivatives of 2-MG (**1-Et**), a branched (**2b-Et**) and linear 2-MG dimer (**2a-Et**), and a branched (**3b-Et**) and linear 2-MG trimer (**3a-Et**). In a following section, we will first discuss in detail the rather complex fragmentation behavior of the TMS derivatives of 2-MG (**1**) and its ethyl derivative (**1-Et**) and will limit the discussion to diagnostic ions with m/z values >140. In subsequent sections, we will then use this information to derive

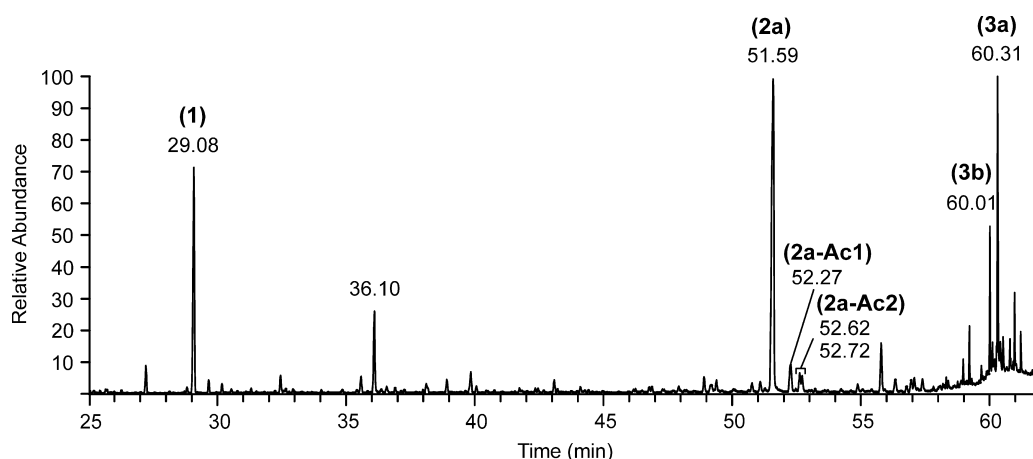


Figure 1. GC/MS TIC obtained for a trimethylsilylated extract of isoprene high-NO_x SOA. Peak identifications: **1**, 2-MG; **2a**, 2-MG linear dimer; **2a-Ac1** and **2a-Ac2**, 2-MG linear dimer mono-acetates; **3a**, 2-MG linear trimer; **3b**, 2-MG branched trimer. The peak eluting at 36.10 min is not discussed in the present work; it was found to correspond to an oxidation product of isoprene but not to be related to 2-MG, and was tentatively identified as 2-hydroxymethyl-3-ketopropanoic acid. Other peaks not marked were also found in a control filter and were identified as fatty acids and monoglycerides thereof. Reprinted from *J. Phys. Chem. A*, **110**, Surratt JD *et al.*, Chemical composition of secondary organic aerosol formed from the photooxidation of isoprene, 9665, Copyright (2006), with permission from American Chemical Society.

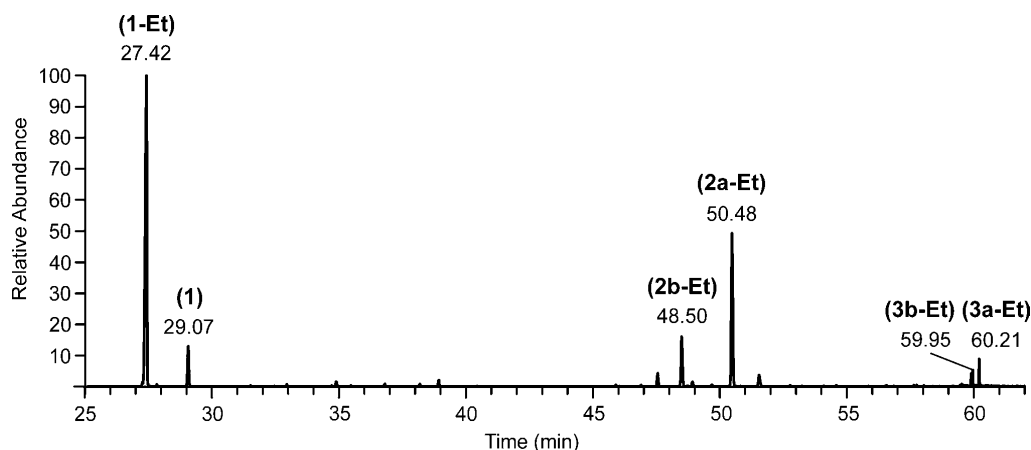


Figure 2. GC/MS extracted ion chromatogram (m/z 219) obtained for an extract of isoprene high- NO_x SOA subjected to a hydrolysis/ethylation procedure prior to trimethylsilylation. Reprinted from *J. Phys. Chem. A*, **110**, Surratt JD *et al.*, Chemical composition of secondary organic aerosol formed from the photooxidation of isoprene, 9665, Copyright (2006), with permission from American Chemical Society.

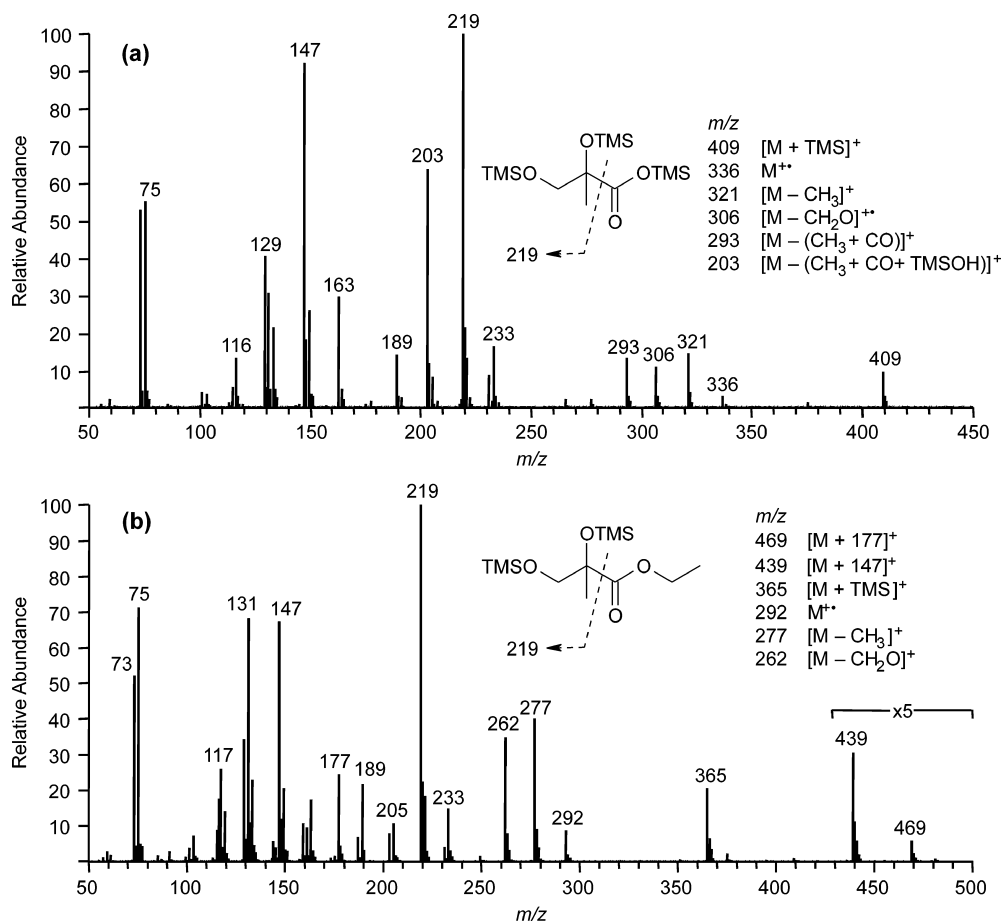


Figure 3. EI mass spectra for the TMS derivatives of (a) 2-MG (**1**) and (b) its ethyl ester derivative (**1-Et**). Part (a) reprinted from *J. Phys. Chem. A*, **110**, Surratt JD *et al.*, Chemical composition of secondary organic aerosol formed from the photooxidation of isoprene, 9665, Copyright (2006), with permission from American Chemical Society.

structural information for 2-MG dimers (**2a,b**), 2-MG trimers (**3a,b**), the ethyl derivatives of 2-MG dimers (**2a,b-Et**), as well as mono-acetate derivatives of the 2-MG linear dimer (**2a-Ac1,2**). In order to support fragmentation pathways, ion trap MS/MS experiments were used; only in the case of the 2-MG monomer was deuterium labeling of the TMS groups carried out.

Fragmentation behavior of 2-methylglyceric acid and its ethyl ester derivative

Figure 3 shows the EI mass spectra of the TMS derivatives of (a) 2-MG (**1**) and (b) its ethyl ester derivative (**1-Et**). The fragmentation pathways of the TMS derivative of 2-MG are summarized in Schemes 1 and 2; all pathways supported by an MS^2 ion trap experiment are indicated

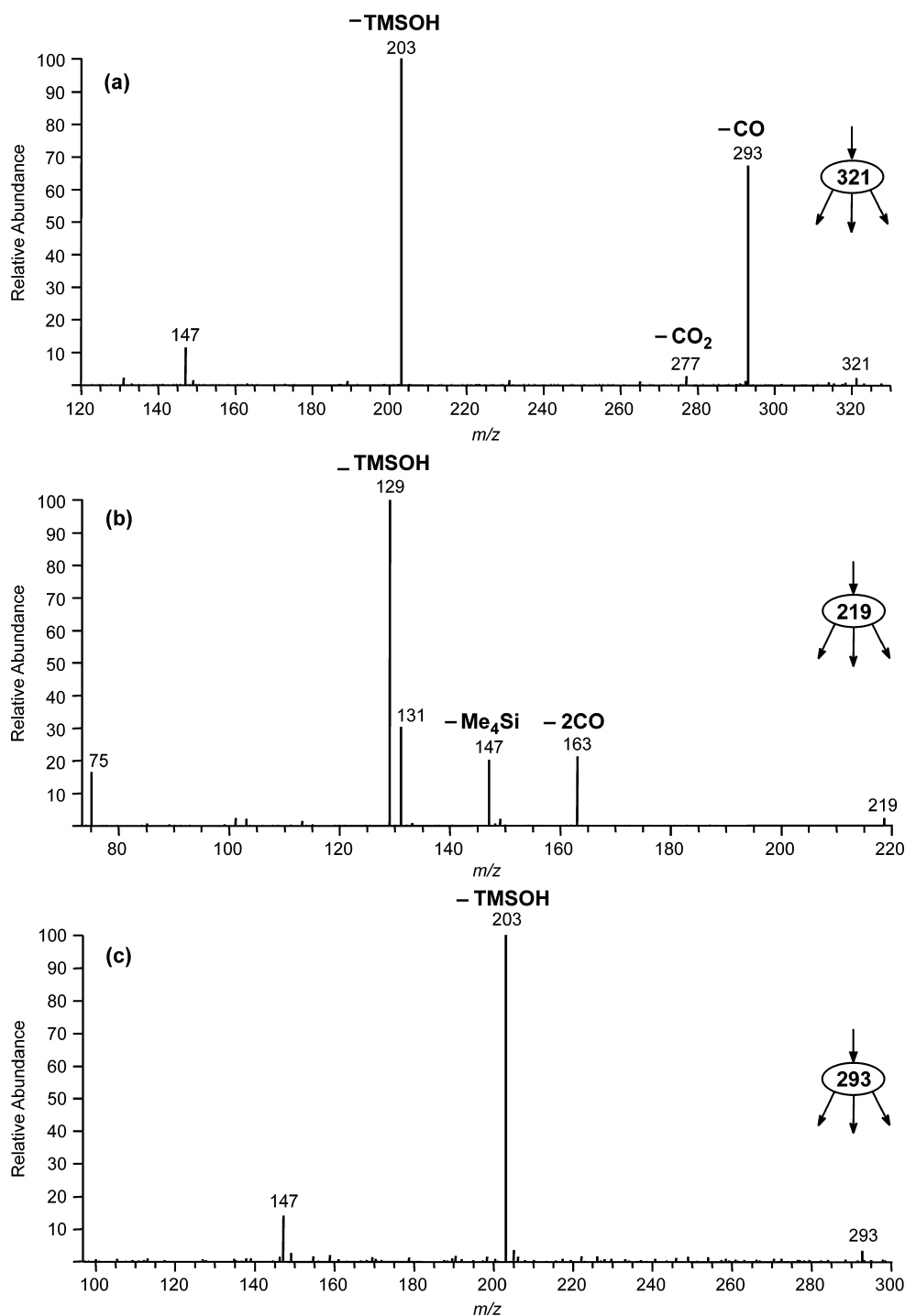
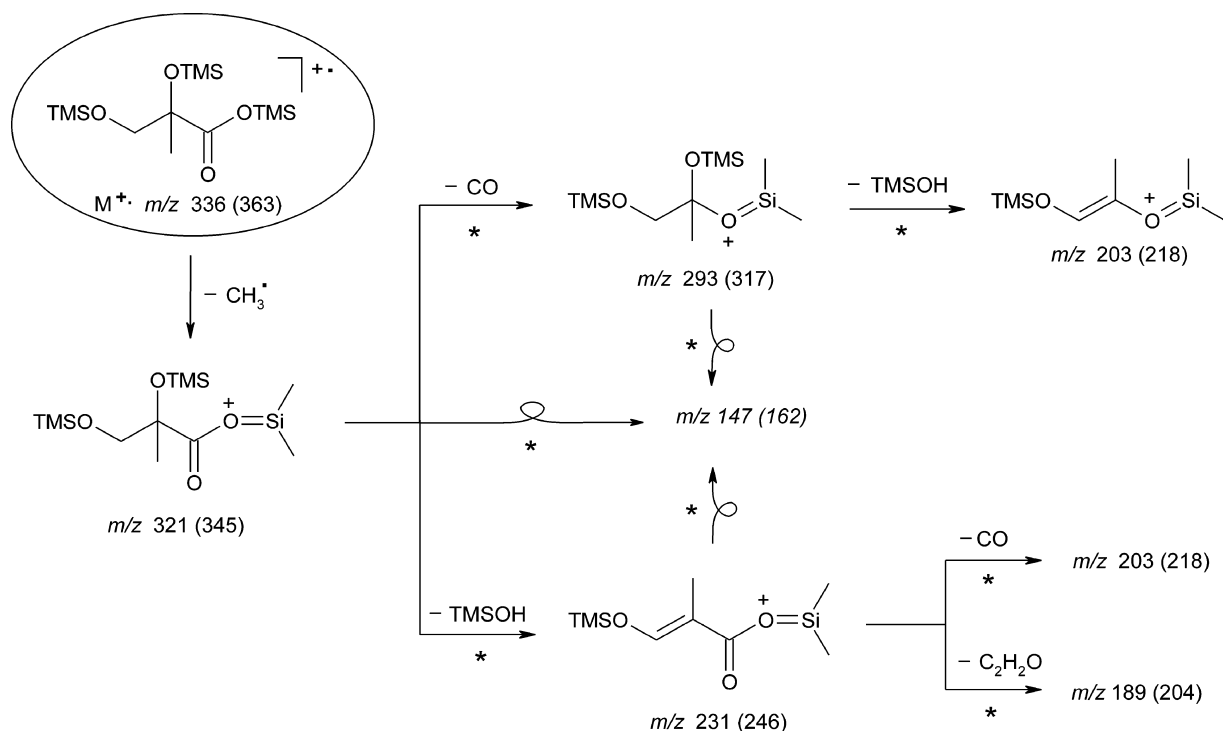


Figure 4. MS² ion trap spectra for selected ions of the TMS derivative of 2-MG: (a) m/z 321, (b) m/z 219 and (c) m/z 293.

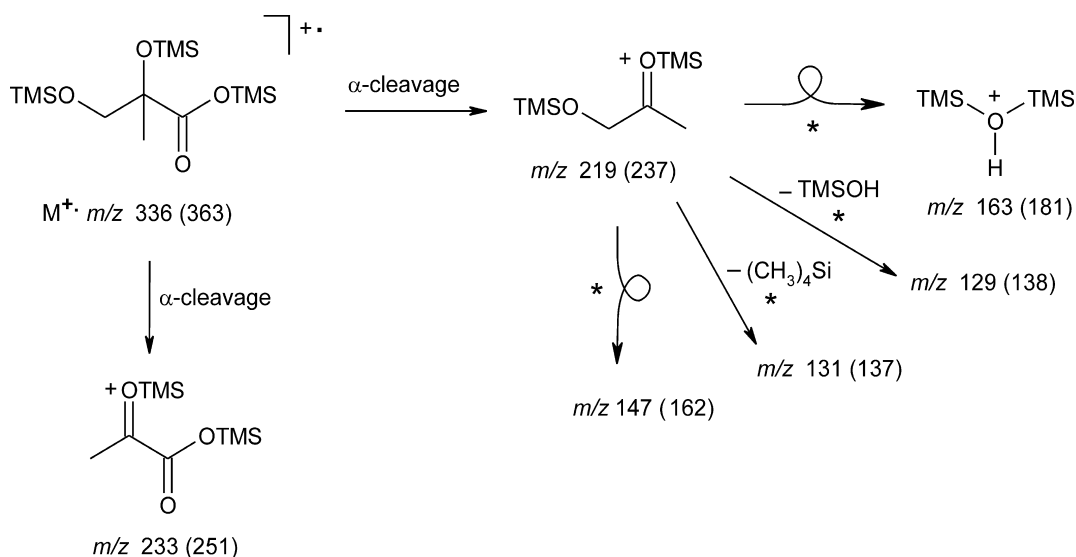
with an asterisk, while mass shifts obtained by introducing a deuterium labeled TMS group are given in parentheses. The molecular ion ($M^{+\bullet}$; m/z 336) of the TMS derivative of 2-MG is very weak, as is generally the case for TMS derivatives of compounds containing multiple hydroxyl groups.^{6,21} The molecular ion region has a signature that is characteristic of a trimethylsilylated carboxylic acid, i.e. the $[M - CH_3]^+$ ion (m/z 321) and the $[M - (CH_3 + CO)]^+$ ion (m/z 293). Proof that m/z 321 is the precursor of m/z 293 was obtained through an MS² ion trap experiment on m/z 321 (Fig. 4(a)). Besides the $M^{+\bullet}$ ion, other useful ions for inferring the MW

(336) are the $[M - CH_3]^+$ ion (m/z 321) and the $[M + TMS]^+$ ion (m/z 409). In addition, the molecular ion region contains a $[M - CH_2O]^+$ ion (m/z 306), which is indicative of a terminal trimethylsilylated hydroxymethyl function and can be explained via a rearrangement reaction of a TMS group to the ionized ester function as outlined in Scheme 3.

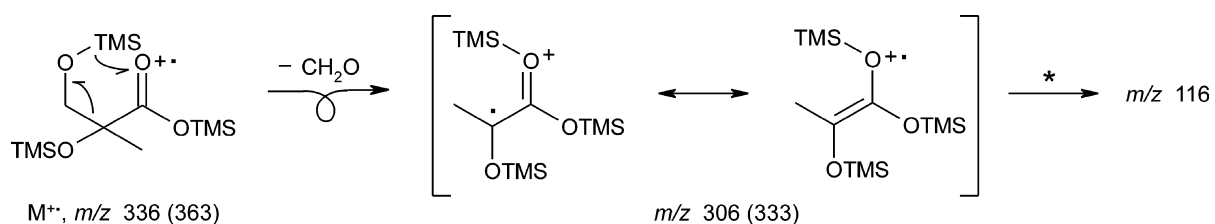
The ion at m/z 219 is the base peak in the mass spectrum and can be explained by a homolytic α -cleavage (Scheme 2). Fragmentation of m/z 219 (Fig. 4(b)) yields the specific signature that was previously reported for the m/z 219 ion of trimethylsilylated 2-methyltetrols,²¹



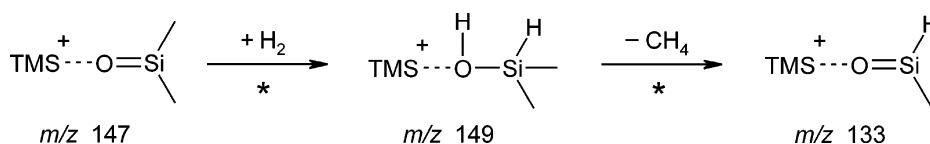
Scheme 1. Main fragmentation pathways for the TMS derivative of 2-methylglyceric acid. All pathways supported by an MS² ion trap experiment are indicated with an asterisk.



Scheme 2. Proposed pathways for *m/z* 233 and 219 formed from the TMS derivative of 2-MG and pathways for formation of *m/z* 219.



Scheme 3. Postulated gas-phase rearrangement process for the TMS derivative of 2-MG resulting in a resonance-stabilized *m/z* 306 ion.



Scheme 4. Hydrogenation reaction of m/z 147 occurring in the ion trap resulting in m/z 149 and 133.

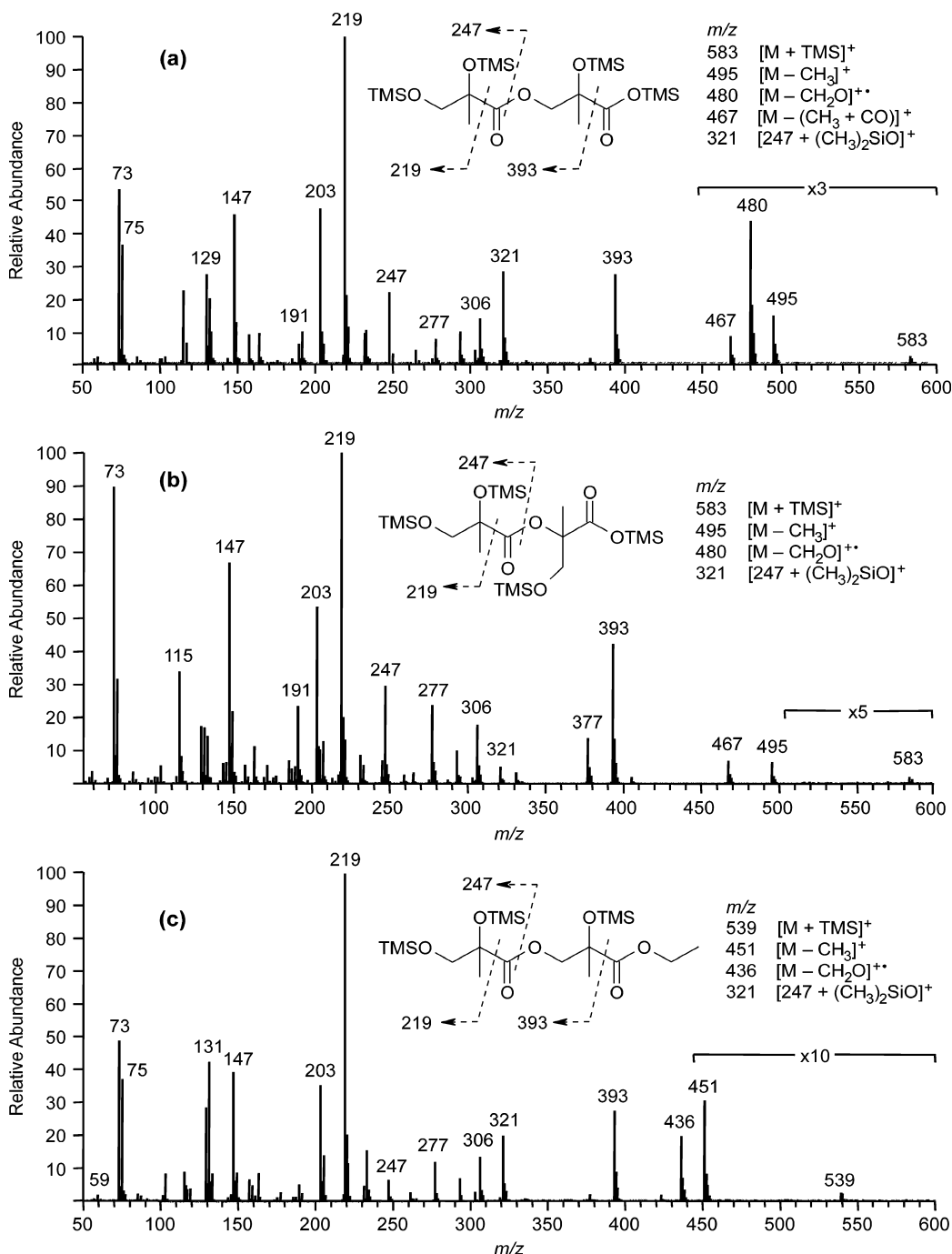


Figure 5. EI mass spectra of the TMS derivatives (a) 2-MG linear dimer (**2a**), (b) 2-MG branched dimer (**2b**), and (c) 2-MG linear dimer ethyl ester (**2a-Et**). Part (a) reprinted from *J. Phys. Chem. A*, **110**, Surratt JD *et al.*, Chemical composition of secondary organic aerosol formed from the photooxidation of isoprene, 9665, Copyright (2006), with permission from American Chemical Society.

and is therefore consistent with a trimethylsilylated 1,2-dihydroxy-2-methylethyl group in the molecule. The m/z 203 ion can be explained by loss of TMSOH from m/z 293 (Scheme 1; Fig. 4(c)), while the m/z 147 ion corresponding to $(\text{CH}_3)_2\text{Si} = \text{O}^+ - \text{TMS}$ is due to interaction between two TMSO groups²² and indicates that the molecule contains at least two TMSO groups. The m/z 147 ion is accompanied by a m/z 149 ion which was shown to be formed from the m/z 147 ion, and is explained by addition of hydrogen in the ion trap, and fragments to m/z 133 through loss of methane (Scheme 4).

Comparison of the spectra of the TMS derivatives of 2-MG (Fig. 3(a)) and its ethyl ester (Fig. 3(b)) shows that ethylation results in the expected mass shifts but has little effect on the fragmentation pathways. MW information is provided by the $\text{M}^{+\bullet}$ ion (m/z 292), the $[\text{M} - \text{CH}_3]^+$ ion (m/z 277), and the $[\text{M} + \text{TMS}]^+$ ion (m/z 365). It is worth noting that the higher m/z region contains additional adduct ions at m/z 439 $[\text{M} + 147]^+$ and m/z 469 $[\text{M} + 177]^+$. Of these ions, m/z 439 can be explained by adduct formation of the 2-MG ethyl ester molecule with m/z 147, which is an abundant ion in the spectrum. The formation of m/z 177 likely involves the further addition of formaldehyde (30 Da), which is generated in the formation of m/z 262 $[\text{M} - \text{CH}_2\text{O}]^+$. The latter ion supports a terminal trimethylsilylated hydroxymethyl function, while the base peak at m/z 219 is consistent with a trimethylsilylated 1,2-dihydroxy-2-methylethyl group.²¹

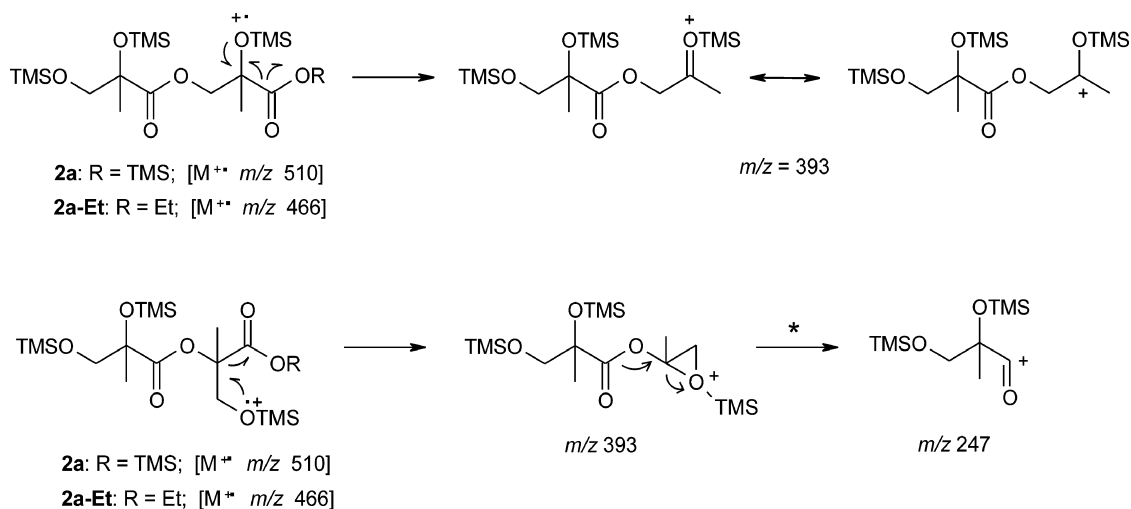
Fragmentation behavior of 2-MG dimers and their ethyl ester derivatives

Figure 5 shows the EI mass spectra of the TMS derivatives of (a) the linear (**2a**) and (b) branched dimer of 2-MG (**2b**) and

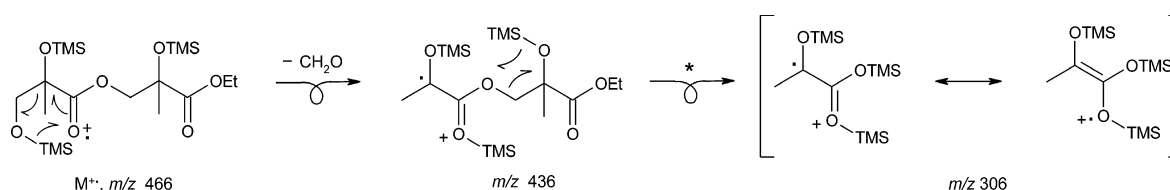
(c) the ethyl ester derivative of the 2-MG linear dimer (**2a-Et**). Examination of the m/z range 450–600 provides information about the MW. In the case of the 2-MG linear dimer (Fig. 5(a); MW 510), these ions include m/z 583 $[\text{M} + \text{TMS}]^+$, m/z 495 $[\text{M} - \text{CH}_3]^+$, and m/z 467 $[\text{M} - (\text{CH}_3 + \text{CO})]^+$. The latter ion supports the presence of a terminal COOTMS group in the molecule as has been discussed above for 2-MG (Scheme 1). In the case of the 2-MG linear dimer ethyl ester (Fig. 5(c)), the MW (466) is supported by m/z 539 $[\text{M} + \text{TMS}]^+$ and m/z 451 $[\text{M} - \text{CH}_3]^+$. The ion at m/z 393 detected for both of the 2-MG linear and branched dimers and their ethyl esters can be readily explained by a homolytic α -cleavage reaction as depicted in Scheme 5.

The mass spectra of the TMS derivatives of the 2-MG linear dimer as well as of its ethyl ester display an abundant $[\text{M} - \text{CH}_2\text{O}]^{+\bullet}$ ion (m/z 480 and m/z 436, respectively), which is consistent with a terminal trimethylsilylated hydroxymethyl function as has been discussed above for the 2-MG monomer (Scheme 2). Subsequent elimination of a neutral (130 Da) through a rearrangement of a TMS group leads to m/z 306, an ion that is also observed for the 2-MG monomer (Fig. 3(a)) and is stabilized by resonance (Scheme 6).

Comparison of the EI spectrum of the TMS derivative of the 2-MG linear dimer (Fig. 5(a)) with that of the branched dimer (Fig. 5(b)) reveals some interesting differences. It can be seen that the $[\text{M} - \text{CH}_2\text{O}]^{+\bullet}$ ion (m/z 480) is absent in the case of the 2-MG branched dimer. However, it is noted that a m/z 306 ion is also present in the 2-MG branched dimer, suggesting that the internal TMS group rearrangement (shown for **2a** in Scheme 6) occurs prior to



Scheme 5. Formation of the m/z 393 characteristic of the 2-MG linear and branched dimers and their ethyl esters via a homolytic α -cleavage reaction.



Scheme 6. Plausible mechanisms for the formation of m/z 436 and 306 from the TMS derivative of 2-MG linear dimer ethyl ester.

CH_2O loss. Furthermore, it can be seen that there is an additional ion at m/z 377 in the latter case, which corresponds to $[\text{M} - (\text{CH}_3 + \text{CO} + \text{TMSOH})]^+$. An MS/MS experiment confirmed that m/z 467 is the precursor for m/z 377; a possible explanation is a favorable 1,3-elimination of TMSOH in the branched carboxylic acid-containing 2-MG residue.

Figure 6 shows the m/z 393 product ion spectra for the two isomeric 2-MG dimers. Interesting differences can be noted, with m/z 247 being most abundant in the branched case; this information will be used in the following section to establish an esterification site in the 2-MG branched

trimer. In the case of the 2-MG branched dimer, m/z 247 can be readily formulated through a charge-directed loss of trimethylsilylated hydroxyacetone (Scheme 5).

Other structurally informative ions in the EI spectra of the TMS derivatives of the 2-MG linear and branched dimers worth discussing are m/z 247 and 321. The m/z 247 ion is explained by an α -cleavage relative to the ester $\text{C}=\text{O}$ bond (Scheme 7) but can also be formed by other pathways (e.g. from m/z 393; Scheme 5) and is characteristic for the presence of an ester linkage in the molecule. The ion at m/z 247 fragments further to m/z 231, 219, 203, and 157, as confirmed

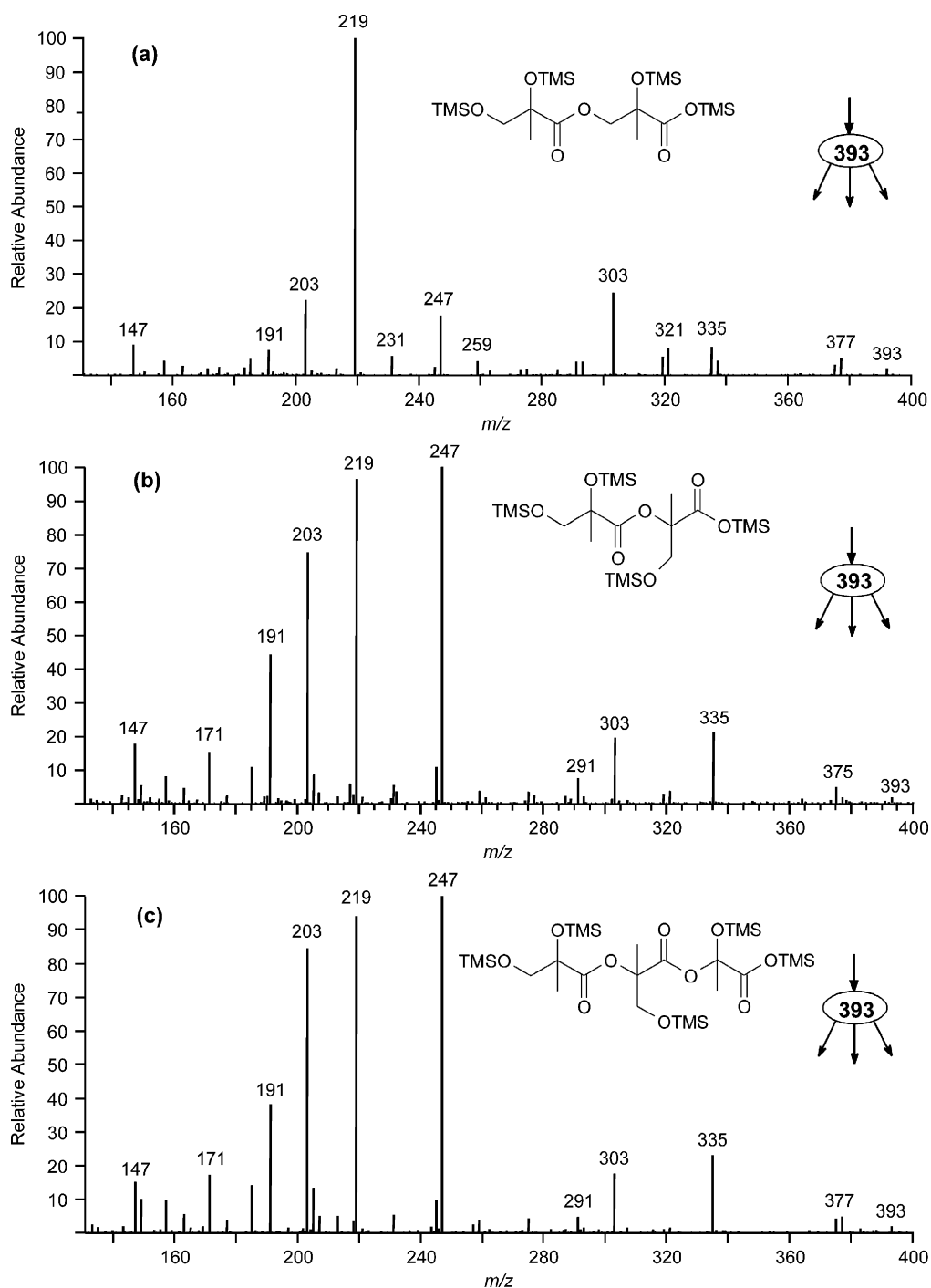


Figure 6. MS² ion trap spectra for m/z 393 of the TMS derivative of (a) the 2-MG linear dimer, (b) the 2-MG branched dimer and (c) the 2-MG branched trimer.

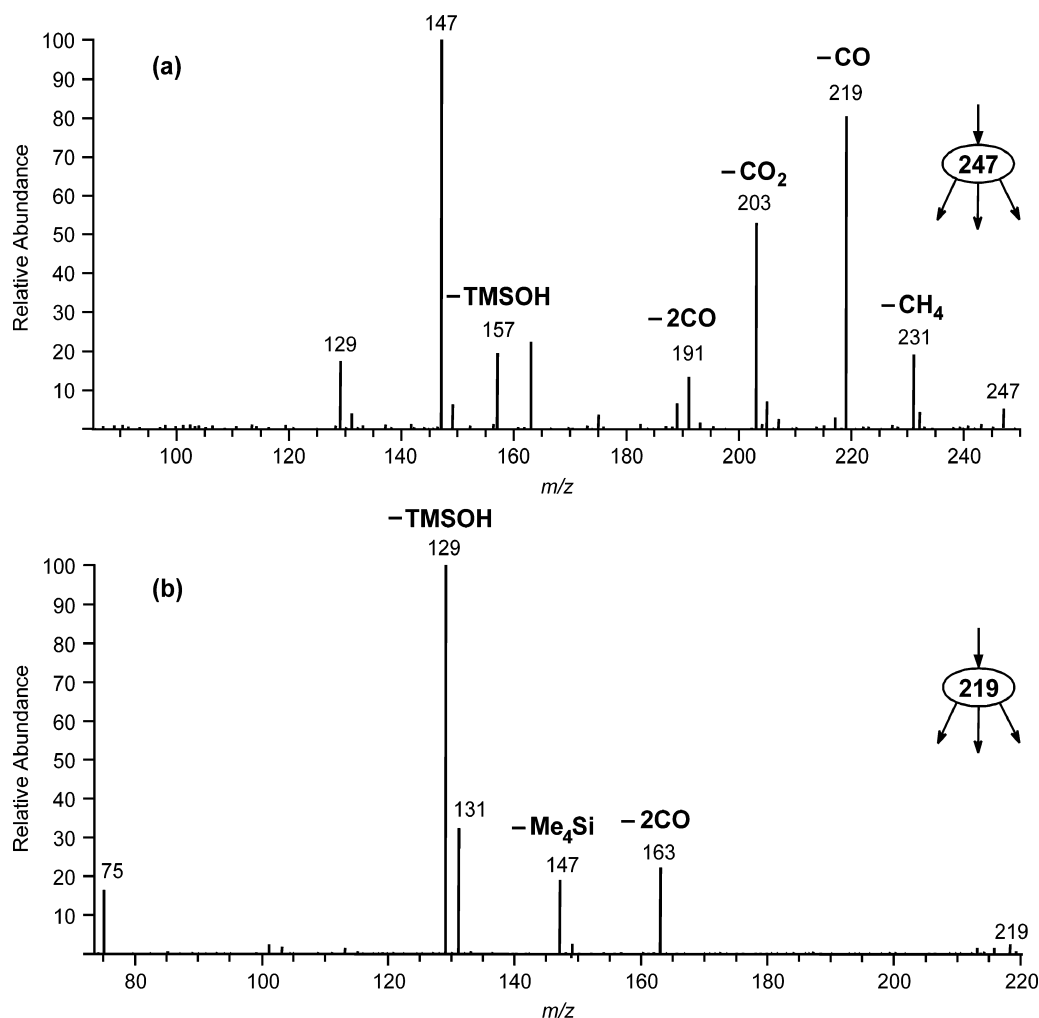
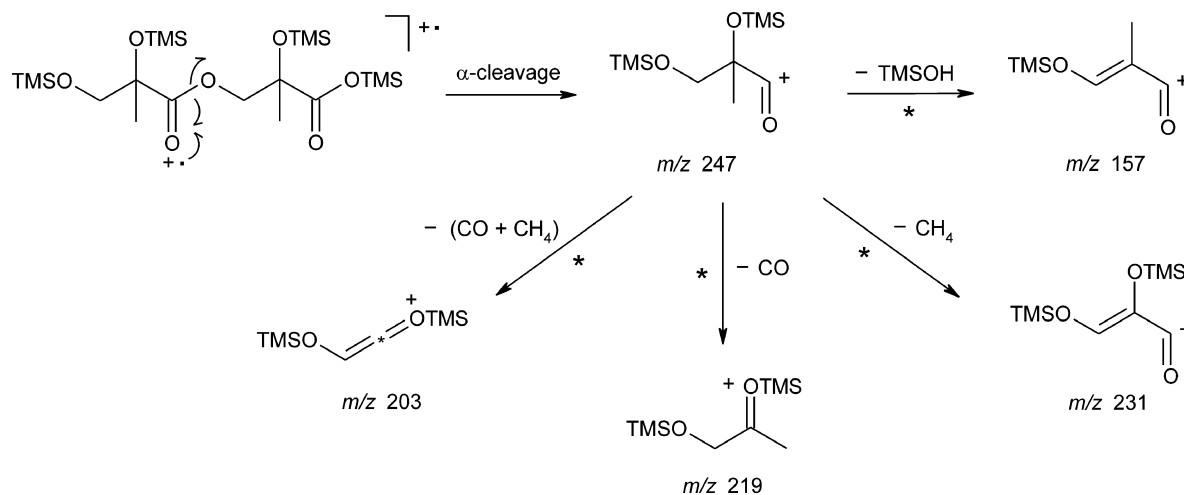


Figure 7. MS² ion trap spectra for selected ions of the TMS derivative of the 2-MG linear dimer: (a) *m/z* 247 and (b) *m/z* 219.



Scheme 7. A plausible formation mechanism for *m/z* 247 and its further fragmentation as confirmed by MS² ion trap experiments.

by MS² experiments (Fig. 7(a); Scheme 7). The MS² ion trap spectrum of *m/z* 219 (Fig. 7(b)) unambiguously proves that its structure is consistent with a trimethylsilylated 1,2-dihydroxy-2-methylethyl group,²¹ which has already been discussed above in the case of 2-MG and its ethyl ester derivative.

Fragmentation behavior of 2-MG trimers and their ethyl esters

Figure 8(a) and (b) shows the EI mass spectra of the TMS derivatives of the two isomeric trimers of 2-MG that were detected in the GC/MS TIC of high-NO_x isoprene SOA (Fig. 1). Since both spectra display the same set of ions

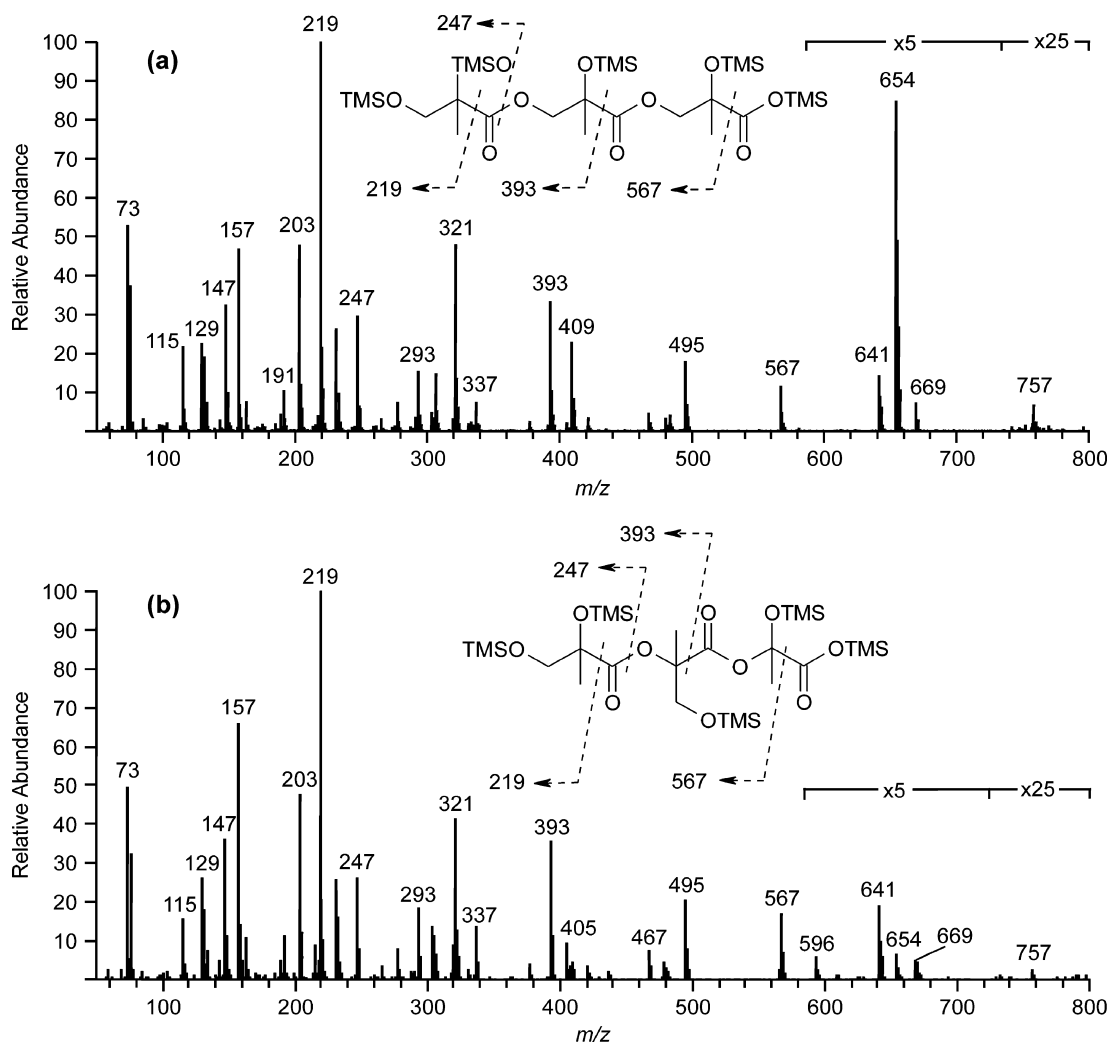


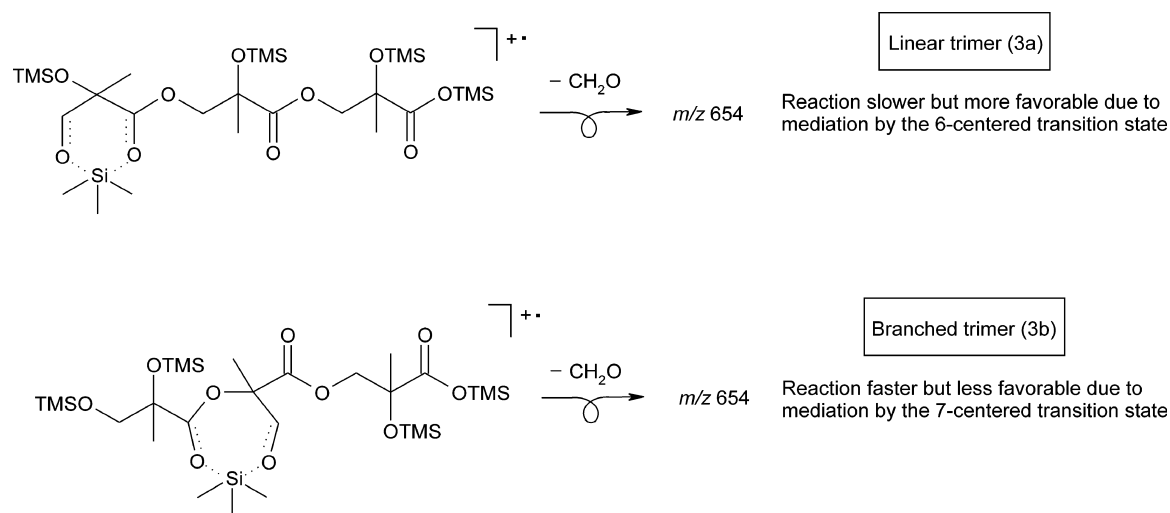
Figure 8. EI mass spectra of the TMS derivatives of 2-MG (a) linear (**3a**) and (b) branched trimer (**3b**).

differing only in terms of their relative abundances, one can conclude that they represent isomeric compounds. The most abundant compound which elutes at the latest retention time (RT = 60.31 min) is attributed to the linear trimer (**3a**), while the other one (RT = 60.01 min) is attributed to a branched trimer (**3b**), given that under the GC conditions employing a nonpolar stationary phase, branched isomers, which have a more compact structure than their linear forms, elute at an earlier retention time. As will be discussed below, evidence for a branched internal 2-MG residue was obtained. However, we have no evidence for the esterification site in the terminal carboxylic acid-containing 2-MG residue and assume that after dimer formation, esterification proceeds by reaction with a terminal hydroxymethyl group of a 2-MG molecule, thus resulting in a linear form, since the formation of linear forms is sterically less hindered.

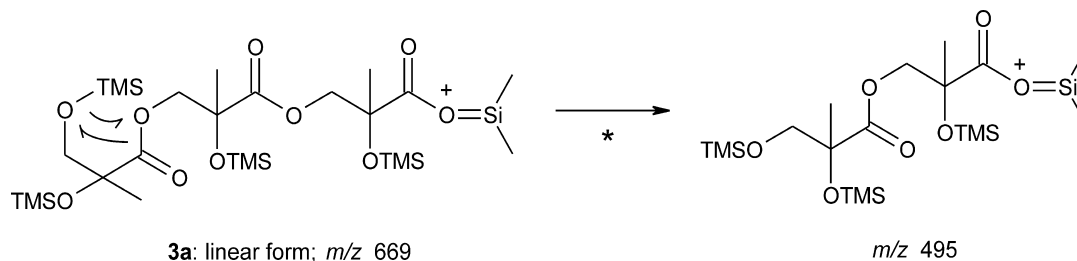
As in the case of the 2-MG dimers, examination of the high m/z range enables us to infer the MW (684). Both isomers reveal a very weak $[M + \text{TMS}]^+$ adduct ion (m/z 757) as well as $[M - \text{CH}_3]^+$ ion (m/z 669) and $[M - (\text{CH}_3 + \text{CO})]^+$ ions (m/z 641). The latter ion also supports a terminal carboxyl group in the underivatized molecules. It can be seen that the abundance of the $[M - \text{CH}_2\text{O}]^+$ ion (m/z 654) is strikingly different and is more abundant for the linear

system compared to the branched one. The same observation was made for the $[M - \text{CH}_2\text{O}]^+$ ion (m/z 610) in the mass spectra of the 2-MG dimers and the ethyl derivatives of 2-MG trimers (results not shown). A possible explanation for this phenomenon is given in Scheme 8. A TMS group transfer may not only proceed from the terminal TMSOCH_2 group but also from an internal TMSOCH_2 group, involve different geometries of the transition state, and take place at a different rate. The interaction between the terminal TMSOCH_2 group and a neighboring ester function involves a 6-centered transition state, while that between the internal TMSOCH_2 group of the branched isomer and a neighboring ester function involves a 7-centered state which is less favorable but may be formed faster.

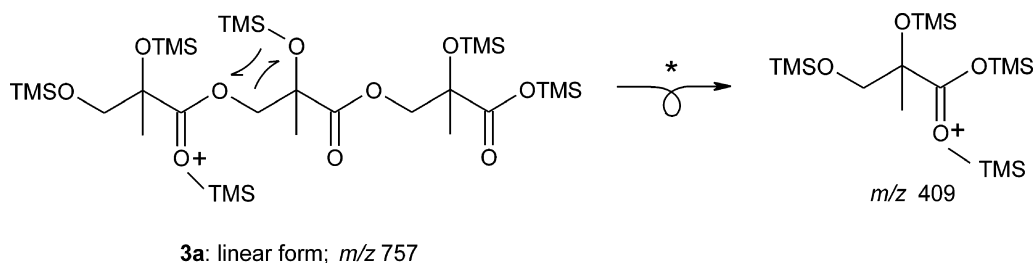
The m/z 393 ion can be explained by an α -cleavage directed by the ionized internal TMSO group of the inner 2-MG residue. Figure 6(c) shows that the m/z 393 product ion profile of the branched trimer is very similar to that of the branched dimer (Fig. 6(b)), suggesting that the branched 2-MG trimer contains an inner branched 2-MG residue. In the following discussion, attention will be given to structurally informative ions, which were not present in the case of the 2-MG dimers. Both the linear and branched 2-MG trimer reveal an ion at m/z 495 which can be explained



Scheme 8. Differences in the geometry of the transition state providing a rational explanation for the more favorable loss of formaldehyde from the $M^{+\bullet}$ ion of the TMS derivative of the 2-MG linear trimer compared to that of the branched form.



Scheme 9. Formation of m/z 495 in the case of the TMS derivative of the 2-MG linear trimer. The same mechanism can be proposed for the 2-MG branched trimer.



Scheme 10. Pathway leading to m/z 409 in the TMS derivative of the 2-MG linear trimer.

from the $[M - \text{CH}_3]^+$ ion by loss of a neutral (174 Da) from the terminal 2-MG residue through a rearrangement of a TMS group (Scheme 9). In addition, ions are present, which are isomer-specific. In the case of the 2-MG linear trimer, an ion can be seen at m/z 409, while the 2-MG branched trimer reveals an ion at m/z 596. The m/z 409 ion can be generated from the $[M + \text{TMS}]^+$ adduct ion by an internal rearrangement of a TMS group resulting in the $[2\text{-MG} + \text{TMS}]^+$ adduct ion (Scheme 10). The m/z 596 ion characteristic of the 2-MG branched trimer is believed to result from a favorable interaction in the $M^{+\bullet}$ ion between the trimethylsilylated hydroxymethyl group of the branched unit and a trimethylsilylated hydroxyl group, leading to loss of $(\text{CH}_3)_4\text{Si}$ (88 Da).

Fragmentation behavior of 2-MG linear dimer mono-acetate derivatives

The two small peaks in the GC/MS TIC of high- NO_x isoprene SOA (Fig. 1) eluting just after the 2-MG linear dimer (**2a**) were

identified as isomeric 2-MG linear dimer mono-acetates (**2a-Ac1,2**). These products were already partially characterized in our previous study using $(-)$ ESI-MS, and are formed by esterification between the 2-MG linear dimer and acetic acid, which is also generated from isoprene in the smog chamber under high- NO_x conditions.¹⁰ As will be discussed below, a more complete characterization of the isomeric 2-MG linear dimer mono-acetates was possible by detailed interpretation of the EI mass spectral data. The EI spectra of the TMS derivatives of the isomeric 2-MG linear dimer mono-acetates are shown in Fig. 9. The peak eluting at a RT of 52.3 min was characterized as the isomer containing an internal acetate group (**2a-Ac1**), while the peak at a RT of 52.6 min was attributed to the isomer containing a terminal acetate group (**2a-Ac2**). The partial splitting noted in the latter chromatographic peak can be explained by diastereoisomerism.

Examination of the high m/z range enables us to infer the MW (480); the EI spectra of the TMS derivatives of both

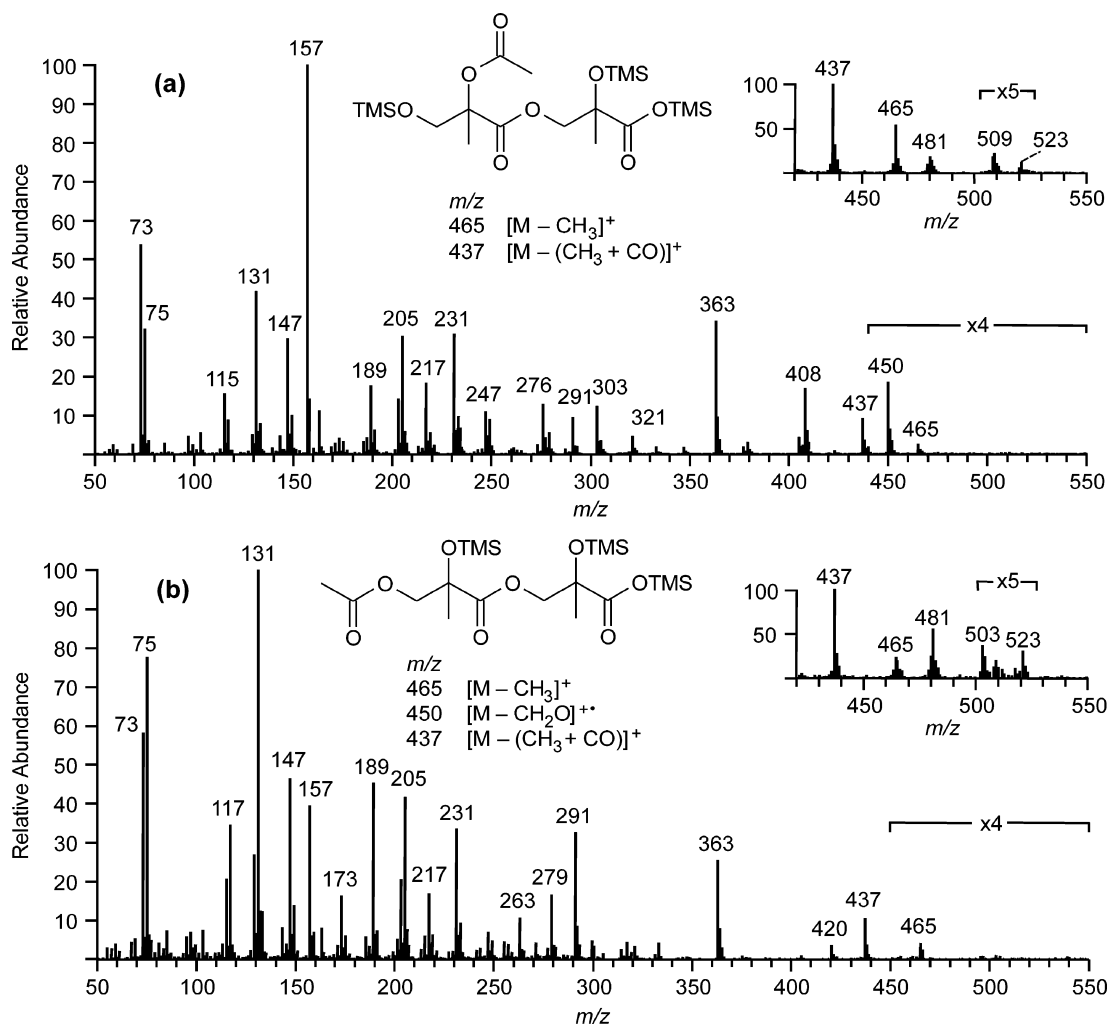
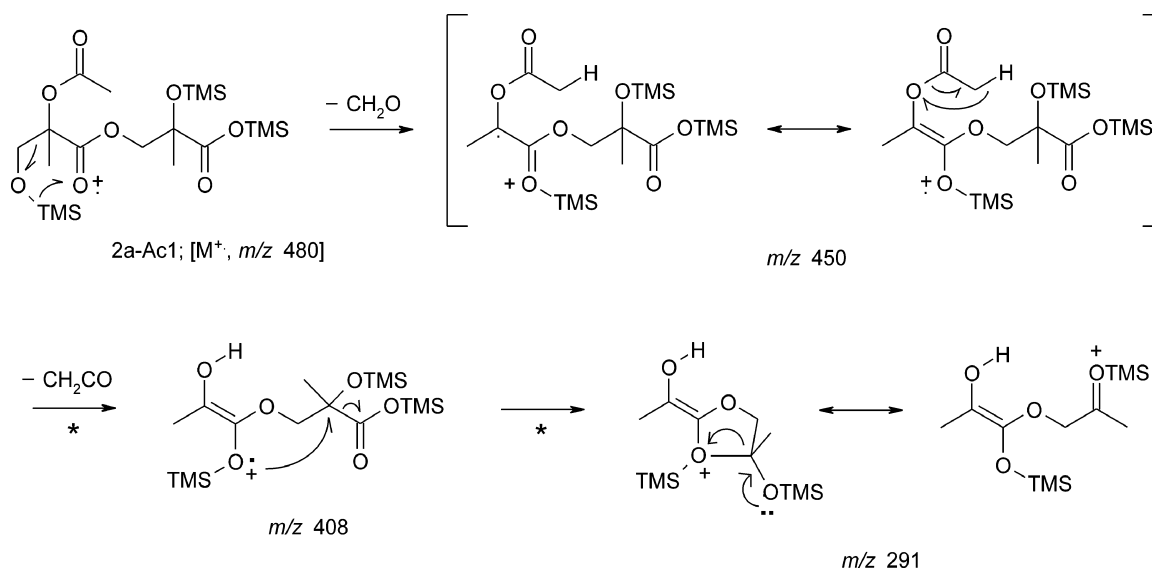


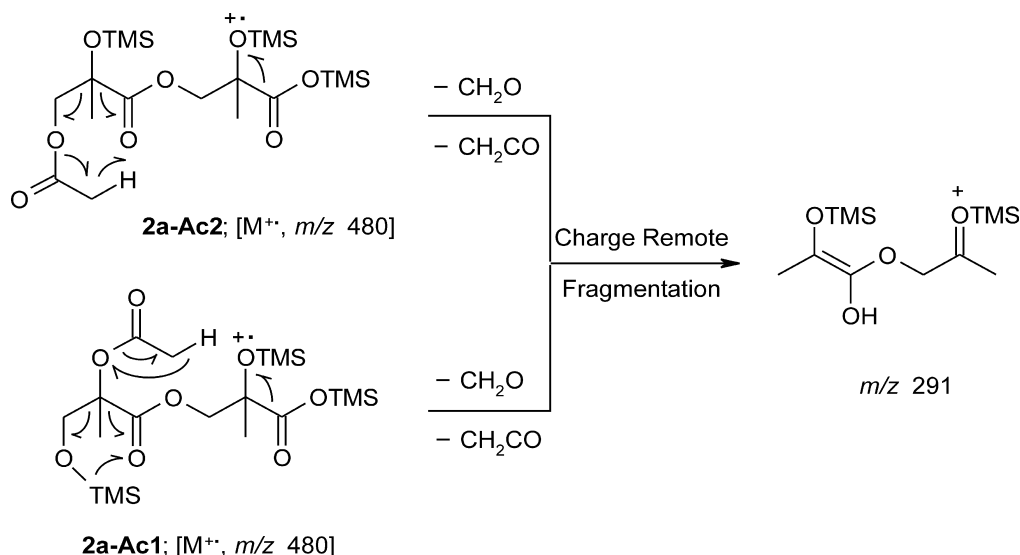
Figure 9. EI mass spectra of the TMS derivatives of 2-MG linear dimer mono-acetates bearing the acetate group at (a) the terminal hydroxymethyl group (**2a-Ac1**) and (b) an internal hydroxyl group (**2a-Ac2**). Insets: CI (methane) data.



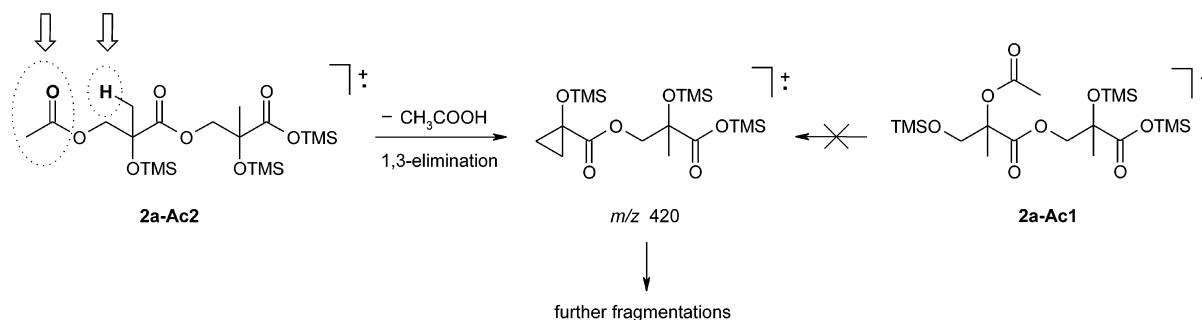
Scheme 11. Mechanisms proposed for the formation of m/z 450, 408, and 291 present in the EI spectrum of the TMS derivative of the 2-MG dimer mono-acetate isomer eluting at RT 52.3 min (**2a-Ac1**).

2-MG linear dimer mono-acetates show $[M - \text{CH}_3]^+$ (m/z 465) and $[M - (\text{CH}_3 + \text{CO})]^+$ ions (m/z 437). Supporting MW information was derived from the CI (methane)

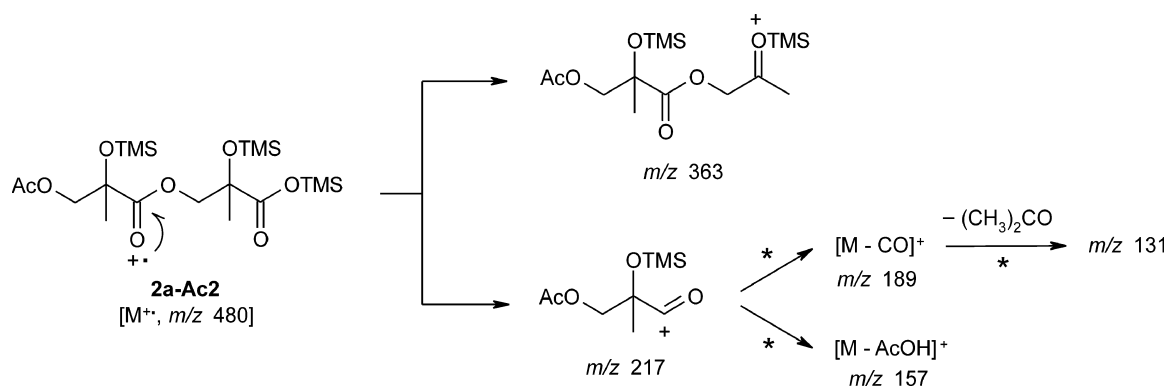
spectra (insets in Fig. 9), which reveal $[M + \text{H}]^+$ (m/z 481), $[M + \text{C}_2\text{H}_5]^+$ (m/z 509), and $[M + \text{C}_3\text{H}_7]^+$ (m/z 523) ions as well as $[\text{MH} - \text{CH}_4]^+$ ions (m/z 465). It can be



Scheme 12. Possible formation pathways for *m/z* 291 in the TMS derivatives of both 2-MG dimer mono-acetate isomers through charge-remote fragmentation reactions.



Scheme 13. Mechanism proposed for the formation of *m/z* 420, an ion characteristic of the TMS derivative of the 2-MG dimer mono-acetate bearing an acetyl group at the terminal hydroxymethyl group of the non-carboxylic acid-containing 2-MG residue (**2a-Ac2**). Parts of the molecule engaged in the elimination process are circled.



Scheme 14. Mechanisms proposed for formation of *m/z* 363, 217, 189, 157, and 131 in the TMS derivative of an 2-MG linear dimer mono-acetate (**2a-Ac2**). The same mechanisms hold for the isomer **2a-Ac1**.

seen that the spectrum of the first-eluting isomer (**2a-Ac1**) contains an ion at *m/z* 450, corresponding to the [M - CH₂O]⁺ ion formed through a rearrangement of a TMS group (Scheme 11). This ion firmly supports the presence of a terminal trimethylsilylated hydroxymethyl group in the non-carboxylic acid-containing 2-MG residue and is consistent with a nonbranched carboxylic acid-containing

2-MG residue. Following the loss of formaldehyde, *m/z* 450 fragments by loss of ketene (42 Da) from the acetate group, resulting in *m/z* 408. Further fragmentation of *m/z* 408 through loss of a TMSO(CO)[•] radical leads to *m/z* 291. It can be seen that *m/z* 291 is also present in the case of the 2-MG dimer mono-acetate isomer eluting at a RT of 52.6 min (**2a-Ac2**); an alternative explanation for *m/z* 291

in both 2-MG dimer mono-acetate isomers through charge-remote rearrangement reactions involving neutral loss of both ketene (42 Da) and formaldehyde (30 Da) is outlined in Scheme 12.

The EI spectrum of the compound corresponding to the 2-MG dimer mono-acetate isomer eluting at a RT of 52.6 min (**2a-Ac2**) (Fig. 9(b)) shows a unique ion at m/z 420, which is explained by loss of acetic acid from the $M^{+\bullet}$ ion (Scheme 13). This favorable elimination of acetic acid involves a hydrogen at a 3-position relative to the acetate group²³ and does not occur in the other isomer (RT 52.3 min) in which only hydrogen atoms at the 2-position are available.

Ions present in the spectra of the TMS derivatives of both isomeric 2-MG linear dimer mono-acetates worth discussing are m/z 363, 217, 189, 157, and 131. Their formation mechanisms are given in Scheme 14. The formation of m/z 217 and 189 in both isomers is consistent with the presence of an acetate group in the non-carboxylic acid-containing 2-MG residue. As expected, m/z 157 is more prominent in the case of the 2-MG dimer mono-acetate bearing an acetyl group at the terminal hydroxymethyl group because of the favorable 1,3-elimination of acetic acid. On the other hand, the formation of m/z 131 due to loss of acetone from m/z 189 seems to be a favored pathway in the case of the 2-MG dimer mono-acetate bearing an internal acetyl group.

CONCLUSIONS

Detailed interpretation of the EI mass spectral data of the TMS derivatives of 2-MG and oligoester derivatives thereof allows one to obtain key structural features of the molecules and as such to elucidate their chemical structures and differentiate isomeric compounds. The m/z 219 ion containing the trimethylsilylated 1,2-dihydroxy-2-methylethyl group is a characteristic ion of 2-MG and its oligomers. Evidence for an ester function in the 2-MG dimers and trimers is indicated by the m/z 247 ion formed by an α -cleavage in the ester group linking the non-carboxylic acid-containing 2-MG residue to the remaining part of the molecules. In addition, evidence for an inner branched 2-MG residue in the case of the 2-MG branched trimer was obtained, while the 2-MG linear and branched dimers could be readily differentiated. Characteristic ions of the terminal carboxyl group are the $[M - CH_3]^+$ and $[M - (CH_3 + CO)]^+$ ions, while the terminal hydroxymethyl group was found to give rise to a $[M - CH_2O]^{+\bullet}$ ion in linear 2-MG oligomers. Furthermore, it was possible to differentiate isomeric mono-acetates of the 2-MG linear dimer containing an acetyl group in the non-carboxylic acid-containing 2-MG residue and locate the position of the acetyl group. We can conclude that the EI spectra of the TMS derivatives contain a wealth of structural information, including information about the MW, ester linkages, terminal carboxylic and hydroxymethyl groups, and esterification sites.

Acknowledgements

Research at the University of Antwerp was supported by the Belgian Federal Science Policy Office through the BIOSOL project (contract SD/AT/02A) and a visiting postdoctoral fellowship to Rafal Szmigielski, and by the Research Foundation – Flanders (FWO)

(grant number G.0091.06). Research at Caltech was funded by the U.S. Environmental Protection Agency under the Science to Achieve Results (STAR) Program grant number RD-83107501-0, managed by EPA's Office of Research and Development (ORD), National Center for Environmental Research (NCER), and by the U.S. Department of Energy, Biological, and Environmental Research Program DE-FG02-05ER63983; this work has not been subjected to the EPA's required peer and policy review and therefore does not necessarily reflect the views of the Agency and no official endorsement should be inferred. Jason Surratt was supported in part by the United States Environmental Protection Agency (EPA) under the STAR Graduate Fellowship Program.

REFERENCES

1. Guenther A, Hewitt CN, Erickson D, Fall R, Geron C, Graedel T, Harley P, Klinger L, Lerdau M, McKay WA, Pierce T, Scholes B, Steinbrecher R, Tallamraju R, Taylor J, Zimmerman P. A global model of natural volatile organic compound emissions. *J. Geophys. Res.* 1995; **100**: 8873.
2. Pandis SN, Paulson SE, Seinfeld JH, Flagan RC. Aerosol formation in the photooxidation of isoprene and β -pinene. *Atmos. Environ.* 1991; **25A**: 997.
3. Claeys M, Graham B, Vas G, Wang W, Vermeylen R, Pashynska V, Cafmeyer J, Guyon P, Andreae MO, Artaxo P, Maenhaut W. Formation of secondary organic aerosols through photooxidation of isoprene. *Science* 2004; **303**: 1173.
4. Claeys M, Wang W, Ion AC, Kourtchev I, Gelencsér A, Maenhaut W. Formation of secondary organic aerosols from isoprene and its gas-phase oxidation products through reaction with hydrogen peroxide. *Atmos. Environ.* 2004; **38**: 4093.
5. Ion AC, Vermeylen R, Kourtchev I, Cafmeyer J, Chi X, Gelencsér A, Maenhaut W, Claeys M. Polar organic compounds in rural PM_{2.5} aerosols from K-pusztá, Hungary, during a 2003 summer field campaign: sources and diel variations. *Atmos. Chem. Phys.* 2005; **5**: 1805.
6. Wang W, Kourtchev I, Graham B, Cafmeyer J, Maenhaut W, Claeys M. Characterization of oxygenated derivatives of isoprene related to 2-methyltetrols in Amazonian aerosols using trimethylsilylation and gas chromatography/ion trap mass spectrometry. *Rapid Commun. Mass Spectrom.* 2005; **19**: 1343.
7. Kourtchev I, Ruuskanen T, Maenhaut W, Kulmala M, Claeys M. Observation of 2-methyltetrols and related photo-oxidation products of isoprene in boreal forest aerosols from Hyytiälä, Finland. *Atmos. Chem. Phys.* 2005; **5**: 2761.
8. Edney EO, Kleindienst TE, Jaoui M, Lewandowski M, Offenberg JH, Wang W, Claeys M. Formation of 2-methyl tetrols and 2-methylglyceric acid in secondary organic aerosol from laboratory irradiated isoprene/NO_x/SO₂/air mixtures and their detection in ambient PM_{2.5} samples collected in the eastern United States. *Atmos. Environ.* 2005; **39**: 5281.
9. Böge O, Miao Y, Plewka A, Herrmann H. Formation of secondary organic particle phase compounds from isoprene gas-phase oxidation products: an aerosol chamber and field study. *Atmos. Environ.* 2006; **40**: 2501.
10. Surratt JD, Murphy SM, Kroll JH, Ng NL, Hildebrandt L, Sorooshian A, Szmigielski R, Vermeylen R, Maenhaut W, Claeys M, Flagan RC, Seinfeld JH. Chemical composition of secondary organic aerosol formed from the photooxidation of isoprene. *J. Phys. Chem. A* 2006; **110**: 9665.
11. Kroll JH, Ng NL, Murphy SM, Flagan RC, Seinfeld JH. Secondary organic aerosol formation from isoprene photooxidation under high-NO_x conditions. *Geophys. Res. Lett.* 2005; **32**: L18808, Doi:10.1029/2005GL023637.
12. Kroll JH, Ng NL, Murphy SM, Flagan RC, Seinfeld JH. Secondary organic aerosol formation from isoprene photooxidation. *Environ. Sci. Technol.* 2006; **40**: 1867, Doi:10.1021/es054301.
13. Dommen J, Metzger A, Duplissy J, Kalberer M, Alfarra MR, Gascho A, Weingartner E, Prevot ASH, Verheggen B, Baltensperger U. Laboratory observation of oligomers in the aerosol

- from isoprene/NO_x photooxidation. *Geophys. Res. Lett.* 2006; **33**: L13805, Doi:10.1029/2006GL026523.
14. Henze DK, Seinfeld JH. Global secondary organic aerosol from isoprene oxidation. *Geophys. Res. Lett.* 2006; **33**: L09812, Doi:10.1029/2006GL025976.
 15. Iinuma Y, Böge O, Gnauk T, Herrmann H. Aerosol-chamber study of the α -pinene/O₃ reaction: influence of particle acidity on aerosol yields and products. *Atmos. Environ.* 2004; **38**: 761.
 16. Gao S, Keywood M, Ng NL, Surratt JD, Varutbangkul V, Bahreini R, Flagan RC, Seinfeld JH. Low-molecular-weight and oligomeric components in secondary organic aerosol from the ozonolysis of cycloalkenes and alpha-pinene. *J. Phys. Chem. A* 2004; **108**: 10147.
 17. Gao S, Ng NL, Keywood M, Varutbangkul V, Bahreini R, Nenes A, He J, Yoo KY, Beauchamp JL, Hodyss RP, Flagan RC, Seinfeld JH. Particle phase acidity and oligomer formation in secondary organic aerosol. *Environ. Sci. Technol.* 2004; **38**: 6582.
 18. Tolocka MP, Jang M, Ginter JM, Cox FJ, Kamens RM, Johnston MV. Formation of oligomers in secondary organic aerosol. *Environ. Sci. Technol.* 2004; **38**: 1428.
 19. Kalberer M, Paulsen D, Sax M, Steinbacher M, Dommen J, Prevot ASH, Fisseha R, Weingartner E, Frankevich V, Zenobi R, Baltensperger U. Identification of polymers as major compounds of atmospheric organic aerosols. *Science* 2004; **308**: 1659.
 20. Jaoui M, Kleindienst TE, Lewandowski M, Edney EO. Identification and quantification of aerosol polar oxygenated compounds bearing carboxylic acid or hydroxy groups. 1. Method development. *Anal. Chem.* 2004; **76**: 4765.
 21. Wang W, Vas G, Dommissie R, Loones K, Claeys M. Fragmentation study of diastereoisomeric 2-methyltetrols, oxidation products of isoprene, as their trimethylsilyl ethers, using gas chromatography/ion trap mass spectrometry. *Rapid Commun. Mass Spectrom.* 2004; **18**: 1787.
 22. Maenhaut-Claeys M, Vandewalle M. Studies in organic mass spectrometry XIX. The fragmentation of the trimethylsilyl derivatives of some 2,3-dialkyl-1,4-cyclopentanediols. *Bull. Soc. Chim. Belges* 1974; **83**: 343.
 23. Liptak M, Heerma W. Fast atom bombardment mass spectrometric study of some N-glycosides and S-glycosides of acetylated hexose isomers. *Rapid Commun. Mass Spectrom.* 1993; **7**: 676.

Appendix F

Measurements of Secondary Organic Aerosol from Oxidation of Cycloalkenes, Terpenes, and *m*-xylene Using an Aerodyne Aerosol Mass Spectrometer*

* This chapter is reproduced by permission from “Measurements of Secondary Organic Aerosol from Oxidation of Cycloalkenes, Terpenes, and *m*-xylene Using an Aerodyne Aerosol Mass Spectrometer” by R. Bahreini, M. D. Keywood, N. L. Ng, V. Varutbangkul, S. Gao, R. C. Flagan, J. H. Seinfeld, *Environmental Science and Technology*, 39: 5674-5688, 2005. Copyright 2005. American Chemical Society.

Measurements of Secondary Organic Aerosol from Oxidation of Cycloalkenes, Terpenes, and *m*-Xylene Using an Aerodyne Aerosol Mass Spectrometer

R. BAHREINI,[†] M. D. KEYWOOD,[†]
N. L. NG,[‡] V. VARUTBANGKUL,[‡] S. GAO,[†]
R. C. FLAGAN,^{†,‡} J. H. SEINFELD,^{*,†,‡}
D. R. WORSNOP,[§] AND J. L. JIMENEZ^{||}

Department of Environmental Science and Engineering, and Department of Chemical Engineering, California Institute of Technology, Mail Code 210-41, 1200 East California Boulevard, Pasadena, California 91125, Aerodyne Research, Inc., 45 Manning Road, Billerica, Massachusetts 01821, and Department of Chemistry & Biochemistry and CIRES, University of Colorado–Boulder, UCB 216, Boulder, Colorado 80309

The Aerodyne aerosol mass spectrometer (AMS) was used to characterize physical and chemical properties of secondary organic aerosol (SOA) formed during ozonolysis of cycloalkenes and biogenic hydrocarbons and photooxidation of *m*-xylene. Comparison of mass and volume distributions from the AMS and differential mobility analyzers yielded estimates of “effective” density of the SOA in the range of 0.64–1.45 g/cm³, depending on the particular system. Increased contribution of the fragment at *m/z* 44, CO₂⁺ ion fragment of oxygenated organics, and higher “ Δ ” values, based on ion series analysis of the mass spectra, in nucleation experiments of cycloalkenes suggest greater contribution of more oxygenated molecules to the SOA as compared to those formed under seeded experiments. Dominant negative “ Δ ” values of SOA formed during ozonolysis of biogenics indicates the presence of terpene derivative structures or cyclic or unsaturated oxygenated compounds in the SOA. Evidence of acid-catalyzed heterogeneous chemistry, characterized by greater contribution of higher molecular weight fragments to the SOA and corresponding changes in “ Δ ” patterns, is observed in the ozonolysis of α -pinene. Mass spectra of SOA formed during photooxidation of *m*-xylene exhibit features consistent with the presence of furandione compounds and nitro organics. This study demonstrates that mixtures of SOA compounds produced from similar precursors result in broadly similar AMS mass spectra. Thus, fragmentation patterns observed for biogenic versus anthropogenic SOA may be useful in determining the sources of ambient SOA.

* Corresponding author phone: (626)395-4635; fax: (626)796-2591; e-mail: seinfeld@caltech.edu.

[†] Department of Environmental Science and Engineering, California Institute of Technology.

[‡] Department of Chemical Engineering, California Institute of Technology.

[§] Aerodyne Research, Inc.

^{||} University of Colorado–Boulder.

1. Introduction

Secondary organic aerosols (SOA) are a significant contributor to the total ambient organic aerosol loading in urban areas as well as regionally and globally. Our understanding of SOA formation processes and their chemical and physical properties is, however, limited. Better understanding of SOA is essential to accurately evaluate the impact of SOA on visibility, climate, and human health and to incorporate this understanding in future regulations. Traditionally, controlled laboratory chamber experiments have been carried out to determine the SOA forming potential, that is, organic yield, of volatile hydrocarbons that are, or have a chemical structure close to, atmospherically relevant compounds (1–6).

Laboratory chamber experiments have been instrumental in identifying specific compounds formed as SOA. Recent studies have demonstrated the presence of polymeric structures in the SOA formed from both anthropogenic and biogenic hydrocarbon precursors (7–11). Formation of such polymeric structures has been suggested to occur by aerosol-phase reactions, possibly acid-catalyzed, such as aldol condensation, gem-diol reaction, and hemiacetal/acetate formation pathways (12). Oligomers have been identified in the SOA formed in both the presence and the absence of inorganic acids (7, 9).

The Aerodyne aerosol mass spectrometer (hereafter referred to as the AMS) provides mass concentration and mass size distribution of nonrefractory components of submicron aerosols in real time (13, 14). Because of the high time and size resolution of the data collected by the AMS, the AMS has been deployed in many field studies, both airborne and ground-based, measuring size-resolved chemical composition of ambient aerosols (14–19). The AMS has also been used in laboratory-chamber studies (20–22). The current work summarizes studies of laboratory-chamber generated SOA using the AMS. A comprehensive series of experiments was conducted to study ozonolysis of cycloalkenes and biogenic precursors to investigate SOA physical and chemical characteristics and effect of heterogeneous reactions on SOA formation. In addition, photooxidation of *m*-xylene, a predominant SOA-forming anthropogenic hydrocarbon, was studied. Experiments were carried out in the absence or presence of seed particles of varying composition. Figure 1 gives the chemical structures of the precursors studied.

To compute a mass yield of SOA, it is necessary to know the SOA density because the volumetric yield is the quantity normally determined in chamber experiments. Estimates of the density of SOA have so far been based on the detailed chemical speciation of the SOA. Because it has been traditionally difficult to identify the complete composition of SOA, the estimated density is uncertain because of the missing contribution of unidentified products. It is demonstrated in the current study that SOA effective density can be estimated by comparing mobility volume distributions with AMS mass distributions measured in parallel. The work presented here demonstrates that information on types of organics present, degree of contribution of higher molecular weight species (or those with higher resistance to fragmentation) to the SOA, and indications of types of SOA precursors can be obtained in the analysis of the AMS organic mass spectra. Because of these specific characteristics observed in the mass spectra, it is then possible to extend the analysis to ambient data where analogies are drawn from patterns observed during laboratory chamber experiments to explore the potential contributions of various precursor classes to the formation of the ambient SOA.

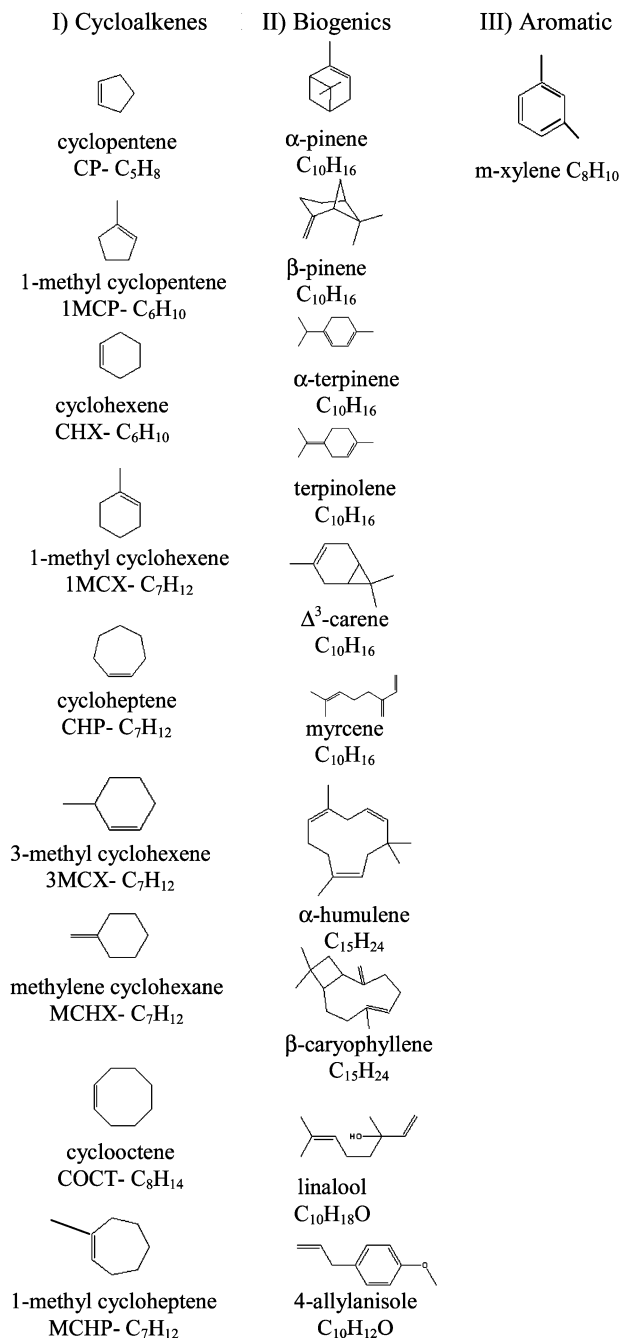


FIGURE 1. Chemical structures of the SOA precursor compounds studied.

2. Experimental Section

Experiments were conducted in Caltech's indoor dual 28 m³ suspended FEP Teflon chambers (23). The AMS was used to measure size-resolved aerosol chemical composition. A complete description of the AMS and its data analysis is given elsewhere (13, 14, 24, 25). In summary, sample (gas and particle phase) is introduced into the differentially pumped chambers of the instrument through a 100 μ m critical orifice. An aerodynamic lens system is used to collimate the particles into a narrow beam. A chopper wheel (~2% duty cycle) is used to chop the particle beam for "time-of-flight" mode measurements (i.e., P-TOF mass distribution measurements) or to block/clear the particle beam for "mass spectrum" mode measurements (MS). Upon impacting on the vaporizer (~650 °C), which is positioned at the end of the P-TOF chamber, the nonrefractory components in/on the aerosols are vaporized, and the vapors are ionized under high vacuum by

electron impact (70 eV). Positive ions are then extracted into the quadrupole mass spectrometer for determination of their mass-to-charge ratio (m/z).

The particle size calibration of the AMS was determined by sampling dry polystyrene latex (PSL) particles (Duke Scientific) and validated using DMA size-selected dry ammonium nitrate and/or ammonium sulfate particles. Ionization efficiency calibration of the AMS, needed to determine the mass concentration of species from raw MS ion signals, was performed on a regular basis by sampling DMA size-selected dry ammonium nitrate particles. Further details of these calibrations and the relevant calculations can be found elsewhere (14, 24).

Aerosol size distributions, in the size range of ~15–775 nm in mobility diameter, were measured by scanning electrical mobility spectrometers (SEMS) (26). Each SEMS system includes a ⁸⁵Kr neutralizer (TSI model 3077), a long cylindrical column differential mobility analyzer (DMA, TSI model 3081), and a condensation particle counter (CPC, TSI model 3760). The flow rates of the SEMS systems are controlled to 2.5 LPM for sheath and excess flows and 0.25 LPM for polydisperse and monodisperse aerosol flows. In addition, the total number concentration of particles in each chamber was measured by additional CPCs (TSI, models 3010 and 3025). A hygroscopic tandem differential mobility analyzer (HTDMA) was used in a number of experiments to determine the hygroscopic behavior of the SOA. Furthermore, bulk filter samples were collected for organic speciation analysis (9, 11).

Gas-phase concentrations of parent hydrocarbons were measured by a gas chromatograph with a flame ionization detector (GC-FID, Hewlett-Packard model 5890, series II Plus). Ozone concentration was measured by a Horiba ambient O₃ monitor (model APOA-360 CE), and concentrations of nitrogen oxides were measured by a Horiba ambient NO–NO₂–NO_x monitor (model APNA-360). Temperature and humidity of the chamber were also measured by Vaisala probes (HMP230 series transmitters). Details on calibration procedures of the above instruments are given elsewhere (6).

During seeded experiments, seed particles were generated by atomizing saltwater solutions using a constant rate atomizer. Nonacidic bulk solutions were made at 0.03 M concentration of the salt (ammonium sulfate or magnesium sulfate); acidic bulk solutions were made of 0.03 M concentration of the salt (ammonium sulfate or magnesium sulfate) and 0.05 or 0.1 M of sulfuric acid. Because the atomized particles are highly charged, they were passed through ²¹⁰Po neutralizers to achieve a more neutral charge distribution and reduce particle loss in the lines. In low relative humidity experiments, particles were also passed through a silica gel diffusion drier before being introduced into the chamber.

The temperature in the chambers was maintained at 20 \pm 2 °C. Relative humidity of the chamber was controlled by controlling the humidity of the flushing air. For dry experiments, chambers were flushed with dry-scrubbed air with RH < 10%. For humid experiments, dry-scrubbed air was passed through a bubbler and a particle filter before being introduced into the chamber at a rate such that the relative humidity achieved in the chamber at 20 °C was ~55 \pm 5%. During photooxidation studies, 300, 40 W each, 350-BL lights were used to illuminate the chambers (23).

Volatile hydrocarbons (Sigma Aldrich) were introduced as liquid samples into injection glass bulbs. The liquid was then heated gently in the bulb, and the vapors were carried to the chamber by passing scrubbed air through the bulb. During dark ozonolysis experiments, cyclohexane, used as the hydroxyl radical (OH) scavenger, was introduced into the chamber in a similar manner. The role of different OH

scavengers in ozonolysis experiments, in terms of producing additional HO₂ and RO₂ radicals that may change the ozonolysis chemistry of alkenes or terpenes, has been the subject of previous studies. Keywood et al. (27) reported that the SOA yield during cyclohexene ozonolysis was 30% lower in the presence of cyclohexane as opposed to 2-butanol as the scavenger. However, Docherty and Ziemann (28) reported that the SOA yield during β-pinene ozonolysis was 3 times higher in the presence of cyclohexane as opposed to propanol as the scavenger. Based on these recent studies, it is apparent that the extent by which the scavenger affects the radical chemistry during ozonolysis experiments depends on the structure of the specific compound being studied. For consistency, however, only cyclohexane was used as the scavenger during the experiments from which we report results. The concentration of cyclohexane injected for each experiment was based on the concentration of the parent hydrocarbon and reaction rates of the parent hydrocarbon and cyclohexane with OH radical such that 99% of the time cyclohexane, rather than the parent hydrocarbon, would react with the OH radical.

During photooxidation studies, NO (502 ppm in nitrogen, Scott-Marrin Inc.), NO₂ (521 ppm in nitrogen, Air Liquide), and propene (500 ppm in nitrogen, Air Liquide) were injected into the chamber.

Concentrations of the parent hydrocarbon and the seed, in the case of seeded experiments, or NO_x levels, in the case of photooxidation experiments, were monitored for at least 1 h to ensure stability of the system before start of the reaction. Start of the reaction in ozonolysis studies was marked by ozone injection using a UV lamp ozone generator (EnMet Corp.). Ozone injection continued until the concentration of ozone exceeded by a factor of 2 or 3 the initial hydrocarbon concentration, depending on the experiment, to ensure full oxidation. During photooxidation experiments, turning on the chamber's UV source lamps marked the beginning of the reaction.

3. Determination of SOA Density and Morphology

As stated above, an estimate of density is needed to convert an apparent volume measurement of SOA into mass concentration, such as in SOA yield calculations using DMA measurements of size distribution. Without all of the significant components of the SOA being identified, the estimation of the density based on the chemical composition may be subject to biases if a class of compounds with different density goes systematically undetected. Comparing parallel AMS mass distribution measurements and DMA volume distributions provides an estimate of aerosol effective density (21, 29, 30). The AMS mass distribution is measured versus vacuum aerodynamic diameter (d_{va}), whereas DMA volume distribution is measured versus electrical mobility diameter (d_m). The vacuum aerodynamic diameter is the diameter of a sphere, in the free molecular regime, with unit density (1 g/cm³) and the same terminal velocity as the particle of interest. The mobility diameter is the diameter of a sphere with the same migration velocity of the particle of interest in a constant electric field at atmospheric pressure. These two measures of particle size are related by "effective density" (ρ_{eff}) or "material density" (ρ_m) as follows:

$$\rho_{eff} = \frac{d_{va}}{d_m} \rho_0 = \rho_m \frac{C_c(d_{ve})}{\delta^3 \chi_t \chi_v C_c(d_m)} \quad (1)$$

where ρ_0 is unit density (1 g cm⁻³), C_c is the Cunningham slip correction factor, d_{ve} is the volume equivalent diameter, δ is the internal void fraction, χ_t is the dynamic shape factor in the transition regime, and χ_v is the dynamic shape factor in the free molecular regime (30). Note that several other

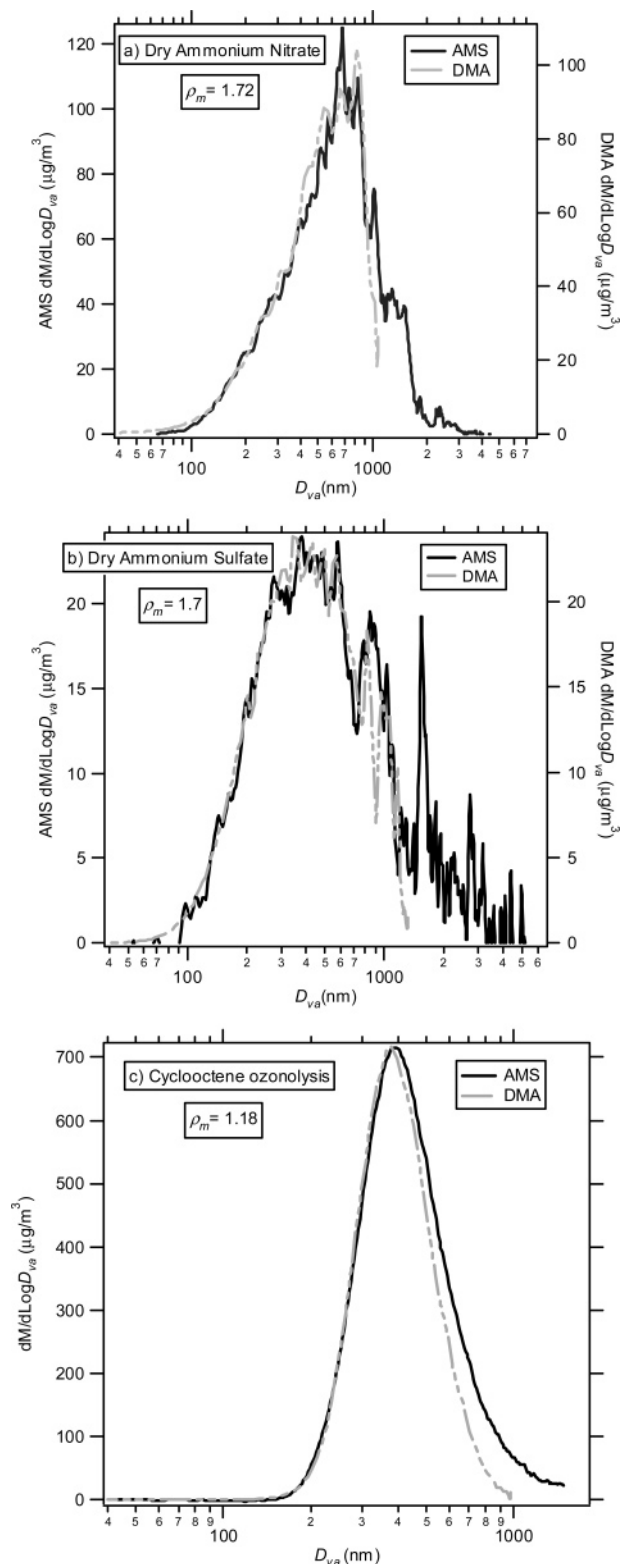


FIGURE 2. Comparison of AMS and DMA mass distributions as a means to deduce aerosol effective density: AMS and DMA mass distributions of (a) dry ammonium nitrate ($\rho_{\text{NH}_4\text{NO}_3} = 1.72$); (b) dry ammonium sulfate ($\rho_{\text{(NH}_4)_2\text{SO}_4} = 1.77$); (c) SOA formed during cyclooctene ozonolysis ($\rho_m = 1.18$).

definitions of effective densities are used in the literature; these definitions are equivalent for spherical particles but can be significantly different when particles are irregular (30). When comparing AMS and DMA aerosol mass distributions to deduce the SOA density, only the rising edge of the small-size bins of the distributions was considered for the following

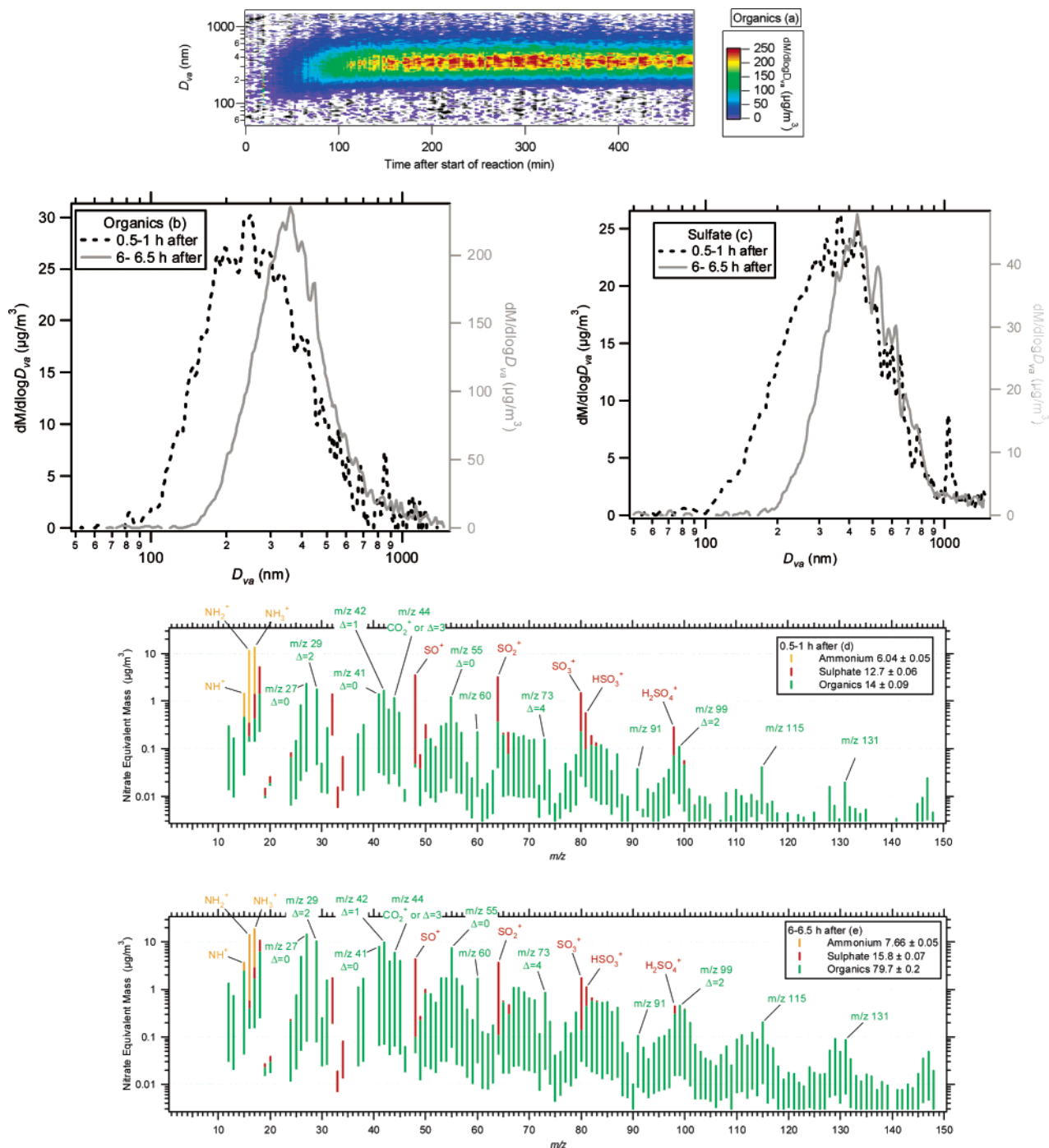


FIGURE 3. Evolution of mass distributions of organics and sulfate (a–c) and the mass spectra (d–e) during cyclohexene ozonolysis. SOA formation led to growth of aerosols with narrower mass distributions and increased organic signal intensities in the mass spectra.

reasons: (1) transmission efficiency in the AMS is 100% for 100–500 nm particles (P. Liu, University of Wyoming, unpublished data) (13), which is also the size range of interest; (2) during some experiments, a longer tail on the AMS mass distributions was observed, which can be an artifact of slower evaporation of some components of the aerosols; (3) during some nucleation experiments, nucleated particles grew to sizes larger than the scan-range of the DMA, thus limiting the comparison only to smaller sizes. As shown in Figure 2a,b, this comparison has been proven successful to better than $\pm 10\%$ for ammonium nitrate and ammonium sulfate aerosols. During seeded experiments, the estimates of ρ_{eff} and mass concentration measurements of the seed and SOA (m_{seed} and m_{SOA}) were used along with the assumption of

unit dynamic shape factor ($\chi = 1$, i.e., particle sphericity) to determine density of SOA (ρ_{SOA}) based on the following relationship, which also assumes volume additivity:

$$\rho_{\text{eff}} = \frac{m_{\text{seed}} + m_{\text{SOA}}}{V_{\text{seed}} + V_{\text{SOA}}} = \frac{m_{\text{seed}} + m_{\text{SOA}}}{\frac{m_{\text{seed}}}{\rho_{\text{seed}}} + \frac{m_{\text{SOA}}}{\rho_{\text{SOA}}}} \quad (2)$$

Typical evolution of the SOA concentration and mass distribution during an experiment is shown in Figure 3a–c; condensation of secondary organics onto the seed causes a shift in the mass distribution of the seed and SOA to larger sizes. During this growth, the width of the mass distribution decreases, indicating condensation is the main mechanism

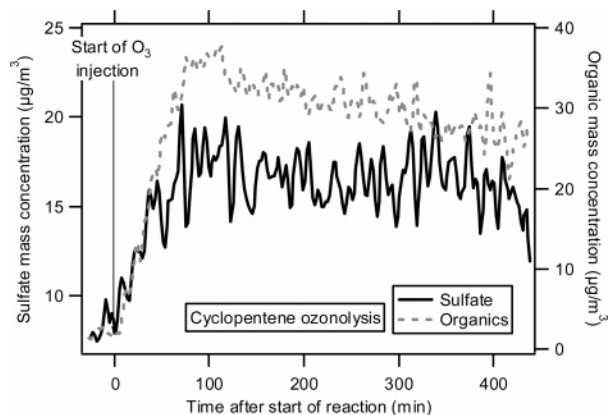


FIGURE 4. Time trends of sulfate and organic mass concentrations during cyclopentene ozonolysis. Sulfate signal increased after SOA formation, indicating improved collection efficiency of organic-coated seed particles.

of growth. Although particle loss to the chamber walls is also expected to narrow the mass distribution, analysis of mass distributions obtained during “wall-loss experiments”, where the loss rate of the seed particles to the chamber walls is characterized, indicates that the width of the distributions does not change appreciably for durations typical of SOA experiments.

Information about morphology of the aerosols can be deduced by comparing the sulfate signal before and after start of the reaction during seeded experiments. Unpublished data from our laboratory experiments have shown collection efficiency of only ~30% in the AMS for dry ammonium sulfate particles, most likely due to bounce of dry and less volatile particles off of the AMS vaporizer (T. Onasch, Aerodyne Research, Inc., personal communication). It has been observed that collection efficiency of ambient particles increases once the AMS inlet temperature approaches the ambient dew point and particles deliquesce and become liquid droplets (16). A similar phenomenon is observed here as SOA condenses on the seed aerosol during the first stages of the reaction. Figure 4 shows the time trend of mass concentration of sulfate and organics for cyclopentene ozonolysis; the sulfate signal increases by a factor of ~2 once ozone injection, and consequently SOA formation starts. As discussed subsequently, this phenomenon was not observed with oxidation of all hydrocarbons, which suggests different particle phases (liquid vs solid) within the AMS vacuum conditions for the SOA formed from different precursors.

4. Analysis of Organics

As gas-phase organics partition into the aerosol phase, different organic peaks appear in the AMS mass spectra (Figure 3d,e). The ion series (or “delta (Δ)”) analysis technique was developed in an attempt to characterize chemical properties and specific features of the EI mass spectra of classes of organic compounds (31). Because of the combination of high-temperature vaporization (650 °C) and relatively hard ionization of molecules in the AMS (electron impact ionization, 70 eV), individual compounds undergo significant fragmentation. Through ion series analysis, it is possible to obtain semiquantitative information about the classes of compounds present in a mixture of organic compounds such as the SOA aerosols studied here. In this analysis, organic compounds are assumed to contain one or several functional groups and saturated and unsaturated hydrocarbon chains. Upon electron impact ionization, the hydrocarbon chain can fragment at different positions, giving rise to mass spectra in which groups of peaks are separated by 14 amu units (for saturated chains). The m/z 's measured for a given compound

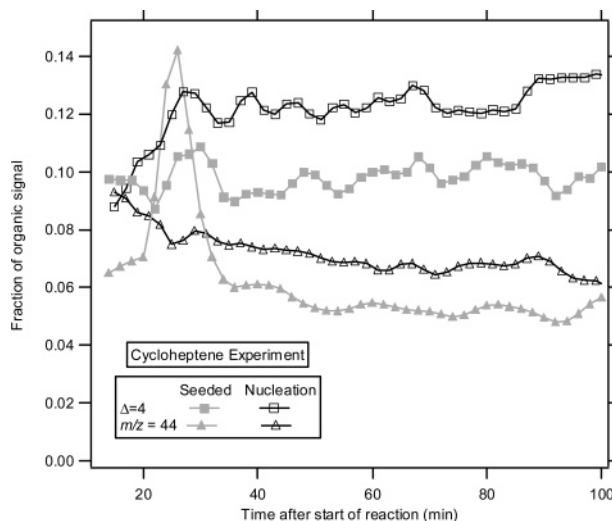


FIGURE 5. Fraction of the organic signal at $\Delta = 4$ (common Δ group for $C_nH_{2n-1}O_2^+$ fragment of acids) and m/z 44 (CO_2^+ fragment of oxygenated organics) in total SOA mass during initial stages of cycloheptene oxidation. Increased contribution of carboxylic acid fragments to total mass during initial stages of nucleation experiments may explain higher SOA density observed in these experiments.

are an indication of the functional groups in the molecule. A delta value ($\Delta = m/z - 14n + 1$, where n is the “nominal” number of CH_2 groups left on the functional group) is calculated for each m/z , which is an indication of the functionality of the fragment. For example, it is observed that unsaturated organics and aromatics yield Δ values ≤ 0 , while oxygenated organics yield Δ values ≥ 2 (31). Although more details will be discussed subsequently, it is worth noting that the SOA generated by the various systems studied here show very different characteristics based on ion series analysis. The patterns determined in chamber experiments can be used in interpreting mass spectra obtained by AMS from ambient aerosols and help provide a better understanding of the main precursors of ambient SOA.

5. Results and Discussion

5.1. Dark Ozonolysis of Cycloalkene Precursors. A series of experiments with C_5 – C_8 cycloalkenes was conducted to investigate the effect of the parent hydrocarbon structure, such as position of the double bond or a methyl substituent, on SOA yield and other physical and chemical properties of SOA (6). These experiments were conducted in the presence of ammonium sulfate seed as well as in the absence of any seed.

As depicted as an example in Figure 4, during all cycloalkene experiments, the sulfate signal of the seed increased after start of reaction, indicating that the particle collection efficiency had increased. This suggests that the SOA formed in cycloalkene ozonolysis is likely in liquid phase and that the aerosols changed as a result of condensation of SOA on the seed particles, such that the probability of bounce of organic-coated seed particles on the vaporizer decreased and thus collection efficiency increased.

The effective density of SOA was determined as described in section 3 and is tabulated in Table 2. Because the organic phase appears to be liquid, it was assumed that the particles are spherical, and thus the effective density should be a good estimate of the true material density. On average, ρ_{SOA} was 1.10 ± 0.04 g/cm³ during seeded experiments in contrast to 1.39 ± 0.05 g/cm³ during nucleation experiments with similar precursor concentrations. The fact that density of the SOA formed during nucleation experiments is ~25% higher than

TABLE 1. Summary of Conducted Experiments

date	parent hydrocarbon	initial concn, ppb	seed aerosol	RH %
10/02/03	cyclopentene, CP	173	(NH ₄) ₂ SO ₄	< 10
05/31/04	CP	192	none	< 10
10/08/03	1-methyl-cyclopentene, 1MCP	171	(NH ₄) ₂ SO ₄	< 10
02/10/03	cyclohexene, CHX	173	(NH ₄) ₂ SO ₄	< 10
02/19/03	CHX	234	(NH ₄) ₂ SO ₄	< 10
09/30/03	CHX	185	(NH ₄) ₂ SO ₄	< 10
05/28/04	CHX	152	none	< 10
02/04/03	cycloheptene, CHP	212	(NH ₄) ₂ SO ₄	< 10
02/19/03	CHP	282	(NH ₄) ₂ SO ₄	< 10
03/24/03	CHP	184	(NH ₄) ₂ SO ₄	< 10
09/30/03	CHP	186	(NH ₄) ₂ SO ₄	< 10
05/28/04	CHP	170	none	< 10
04/11/03	cyclooctene, COCT	195	(NH ₄) ₂ SO ₄	< 10
10/02/03	COCT		(NH ₄) ₂ SO ₄	< 10
05/31/04	COCT	177	none	< 10
01/27/03	1-methyl-cyclohexene, 1MCX	213	(NH ₄) ₂ SO ₄	< 10
01/29/03	1MCX	205	(NH ₄) ₂ SO ₄	< 10
02/10/03	1MCX	148	(NH ₄) ₂ SO ₄	< 10
03/03/03	1MCX	257	(NH ₄) ₂ SO ₄	< 10
10/06/06	1MCX	202	(NH ₄) ₂ SO ₄	< 10
06/07/04	1MCX	159	none	< 10
10/06/03	3-methyl-cyclohexene, 3MCX	183	(NH ₄) ₂ SO ₄	< 10
06/07/04	3MCX	178	none	< 10
10/08/03	1-methyl-cycloheptene, 1MCHP	170	(NH ₄) ₂ SO ₄	< 10
06/02/04	1MCHP	169	none	< 10
02/04/03	methylene cyclohexane, MCHX	218	(NH ₄) ₂ SO ₄	< 10
10/04/03	MCHX	181	(NH ₄) ₂ SO ₄	< 10
06/02/04	MCHX	188	none	< 10
05/18/04	<i>m</i> -xylene	143	(NH ₄) ₂ SO ₄	55
05/18/04	<i>m</i> -xylene	137	(NH ₄) ₂ SO ₄ +H ₂ SO ₄ ^a	55
03/24/03	α -pinene	186	(NH ₄) ₂ SO ₄	< 10
10/31/03	α -pinene	111	(NH ₄) ₂ SO ₄	55
10/31/03	α -pinene	113	(NH ₄) ₂ SO ₄ +H ₂ SO ₄ ^b	55
11/03/03	α -pinene	71	(NH ₄) ₂ SO ₄	55
11/03/03	α -pinene	72	(NH ₄) ₂ SO ₄ +H ₂ SO ₄ ^b	55
11/25/03	α -pinene	48	MgSO ₄	55
11/25/03	α -pinene	47	MgSO ₄ +H ₂ SO ₄ ^b	55
11/27/03	α -pinene	96	MgSO ₄	55
11/27/03	α -pinene	88	MgSO ₄ +H ₂ SO ₄ ^b	55
11/29/03	α -pinene	52	MgSO ₄	55
11/29/03	α -pinene	51	MgSO ₄ +H ₂ SO ₄ ^b	55
03/15/03	β -pinene	196	none	< 10
03/31/03	terpinolene	97	(NH ₄) ₂ SO ₄	< 10
04/11/03	terpinolene	188	(NH ₄) ₂ SO ₄	< 10
06/04/04	terpinolene	200	none	< 10
03/31/03	α -terpinene	58	none	< 10
04/04/03	Δ^3 -carene	90	(NH ₄) ₂ SO ₄	< 10
04/02/03	myrcene	83	(NH ₄) ₂ SO ₄	< 10
04/04/03	allylanisole	120	(NH ₄) ₂ SO ₄	< 10
04/02/03	linalool	72	(NH ₄) ₂ SO ₄	< 10
03/28/03	β -caryophyllene	89	none	< 10
03/28/03	α -humulene	103	none	< 10

^a Acidic seed made from 0.03 M salt+0.1 M H₂SO₄ solution. ^b Acidic seed made from 0.03 M salt+0.05 M H₂SO₄ solution.

TABLE 2. Estimated Effective Density of SOA during Cycloalkene Ozonolysis Experiments in the Presence or Absence of Seed Aerosol^a

ρ_{SOA}^{SOA} (g/cm ³)	CP	CHX	CHP	COCT	1MCP	1MCX	3MCX	MCHX	1MCHP
seeded	1.15	1.13 (0.04)	1.14 (0.05)	1.14 (<0.01)	1.07	1.06 (0.08)	1.06	1.08 (0.06)	1.11
nucleation	1.42	1.45	1.4	1.38	N/A	1.3	1.43	N/A	1.35

^a The corresponding standard deviations of the average when multiple experiments were considered are indicated in parentheses. (See Figure 1 for list of compounds.)

that of SOA formed during seeded experiments may suggest that either the particles sampled during seeded experiments are not spherical or the chemistry leading to the presence of organics in the aerosol phase is different under the two systems, such that it leads to formation of denser organic

species during nucleation experiments. As shown in Figure 5 as an example, the fragments that are dominant for oxygenated organics, mainly C_nH_{2n-1}O₂⁺ fragments with $\Delta = 4$ and CO₂⁺ fragment (m/z 44) from thermal decomposition of oxygenated organics on the AMS vaporizer, indeed

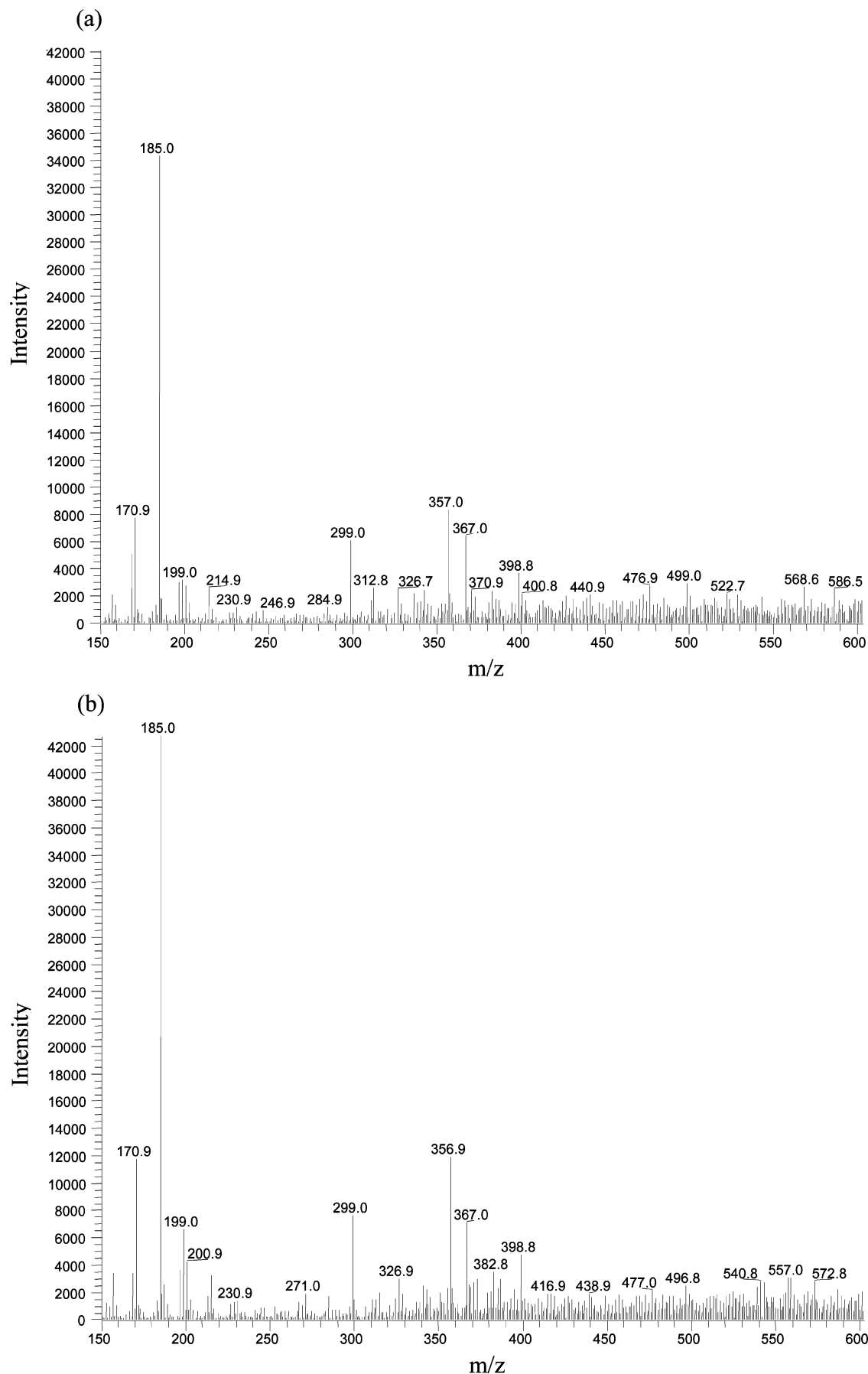


FIGURE 6. Ion trap mass spectra (negative-ion mode) of SOA from α -pinene (100 ppb) ozonolysis: (a) in the presence of MgSO_4 seed particles; (b) in the absence of any seed particles. The mass spectrum of SOA formed during nucleation exhibits higher signal intensity for acids (m/z 171, 185, 199) and oligomers (m/z 299, 357, and 399) than the seeded experiment.

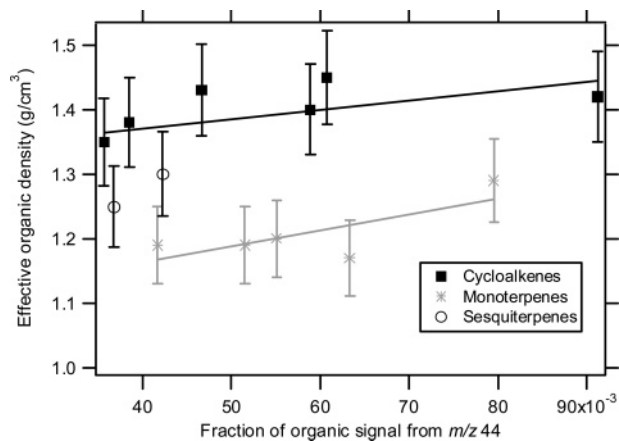


FIGURE 7. Relationship between SOA effective density with relative contribution of m/z 44 signal to total organic signal for different classes of parent hydrocarbons. Increased SOA effective density is observed with increased contribution of m/z 44 (CO_2^+ fragment of oxygenated organics) to total organic signal.

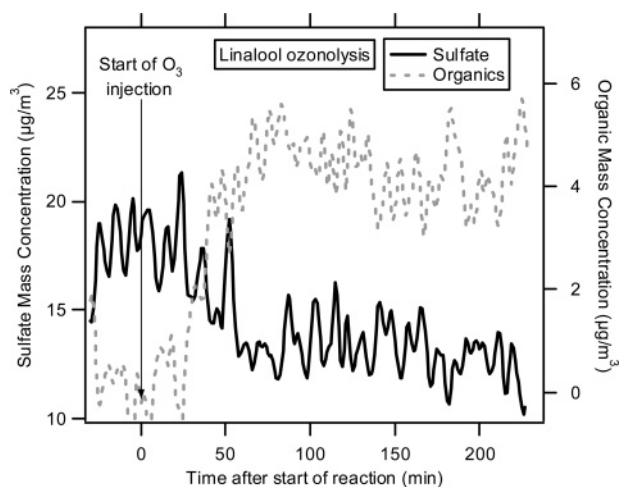


FIGURE 8. Time trends of sulfate and organic mass concentrations in ozonolysis of linalool. Decrease in sulfate signal after SOA formation indicates poorer collection efficiency of particles and may suggest formation of solid SOA within the AMS.

contribute to a greater extent to the total SOA mass for nucleation-generated SOA of cycloheptene.

Consistent observations of increased ion signal intensities of organic acids in the SOA during nucleation experiments have also been made in the ozonolysis of α -pinene by ion

trap mass spectrometry (electrospray ionization source, direct infusion injection of the SOA sample). Although this observation was made in a different system (ozonolysis of α -pinene rather than cycloalkenes), it is still consistent with the qualitative trends of the AMS observations presented here. For example, it is seen in the negative-ion mode mass spectra in Figure 6 that ion signals at m/z 171, 185, and 199 (corresponding to norpinic acid, pinic acid, and hydroxy pinonic acid, respectively, and likely their isomers, all gas-phase oxidation products) increase by 50%, 24%, and 130%, respectively, in the nucleation experiment (Figure 6b) as compared to the nonacid seeded one (Figure 6a). It is also seen in Figure 6b that ion signal intensities of some oligomers (m/z 299, 357, and 399) increase by at least 25% in the nucleation experiment, which may explain in part its higher SOA yield as compared to that in the nonacid seeded experiment (11).

There is a trend of increasing SOA effective density with increasing contribution of m/z 44 to the total organic signal in the oxidation of many of the hydrocarbon precursors studied here (Figure 7). Although it is not possible to rule out completely the possibility of shape effects on lower estimates of SOA effective density during seeded experiments, the AMS mass spectra provided the evidence that there is an increased contribution of more oxygenated organics, which are generally denser, to the total SOA during nucleation experiments.

During the course of the cycloalkene ozonolysis experiments, the specific features of the organic mass spectra did not exhibit much change in time, as shown in Figure 3d,e, except for an increase in absolute intensity of organic peaks relative to the sulfate peaks.

5.2. Dark Ozonolysis of Biogenic Precursors. SOA formation during ozonolysis of biogenic precursors, monoterpenes, sesquiterpenes, and oxygenated terpenes, was studied. The phase/morphology of the SOA produced is such that the seed signal decreased after the start of condensation of organics, indicating less efficient collection of SOA-coated sulfate particles. One possible explanation is that the SOA formed during ozonolysis of biogenics is in solid phase under the vacuum conditions of the AMS; therefore, there is a greater probability of bounce of these SOA-coated particles on the AMS vaporizer. For example, it is shown in Figure 8 that after start of condensation of SOA from ozonolysis of linalool, the sulfate signal of the seed decreased by $\sim 26\%$, which cannot be explained only by particle loss to the walls.

The effective density of SOA formed from ozonolysis of biogenic hydrocarbons was calculated following the method outlined in section 3. Because the particles are likely in solid phase within the AMS and potentially nonspherical, the estimated densities are a lower bound of the true material densities (30). On average, biogenically derived SOA have

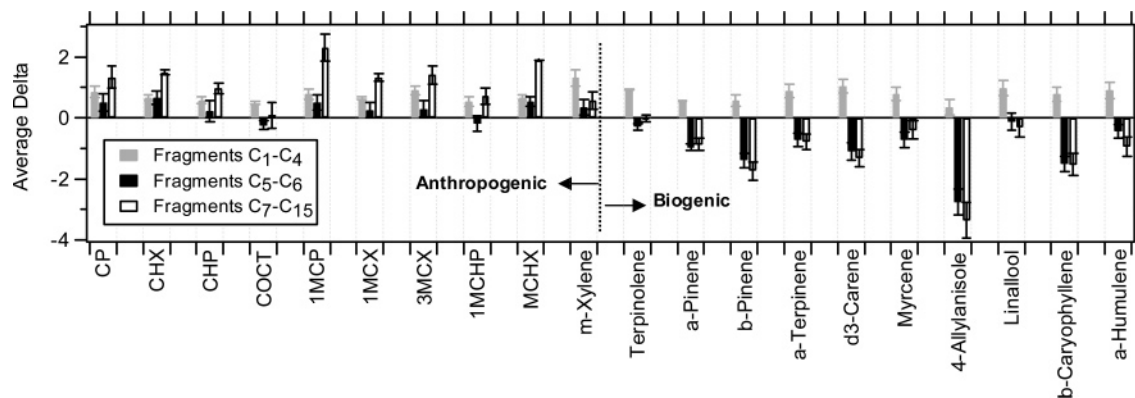


FIGURE 9. Average Δ values of different size fragments for anthropogenic and biogenic SOA. In contrast to anthropogenic SOA, larger fragments of biogenic SOA have dominantly negative Δ values, indicating the presence of terpene derivative structures and unsaturated or cyclic oxygenated compounds.

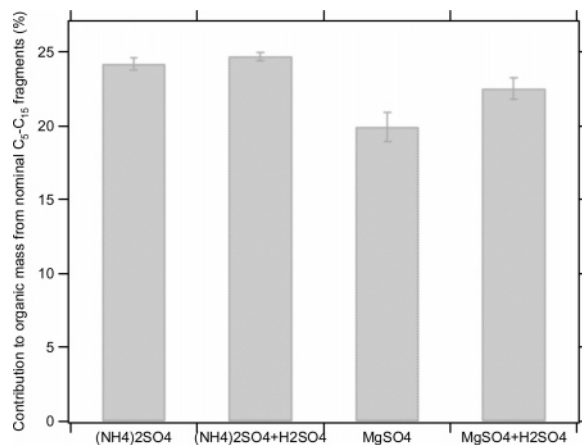


FIGURE 10. Relative contribution of higher molecular weight fragments to total organic mass during ozonolysis of α -pinene in the presence of different seed particles. Increased fraction of larger fragments to SOA formed during acidic MgSO_4 experiment indicates greater extent of acid-catalyzed reactions that form higher molecular weight species.

lower “effective” densities as compared to the SOA formed from nucleation-oxidation of cycloalkenes (Table 3), which

TABLE 3. Estimated Effective Density of SOA during Biogenic Ozonolysis Experiments^a

parent HC	ρ^{SOA} (g/cm ³)	parent HC	ρ^{SOA} (g/cm ³)
terpinolene ^b	1.29 (0.03)	4-allylanisole	1.04
α -pinene ^c	1.19	linalool	0.64
β -pinene	1.20	β -caryophyllene	1.3
Δ^3 -carene	1.19	α -humulene	1.25
myrcene	1.17		

^a The corresponding standard deviations of the average when multiple experiments were considered are indicated in parentheses. These densities are lower limits of the true material densities, as shape effects for these experiments tend to reduce the measured effective densities. All estimates are based on seeded experiments except for β -pinene, β -caryophyllene, and α -humulene (see Table 1). ^b Seeded experiments. ^c Experiment on 03/24/03.

may be due to real differences in material density as well as shape effects.

The biogenic precursors studied here showed distinct characteristics in the ion series pattern when compared to those of cycloalkene and *m*-xylene SOA. Generally, fragments in different *m/z* ranges exhibit different patterns of Δ values.

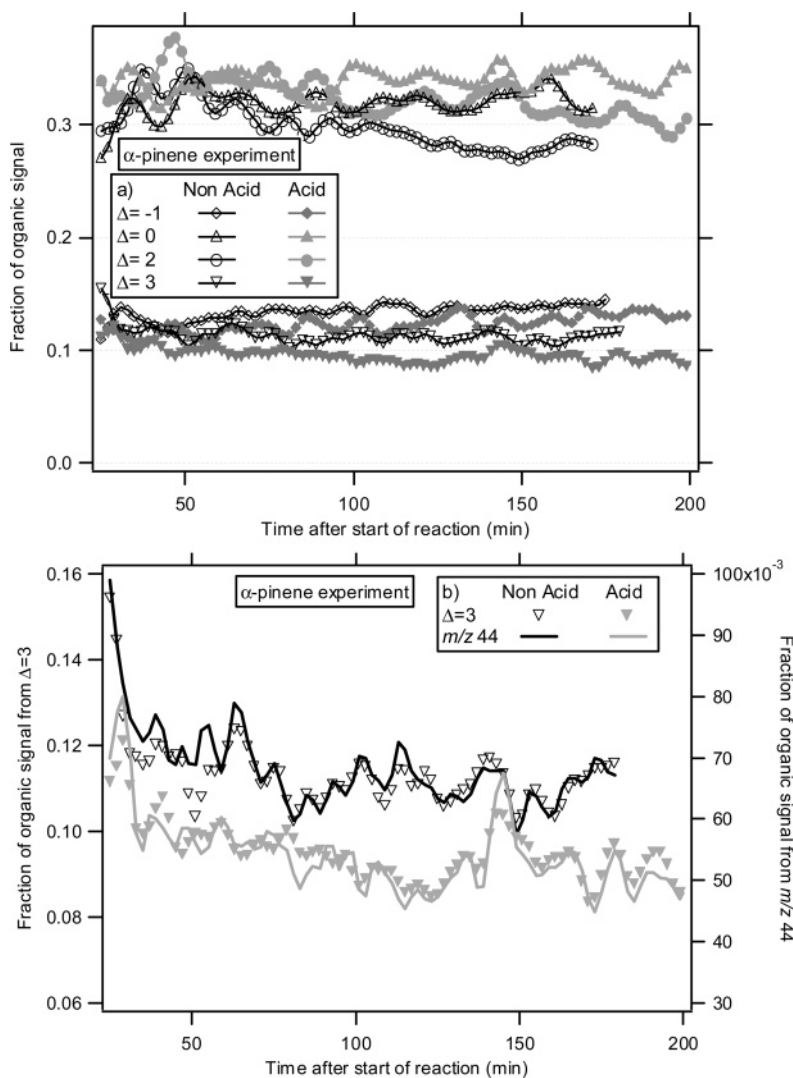


FIGURE 11. (a) Relative contribution of different Δ groups to total SOA mass formed from ozonolysis of α -pinene in the presence of MgSO_4 or $\text{MgSO}_4 + \text{H}_2\text{SO}_4$ seed aerosols. (b) Fraction of organic signal due to *m/z* 44 and $\Delta = 3$ during ozonolysis of α -pinene in the presence of MgSO_4 or $\text{MgSO}_4 + \text{H}_2\text{SO}_4$ seed. Increased contribution of $\Delta = 0$ and decreased contribution of $\Delta = -1$ and $\Delta = 3$ (or *m/z* 44) to total mass during acid experiment are consistent with acid-catalyzed reactions.

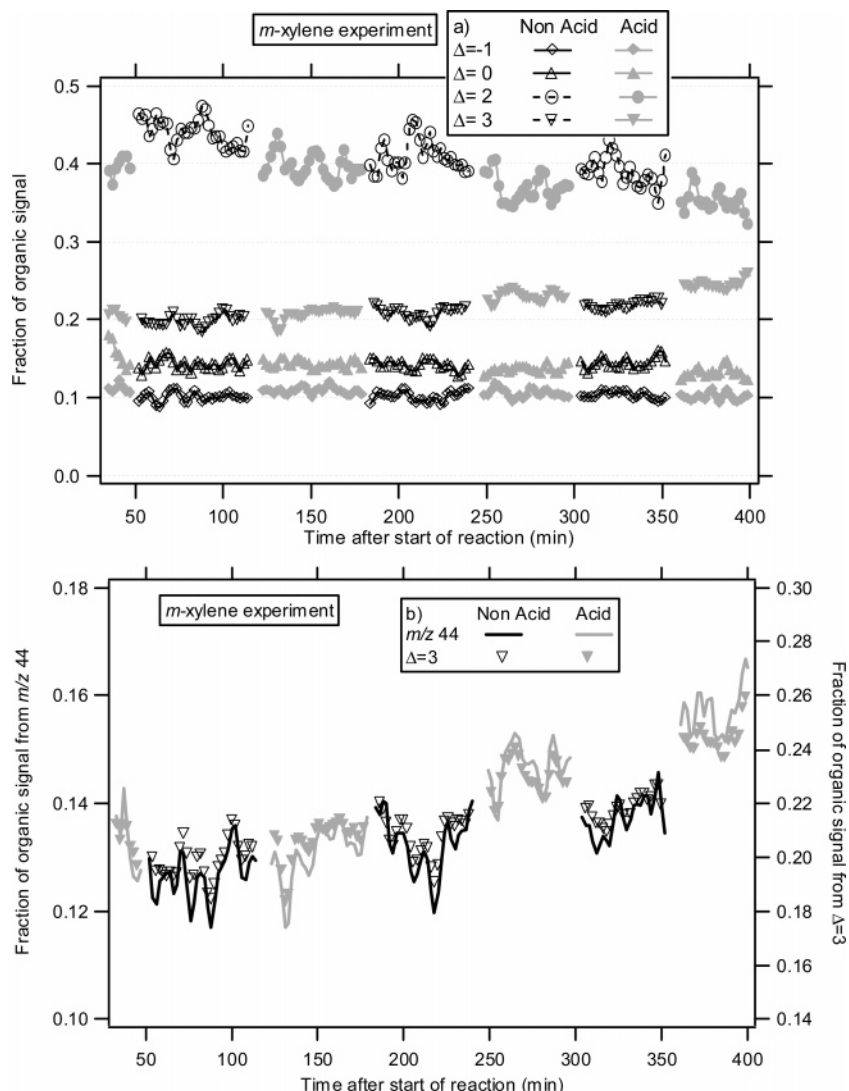


FIGURE 12. (a) Relative contribution of different Δ groups to total SOA mass formed from photooxidation of *m*-xylene in the presence of $(\text{NH}_4)_2\text{SO}_4$ or $(\text{NH}_4)_2\text{SO}_4 + \text{H}_2\text{SO}_4$ seed aerosols. (b) Fraction of organic signal due to m/z 44 and $\Delta = 3$ during photooxidation of *m*-xylene in the presence of $(\text{NH}_4)_2\text{SO}_4$ or $(\text{NH}_4)_2\text{SO}_4 + \text{H}_2\text{SO}_4$ seed aerosols. Increased contribution of $\Delta = 3$ to total signal correlates well with increased contribution of CO_2^+ fragment of oxygenated organics (m/z 44).

Here, three categories with different fragment size, with the nominal ranges of $\text{C}_1\text{--C}_4$, $\text{C}_5\text{--C}_6$, and $\text{C}_7\text{--C}_{15}$, are considered because the Δ patterns shift from fragments of $\text{C}_1\text{--C}_4$ category to those of $\text{C}_7\text{--C}_{15}$. As shown in Figure 9, the larger fragments of SOA from biogenic precursors show a sharp contrast to cycloalkene and *m*-xylene SOA in that these larger fragments have dominantly negative Δ values. An exception to this observation is terpinolene; however, the backbone of terpinolene molecule is more similar to that of a methylene-substituted cycloalkene. Thus, it is not surprising that the fragmentation pattern of SOA formed from terpinolene ozonolysis is closer to that of SOA formed from ozonolysis of cycloalkenes. Dominant negative Δ values are indicative of organic molecules that are terpene derivatives or have unsaturated or cyclic oxygenated structures.

The bicyclic compounds studied here, α -pinene, β -pinene, and Δ^3 -carene, have similar average Δ values for larger fragment sizes, as shown in Figure 9, due to the similarity in their structures. A quite different precursor studied was 4-allylanisole, the SOA from which exhibits a very dominant low Δ value in its fragmentation pattern. We conclude that the benzyl fragment (m/z 77, $\Delta = -6$) and $\text{CH}_3\text{OC}_6\text{H}_4\text{CH}_2^+$ fragment (m/z 121, $\Delta = -4$) are the dominant contributors to the low average Δ values. Among all of the biogenic

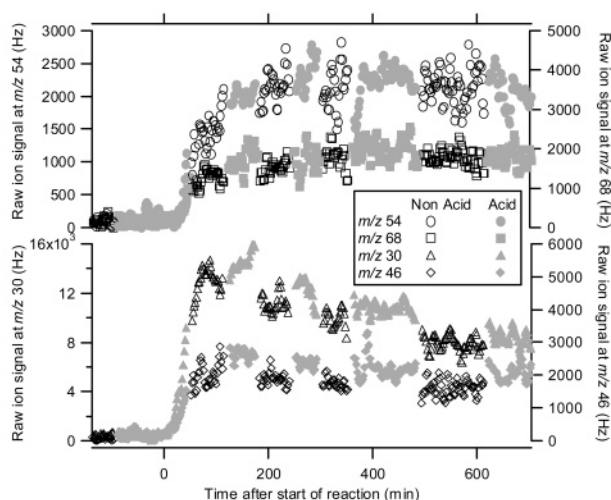


FIGURE 13. Time trend of main fragments of 2,5-furandione (m/z 54), 3-methyl-2,5-furandione (m/z 68), and nitrate (m/z 30 and 46) during photooxidation of *m*-xylene. Increase in the intensity of these fragments after start of reaction is consistent with the presence of furandione compounds and nitro-compounds in SOA.

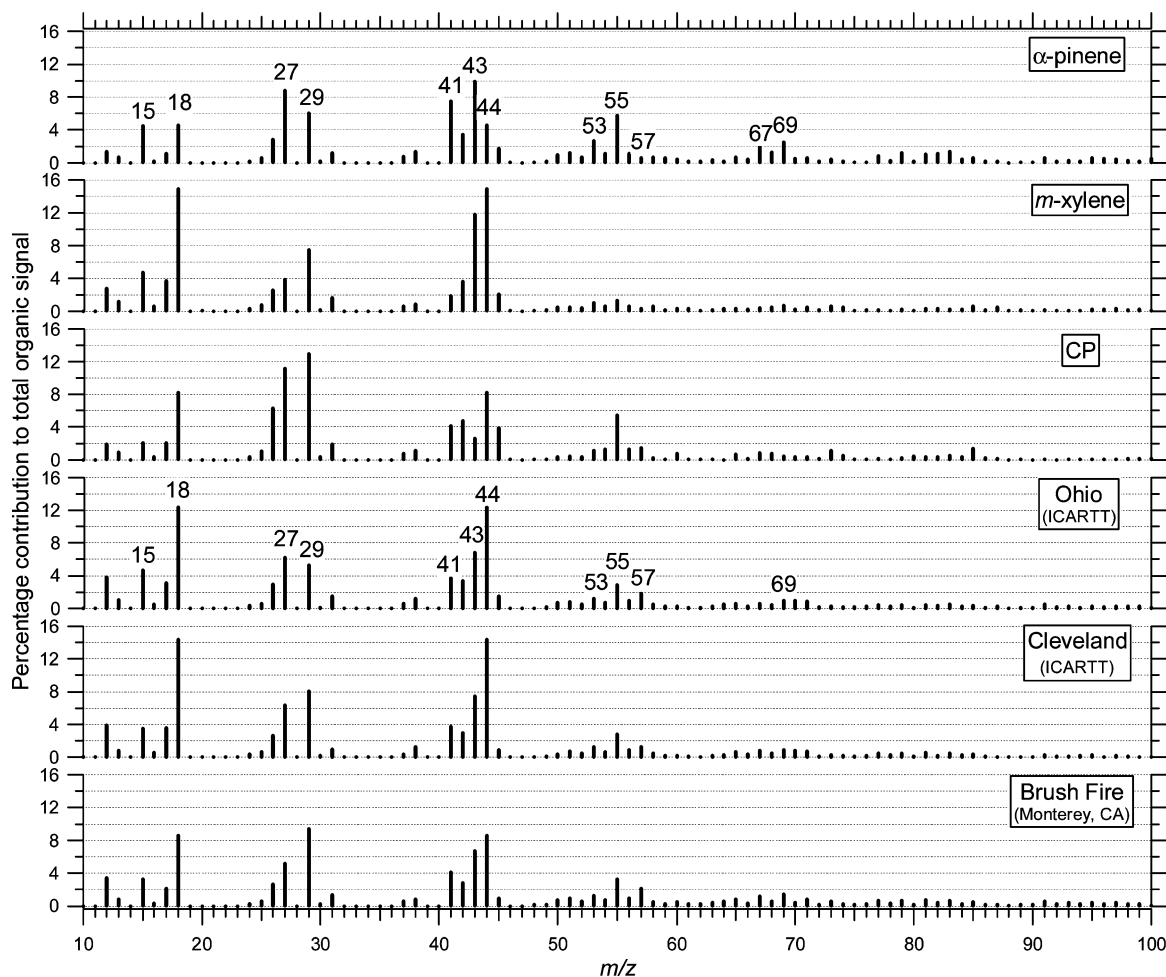


FIGURE 14. Mass spectra of SOA formed during α -pinene, *m*-xylene, and cyclopentene oxidation experiments as well as ambient organic mass spectra of Ohio background pollution, Cleveland, OH pollution, and brush fire plumes. Common dominant fragments at m/z 41, 43, 44, and 55 are observed in all mass spectra.

TABLE 4. Estimated pH Values of Seed Particles and Their Relative Bulk Concentrations

	$(\text{NH}_4)_2\text{SO}_4$ (0.03 M)	$(\text{NH}_4)_2\text{SO}_4 + \text{H}_2\text{SO}_4$ (0.03 M + 0.05 M)	MgSO_4 (0.03 M)	$\text{MgSO}_4 + \text{H}_2\text{SO}_4$ (0.03 M + 0.05 M)
pH (RH = 55%)	4.6	2.4	6.5	-0.3

precursors studied here, the SOA formed from ozonolysis of linalool exhibits the smallest contribution of larger fragments to the total SOA mass (only 4.5% from C_7 – C_{15} fragments). Because of the chemical structure and position of the double bonds in linalool, it is suspected that the primary ozonolysis products of linalool are only small-oxygenated molecules that only partition into the aerosol phase to a small extent. This hypothesis is further supported by low SOA yield observed for linalool. It is also interesting to note that the SOA formed from linalool yielded the lowest estimate of effective density of all systems studied, which may suggest the growth of somewhat nonspherical or porous particles. During the oxidation of biogenic precursors that have similar molecular weight and similar structures, α -pinene, Δ^3 -carene, α -terpinene, and terpinolene, it was observed that the organic yield was proportional to the mass fraction of larger organic fragments (C_5 – C_{15}). This is an indication that the SOA systems that have greater organic yields also contain greater amounts of larger organic molecules, and possibly have a higher contribution of oligomeric structures (or of molecules that are more resistant to fragmentation) to the total SOA mass.

It is suspected that the reactions leading to formation of higher molecular weight SOA species are catalyzed in the

presence of acids or bases (9, 12). To assess the effect of seed particle acidity on SOA formation, α -pinene ozonolysis was carried out in the presence of both neutral and acidic ammonium sulfate seed as well as magnesium sulfate seed. The choice of these seeds allowed the study of the effect of seed type and pH on possible aerosol-phase reactions. The pH values of the bulk solutions from which the seeds were prepared from (at 55% relative humidity) are tabulated in Table 4 (9). During acid runs, sulfate fragmentation patterns in the mass spectra were analyzed to ascertain the acidity of the seed. Sulfate fragmentation patterns for pure and acidic ammonium sulfate were very similar because the most probable form of the anion in both systems is bisulfate. However, during acid MgSO_4 experiments, at least an order of magnitude increase in signals at fragments that are dominant for H_2SO_4 , m/z 81 (HSO_3^+) and m/z 98 (H_2SO_4^+), relative to the SO^+ fragment was observed.

As mentioned earlier, recent studies have shown evidence of polymerization and presence of high molecular weight species in SOA (9, 11, 12). Organic mass spectra obtained from the AMS are also suggestive of the presence of higher molecular weight fragments in SOA. Figure 10 indicates the relative contribution of higher molecular weight fragments

to the total organic mass observed during α -pinene ozonolysis experiments in the presence of different seeds. The difference in contribution of larger fragments to the organic mass can be an indication of the presence of higher molecular weight species in the SOA or presence of molecules that are more resistant to fragmentation. The difference between experiments with ammonium sulfate and acidic ammonium sulfate is statistically insignificant. In addition, the fragmentation patterns of SOA, analyzed with the time series of Δ values, during these experiments are very similar. This can be explained because the pH difference between the ammonium sulfate and acidic ammonium sulfate solutions used is only ~ 2.2 , and thus the sensitivity of the two systems to acid-catalyzed reactions is not significantly different. The contribution of larger organic fragments to the organic mass increased, however, by 13% in the presence of acidic MgSO_4 seed as compared to pure MgSO_4 seed. This indicates that acid-catalyzed heterogeneous reactions that form high molecular weight species occur to a greater extent in the presence of acidic MgSO_4 seed, leading to a greater contribution of larger fragments to the total organic mass. Similar observations have been made during these experiments in terms of percentage of increased organic yield of α -pinene in the presence of ozone and the same pairs of seed: presence of sulfuric acid with MgSO_4 seed led to an increased organic yield of 7–15%, while presence of sulfuric acid with ammonium sulfate seed led to an increased yield of $<5\%$ (9). Because of slower evaporation of the MgSO_4 (neutral or acidic) seed on the AMS vaporizer as compared to ammonium sulfate, and to avoid build up of the salt on the vaporizer, the vaporizer temperature was increased to $\sim 750^\circ\text{C}$ during experiments with MgSO_4 seed. Because organic species are expected to fragment to a greater extent at higher temperatures (32), it is possible to compare mass spectra of SOA only from experiments during which the AMS vaporizer is operated at the same temperature. For example, the degree, if any, to which slightly more acidic pure ammonium sulfate seed might have increased the degree of polymerization as compared to pure MgSO_4 seed cannot be inferred from Figure 10 because the AMS vaporizer was operated at a higher temperature with MgSO_4 seed and thus shifted the fragmentation of SOA toward smaller fragments.

Differences of fragmentation patterns are observed, as shown in Figure 11. For example, the contribution of $\Delta = -1$ and $\Delta = 3$ during acid MgSO_4 runs is lower, while that of $\Delta = 0$ is higher when comparing to the nonacid MgSO_4 runs (Figure 11a). These variations are consistent with suggested acid-catalyzed reaction mechanisms, for example, acid-catalyzed gem-diol reactions as well as acid dehydration of monomers in α -pinene ozonolysis. Polymerization through gem-diol reaction involves the reaction of hydroxyl and carbonyl groups of monomers. Such reaction of α -pinene oxidation products, which still contain one of the cyclic structures of α -pinene, would result in lower contribution of $\Delta = -1$ patterns to the oligomers. Acid dehydration in the aerosol phase would also lead to less contribution of organic acids/diacids to the total organic mass, and therefore less contribution of m/z 44 (CO_2^+ ion fragment) and $\Delta = 3$ to the total organic signal. Figure 11b shows the correlation of the reduction in $\Delta = 3$ fragments with decrease in CO_2^+ signal (m/z 44), which is attributed to thermal decomposition of oxygenated organic molecules, such as carboxylic acids or peroxides. This reduction is thus consistent with the acid dehydration mechanism. Furthermore, Tolocka et al. (10) outlined a mechanism of acid-catalyzed ring cleavage of primary ozonolysis products of α -pinene. The ring cleavage, which leads to smaller unsaturated oxidized molecules (such as ketones, aldehydes, or alcohols) with dominant $\Delta = 0$ patterns, may explain the increased contribution of $\Delta = 0$ patterns under acidic conditions (Figure 11a).

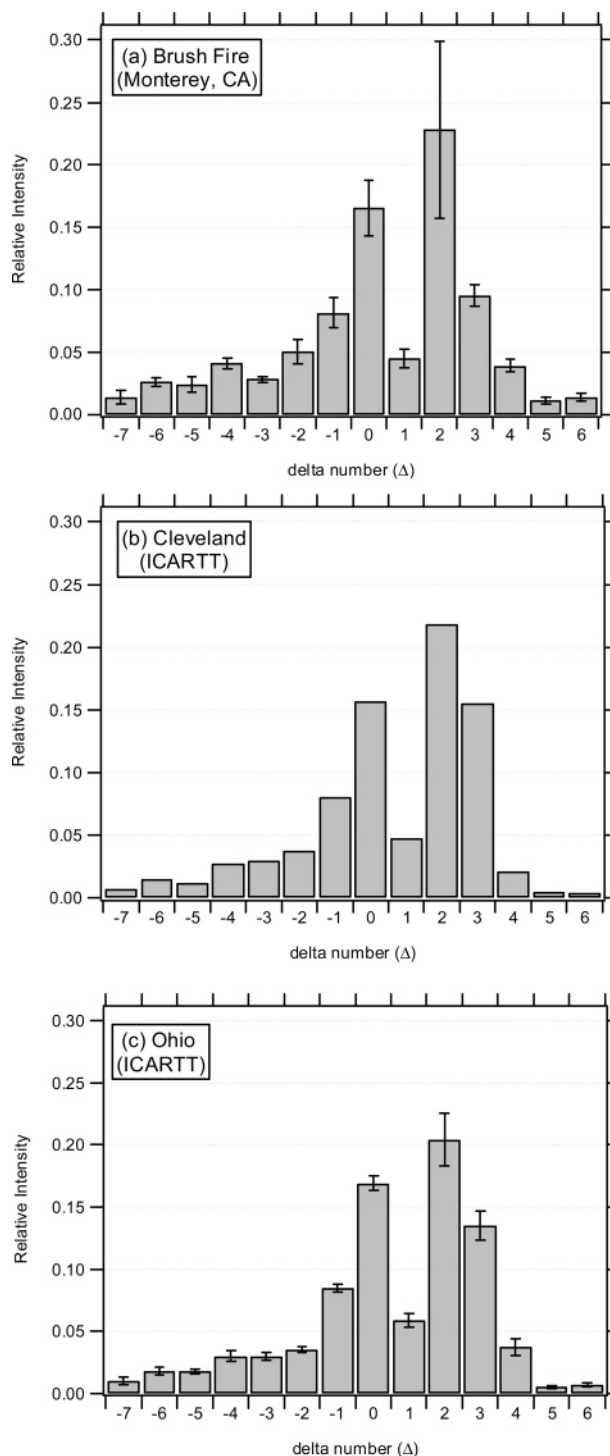


FIGURE 15. Δ analysis of mass spectra obtained from brush fire, Cleveland, and background Ohio pollution plumes. Organic composition in all of these air masses is very similar and dominated by fragments with $\Delta = 2, 0,$ and 3 . In cases when similar air masses were sampled in more than one occasion, the error bars represent the standard deviation of the average to indicate the extent of variation in the averaged Δ values.

5.3. Photooxidation of *m*-Xylene. The photooxidation of *m*-xylene was studied in the presence of pure and acidic ammonium sulfate seed, 45 ppb of NO , 15 ppb of NO_2 , and 240 ppb of propene. Due to the nature of photooxidation experiments, that is, simultaneous reactions in the two chambers with different seed aerosols, the AMS sampled alternatively from each chamber. In contrast to the morphology of SOA formed during cycloalkene ozonolysis but

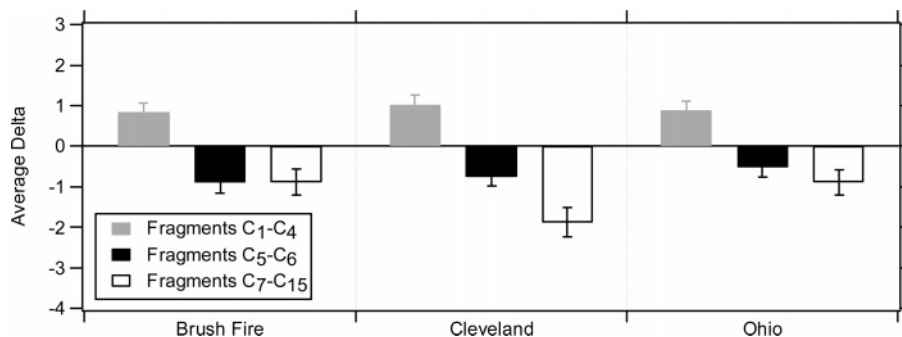


FIGURE 16. Average Δ values of different size fragments of ambient organic mass spectra obtained in brush fire, Cleveland pollution, and background Ohio pollution plumes. Larger fragments in these mass spectra exhibit negative Δ values. The error bars represent the standard deviation of the averaged Δ values in each category.

similar to biogenic SOA, SOA condensed on the seed during *m*-xylene photooxidation caused the sulfate seed signal to decrease, indicating poorer collection efficiency of the seed after SOA condensation likely due to formation of solid-phase SOA under the AMS vacuum conditions.

Figure 12 shows the evolution of the contribution of different ion series to the total organic signal during the experiment. Similar to pure ammonium sulfate and acidic ammonium sulfate experiments with α -pinene, there is little variation between the two seed types. Unlike ozonolysis of α -pinene, however, the contribution of $\Delta = 3$ increased by $\sim 16\%$ and $\sim 30\%$, during nonacid and acid experiments, respectively, over a similar time period after the start of reaction, as did the contribution of organic signal from m/z 44 (CO_2^+ ion fragment), indicating a more prolonged oxidation process of the organics during the photooxidation study (Figure 12b).

Previous work on composition of SOA formed under low-humidity photooxidation of *m*-xylene identified 3-methyl-2,5-furandione, *m*-toluic acid, and 2,5-furandione together with some nitrophenol compounds as the dominant species, contributing, respectively, to 61%, 9.2%, 5.2%, and 5.8% of the identified mass (33). The mass spectra obtained by the AMS exhibited increase in signals at m/z 54 and 68 that are consistent with the presence of 2,5-furandione and 3-methyl-2,5-furandione (Figure 13). Based on the contribution of m/z 68 to the total organic signal while sampling from the chamber and for pure 3-methyl-2,5-furandione during an off-line calibration procedure, the estimated mass of 3-methyl-2,5-furandione in *m*-xylene experiment was at most $\sim 6\%$ of the total organic mass. It is not possible though to compare this estimate directly with that of Forstner et al. (33) because of the following reasons: (1) the humidity levels in the two sets of experiments are not the same; this is an important factor to consider because anhydrides tend to form carboxylic acids in the presence of water molecules (34); (2) percentage of the identified mass relative to total SOA mass has not been reported by Forstner et al. Also shown in Figure 13 are the time trends of fragments at m/z 30 and 46, two dominant fragments of nitrate. The increased signal intensity of these fragments after start of the reaction is consistent with the presence of nitro compounds in the SOA. The mass of 2,6-dimethyl-4-nitrophenol, identified in previous photooxidation studies of *m*-xylene, was estimated to be at most $\sim 2\%$ of the total organic mass based on the contribution of m/z 137 and 167 fragments to the total organic signal during an off-line calibration of pure 2,6-dimethyl-4-nitrophenol by the AMS. Although care has been taken to use fragments that do not have signal contributions from known inorganic compounds, the calculated contributions of 3-methyl-2,5-furandione and 2,6-dimethyl-4-nitrophenol to the total organic mass may be overestimated because some other

organic species may also fragment at the masses used in these calculations.

6. Common Features in Different Systems

The patterns observed in the mass spectra of chamber-derived SOA for groups of precursors such as cycloalkenes and terpenes demonstrate that similar mixture of species produce roughly similar mass spectra in the AMS. Organic mass spectra obtained from oxidation of α -pinene, *m*-xylene, and cyclopentene are compared in Figure 14 with those obtained in the ambient, sampling Ohio background pollution, measured airborne during August 2004, Cleveland, OH pollution, obtained on the ground at the Cleveland International Airport during August 2004, and brush-fire plumes, obtained in the vicinity of Monterey, CA during July 2003. All of the ambient samples are dominated by signals at m/z 18 and 44 (similar to *m*-xylene and cyclopentene), and yet there is significant contribution from fragments at m/z 27, 29, 41, 43, and 55 in all cases. Furthermore, ambient mass spectra show a more dominant feature at m/z 57 as compared to chamber-derived SOA, indicating greater presence of the alkyl groups in the ambient organic aerosols. The mass spectrum of the brush-fire plume also indicates signals at m/z 67 and 69, similar to that of α -pinene, which are common for unsaturated hydrocarbons, unsaturated alcohols, or unsaturated carbonyl groups.

Similarities between organic composition of the brush fire, Cleveland pollution, and background Ohio pollution plumes are apparent in the distribution of Δ values obtained from the corresponding mass spectra as well (Figure 15). The dominant fragments in these mass spectra are those with $\Delta = 2$ (alkyl groups and saturated carbonyls), $\Delta = 0$ (unsaturated hydrocarbons, unsaturated alcohols, and unsaturated carbonyls), $\Delta = 3$ (oxygenated organics and nitro compounds), and $\Delta = -1$. In addition, the organic mass spectra obtained from brush fire plumes show more contribution from fragments with negative Δ values as compared to the mass spectra of Cleveland and background Ohio pollution, indicating the presence of more terpene derivative, aromatic, unsaturated, or cyclic structures. Similar dominance of fragments with Δ values of $\Delta = 0, 2$, and 3 has been observed in the organic mass spectra obtained during other ambient studies (17, 35). The average Δ values of different size fragments from ambient organic mass spectra are compared in Figure 16. Commonly, the larger fragments exhibit negative average Δ values, indicating dominance of unsaturated, aromatic, or cyclic structures, while the smaller fragments have positive Δ values, indicating dominance of more saturated and oxygenated structures.

In previous studies with the AMS, fragments at m/z 44 (CO_2^+ fragment of oxygenated organics) and m/z 57 (common fragment of alkyl groups) have been identified as indicators

TABLE 5. Relative Contribution of Different Fragments to the Total Organic Signal (See Table 1 for List of Compounds and Experiments)

hydrocarbon	m/z 44	m/z 57	hydrocarbon	m/z 44	m/z 57
CHX ^a	0.061	0.018	β -pinene	0.055	0.006
1MCX ^a	0.043	0.019	α -terpinene	0.058	0.008
CHP ^a	0.059	0.020	terpinolene ^d	0.080	0.008
MCHX ^a	0.067	0.021	myrcene	0.063	0.011
COCT ^a	0.039	0.017	linalool	0.056	0.011
m-xylene ^b	0.149	0.004	α -humulene	0.037	0.012
α -pinene ^c	0.042	0.006	β -caryophyllene	0.042	0.008

^a Nucleation experiment. ^b Seeded experiment with ammonium sulfate. ^c Experiment on 3/24/03. ^d Seeded experiment.

for oxygenated and hydrocarbon-like organic aerosols, respectively (14, 19, 36–38). Keeping in mind that the spectra obtained in chamber studies are all SOA spectra, for comparison purposes and as a reference, the relative contributions of these fragments to the total organic mass in several systems studied here are presented in Table 5.

Acknowledgments

This research was funded by the U.S. Environmental Protection Agency Science to Achieve Results (STAR) Program grant number RD-83107501-0, managed by EPA's Office of Research and Development (ORD), National Center for Environmental Research (NCER), U.S. Department of Energy Biological and Environmental Research Program DE-FG03-01ER63099, and by the National Science Foundation grant ATM-0340832. We thank J. D. Allan (UMIST) for fundamental AMS data analysis software, M. R. Canagaratna and T. Onasch (Aerodyne Research, Inc.) for developing the software for ion series analysis of AMS data, and F. Brechtel (Caltech and Brechtel Manufacturing Inc.) for helpful discussions.

Literature Cited

- Pandis, S. N.; Paulson, S. E.; Seinfeld, J. H.; Flagan, R. C. Aerosol formation in the photooxidation of isoprene and β -pinene. *Atmos. Environ.* **1991**, *25*, 997–1008.
- Hoffmann, T.; Odum, J. R.; Bowman, F. M.; Collins, D.; Klockow, D.; Flagan, R. C.; Seinfeld, J. H. Formation of organic aerosols from the oxidation of biogenic hydrocarbons. *J. Atmos. Chem.* **1997**, *26*, 189–222.
- Odum, J. R.; Jungkamp, T. P. W.; Griffin, R. J.; Flagan, R. C.; Seinfeld, J. H. The atmospheric aerosol-forming potential of whole gasoline vapor. *Science* **1997**, *276*, 96–99.
- Odum, J. R.; Jungkamp, T. P. W.; Griffin, R. J.; Forstner, H. J. L.; Flagan, R. C.; Seinfeld, J. H. Aromatics, reformulated gasoline, and atmospheric organic aerosol formation. *Environ. Sci. Technol.* **1997**, *31*, 1890–1897.
- Griffin, R. J.; Cocker, D. R.; Flagan, R. C.; Seinfeld, J. H. Organic aerosol formation from the oxidation of biogenic hydrocarbons. *J. Geophys. Res.* **1999**, *104*, 3555–3567.
- Keywood, M. D.; Varutbangkul, V.; Bahreini, R.; Flagan, R. C.; Seinfeld, J. H. Secondary organic aerosol formation from the ozonolysis of cycloalkenes and related compounds. *Environ. Sci. Technol.* **2004**, *38*, 4157–4164.
- Kalberer, M.; Paulsen, D.; Sax, M.; Steinbacher, M.; Dommen, J.; Prevot, A. S. H.; Finessa, R.; Weingartner, E.; Frankevich, V.; Zenobi, R.; Baltensperger, U. Identification of polymers as major components of atmospheric organic aerosols. *Science* **2004**, *303*, 1659–1662.
- Limbeck, A.; Kulmala, M.; Puxbaum, H. Secondary organic aerosol formation in the atmosphere via heterogeneous reaction of gaseous isoprene on acidic particles. *Geophys. Res. Lett.* **2003**, *30*, 1996.
- Gao, S.; Ng, N. L.; Keywood, M.; Varutbangkul, V.; Bahreini, R.; Nenes, A.; He, J.; Yoo, K. Y.; Beauchamp, J. L.; Hodyss, R. P.; Flagan, R. C.; Seinfeld, J. H. Particle phase acidity and oligomer formation in secondary organic aerosol. *Environ. Sci. Technol.* **2004**, *38* (24), 6582–6589.
- Tolocka, M. P.; Jang, M.; Ginter, J. M.; Cox, F. J.; Kamens, R. M.; Johnston, M. V. Formation of oligomers in secondary organic aerosol. *Environ. Sci. Technol.* **2004**, *38*, 1428–1434.

- Gao, S.; Keywood, M.; Ng, N. L.; Surratt, J.; Varutbangkul, V.; Bahreini, R.; Flagan, R. C.; Seinfeld, J. H. Low-molecular-weight and oligomeric components in secondary organic aerosol from the ozonolysis of cycloalkenes and α -pinene. *J. Phys. Chem.* **2004**, *108* (46), 10147–10164.
- Jang, M.; Czoschke, N. M.; Lee, S.; Kamens, R. M. Heterogeneous atmospheric aerosol production by acid-catalyzed particle-phase reactions. *Science* **2002**, *298*, 814–817.
- Jayne, J. T.; Leard, D. C.; Zhang, X.; Davidovits, P.; Smith, K. A.; Kolb, C. E.; Worsnop, D. W. Development of an Aerosol Mass Spectrometer for size and composition analysis of submicron particles. *Aerosol Sci. Technol.* **2000**, *33*, 49–70.
- Jimenez, J. L.; Jayne, J. T.; Shi, Q.; Kolb, C. E.; Worsnop, D. R.; Yourshaw, I.; Seinfeld, J. H.; Flagan, R. C.; Zhang, X.; Smith, K. A.; Morris, J.; Davidovits, P. Ambient aerosol sampling with an Aerosol Mass Spectrometer. *J. Geophys. Res.* **2003**, *108*, 8425.
- Bahreini, R.; Jimenez, J. L.; Wang, J.; Flagan, R. C.; Seinfeld, J. H.; Jayne, J. T.; Worsnop, D. R. Aircraft-based aerosol size and composition measurements during ACE-Asia using an Aerodyne aerosol mass spectrometer. *J. Geophys. Res.* **2003**, *108*, 8645.
- Allan, J. D.; Bower, K. N.; Coe, H.; Boudries, H.; Jayne, J. T.; Canagaratna, M. R.; Millet, D. B.; Goldstein, A. H.; Quinn, P. K.; Weber, R. J.; Worsnop, D. R. Submicron aerosol composition at Trinidad Head, California, during ITCT 2K2: Its relationship with gas-phase volatile organic carbon and assessment of instrument performance. *J. Geophys. Res.* **2004**, *109*, D23S24.
- Drewnick, F.; Schwab, J. J.; Jayne, J. T.; Canagaratna, M.; Worsnop, D. R.; Demerjian, K. L. Measurements of ambient aerosol composition during PMTACS-NY 2001 using an aerosol mass spectrometer. Part I: Mass Concentrations. *Aerosol Sci. Technol.* **2004**, *38*, 92–103.
- Drewnick, F.; Schwab, J. J.; Jayne, J. T.; Canagaratna, M.; Worsnop, D. R.; Demerjian, K. L. Measurements of ambient aerosol composition during PMTACS-NY 2001 using an aerosol mass spectrometer. Part II: Chemically speciated mass distributions. *Aerosol Sci. Technol.* **2004**, *38*, 104–117.
- Zhang, Q.; Stanier, C. O.; Canagaratna, M.; Jayne, J. T.; Worsnop, D. R.; Pandis, S. N.; Jimenez, J. L. Insights into the chemistry of nucleation bursts and new particle growth events in Pittsburgh based on aerosol mass spectrometry. *Environ. Sci. Technol.* **2004**, *38*, 4797–4809.
- O'Dowd, C. D.; Jimenez, J. L.; Bahreini, R.; Flagan, R. C.; Seinfeld, J. H.; Hameri, K.; Pirjola, L.; Kulmala, M.; Jennings, S. G.; Hoffmann, T. Marine aerosol formation from biogenic iodine emissions. *Nature* **2002**, *417*, 632–636.
- Jimenez, J. L.; Bahreini, R.; Cocker, D. R.; Zhuang, H.; Varutbangkul, V.; Flagan, R. C.; Seinfeld, J. H.; O'Dowd, C. D.; Hoffmann, T. New Particle Formation from Photooxidation of Diiodomethane (CH₂I₂). *J. Geophys. Res.* **2003**, *108*, 4318.
- Alfarra, M. R.; Paulsen, D.; Gysel, M.; Garforth, A. A.; Dommen, J.; Prevot, A. S. H.; Worsnop, D. R.; Baltensperger, U.; Coe, H. A mass spectrometric study of secondary organic aerosols formed from the photooxidation of anthropogenic and biogenic precursors in a reaction chamber. *Environ. Sci. Technol.*, submitted.
- Cocker, D. R.; Flagan, R. C.; Seinfeld, J. H. State-of-the-art chamber facility for studying atmospheric aerosol Chemistry. *Environ. Sci. Technol.* **2001**, *35*, 2594–2601.
- Allan, J. D.; Jimenez, J. L.; Coe, H.; Bower, K. N.; Williams, P. I.; Worsnop, D. R. Quantitative sampling using an Aerodyne Aerosol Mass Spectrometer. Part 1: Techniques of data interpretation and error analysis. *J. Geophys. Res.* **2003**, *108*, 4090.
- Allan, J. D.; Delia, A. E.; Coe, H.; Bower, K. N.; Alfarra, M. R.; Jimenez, J. L.; Middlebrook, A. M.; Drewnick, F.; Onasch, T. B.; Canagaratna, M. R.; Jayne, J. T.; Worsnop, D. R. A generalized method for the extraction of chemically resolved mass spectra from aerodyne aerosol mass spectrometer data. *J. Aerosol Sci.* **2004**, *35*, 909–922.
- Wang, S. C.; Flagan, R. C. Scanning electrical mobility spectrometer. *J. Aerosol Sci.* **1989**, *20*, 1485–1488.
- Keywood, M. D. K.; Kroll, J. H.; Varutbangkul, V.; Bahreini, R.; Flagan, R. C.; Seinfeld, J. H. Secondary Organic Aerosol Formation from Cyclohexene Ozonolysis: Effect of OH Scavenger and the Role of Radical Chemistry. *Environ. Sci. Technol.* **2004**, *38*, 3343–3350.
- Docherty, K. S.; Ziemann, P. J. Effects of stabilized Criegee intermediate and OH radical scavengers on aerosol formation from reactions of β -pinene with O₃. *Aerosol Sci. Technol.* **2003**, *37*, 877–891.
- Jimenez, J. L.; Bahreini, R.; Cocker, D. R.; Zhuang, H.; Varutbangkul, V.; Flagan, R. C.; Seinfeld, J. H.; O'Dowd, C. D.;

- Hoffmann, T. New particle formation from photooxidation of diiodomethane (CH₂I₂). *J. Geophys. Res.* **2003**, *108*, 4733.
- (30) DeCarlo, P.; Slowik, J. G.; Worsnop, D. R.; Davidovits, P.; Jimenez, J. L. Particle morphology and density characterization by combined mobility and aerodynamic measurements. Part I: Theory. *Aerosol Sci. Technol.* **2004**, *38*, 1185–1205.
- (31) McLafferty, F. W.; Turecek, F. *Interpretation of Mass Spectra*; University Science Books: Sausalito, CA, 1993.
- (32) Alfarra, R. M. Insights Into Atmospheric Organic Aerosols Using An Aerosol Mass Spectrometer. Ph.D. Thesis, University of Manchester, 2004.
- (33) Forstner, H. J. L.; Flagan, R. C.; Seinfeld, J. H. Secondary organic aerosol from the photooxidation of aromatic hydrocarbons: molecular composition. *Environ. Sci. Technol.* **1997**, *31*, 1345–1358.
- (34) Koehler, C. A.; Fillo, J. D.; Ries, K. A.; Sanchez, J. T.; Haan, D. O. D. Formation of secondary organic aerosol by reactive condensation of furandiones, aldehydes, and water vapor onto inorganic aerosol seed particles. *Environ. Sci. Technol.* **2004**, *38*, 5064–5072.
- (35) Schneider, J.; Bormann, S.; Wollny, A. G.; Blasner, M.; Mihalopoulos, N.; Oikonomou, K.; Sciare, J.; Teller, A.; Levin, Z.; Worsnop, D. R. Online mass spectrometric aerosol measurements during the MINOS campaign (Crete, August 2001). *Atmos. Chem. Phys.* **2004**, *4*, 65–80.
- (36) Zhang, Q.; Alfarra, M. R.; Worsnop, D. R.; Allan, J. D.; Coe, H.; Canagaratna, M. R.; Jimenez, J. L. Deconvolution and quantification of primary and oxygenated organic aerosols based on aerosol mass spectrometry. Part I: Development and validation of the method. *Environ. Sci. Technol.*, **2005**, *39* (13), 4938–4952.
- (37) Canagaratna, M.; Jayne, J. T.; Ghertner, D. A.; Herndon, S.; Shi, Q.; Jimenez, J. L.; Silva, P. J.; Williams, P.; Lanni, T.; Drewnick, F.; Demerjian, K. L.; Kolb, C. E. Chase Studies of Particulate Emissions from in-use New York City Vehicles. *Aerosol Sci. Technol.* **2004**, *38*, 555–573.
- (38) Alfarra, M. R.; Coe, H.; Allan, J. D.; Bower, K. N.; Boudries, H.; Canagaratna, M. R.; Jimenez, J. L.; Jayne, J. T.; Garforth, A. A.; Li, S.; Worsnop, D. R. Characterization of urban and rural organic particulate in the Lower Fraser Valley using two Aerodyne Aerosol Mass Spectrometers. *Atmos. Environ.* **2004**, *38*, 5745–5758.

Received for review December 7, 2004. Revised manuscript received April 27, 2005. Accepted May 19, 2005.

ES048061A

Appendix G

Secondary Aerosol Formation from Atmospheric Reactions of Aliphatic Amines^{*}

^{*} This chapter is reproduced by permission from “Secondary Aerosol Formation from Atmospheric Reactions of Aliphatic Amines” by S. M. Murphy, A. Sorooshian, J. H. Kroll, N. L. Ng, P. Chhabra, C. Tong, J. D. Surratt, E. Knipping, R. C. Flagan, J. H. Seinfeld, *Atmospheric Chemistry and Physics*, 7, 2313-2337, 2007. © 2007 Author(s). This work is licensed under a Creative Commons License.

Secondary aerosol formation from atmospheric reactions of aliphatic amines

S. M. Murphy¹, A. Sorooshian¹, J. H. Kroll², N. L. Ng¹, P. Chhabra¹, C. Tong¹, J. D. Surratt¹, E. Knipping³, R. C. Flagan¹, and J. H. Seinfeld¹

¹Division of Chemistry and Chemical Engineering, California Institute of Technology, Pasadena, CA 91125, USA

²Current Address: Aerodyne Research Inc., Billerica, MA, USA

³Electric Power Research Institute, Palo Alto, CA, USA

Received: 17 December 2006 – Published in Atmos. Chem. Phys. Discuss.: 10 January 2007

Revised: 13 April 2007 – Accepted: 13 April 2007 – Published: 8 May 2007

Abstract. Although aliphatic amines have been detected in both urban and rural atmospheric aerosols, little is known about the chemistry leading to particle formation or the potential aerosol yields from reactions of gas-phase amines. We present here the first systematic study of aerosol formation from the atmospheric reactions of amines. Based on laboratory chamber experiments and theoretical calculations, we evaluate aerosol formation from reaction of OH, ozone, and nitric acid with trimethylamine, methylamine, triethylamine, diethylamine, ethylamine, and ethanolamine. Entropies of formation for alkylammonium nitrate salts are estimated by molecular dynamics calculations enabling us to estimate equilibrium constants for the reactions of amines with nitric acid. Though subject to significant uncertainty, the calculated dissociation equilibrium constant for diethylammonium nitrate is found to be sufficiently small to allow for its atmospheric formation, even in the presence of ammonia which competes for available nitric acid. Experimental chamber studies indicate that the dissociation equilibrium constant for triethylammonium nitrate is of the same order of magnitude as that for ammonium nitrate. All amines studied form aerosol when photooxidized in the presence of NO_x with the majority of the aerosol mass present at the peak of aerosol growth consisting of aminium (R₃NH⁺) nitrate salts, which repartition back to the gas phase as the parent amine is consumed. Only the two tertiary amines studied, trimethylamine and triethylamine, are found to form significant non-salt organic aerosol when oxidized by OH or ozone; calculated organic mass yields for the experiments conducted are similar for ozonolysis (15% and 5% respectively) and photooxidation (23% and 8% respectively). The non-salt organic aerosol formed appears to be more stable than the nitrate salts and does not quickly repartition back to the gas phase.

Correspondence to: J. H. Seinfeld
(seinfeld@caltech.edu)

1 Introduction

Amines are emitted into the atmosphere from a variety of sources including meat cooking, biomass burning, motor vehicle exhaust, industrial processes, and marine organisms. The dominant anthropogenic source is emissions from animal husbandry operations (Table 1). While amine emissions from animal husbandry are typically reported to be two to three orders of magnitude less than those of ammonia (Ngwabie and Hintz, 2005; Schade and Crutzen, 1995), at least one study has reported gas-phase concentrations of amines in the hundreds of ppb in areas of intense animal husbandry (Raubaud et al., 2003). Though emission estimates vary widely, amines have been detected in marine, rural, and urban atmospheres in the gas phase, particle phase and within aqueous fog and rain drops (Zhang and Anastasio, 2003). Mass spectrometric studies by both Murphy (1997) and Angelino (2001) have shown that molecular ions typically associated with amines are present in ambient particles, especially in air masses from agricultural regions. Tan et al. (2002) identified particle phase amines during multiple smog events in Toronto's winter atmosphere. Recent field studies suggest that organic nitrogen species could be an appreciable fraction of organic aerosol mass (Beddows et al., 2004; Mace et al., 2003; Makela et al., 2001; McGregor and Anastasio, 2001; Neff et al., 2002; Simoneit et al., 2003; Tan et al., 2002), although the relative importance of amines as a source of particulate organic nitrogen remains unclear.

During the 1970's, interest in the gas-phase atmospheric chemistry of amines focused on carcinogenic nitrosamines formed when amines are photooxidized (Pitts et al., 1978). It was subsequently determined that gas-phase nitrosamines photolyze rapidly in the troposphere and are believed to pose a minimal threat to human health. More recently, toxicology studies have demonstrated that particulate organic nitrogen species are associated with adverse health effects (Hamoir et

Table 1. Summary of structures of amines studied and estimated global emissions from animal husbandry.

Amine (abbrev)	Formula	Estimated Global Emissions, Gg N y ⁻¹ (Schade and Crutzen, 1995)
Ammonia	NH ₃	23 300
Methylamine (MA)	CH ₃ NH ₂	24±15
Trimethylamine (TMA)	(CH ₃) ₃ N	108±30
Diethylamine (DEA)	(CH ₃ CH ₂) ₂ NH	–
Triethylamine (TEA)	(CH ₃ CH ₂) ₃ N	–
Ethanolamine (MEA)	(CH ₂ OH)CH ₂ NH ₂	–

al., 2003). Nemmar (2002) found that particles coated with amines produced a significant increase in the rate of blood clots (by nearly 4 times) when installed in the trachea of hamsters; in contrast, the effects of particles coated with carboxylic acids and unmodified polystyrene particles were not statistically significant when compared to the control group of hamsters.

Amines are oxidized in the atmosphere by the hydroxyl radical (OH), ozone (O₃), and possibly by the nitrate radical (NO₃), with measured rate constants suggesting that the reaction rates of ozone and OH with amines are competitive during the day if ozone levels are in the tens to hundreds of ppb (Tuazon et al., 1994). The nitrate radical may play a significant role in amine oxidation at night, though very little is known about this pathway. While many of the gas-phase oxidation pathways involving OH and ozone have been elucidated, secondary aerosol formation resulting from the photooxidation of amines has received limited attention. Also, because amines are basic compounds, they can form particulate salts through reactions with gas-phase acids present in the atmosphere (HNO₃, H₂SO₄),



Reactions (R1) and (R2) are analogous to those of ammonia to form ammonium sulfate and ammonium nitrate. While the equilibria between gas-phase ammonia and nitric or sulfuric acid to form particle-phase salts have been thoroughly investigated and the thermodynamic parameters governing these reactions are well known (Mozurkewich, 1993; Stelson and Seinfeld, 1982), similar thermodynamic parameters for amine systems were not available prior to this study.

There have been a limited number of laboratory chamber experiments in which aerosol resulting from amine photooxidation was observed (Angelino et al., 2001; Pitts et al., 1978). Aerosol yields, the relative importance of acid-base chemistry, and the oxidative pathways leading to particle formation remain poorly understood. The goal of the present work is to use controlled laboratory chamber studies to evaluate the aerosol forming potential, by acid-base reactions, photooxidation and ozonolysis, of aliphatic amines known to be

present in the atmosphere. The amines studied (with abbreviation used) are: trimethylamine (TMA), methylamine (MA), triethylamine (TEA), diethylamine (DEA), ethylamine (EA), and monoethanolamine (MEA), which will be referred to as ethanolamine in this paper.

2 Experimental

All experiments (Table 2) were carried out in the Caltech dual 28 m³ FEP Teflon chambers (Cocker et al., 2001; Keywood et al., 2004). The chambers are surrounded by banks of black lights (276GE350BL) which output ultraviolet light predominantly between 300 and 400 nm, with a maximum at 354 nm. Ports allow for the introduction of clean, dry (<10% RH) air, gas-phase reagents, inorganic seed aerosol, and for measurement of NO, NO_x, O₃, RH, temperature, and particulate mass, size, number concentration, and chemistry. Temperature is held at 20°C, increasing to 25°C during photooxidation experiments using the black lights. Commercial monitors (Horiba) are used to measure O₃ (by UV absorption) and NO/NO_x (NO_x conversion to NO by activated carbon, followed by NO + O₃ chemiluminescence). Both amines and nitric acid (when added) were injected into the chamber by passing a stream of dry, clean air over a known volume of high purity liquid phase compound. The purity and source of the amines used in this study are: trimethylamine (45% solution in H₂O, Fluka), methylamine (40 wt.% solution in H₂O, Sigma-Aldrich), triethylamine (>99.5% purity, Sigma Aldrich), diethylamine (>99.5% purity, Sigma Aldrich), ethylamine (70 wt.% solution in H₂O, Aldrich), ethanolamine, (≥99% purity, Sigma Aldrich). Gas-phase concentrations of amines and nitric acid were not directly measured and were instead estimated based on the volume of liquid phase amine injected; these concentrations represent the maximum possible within the chamber in the absence of wall loss.

“Seed” aerosol was generated by atomizing a solution of 0.015 M ammonium sulfate or 0.75 M ammonium nitrate. Particle-phase measurements were made by an Aerodyne Time of Flight Aerosol Mass Spectrometer (cToF-AMS), a Particle-Into-Liquid Sampler coupled to Ion

Table 2. Initial conditions of all experiments conducted.

Exp.	Amine	Estimated Initial (ppb) Mixing Ratios	Oxidant	Initial NO _x Mixing Ratios (ppb)	HNO ₃ Injected (ppb)	Atomized Seed Aerosol
1	Trimethylamine	100	NO _x , Propene	100 (NO ₂)	–	–
2	Trimethylamine	100	NO _x , Propene	100 (NO ₂)	10	–
3	Trimethylamine	100	H ₂ O ₂	100 (NO ₂)	10	–
4	Trimethylamine	100	Ozone	–	18	–
5	Methylamine	100	NO _x	100 (NO ₂)	10	–
6	Methylamine	100	H ₂ O ₂	100 (NO)	10	–
7	Methylamine	100	Ozone	–	–	(NH ₄) ₂ SO ₄
8	Triethylamine	500	H ₂ O ₂	–	–	–
9	Triethylamine	500	H ₂ O ₂	400 (NO)	–	–
10	Triethylamine	100	NO _x	100 (NO)	–	–
11	Triethylamine	100	NO _x	100 (NO) 100 (NO ₂)	–	–
12	Triethylamine	100	NO _x	140 (NO ₂)	–	–
13	Triethylamine	100	NO _x	100 (NO ₂)	–	–
14	Triethylamine	100	NO _x	100 (NO ₂)	10	–
15	Triethylamine	50	NO _x , Propene	100 (NO ₂)	100	–
16	Triethylamine	100	O ₃	–	8	–
17	Triethylamine	100	HNO ₃	–	100	–
18	Triethylamine	20 ppb TEA aliquots	–	–	–	NH ₄ NO ₃
19	Triethylamine	100 ppb NH ₃ inject TEA in aliquots	–	–	5 (twice)	–
20	Triethylamine	50 ppb TEA 50 ppb NH ₃	–	–	8	–
21	Diethylamine	100	H ₂ O ₂	–	–	–
22	Diethylamine	100	H ₂ O ₂	80 (NO)	–	–
23	Diethylamine	100	NO _x , Propene	100 (NO)	–	–
24	Diethylamine	100	NO _x	100 (NO)	–	–
25	Diethylamine	100	NO _x	100 (NO ₂)	–	(NH ₄) ₂ SO ₄
26	Diethylamine	100	NO _x	100 (NO ₂)	10	–
27	Ethylamine	100	NO _x	100 (NO ₂)	10	–
28	Ethanolamine	100	NO _x , Propene	140 NO 140 NO ₂	–	–
29	Ethanolamine	100	NO _x , Propene	135 NO ₂	–	–
30	Ethanolamine	300	NO _x , Propene	100 (NO ₂)	–	–
31	Ethanolamine	100	–	–	–	(NH ₄) ₂ SO ₄ mixed with H ₂ SO ₄ (aq)
32	Ethanolamine	100	H ₂ O ₂	100	100	–
33	Ethanolamine	100	O ₃	–	–	–
34	NH ₃	100	NO _x , Propene	100 (NO ₂)	10	–

Chromatography (PILS-IC), and a differential mobility analyzer (DMA, TSI 3760). During experiment number 20 (Table 2), chamber particles were collected onto a Teflon (PALL Life Sciences, 47-mm diameter, 1.0- μ m pore size) filter for analysis by mass spectrometry using both Matrix Assisted Laser Desorption Ionization (MALDI) and electrospray ionization (ESI) to determine how spectra from these ionization techniques compared to the electron impact ionization spectra of the cToF-AMS. Details of the extraction and analysis methodology used for the Teflon filter are given in Surratt et al. (2006).

2.1 PILS-IC

The particle-into-liquid sampler coupled with ion chromatography is a quantitative technique for measuring water-soluble ions, including inorganic, organic acid, and amine ions in aerosol particles. The PILS-IC used in this study (Sorooshian et al., 2006) is based on the prototype design (Weber et al., 2001) with key modifications, including integration of a liquid sample fraction collector and real-time control of the steam injection tip temperature. Chamber air is sampled through a 1 μ m cut-size impactor and a set of three denuders (URG and Sunset Laboratories) to remove in-

organic (basic and acidic) and organic gases that would otherwise bias aerosol measurements. Sample air mixes with steam in a condensation chamber where rapid adiabatic mixing produces a high water supersaturation. Droplets grow sufficiently large to be collected by inertial impaction before being delivered to vials held on a rotating carousel. The contents of the vials are subsequently analyzed off-line using a dual IC system (ICS-2000 with 25 μ L sample loop, Dionex Inc.) for simultaneous anion and cation analysis.

Data for the following ions are reported: acetate, formate, nitrate, sulfate ammonium, methylammonium, dimethylammonium, trimethylammonium, ethylammonium, diethylammonium, and triethylammonium. The PILS-IC technique cannot be used to speciate many of the organic compounds that make up the total aerosol mass since these are not sufficiently ionic in water to have affinity for the IC columns used (anion: Dionex AS-11 column 2 \times 250 mm, ASRS Ultra II 2-mm suppressor, potassium hydroxide eluent; cation: CS12A column 2 \times 250 mm, CSRS Ultra II 2-mm suppressor, methanesulfonic acid eluent); nevertheless, all of the amine salts formed in the experiments reported here were successfully speciated. It should be noted that ammonium, methylammonium, and ethylammonium co-elute; additional co-eluting pairs are diethylammonium:trimethylammonium

and potassium:dimethylammonium. While potassium was never expected to be present and ammonium formation was not anticipated for many of the experiments, background levels of these species in the IC baseline noise did interfere with quantification of co-eluting species. The limit of detection (LOD) for each ion (NH_4^+ , NO_3^- , acetate, formate, and the six aforementioned amine species) is defined in this study as the air-equivalent concentration of the lowest concentration standard that is distinct from baseline noise in the IC plus three times the standard deviation ($n=3$) of this measurement. The LOD's for the ions measured using the PILS-IC technique for this study are all below $0.1 \mu\text{g m}^{-3}$, with the exceptions of trimethylamine and triethylamine, which have LOD's of 0.60 and $0.89 \mu\text{g m}^{-3}$, respectively. In all experiments, chamber air containing gas-phase amine and nitric acid (when added) was run through a particle filter and sampled by the PILS-IC; none of the amines was ever detected in these filtered vials, confirming that the carbon denuder was able to completely remove gas-phase species and that the PILS-IC signal is entirely a result of aerosol-phase compounds.

2.2 Aerodyne cToF-AMS

The design parameters and capabilities of the cToF-AMS instrument are described in detail elsewhere (Drewnick et al., 2004a, b). Briefly, chamber air enters the instrument through a $100 \mu\text{m}$ critical orifice at a flowrate of $1.4 \text{ cm}^3 \text{ s}^{-1}$. Particles with a vacuum aerodynamic diameter between roughly 50 and 800 nm are efficiently focused by an aerodynamic lens, passed through a 1% chopper, and then impacted onto a tungsten vaporizer. The chopper can be operated in three modes: (1) completely blocking the beam to gather background mass spectra; (2) out of the beam's path to collect ensemble average mass spectra over all particles sizes; (3) chopping the beam to create size-resolved mass spectra. The vaporizer is set at $\sim 550 \text{ }^\circ\text{C}$ to ensure complete volatilization of the aerosol. Once vaporized, molecules undergo electron impact ionization at 70 eV and are orthogonally pulsed every $19 \mu\text{s}$ into the time of flight mass analyzer. The resolution of the mass analyzer is ~ 800 ($M/\Delta M$). For all mass spectra shown in this work the ion signal is represented as sticks, the height of which represent the raw ion signal integrated over 1 amu bins. These stick mass spectra are divided into different chemical species based on the methodology of Allan et al. (2003), with exceptions noted in the text. The limits of detection, calculated as three times the standard deviation of the noise for particle filtered air are $<0.05 \mu\text{g m}^{-3}$ for all species measured.

2.3 Effective density

Calculating the density of aerosol particles is important for two reasons. First, multiplying the aerosol volume measured by the DMA by the material density allows one to calculate aerosol mass yields. (The cToF-AMS cannot be used to di-

rectly quantify aerosol mass because the fraction of particles that bounce off of the vaporizer is unknown and the PILS-IC does not measure the mass of non-ionic species) Second, changes in the density give an indication of alterations in particle morphology during secondary aerosol formation.

The effective density (ρ_{eff}) is a function of the vacuum aerodynamic diameter (d_{va}) measured by the cToF-AMS and the mobility diameter (d_{m}) measured by the DMA (DeCarlo et al., 2004),

$$\rho_{\text{eff}} = \frac{d_{\text{va}}}{d_{\text{m}}} \rho_0 = \rho_{\text{m}} \frac{C_c(d_{\text{ve}})}{\delta^3 \chi_t \chi_v C_c(d_{\text{m}})} \quad (1)$$

where ρ_0 is unit density (1 g cm^{-3}), ρ_{m} is the material density, C_c is the slip correction factor, d_{ve} is the volume equivalent diameter, δ is a measure of the internal void space defined by $\delta = (\rho_{\text{m}}/\rho_{\text{p}})^{1/3}$ where ρ_{p} is the particle density, χ_t is the dynamic shape factor in the transition regime, and χ_v is the dynamic shape factor in the free molecular regime.

As described in Bahreini et al. (2005) and Decarlo et al. (2004), the effective density is equivalent to the material density if the shape factor and slip correction factor are unity and the internal void fraction is zero. These assumptions are probably slightly incorrect for amine salts and amine oxidation products, given that ammonium nitrate particles have an effective density 20 percent less than the material density of ammonium nitrate when ρ_{eff} is calculated using simultaneous cToF-AMS and DMA measurements (Jayne et al., 2000). Indeed the effective densities calculated in this way for the ammonium nitrates are less than the literature values. While there is no need to use effective densities to calculate the mass of pure salts (the PILS-IC is able quantitatively measure these), it is necessary to use effective densities (as an approximation of the material density) to calculate the mass of aerosol formed during photooxidation and ozonolysis because non-ionic species are present.

To calculate the effective density, one represents the DMA volume distribution, normally expressed as $dV/d\log(d_{\text{m}})$, as $dV/d\log(\rho_{\text{eff}}d_{\text{m}})$ and adjusts ρ_{eff} until this distribution (with peak height normalized to 1) aligns in diameter space with the mass distribution from the cToF-AMS, $dM/d\log(d_{\text{va}})$ (peak height also normalized to 1). The two distributions align when the correct effective density is used because $\rho_{\text{eff}}d_{\text{m}} = d_{\text{va}}\rho_0$ (if unity shape and slip correction factors and zero internal void fraction are assumed). Figure 1a shows the calculated effective density of triethylammonium nitrate (TEAN) is $1.0 \pm 0.1 \text{ g cm}^{-3}$ while the effective density of the aerosol formed from photolysis of TEA (mixed TEAN and products from TEA oxidation) has a slightly increased effective density of $1.1 \pm 0.1 \text{ g cm}^{-3}$.

2.4 Oxidation experiments

Three types of amine oxidation experiments were conducted in this study: (1) Photooxidation in the absence of NO_x , (2)

Photooxidation in the presence of NO_x , and (3) dark ozonolysis. Hydrogen peroxide (H_2O_2) was used as the OH radical precursor for all of the NO_x -free photooxidation experiments and many of the high NO_x experiments (see Table 2 for details). H_2O_2 is introduced by bubbling 5 L min^{-1} of humidified room-temperature air for 2.5 h through a 50% H_2O_2 solution (Aldrich), through a particle filter to avoid the introduction of droplets, and finally into the chamber. The mixing ratio of H_2O_2 achieved using this method has been previously estimated to be between 3 and 5 ppm (Kroll et al., 2006). To minimize potential uptake of H_2O_2 by the aerosol, all experiments were carried out under dry ($\text{RH} < 10\%$) conditions. To determine if the presence of hydrogen peroxide significantly affected the particle-phase chemistry, numerous high NO_x photooxidation experiments were conducted in the absence of H_2O_2 , some with the gas-phase amine and NO_x alone, and others where propene was added to generate higher levels of OH in the chamber and increase the rate of oxidation (see Table 2 for details). For all photooxidation studies, H_2O_2 , NO_x , propene, or a combination of these was injected first. For many experiments using NO_x , this step was followed by the injection of nitric acid or, occasionally, ammonium sulfate (see Table 2 for details). After the HNO_3 or ammonium sulfate had mixed throughout the chamber, the amine was added. When nitric acid is present, formation of ammonium nitrate salt occurs once the amine is injected. By using a similar concentration of HNO_3 in all experiments, we were able to roughly control the size distribution of the aerosol. Nucleating the ammonium nitrate before the start of oxidation also allowed us to measure the chemistry of pure salt particles in situ with the cToF-AMS and PILS-IC. Photooxidation reactions were initiated by irradiation from the black lights surrounding the chamber. Ozonolysis experiments were conducted in the dark in the absence of an OH scavenger. The order of reactant introduction for ozonolysis experiments was: nitric acid, amine, and finally ozone. Between experiments, the chamber was continuously flushed with clean air and irradiated with UV light. Contamination from previous experiments was occasionally observed and has been accounted for in the analyses.

3 Atmospheric reaction pathways of amines

At the outset, it is useful to frame the results of this study by outlining a hypothesis for the atmospheric reaction pathways of amines. Direct or indirect evidence of most of these pathways has been observed during the chamber experiments in this study.

Because amines are one of relatively few basic atmospheric compounds, they have the potential to undergo rapid acid-base reactions to form salt particles in the presence of nitric or sulfuric acid. Formation of salt particles depends on temperature, the identity of the amine, and the concentrations and identities of acidic species present. Formation

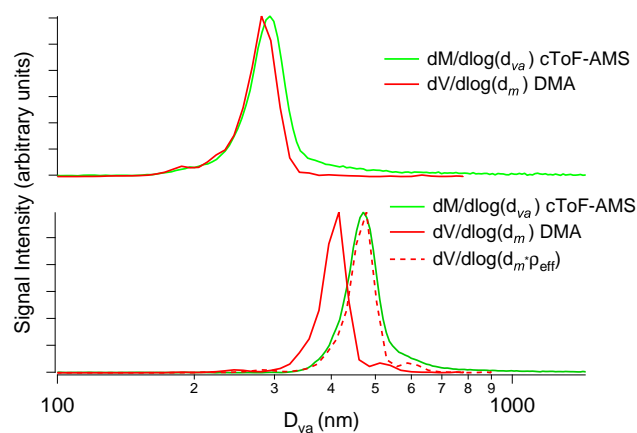


Fig. 1. Calculation of the effective density (data from exp. 14, Table 2). Panel (a) Volume distribution from the DMA ($dV/d\log(d_m)$, solid red line) and mass distribution from the cToF-AMS ($dM/d\log(d_{va})$, solid green line) of triethylammonium nitrate (TEAN). The fact that the two distributions are aligned indicates the effective density of TEAN is ~ 1 . The slight tailing of the cToF-AMS signal could be caused by slow vaporization or higher uncertainty in the size calibration for larger particles. Panel (b) The same distributions shown in (a) after products from TEA photooxidation have condensed onto the nitrate salt shown in (a) for 7 h. The particles have grown larger from the condensation process. The dashed red line ($dV/d\log(\rho_{\text{eff}} d_m)$) is created by adjusting the effective density (ρ_{eff}) until the dotted red line aligns with the solid green line ($\rho_{\text{eff}} = 1.1 \text{ g cm}^{-3}$).

of ammonium salts also depends indirectly on the concentration of ammonia, which will compete with amines for acidic molecules. Once ammonium-salt particles are formed, they can revolatilize, undergo particle-phase reactions (including oxidation), or serve as a site for condensation of other organic species. Condensation of organics onto the salts particles may form a barrier that prevents the salts from remaining at equilibrium with the gas phase.

Gas-phase amines can be oxidized by OH, O_3 and possibly NO_3 (OH and O_3 are known to be competitive oxidation agents of amines at atmospherically relevant concentrations while the rate of NO_3 oxidation remains unexplored). Specifics of the known oxidation pathways will be discussed thoroughly in Sect. 5. Briefly, the products formed depend on the oxidizing species and the NO_x level. Many of the oxidation products of amines are themselves basic and can undergo reactions with atmospheric acids to form additional salts. Other oxidation products are sufficiently non-volatile to condense directly onto particles without forming salts. Finally, it is possible that certain amines, or their oxidation products, that are too volatile to condense onto dry particles will condense into, and ionize within, aqueous aerosols. Once condensed, amines and their oxidation products may undergo particle-phase reactions to form high molecular weight compounds, or they may be further oxidized into volatile species.

Table 3. Theoretically calculated dissociation constants for different nitrate systems. $K_{p,298}$ for ammonium nitrate = $7.14\text{E-}7 \text{ Pa}^2$.

Species	$K_{p,298} \text{ (Pa}^2\text{)}$	
	$\Delta H^\circ f$ from Cottrell and Gill (1951)	$\Delta H^\circ f$ from NBS (1982)
Methylammonium nitrate	7.90E-06	8.56E-09
Dimethylammonium nitrate	1.01E-05	3.95E-09
Trimethylammonium nitrate	2.27E+00	5.29E-07
Ethylammonium nitrate	3.29E-06	9.56E-07
Diethylammonium nitrate	3.11E-10	3.30E-11
Triethylammonium nitrate	1.37E-05	1.18E-12

The remainder of the paper is divided into two main sections. In the first section, we investigate salt aerosol formation from acid-base reactions of amines through both laboratory chamber experiments and theoretical estimates. In the second section, aerosol formation resulting from photooxidation and ozonolysis of amines under varying NO_x conditions is addressed.

4 Salt aerosol formation from acid-base reactions of amines

4.1 Detection of aminium nitrate salts

As described in the Experimental section, nitrate salts were formed by adding the amine of interest to a chamber containing gaseous nitric acid (HNO_3). In all cases, particle nucleation occurred within a few minutes of amine injection. All of the aminium nitrate salts investigated were detected by the cToF-AMS, PILS-IC, and DMA instruments. The mass spectra for the nitrate salts of the amines studied are shown in Fig. 2. The spectra are similar to reference electron impact spectra in the NIST database for the gas-phase amines except for additional intensity at m/z 30 and m/z 46 caused by NO^+ and NO_2^+ ion fragments from nitrate (Stein, 2005). The only previous chamber study to focus on aerosol-phase amines was conducted by Angelino et al. (2001) using a laser desorption aerosol time of flight mass spectrometer (ATOFMS). In their study, the spectra of dialkyl ammonium salts exhibited prominent peaks $(M+13)^+$, attributed to ion-molecule reactions within the ionization region of the instrument. We do not observe peaks larger than the molecular ion for any of the salts, indicating that ion-molecule reactions do not occur in the ionization region of the Aerodyne cToF-AMS; this absence of ion-molecule reactions dramatically simplifies mass spectral interpretation.

Though we did not observe ion-molecule reactions, it is important to note that we did observe a dramatic increase in the number of ions detected by the cToF-AMS when the voltages that extract ions from the electron impact region into the flight chamber of the mass spectrometer were al-

tered by a few percent. When the voltages were in this altered state, we observed a further increase in both molecular and fragment amine ions with increasing vaporizer temperature above 550°C . No such correlation between increased vaporizer temperature and ion signal is observed when the extraction voltages are not in the altered state. Because altering the extraction voltages allows ions formed on the vaporizer surface to enter the mass spectrometer and because amines have low ionization potentials, we believe that the additional ions are formed on the high temperature tungsten surface of the vaporizer. The artificial signal enhancement (increased ion rate) caused by this proposed surface ionization indicates that there is a potential for overestimates of amine concentrations measured by the Aerodyne cToF-AMS if the instrument is not carefully calibrated and tuned. Similar effects caused by the unusually low ionization energy of amines may also occur in other aerosol mass spectrometry instruments. We observed enhancement of up to an order of magnitude by changing the voltages in the instrument a few percent. The m/z with the most prominent increase in ion rate was that corresponding to the molecular ion of the amine being studied. The fact that the molecular ion showed the most dramatic increase further supports the hypothesis that a non-electron impact surface ionization is occurring; 70 eV electron impact ionization typically induces alpha cleavage of amines and little, non-fragmented, molecular ion signal is observed. It should be noted that we have not observed an increase in detected ions when the extraction voltages are shifted when studying aerosol that does not contain amines. Though not investigated further, these observations raise the possibility that this type of tuning might be intentionally used to detect the presence of molecular amine ions.

4.2 Atmospheric formation of aminium nitrate salts: theory

Having confirmed that aminium nitrate salts can be generated and detected, we wish to estimate the potential atmospheric importance of aminium nitrate salts relative to ammonium nitrate (typically assumed to be the dominant atmospheric nitrate salt in the fine mode). Based on theory, we estimate the dissociation constants ($K_p = p_{\text{HNO}_3} p_{\text{amine}}$)

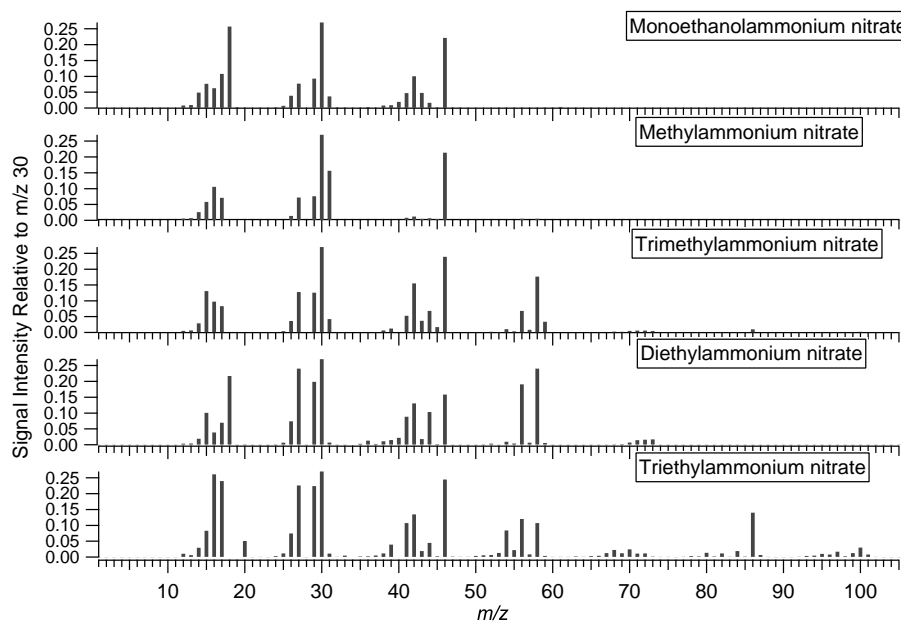


Fig. 2. Mass spectra for the nitrate salts of the amines studied. On the $\sim 550^\circ\text{C}$ surface of the vaporizer, all nitrate salts decompose into nitric acid and the parent amine. Signals at m/z 30 and 46 are generated from the nitrate fragments NO^+ and NO_2^+ and are common to all spectra. Signal at m/z 30 is a combination of signal from NO^+ and from amine fragments resulting from rearrangements after electron impact ionization. For all spectra, molecular ions have significantly less signal intensity than the fragments resulting from the cleavage of the chemical group alpha to the nitrogen (alpha cleavage). For the ethyl amines, loss of methyl groups alpha to the nitrogen give fragments at $[\text{M}-15]^+$ while for the methyl amines, loss of hydrogen atoms alpha to the nitrogen give fragments at $[\text{M}-1]^+$.

for the gas-particle equilibrium of all amines studied except for ethanolamine, while noting that the estimates have large uncertainties resulting from discrepancies in the literature values for the heats of formation of the aminium nitrate salts. If the required thermodynamic parameters are known, the dissociation constant for a given amine-nitric acid system can be obtained using the integrated form of the Van't Hoff equation,

$$\ln K_p = \frac{\Delta S_{\text{diss}}^\circ - \Delta C_{\text{P,diss}}}{R} - \frac{\Delta H_{\text{diss}}^\circ - T_0 \Delta C_{\text{P,diss}}}{RT} + \frac{\Delta C_{\text{P,diss}}}{R} \ln \left(\frac{T}{T_0} \right) \quad (2)$$

Entropies of formation for aminium nitrate salts have apparently not been reported in the literature; we estimate them using a molecular dynamics approach described in the Appendix. Also given in the Appendix are literature sources and values for the other thermodynamic parameters in Eq. (2). The calculated dissociation constants for all of the amines studied (except ethanolamine, for which the entropy was not estimated) are given in Table 3. Even if we assume that the estimated entropies are accurate, the results in Table 3 show that discrepancies in the literature values for the heats of formation lead to significant uncertainty in the calculated dissociation constants. While this uncertainty precludes us from gaining meaningful insight into how MA, DMA, or TEA might compete with ammonia for HNO_3 in the atmosphere,

we are able to draw conclusions about the other salts. As mentioned earlier, most studies show that ambient ammonia concentrations tend to be an order of magnitude greater than amine concentrations, except perhaps in the immediate vicinity of an amine emissions source. Given this, and assuming that the calculated entropies are reasonable, it is improbable that nitrate salts of TMA or EA would form in the presence of typical ambient ammonia levels, because the K_p values for these two systems are greater than or equal to that of ammonium nitrate, independent of the precise value of the heat of formation. By contrast, the value of the dissociation constant for DEA is 2 to 3 orders of magnitude smaller than that of ammonium nitrate (independent of the uncertainty in the heat of formation), indicating that formation of DEAN particles under typical atmospheric mixing ratios is possible.

4.3 Atmospheric formation of aminium nitrate salts; experimental

We conducted chamber experiments to evaluate and constrain the theoretical estimate for the dissociation constant of triethylammonium nitrate (TEAN), the highest molecular weight aminium nitrate studied.

The first experiment was carried out to study TEAN formation at atmospherically relevant ratios of ammonia:TEA (Fig. 3). Initially, 100 ppb of gas-phase ammonia was mixed in a chamber containing ~ 5 ppb of nitric acid, leading to

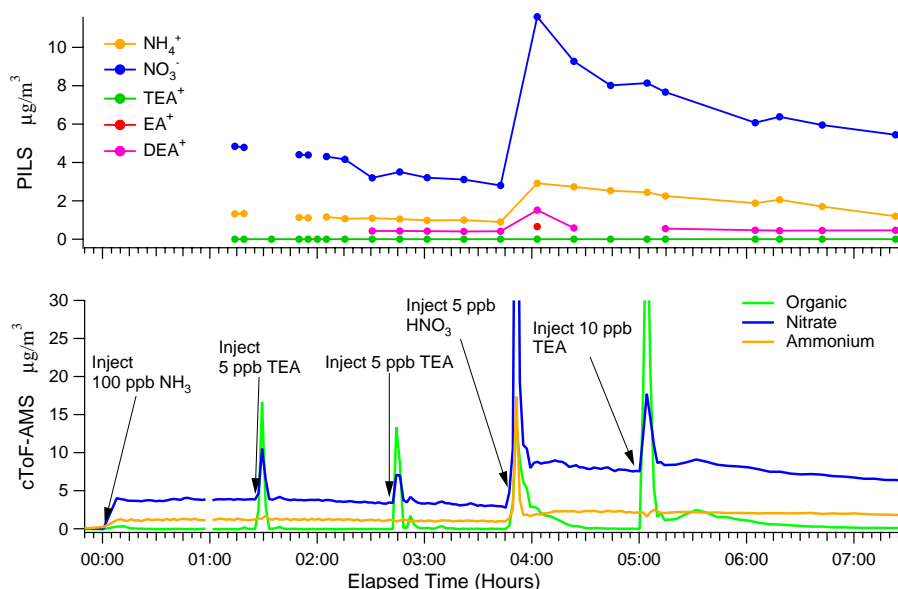


Fig. 3. Time series from exp. 19 in Table 2 of the cToF-AMS (bottom) and the PILS-IC (top) showing rapid particle growth and evaporation after TEA and nitric acid were added in small aliquots to a chamber containing equilibrated ammonium nitrate particles. The transient spikes in particle loading do not appear in the PILS-IC data because of the relatively long averaging time (5 min) of measurements and because the PILS-IC inlet is not in the path of the highly concentrated injection plume.

nucleation of ammonium nitrate particles. Once the ammonium nitrate particle concentration and mass had stabilized, aliquots of TEA were injected into the chamber. As can be seen in Fig. 3, the concentration of TEAN salt, indicated by simultaneous shifts in the nitrate and organic signals, increased dramatically when TEA was added because the injection plume provided a high concentration region for particle formation. As the amine mixed throughout the chamber and became more dilute, the equilibrium shifted back to the gas phase, the salt returned to pure ammonium nitrate, and the organic signal = 0. This sequence of events occurred after each injection, including a second addition of 5 ppb of nitric acid to the chamber.

After concluding that TEA would be unable to form nitrate salts at ratios of TEA:NH₃ typically found in the atmosphere (except possibly near emissions sources), we developed an experimental technique to estimate the gas-particle equilibrium constant for TEAN. The procedure consists of adding an equimolar mixture of amine and ammonia to a chamber containing nitric acid (it is necessary to inject both ammonia and amine because we are unable to accurately measure gas-phase amine or nitric acid concentrations). Once ammonia, TEA, and nitric acid are injected, the following equilibria are established:

$$K_{P1} = p_{\text{HNO}_3} p_{\text{NH}_3} \quad (3)$$

$$K_{P2} = p_{\text{HNO}_3} p_{\text{TEA}} \quad (4)$$

where p_{HNO_3} , p_{NH_3} , and p_{TEA} are the partial pressures of nitric acid, ammonia, and triethylamine, and K_{P1} and K_{P2}

are the dissociation constants for ammonium nitrate and triethylammonium nitrate, respectively. Using the values in Table A1 in Eq. (2), K_{P1} for the ammonium nitrate system is calculated to be $1.916\text{E-}7 \text{ Pa}^2$ at 293 K. The partial pressures of NH₃ and TEA can be determined by subtracting the measured mass of each species in the aerosol phase from that which was injected, assuming negligible wall loss. Thus K_{P2} and p_{HNO_3} are the two unknown quantities to be determined. Although the PILS-IC can measure the amount of nitrate in the aerosol phase, this measurement was not used to calculate p_{HNO_3} , as nitric acid is subject to significant wall losses.

We report here an experiment in which 50 ppb of TEA and 50 ppb of ammonia were added simultaneously to a chamber containing 8 ppb of nitric acid. Upon injection of the amine/ammonia mixture, a rapid particle nucleation event was detected by the cToF-AMS (similar to those shown in Fig. 3). As the plume of ammonia and TEA mixed through the chamber, the mass loading of particles detected by the cToF-AMS decreased, and the other particle instruments (PILS-IC and DMA, which are not aligned with the injection port) began to detect particle loadings consistent with those of the cToF-AMS. After all of the instruments gave consistent readings and the particle concentration was stable (other than a slow decrease from wall loss), the triethylammonium and ammonium contents of the aerosol-phase were measured by the PILS-IC, which unambiguously and quantitatively detects these two species. The dissociation constant of triethylammonium nitrate determined from this experiment, using Eq. (4), is $1.85\text{E-}7 \text{ Pa}^2$. Although wall losses and slight

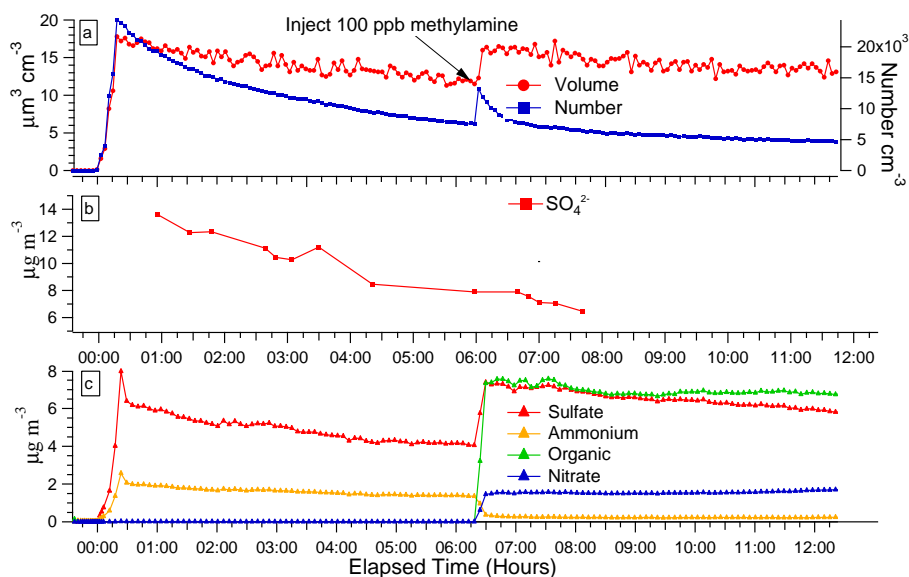


Fig. 4. Time Series of data from the DMA Panel (a), PILS-IC Panel (b), and cToF-AMS Panel (c) showing rapid replacement of ammonium sulfate by methylammonium sulfate during the injection of 100 ppb of methylamine into a chamber containing ammonium sulfate seed and ozone. The increase in the ratio of organic signal to sulfate signal near the end of the experiment results from the slow reaction of methylamine with ozone forming a small mass of organic aerosol.

contamination from other amine compounds from previous experiments influenced this result, the likely effect of these influences is judged to be too small to affect the conclusion that the dissociation constant for TEAN is close to that of ammonium nitrate. This conclusion is consistent with the previous experiment and the estimated dissociation constant falls within the large range of values predicted theoretically.

The two chamber experiments described above confirm that TEA does not form nitrate salts unless the ammonia concentration is roughly equivalent to that of TEA or there is a large excess of nitric acid. Experimental testing of all of the amines was beyond the scope of this study and further studies of this type are warranted, but these initial results indicate that the calculated dissociation constants, although subject to considerable uncertainty, are reasonable.

4.4 Aminium sulfate salts

Amines have the potential to form sulfate salts analogous to ammonium sulfate. Although nitrate salts are probably more relevant in agricultural settings, aminium sulfate salts may form in the presence of high sulfate concentrations. Figure 4 shows results from the addition of 100 ppb methylamine (MA) to pure ammonium sulfate seed in a dry (less than 10% RH) chamber (the chamber also contained ozone because the experiment was designed for MA ozonolysis). The DMA data show a $3 \mu\text{m}^3 \text{cm}^{-3}$ increase in particle volume and new particle formation when methylamine is injected. The new particles are formed from the reaction of methylamine with residual nitric acid in the chamber.

Intriguingly, the mass of methylammonium (labeled “organic” in Fig. 4) detected by the cToF-AMS is roughly 8 times the mass needed to neutralize the nitrate. Additionally, the time series from the cToF-AMS also shows a sharp decrease in the ammonium signal as the methylamine signal increases. The effective density of the particles decreases slightly ($\sim 0.1 \pm 0.1 \text{ g cm}^{-3}$) as the organic signal increases. All of these trends indicate that the methylamine is displacing ammonia and forming methylammonium sulfate. One oddity is the apparent increase in sulfate observed by the cToF-AMS. The sulfate time series from the PILS-IC shows that there is no increase in sulfate loading after methylamine is injected (the growth of methylammonium cannot be followed by the PILS-IC because the IC column used is unable to distinguish between ammonium and methylammonium cations). The increase in sulfate signal from the cToF-AMS can most easily be explained as an artifact, often seen in chamber studies, resulting from an increase in collection efficiency as the physical properties of the aerosol change (Bahreini et al., 2005; Huffman et al., 2005). We hypothesize that replacement of the ammonium cation by methylammonium alters the physical characteristics of the particle which, in turn, causes fewer particles to bounce from the vaporizer surface, increasing collection efficiency. All of the signals from the cToF-AMS (sulfate, organic, nitrate and ammonium) have been scaled by a factor that causes the cToF-AMS sulfate mass to match the PILS-IC sulfate mass after the increase in collection efficiency. Accordingly, the masses shown for the cToF-AMS before the collection efficiency increase are low.

Though the gas-phase concentration of methylamine in this experiment is relatively large, a nearly complete conversion from ammonium sulfate to methylammonium sulfate was observed. The extent of this type of displacement at lower gas-phase amine concentrations, for other amines, and as a function of RH all warrant further study.

5 Aerosol formation from photooxidation and ozonolysis of amines

We begin this section by describing common trends observed during the oxidation experiments of all amines. The following subsections give the data and details for the oxidation of individual amines.

During all of the photooxidation experiments with NO_x , we observed aerosol growth resulting from a combination of aminium nitrate salt formation and condensation of non-volatile oxidized compounds (growth from the dissolution of water soluble amines was limited by the low, <10%, RH of the chamber). For all of the amines studied, some of the aminium nitrate salt that was initially formed during photooxidation partitioned back into the gas-phase as more of the parent amine was reacted away. The particle-phase salt repartitions back to the gas phase because the continued oxidation of the parent amine depletes its concentration in the gas phase and drives the equilibrium back towards gas-phase amine and nitric acid. For methylamine, ethylamine, ethanolamine, and diethylamine nearly 100 percent of the nitrate salt revolatilized while for trimethylamine and triethylamine the nitrate salts appeared to be more stable and did not return completely to the gas phase. All experiments were carried out until the mass of aerosol was stable, no further growth or decay other than a slow decay caused by particle loss to the walls. Based on estimates of the OH concentration in our chamber (Kroll et al., 2006) and measured ozone concentrations, the cessation of aerosol growth is not caused by a depletion of oxidant. Typically, one defines a mass yield of secondary organic aerosol (ratio of organic aerosol mass to the mass of hydrocarbon reacted), but for the amines the mass yield of aerosol depends on the concentration of nitric acid in the system. If ample nitric acid is formed during photooxidation, nearly all of the amine will form aminium nitrate salts, while in the absence of nitric acid, nitrate salts are not formed and the yield reflects the formation of non-volatile compounds from reaction of OH and O_3 with the amine. Additional complexity arises because many of the oxidation products of amines are themselves basic and can form salts with nitric acid (e.g. amides and imines can all form salts with HNO_3). These factors create a situation in which the yield of aerosol is related in a complex manner to the rate of formation of nitric acid in the system.

If all of the nitrate salts return to the gas phase as the parent amine is reacted away, the final aerosol mass yield would be relatively independent of the nitric acid concentra-

tion. Intriguingly, this is not the case for experiments involving TMA or TEA, as the PILS-IC detects significant loadings of salt at the end of these experiments. As described in detail later in this section, TMA and TEA are the only two amines that formed significant non-salt organic aerosol during oxidation. One explanation for the persistence of the aminium nitrate salts in these two systems is that the salt has been “trapped” inside an external layer of oxidized aerosol and is no longer in equilibrium with the gas phase. However, the timescale for diffusion through the organic layers formed in these experiments, which are less than 200 nm thick, is small and, unless the gas phase amine was completely insoluble in the organic layer, it is improbable that this layer could “trap” the salt for any significant amount of time. It is possible that mixing of organic material with the salt in the particle phase somehow lowers the volatility of the salt. Another possibility is that gas-phase concentrations of nitric acid are sufficiently high to force the equilibrium towards the particle phase even when the concentration of the parent amine is very low. Finally, given the large uncertainties in the calculated gas-particle equilibrium constants for the amines, it is possible that certain amines favor the particle phase even at very low gas-phase concentrations.

Regardless of the mechanism by which the salts persist, the formation of nitrate salts biases the calculated mass yields of the photooxidation experiments to be higher than they would be as a result of oxidation alone. In an attempt to estimate the purely oxidative yield in the absence of salt formation we conducted ozonolysis experiments and photooxidation experiments in the absence of NO_x . The aerosol mass yields for the different amines during photooxidation (with and without NO_x) and ozonolysis are given in Table 4. It is important to note that these yields are derived from experiments run under a single set of conditions and are given to show relative differences in the behavior of the different amines; they are not quantitative yield estimates for the individual amines. Indeed, runs conducted with higher initial concentrations of amine give higher yields because of the increased particle-phase organic mass into which organics can condense (Seinfeld and Pankow, 2003). It is even possible that the mass of salt formed can affect the yield if the condensable organics formed are soluble in the nitrate salts. Because of the exploratory nature of this study and because of the complex behavior of amines forming aerosol both through salt formation and oxidation, we do not attempt to derive yield curves from these data.

The non-salt photooxidation yields given in Table 4 were obtained using the following method: first, the aerosol volume measured by the DMA was multiplied by the effective density; second, the salt fraction of the aerosol mass was determined as (PILS-IC mass)/(DMA volume \times effective density). Finally, the wall-loss corrected DMA volume was multiplied by the effective density and then by the fraction of non-salt aerosol mass to give the mass of non-salt secondary organic aerosol (SOA). The yields were calculated using data

Table 4. Estimated percent mass yields^a of non-salt aerosol during ozonolysis and photooxidation. All yields have an uncertainty of ~25% of their magnitude.

Amine	Ozonolysis Yield	High NO _x Photooxidation Yield	Zero NO _x Photooxidation Yield
Trimethylamine	15	23 ^b	–
Methylamine	<1	<1 ^b	–
Triethylamine	5	8 ^c	12 ^b
Diethylamine	<1	<1 ^b	<1 ^b
Ethylamine	–	<1 ^c	–
Ethanolamine	3	2 ^c	–

^aAll yields for high NO_x and ozonolysis are derived from experiments using 100 ppb initial concentrations of amine (high NO_x photooxidations were run with 100 ppb of NO_x). The zero NO_x yields are from experiments using 500 ppb initial amine concentrations. These yields are given to demonstrate trends in the aerosol forming potential of the different amines and are not meant to represent definitive yields for the systems shown.

^bH₂O₂ as OH precursor.

^cPhotooxidation without H₂O₂. Photooxidation of 500 ppb TEA using H₂O₂ gave a mass yield of non-salt organic aerosol of > 20%.

^dThe effective densities used for the yield calculations are: TMA Ozonolysis: 1.4; TMA High NO_x photox: 1.3; TEA Ozonolysis: 1.2; TEA High NO_x photox: 1.1; TEA Low NO_x photox: 1.1. All effective densities are given in g cm⁻³ with uncertainties of ±0.1 g cm⁻³.

from the period after aerosol growth and decay appeared to have ceased other than from loss to the chamber walls. These yield results will be discussed in detail later, although it is immediately evident that while all of the amines can generate aerosol mass by forming nitrate salts, several do not form aerosol mass through oxidation.

Before discussing results from individual photooxidation and ozonolysis experiments, it is useful to consider the general mechanisms by which OH and ozone oxidize aliphatic amines. The gas-phase chemistry of amine oxidation by OH (in the presence of NO_x) and by ozone (without NO_x) have been studied (Schade and Crutzen, 1995; Tuazon et al., 1994), and the major products formed by these reactions have been identified. For many of the oxidation pathways, the products of OH and ozone oxidation are similar, if not identical. The gas-phase products formed from oxidation of aliphatic amines by OH in low NO_x environments are unknown.

Figure 5a shows the most common oxidation pathways for OH attack of an aliphatic amine in the presence of NO_x (Angelino et al., 2001; Schade and Crutzen, 1995). Abstraction of hydrogen from the secondary carbon is believed to be the dominant pathway (Finlayson-Pitts and Pitts, 1986). Abstraction of a hydrogen atom bound directly to the nitrogen in a primary or secondary amine is also possible but is believed to play a less significant role (Schade and Crutzen, 1995). The gas-phase oxidation products formed are amides, nitramines, and imines. All of the products shown have the potential to partition to the aerosol phase, although amides are particularly water soluble and have the lowest vapor pressures. An unexpected product, alkylamine-N-oxide, was first detected by Angelino et al. (2001) in the aerosol phase and was again detected in the particle phase during the current study.

Figure 5b shows the pathways for ozone reaction with an aliphatic amine. While the loss of an alkyl group from the high energy amine oxide generates products distinct from those generated by reaction with OH, rearrangement of the amine oxide and subsequent loss of OH leads to alkoxy radicals similar to those generated from hydrogen abstraction by OH followed by loss of an oxygen atom to NO. Following this branch of the reaction diagram leads to similar, and in many cases identical, products as those formed by reaction with OH.

Figure 5c shows the beginning of the reaction pathways for amine oxidation by OH in the absence of NO_x. Presumably, a number of the condensable species in this system consist of hydroperoxides and alkyl peroxides. Many of the same products formed in the high NO_x and ozone systems are formed if, rather than forming peroxides, RO₂ + RO₂ and RO₂+HO₂ reactions form alkoxy radicals.

Many of the photooxidation experiments reported here employed hydrogen peroxide (H₂O₂) as an OH source. As detailed in the Experimental section, a relatively large amount (3–5 ppm) of hydrogen peroxide must be introduced into the chamber to achieve sufficient levels of OH for rapid reaction. Because the reaction between OH and H₂O₂ forms HO₂ and because hydrogen peroxide itself may affect the chemistry of the aerosol formed, we conducted additional photooxidation experiments using mixtures of propene and NO_x as well as NO_x alone. We found no major differences in chemistry between the systems with and without H₂O₂, although the reactions occurred much faster in the presence of hydrogen peroxide, as expected. All of the ozonolysis reactions were carried out in the absence of NO_x.

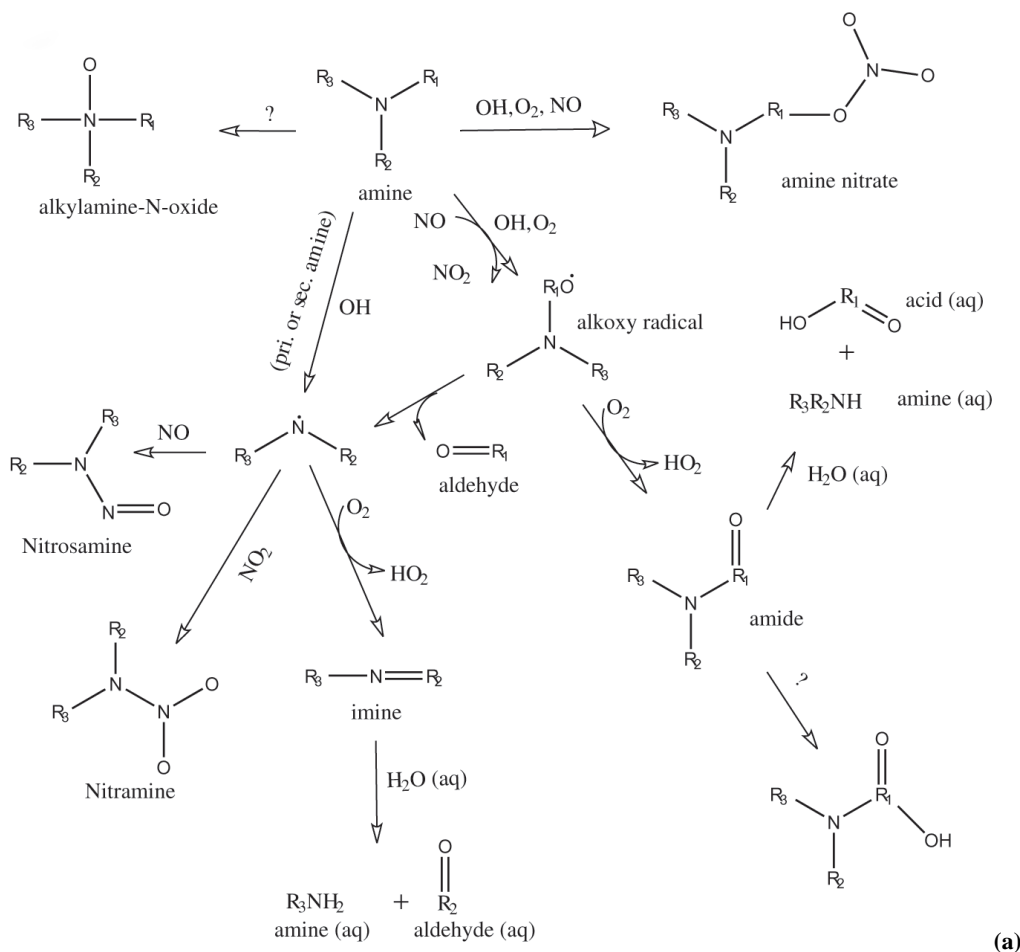


Fig. 5a. Mechanism of amine oxidation by OH in the presence of NO_x (Schade and Crutzen, 1995).

5.1 Experimental protocol

The same procedure was used for all photooxidation and ozonolysis experiments. For photooxidation experiments, the first step is the injection of either: H₂O₂, a H₂O₂ and NO_x mixture, a NO_x and propene mixture, or NO_x alone. Table 2 gives the oxidant used and NO_x mixing ratio for each photooxidation experiment. For all types of experiments, except NO_x-free photooxidations, the next step was to add a small amount (~10 ppb) of HNO₃. Once the HNO₃ had mixed, the amine was injected at a much higher concentration than the nitric acid (typically ~100 ppb) causing nucleation of aminium nitrate salt while the vast majority of the amine remained in the gas phase. The concentration of nucleated salt particles was always observed to peak soon after the injection of the amine, followed by a sharp decrease in mass as mixing occurred and gas-particle equilibrium was established.

After the concentration of the nucleated particles became steady and sufficient time had elapsed to collect composition data with the cToF-AMS and the PILS-IC, oxidation was ini-

tiated. For photooxidation experiments, oxidation was initiated by turning on the black lights surrounding the chamber, while for ozonolysis ozone was injected into the chamber. All experiments were continued until there were no further changes in particle mass or volume, except for slow decay in mass and volume caused by particle loss to the chamber walls.

5.2 Trimethylamine (TMA) photooxidation

Trimethylamine (TMA) is one of the more abundant ambient alkyl amines near animal husbandry operations (Rabaud et al., 2003; Schade and Crutzen, 1995). Figure 6 shows the time profiles for NO_x, O₃, particle volume (DMA), ionic particle mass (PILS-IC), and particle mass (cToF-AMS) during the photooxidation of TMA. For this experiment (number 3, Table 2), 300 ppb of NO₂, 10 ppb of HNO₃ and 100 ppb of TMA were used. As expected, trimethylammonium nitrate (TMAN) salt began to nucleate soon after the injection of TMA. Approximately 30 min after the TMA injection the aerosol mass stabilized as the system reached gas-particle

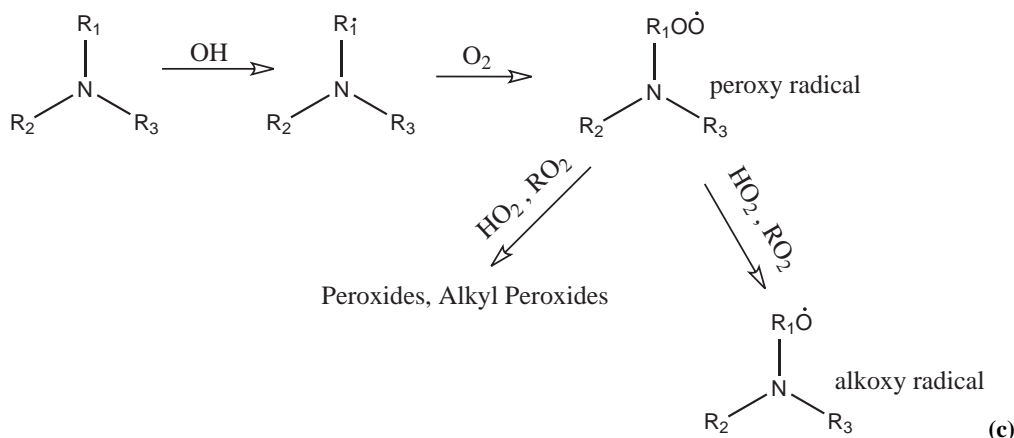
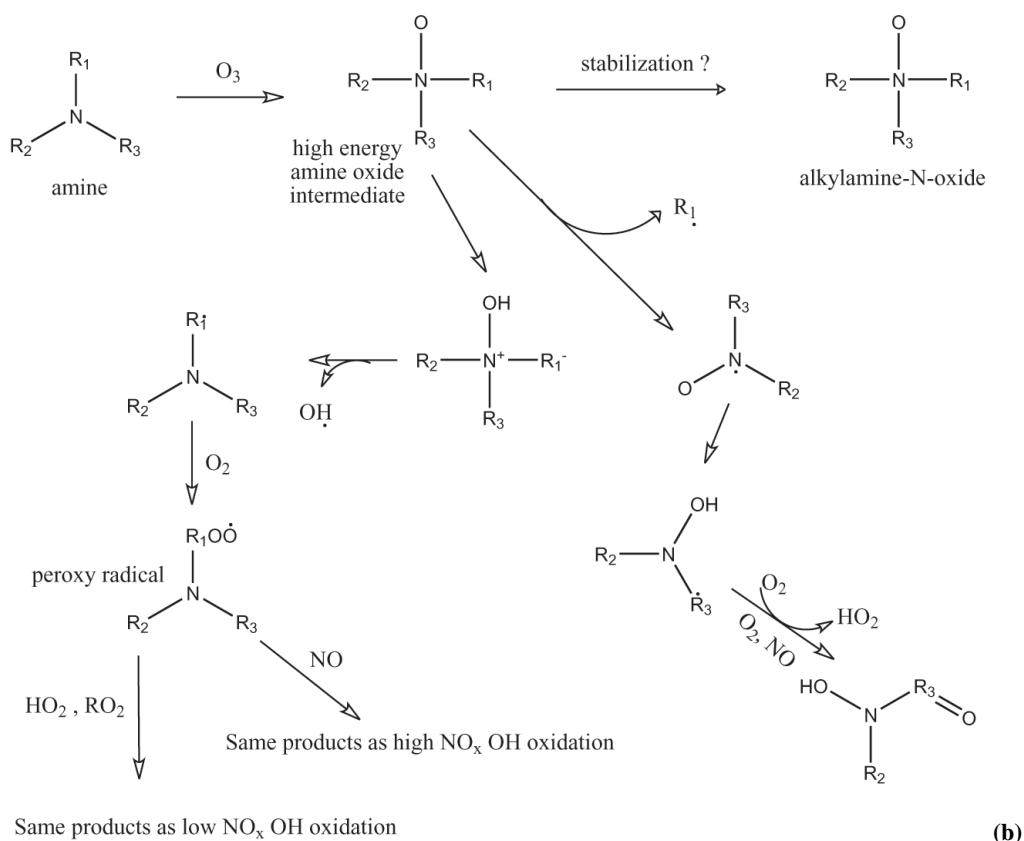


Fig. 5b+c. Mechanism of amine oxidation by (b) Ozone, in the absence of NO_x (Tuazon et al., 1994), (c) OH in the absence of NO_x . A ? indicates an unknown oxidation mechanism to form the product shown.

equilibrium. The composition of the TMAN particles was measured for an additional 30 min with the cToF-AMS and the PILS-IC before the black lights surrounding the chamber were turned on, initiating photooxidation.

When photooxidation begins, because of the large excess of TMA injected relative to HNO_3 , much of the nitric acid has been converted into particle-phase nitrate. Assuming negligible wall loss, ~ 90 ppb of TEA remains in the gas

phase at the time the lights are turned on. Upon irradiation, there is a brief spike in NO from the photolysis of NO_2 ; as the TMA is oxidized by OH, RO_2 radicals are formed that convert the NO back to NO_2 , and ozone formation begins. NO_x gradually decreases throughout the course of the experiment as NO_2 is converted to HNO_3 by reaction with OH. Particle formation begins within ~ 10 min of the start of irradiation.

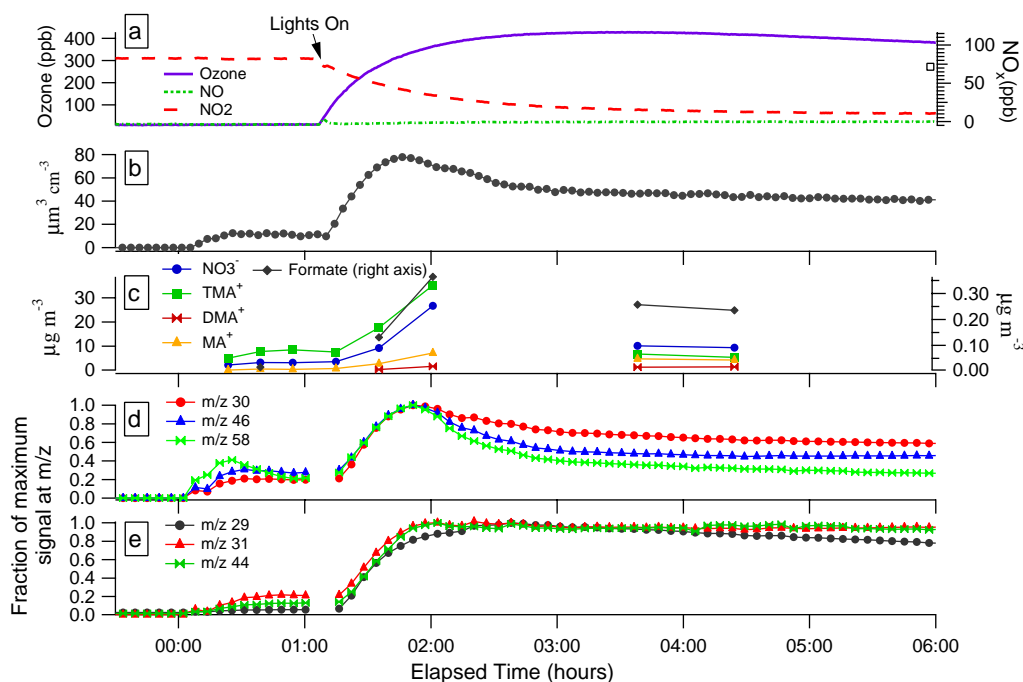


Fig. 6. Photooxidation of trimethylamine (experiment 3 from Table 2). Panel (a) NO_x and ozone concentrations. Panel (b) Particle volume measured by the DMA. Panel (c) Growth of ionic species measured by the PILS-IC. Panels (d) and (e) Fragment ions from the cToF-AMS. When injected, the TMA reacts with nitric acid in the chamber to form trimethylammonium nitrate. Upon activation of the black lights, there is an initial burst of particle growth followed by a rapid decay in particle mass and volume. The PILS-IC data show that much of the decay is a result of volatilization of the trimethylammonium nitrate salt. The cToF-AMS traces show that while m/z 's corresponding to trimethylammonium nitrate salt fragments (30 NO^+ , 46 NO_2^+ , $58 ((\text{CH}_3)_2\text{NCH}_2^+)$) rapidly decrease after the peak in growth, m/z 's corresponding to methylammonium nitrate ($31 \text{ CH}_3\text{NH}_2^+$) and oxidized fragments (29 HCO^+ , 44 CO_2^+) are level or decrease much more gradually.

Figure 6c-e shows the particle composition as measured by the cToF-AMS and the PILS-IC instruments. The PILS-IC data show that at the peak of particle growth, $62 \mu\text{g m}^{-3}$ of the particle mass consists of TMAN salt. The volume measured by the DMA is $78 \mu\text{m}^3 \text{cm}^{-3}$ at the peak of particle growth. Based on a calculated effective density of (1.3 ± 0.2) , nearly 80% of the particle mass is composed of the nitrate salt at the peak of particle growth. In addition to the salt present at the start of irradiation, additional salt is formed as TMA reacts with nitric acid formed as OH reacts with NO_2 . After the peak of particle growth, both the mass and volume of aerosol drop dramatically. The drop in particle mass can be accounted for almost entirely by the volatilization of TMAN, and after 4.4 h of reaction TMAN salt accounts for less than 35% of the particle mass. Volatilization of TMAN is a direct consequence of the gas-particle equilibrium of the nitrate salt; as oxidation proceeds and gas-phase TMA is reacted away (and as nitric acid is lost to the walls of the chamber), the equilibrium for the salt shifts back towards the gas phase. Figure 6d-e shows time traces of signals from the cToF-AMS associated with trimethylammonium (m/z 58 $(\text{CH}_3)_2\text{NCH}_2^+$), methylammonium (m/z 31 CH_3NH_2^+), nitrate (m/z 30 NO^+ , m/z 46 NO_2^+) and oxidized fragments

(m/z 44 CO_2^+ , m/z 29 CHO^+). The signals associated with trimethylammonium and nitrate all decrease quickly after the peak of particle growth while those associated with oxidized fragments and methylamine are relatively flat (some show slight decreases associated with the slow loss of particles to the chamber walls). The time trends of these fragments lend support to the hypothesis that TMAN salt is repartitioning to the gas phase while compounds formed from TMA oxidation are condensing.

Over the course of the reaction, both the cToF-AMS and the PILS-IC detected signals consistent with the presence of particle-phase methylammonium. Based on the PILS-IC data, nearly 10% of the particle mass at the peak of aerosol growth is methylammonium. The most plausible explanation for the detection of this species is that imines formed in the gas phase (see Fig. 5a) partition to the particle phase through either nitrate salt formation or direct condensation. Imines exposed to liquid water readily decompose into an amine and an aldehyde (Fig. 5a). It is possible that this reaction occurs in the particle phase, though it is unclear if sufficient particle-phase water existed to drive this reaction. The experiments are carried out at low RH ($< 10\%$) but both the TEA and nitric acid were bubbled into the chamber from aqueous

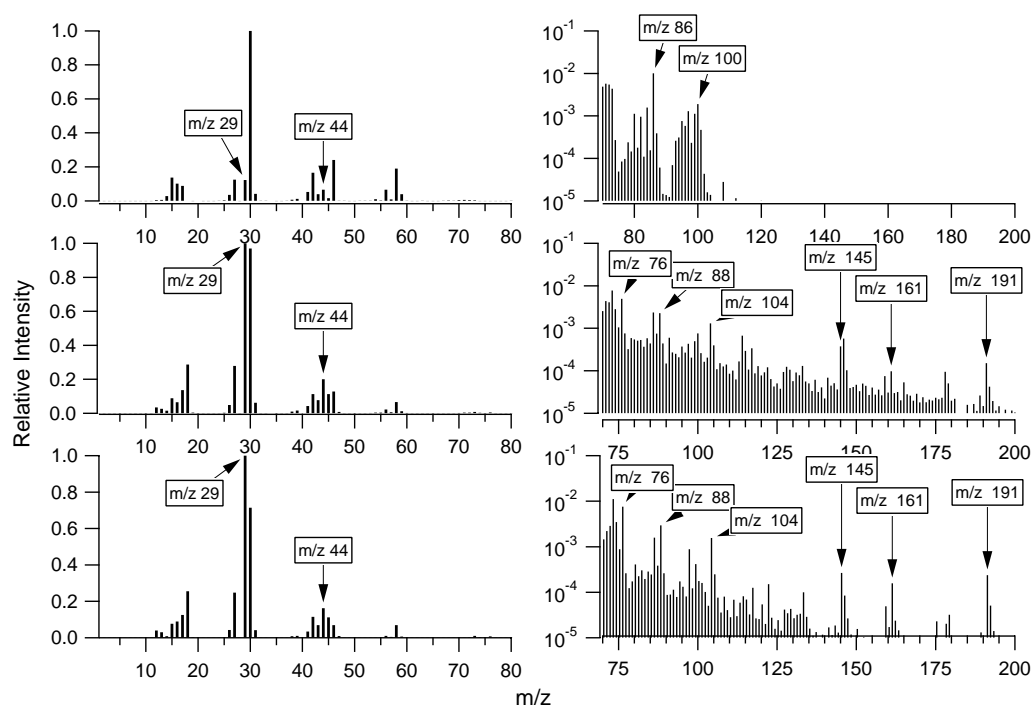


Fig. 7. Aerosol mass spectra from the cToF-AMS during different stages of trimethylamine photooxidation (Fig. 6) and ozonolysis (Fig. 8). The top panel shows trimethylammonium nitrate before oxidation while the middle panel is from the end of the photooxidation experiment (8 h elapsed time). The bottom panel shows the spectra from aerosol formed from TMA after ~ 3 h of ozone exposure. The right and left panels show different m/z ranges of the same spectra. The major peaks shift during the photooxidation from peaks corresponding to the trimethylammonium nitrate salt to more oxidized peaks (29 HCO^+ , 44 CO_2^+). There is also a significant increase in the fraction of higher molecular weight species.

solutions and the efflorescence behavior of aminium nitrate particles is unknown (although if their behavior is similar to that of ammonium nitrate, the particles may retain water at low RH). Independent of the amount of particle water, because the PILS-IC dissolves collected aerosol particles into water droplets, the imines would almost certainly react with water inside of the instrument if this reaction had not already occurred in the chamber. The fact that more methylammonium nitrate is detected by the PILS-IC than dimethylammonium nitrate further supports the imine reaction pathway because this pathway does not lead to dimethylammonium nitrate. The PILS-IC data also show an increase in the abundance of formate, which is a byproduct of hydrolysis of imines. While the cToF-AMS peak at m/z 31 could be a fragment from oxidized forms of TMA and not from methylammonium, it is improbable that this peak is a fragment from TMAN itself because it does not follow the same time profiles as m/z 58 (the dominant peak for TMAN). It is improbable that this peak is a fragment from TMAN itself because it does not follow the same time profiles as m/z 58 (the dominant peak for TMAN). The small amounts of dimethylammonium nitrate detected by the PILS-IC could be formed through hydrolysis of amides in the particle phase as shown in Fig. 5a.

Figure 7 shows the spectra from the cToF-AMS during different stages of the same photooxidation experiment discussed above (experiment 3, Table 2). As in Fig. 6, the growing importance of oxidized fragments relative to trimethylammonium nitrate fragments is evident. Of note is the relative prominence of m/z 88, which is the expected dominant peak (resulting from alpha-cleavage) of the carboxylic acid of TMA (shown in the bottom of Fig. 5a). Also of note is the increase in abundance of higher molecular weight species which could be the result of particle-phase reactions or multiple oxidations in the gas phase. The gas-phase route seems somewhat implausible for molecular weights above 150 ($\text{RO}_2 + \text{RO}_2 = 148 \text{ amu}$ for TMA) because formation of these high molecular weight compounds would require multiple $\text{RO}_2 + \text{RO}_2$ or $\text{RO}_2 + \text{HO}_2$ reactions.

5.3 Trimethylamine (TMA) ozonolysis

During the photooxidation of trimethylamine a large amount of ozone is formed, and, based on reported rate constants (Atkinson et al., 1978; Tuazon et al., 1994), ozone and OH reactions with TMA are competitive under these conditions. To determine if the products of the ozone reaction form aerosol, we conducted a TMA ozonolysis experiment.

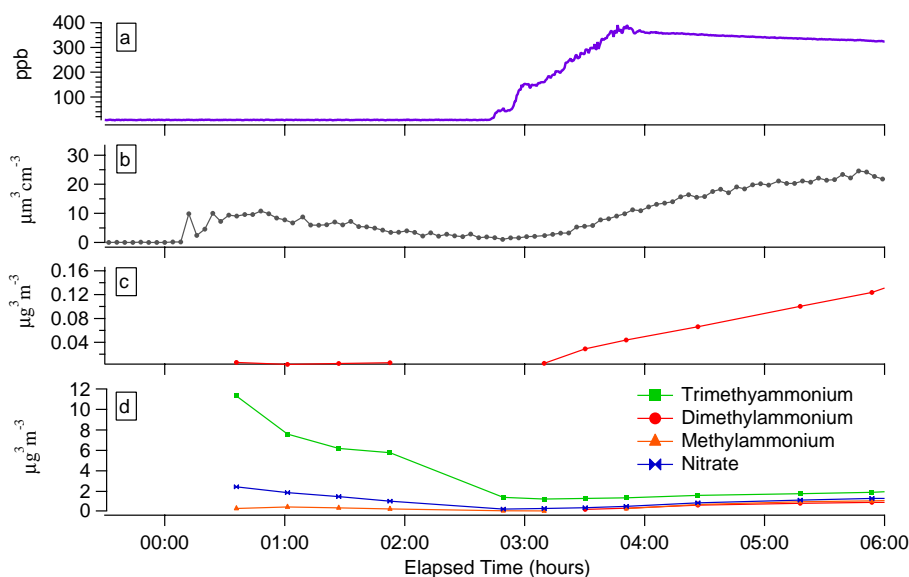


Fig. 8. Ozonolysis of trimethylamine (exp. 4, Table 2). Trimethylamine is injected into a chamber containing 18 ppb of nitric acid at time =0. The salt is allowed to decay away before 400 ppb of ozone is injected over ~ 1 h. Panel (a) Ozone concentration. Panel (b) DMA volume showing significant aerosol growth as the TMA is oxidized. Panel (c) Formate concentration measured by the PILS-IC. Panel (d) Ions measured by the PILS-IC, showing that there is little increase in salt concentrations during the ozonolysis.

Figure 8 shows the time series of the DMA, cToF-AMS, and PILS-IC for this experiment. At time =0, 100 ppb of TMA was added to 16 ppb of HNO_3 already in the chamber, forming trimethylammonium nitrate (TMAN). The TMAN salt remained in the chamber for ~ 3 h during which time nearly all of it deposited on the chamber walls or volatilized. Oxidation was initiated by adding 200 ppb of ozone to the remaining gas-phase TMA in the system (~ 85 ppb assuming negligible wall loss of gas phase TMA and assuming all of the particulate TMAN was lost to the walls). During the ozonolysis, the vast majority ($>90\%$) of the aerosol formed was non-ionic and accordingly was not detected by the PILS-IC. After 3 h of ozonolysis, aerosol growth had reached a peak. At this point, nitric acid was added (not shown in Fig. 8) to induce nitrate salt formation of gas-phase products too volatile to condense. The addition of nitric acid led to $9 \mu\text{m}^3 \text{cm}^{-3}$ of aerosol growth, which was predominantly TMAN with a small contribution from methylammonium nitrate.

Though a large excess of ozone remained after the peak of aerosol growth, the aerosol formed appeared to be stable towards further oxidation and did not rapidly revolatilize. The mass yield of non-salt aerosol (before additional nitric acid was injected) was $\sim 15\%$ (assuming 85 ppb as the starting concentration of amine). Interestingly, the yield from the ozonolysis is similar to the 23% yield of oxidized (non-salt) SOA formed during photooxidation with NO_x .

The bottom panel of Fig. 7 shows a spectrum from the cToF-AMS after three hours of ozone oxidation. The similarity between this spectrum and that in the middle panel of the figure (after photooxidation) is striking, with the one

obvious difference being that the nitrate fragments (m/z 30 and 46) are less prominent because nitrate salts represent a smaller fraction of the particulate mass in the ozonolysis experiment. The similarity of the spectra indicates that ozonolysis generates similar condensable compounds to those from photooxidation. It should be noted that OH can be created during ozonolysis (see Fig. 5) and some of the compounds formed in ozonolysis could potentially be formed from amine reaction with OH.

5.4 Methylamine (MA) photooxidation

In addition to being formed through oxidation and hydrolysis of TMA, methylamine (MA) is itself a major emission from animal husbandry operations. In the study of Schade and Crutzen (1995) methylamine and trimethylamine were the only two aliphatic amines detected near animal husbandry operations. Figure 9 shows the time series for the photooxidation of methylamine (experiment 6, Table 2) using H_2O_2 as the OH precursor. Nitric acid, in the amount of 10 ppb, was added before methylamine was injected, and NO_x was added as 100 ppb of NO, instead of as NO_2 . Injection of the methylamine caused the nucleation of methylammonium nitrate, which was allowed to equilibrate and mix for approximately two hours before the black lights were turned on 2.5 h after injection of the amine. When irradiation began, NO was quickly converted to NO_2 through reactions with RO_2 and HO_2 . As NO was removed, ozone formation began, NO_2 started to convert to HNO_3 , and aerosol formation began. The aerosol volume shows the same behavior as that during

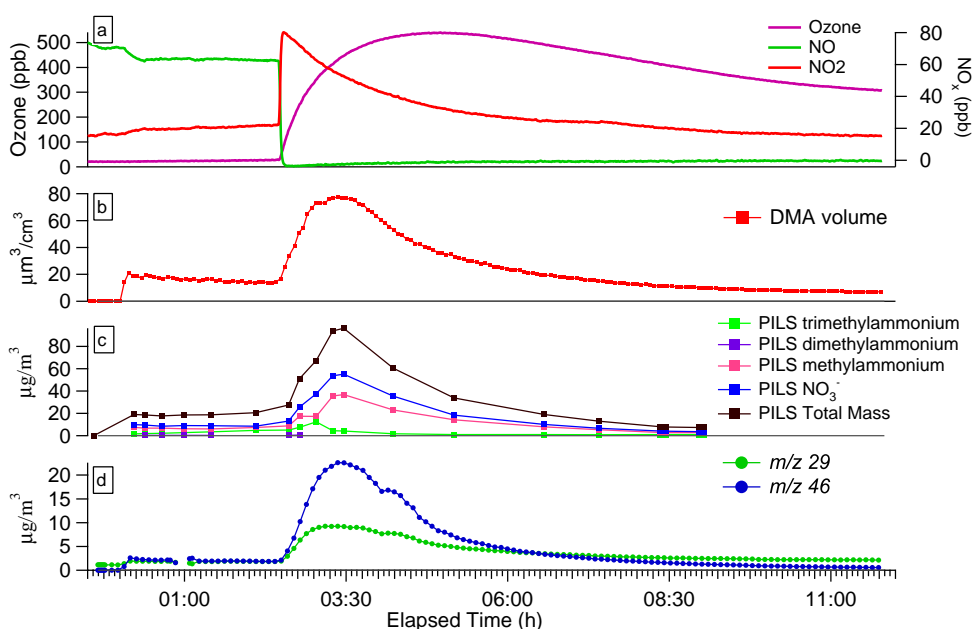


Fig. 9. Methylamine photooxidation (exp. 6, Table 2). Panel (a) Ozone and NO_x concentrations. Panel (b) Time series for the DMA volume showing rapid decay after the peak of aerosol growth. Panel (c) Time series for the PILS-IC showing that most of the rapid mass decay is due to vaporization of the methylammonium nitrate salt. Panel (d) Fragment ions from the cToF-AMS. Signal from *m/z* 29 which is a mix of oxidized organic fragments (CHO⁺) and salt fragments gradually grows more important than signal from from salt alone (*m/z* 46 NO₂⁺).

the TMA photooxidation, growing to a peak as methylammonium nitrate is formed then rapidly decaying as gas-phase methylamine is oxidized. Subtracting the mass of all the ionic species detected by the PILS-IC from the aerosol mass calculated by multiplying the DMA volume by the effective density of 1.1 ± 0.2 , one finds that nearly 100% of the aerosol formed at the peak of aerosol growth is methylammonium nitrate. There is a small signal in the PILS-IC from contaminant TMA which decreases as the experiment progresses. In contrast to the TMA photooxidation, there is little aerosol remaining after the rapid decay of the salt; $< 1 \mu\text{g m}^{-3}$ of non-salt organic aerosol is present in the system after 4 h of photooxidation relative to more than $20 \mu\text{g m}^{-3}$ remaining for the TMA with similar starting concentrations of amine. Though the mass of non-salt aerosol formed from the photooxidation was small, Panel (D) of Fig. 9 shows that the relative importance of non-salt organic aerosol increases throughout the experiment. Methanimine, one of the most abundant gas-phase products from methylamine photooxidation is known to polymerize on surfaces and may be a source of the non-ionic aerosol detected (Schade and Crutzen, 1995).

5.5 Methylamine (MA) ozonolysis

Because the vast majority of the aerosol formed during the photooxidation of methylamine is methylammonium nitrate, we performed an ozonolysis experiment to confirm that methylamine is unable to generate significant aerosol mass through oxidative routes. Time series from the ozonolysis

have already been shown, though in the context of sulfate salt formation, in Fig. 4. Ammonium sulfate seed was added to the methylamine-ozonolysis system to provide a surface for condensation if the system did not generate enough condensable products to induce nucleation. Ozone, in the amount of 200 ppb, was added to the chamber along with ~ 100 ppb of methylamine. As discussed previously, the methylamine replaced the ammonium from the ammonium sulfate seed, but after this initial phase of growth by displacement, negligible further growth was observed, confirming the result of negligible non-salt organic mass yield observed during the photooxidation.

5.6 Triethylamine (TEA) photooxidation

Results from the photooxidation of 500 ppb of triethylamine with NO_x using hydrogen peroxide as an OH precursor are shown in Fig. 10. For all TEA photooxidations, independent of OH source or starting concentration, rapid decay of aerosol mass after the peak growth was not observed. The reason for the observed stability of the salt formed is unclear. It probably indicates that TEAN has a smaller dissociation constant than the other amines studied. It could also indicate that there is interaction between the organic material and the salt lowering the volatility of the TEAN. Finally, it could be the result of salt formation by products of TEA oxidation. During all TEA photooxidations, diethylammonium and ethylammonium were detected by the PILS-IC with diethylammonium being formed at higher

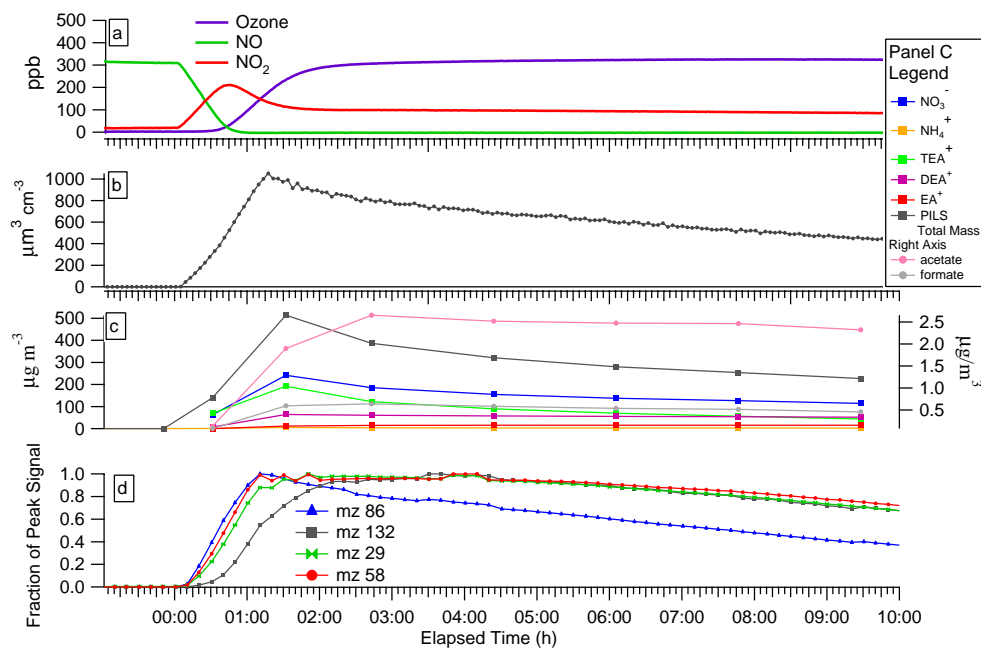


Fig. 10. Photooxidation of 500 ppb triethylamine (TEA) (exp. 9, Table 2). Irradiation is initiated at $t=0$. Panel (a) Evolution of ozone and NO_x . Panel (b) DMA volume. Panel (c) Time profile of species detected by the PILS-IC showing that diethylammonium and ethylammonium are formed during the photooxidation, with significantly more diethylammonium being formed. Panel (d) Fragments from the cToF-AMS. The most intense fragment of TEA (m/z 86 $\text{N}(\text{CH}_2\text{CH}_3)_2\text{CH}_2^+$) grows in first followed by the major peak for DEA (m/z 58 $\text{NH}(\text{CH}_2\text{CH}_3)\text{CH}_2^+$) and oxidized fragments (m/z 29 CHO^+). Higher molecular weight fragments (m/z 132) grow in more slowly.

concentrations in the particle phase than ethylammonium. Based on our knowledge of the gas-phase oxidation reactions, it seems most plausible that the diethylammonium is formed by the particle-phase hydrolysis of N,N diethylacetamide (the amide shown in Fig. 5a if all R groups are ethyl groups. As mentioned earlier, it is possible that hydrolysis of the amide occurs in the PILS-IC instrument itself rather than in the chamber.) The detection of acetate by the PILS-IC during the experiment is consistent with the proposed mechanism of diethylammonium formation from hydrolysis of N,N diethylacetamide. The ethylammonium detected by the PILS-IC could be formed in two ways. First, it could result from aqueous reaction of the imine as shown in Fig. 5a (if all R groups being ethyl). Second, it could be the result of two successive amide hydrolysis reactions. The detection of higher levels of diethylammonium than ethylammonium contrasts with the results from the oxidation of trimethylamine for which higher levels of methylamine were detected than for dimethylamine. This difference suggests that more aerosol is formed through the imine route for trimethylamine whereas more aerosol is formed through the amide route for triethylamine.

During one photooxidation of TEA (experiment 20), a filter of the aerosol was collected and analyzed by LC/MS with electrospray ionization. All of the mass spectral peaks observed using LC/MS were consistent with the nitrate salt and

oxidation products already discussed, except for a peak at m/z 118 detected in the positive mode. Peaks detected in the positive mode from electrospray ionization are typically $[\text{M}+\text{H}]^+$ ions, making the molecular weight of the species detected 117 amu. This molecular weight is consistent with triethylamine-N-oxide (shown in Figs. 5a and b with R=ethyl group), a species that was previously detected by Angelino et al. (2001). There is not a significant peak in the spectrum from the cToF-AMS at m/z 117 (or m/z 116 which would be the expected largest fragment ion peak resulting from the alpha cleavage of a hydrogen from triethylamine-N-oxide); this is not particularly surprising because a high energy oxide of this type would be expected to fragment under electron impact ionization if it had not already thermally fragmented on the vaporizer. The extracted ion chromatogram (EIC) of m/z 118 from the LC/MS system gives three distinct peaks with retention times of 1.38, 2.00, and 2.30 min, indicating the presence of three distinct isomers of this species. The structures of these isomers remain unknown.

5.7 Triethylamine (TEA) ozonolysis

Ozonolysis of TEA was conducted using the same procedure as for the ozonolysis of TMA and MA. First, nucleation of triethylammonium nitrate (TEAN) was initiated by adding 100 ppb of TEA to a chamber containing 8 ppb of nitric acid. After allowing the TEAN to equilibrate for 2 h,

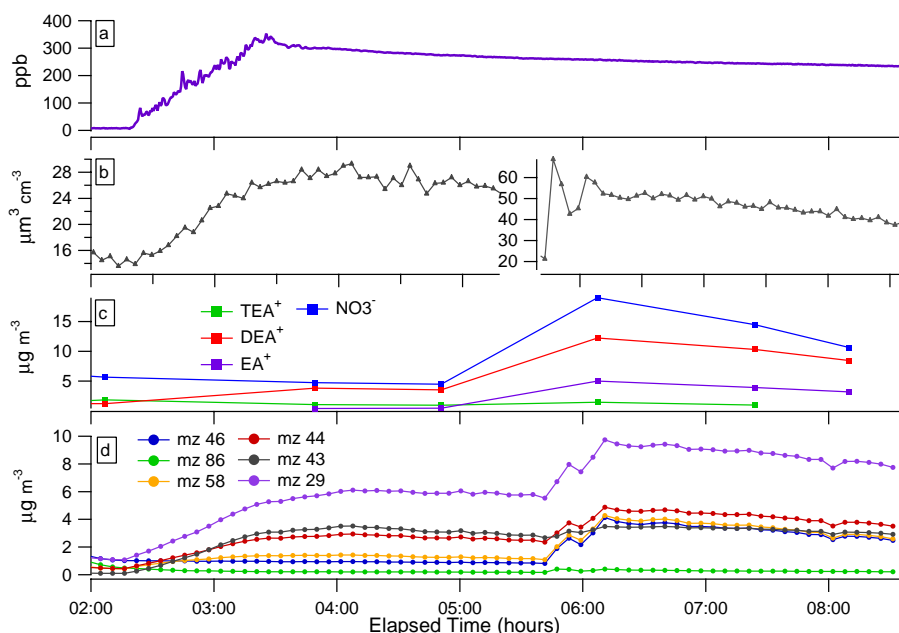


Fig. 11. Ozonolysis of triethylamine (TEA) (exp. 16, Table 2). At $t=0$ (not shown) 100 ppb of TEA is injected into a chamber containing 8 ppb of nitric acid, nucleating triethylammonium nitrate (TEAN) particles, which are still present when ozone is injected at $t=2$ h 12 min. After growth of secondary aerosol formed through ozonolysis had ceased, an additional 8 ppb of nitric acid was injected at 5 h 31 min. Panel (a) Time series of ozone mixing ratio Panel (b) Aerosol volume as measured by the DMA (the time axis is coincident with all of the other panels, two y-axes have been used to show more precisely the growth resulting from ozonolysis). Panel (c) Ionic species measured by the PILS-IC showing an increase in DEA throughout the reaction and condensation of EA when additional HNO_3 is added Panel (d) Ion fragments detected by the cToF-AMS: m/z 46 NO_2^+ , m/z 86 $\text{N}(\text{CH}_2\text{CH}_3)_2\text{CH}_2^+$ (largest peak from triethylammonium), m/z 58 $\text{NH}(\text{CH}_2\text{CH}_3)\text{CH}_2^+$ (largest peak from Diethylammonium), m/z 44 CO_2^+ , m/z 43 $\text{C}_2\text{H}_3\text{O}^+$, m/z 29 CHO^+ .

350 ppb of ozone was slowly added to the chamber causing further aerosol growth that peaked, after ~ 3 h of ozone exposure, at a maximum of $15 \mu\text{m}^3 \text{cm}^{-3}$, or $\sim 18 \mu\text{g}^3 \text{m}^{-3}$ (effective density = 1.2 ± 0.2) of additional growth. The mass yield from ozonolysis is 5%.

During ozonolysis, diethylammonium and ethylammonium were formed as they were during photooxidation, but there was no corresponding growth in the nitrate signal (either on the cToF-AMS or the PILS-IC) indicating that these compounds condensed in the particle phase in a form other than nitrate salts. At the peak of aerosol growth (3 h of oxidation), diethylammonium constituted 23% of the aerosol mass formed after ozone injection and ethylammonium accounted for 3% of the mass from ozonolysis. After the aerosol growth had peaked, an additional 8 ppb of nitric acid was added causing a further $30 \mu\text{g} \text{m}^{-3}$ of aerosol growth. The aerosol generated by this second addition of nitric acid was a mix of diethylammonium ($8.7 \mu\text{g} \text{m}^{-3}$), ethylammonium ($4.5 \mu\text{g} \text{m}^{-3}$), triethylammonium ($0.5 \mu\text{g} \text{m}^{-3}$), and nitrate ($14.5 \mu\text{g} \text{m}^{-3}$). The near perfect ion balance between the positive amine ions and the negative nitrate ions (3% negative charge imbalance) substantiates that all of the additional growth was in the form of nitrate salts. The negligible increase in triethylammonium mass during the second

addition of nitric acid indicates that nearly all of the starting TEA had been oxidized. The final aerosol, composed of nitrate salts and oxidized SOA, did not rapidly decay. The PILS-IC data showed that nitrate decayed 7 percent faster than ethylammonium and 14 percent faster than diethylammonium further supporting the idea that these species are not entirely nitrate salts and that nitrate salts decay more rapidly than SOA formed through oxidation.

5.8 Diethylamine (DEA) photooxidation

Figure 12 shows the photooxidation of 100 ppb of diethylamine, conducted in the same manner as the previously discussed photooxidations using hydrogen peroxide as an OH precursor. Diethylammonium nitrate nucleates upon injection of DEA followed by a burst of aerosol mass when the lights are turned on that quickly decays away. The rapid decay is similar to the behavior of TMA and MA during photooxidation, with DEA being more similar to MA in that nearly all of the aerosol formed is nitrate salt. Experiments using different OH sources also yielded negligible non-salt aerosol. This is an intriguing result, because by molecular weight alone, DEA would be predicted to form more secondary organic aerosol when oxidized than TMA. Clearly, in this case, the chemical nature of the compound is more

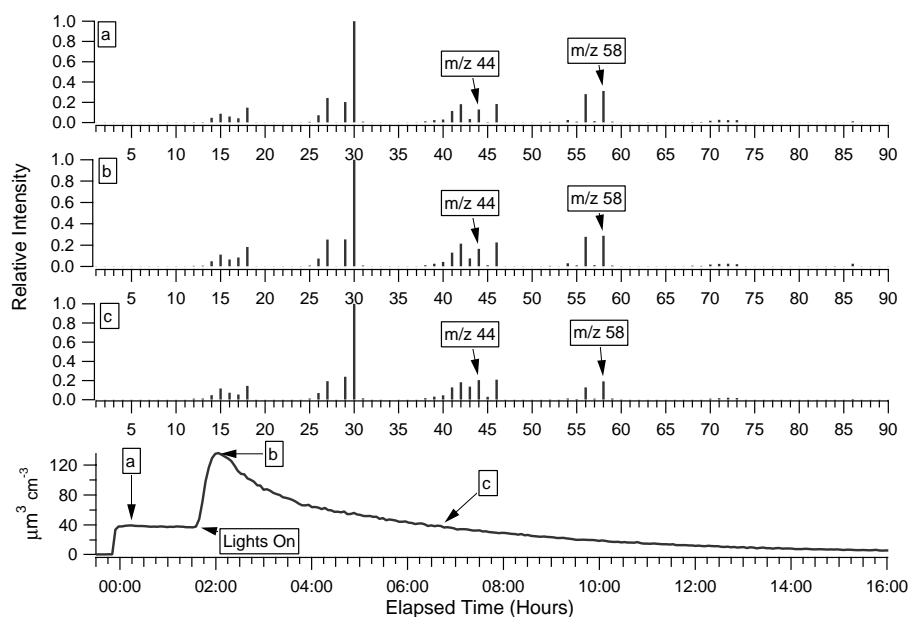


Fig. 12. Photooxidation of diethylamine (exp. 22, Table 2). The volume trace from the DMA (bottom panel) shows that the aerosol formed decays quickly back to the volume present before the irradiation. The prominent peaks in the cToF-AMS spectra (Panels a–c) show little change throughout the course of the experiment, except for a slight increase in the relative intensity of oxidized peaks at m/z 44 (CO_2^+) and m/z 43 ($\text{C}_2\text{H}_3\text{O}^+$). There was also little change in the high m/z spectra indicating negligible growth of high molecular weight species.

important than molecular weight alone. Though the specific reactions that lead to the difference in yield between TEA and DEA remain unclear, Fig. 5 shows that there are several compounds that can be formed by tertiary amines through the loss of one of the alkyl groups, a reaction pathway that is not available for secondary or primary amines. Though believed to be a minor channel, OH can also extract a hydrogen atom directly from the nitrogen of primary and secondary amines; it is possible that this reaction pathway leads to more volatile compounds. Because photooxidation yielded no non-salt organic aerosol, an ozonolysis experiment was not conducted for DEA.

5.9 Ethylamine (EA) photooxidation

One photooxidation of ethylamine was conducted and yielded negligible non-salt aerosol mass. Though there was contamination from a previous DEA experiment, it is doubtful that this affected the amount of organic aerosol formed. Ethylamine ozonolysis was not pursued because of the negligible non-salt yield during photooxidation.

5.10 Ethanolamine (MEA) photooxidation and ozonolysis

Figure 13 shows the photooxidation of ethanolamine. Aerosol growth follows the same pattern as for the other amines with the majority of the initial growth being composed of nitrate salts that repartition back to the gas phase as the amine reacts away. Non-salt organic aerosol forms

(~2% mass yield), but the yield is small as it is for the other non-tertiary amines studied. The cToF-AMS data show that oxidized fragments (m/z 44, CO_2^+) grow in more gradually and decay less than fragments associated with ethanolammonium nitrate (m/z 46 NO_2^+ and m/z 30 NO^+ and the major ion fragment from ethanolammonium itself). The PILS-IC shows growth of diethylammonium though this is probably a result of contamination because it is unclear how ethanolamine could react to form diethylammonium. The yield from ozonolysis of ethanolamine was small (~3%), as expected from the small yield observed during photooxidation.

5.11 Photooxidation in the absence of NO_x

NO_x -free photooxidation experiments were conducted for both TEA and DEA. In both cases, negligible mass from nitrate salts was detected by the PILS-IC. Following the trends of the high NO_x photooxidation and ozonolysis results, 500 ppb of TEA formed $260 \mu\text{g m}^{-3}$ of aerosol (mass yield of ~12%) while 500 ppb DEA formed less than $2 \mu\text{g m}^{-3}$ (mass yield of ~0.1%). The cToF-AMS mass spectrum from the NO_x -free photooxidation of TEA is shown in Fig. 14. No dramatic changes in the mass spectrum occur during the course of the experiment.

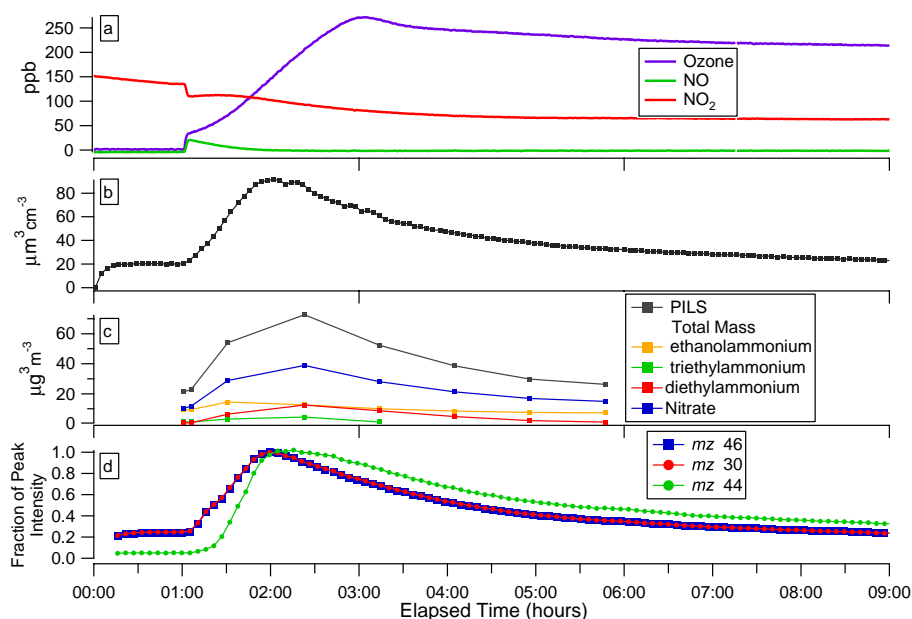


Fig. 13. Photooxidation of 100 ppb of ethanolamine (MEA) (exp. 29, Table 2). Ethanolamine is injected at $t=0$ forming ethanolammonium nitrate. Panel (a) Evolution of ozone and NO_x mixing ratios. Panel (b) DMA volume. Panel (c) PILS-IC data. Panel (d) Fragments from the cToF-AMS. Oxidized fragment ions (m/z 44 CO_2^+) grow in slowly and decay less quickly than nitrate fragment ions (m/z 46 NO_2^+ and m/z 30 NO^+) or ethanolammonium fragment ions (m/z 30 is the base peak for ethanolammonium in the cToF-AMS).

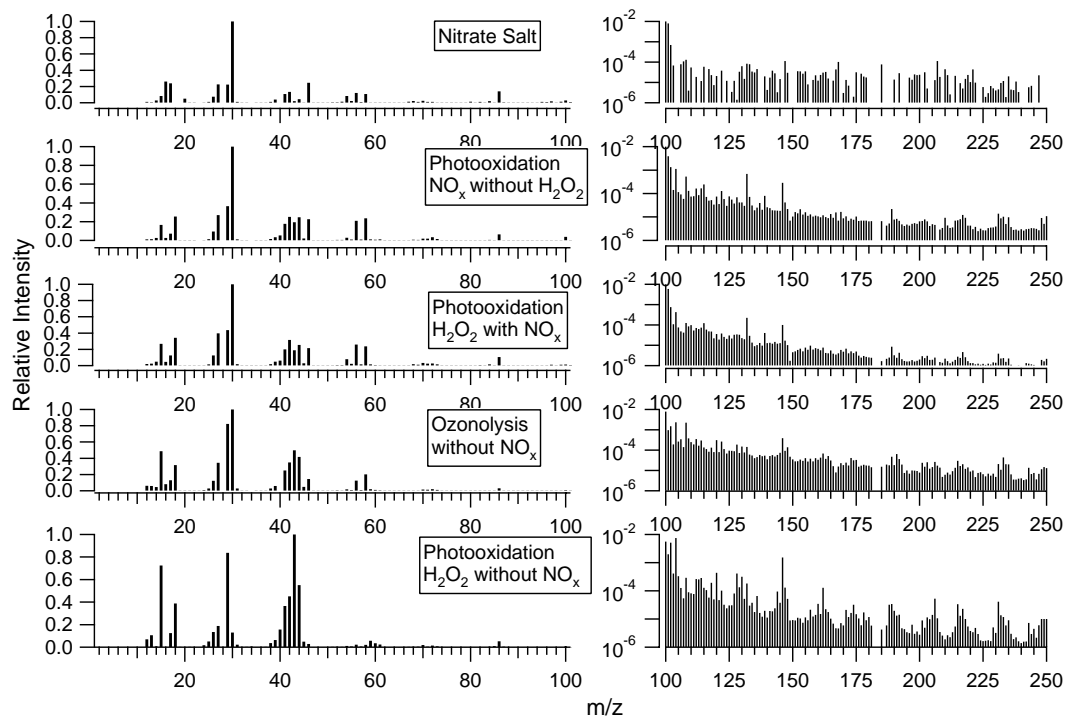


Fig. 14. cToF-AMS spectra (normalized to the largest peak) of aerosol generated from TEA oxidation under various conditions. In all cases, except for hydrogen peroxide without NO_x , the nitrate salt was intentionally formed by mixing TEA with nitric acid in the chamber before the start of oxidation. All spectra were collected after the peak of aerosol growth had been reached.

5.12 Effect of oxidation conditions on particle chemistry

Figure 14 shows cToF-AMS spectra from particles formed by oxidation of TEA using four different systems: (1) photooxidation with NO_x alone, (2) photooxidation with NO_x using H_2O_2 as an OH precursor, (3) ozonolysis in the absence of NO_x , and (4) photooxidation in the absence of NO_x using H_2O_2 as an OH precursor. Because the cToF-AMS uses electron impact ionization, differences in the peak height ratios can be used to assess chemical similarity between the systems even though the spectra are highly fragmented. Aerosol formed in the two different photooxidation systems containing NO_x have similar spectra with large peaks corresponding to fragments from the nitrate salt mixed with oxidized fragments (m/z 29 HCO^+ , m/z 44 COO^+ , m/z 43 $\text{C}_2\text{H}_3\text{O}^+$, etc.). The spectrum of aerosol generated by photooxidation (using hydrogen peroxide as an OH precursor) in the absence of NO_x is the most distinct from all other spectra, with dramatically different peak height ratios (m/z 43 is the most intense signal) and more high molecular weight fragments than the other systems. The ozone spectrum shows characteristics of both the high and low NO_x spectra including a relatively large, yet not dominant, m/z 43 peak.

The spectra from different oxidation systems show that in addition to affecting how much nitrate salt is formed, oxidant (OH, O_3) and NO_x levels also affect the chemical composition of the oxidized aerosol. At the same time, the similarities between the spectra from high NO_x photooxidation systems with and without H_2O_2 indicate that similar species condense independent of the OH source. All of the amines studied formed aerosol with similar spectra during photooxidation whether or not hydrogen peroxide was used as an OH precursor.

5.13 Effective density shifts

During the photooxidations of TEA and TMA the effective density of the aerosol continually increased as non-salt organic mass condensed. Figure 1 shows the increase observed during the photooxidation of TEA. The effective density of the aerosol formed during ozonolysis was higher than that of the salt for both TEA and TMA. Additionally, TEA formed aerosol with a higher effective density than TEAN when photooxidized in the absence of NO_x . The increases in effective densities observed in particles with a higher fraction of non-salt mass indicates that either: (1) the non-salt aerosol is more dense; or (2) the salt aerosol is either non-spherical or has void volumes, and the condensation of organic aerosol onto the salt alters these physical characteristics. In either case, it is evident that the physical morphology of the particles depends on the ratio of non-salt to salt mass.

6 Implications

Amines can undergo similar acid-base reactions as ammonia to form atmospheric nitrate and sulfate salts when in the presence of HNO_3 or H_2SO_4 . Whether amines, in fact, will form such aminium salts depends not only on the concentration of the amine and the acid, but also on the concentration of ammonia which competes for acidic molecules. Thermodynamic calculations using entropies estimated from quantum mechanics and molecular dynamics indicate that diethylammonium nitrate will be able to form when ammonia mixing ratios are greater than those of diethylamine. Triethylamine was shown experimentally to have a dissociation equilibrium constant similar to that of ammonia. Ethylammonium nitrate and trimethylammonium nitrate are predicted to be unable to form unless their mixing ratios are near to or greater than that of ammonia. We note that thermodynamic parameters for the aminium salts have large uncertainties that preclude us from making conclusions regarding the formation, in the presence of ammonia, of the other aminium salts studied.

Gas-phase amines are subject to atmospheric oxidation by the OH radical and ozone, leading to secondary organic aerosol formation. If nitric or sulfuric acid is present during the oxidation, aminium salts of the parent amine can form simultaneously with the SOA resulting from oxidation. The products of amine oxidation can also be basic and form additional aminium salts. Aminium salts will most often form in source-rich areas. As the parent amine is reacted away or as the air mass undergoes dilution, aminium salts can be expected to repartition back to the gas phase. SOA resulting from amine oxidation appears to be more stable in the particle phase than the aminium salts.

Table 4 gives the non-salt organic aerosol yields for all of the amines studied under a number of different oxidative conditions. While the yields shown are only applicable to the amine:oxidant and oxidant: NO_x ratios of the particular experiments, we can draw the general conclusion that the tertiary amines (TMA and TEA) are able to form significant yields of non-salt SOA while the primary and secondary amines studied are not. Ethanolamine showed a small growth during ozonolysis which may be an indication that adding functional groups to the amines increases their organic (non-salt) aerosol yield.

Appendix A

Thermodynamic data for amine systems

Table A1 lists available thermodynamic data for common amine systems. Multiple heats of formation values of alkylammonium nitrates are listed to highlight their uncertainty. Data on entropy and heat capacities for alkylammonium nitrates, with the exception of ammonium nitrate, do not appear to be available.

Table A1. Thermodynamic data for various amine nitrate systems. Amines and nitric acid are in the gas phase and nitrates are solid.

Substance	ΔH_f° (kJ/mol)	S° (J/mol K)	C_p (J/mol K)
ammonia	-45.90 ^d	192.77 ^e	35.65 ^d
methylamine	-23.0 ^f	243 ^g	53 ^g
dimethylamine	-18.5 ^f	273 ^g	70.8 ^g
trimethylamine	-23.7 ^f	287 ^g	91.8 ^g
ethylamine	-47.5 ^f	285 ^g	72.7 ^g
diethylamine	-72.6 ^f	352 ^g	115.7 ^g
triethylamine	-92.4 ^f	405 ^g	160.9 ^g
ethanolamine	-210.2 ^j	321 ^j	85.3 ^j
ammonium nitrate	-365.61 ^a	146.44 ^b 141.56*	140 ^c
methylammonium nitrate	-337 ^h -354.4 ^k	194.7*	
dimethylammonium nitrate	-331 ^h -350.2 ^k	229.9*	
trimethylammonium nitrate	-306 ^h -343.9 ^k	243.5*	
ethylammonium nitrate	-364 ^h -366.9 ^k	237.2*	206 ⁱ
diethylammonium nitrate	-413 ^h -418.8 ^k	299.9*	
triethylammonium nitrate	-407 ^h -447.7 ^k	350.3*	
ethanolammonium nitrate	-576 ^h -577 ^k		
nitric acid	-134.31 ^d	266.39 ^d	53.31 ^d

*values estimated from quantum mechanics/molecular dynamics

^aCox et al. (1979), ^bEichenauer and Liebscher (1965), ^cWagman et al. (1968), ^dChase et al. (1998), ^eHaar (1968), ^fSchmitz et al. (2001), ^gPerry et al. (1997), ^hCottrell and Gill (1951), ⁱAllen et al. (1985), ^jYaws (2003), ^kWagman et al. (1982)

One approach is to extract the entropy information from atomistic classical and quantum simulation. Lin et al. (2003) developed a 2-phase thermodynamic approach for calculating the thermodynamic properties of complex systems from single molecular dynamics simulation trajectories. In general the Fourier transform of the velocity autocorrelation function, obtained from a molecular dynamics trajectory is used to obtain the vibrational density of states, which is then used to calculate the thermodynamic properties by applying quantum statistics assuming each vibrational mode is a harmonic oscillator. This approach is quite accurate for solids, but leads to significant errors for liquids. Lin et al. (2003) extend this approach to fluids by applying the 2-phase model in which the density of states of the fluid systems are partitioned into gas and solid like components. However, for ammonium nitrates that are solids in ambient conditions, the harmonic approximation is sufficiently accurate for entropy estimation.

Of the alkylammonium nitrates, crystal structures were only found for ammonium nitrate (Herrmann et al., 1994) and methylammonium nitrate (Mylrajan et al., 1985). For the compounds with experimental crystal structures, the periodic quantum mechanical (QM) Mulliken charge distribution were determined by the SeqQuest program (Feibelman, 1987; Verdozzi et al., 2002). For the compounds lacking experimental crystal structure, the solid structures were es-

timated by modifying the methylammonium nitrate crystal. For instance, methyl groups were replaced by ethyl groups in order to create the ethylammonium nitrate crystal structure. The QM charges were obtained using Density Functional Theory (DFT), B3LYP (Becke, 1993) functions as implemented in the Jaguar program (Jaguar, 2005) using basis sets aug-cc-pvtz (Kendall et al., 1992). Solid structures were built using this method for di and trimethylammonium nitrate, mono, di and triethylammonium nitrate in CERIOUS2 (Cerius2, 1999). Molecular dynamic (MD) simulation at constant pressure, temperature and number of particles (NPT) were performed to equilibrate these solid structures. NVT simulations were then carried out for these experimental crystals or equilibrated solids for a total of 50 ps. Long-range interactions are included using the Ewald sum method and the Nose-Hoover thermostat. Using the MD trajectories, the density of states can be obtained, and the entropies can then be determined from quantum statistics (Lin et al., 2003).

The QM entropy is expected to be quite accurate for crystalline systems. Indeed, the QM entropy agrees rather well with the experimental values for ammonium nitrate (141.56 J/molK vs. 146.44 J/molK). Unfortunately, experimental entropy is available only for ammonium nitrate so further comparison cannot be done. Since crystal structure was also available for methylammonium nitrate, we expect

its QM entropy to be reasonably accurate. For other aminium nitrates, the accuracy of the calculated entropies remains undetermined although we observed a sensible correlation between the “flexibility” of the alkyl groups and the entropies.

Acknowledgements. This work was supported by the Electric Power Research Institute.

Edited by: A. Laaksonen

References

- Allan, J. D., Jimenez, J. L., Williams, P. I., Alfarra, M. R., Bower, K. N., Jayne, J. T., Coe, H., and Worsnop, D. R.: Quantitative sampling using an Aerodyne aerosol mass spectrometer: 1. Techniques of data interpretation and error analysis, *J. Geophys. Res.*, 108(D3), 4090, doi:10.1029/2002JD002358, 2003.
- Allen, M., Evans, D. F., and Lumry, R.: Thermodynamic properties of the ethylammonium nitrate + water-system – partial molar volumes, heat-capacities, and expansivities, *J. Solution. Chem.*, 14(8), 549–560, 1985.
- Angelino, S., Suess, D. T., and Prather, K. A.: Formation of aerosol particles from reactions of secondary and tertiary alkylamines: Characterization by aerosol time-of-flight mass spectrometry, *Environ. Sci. Technol.*, 35(15), 3130–3138, 2001.
- Atkinson, R., Perry, R. A., and Pitts, J. N.: Rate constants for reactions of OH radical with (CH₃)₂NH, (CH₃)₃N, and C₂H₅NH₂ over temperature range 298–426 degrees K, *J. Chem. Phys.*, 68(4), 1850–1853, 1978.
- Bahreini, R., Keywood, M. D., Ng, N. L., Varutbangkul, V., Gao, S., Flagan, R. C., Seinfeld, J. H., Worsnop, D. R., and Jimenez, J. L.: Measurements of secondary organic aerosol from oxidation of cycloalkenes, terpenes, and m-xylene using an Aerodyne aerosol mass spectrometer, *Environ. Sci. Technol.*, 39(15), 5674–5688, 2005.
- Becke, A. D.: Density-functional thermochemistry III. The role of exact exchange, *J. Chem. Phys.*, 98(7), 5648–5652, 1993.
- Beddows, D. C. S., Donovan, R. J., Harrison, R. M., Heal, M. R., Kinnorsley, R. P., King, M. D., Nicholson, D. H., and Thompson, K. C.: Correlations in the chemical composition of rural background atmospheric aerosol in the UK determined in real time using time-of-flight mass spectrometry, *J. Environ. Monit.*, 6(2), 124–133, 2004.
- Cerius2, v. 4.0, Accelrys, San Diego, CA, 1999.
- Chase, M. W.: NIST-JANAF thermochemical tables, fourth edition, *J. Phys. Chem. Ref. Data*, Monograph 9, 1343–1290, 1998.
- Cocker, D. R., Flagan, R. C., and Seinfeld, J. H.: State-of-the-art chamber facility for studying atmospheric aerosol chemistry, *Environ. Sci. Technol.*, 35(12), 2594–2601, 2001.
- Cottrell, T. L. and Gill, J. E.: The preparation and heats of combustion of some amine nitrates, *J. Chem. Soc.*, (Jul), 1798–1800, 1951.
- Cox, J. D., Harrop, D., and Head, A. J.: Standard enthalpy of formation of ammonium-nitrate and of the nitrate ion, *J. Chem. Thermodyn.*, 11(8), 811–814, 1979.
- DeCarlo, P. F., Slowik, J. G., Worsnop, D. R., Davidovits, P., and Jimenez, J. L.: Particle morphology and density characterization by combined mobility and aerodynamic diameter measurements. Part 1: Theory, *Aerosol Sci. Technol.*, 38(12), 1185–1205, 2004.
- Drewnick, F., Jayne, J. T., Canagaratna, M., Worsnop, D. R., and Demerjian, K. L.: Measurement of ambient aerosol composition during the PMTACS-NY 2001 using an aerosol mass spectrometer. Part II: Chemically speciated mass distributions, *Aerosol Sci. Technol.*, 38, 104–117, 2004a.
- Drewnick, F., Schwab, J. J., Jayne, J. T., Canagaratna, M., Worsnop, D. R., and Demerjian, K. L.: Measurement of ambient aerosol composition during the PMTACS-NY 2001 using an aerosol mass spectrometer. Part I: Mass concentrations, *Aerosol Sci. Technol.*, 38, 92–103, 2004b.
- Eichenau, W. and Liebsche, D.: Die molwärme des ammonium-nitrats zwischen 11 und 280 degrees K, *Zeitschrift für Naturforschung Part a-Astrophysik Physik und Physikalische Chemie*, A 20(1), 160, 1965.
- Feibelman, P. J.: Force and total-energy calculations for a spatially compact adsorbate on an extended, metallic crystal surface, *Phys. Rev. B*, 35(6), 2626–2646, 1987.
- Finlayson-Pitts, B. J. and Pitts, J. N. J.: *Atmospheric chemistry: Fundamentals and experimental techniques*, Wiley, New York, 1986.
- Haar, L.: Thermodynamic properties of ammonia as an ideal gas, *J. Res. Nbs. A. Phys. Ch.*, A 72(2), 207, 1968.
- Hamoir, J., Nemmar, A., Halloy, D., Wirth, D., Vincke, G., Vanderplassen, A., Nemery, B., and Gustin, P.: Effect of polystyrene particles on lung microvascular permeability in isolated perfused rabbit lungs: Role of size and surface properties, *Toxicol. Appl. Pharmacol.*, 190(3), 278–285, 2003.
- Herrmann, M., Engel, W., Schneider, J., and Goebel, H.: Rietveld refinement of the phase of NH₄NO₃ measured in-situ under different diffraction geometries, *Materials Science Forum*, 166, 489–494, 1994.
- Huffman, J. A., Jayne, J. T., Drewnick, F., Aiken, A. C., Onasch, T., Worsnop, D. R., and Jimenez, J. L.: Design, modeling, optimization, and experimental tests of a particle beam width probe for the Aerodyne aerosol mass spectrometer, *Aerosol Sci. Technol.*, 39(12), 1143–1163, 2005.
- Jaguar, v. 6.5, Schrodinger, LLC, New York, NY, 2005.
- Jayne, J. T., Leard, D. C., Zhang, X. F., Davidovits, P., Smith, K. A., Kolb, C. E., and Worsnop, D. R.: Development of an aerosol mass spectrometer for size and composition analysis of submicron particles, *Aerosol Sci. Technol.*, 33(1–2), 49–70, 2000.
- Kendall, R. A., Dunning Jr., T. H., and Harrison, R. J.: Electron affinities of the first-row atom revisited. Systematic basis sets and wave functions, *J. Chem. Phys.*, 96(9), 6796–6806, 1992.
- Keywood, M. D., Varutbangkul, V., Bahreini, R., Flagan, R. C., and Seinfeld, J. H.: Secondary organic aerosol formation from the ozonolysis of cycloalkenes and related compounds, *Environ. Sci. Technol.*, 38(15), 4157–4164, 2004.
- Kroll, J. H., Ng, N. L., Murphy, S. M., Flagan, R. C., and Seinfeld, J. H.: Secondary organic aerosol formation from isoprene photooxidation, *Environ. Sci. Technol.*, 40(6), 1869–1877, 2006.
- Lin, S.-T., Blanco, M., and Goddard III, W. A.: The two-phase model for calculating thermodynamic properties of liquids from molecular dynamics: Validation for the phase diagram of Lennard-Jones fluids, *J. Chem. Phys.*, 119(22), 11 792–11 805, 2003.
- Mace, K. A., Artaxo, P., and Duce, R. A.: Water-soluble organic nitrogen in Amazon basin aerosols during the dry (biomass burning) and wet seasons, *J. Geophys. Res.*, 108(D16), 4512,

- doi:10.1029/2003JD003557, 2003.
- Makela, J. M., Yli-Koivisto, S., Hiltunen, V., Seidl, W., Swietlicki, E., Teinila, K., Sillanpaa, M., Koponen, I. K., Paatero, J., Rosman, K., and Hameri, K.: Chemical composition of aerosol during particle formation events in boreal forest, *Tellus B*, 53(4), 380–393, 2001.
- McGregor, K. G. and Anastasio, C.: Chemistry of fog waters in California's central valley: 2. Photochemical transformations of amino acids and alkyl amines, *Atmos. Environ.*, 35(6), 1091–1104, 2001.
- Mozurkewich, M.: The dissociation-constant of ammonium-nitrate and its dependence on temperature, relative-humidity and particle-size, *Atmos. Environ. A-Gen.*, 27(2), 261–270, 1993.
- Murphy, D. M. and Thomson, D. S.: Chemical composition of single aerosol particles at Idaho hill: Positive ion measurements, *J. Geophys. Res.*, 102(D5), 6341–6352, 1997.
- Mylrajan, M., Srinivasan, T. K. K., and Sreenivasamurthy, G.: Crystal structure of monomethylammonium nitrate, *J. Cryst. Spectrosc.*, 15(5), 493–500, 1985.
- Neff, J. C., Holland, E. A., Dentener, F. J., McDowell, W. H., and Russell, K. M.: The origin, composition and rates of organic nitrogen deposition: A missing piece of the nitrogen cycle?, *Bio-geochemistry*, 57(1), 99–136, 2002.
- Nemmar, A., Hoylaerts, M. F., Hoet, P. H. M., Dinsdale, D., Smith, T., Xu, H. Y., Vermeylen, J., Nemery, B., and Nemery, B.: Ultra-fine particles affect experimental thrombosis in an in vivo hamster model, *Am. J. Resp. Crit. Care.*, 166(7), 998–1004, 2002.
- Ngwabie, N. M. and Hintz, T.: Mxing ratio measurements and flux estimates of volatile organic compounds (voc) from a cowshed with conventional manure treatment indicate significant emissions to the atmosphere, *Geograph. Res. Abstr.*, 7(01175), 2005.
- Perry, R. H., Green, D. W., and Maloney, J. O.: Perry's chemical engineers' handbook, McGraw-Hill, New York, 1997.
- Pitts, J. N., Grosjean, D., Vancauwenberghe, K., Schmid, J. P., and Fitz, D. R.: Photo-oxidation of aliphatic-amines under simulated atmospheric conditions – formation of nitrosamines, nitramines, amides, and photo-chemical oxidant, *Environ. Sci. Technol.*, 12(8), 946–953, 1978.
- Rabaud, N. E., Ebeler, S. E., Ashbaugh, L. L., and Flocchini, R. G.: Characterization and quantification of odorous and non-odorous volatile organic compounds near a commercial dairy in California, *Atmos. Environ.*, 37(7), 933–940, 2003.
- Schade, G. W. and Crutzen, P. J.: Emission of aliphatic-amines from animal husbandry and their reactions – potential source of N₂O and HCN, *J. Atmos. Chem.*, 22(3), 319–346, 1995.
- Schmitz, L. R., Chen, K. H., Labanowski, J., and Allinger, N. L.: Heats of formation of organic molecules calculated by density functional theory. III - amines, *J. Phys. Org. Chem.*, 14(2), 90–96, 2001.
- Seinfeld, J. H. and Pankow, J. F.: Organic atmospheric particulate material, *Annu. Rev. Phys. Chem.*, 54, 121–140, 2003.
- Simoneit, B. R. T., Rushdi, A. I., Bin Abas, M. R., and Didyk, B. M.: Alkyl amides and nitriles as novel tracers for biomass burning, *Environ. Sci. Technol.*, 37(1), 16–21, 2003.
- Sorooshian, A., Brechtel, F. J., Ma, Y. L., Weber, R. J., Corless, A., Flagan, R. C., and Seinfeld, J. H.: Modeling and characterization of a particle-into-liquid sampler (pils), *Aerosol Sci. Technol.*, 40(6), 396–409, 2006.
- Stein, S. E.: Mass spectra by NIST mass spec data center, NIST chemistry webbook, NIST standard reference database number 69, Eds. Linstrom PJ, Mallard WG, National Institute of Standards and Technology, Gaithersburg MD, (<http://webbook.nist.gov>), 2005.
- Stelson, A. W. and Seinfeld, J. H.: Relative-humidity and temperature-dependence of the ammonium-nitrate dissociation-constant, *Atmos. Environ.*, 16(5), 983–992, 1982.
- Surratt, J. D., Murphy, S. M., Kroll, J. H., Ng, N. L., Hildebrandt, L., Sorooshian, A., Szmigielski, R., Vermeylen, R., Maenhaut, W., Claeys, M., Flagan, R. C., and Seinfeld, J. H.: Chemical composition of secondary organic aerosol formed from the photooxidation of isoprene, *J. Phys. Chem. A*, 110(31), 9665–9690, 2006.
- Tan, P. V., Evans, G. J., Tsai, J., Owega, S., Fila, M. S., and Malpica, O.: On-line analysis of urban particulate matter focusing on elevated wintertime aerosol concentrations, *Environ. Sci. Technol.*, 36(16), 3512–3518, 2002.
- Tuazon, E. C., Atkinson, R., Aschmann, S. M., and Arey, J.: Kinetics and products of the gas-phase reactions of O₃ with amines and related-compounds, *Res. Chem. Intermed.*, 20(3–5), 303–320, 1994.
- Verdozzi, C., Schultz, P. A., Wu, R., Edwards, A. H., and Kiousis, N.: Layer intermixing during metal/metal oxide adsorption: Ti/sapphire(0001), *Phys. Rev. B*, 66, 125408, 2002.
- Wagman, D. D., Evans, W. H., Parker, V. B., Halow, I., Bailey, S. M., and Schumm, R. H.: Selected values of chemical thermodynamic properties; tables for the first thirty-four elements in the standard order of arrangement, NBS Technical Note, 270(3), 1968.
- Wagman, D. D., Evans, W. H., Parker, V. B., Schumm, R. H., Halow, I., Bailey, S. M., Churney, K. L., and Nuttall, R. L.: The nbs tables of chemical thermodynamic properties – selected values for inorganic and C-1 and C-2 organic-substances in si units, *J. Phys. Chem. Ref. Data*, 11(2), 91–110, 1982.
- Weber, R. J., Orsini, D., Daun, Y., Lee, Y. N., Klotz, P. J., and Brechtel, F.: A particle-into-liquid collector for rapid measurement of aerosol bulk chemical composition, *Aerosol Sci. Technol.*, 35(3), 718–727, 2001.
- Yaws, C. L.: Yaws' handbook of thermodynamic and physical properties of chemical compounds, Knovel, 2003.
- Zhang, Q. and Anastasio, C.: Free and combined amino compounds in atmospheric fine particles (pm_{2.5}) and fog waters from northern California, *Atmos. Environ.*, 37(16), 2247–2258, 2003.

Appendix H

Hygroscopicity of Secondary Organic Aerosols Formed by Oxidation of Cycloalkenes, Monoterpenes, Sesquiterpenes, and Related Compounds*

* This chapter is reproduced by permission from “Hygroscopicity of Secondary Organic Aerosols Formed by Oxidation of Cycloalkenes, Monoterpenes, Sesquiterpenes, and Related Compounds” by V. Varutbangkul, F. J. Brechtel, R. Bahreini, N. L. Ng, M. D. Keywood, J. H. Kroll, R. C. Flagan, J. H. Seinfeld, A. Lee, A. H. Goldstein, *Atmospheric Chemistry and Physics*, 6, 2367-2388, 2006. © 2006 Author(s). This work is licensed under a Creative Commons License.

Hygroscopicity of secondary organic aerosols formed by oxidation of cycloalkenes, monoterpenes, sesquiterpenes, and related compounds

V. Varutbangkul¹, F. J. Brechtel^{2,3}, R. Bahreini^{3,4}, N. L. Ng¹, M. D. Keywood^{3,5}, J. H. Kroll³, R. C. Flagan^{1,3}, J. H. Seinfeld^{1,3}, A. Lee⁶, and A. H. Goldstein⁶

¹Department of Chemical Engineering, California Institute of Technology, Pasadena, CA, USA

²Brechtel Manufacturing Inc., Hayward, CA, USA

³Department of Environmental Science and Engineering, California Institute of Technology, Pasadena, CA, USA

⁴National Oceanic and Atmospheric Administration (NOAA), Boulder, CO, USA

⁵Commonwealth Scientific and Industrial Research Organisation, Melbourne, Australia

⁶Department of Environmental Science, Policy and Management, University of California, Berkeley, CA, USA

Received: 14 December 2005 – Published in Atmos. Chem. Phys. Discuss.: 9 February 2006

Revised: 21 April 2006 – Accepted: 5 May 2006 – Published: 29 June 2006

Abstract. A series of experiments has been conducted in the Caltech indoor smog chamber facility to investigate the water uptake properties of aerosol formed by oxidation of various organic precursors. Secondary organic aerosol (SOA) from simple and substituted cycloalkenes (C₅–C₈) is produced in dark ozonolysis experiments in a dry chamber (*RH*~5%). Biogenic SOA from monoterpenes, sesquiterpenes, and oxygenated terpenes is formed by photooxidation in a humid chamber (~50% *RH*). Using the hygroscopicity tandem differential mobility analyzer (HTDMA), we measure the diameter-based hygroscopic growth factor (*GF*) of the SOA as a function of time and relative humidity. All SOA studied is found to be slightly hygroscopic, with smaller water uptake than that of typical inorganic aerosol substances. The aerosol water uptake increases with time early in the experiments for the cycloalkene SOA, but decreases with time for the sesquiterpene SOA. This behavior could indicate competing effects between the formation of more highly oxidized polar compounds (more hygroscopic), and formation of longer-chained oligomers (less hygroscopic). All SOA also exhibit a smooth water uptake with *RH* with no deliquescence or efflorescence. The water uptake curves are found to be fitted well with an empirical three-parameter functional form. The measured pure organic *GF* values at 85% *RH* are between 1.09–1.16 for SOA from ozonolysis of cycloalkenes, 1.01–1.04 for sesquiterpene photooxidation SOA, and 1.06–1.10 for the monoterpene and oxygenated terpene SOA. The *GF* of pure SOA (*GF*_{org}) in experiments in which inorganic seed aerosol is used is determined by assuming volume-weighted water uptake (Zdanovskii-Stokes-Robinson or “ZSR” approach) and using the size-resolved

organic mass fraction measured by the Aerodyne Aerosol Mass Spectrometer. Knowing the water content associated with the inorganic fraction yields *GF*_{org} values. However, for each precursor, the *GF*_{org} values computed from different HTDMA-classified diameters agree with each other to varying degrees. Comparing growth factors from different precursors, we find that *GF*_{org} is inversely proportional to the precursor molecular weight and SOA yield, which is likely a result of the fact that higher-molecular weight precursors tend to produce larger and less hygroscopic oxidation products.

1 Introduction

The ability of atmospheric aerosol to absorb water is a property with far-reaching implications. Water uptake affects the particle size and phase and therefore influences many physicochemical characteristics of the aerosol, including respiratory tract deposition (Finlay et al., 1997; Broday and Georgopoulos, 2001; Chan et al., 2002), optical properties (Heintzenberg et al., 2001), atmospheric lifetime, and chemical reactivity, especially with respect to heterogeneous chemistry. In addition, the hygroscopic behavior of a particle also determines its ability to serve as a cloud condensation nucleus (CCN). Changes in aerosol water uptake behavior can therefore lead to changes in both direct and indirect radiative forcing of climate (IPCC, 2001).

The hygroscopicity of a particle depends on its chemical composition. While the water uptake properties of atmospherically relevant inorganic salts as a function of relative humidity are generally well-known (Tang, 1976; Tang and Munkelwitz, 1994; Weis and Ewing, 1999), the effects of

Correspondence to: J. H. Seinfeld
 (seinfeld@caltech.edu)

organics on the overall hygroscopic properties are not yet fully understood. Organic compounds are ubiquitous in the atmospheric aerosol. The presence of organic compounds can alter the hygroscopic behavior of inorganic aerosol, sometimes in unanticipated ways (Saxena et al., 1995; Hansson et al., 1998; Li et al., 1998; Ansari and Pandis, 2000; Cruz and Pandis, 2000). A review of recent laboratory and field studies on aerosol hygroscopic properties has been compiled by Jacobson et al. (2000) and Kanakidou et al. (2005).

Secondary organic aerosol (SOA) is formed by the gas-particle partitioning of low-volatility oxidation products of gaseous organic species and can make up a significant fraction of the organic aerosol mass in urban areas (Turpin et al., 1991; Cabada et al., 2002, 2004; Lim and Turpin, 2002). Biogenic terpenes have been identified as precursors of SOA, predominantly in rural or forested areas (Kavouras et al., 1999a, b; Yu et al., 1999; Janson et al., 2001; Pio et al., 2001; Sellegri et al., 2005). As with organic aerosols generally, knowledge of water uptake properties of the SOA is imperative for understanding aerosol evolution and its effect on the regional visibility, cloud formation, and climate.

To date, there have been few laboratory studies on the hygroscopicity of SOA. Those that exist are based on a limited number of hydrocarbon precursors, and some provide data on growth factors (*GF*, defined as the ratio between wet and dry particle diameters) only at a single *RH*. A summary of these studies, as well as two dealing with SOA cloud condensation nuclei (CCN) properties, which are related to hygroscopicity in the sub-saturated regime as measured by the HTDMA, are listed in Table 1. Virkkula et al. (1999) measured hygroscopic growth factors of about 1.1 at ~85% *RH* for nucleated SOA from ozonolysis of α -pinene, β -pinene, and limonene. In experiments with seed aerosol, they found that *GF* was inversely proportional to the organic volume fraction and not the organic layer thickness, indicating that water uptake could be represented by additive uptake of the inorganic and organic fractions. Kleindienst et al. (1999) irradiated toluene, *p*-xylene, and 1,3,5-trimethylbenzene in the presence of NO_x and $(\text{NH}_4)_2\text{SO}_4$ seed, collected the particles onto a Teflon filter, and measured the mass changes due to liquid water content of the deposited particles with varying *RH*. They observed water uptake that was slightly less than that of pure $(\text{NH}_4)_2\text{SO}_4$ but with the same deliquescence point as $(\text{NH}_4)_2\text{SO}_4$. In a subsequent work, simulated automobile exhaust was similarly photooxidized to nucleate fine particles for analogous bulk liquid water content analysis (Kleindienst et al., 2002). The total amount of organic mass deposited on the filter was not reported; hence the volumetric growth factor could not be inferred, but the general shape of the water uptake curve was similar to those of many pure organic compounds, in that no deliquescence behavior was detected.

Cocker et al. (2001a) found that SOA formed by ozonolysis of α -pinene reduces the *GF* of the $(\text{NH}_4)_2\text{SO}_4$ seed. In subsequent work, *GF* of pure nucleated SOA

from photooxidation of *m*-xylene, photooxidation of 1,3,5-trimethylbenzene, and ozonolysis of α -pinene was observed to increase with time in the first seven hours of oxidation (Cocker et al., 2001c). Saathoff et al. (2003) performed α -pinene ozonolysis experiments with and without seed (diesel soot, "Palas" soot, and $(\text{NH}_4)_2\text{SO}_4$) and also found that the aerosol *GF* increased with time before leveling off in all cases. The final growth factors for 200-nm particles were 1.106 at 85% *RH* for the nucleated SOA, ~1.55 at 90.3% *RH* for the SOA deposited on $(\text{NH}_4)_2\text{SO}_4$ seed, 1.08 at 90% *RH* for SOA on diesel soot seeds (although significant nucleation occurred in both of the previous seeded cases, so the growth factors measured may not be representative due to the difference in condensational dynamics induced by presence of freshly formed particles), and ~0.95 at 90.1% *RH* for SOA on "Palas" soot seed. In both experiments involving soot, the condensed organics increased the particle size after humidification compared to an otherwise collapsing soot seed, which is caused by structural rearrangement and compaction of the fractal agglomerates. No deliquescence or efflorescence behavior was observed during *RH* variation for the nucleated aerosol, but SOA on $(\text{NH}_4)_2\text{SO}_4$ deliquesced at 80% *RH*, similar to pure seed. Baltensperger et al. (2005) reported that the water uptake of nucleated SOA from photooxidation of 1,3,5-trimethylbenzene and α -pinene also increased with time but eventually leveled off. The SOA was found to have a smooth water uptake curve with no deliquescence behavior.

Related to the SOA uptake of water in the sub-saturated regime is the ability for the SOA to act as CCN. VanReken et al. (2005) measured the CCN activation at four supersaturations of SOA formed from ozonolysis of four monoterpenes and a terpenoid alcohol. They found that α -pinene SOA is the least CCN active, and limonene SOA is the most CCN active (across all four supersaturations studied), and that each type of SOA becomes less CCN active with time. Huff Hartz et al. (2005) generated SOA by ozonolysis of four monoterpenes and three sesquiterpenes and found that the monoterpene SOA activates like highly water-soluble organics, while sesquiterpene SOA is less CCN active.

To summarize, these laboratory studies indicate that SOA is slightly hygroscopic; with the exception of the recent work by Baltensperger et al. (2005) and a single α -pinene ozonolysis experiment by Saathoff et al. (2003), the quantitative change in SOA water uptake with *RH* has in general not been measured fully. SOA coatings on inorganic aerosol are found to allow water uptake at lower *RH*s than the pure inorganic portion alone, which suggests that SOA can play an important role in extending the range of *RH*s over which particle-bound water influences aerosol properties, such as density, light scattering, or refractive index. In fact, field measurements have shown that there is a substantial decrease in the *RH* dependence of light scattering with increasing organic mass fraction (Quinn et al., 2005).

The range of growth factors measured in the previous works is typically consistent with those of the "less

Table 1. Previous studies involving hygroscopicity or CCN activity of secondary organic aerosols.

Work	Precursor	Oxidant, etc.	Seed	Technique	Summary of Results
Virkkula et al. (1999)	α -pinene, β -pinene, limonene	O ₃	(NH ₄) ₂ SO ₄ & nucleation	TDMA	Nucleated SOA GF = 1.10 at ~85% RH. For seed experiments, GF was inversely proportional to organic volume fraction, not organic layer thickness. Organic & inorganic took up water independently.
Kleindienst et al. (1999)	toluene, p-xylene, 1,3,5-TMB	NO _x + OH + hv	(NH ₄) ₂ SO ₄	LWC analyzer on bulk filter	Water uptake at 5-95% slightly lower than pure (NH ₄) ₂ SO ₄ ; no significant contributions from organics. DRH same as (NH ₄) ₂ SO ₄ . Total organic mass deposited on filter not reported.
Cocker et al. (2001a)	α -pinene	O ₃	(NH ₄) ₂ SO ₄ & nucleation	TDMA	(NH ₄) ₂ SO ₄ particle GF is reduced by organics; GF decreases with increasing organic fraction
Cocker et al. (2001c)	m-xylene, 1,3,5-TMB	NO _x + OH + hv	nucleation	TDMA	GF of SOA increased with time in the first 7 hours of oxidation and leveled off after.
Kleindienst et al. (2002)	simulated automobile exhaust	NO _x + OH + hv	nucleation	LWC analyzer on bulk filter	Smooth water uptake, no deliquescence. Total amount of organic mass deposited on the filter not reported. (Not quantitative)
Saathoff et al. (2003)	α -pinene	O ₃	nucleation, (NH ₄) ₂ SO ₄ , diesel soot, "Palas" soot,	TDMA	GF increased with time for the first 2 hours before leveling off. At 200 nm, GF = 1.106 at 85% RH for nucleated SOA, ~1.55 for SOA with (NH ₄) ₂ SO ₄ seed, 1.08 for SOA with Diesel soot seed, and ~0.95 for SOA on "Palas" soot seed (last three at 90% RH). No deliquescence for nucleated aerosol. SOA on (NH ₄) ₂ SO ₄ deliquesced at 80% RH.
Baltensperger et al. (2005)	1,3,5-TMB	NO _x + OH + hv	nucleation	TDMA	GF increased with time but leveled off after 7 hr. Smooth water uptake curve.
VanReken et al. (2005)	α -pinene, β -pinene, Δ^3 -carene, limonene, terpinene-4-ol	O ₃	nucleation	CCN counter	α -pinene SOA is least CCN active, and limonene SOA is most active (across four supersaturations studied). SOA becomes less CCN-active with time.
Huff Hartz et al. (2005)	α -pinene, β -pinene, Δ^3 -carene, limonene, β -caryophyllene, α -humulene, α -cedrene	O ₃	Nucleation & "self-seeding"	CCN counter	Monoterpene SOA is CCN active and activates like highly water-soluble organics (cut D _p ~48 nm at S = 1%). Sesquiterpene SOA is less active (~120 nm at S = 1%).

hygroscopic" mode found in ambient measurements, in which the observed water uptake and the relative number concentrations of particles in the "more" and "less" hygroscopic modes were found to depend on the time of day and type of air mass (Svenningsson et al., 1992; Covert and Heintzenberg, 1993; Zhang et al., 1993; Swietlicki et al., 1999; Cocker et al., 2001d; Busch et al., 2002; Massling et al., 2003; Ferron et al., 2005). This suggests that the ob-

served low-hygroscopicity fraction in ambient aerosol can be attributed to the presence of secondary organic species, in addition to other types of organics or primary soot, which may also be a significant contributor in urban areas. Changes in traffic patterns, such as rush hour traffic, and the distribution and strength of other aerosol precursors, such as terpene-emitting plants, relative to diurnal transport patterns can result in secondary organic aerosol (SOA) contributing

to ambient aerosol mass to varying degrees, which may explain the observed time dependence in growth factors and hygroscopic mode concentrations.

We report here a comprehensive study performed at the Caltech indoor chamber facility to investigate the hygroscopic behavior of SOA formed by ozonolysis of cycloalkenes and photooxidation of terpenes. Cycloalkenes are a class of compounds that can serve as a model for many atmospheric hydrocarbons with similar molecular skeletons, particularly the anthropogenic pollutants in urban and industrial areas. Terpenes are biogenic hydrocarbons that share a building block of isoprene (C_5H_8). They are emitted by conifers and broad-leaved trees, and along with isoprene, are among the most abundant reactive organic gases globally (Guenther et al., 1995; Andreae and Crutzen, 1997; Simpson et al., 1999). Terpenes have been observed to be very reactive even at ambient concentrations of oxidants (Holzinger et al., 2005) and to form aerosol with high mass yields (Griffin et al., 1999). The goal of this study is to measure the hygroscopic growth factors of the SOA formed by the oxidation of these parent species, both in pure form (nucleation experiments) and mixed organic-inorganic form (seeded experiments). The relationship between the SOA hygroscopicity and properties of the precursor is explored.

2 Experimental methods

2.1 SOA generation in the smog chamber

The specifications of the Caltech Indoor Chamber Facility have been described in detail elsewhere (Cocker et al., 2001b; Keywood et al., 2004) and so will only be briefly summarized here. The facility consists of two 28-m³ suspended flexible Teflon chambers, which are continuously flushed with clean, particle-free air for at least 36 h before an experiment. The chambers are preconditioned with the appropriate *RH*, either by passing the flushing air through a silica gel cartridge to achieve air with <10% *RH* for dry experiments, or by passing the flushing air through a sintered stainless steel bubbler placed in a bottle of Milli-Q deionized water (Millipore Corp., Billerica, Massachusetts) to obtain about 50% *RH* in humid experiments.

2.1.1 Cycloalkene ozonolysis

The experimental procedure for the cycloalkene ozonolysis experiments is described in detail in Keywood et al. (2004). To summarize, about 20 000 particles/cm³ of ammonium sulfate seed aerosol is atomized using a stainless steel constant-flow atomizer from a 0.03 M $(NH_4)_2SO_4$ solution, dried using a diffusion dryer, and introduced into a clean chamber. The initial dry seed size distribution has a mode diameter of approximately 70–80 nm and geometric standard deviation (σ_g) of ~ 1.75 . Approximately 200 ppb of the cycloalkene parent compound of interest is then volatilized in a glass bulb

and injected in a stream of air along with cyclohexane, which serves as a hydroxyl radical scavenger. The amount of cyclohexane injected is such that the reaction rate of OH radicals with cyclohexane is 100 times faster than that with the cycloalkene being studied. When both concentrations have reached steady state, 400–600 ppb of ozone are injected using a UV lamp ozone generator (EnMet Corp, Michigan) to start the oxidation reaction in an excess-ozone regime. The experiments are performed in the dark at <10% *RH* and $20 \pm 1^\circ C$. For nucleation experiments, no seed aerosol is used, and pure organic particles are formed when oxidation products nucleate.

Four simple and five substituted cycloalkenes are studied in this work: cyclopentene, cyclohexene, cycloheptene, cyclooctene, 1-methyl cyclopentene, 1-methyl cyclohexene, 1-methyl cycloheptene, 3-methyl cyclohexene, and methylene cyclohexane. The molecular structures and relevant properties of these compounds as well as the terpene precursors (see below) are shown in Table 2.

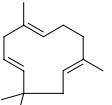
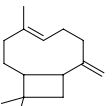
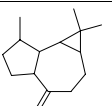
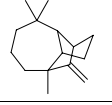
Hypothetically, the reaction mechanism of the cycloalkene ozonolysis could be dependent on humidity. For example, higher *RH* could increase the reaction rate of stabilized Criegee intermediates with water molecules, potentially changing the distribution of semivolatile species. However, it has been suggested that the effect of water on the stabilized Criegee intermediate of smaller cycloalkenes (carbon number of 8 or less) would be minor, since the dominant reaction pathway is through that of the excited Criegee intermediate that readily break down into other products (Chuong et al., 2004). In the end, it is unlikely that such minor effects on chemical composition would be captured by the hygroscopicity measurement. Because of this and the fact that the cycloalkene family was meant to be a set of “model compounds” rather than representative of atmospherically relevant species like the biogenics, the dry condition was deemed sufficient for the hygroscopicity and yield measurements.

2.1.2 Terpene photooxidation

Photooxidation experiments of eight monoterpenes, four sesquiterpenes, and three oxygenated terpenes are performed individually in a humid chamber (*RH* $\sim 50\%$). Deliquesced $(NH_4)_2SO_4$ seed is generated by atomization as above but without the diffusion dryer, resulting in an initial size distribution in the chamber with a mode diameter of approximately 80–100 nm and geometric standard deviation of ~ 1.80 . $(NH_4)_2SO_4$ seed is used for experiments with monoterpenes and oxygenated terpenes, which include α -pinene, β -pinene, Δ^3 -carene, limonene, α -terpinene, γ -terpinene, terpinolene, myrcene, methyl chavicol, verbenone, and linalool. The initial concentrations of these compounds are approximately 120 ppb.

Because the higher-molecular-weight sesquiterpenes react extremely quickly with the OH radical to form low-volatility condensable products that readily form fresh particles even

Table 2. Hydrocarbon precursors studied.

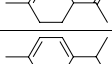
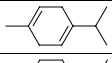
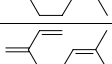
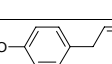
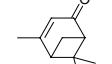
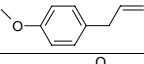
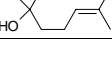
Parent Hydrocarbon	Molecular structure	Molecular formula	Molecular Weight (g/mol)	Reported Purity	Supplier
Cycloalkenes					
cyclopentene		C ₅ H ₈	68.12	96%	Aldrich
cyclohexene		C ₆ H ₁₀	82.15	≥99%	Aldrich
cycloheptene		C ₇ H ₁₂	96.17	97%	Aldrich
cyclooctene		C ₈ H ₁₄	110.20	95%	Aldrich
Substituted cycloalkenes & related compounds					
1-methyl cyclopentene		C ₆ H ₁₀	82.15	98%	Aldrich
1-methyl cyclohexene		C ₇ H ₁₂	96.17	97%	Aldrich
1-methyl cycloheptene		C ₈ H ₁₄	110.20	98%	Chemsampco
3-methyl cyclohexene		C ₇ H ₁₂	96.17	95%	TCI America
methylene cyclohexane		C ₇ H ₁₂	96.17	98%	Aldrich
Sesquiterpenes					
α-humulene		C ₁₅ H ₂₄	204.35	not reported	Sigma
β-caryophyllene		C ₁₅ H ₂₄	204.35	not reported	Aldrich
aromadendrene		C ₁₅ H ₂₄	204.35	≥ 97%	Fluka
longifolene		C ₁₅ H ₂₄	204.35	≥ 99%	Fluka

in the presence of seed, photooxidation experiments of α -humulene, β -caryophyllene, longifolene, and aromadendrene are performed without preexisting seed. In this way, a cleaner system with only pure nucleated SOA particles is achieved. An initial mixing ratio of ~ 40 ppb of these sesquiterpenes is used in each experiment.

All terpene injections are carried out with clean humid air ($RH \sim 50\%$) to prevent the particles in the chamber from efflorescing. Nitrous acid (HONO) is used as the OH radical source. HONO is prepared by drop-wise addition of 2 mL of 1% NaNO₂ into 15 mL of 10% H₂SO₄, which also produces NO_x as a byproduct. After the terpene injection, HONO is

introduced into the chamber by passing air over the mixture until the steady-state volumetric mixing ratio of NO_x is equal to that of the parent terpene. Ultraviolet lights are switched on to photolyze HONO into OH and NO, which marks the beginning of the experiment. In general, approximately 1–2°C of temperature increase is measured during the course of an experiment (due to heating from the lights). The RH never drops below 40%, the efflorescence RH of (NH₄)₂SO₄; thus, the seed aerosol always exists in the deliquesced state.

Table 2. Continued.

Parent Hydrocarbon	Molecular structure	Molecular formula	Molecular Weight (g/mol)	Reported Purity	Supplier
Monoterpenes					
α -pinene		C ₁₀ H ₁₆	136.24	≥99%	Aldrich
β -pinene		C ₁₀ H ₁₆	136.24	≥99%	Fluka
Δ^3 -carene		C ₁₀ H ₁₆	136.24	99%	Aldrich
limonene		C ₁₀ H ₁₆	136.24	97%	Aldrich
α -terpinene		C ₁₀ H ₁₆	136.24	≥97%	Fluka
γ -terpinene		C ₁₀ H ₁₆	136.24	≥ 98.5%	Fluka
terpinolene		C ₁₀ H ₁₆	136.24	≥97%	Fluka
myrcene		C ₁₀ H ₁₆	136.24	90%	Fluka
Oxygenated terpenes					
methyl chavicol (4-allylanisole)		C ₁₀ H ₁₂ O	148.20	≥ 98.5	Fluka
verbenone		C ₁₀ H ₁₄ O	150.22	99%	Fluka
linalool		C ₁₀ H ₁₈ O	154.25	97%	Fluka

2.2 Analytical instrumentation

2.2.1 Chamber instrumentation

During the experiments, the aerosol size distribution is monitored using a scanning differential mobility analyzer (DMA) (Wang and Flagan, 1990). A condensation particle counter (CPC) 3010 or 3025 (TSI Inc., St. Paul, MN) provided another independent measurement for the particle number concentration. An Aerodyne quadrupole aerosol mass spectrometer (AMS) (Jayne et al., 2000; Allan et al., 2003) is used to measure the size-resolved aerosol chemical composition for most of the experiments. Bahreini et al. (2005) reported detailed findings from the AMS from the cycloalkene experiments, including its use in the estimation of aerosol density. The sampling and analysis are carried out in a similar manner for the biogenic photooxidation experiments.

To measure the gas-phase concentrations of the precursor hydrocarbon, a Hewlett Packard 5890 series II gas chromatograph with flame ionization detector (GC-FID) is used (now Agilent Technologies Inc., Palo Alto, CA). In experiments involving terpenes, a proton transfer reaction mass spectrometer, or PTR-MS, (Ionicon Analytik, Innsbruck, Aus-

tria) (Lindinger et al., 1998) is used to monitor the evolution of gas-phase precursors. Details on the PTR-MS calibration techniques for these terpenes can be found in Lee et al. (2006). Ozone, NO, and NO₂ concentrations are measured using a Horiba APOA-360 ozone monitor and an APNA-360 NO_x monitor, respectively (Horiba Instruments Inc., Irvine, CA). The temperature and *RH* are measured using Vaisala HMP233 hygrometer probes and transmitters (Vaisala Inc., Woburn, MA). The aerosol hygroscopicity is measured using the hygroscopicity tandem differential mobility analyzer (HTDMA), which is described in more detail below.

2.2.2 Hygroscopicity Tandem differential mobility analyzer (HTDMA)

The HTDMA (Liu et al., 1978; Rader and McMurry, 1986; McMurry and Stolzenburg, 1989) is a widely-used method of measuring changes of submicron particle size with *RH*. The instrument used here is based on that described previously (Cocker et al., 2001b, d), but with improvements in the aerosol charging, *RH* measurement, CPC unit, data acquisition boards, and LabVIEW program. A schematic of the

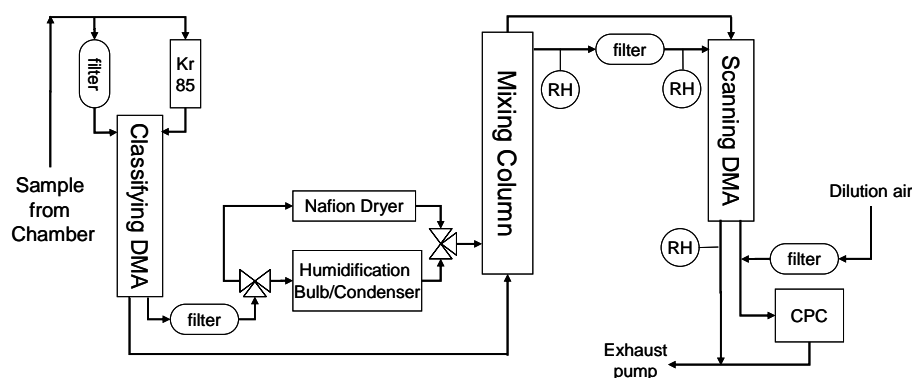


Fig. 1. Schematic of the HTDMA system used.

setup is illustrated in Fig. 1. SOA from the chamber is first passed through a TSI ^{85}Kr charger (Model 3077, TSI Inc., St. Paul, MN) to achieve equilibrium charge distribution and is then classified at constant voltage in the first cylindrical DMA (Model 3071, TSI Inc., St. Paul, MN) to a specified diameter, usually 60, 180, or 300 nm, depending on the size distribution of the aerosol in the chamber.

Changing the RH of the carrier air is achieved by passing the filtered excess flow from the classifying DMA through either a humidification or a drying system. The humidification system consists of a water saturator bath, followed by a temperature-controlled condenser. By adjusting the temperature of the ethylene glycol fluid flowing through the condenser coil from 2°C to room temperature ($\sim 20^\circ\text{C}$) using a refrigerated bath/circulator (RTE Series, Neslab Instruments Inc., Portsmouth, NH), the equilibrium RH of the carrier air can be varied roughly between 25–92%. The drying system consists of a 200-tube Nafion membrane dryer (Model PD-200T-12SS, Perma Pure LLC, Toms River, NJ), which uses a stream of dry air at 0.5 atm pressure as the purge air to carry away moisture across the membrane from the sample air. The system is able to dry humid air from the chamber down to $\sim 8\%$ RH . Both the humidification and the drying system can be completely bypassed, allowing verification of the classified aerosol size (at the chamber RH of either $< 10\%$ or $\sim 50\%$).

Monodisperse aerosol from the classifying DMA is mixed with the RH -conditioned air in an insulated, laminar flow mixing column, which has a residence time of approximately 38 s. The particles experience hygroscopic growth (or shrinkage) in this column and enter the second DMA, operating in scanning mode to measure the new aerosol size distribution. The scanning DMA sheath flow is also drawn from the humidification column; in this manner, the gaseous organic oxidation products are preserved, and re-partitioning of these species between the particle and gas phase, which may alter the aerosol water affinity and content, is reduced. Two Vaisala hygrometer probes (Models HMM211 and HMP233, Vaisala Inc., Woburn, MA) are used to measure the tempera-

ture and RH immediately before and after the scanning DMA on the sheath and excess flows. Classified particles from the scanning DMA are detected with a TSI Model 3760A CPC with dilution flow from filtered room air. Both DMAs are operated at 2.5 L/min sheath and excess flow rates and 0.25 L/min aerosol and monodisperse flow rates. The particle size classification by the DMAs has been validated by sampling polystyrene latex (PSL) spheres of known sizes (Duke Scientific Corp., Palo Alto, CA).

Inversion of the scanning DMA data (Collins et al., 2002) yields the size distribution of the grown droplets, which can then be fitted with a lognormal curve to obtain a mode diameter corresponding to the peak of the distribution. The hygroscopic growth factor (GF) at a certain RH is then defined as the ratio of the diameter of the humidified particle, $D_{p,wet}$, to that of the dry classified particle, $D_{p,dry}$:

$$GF = \frac{D_{p,wet}}{D_{p,dry}} \quad (1)$$

During the dry cycloalkene ozonolysis experiments, the mixing column RH is set at a constant elevated value between 85–90% in order to measure the change in aerosol hygroscopicity as the condensation of low-volatility organic oxidation products progresses. After the chamber aerosol has grown to a maximum volume, the RH in the HTDMA is then varied between $< 10\%$ (no humidification) and 92% in order to measure the dependence on SOA growth factor on RH . Figure 2a shows an image plot of the resulting droplet size distribution and the RH variation scheme. The thick black line marks the monodisperse particle size classified in the first DMA. The results on the growth factors will be discussed in the next section.

For terpene photooxidation experiments, which are performed in a humid chamber, the drying system is used instead to remove the water in the gas stream between the classifying and scanning DMA. After the maximum aerosol volume has been reached in the chamber, the RH is then varied in a similar manner as in the dry experiments (Fig. 2b). Note that the reported growth factors for these humid photooxidation

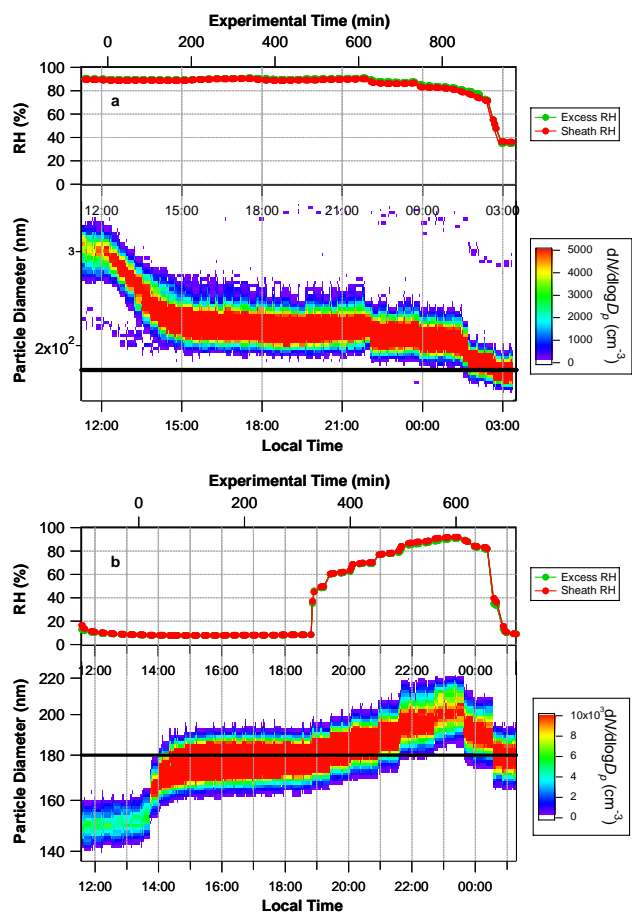


Fig. 2. Image plots of raw TDMA data and the variations in RH in a typical operating scheme for (a) cycloalkene ozonolysis experiments (dry) and (b) terpene photooxidation experiments (humid). The data shown here are from ozonolysis of 181 ppb of methylene cyclohexane in the presence of $(\text{NH}_4)_2\text{SO}_4$ seed and photooxidation of 105 ppb verbenone in the presence of $(\text{NH}_4)_2\text{SO}_4$ seed, respectively. The thick black line in each image plot denotes the classified particle size of 180 nm.

experiments are obtained by dividing the diameter of the grown droplet at a certain RH by the final dried diameter of the aerosol (rather than the diameter of the classified aerosol, which still contains some water).

The humidity probes are regularly calibrated against a set of saturated salt solutions in the range of 11%–93% RH . The HTDMA measurement is validated with ammonium sulfate, the growth factor of which as a function of RH is well-known. The HTDMA is found to be able to reproduce the hygroscopic growth curve that agrees to within 0.01 in GF compared to theoretically calculated GF of 1.484 at 80% RH (Nenes et al., 1998), equivalent to an error of about 1.5% ($n=18$). The precision of the measurement, measured from the same $(\text{NH}_4)_2\text{SO}_4$ experiment, is 1% ($n=18$). To capture the growth factors at different particle sizes, the HTDMA is set to switch between classifying 180-nm and 300-nm parti-

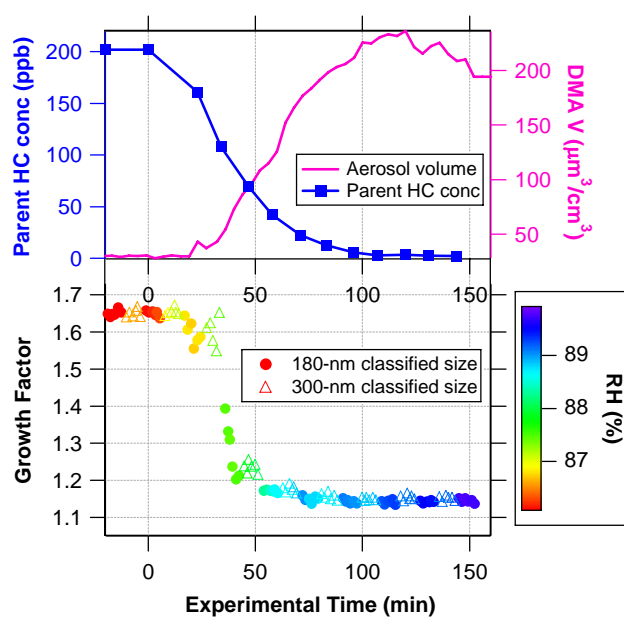


Fig. 3. Aerosol hygroscopic growth factor decreases as the precursor cycloalkene is consumed and the gas-to-particle partitioning of organic products occurs onto $(\text{NH}_4)_2\text{SO}_4$ seed. The data points shown are from a 202 ppb 1-methyl cyclohexene + ozone experiment.

cles after three complete up- and down-scan cycles at each size, with a 70-s delay between the switch and the start of scanning at the new size to prevent contamination. For nucleated SOA, 60-nm particles are selected.

3 Results and discussion

3.1 Cycloalkene ozonolysis

3.1.1 Seeded experiments: SOA formation on inorganic substrate

At the beginning of a seeded experiment, the aerosol GF at a fixed RH is equal to that of pure $(\text{NH}_4)_2\text{SO}_4$ but quickly decreases as the less-hygroscopic organic oxidation products partition into the particle phase (Fig. 3). A similar reduction in hygroscopicity of SOA containing seed aerosol has been observed in the oxidation of α -pinene, β -pinene, and limonene (Virkkula et al., 1999; Cocker et al., 2001a). In our experiments, the GF of 180-nm classified particles decreases at a faster rate than that of 300-nm particles due to preferential condensation of organic material on smaller particles.

During the period of rapid decline in particle hygroscopicity, we also observe bimodal humidified droplet spectra in the HTDMA (Fig. 4), similar to those observed for ambient aerosol (Svenningsson et al., 1992; Covert and Heintzenberg, 1993; Zhang et al., 1993; Swietlicki et al., 1999; Cocker et al., 2001d; Busch et al., 2002; Massling et al., 2003;

Ferron et al., 2005). For most parent cycloalkenes, the dominance in number concentration shifts from the more hygroscopic mode to the less hygroscopic mode, such that the less hygroscopic mode dominates the droplet distribution in the end (Fig. 4a). However, for a few parent compounds with low SOA yield, e.g. cyclopentene and 1-methyl cyclopentene (Keywood et al., 2004), the more hygroscopic mode can remain dominant even after the maximum organic volume is achieved, resulting in clear bimodal structure during the entire experiment (Fig. 4b).

The bimodal droplet distribution is most likely caused by significant differences in the organic volume fractions in the particles selected by the classifying DMA early in experiment, which could, in turn, be caused by a number of factors. First, classified particles of a certain diameter could have been formed in the chamber from an array of different seed diameters, with initially larger seeds having gained a relatively small amount of organics (becoming the more hygroscopic mode), and initially smaller seeds having gained relatively more organics (becoming the less hygroscopic mode). Such different particle growth trajectories, which also results in the narrowing aerosol size distribution as measured by the DMA, can lead to monodisperse particles having a range of organic fractions. While this phenomenon was probably occurring in the chamber to some degree, it is unlikely that a smooth range of organic fractions could give rise to a distinctly bimodal droplet distribution.

The relatively slow ozone injection, which takes up to 2.5 h to complete, can also cause the chamber to be slightly inhomogeneous, especially near the injection port where ozone is constantly introduced. Different histories of exposure to ozone and therefore to oxidation products stemming from this lack of complete mixing can also lead to different organic fractions in particles of the same size. Finally, because the DMA selects particles by their electrical mobility, larger, doubly-charged particles with the same electrical mobility as that of the expected singly-charged particles can be transmitted through the classifying DMA. Thus, the droplet distribution detected by the scanning DMA would reflect the hygroscopic growth of both the singly-charged particles of the expected size and a small fraction of multiply-charged larger particles that, as a result of the aforementioned preferential condensation of organic vapors onto smaller particles, have a lower organic fraction. Using the aerosol size distribution in the chamber and approximating the size-dependent equilibrium charge distribution according to Wiedensohler (1988), we can estimate the influence of doubly-charged 289-nm particles transmitted at the same voltage as singly-charged 180-nm particles to be about 10% of the number of singly-charged particles. While this fraction will increase as the experiment progresses due to larger number of particles at 289 nm, the relative difference between the organic fractions at 180 and 289 nm also decreases quickly with time, and the organic fractions of both sizes quickly approach unity for most compounds. Thus, the “error” in *GF* due to doubly-

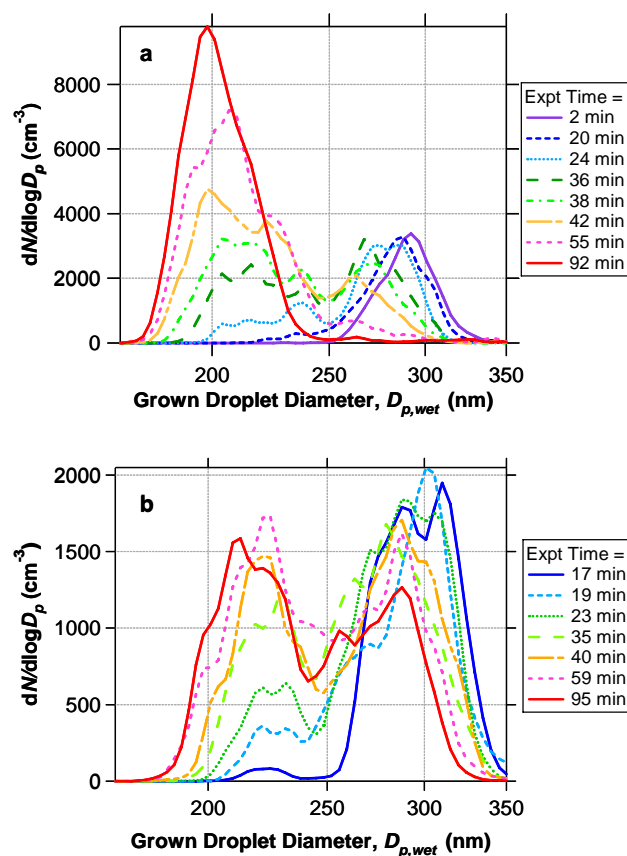


Fig. 4. Bimodal size distribution of grown droplets at classified diameter of 180 nm, observed during early times in experiments. The curve corresponding to the latest time in each case is the final shape of the droplet spectrum. **(a)** For most compounds, the bimodal shape shifts such that the less hygroscopic mode dominates the droplet spectrum at the end of the experiment. The curves shown are from ozonolysis of 202 ppb of 1-methyl cyclohexene, at an *RH* of 88%. **(b)** In experiments with low-aerosol-yield precursors, such as cyclopentene or 1-methyl cyclopentene, both modes remain comparable in size even after the organic volume has leveled off. The curves shown are from ozonolysis of 186 ppb of 1-methyl cyclopentene.

charged particles will be minimal by the time the organic volume levels off and when the *RH* ramping in the HTDMA starts.

In the seeded, humid terpene experiments (discussed in the Sect. 3.2.2 below), a bimodal distribution of the dried aerosol is not observed at early times as in the case of cycloalkene ozonolysis SOA grown droplets. This observation suggests that the inhomogeneity in the chamber due to slow ozone injection is probably the most likely cause of this phenomenon in the cycloalkene seeded experiments. Regardless of the exact cause of the bimodal structure at early times, the droplet distribution evolves to an essentially unimodal distribution by the end of most experiments. The SOA *GF* approaches an asymptote as the aerosol volume reaches the maximum,

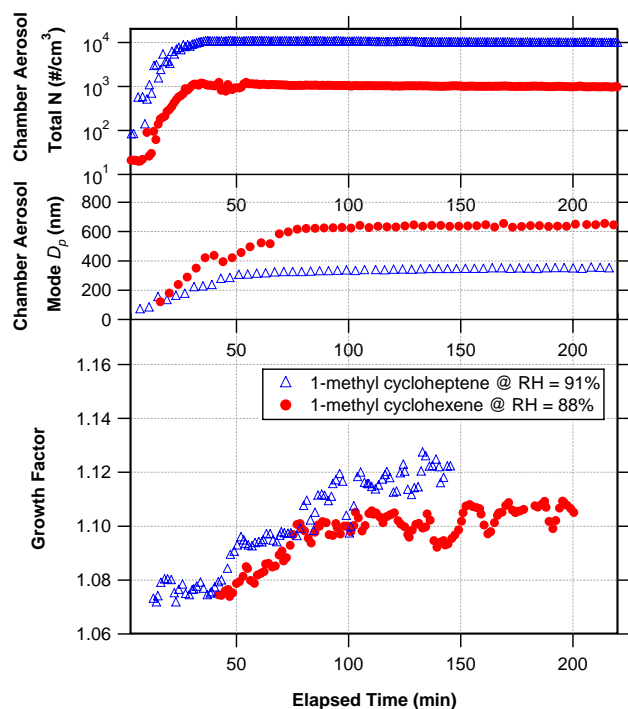


Fig. 5. Time series of the particle number concentration (as measured by CPC) and mode diameter of the chamber aerosol and the TDMA growth factor in two cycloalkene ozonolysis nucleation experiments. The growth factor of the nucleated SOA increases with time early in the experiment, consistent with further oxidation of organic products into more polar and more hydrophilic species. The *GF* data shown are from 180-nm classified diameter.

with almost no difference between the two classified sizes (Fig. 3).

3.1.2 Nucleation experiments: pure SOA

In order to measure the growth factor as a function of *RH* for pure SOA products, cycloalkene ozonolysis experiments were also performed in the absence of seed particles. By sampling nucleated SOA from these systems, we can directly obtain SOA *GF* with minimal uncertainties. The ozonolysis products of all of the cycloalkene species studied except for 1-methyl cyclopentene and methylene cyclohexane nucleate and grow large enough particles to be sampled by the HTDMA. These two excepted compounds generally form products with low molecular weights and/or high volatilities, which do not trigger formation of significant numbers of particles. The ozonolysis of methylene cyclohexane forms no particles, and that of 1-methyl cyclopentene forms less than 80 particles/cm³, which are too few to yield quantitative results in the HTDMA.

The water uptake of pure nucleated SOA formed by cycloalkene ozonolysis increases slightly with time early in experiment as shown in Fig. 5. This behavior is similar

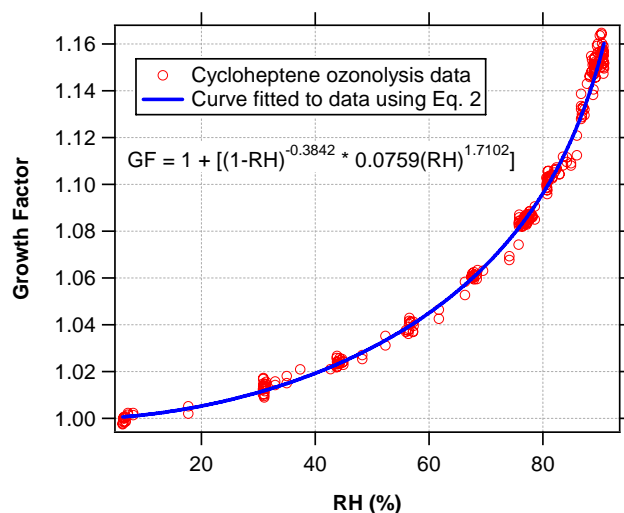


Fig. 6. Hygroscopic growth factor as a function of *RH* for nucleated SOA formed by ozonolysis of 170 ppb of cycloheptene. The growth curve is smooth, and no deliquescence or efflorescence is observed. The fitted curve is the empirical three-parameter fit of the form of Eq. (2).

to observations made in other works for α -pinene ozonolysis (Cocker et al., 2001a; Saathoff et al., 2003), and *m*-xylene, 1,3,5-trimethylbenzene, and α -pinene photooxidation (Cocker et al., 2001c; Baltensperger et al., 2005). The likely reason for this trend is the formation of more highly oxidized species in the aerosol, which tend to be more hygroscopic.

When the maximum organic aerosol volume is achieved, the *RH* in the HTDMA humidification chamber is ramped up and down to study the variation in *GF* with *RH*. All of the SOA formed in the cycloalkene ozonolysis exhibit slight hygroscopicity with no observable deliquescence behavior. Figure 6 shows an example of the hygroscopic growth curve of the nucleated SOA from cycloheptene ozonolysis. In order to fit a curve through the experimental data, we use an equation of the following empirical functional form:

$$GF = 1 + \left[\left(1 - \frac{RH}{100} \right)^{-A} \times B \left(\frac{RH}{100} \right)^C \right] \quad (2)$$

where *RH* is the relative humidity expressed between 0 and 100, and *A*, *B*, and *C* are positive empirical parameters. The first part of the product term is the functional form previously used to model the “more hygroscopic” portion of aerosol over the Northeastern Atlantic during ACE-2 (Swietlicki et al., 2000). The second part of the product term is the general power-law form commonly used to represent dicarboxylic acid hygroscopic behavior in a limited range of *RH* (Wise et al., 2003). While each of these functional forms does not satisfactorily fit our experimental data in their entire range, the product of the two proves to be quite robust in representing our data. A fit of the cycloheptene ozonolysis SOA data is

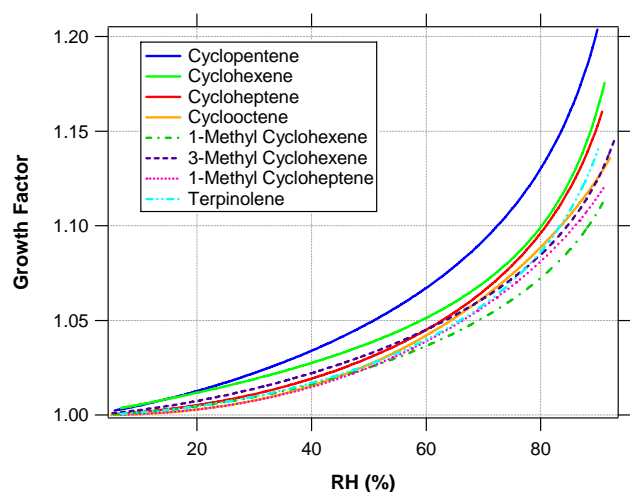


Fig. 7. Fitted curves of hygroscopic growth factors as a function of RH for nucleated SOA formed by ozonolysis of various cycloalkenes. Fitting parameters used to generate the curves are given in Table 3. In general, pure cycloalkene ozonolysis SOA is slightly hygroscopic, with GF between 1.09–1.16 at 85% RH .

also shown in Fig. 6. Table 3 shows the fit parameters of SOA hygroscopicity data obtained for all cycloalkene compounds studied. From these parameters and Eq. (2), the growth factor of each type of SOA at a given RH can be computed. These interpolated GF values at 50% and 85% RH are also shown in Table 3. In general, pure cycloalkene ozonolysis SOA is slightly hygroscopic, and the water uptake behavior varies somewhat within the family, with GF values between 1.09–1.16 at 85% RH . Figure 7 shows the fitted hygroscopic growth curve for all the nucleated cycloalkenes. Comparison of GF from different systems will be discussed in Sect. 3.4.

3.2 Terpene photooxidation

3.2.1 Sesquiterpenes – nucleated SOA

In the beginning of humid photooxidation experiments involving terpenes, the chamber aerosol is dried before entering the second DMA of the HTDMA to $\sim 8\%$. Assuming that all the SOA-bound water is removed at this low RH , and that the change in particle volume due to mixing of water and SOA products is negligible, we can calculate the percent water content (by volume), $\%WC$, of the chamber aerosol by:

$$\%WC = \left[1 - \left(\frac{D_{p,dry}}{D_{p,classified}} \right)^3 \right] * 100 \quad (3)$$

where $D_{p,dry}$ is the particle diameter measured at 8% RH , and $D_{p,classified}$ is the particle diameter selected by the first DMA. Figure 8 shows that the percent water content of the nucleated sesquiterpene SOA in the chamber decreases as a function of time early in the experiment and levels off within

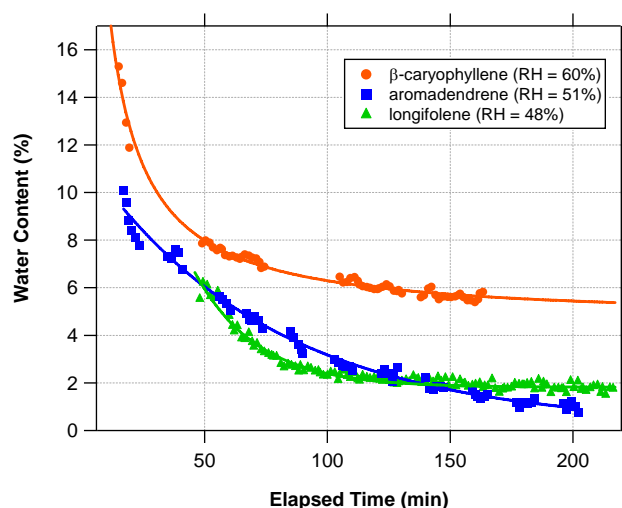


Fig. 8. The percent volumetric water content (at chamber RH) of nucleated sesquiterpene photooxidation SOA decreases with time during the experiment, suggesting that the SOA is becoming less hygroscopic. This behavior is consistent with the continued formation of less hygroscopic oligomeric species. The data shown are from 180-nm classified particles.

~ 4 h. While the increase in temperature due to the UV lights does result in a slight decrease in the chamber RH , this reduction is generally less than 4–5% and occurs in the region where water uptake is not a strong function of RH . This slight decline in chamber RH is not nearly large enough to account for the magnitude of the reduction in aerosol water content observed. Therefore, the diminishing percentage of water must mainly be a result of the decreasing hygroscopicity of the SOA itself. VanReken et al. (2005) reported a similar decrease in CCN activity of SOA formed from ozonolysis of various monoterpenes, which is indicative of decreasing hygroscopicity as well. Such behavior is consistent with gradual, but significant, oligomer formation in SOA, which has recently been observed even in the absence of highly acidic seed (Gao et al., 2004a, b; Kalberer et al., 2004). Oligomeric species formed by heterogeneous reactions between smaller oxidation products are expected to have lower hygroscopicity due to their high molecular weights and relatively low polarity.

While the decline in aerosol water content with time could intuitively be explained by the formation of particle-phase oligomers, it is the reverse of the trend we observed in the cycloalkene ozonolysis case, as well as in other studies previously mentioned, in which particle hygroscopicity is observed to increase with time. The increase in water uptake has generally been attributed to the further extent of organic oxidation, leading to more polar products in the particle phase. Thus, we postulate that the temporal variation in particle hygroscopicity is governed by the competing effects of formation of less hygroscopic oligomers and more

Table 3. Summary of nucleation experiments performed and fitting results of the final hygroscopic growth curve.

Experimental Conditions						Fitting parameters from Eq. 2			Growth factors interpolated from fit (see Fig. 16)	
Parent Hydrocarbon	ΔHC^a (ppb)	T (K)	RH (%)	Peak ΔM_o^b ($\mu\text{g}/\text{m}^3$)	SOA Yield	A	B	C	GF @ 50%	GF @ 85%
Cycloalkenes (ozonolysis in dry chamber)										
cyclopentene	192	294	6	17	0.031	0.4428	0.0841	1.2347	1.049	1.159
cyclohexene	151	293	3	60	0.116	0.5410	0.0519	0.9920	1.038	1.123
cycloheptene	170	293	6	78	0.115	0.3842	0.0759	1.7102	1.030	1.119
cyclooctene	177	293	2	160	0.197	0.1025	0.1269	2.3475	1.027	1.105
Substituted cycloalkenes & related compounds (ozonolysis in dry chamber)										
1-methyl cyclohexene	159	293	6	170	0.267	0.2817	0.0674	1.7026	1.025	1.087
3-methyl cyclohexene	178	293	6	80	0.112	0.3152	0.0703	1.4334	1.032	1.101
1-methyl cycloheptene	188	293	3	450	0.522	0.1263	0.1095	2.2474	1.025	1.097
terpinolene	200	294	2	195	0.172	0.4135	0.0646	1.6842	1.027	1.108
Sesquiterpenes (photooxidation in humid chamber)										
α -humulene	46	294	54	254	0.65	0.0000	0.0611	3.4509	1.006	1.035
β -caryophyllene	37	295	57	210	0.68	0.0000	0.0588	2.4384	1.011	1.040
aromadendrene	34	294	47	87	0.374	0.3329	0.0258	2.0226	1.008	1.035
longifolene	34	294	50	149	0.649	N/A ^c	N/A ^c	N/A ^c	1.010 ^d	1.010 ^d

a: Cycloalkene ΔHC is measured by GC-FID. Terpene ΔHC is measured by PTR-MS
b: measured by AMS in total MS mode
c: The hygroscopic growth curve could not be fitted with Eq. 1 due to irregular shape (see text for details)
d: GF interpolated from a fifth-order polynomial fit: $GF = 1.0112 - (2.17\text{e-}3*\text{RH}) + (1.40\text{e-}4*\text{RH}^2) - (3.48\text{e-}6*\text{RH}^3) + (3.63\text{e-}8*\text{RH}^4) - (1.32\text{e-}10*\text{RH}^5)$

hygroscopic polar oxidized species. It appears that in the case of SOA from photooxidized sesquiterpenes, oligomer formation dominates, either in terms of relative formation rate or the absolute amount. It is unlikely that the nature of our measurement, i.e., drying wet particles to extract hygroscopicity data rather than humidifying dry particles as is commonly done, should introduce any undue artifacts such that the temporal trend would be reversed. As discussed below, the sesquiterpene SOA growth factor is not found to be a function of particle size; thus, we can also eliminate the possibility that the decreasing water content at a certain particle size could stem from smaller particles with a vastly different organic chemical composition growing into the classified size bin.

After particle nucleation has stopped and the particle growth has reached the maximum (about 4–5 h after inception of photooxidation), the HTDMA RH is varied using both the drying and humidification systems. The growth factor, defined relative to the final dried particle diameter, is independent of the classified particle size, as shown in Fig. 9. This suggests that the aerosol chemical composition does not vary with particle size, which agrees with one's intuition

about the system. Thus, we can combine the GF results from any classified size into one single hygroscopic growth curve. Figure 10 shows the hygroscopic growth curves of the four sesquiterpenes studied. In general, sesquiterpene SOA has very low hygroscopicity, showing smooth but very small water uptake, with growth factors between 1.01–1.04 at 85% RH. The shapes of the curves for SOA from α -humulene, β -caryophyllene, and aromadendrene are similar, but that for longifolene exhibits an unexpected behavior, in which the increase in GF with RH is not monotonic. This could be indicative of the presence of void volumes in the particle, which can lead to compaction of the structure after a certain degree of water uptake. This type of behavior has been observed for nucleated particles from the photolysis of CH_2I_2 , a compound emitted by marine microalgae, in the presence of ozone (Jimenez et al., 2003). However, the degree of compaction following humidification is much higher for CH_2I_2 aerosol, which is composed of highly fractal agglomerates. For longifolene, the void volume hypothesis is also consistent with the atypical observation that the precursor concentration in the chamber continues to decrease at the end of the experiment without detectable change in aerosol volume as

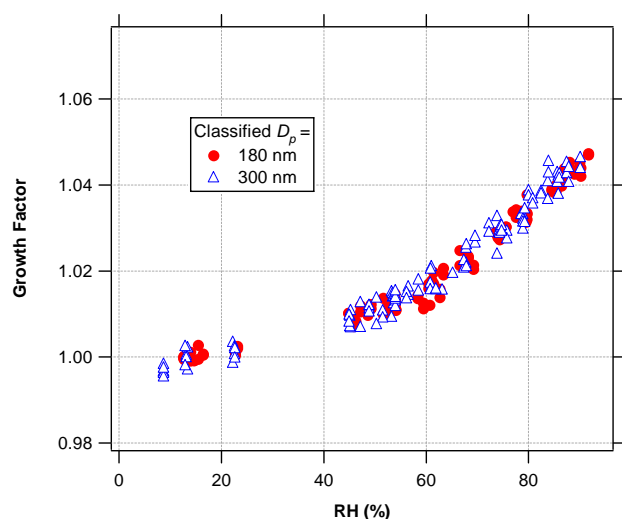


Fig. 9. Different classified diameters of pure β -caryophyllene photooxidation SOA exhibit similar hygroscopic growth factors, suggesting that the aerosol composition is independent of particle size.

measured by the DMA. If there are void volumes in a particle, additional aerosol mass can condense into those voids, resulting in denser particles with no change in apparent volume. We cannot explain, however, why only longifolene forms particles with such properties.

Fitting of the sesquiterpene hygroscopic growth curves are also performed using Eq. (2). For longifolene, a fifth-order polynomial can satisfactorily fit the experimental data. All fit parameters and interpolated GF at reference RH s are presented in Table 3.

3.2.2 Monoterpenes and oxygenated terpenes – SOA on inorganic seed

For the photooxidation of monoterpenes and oxygenated terpenes, wet $(\text{NH}_4)_2\text{SO}_4$ seed is used to provide a substrate onto which the organic oxidation products can condense. The HTDMA is still operated in the drying mode at the beginning of the experiment, allowing us to obtain the water content as in the sesquiterpene case. The percentage starts out as that of the pure $(\text{NH}_4)_2\text{SO}_4$ seed at the chamber RH and then decreases as the less-hygroscopic organics are deposited on the aerosol (Fig. 2b and Fig. 11). As mentioned earlier, a bimodal distribution of the aerosol following change in the RH is not observed at early times as in the case of cycloalkene ozonolysis SOA grown droplets.

In the terpene oxidation experiments, because the seed aerosol is deliquesced and the chamber RH does not drop below the efflorescence point of $(\text{NH}_4)_2\text{SO}_4$ of 40%, the seed should remain deliquesced throughout the experiment. Therefore, the measured growth factors in the HTDMA (down to 40% RH) include the water associated with the $(\text{NH}_4)_2\text{SO}_4$ fraction according to the “wet” or efflorescence

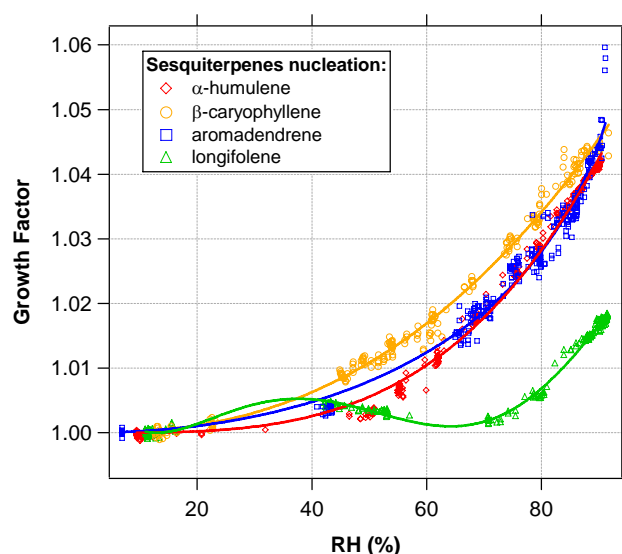


Fig. 10. Hygroscopic growth curves for nucleated SOA formed by sesquiterpene photooxidation. Sesquiterpene SOA exhibits very low hygroscopicity, showing smooth but very small water uptake, with growth factors mostly between 1.01–1.04 at 85% RH . While the shapes of the curves for SOA from α -humulene, β -caryophyllene, and aromadendrene are similar, the curve for longifolene exhibits an unexpected behavior, in which the increase in GF with RH is not monotonic. This could be indicative of the presence of void volumes in the particle, which can lead to compaction of the structure after a certain degree of water uptake.

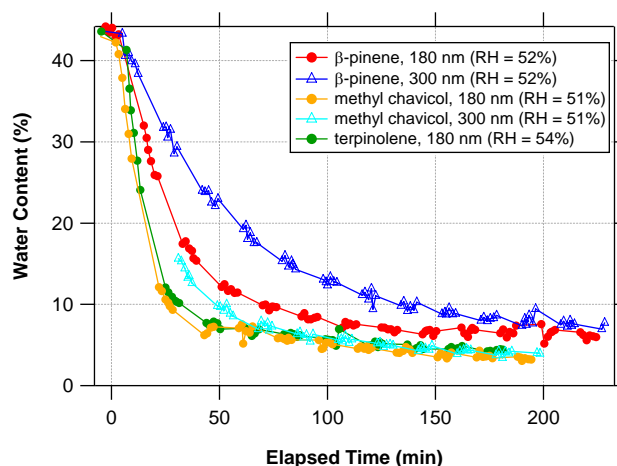


Fig. 11. The percent volumetric water content (at chamber RH) at a particular particle size of SOA formed by photooxidation of monoterpene and oxygenated terpene decreases with time early in experiment due to the deposition of less-hygroscopic organic species onto the seed. The water content levels off after a ~ 4 h as the organic deposition is completed. All SOA from monoterpene and oxygenated terpene photooxidation exhibit this behavior, although only a selected few are shown here. Line between points are for guiding the eye only.

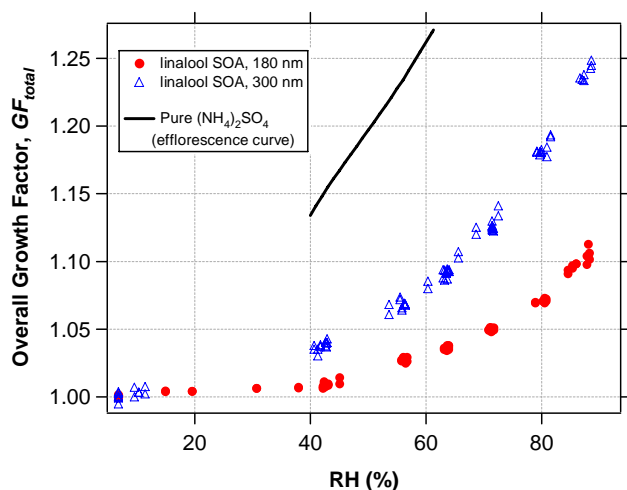


Fig. 12. Hygroscopic growth curve for linalool photooxidation SOA, measured at 180 nm and 300 nm. The differing hygroscopicity reflects the different organic fractions at each size.

branch of the hysteresis curve. As shown in Fig. 12 for linalool SOA, the variation of monoterpene and oxygenated terpene SOA growth factors with RH is also smooth. The 180-nm classified particles are less hygroscopic than the 300-nm classified particles due to the higher organic fractions in the smaller particles, but usually the difference in hygroscopicity is not as pronounced as in the illustrated case of linalool, for which the organic fractions of the 180-nm and 300-nm classified particles are more different (0.994 and 0.963, respectively, see Table 5).

Figure 13 shows the raw growth curves for the suite of monoterpene and oxygenated terpene SOA studied. Reported data are from 180-nm classified diameter, unless otherwise noted. All GF values from various terpene precursors are contained within a relatively narrow envelope between 1.06–1.10 at 85% RH . This agrees with the GF range of ~ 1.08 – 1.11 previously reported for a few biogenic SOA (Virkkula et al., 1999; Cocker et al., 2001a, c; Saathoff et al., 2003).

In order to obtain the hygroscopic growth factor of the pure SOA portion, we must remove the effect of the inorganic seed on the overall measured growth factor. This can be achieved to first order by assuming that the water uptake by the inorganic and organic fractions is independent and additive. This is also known as the volume-weighted, volume-additivity, or Zdanovskii-Stokes-Robinson (ZSR) assumption (Stokes and Robinson, 1966). The additivity of water associated with two different fractions is expressed as:

$$GF_{\text{total}}^3 = \varepsilon_{\text{org}} GF_{\text{org}}^3 + (1 - \varepsilon_{\text{org}}) GF_{\text{AS}}^3 \quad (4)$$

where ε_{org} is the organic volumetric fraction, and GF_{total} , GF_{org} , and GF_{AS} are the hygroscopic growth factors at a given RH of the entire particle (i.e. the overall growth factor),

the organic (SOA) portion, and the pure $(\text{NH}_4)_2\text{SO}_4$, respectively. We can theoretically determine GF_{AS} using the ISOR-ROPIA thermodynamic model (Nenes et al., 1998), measure GF_{total} in experiment with the HTDMA, and obtain ε_{org} with the AMS as described below. Using this information and Eq. (4), we can determine GF_{org} .

The AMS operating in time-of-flight (TOF) mode provides quantitative data on non-refractory components of aerosols as a function of size, from which we can calculate the size-dependent organic mass fraction $\varepsilon_{\text{org},m}$ as the ratio between the organic mass over the total aerosol mass:

$$\varepsilon_{\text{org},m} = \frac{M_{\text{org}} + M_{\text{NO}_3}}{M_{\text{NH}_4} + M_{\text{SO}_4} + M_{\text{org}} + M_{\text{NO}_3}} \quad (5)$$

where M_i is the absolute mass of species i measured at a given particle size. Note that we assume that nitrates measured by the AMS are fragments of organic nitrates. This assumption is supported by the observation that the nitrate signal (in total MS mode) correlates very well with the organic signal, and that both the nitrates and organics have the same mass distributions. Figure 14 shows the organic mass fraction as a function of particle size at various times during the linalool photooxidation experiment. Again, smaller particles have higher organic mass fractions due to preferential condensation of organic vapors onto smaller particles, which have higher surface area concentrations. The organic mass fraction across all sizes increases quickly as the experiment progresses and more organics condense onto the particles (Fig. 14a). The RH ramp at the end of each experiment is performed when the organic fraction at a given particle size no longer changes with time, and the average organic mass fraction over the ramping time period is used in the calculation of pure SOA growth factor (black curve in Fig. 14b). Because Eq. (4) calls for an organic *volumetric* fraction, ε_{org} , we convert the AMS-derived organic mass fraction $\varepsilon_{\text{org},m}$ to ε_{org} using the following relationship:

$$\varepsilon_{\text{org}} = \frac{1}{1 + \left(\frac{1 - \varepsilon_{\text{org},m}}{\varepsilon_{\text{org},m}} \right) \left(\frac{\rho_{\text{org}}}{\rho_{\text{AS}}} \right)} \quad (6)$$

where ρ_{org} is the density of the pure SOA portion of the aerosol, and ρ_{AS} is the density of ammonium sulfate (1.77 g/cm^3).

We note that while the HTDMA measures particle size as electrical mobility equivalent diameter, D_p , the AMS measures particle size as the vacuum aerodynamic diameter, D_{va} . The electrical mobility equivalent diameter is the diameter of a spherical particle with the same electrical migration mobility at atmospheric pressure as the particle of interest. The vacuum aerodynamic diameter is defined as the diameter of a unit-density sphere having the same terminal velocity in the free-molecular regime as the particle of interest. These two measures of particle size are related by the “effective density” as (DeCarlo et al., 2004):

$$D_{va} = D_p \frac{\rho_{\text{eff}}}{\rho_0} \quad (7)$$

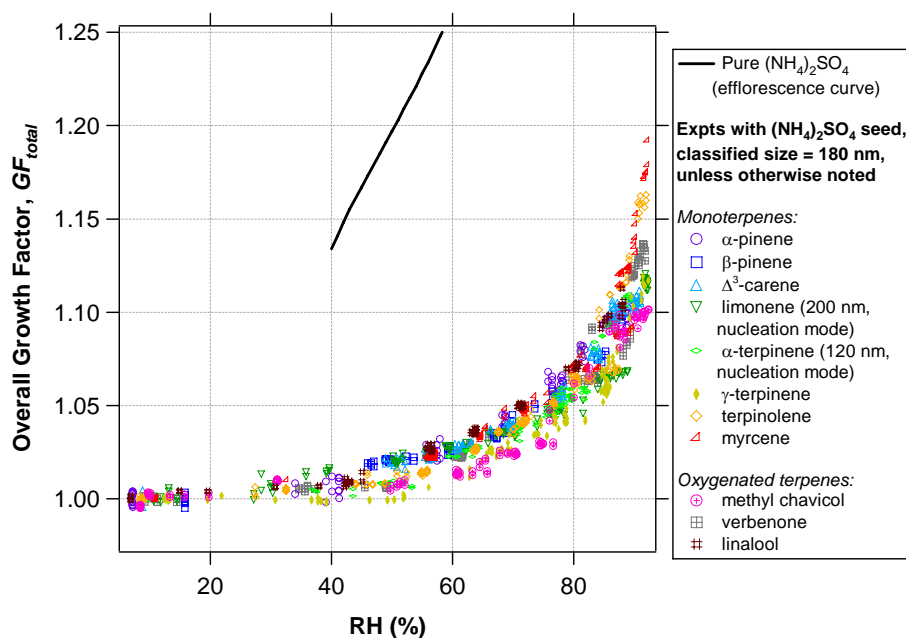


Fig. 13. Raw hygroscopic growth factors of SOA from monoterpene and oxygenated terpene photooxidation (with $(\text{NH}_4)_2\text{SO}_4$ seed). Reported data are from 180-nm classified diameter, unless otherwise noted. All the growth factors from various terpene precursors are contained within a relatively narrow envelope between 1.06–1.10 at 85% RH.

Table 4. Effective particle density and SOA density for monoterpene and oxygenated terpene precursors used in seeded experiments, in which AMS measurements were available. The calculations of both densities are performed in the same manner as in Bahreini et al. (2005).

Parent hydrocarbon	Effective particle density, ρ_{eff} (g/cm^3)	SOA density, ρ_{org} (g/cm^3)
limonene	1.30	1.30
α -terpinene	1.20	1.20
terpinolene	1.40	1.39
methyl chavicol	1.30	1.28
verbenone	1.30	1.27
linalool	1.30	1.27
Average		1.30

where $\rho_0=1 \text{ g}/\text{cm}^3$, and ρ_{eff} is the effective density of the aerosol, which is equivalent to the true material density of the aerosol assuming particle sphericity. The effective density can be estimated by matching the AMS and the corresponding DMA volume distributions at the rising edge (Bahreini et al., 2005). The density of the pure organic portion ρ_{org} can then be calculated from this ρ_{eff} using simple mass-weighting. The effective density and SOA density

for monoterpenes and oxygenated terpene experiments for which AMS measurements are available are listed in Table 4. These values are used to convert between the AMS-based D_{va} and HTDMA-based D_p . Thus, the organic mass fractions at the final HTDMA-dried particle sizes of 178 nm and 291 nm (for linalool experiment) are taken at AMS vacuum aerodynamic diameters of 232 nm and 378 nm, respectively, as shown by vertical dashed lines in Fig. 14b.

Table 5. Summary of experiments with $(\text{NH}_4)_2\text{SO}_4$ seed and the fitting results of the hygroscopic growth curve. Pure SOA growth factors (GF_{org}) are calculated from measured organic fractions at different TDMA-classified sizes.

Experimental Conditions							Fitting parameters from Eq. 2			GF interpolated from fit (Fig. 16)		ΔGF_c	
Parent Hydrocarbon	ΔHC (ppb)	T (K)	RH (%)	Peak ΔM_{O} ^a ($\mu\text{g}/\text{m}^3$)	SOA Yield	$D_{p,\text{classified}}$ (nm)	ϵ_{org}	A	B	C	GF @ 50%		GF @ 85%
Monoterpenes (photooxidation in humid chamber)													
α -pinene	108	293	44	199 ^b	0.337	180	0.996 ^d	0.0000	0.1447	3.2783	1.015	1.085	0.004
						300	0.982 ^d	0.0000	0.1443	3.0028	1.018	1.089	
β -pinene	170	293	50	293 ^b	0.318	180	0.996 ^d	0.5108	0.0367	1.5177	1.018	1.076	-0.005
						300	0.982 ^d	0.6526	0.0243	1.0138	1.019	1.071	
Δ^3 -carene	109	294	53	236 ^b	0.399	180	0.996 ^d	0.1825	0.0912	2.8905	1.014	1.081	0.000
						300	0.982 ^d	0.0999	0.1098	3.0357	1.014	1.081	
limonene	120	294	45	435	0.645	200 ^c	1.000	0.8133	0.0153	0.5882	1.018	1.065	0.023, 0.046
						300	0.999	0.4907	0.0424	1.2047	1.026	1.088	
						400	0.996	0.7191	0.0326	0.8574	1.030	1.111	
α -terpinene	103	293	47	217	0.372	120 ^c	1.000	0.6083	0.0378	2.4262	1.011	1.081	0.025
						230	0.990	0.9616	0.0219	1.5472	1.015	1.106	
γ -terpinene	119	294	48	193 ^b	0.301	180	0.996 ^d	0.5771	0.0319	2.8239	1.007	1.060	0.050
						300	0.982 ^d	0.6638	0.0515	3.0681	1.010	1.110	
terpinolene	110	294	50	190 ^b	0.319	180	0.990	0.9246	0.0172	1.5134	1.011	1.077	0.049
						300	0.973	0.9546	0.0275	1.7925	1.015	1.126	
myrcene	112	294	53	272 ^b	0.446	180	0.996 ^d	0.9703	0.0145	0.5806	1.019	1.083	0.011
						300	0.982 ^d	0.7255	0.0311	1.6379	1.017	1.094	
Oxygenated terpenes (photooxidation in humid chamber)													
methyl chavicol	79	294	49	125	0.259	180	0.999	0.0000	0.1509	4.8326	1.005	1.069	0.013
						300	0.994	0.0000	0.1904	5.1972	1.005	1.082	
verbenone	105	294	46	129	0.198	180	0.994	0.4884	0.0453	2.4240	1.012	1.077	0.049
						300	0.973	0.9167	0.0268	1.2082	1.022	1.126	
linalool	124	295	40	146	0.184	180	0.994	0.2092	0.0894	2.6252	1.017	1.087	0.104
						300	0.963	0.1191	0.2322	2.5935	1.042	1.191	

a: Measured by AMS in total MS mode, unless otherwise noted

b: Calculated by multiplying the final DMA volume by the average SOA density of 1.30 g/cm³ from AMS

c: At the peak of a small “nucleation mode” (already pure SOA), which formed despite the presence of seed

d: AMS data are not available from α -pinene, β -pinene, Δ^3 -carene, γ -terpinene, and myrcene experiments. The average organic mass fractions of 0.996 and 0.982 are used for the 180-nm and 300-nm classified particles, respectively.

The resulting organic volume fractions at different classified sizes are reported in Table 5. The relatively high ϵ_{org} values (0.990–1.000 at 180-nm classified size) indicate that the SOA selected by the HTDMA is almost entirely composed of organics, with a virtually negligible $(\text{NH}_4)_2\text{SO}_4$ core. Even the 300-nm particles have relatively high organic fractions (0.963–0.999). Thus, GF_{total} is already a relatively accurate approximation of GF_{org} even without explicit volume-weighting analysis. For completeness, however, we will proceed with determination of GF_{org} according to Eq. (4).

Figure 15 shows the original hygroscopic growth curves (with inorganic seed) and the calculated GF_{org} curves from different classified diameters of (a) Δ^3 -carene SOA, (b) linalool SOA, and (c) limonene SOA. The GF_{org} curves are seen as “shifted” downward when the water uptake of $(\text{NH}_4)_2\text{SO}_4$ is taken into account using Eq. (4). However, while it is expected that the GF_{org} curves calculated from the different classified diameters would collapse together, this may occur to varying degrees. For Δ^3 -carene SOA (Fig. 15a), the GF_{org} curves calculated from 180-nm or 300-

nm classified sizes are practically identical. For linalool SOA (Fig. 15b), there is a large discrepancy between the two curves. For the limonene SOA (Fig. 15c), we are able to directly measure GF_{org} by classifying 200-nm particles, which are in a small mode grown from particles that nucleated despite the presence of seed. The figure illustrates that the GF_{org} values calculated from the 300 nm and 400 nm classified sizes are close to the directly measured GF_{org} at the pure organic mode at 200 nm, but not exactly equal. The possible reasons for this variation in the ability to match GF_{org} curves derived from different classified sizes are discussed below. Each obtained GF_{org} curve can still be fitted with the three-parameter functional form of Eq. (2). Table 5 lists the resulting fit parameters and the interpolated GF_{org} at reference RHs from different classified diameters for monoterpene and oxygenated terpene experiments. In general, the growth factors for pure monoterpene and oxygenated terpene SOA are between 1.06–1.11, which is practically identical to the raw growth data when the $(\text{NH}_4)_2\text{SO}_4$ growth is not taken into account. This range is higher than that for sesquiterpene SOA

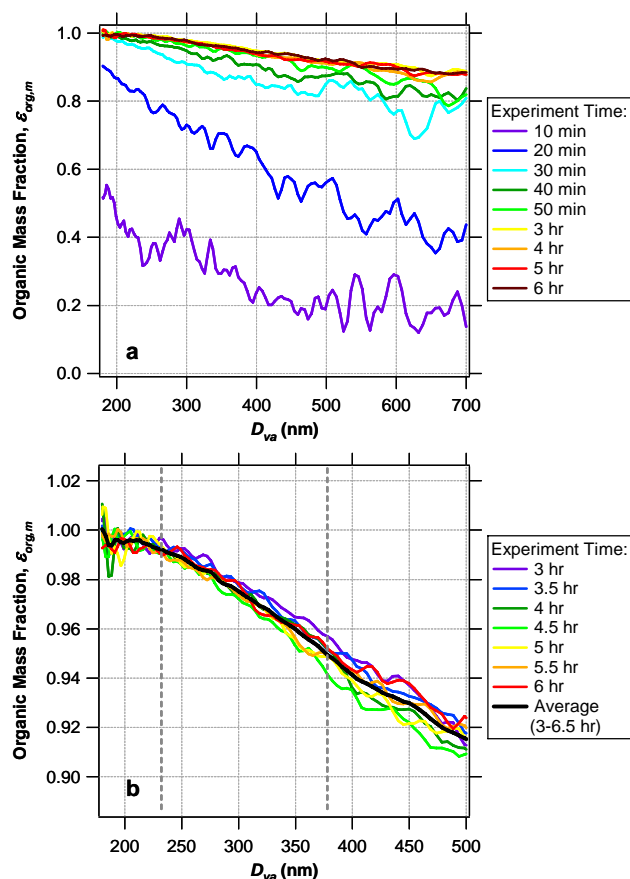


Fig. 14. Size-dependent organic mass fraction vs. particle vacuum aerodynamic diameter, as measured by the AMS at various times during linalool photooxidation experiment. Smaller particles have higher organic mass fractions due to preferential condensation of organic vapors onto smaller particles, which have higher surface area concentration. The organic mass fraction across all sizes increases as the experiment progresses and more organics condense onto the particles. **(a)** The organic fraction curves shown at times less than 1 h are calculated by averaging 4 min of AMS data, while those at times more than 1 h are calculated by averaging 30 min of data. **(b)** TDMA ramping for this linalool experiment occurs between 3–7 h, when the organic fraction at a given size no longer changes with time, and the average organic mass fraction over this long time is used in the calculation of pure SOA growth factor (intersection between the black average curve and the dashed line showing classified sizes at $D_{va}=232$ nm and 378 nm).

($GF=1.01$ – 1.04), which is intuitive due to the higher molecular weights of sesquiterpene precursors. Larger precursors should produce larger oxidation products, which given the same functionalities would tend to be less hygroscopic.

One possible cause for the finding that GF_{org} values calculated from different classified diameters do not fall onto a single curve for certain SOA precursors is inaccuracy of the volume-weighting approach to describe water uptake of an inorganic-organic mixture. The method has been shown

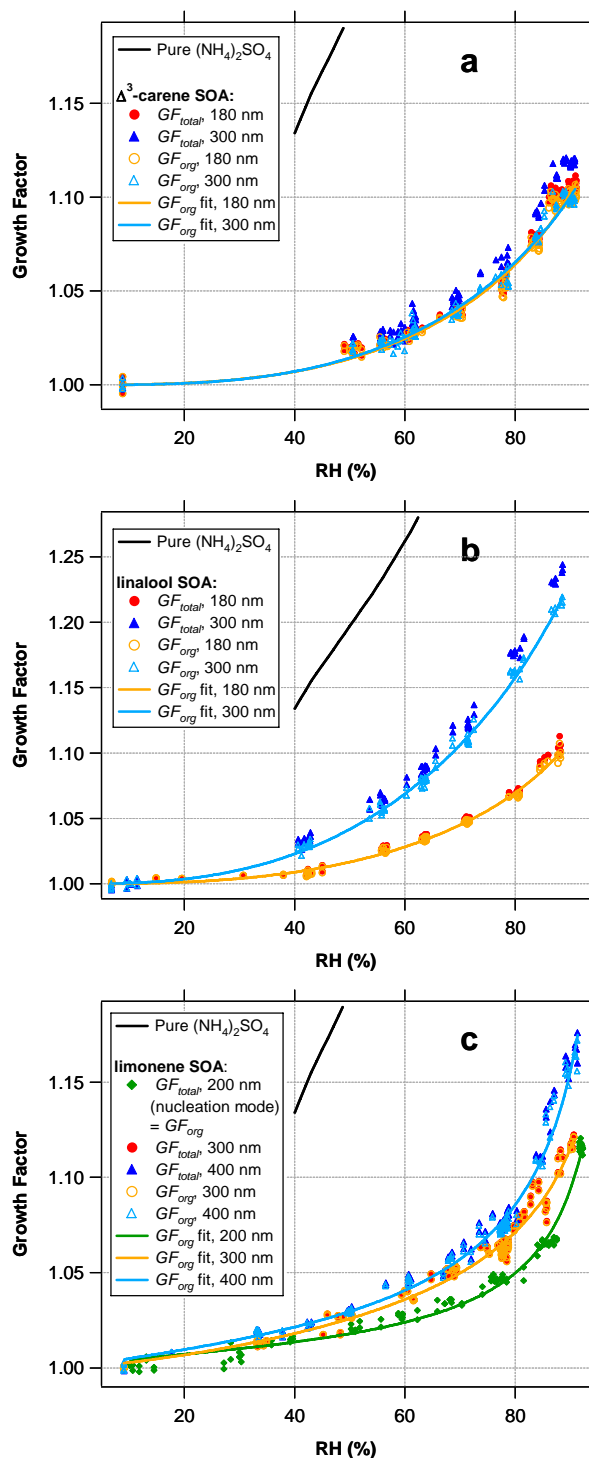


Fig. 15. Hygroscopic growth curves of **(a)** Δ^3 -carene, **(b)** linalool, and **(c)** limonene photooxidation SOA, with and without accounting for the effect of water uptake by inorganic seed. For a given precursor, the resulting “pure SOA” growth curves from the different classified sizes collapse together to various degrees. Possible reasons for this behavior are discussed in the text.

to work with relatively dilute solutions, where the inorganic and organic species do not thermodynamically interact with each other (Choi and Chan, 2002; Prenni et al., 2003; Wise et al., 2003). However, the SOA we are studying has very high organic fractions and correspondingly low water content, and thus could involve some non-ideal solution thermodynamics, the effect of which may not be captured by the assumption of volume additivity. Khlystov et al. (2005) also reported discrepancies between measured water content of ambient aerosol and that predicted by the ZSR method. The authors used models that assumed organics do not contribute to water absorption and only took into account the water uptake by inorganics. Their results indicate that the models underestimated the water uptake compared to the measured values; however, no correlation was found between the organic mass and the scaled excess water (measured minus predicted). This indicates that volume additivity may not apply, and complex interactions between the organic and inorganics may be occurring, leading to the water uptake of the inorganic portion being enhanced or suppressed. On the other hand, our mixed particles have very low inorganic content to add to the solute amount, and the organic oxidation products are not likely to be nearly as soluble in water as $(\text{NH}_4)_2\text{SO}_4$. A first-order calculation, using pinonic acid as a model compound to represent particle-phase oxidation products, suggests that the solution molality would be on the order of 0.02 molal. While the molality could potentially be an order of magnitude or so higher depending on the organic composition and solubility, it is likely not large enough to be in the regime where organic/inorganic interactions could become significant.

For ease of discussion, we define the discrepancy ΔGF_c between the GF_{org} at 85% derived from different classified sizes (nominally 300 and 180 nm) as follows:

$$\Delta GF_c = GF_{\text{org},300\text{nm}} - GF_{\text{org},180\text{nm}} \quad (8)$$

Linalool, γ -terpinene, terpinolene, and verbenone are the precursors that show significantly different GF_{org} derived from different classified sizes ($\Delta GF_c > 0.04$), while α -pinene, β -pinene, Δ^3 -carene, myrcene, and methyl chavicol are those whose GF_{org} curves from different classified sizes agree well with each other ($\Delta GF_c < 0.015$). Limonene and α -terpinene exhibit deviations that are in between these two extremes. Note that the compounds with high ΔGF_c tend to also show relatively different raw growth curves from 180-nm and 300-nm classified sizes. The corresponding ε_{org} at the two sizes are also more different than with other compounds. If either the AMS overestimates the organic fraction of larger particles or the HTDMA overestimates GF at the larger sizes or underestimates GF at smaller sizes, this would result in higher ΔGF_c .

Since we utilize the size-resolved organic fraction data derived from the AMS, we are also subject to the uncertainties inherently present in AMS measurements and the assumptions made in the analysis that can manifest into errors in

the GF_{org} calculation, for example, uncertainties in collection efficiency due to bounce of particles on the AMS vaporizer, the relative ionization efficiency used for organic species, handling of interferences due to organic nitrates, or using a unity shape factor (i.e. assuming particle sphericity) when interpreting the mass distributions. All of these could potentially impact the estimated speciated mass; however, because the organic fraction is expressed as a ratio between the organic and total mass, the errors affecting absolute mass must be quite large in order to impact the organic fraction significantly. To match the GF_{org} curves from two classified sizes for linalool, for example, ε_{org} at 300 nm would need to be ~ 0.83 rather than 0.963, which is well outside the measurement uncertainty of the AMS. At the same time, the growth curves for the two sizes as measured by the HTDMA (Fig. 12) are also quite different and beyond the measurement uncertainty of the HTDMA (± 0.02 in GF , from the deviation of observed vs. theoretical pure growth curves). Although another possible reason for the high ΔGF_c is that different organic species condense onto seeds of different size ranges, this would seem unlikely.

3.3 Mass transfer considerations

In any hygroscopic growth measurement, one must also consider the possibility that the aerosol measured is not at equilibrium with the new RH . While mass transfer analysis shows that sub-micrometer particles only require time scales of less than a second to attain equilibrium sizes following humidification or dehumidification (Kerminen, 1997), it has been suggested that an organic layer present on the particle may reduce the rate of water transport across the surface by acting as a physical barrier (Xiong et al., 1998; Chuang, 2003). If insufficient time is allowed for particles to achieve their final sizes in the RH conditioner and mixing chamber, in which particle growth or evaporation is induced, the size distribution attained by the time the particles are sized in the scanning DMA may not be the equilibrium size distribution. However, this is unlikely to be the cause of the non-collapsing GF_{org} curves because the organic fractions for all types and sizes of SOA are consistently high. The difference between organic layer thicknesses corresponding to organic fractions of 0.963 and 0.994 is negligible, and it is unlikely that only particles of a certain classified size in the HTDMA would suffer from mass transfer limitation but not at another size.

In addition, it has been shown that the characteristic diffusion time scale for gas-phase species (such as of water vapor) to a particle, the time scale to achieve equilibrium in the gas-particle interface, and the time scale of aqueous-phase diffusion in a droplet all vary with the square of the particle diameter (Seinfeld and Pandis, 1998). Thus, if mass transfer limitation occurs in the particles we study, a 300-nm particle should suffer a delay in growth that is ~ 2.8 times as long as that of a 180-nm particle. The very slightly lower absolute

organic fractions in the larger particle would not be low enough to alleviate the greater mass transfer delay. Therefore, if mass transfer limitation was a factor in our measurements, we would expect that, relative to the 180-nm particles, the 300-nm particles would not reach a sufficiently large final droplet size when exposed to the same elevated humidity. On the contrary, for the four compounds with the disagreement behavior, GF_{org} values calculated from 300-nm classified particles are consistently greater than those from 180-nm particles, indicating that the 300-nm particles “grew too much”, reaching larger final size change ratios than would be expected when comparing to 180-nm particles of similar organic fraction. This is the opposite trend as would be expected for a mass-transfer-limited case. Hence, we believe that mass transfer limitations are not an issue in our HTDMA for the current study. As such, we do not currently have a likely explanation for the discrepancy between the GF_{org} derived from different classified sizes in certain compounds.

3.4 Comparison of growth factors from various systems

To explain the growth factors from the various precursor compounds, we attempt to correlate GF_{org} with features of the precursor. Figure 16 shows the SOA growth factors at 50% and 85% RH plotted against (a) the precursor molecular weight and (b) the organic mass yield from the nucleated cycloalkene ozonolysis and sesquiterpenes photooxidation SOA, and monoterpene and oxygenated terpene photooxidation SOA on $(NH_4)_2SO_4$ seed. For the latter case, GF_{org} calculated from the lowest classified size is shown. The peak organic mass yield Y is defined as the ratio of the mass of the organics formed (ΔM_O) to the mass of the parent hydrocarbon consumed (ΔHC) during the experiment:

$$Y = \frac{\Delta M_O}{\Delta HC} \quad (9)$$

For experiments in which AMS data are available, ΔM_O is taken from the peak total organic signal. Otherwise, it is calculated from the DMA-derived total aerosol volume change, multiplied by the averaged terpene SOA density of 1.30 g/cm^3 . At both reference RH s, we observe a general anti-correlation between GF_{org} and both precursor molecular weight and SOA yield. This is understandable because higher-molecular weight precursors will tend to produce larger oxidation products, which are less hygroscopic given similar functional groups. Since the larger oxidation products also tend to be less volatile, they also result in higher SOA yields.

4 Conclusions

The hygroscopic growth of SOA formed by ozonolysis of cycloalkenes and photooxidation of sesquiterpene and monoterpenes is studied. In all cases, the SOA are slightly hygroscopic, but considerably less so than inorganic salts

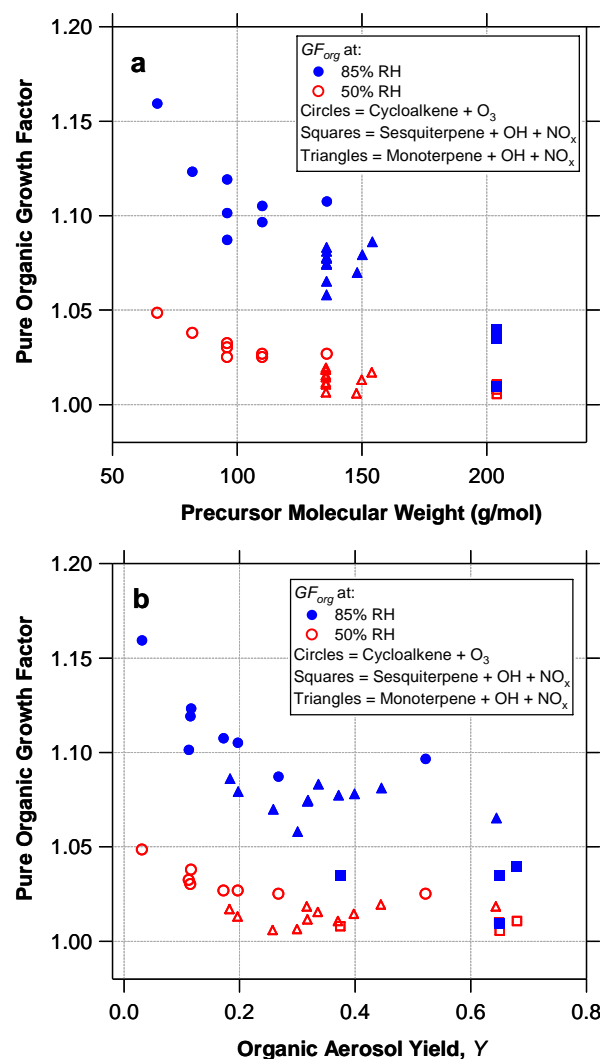


Fig. 16. SOA growth factor versus (a) the molecular weight and (b) the SOA yield of the precursor.

such as $(NH_4)_2SO_4$, and show smooth water uptake curves with no deliquescence or efflorescence behavior. In the seeded cycloalkene experiments, bimodal droplet distributions are observed early in the experiment, due to the differing organic mass fractions in monodisperse particles caused by different particle growth trajectories. In cycloalkene nucleation experiments, the water uptake is seen to increase with time, indicative of further oxidation of organic products into more polar and more hygroscopic species. For the SOA formed by photooxidation of sesquiterpene SOA, however, the hygroscopicity decreases with time, which could be explained by the formation of higher-molecular weight and less hydrophilic oligomers. Thus, the temporal variation of SOA hygroscopicity is probably a result of these two competing effects.

The SOA growth factor as a function of RH is measured, and the growth curve is fitted with an empirical three-

parameter functional form, from which the *GF* at any *RH* can be interpolated. *GF* values of the pure organic portion of the SOA at 85% *RH* are between 1.09–1.16 for the C₅–C₈ cycloalkenes, 1.06–1.10 for the monoterpenes and oxygenated terpenes, and 1.01–1.04 for the sesquiterpenes. In the monoterpene and oxygenated terpene case, volume-weighting analysis is performed to compute the growth factor of the pure SOA from the growth measured with inorganic seed. This approach results in mixed success as observed by the pure organic growth curves from different classified sizes agreeing to varying degrees. Finally, we observe an anti-correlation between the pure SOA growth factor and the precursor molecular weight and SOA yield that is consistent with the fact that higher-molecular weight precursors tend to produce larger, less hygroscopic oxidation products.

The implication of these measurements to modeling of atmospheric aerosol is that the presence of SOA in a particle can significantly reduce the hygroscopicity of the aerosol at high *RH*s from that for pure inorganics. We find the SOA to lack a clear deliquescence *RH* and to continually uptake water even at *RH*s lower than the deliquescence *RH* of atmospherically relevant inorganic substances. These observations suggest that SOA can play an important role in extending the range of *RH*s over which particle-bound water influences aerosol physicochemical and optical properties.

Acknowledgements. This research was funded by the U.S. Environmental Protection Agency Science to Achieve Results (STAR) Program grant number RD-83107501-0, managed by EPA's Office of Research and Development (ORD), National Center for Environmental Research (NCER), and by U.S. Department of Energy Biological and Environmental Research Program DE-FG02-05ER63983. The University of California contributions to this work were supported by the National Science Foundation Atmospheric Chemistry Program (Awards ATM-0119510 and ATM-0443448) and the California Air Resources Board (Contract 00-732). F. J. Brechtel was supported by the National Science Foundation Atmospheric Chemistry Program under Award ATM-0333817. The authors thank D. Collins of Texas A&M University and C. Stanier of University of Iowa for helpful discussions.

Edited by: T. Koop

References

- Allan, J. D., Alfarra, M. R., Bower, K. N., Williams, P. I., Gallagher, M. W., Jimenez, J. L., McDonald, A. G., Nemitz, E., Canagaratna, M. R., Jayne, J. T., Coe, H., and Worsnop, D. R.: Quantitative sampling using an Aerodyne aerosol mass spectrometer – 2. Measurements of fine particulate chemical composition in two U.K. cities, *J. Geophys. Res.-Atmos.*, 108, 4091, doi:10.1029/2002JD002359, 2003.
- Andreae, M. O. and Crutzen, P. J.: Atmospheric aerosols: Biogeochemical sources and role in atmospheric chemistry, *Science*, 276, 1052–1058, 1997.
- Ansari, A. S. and Pandis, S. N.: Water absorption by secondary organic aerosol and its effect on an inorganic aerosol behavior, *Environ. Sci. Technol.*, 34, 71–77, 2000.
- Bahreini, R., Keywood, M. D., Ng, N. L., Varutbangkul, V., Gao, S., Flagan, R. C., Seinfeld, J. H., Worsnop, D. R., and Jimenez, J. L.: Measurements of secondary organic aerosol from oxidation of cycloalkenes, terpenes, and m-xylene using an Aerodyne aerosol mass spectrometer, *Environ. Sci. Technol.*, 39, 5674–5688, 2005.
- Baltensperger, U., Kalberer, M., Dommen, J., Paulsen, D., Alfarra, M. R., Coe, H., Fisseha, R., Gascho, A., Gysel, M., Nyeki, S., Sax, M., Steinbacher, M., Prevot, A. S. H., Sjoren, S., Weingartner, E., and Zenobi, R.: Secondary organic aerosols from anthropogenic and biogenic precursors, *Faraday Discuss.*, 130, 265–278, doi:10.1039/b417367h, 2005.
- Brodsky, D. M. and Georgopoulos, P. G.: Growth and deposition of hygroscopic particulate matter in the human lungs, *Aerosol Sci. Technol.*, 34, 144–159, 2001.
- Busch, B., Kandler, K., Schutz, L., and Neusüss, C.: Hygroscopic properties and water-soluble volume fraction of atmospheric particles in the diameter range from 50 nm to 3.8 μ m during LACE 98, *J. Geophys. Res.-Atmos.*, 107, 8119, doi:10.1029/2000JD000228, 2002.
- Cabada, J. C., Pandis, S. N., and Robinson, A. L.: Sources of atmospheric carbonaceous particulate matter in Pittsburgh, Pennsylvania, *J. Air Waste Manage. Assoc.*, 52, 732–741, 2002.
- Cabada, J. C., Pandis, S. N., Subramanian, R., Robinson, A. L., Polidori, A., and Turpin, B.: Estimating the secondary organic aerosol contribution to PM_{2.5} using the EC tracer method, *Aerosol Sci. Technol.*, 38, 140–155, 2004.
- Chan, H. K., Eberl, S., Daviskas, E., Constable, C., and Young, I.: Changes in lung deposition of aerosols due to hygroscopic growth: A fast SPECT study, *Journal of Aerosol Medicine-Deposition Clearance and Effects in the Lung*, 15, 307–311, 2002.
- Choi, M. Y. and Chan, C. K.: The effects of organic species on the hygroscopic behaviors of inorganic aerosols, *Environ. Sci. Technol.*, 36, 2422–2428, 2002.
- Chuang, P. Y.: Measurement of the timescale of hygroscopic growth for atmospheric aerosols, *J. Geophys. Res.-Atmos.*, 108, 4282, doi:10.1029/2002JD002757, 2003.
- Cocker, D. R., Clegg, S. L., Flagan, R. C., and Seinfeld, J. H.: The effect of water on gas-particle partitioning of secondary organic aerosol. Part I: Alpha-pinene/ozone system, *Atmos. Environ.*, 35, 6049–6072, 2001a.
- Cocker, D. R., Flagan, R. C., and Seinfeld, J. H.: State-of-the-art chamber facility for studying atmospheric aerosol chemistry, *Environ. Sci. Technol.*, 35, 2594–2601, 2001b.
- Cocker, D. R., Mader, B. T., Kalberer, M., Flagan, R. C., and Seinfeld, J. H.: The effect of water on gas-particle partitioning of secondary organic aerosol: II. m-xylene and 1,3,5-trimethylbenzene photooxidation systems, *Atmos. Environ.*, 35, 6073–6085, 2001c.
- Cocker, D. R., Whitlock, N. E., Flagan, R. C., and Seinfeld, J. H.: Hygroscopic properties of Pasadena, California aerosol, *Aerosol Sci. Technol.*, 35, 637–647, 2001d.
- Collins, D. R., Flagan, R. C., and Seinfeld, J. H.: Improved inversion of scanning DMA data, *Aerosol Sci. Technol.*, 36, 1–9, 2002.
- Covert, D. S. and Heintzenberg, J.: Size distributions and chemical-properties of aerosol at Ny Alesund, Svalbard, *Atmos. Environ. Part A-General Topics*, 27, 2989–2997, 1993.
- Cruz, C. N. and Pandis, S. N.: Deliquescence and hygroscopic

- growth of mixed inorganic-organic atmospheric aerosol, *Environ. Sci. Technol.*, 34, 4313–4319, 2000.
- DeCarlo, P., Slowik, J. G., Worsnop, D. R., Davidovits, P., and Jimenez, J. L.: Particle morphology and density characterization by combined mobility and aerodynamic diameter measurements. Part I: theory, *Aerosol Sci. Technol.*, 38, 1185–1205, 2004.
- Ferron, G. A., Karg, E., Busch, B., and Heyder, J.: Ambient particles at an urban, semi-urban and rural site in central Europe: hygroscopic properties, *Atmos. Environ.*, 39, 343–352, 2005.
- Finlay, W. H., Stapleton, K. W., and Zuberbuhler, P.: Errors in regional lung deposition predictions of nebulized salbutamol sulphate due to neglect or partial inclusion of hygroscopic effects, *Int. J. Pharm.*, 149, 63–72, 1997.
- Gao, S., Keywood, M., Ng, N. L., Surratt, J., Varutbangkul, V., Bahreini, R., Flagan, R. C., and Seinfeld, J. H.: Low-molecular-weight and oligomeric components in secondary organic aerosol from the ozonolysis of cycloalkenes and alpha-pinene, *J. Phys. Chem. A*, 108, 10 147–10 164, 2004a.
- Gao, S., Ng, N. L., Keywood, M., Varutbangkul, V., Bahreini, R., Nenes, A., He, J. W., Yoo, K. Y., Beauchamp, J. L., Hodyss, R. P., Flagan, R. C., and Seinfeld, J. H.: Particle phase acidity and oligomer formation in secondary organic aerosol, *Environ. Sci. Technol.*, 38, 6582–6589, 2004b.
- Griffin, R. J., Cocker, D. R., Flagan, R. C., and Seinfeld, J. H.: Organic aerosol formation from the oxidation of biogenic hydrocarbons, *J. Geophys. Res.-Atmos.*, 104, 3555–3567, 1999.
- Guenther, A., Hewitt, C. N., Erickson, D., Fall, R., Geron, C., Graedel, T., Harley, P., Klinger, L., Lerdau, M., McKay, W. A., Pierce, T., Scholes, B., Steinbrecher, R., Tallamraju, R., Taylor, J., and Zimmerman, P.: A global-model of natural volatile organic-compound emissions, *J. Geophys. Res.-Atmos.*, 100, 8873–8892, 1995.
- Hansson, H. C., Rood, M. J., Koloutsou-Vakakis, S., Hameri, K., Orsini, D., and Wiedensohler, A.: NaCl aerosol particle hygroscopicity dependence on mixing with organic compounds, *J. Atmos. Chem.*, 31, 321–346, 1998.
- Hartz, K. E. H., Rosenorn, T., Ferchak, S. R., Raymond, T. M., Bilde, M., Donahue, N. M., and Pandis, S. N.: Cloud condensation nuclei activation of monoterpene and sesquiterpene secondary organic aerosol, *J. Geophys. Res.-Atmos.*, 110, D14208, doi:10.1029/2004JD005754, 2005.
- Heintzenberg, J., Massling, A., and Birmili, W.: The connection between hygroscopic and optical particle properties in the atmospheric aerosol, *Geophys. Res. Lett.*, 28, 3649–3651, 2001.
- Holzinger, R., Lee, A., Paw, K. T., and Goldstein, A. H.: Observations of oxidation products above a forest imply biogenic emissions of very reactive compounds, *Atmos. Chem. Phys.*, 5, 67–75, 2005, <http://www.atmos-chem-phys.net/5/67/2005/>.
- Intergovernmental Panel on Climate Change: Climate change 2001, Cambridge University Press, Cambridge, UK, 2001.
- Jacobson, M. C., Hansson, H. C., Noone, K. J., and Charlson, R. J.: Organic atmospheric aerosols: review and state of the science, *Rev. Geophys.*, 38, 267–294, 2000.
- Janson, R., Rosman, K., Karlsson, A., and Hansson, H. C.: Biogenic emissions and gaseous precursors to forest aerosols, *Tellus Ser. B-Chem. Phys. Meteorol.*, 53, 423–440, 2001.
- Jayne, J. T., Leard, D. C., Zhang, X. F., Davidovits, P., Smith, K. A., Kolb, C. E., and Worsnop, D. R.: Development of an aerosol mass spectrometer for size and composition analysis of submicron particles, *Aerosol Sci. Technol.*, 33, 49–70, 2000.
- Jimenez, J. L., Bahreini, R., Cocker, D. R., Zhuang, H., Varutbangkul, V., Flagan, R. C., Seinfeld, J. H., O'Dowd, C. D., and Hoffmann, T.: New particle formation from photooxidation of diodomethane (CH₂I₂), *J. Geophys. Res.-Atmos.*, 108, doi:10.1029/2002JD002452, 2003.
- Kalberer, M., Paulsen, D., Sax, M., Steinbacher, M., Dommen, J., Prevot, A. S. H., Fisseha, R., Weingartner, E., Frankevich, V., Zenobi, R., and Baltensperger, U.: Identification of polymers as major components of atmospheric organic aerosols, *Science*, 303, 1659–1662, 2004.
- Kanakidou, M., Seinfeld, J. H., Pandis, S. N., Barnes, I., Dentener, F. J., Facchini, M. C., Van Dingenen, R., Ervens, B., Nenes, A., Nielsen, C. J., Swietlicki, E., Putaud, J. P., Balkanski, Y., Fuzzi, S., Horth, J., Moortgat, G. K., Winterhalter, R., Myhre, C. E. L., Tsigaridis, K., Vignati, E., Stephanou, E. G., and Wilson, J.: Organic aerosol and global climate modelling: a review, *Atmos. Chem. Phys.*, 5, 1053–1123, 2005, <http://www.atmos-chem-phys.net/5/1053/2005/>.
- Kavouras, I. G., Mihalopoulos, N., and Stephanou, E. G.: Formation and gas/particle partitioning of monoterpenes photooxidation products over forests, *Geophys. Res. Lett.*, 26, 55–58, 1999a.
- Kavouras, I. G., Mihalopoulos, N., and Stephanou, E. G.: Secondary organic aerosol formation vs primary organic aerosol emission: in situ evidence for the chemical coupling between monoterpene acidic photooxidation products and new particle formation over forests, *Environ. Sci. Technol.*, 33, 1028–1037, 1999b.
- Kerminen, V. M.: The effects of particle chemical character and atmospheric processes on particle hygroscopic properties, *J. Aerosol Sci.*, 28, 121–132, 1997.
- Keywood, M. D., Varutbangkul, V., Bahreini, R., Flagan, R. C., and Seinfeld, J. H.: Secondary organic aerosol formation from the ozonolysis of cycloalkenes and related compounds, *Environ. Sci. Technol.*, 38, 4157–4164, 2004.
- Khlystov, A., Stanier, C. O., Takahama, S., and Pandis, S. N.: Water content of ambient aerosol during the Pittsburgh air quality study, *J. Geophys. Res.-Atmos.*, 110, D07S10, doi:10.1029/2004JD004651, 2005.
- Kleindienst, T. E., Corse, E. W., Li, W., McIver, C. D., Conver, T. S., Edney, E. O., Driscoll, D. J., Speer, R. E., Weathers, W. S., and Tejada, S. B.: Secondary organic aerosol formation from the irradiation of simulated automobile exhaust, *J. Air Waste Manage. Assoc.*, 52, 259–272, 2002.
- Kleindienst, T. E., Smith, D. F., Li, W., Edney, E. O., Driscoll, D. J., Speer, R. E., and Weathers, W. S.: Secondary organic aerosol formation from the oxidation of aromatic hydrocarbons in the presence of dry submicron ammonium sulfate aerosol, *Atmos. Environ.*, 33, 3669–3681, 1999.
- Lee, A., Goldstein, A. H., Keywood, M. D., Gao, S., Kroll, J. H., Varutbangkul, V., Bahreini, R., Ng, N. L., Flagan, R. C., and Seinfeld, J. H.: Gas-phase products and secondary aerosol yields from the ozonolysis of ten different terpenes, *J. Geophys. Res.-Atmos.*, 111, art. no. D07302, doi:10.1029/2005JD006437, 2006.
- Li, Z. D., Williams, A. L., and Rood, M. J.: Influence of soluble surfactant properties on the activation of aerosol particles containing inorganic solute, *J. Atmos. Sci.*, 55, 1859–1866, 1998.

- Lim, H. J. and Turpin, B. J.: Origins of primary and secondary organic aerosol in Atlanta: results of time-resolved measurements during the Atlanta supersite experiment, *Environ. Sci. Technol.*, 36, 4489–4496, 2002.
- Lindinger, W., Hansel, A., and Jordan, A.: Proton-transfer-reaction mass spectrometry (PTR-MS): On-line monitoring of volatile organic compounds at pptv levels, *Chem. Soc. Rev.*, 27, 347–354, 1998.
- Liu, B. Y. H., Pui, D. Y. H., Whitby, K. T., Kittelson, D. B., Kousaka, Y., and McKenzie, R. L.: Aerosol mobility chromatograph – new detector for sulfuric-acid aerosols, *Atmos. Environ.*, 12, 99–104, 1978.
- Massling, A., Wiedensohler, A., Busch, B., Neusüss, C., Quinn, P., Bates, T., and Covert, D.: Hygroscopic properties of different aerosol types over the Atlantic and Indian oceans, *Atmos. Chem. Phys.*, 3, 1377–1397, 2003, <http://www.atmos-chem-phys.net/3/1377/2003/>.
- McMurry, P. H. and Stolzenburg, M. R.: On the sensitivity of particle-size to relative-humidity for Los Angeles aerosols, *Atmos. Environ.*, 23, 497–507, 1989.
- Nenes, A., Pandis, S. N., and Pilinis, C.: ISORROPIA: A new thermodynamic equilibrium model for multiphase multicomponent inorganic aerosols, *Aquat. Geochem.*, 4, 123–152, 1998.
- Pio, C., Alves, C., and Duarte, A.: Organic components of aerosols in a forested area of central Greece, *Atmos. Environ.*, 35, 389–401, 2001.
- Prenni, A. J., De Mott, P. J., and Kreidenweis, S. M.: Water uptake of internally mixed particles containing ammonium sulfate and dicarboxylic acids, *Atmos. Environ.*, 37, 4243–4251, 2003.
- Quinn, P. K., Bates, T. S., Baynard, T., Clarke, A. D., Onasch, T. B., Wang, W., Rood, M. J., Andrews, E., Allan, J., Carrico, C. M., Coffman, D., and Worsnop, D.: Impact of particulate organic matter on the relative humidity dependence of light scattering: A simplified parameterization, *Geophys. Res. Lett.*, 32, L22809, doi:10.1029/2005GL024322, 2005.
- Rader, D. J. and McMurry, P. H.: Application of the tandem differential mobility analyzer to studies of droplet growth or evaporation, *J. Aerosol Sci.*, 17, 771–787, 1986.
- Saathoff, H., Naumann, K. H., Schnaiter, M., Schock, W., Mohler, O., Schurath, U., Weingartner, E., Gysel, M., and Baltensperger, U.: Coating of soot and $(\text{NH}_4)_2\text{SO}_4$ particles by ozonolysis products of alpha-pinene, *J. Aerosol Sci.*, 34, 1297–1321, 2003.
- Saxena, P., Hildemann, L. M., McMurry, P. H., and Seinfeld, J. H.: Organics alter hygroscopic behavior of atmospheric particles, *J. Geophys. Res.-Atmos.*, 100, 18 755–18 770, 1995.
- Seinfeld, J. H. and Pandis, S. N.: *Atmospheric chemistry and physics*, John Wiley & Sons, Inc., 1998.
- Sellegri, K., Hanke, M., Umann, B., Arnold, F., and Kulmala, M.: Measurements of organic gases during aerosol formation events in the boreal forest atmosphere during QUEST, *Atmos. Chem. Phys.*, 5, 373–384, 2005, <http://www.atmos-chem-phys.net/5/373/2005/>.
- Simpson, D., Winiwarer, W., Borjesson, G., Cinderby, S., Ferreiro, A., Guenther, A., Hewitt, C. N., Janson, R., Khalil, M. A. K., Owen, S., Pierce, T. E., Puxbaum, H., Shearer, M., Skiba, U., Steinbrecher, R., Tarrason, L., and Oquist, M. G.: Inventorying emissions from nature in Europe, *J. Geophys. Res.-Atmos.*, 104, 8113–8152, 1999.
- Stokes, R. H. and Robinson, R. A.: Interactions in aqueous nonelectrolyte solutions. I. Solute-solvent equilibria, *J. Phys. Chem.*, 70, 2126–2131, 1966.
- Svenningsson, I. B., Hansson, H. C., Wiedensohler, A., Ogren, J. A., Noone, K. J., and Hallberg, A.: Hygroscopic growth of aerosol-particles in the Po Valley, *Tellus Ser. B-Chem. Phys. Meteorol.*, 44, 556–569, 1992.
- Swietlicki, E., Zhou, J. C., Berg, O. H., Martinsson, B. G., Frank, G., Cederfelt, S. I., Dusek, U., Berner, A., Birmili, W., Wiedensohler, A., Yuskiewicz, B., and Bower, K. N.: A closure study of sub-micrometer aerosol particle hygroscopic behaviour, *Atmos. Res.*, 50, 205–240, 1999.
- Swietlicki, E., Zhou, J. C., Covert, D. S., Hameri, K., Busch, B., Vakeva, M., Dusek, U., Berg, O. H., Wiedensohler, A., Aalto, P., Makela, J., Martinsson, B. G., Papaspiropoulos, G., Mentes, B., Frank, G., and Stratmann, F.: Hygroscopic properties of aerosol particles in the northeastern Atlantic during ACE-2, *Tellus Ser. B-Chem. Phys. Meteorol.*, 52, 201–227, 2000.
- Tang, I. N.: Water transformation and growth of aerosol particles composed of mixed salts, *J. Aerosol Sci.*, 361–371, 1976.
- Tang, I. N. and Munkelwitz, H. R.: Water activities, densities, and refractive-indexes of aqueous sulfates and sodium-nitrate droplets of atmospheric importance, *J. Geophys. Res.-Atmos.*, 99, 18 801–18 808, 1994.
- Turpin, B. J., Huntzicker, J. J., Larson, S. M., and Cass, G. R.: Los Angeles summer midday particulate carbon – primary and secondary aerosol, *Environ. Sci. Technol.*, 25, 1788–1793, 1991.
- VanReken, T. M., Ng, N. L., Flagan, R. C., and Seinfeld, J. H.: Cloud condensation nucleus activation properties of biogenic secondary organic aerosol, *J. Geophys. Res.-Atmos.*, 110, D07206, doi:10.1029/2004JD005465, 2005.
- Virkkula, A., Van Dingenen, R., Raes, F., and Hjorth, J.: Hygroscopic properties of aerosol formed by oxidation of limonene, alpha-pinene, and beta-pinene, *J. Geophys. Res.-Atmos.*, 104, 3569–3579, 1999.
- Wang, S. C. and Flagan, R. C.: Scanning electrical mobility spectrometer, *Aerosol Sci. Technol.*, 13, 230–240, 1990.
- Weis, D. D. and Ewing, G. E.: Water content and morphology of sodium chloride aerosol particles, *J. Geophys. Res.-Atmos.*, 104, 21 275–21 285, 1999.
- Wiedensohler, A.: An approximation of the bipolar charge-distribution for particles in the sub-micron size range, *J. Aerosol Sci.*, 19, 387–389, 1988.
- Wise, M. E., Surratt, J. D., Curtis, D. B., Shilling, J. E., and Tolbert, M. A.: Hygroscopic growth of ammonium sulfate/dicarboxylic acids, *J. Geophys. Res.-Atmos.*, 108, 4638, doi:10.1029/2003JD003775, 2003.
- Xiong, J. Q., Zhong, M. H., Fang, C. P., Chen, L. C., and Lippmann, M.: Influence of organic films on the hygroscopicity of ultrafine sulfuric acid aerosol, *Environ. Sci. Technol.*, 32, 3536–3541, 1998.
- Yu, J. Z., Griffin, R. J., Cocker, D. R., Flagan, R. C., Seinfeld, J. H., and Blanchard, P.: Observation of gaseous and particulate products of monoterpene oxidation in forest atmospheres, *Geophys. Res. Lett.*, 26, 1145–1148, 1999.
- Zhang, X. Q., McMurry, P. H., Hering, S. V., and Casuccio, G. S.: Mixing characteristics and water-content of submicron aerosols measured in Los Angeles and at the Grand Canyon, *Atmos. Environ. Part A-General Topics*, 27, 1593–1607, 1993.

Appendix I

Gas-Phase Products and Secondary Aerosol Yields from the Ozonolysis of Ten Different Terpenes^{*}

^{*} This chapter is reproduced by permission from “Gas-Phase Products and Secondary Aerosol Yields from the Ozonolysis of Ten Different Terpenes” by A. Lee, A. H. Goldstein, M. D. Keywood, S. Gao, V. Varutbangkul, R. Bahreini, N. L. Ng, R. C. Flagan, J. H. Seinfeld, *Journal of Geophysical Research-Atmosphere*, 111 (D7): Art. No. D07302, doi: 10.1029/2005JD006437, 2006. Copyright 2006, American Geophysical Union.

Gas-phase products and secondary aerosol yields from the ozonolysis of ten different terpenes

Anita Lee,¹ Allen H. Goldstein,¹ Melita D. Keywood,² Song Gao,² Varuntida Varutbangkul,² Roya Bahreini,² Nga L. Ng,² Richard C. Flagan,² and John H. Seinfeld²

Received 29 June 2005; revised 14 November 2005; accepted 30 December 2005; published 5 April 2006.

[1] The ozonolyses of six monoterpenes (α -pinene, β -pinene, 3-carene, terpinolene, α -terpinene, and myrcene), two sesquiterpenes (α -humulene and β -caryophyllene), and two oxygenated terpenes (methyl chavicol and linalool) were conducted individually in Teflon chambers to examine the gas-phase oxidation product and secondary organic aerosol (SOA) yields from these reactions. Particle size distribution and number concentration were monitored and allowed for the calculation of the SOA yield from each experiment, which ranged from 1 to 54%. A proton transfer reaction mass spectrometer (PTR-MS) was used to monitor the evolution of gas-phase products, identified by their mass to charge ratio (m/z). Several gas-phase oxidation products, formaldehyde, acetaldehyde, formic acid, acetone, acetic acid, and nopinone, were identified and calibrated. Aerosol yields, and the yields of these identified and calibrated oxidation products, as well as many higher m/z oxidation products observed with the PTR-MS, varied significantly between the different parent terpene compounds. The sum of measured oxidation products in the gas and particle phase ranged from 33 to 77% of the carbon in the reacted terpenes, suggesting there are still unmeasured products from these reactions. The observations of the higher molecular weight oxidation product ions provide evidence of previously unreported compounds and their temporal evolution in the smog chamber from multistep oxidation processes. Many of the observed ions, including m/z 111 and 113, have also been observed in ambient air above a Ponderosa pine forest canopy, and our results confirm they are consistent with products from terpene + O₃ reactions. Many of these products are stable on the timescale of our experiments and can therefore be monitored in field campaigns as evidence for ozone oxidative chemistry.

Citation: Lee, A., A. H. Goldstein, M. D. Keywood, S. Gao, V. Varutbangkul, R. Bahreini, N. L. Ng, R. C. Flagan, and J. H. Seinfeld (2006), Gas-phase products and secondary aerosol yields from the ozonolysis of ten different terpenes, *J. Geophys. Res.*, *111*, D07302, doi:10.1029/2005JD006437.

1. Introduction

[2] Biogenic emissions of terpene compounds influence atmospheric chemistry through the formation of tropospheric ozone and the production of secondary organic aerosol (SOA). Terpenes encompass several wide classes of compounds, including monoterpenes (C₁₀H₁₆), sesquiterpenes (C₁₅H₂₄), and oxygenated terpenes (e.g., C₁₀H₁₈O, C₁₀H₁₂O). These compounds are emitted from conifers as well as broad-leaved trees as a function of temperature, or both temperature and light [Kesselmeier and Staudt, 1999]. They react with OH, O₃, and NO₃, the common atmo-

spheric oxidants, with lifetimes that range from minutes to days [Atkinson and Arey, 2003]. Several monoterpene oxidation products are known to undergo gas-particle partitioning and have been found in ambient air in the gas and particle phases [Yu *et al.*, 1999b], [Kavouras *et al.*, 1999].

[3] Experiments examining terpene oxidation have been conducted after F. W. Went first suggested that blue hazes in forested regions were products of these reactions [Went, 1960]. Early experiments determined rate constants for the reaction of many different terpenes with the major atmospheric oxidants [e.g., Atkinson *et al.*, 1990; Shu and Atkinson, 1995], and yields of SOA and gas-phase carbonyl products from the oxidation of common monoterpene species, such as α - and β -pinene [e.g., Hatakeyama *et al.*, 1989; Pandis *et al.*, 1991; Zhang *et al.*, 1992; Hakola *et al.*, 1994]. Studies on the yields of OH from the ozonolysis of terpenes and other alkenes, from the decomposition of activated carbonyl oxides, or Criegee intermediates (CI), have also been conducted and found to occur at atmospheric

¹Department of Environmental Science, Policy and Management, University of California, Berkeley, California, USA.

²Department of Environmental Science and Engineering and Department of Chemical Engineering, California Institute of Technology, Pasadena, California, USA.

pressure, with yields, for some terpenes, near unity [e.g., Atkinson *et al.*, 1992; Kroll *et al.*, 2001; Aschmann *et al.*, 2002]. Thus, for ozonolysis experiments, an OH scavenger is often added to the chamber to avoid the confounding effects of simultaneous O₃ and OH oxidation reactions. Recent work has suggested that the choice of OH scavenger influences SOA yield in alkene ozonolysis [Docherty and Ziemann, 2003; Keywood *et al.*, 2004a]. Keywood *et al.* [2004a] determined that the main influence of the scavenger results from the production of HO₂ radicals, altering the HO₂/RO₂ ratio, with higher ratios (ratio from CO > 2-butanol > cyclohexane) resulting in enhanced SOA production. Additionally, the structure of the parent compound, e.g., cyclic or acyclic, determined the sensitivity of SOA yield to the type of OH scavenger used [Jenkin, 2004; Keywood *et al.*, 2004a]. Recently, the predominance of organic peroxides found in monoterpene-generated SOA provided evidence for oligomer formation from heterogeneous reactions between hydroperoxides and aldehydes [Docherty *et al.*, 2005], catalyzed by the acidic component of the aerosol phase [Jang *et al.*, 2002].

[4] Ambient air temperature is known to affect the partitioning of semivolatile oxidation products between the gas and particle phases. Relative humidity has also been shown to affect the yields of nopinone and pinonaldehyde from β -pinene and α -pinene, respectively. The reaction between water and the stabilized C₉-CI resulted in additional formation of nopinone [Winterhalter *et al.*, 1999] or pinonaldehyde [Baker *et al.*, 2001; Warscheid and Hoffmann, 2001], with SOA yields doubling from dry to humid conditions. Additionally, Baker *et al.* [2001] found that the pinonaldehyde formation yield was independent of RH over a range of ~5–50%, suggesting that the Criegee intermediates react dominantly with water, even at relatively low RH values. Numerous other gas-phase oxidation products have been identified from the ozonolysis of terpenes, including low molecular weight products, e.g., formaldehyde, acetone, and formic acid, and higher molecular weight products that are often specific to the parent terpene, such as nopinone and pinonaldehyde, mentioned above, as well as other multifunctional compounds with carbonyl, carboxyl, or hydroxyl groups [e.g., Calogirou *et al.*, 1999, and references therein; Yu *et al.*, 1999a; Jang and Kamens, 1999].

[5] Recent field studies have provided observational support that terpenes can be oxidized within a forest canopy before detection by above-canopy flux techniques. In an orange grove in Spain, β -caryophyllene, a reactive sesquiterpene, was observed in branch enclosures but not in simultaneous measurements above the canopy, suggesting that β -caryophyllene was oxidized within the canopy [Ciccioli *et al.*, 1999]. In a California Ponderosa pine forest, chemical O₃ flux to the ecosystem scaled exponentially with temperature in a similar manner as monoterpenes [Kurpius and Goldstein, 2003], and from the same site, elevated monoterpene fluxes to the atmosphere from the mastication of Ponderosa pine trees [Schade and Goldstein, 2003] resulted in increased chemical O₃ flux to the ecosystem [Goldstein *et al.*, 2004], suggesting a linkage between chemical ozone loss in the canopy and terpene emissions. In subsequent work, Holzinger *et al.* [2005] observed large quantities of previously unmeasured

oxidation products above the same Ponderosa pine forest canopy. In a northern Michigan forest, elevated nighttime OH concentrations correlated with O₃ mixing ratios, suggesting that OH was produced from reactions between O₃ and unmeasured terpenes [Faloona *et al.*, 2001]. From the same forest, higher than expected OH reactivity was observed and scaled exponentially with temperature in a similar manner as biogenic emissions [Di Carlo *et al.*, 2004]. Taken together, these results provide convincing evidence of chemical loss of reactive compounds within the forest canopy through oxidation by OH and O₃.

[6] Here, we report the results from a series of chamber experiments conducted in March and April of 2003, examining the gas-phase oxidation products and gas and particle-phase yields obtained from terpene + O₃ reactions, in the presence of an OH scavenger and ammonium sulfate seed aerosol. The suite of terpene compounds used in these experiments is representative of emissions from Ponderosa pine trees [e.g., Lee *et al.*, 2005] and other terpene-emitting vegetation, [e.g., Kesselmeier and Staudt, 1999; Fuentes *et al.*, 2000; Geron *et al.*, 2000, and references therein]. We focus primarily on the time evolution and yields of gas-phase oxidation products, and propose structures and partial formation mechanisms for many of the observed products from myrcene, terpinolene, and α -terpinene. The gas-phase oxidation products observed from terpene + O₃ experiments, identified by their mass to charge ratio (*m/z*), provided a guide to the interpretation of the oxidation product masses observed in and above the Ponderosa pine forest canopy by PTR-MS [Holzinger *et al.*, 2005]. Additionally, the molar yields of the low molecular weight gas-phase oxidation products, such as formaldehyde, acetaldehyde, formic acid, acetone, and acetic acid, are useful for understanding and modeling the impacts of terpene emissions to the atmosphere. The high variability in yield of gas-phase oxidation products and SOA between the different terpene compounds tested highlights the variable impacts of the different terpenes on regional atmospheric chemistry and suggests that this species variability should be accounted for in models of gas and particle-phase products from terpene oxidation.

2. Experiment

[7] The ozonolysis experiments were conducted at the Caltech Indoor Chamber Facility, which has been described in detail elsewhere [Cocker *et al.*, 2001; Keywood *et al.*, 2004b]. Briefly, the facility consists of two suspended 28 m³ flexible Teflon chambers that maintain atmospheric pressure at all times. Temperature and relative humidity (RH) inside the chamber were measured using combined temperature and RH probes (Vaisala HMP233 series transmitters, Woburn, Massachusetts). The accuracy of the probe is 0.001°C and 2% RH, when calibrated against salt solutions. Experiments were conducted at 20 ± 1°C and <10% RH with a drift within 5% (see Table 2 in section 3.1). O₃ concentrations were measured using an ambient O₃ monitor (Horiba APOA-360, Irvine, California), and calibrated using an internal O₃ generator and N₂ as zero air. The uncertainty in the O₃ measurement was ±3%. These experiments were conducted under low NO_x conditions, with concentrations <5 ppb.

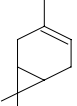
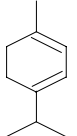
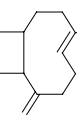
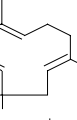
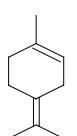
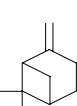
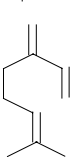
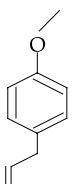
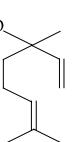
Compound	Structure	Formula	m/z	k_{ozone} ($\text{cm}^3 \text{molec}^{-1} \text{s}^{-1}$)	Description
3-carene		$\text{C}_{10}\text{H}_{16}$	137	3.7×10^{-17}	bicyclic, internal double bond
α -terpinene		$\text{C}_{10}\text{H}_{16}$	137	2.1×10^{-14}	monocyclic, 2 internal double bonds
β -caryophyllene		$\text{C}_{15}\text{H}_{24}$	205	1.16×10^{-14}	bicyclic, 1 internal, 1 external double bond
α -humulene		$\text{C}_{15}\text{H}_{24}$	205	1.17×10^{-14}	monocyclic, 3 internal double bonds
α -pinene		$\text{C}_{10}\text{H}_{16}$	137	8.4×10^{-17}	bicyclic, internal double bond
terpinolene		$\text{C}_{10}\text{H}_{16}$	137	1.9×10^{-15}	monocyclic, 1 internal, 1 external double bond
β -pinene		$\text{C}_{10}\text{H}_{16}$	137	1.5×10^{-17}	bicyclic, 1 external double bond
myrcene		$\text{C}_{10}\text{H}_{16}$	137	4.7×10^{-16}	acyclic, 3 double bonds
methyl chavicol		$\text{C}_{10}\text{H}_{12}\text{O}$	149		aromatic, oxygenated, 1 external double bond
linalool		$\text{C}_{10}\text{H}_{18}\text{O}$	155		acyclic, oxygenated, 2 double bonds

Figure 1. Parent terpene compounds used in the experiments, listed in order of decreasing aerosol production. Rate constants were obtained from *Atkinson and Arey* [2003, and references therein].

[8] Particle size distribution and number concentration were measured separately from each chamber using two cylindrical scanning electrical mobility spectrometers. Particle phase instrumentation and calibration, and generation of ammonium sulfate, $(\text{NH}_4)_2\text{SO}_4$, seed aerosol are described in more detail elsewhere [Keywood *et al.*, 2004b]. The presence of seed aerosol generally suppressed nucleation, and acted as a surface for the condensation of oxidation products, contributing to the measured yield of

secondary organic aerosol. The initial volume of the aerosol was accurately known as the seed aerosol was intentionally prepared within the measurement size range of the SEMS. The starting concentration of seed aerosol was about 20,000 particles cm^{-3} , with a mean diameter of 80–100 nm.

[9] Ten different terpene compounds were reacted in these experiments: six monoterpenes (α -pinene, β -pinene, 3-carene, terpinolene, α -terpinene, and myrcene), two sesquiterpenes (α -humulene and β -caryophyllene), and two

oxygenated terpenes (methyl chavicol, also known as 4-allylanisole, and linalool). Figure 1 lists the structures and m/z of the parent terpenes used and the rate constants for their reactions with ozone (k_{O_3}). Gas-phase concentrations of the parent terpene were monitored using two instruments: a Hewlett Packard gas chromatograph with a flame ionization detector (GC-FID) using a 60 m \times 0.32 μm DB-5 column (J&W Scientific, Davis, California), and a proton transfer reaction mass spectrometer, or PTR-MS (Ionicon Analytik, Innsbruck, Austria) [Lindinger *et al.*, 1998]. Air from the reaction chamber was sampled using SilcoSteel (Restek Corporation, Bellefonte, Pennsylvania) tubing, and pulled through a 2 μm pore size PTFE particulate filter (Pall Corporation, East Hills, New York) before analysis by PTR-MS, which measured parent terpenes as well as gas-phase oxidation products. The PTR-MS is a quadrupole mass spectrometer that uses hydronium ions (H_3O^+) to chemically ionize the compound of interest through a proton transfer reaction. Thus any compound that has a proton affinity higher than that of water can be detected by the PTR-MS, and is identified by its mass to charge ratio (m/z). Because compounds are identified by their molecular weight plus 1 (H^+), the PTR-MS is unable to distinguish between different compounds with the same molecular weight. However, because of the controlled nature of these laboratory chamber experiments, where one terpene at a time is reacted with O_3 , increasing count rates of certain ions are indicative of oxidation products from these reactions. Knowledge of the structures of the parent terpene allows for the deduction of possible identities of the oxidation products from reasonable oxidation mechanisms. However, structurally different oxidation products that have the same mass cannot be distinguished from one another by PTR-MS.

[10] Microliter volumes of individual liquid monoterpenes and oxygenated terpenes were injected into a 250 mL glass bulb and gently heated as a stream of clean air passed through the bulb, vaporizing the terpene and carrying it into the chamber. Cyclohexane was injected in the same way. Because of their high boiling points ($>250^\circ\text{C}$), liquid sesquiterpenes were injected with cyclohexane simultaneously, using the cyclohexane as a carrier for the sesquiterpenes. The starting concentration of the parent hydrocarbon was measured by GC-FID and PTR-MS (monoterpenes), or by PTR-MS (sesquiterpenes and oxygenated terpenes), and was allowed to stabilize before the injection of O_3 initialized the reaction. O_3 was generated using a UV lamp ozone generator (EnMet Corporation, Michigan) and was injected into the chamber at 5 L min^{-1} . The total concentration of O_3 was sufficient to exceed the parent terpene concentration by at least a factor of 3 in each experiment.

2.1. Gas-Phase Measurements and Calibrations

[11] For calibrations, each pure terpene compound was diluted in cyclohexane and injected into a Teflon bag filled to a final volume of 50 L. All parent terpene compounds were obtained from Fluka Chemicals through Sigma-Aldrich (St. Louis, Missouri). The monoterpenes were calibrated from the same Teflon bag simultaneously by GC-FID and PTR-MS, and the sesquiterpenes and oxygenated terpenes were only calibrated using PTR-MS. Calibra-

tion curves were generated from measurements at three different terpene concentrations. The five low molecular weight oxidation products: formaldehyde, acetaldehyde, formic acid, acetone, and acetic acid, and two higher molecular weight oxidation products, nopinone, from β -pinene oxidation, and α -pinene oxide, from α -pinene oxidation, were also calibrated in the PTR-MS using Teflon bags. Nopinone was diluted in cyclohexane before injection into the bag, and the other five oxidation products were diluted in ultrapure water prepared by the Millipore Milli-Q system (Billerica, Massachusetts). Two different Teflon bags were used for the calibrations to separate cyclohexane-based and water-based solutions. The standard error of the slope of the calibration curves for all terpene compounds and (calibrated) oxidation products was $<3\%$, except for α -humulene (standard error $\sim 7\%$), and acetaldehyde (standard error $\sim 4\%$). Additional sources of error include the accuracies of the syringe, the volumetric flask used for the terpene dilutions, and the flow controller, together contributing an uncertainty of 3–5%.

[12] The concentrations of compounds for which pure commercial standards were not available were estimated on the basis of the rate constant (k) of the proton transfer reaction, according to the equation [Lindinger *et al.*, 1998]:

$$[R] = \frac{[RH^+]}{[H_3O^+]_0 kt} \quad (1)$$

where $[R]$ is the unknown concentration of the compound of interest, and $[RH^+]$ is the signal of the protonated compound, $[H_3O^+]$ is the primary ion signal, and t is the reaction time in the drift tube. Because the proton transfer reaction rate constants are not known for all compounds, an estimated rate constant (k) of $2 \times 10^{-9} \text{ cm}^3 \text{ molecule}^{-1} \text{ s}^{-1}$ was used for those compounds without a measured rate constant. The rate constants for the proton transfer reaction of most compounds are generally within $\pm 20\%$ of the estimated k .

[13] Between experiments, the chambers were continuously flushed with clean compressed air that passed through four scrubbing cartridges containing activated carbon, silica gel, Purafil, and molecular sieves, respectively, and a HEPA filter before entering the Teflon chambers. The chambers were flushed for 36 h before the start of an experiment, which reduced O_3 and particle concentrations to below 1 ppb and 100 particles cm^{-3} , respectively. Hydrocarbon concentrations inside the chamber, before the injection of the terpene, were below detection limit for all parent terpenes. Higher background counts from the blank chamber air were observed for the low molecular weight oxidation products, resulting in higher detection limits for those compounds. The detection limit ($1\sigma_{\text{background counts/sensitivity}}$) for the terpenes was <70 ppt, for nopinone: 20 ppt, for acetaldehyde and acetone: <1 ppb, for formic acid and acetic acid: <2 ppb, and for formaldehyde: 4 ppb. Starting concentrations for formaldehyde and formic acid, m/z 31 and 47, respectively, were <10 ppb, calculated from count rate divided by the sensitivity of the PTR-MS to those compounds. The background count rate on m/z 31 does not result from formaldehyde, but rather from interference from other ions, such as the ^{15}N isotope of NO^+ . Additionally, back reactions between protonated formaldehyde

(CH_2OH^+) and H_2O make PTR-MS measurements of formaldehyde in ambient air difficult because of low formaldehyde mixing ratios and high water content of ambient air. Because of the use of relatively dry air in the chamber, and because of the high formaldehyde mixing ratios in the chamber (7–100 ppb), we were able to detect and calibrate for formaldehyde using the PTR-MS. Starting concentrations for acetaldehyde, acetone, and acetic acid were <5 ppb. Background counts were subtracted from the signal for all parent terpenes and oxidation products.

2.2. Cyclohexane Measurements

[14] Cyclohexane was used both as an OH scavenger and as the solvent for diluting pure terpene compounds for calibration. OH yields from the ozonolysis of biogenic terpenes have already been characterized [Aschmann *et al.*, 2002]. Cyclohexane was injected at sufficient concentrations so that the reaction of OH with cyclohexane exceeded that of OH with the terpene by a factor of 100. Cyclohexane was used because, as an alkane, it does not have a proton affinity high enough to be ionized and detected by PTR-MS, so the use of high concentrations of cyclohexane to scavenge OH would not saturate the instrument. However, the m/z 85 ion was detected and produced a linear response in the PTR-MS, but with a sensitivity to the cyclohexane concentration that was 1000 times lower than the sensitivity to monoterpenes. Thus, because of the high concentrations of cyclohexane used during the experiments, cyclohexane was likely detected at m/z 85. Additionally, reaction products from cyclohexane + OH reactions were detected by PTR-MS at significantly higher count rates compared to the terpene + O_3 oxidation products. The main oxidation products observed by PTR-MS from the reaction of cyclohexane + OH occurred at m/z 99 and 100, which indicated the formation of cyclohexanone and its ^{13}C isotope ($\text{C}_6\text{H}_{10}\text{O}$). If any oxidation products from the terpene + O_3 reactions occurred on m/z 99 or 100, those signals would be smaller than and indistinguishable from the cyclohexanone. However, given the structures of the parent terpenes, $\text{C}_{10}\text{H}_{16}$, $\text{C}_{15}\text{H}_{24}$, $\text{C}_{10}\text{H}_{12}\text{O}$, $\text{C}_{10}\text{H}_{18}\text{O}$ (see Figure 1), it seems unlikely that an unfragmented oxidation product from reactions with O_3 would occur significantly at m/z 99, which would require a formula of $\text{C}_6\text{H}_{10}\text{O}$ or $\text{C}_5\text{H}_6\text{O}_2$. Cyclohexanone and cyclohexanol have been identified as the main products from cyclohexane + OH, with yields of 0.53 and 0.35 respectively [Berndt *et al.*, 2003]. Further reaction of cyclohexanol with OH results in additional formation of cyclohexanone with a yield of 0.58 [Berndt *et al.*, 2003]. Cyclohexanol was not detected by PTR-MS at its protonated parent mass (m/z 101), perhaps because the cyclohexanol becomes dehydrated at a 100% efficiency during the proton transfer reaction. The resulting dehydrated ion would occur at m/z 83, which is already swamped by interference from the cyclohexane impurities, thus the cyclohexanol was not quantifiable. The cyclohexoxy radical formed from cyclohexane + OH may also decompose by ring cleavage and isomerize to produce a hydroxy-dicarbonyl ($\text{C}_6\text{H}_{10}\text{O}_3$), with m/z of 131 that would dehydrate in the PTR-MS producing a fragment ion at m/z 113. Because m/z 113 was not observed ubiquitously as a product ion from all experiments, and m/z 131 was not observed as a product from any experiments, we conclude

that the $\text{C}_6\text{H}_{10}\text{O}_3$ hydroxy-dicarbonyl does not interfere with the signal observed at m/z 113. Additionally ozonolysis experiments without the use of cyclohexane were performed on α -pinene and β -pinene, and the yields of m/z 113 from α -pinene with and without cyclohexane were identical ($0.6 \pm 0.1\%$), and for β -pinene was $0.4 \pm 0.1\%$ with cyclohexane and $0.3 \pm 0.1\%$ without cyclohexane.

[15] The purity of the cyclohexane (Sigma-Aldrich, St. Louis, Missouri) used was 99.9%, with a 0.1% impurity that was detected by the PTR-MS predominantly at m/z 83 and 41 (Table 1). Although cyclohexene, occurring at m/z 83, is a likely candidate for the main cyclohexane impurity, the GC-FID did not detect any cyclohexene associated with the cyclohexane. This suggests that cyclohexene was not an impurity from cyclohexane and would not interfere with the terpene ozonolysis experiments. Another possible candidate for the cyclohexane impurity is cyclohexanol, as the ions associated with this compound are expected to be m/z 101 and 83. M/z 101 was not correlated with cyclohexane, thus, if the impurity is indeed cyclohexanol, it would require that the cyclohexanol become dehydrated at 100% efficiency in the PTR-MS. The signals of all additional masses associated with cyclohexane did not change during the terpene ozonolysis, indicating that these compounds were not interfering with the experiments by reacting with ozone and producing additional oxidation products. Masses listed in Table 1 in association with cyclohexane were not observed as fragments of the parent terpene compounds.

3. Results and Discussion

3.1. Aerosol Yields

[16] The initial experimental conditions and SOA yields are stated in Table 2. SOA mass yields from all compounds were calculated from the volumetric yields assuming an average aerosol density of 1.25 g cm^{-3} [Bahreini *et al.*, 2005; Ng *et al.*, 2006]. Yields of SOA varied significantly between the different terpene compounds. The terpene compounds listed in all tables are ordered with respect to decreasing aerosol yield. In general, the presence of an exocyclic double bond resulted in a reduction of SOA yield, compared to a compound with the same carbon number and an endocyclic double bond, supporting the results of Keywood *et al.* [2004b]. Terpene compounds with high aerosol yields (>40%) possessed one or more double bonds internal to the ring structure, such as 3-carene, α -terpinene, α -humulene, and α -pinene. β -caryophyllene, a sesquiterpene, has one internal and one external double bond, similar to terpinolene, but had higher SOA yields likely because of the lower volatility of the higher molecular weight oxidation products. Additionally, the oxidation of terpinolene at the external double bond results in the loss of 3 carbons, increasing the volatility of the terpinolene oxidation products, whereas the oxidation of β -caryophyllene at the external double bond results in the loss of one carbon. The ozonolysis of β -pinene, with one external double bond, resulted in intermediate SOA yields, and the reaction with ozone of the acyclic terpenes (myrcene and linalool) and methyl chavicol, with one external double bond and a benzene ring, resulted in the lowest aerosol yields.

[17] Table 2 compares SOA yields we obtained with those reported in the literature, and lists the OH scavengers and

Table 1. Molecular Weights Associated With Different Compounds Detected by PTR-MS

	<i>m/z</i> (mass + 1)	Structure	Description
Primary signal			
21		H ₂ ¹⁸ OH ⁺	isotope of primary ion
37		H ₂ OH ₂ OH ⁺	primary ion water cluster
Cyclohexane ^a			
39, 40, 41, 43, 44, 53, 56, 57, 58, 69, 83, 84, 85, 86		C ₆ H ₁₀ OH ⁺	cyclohexane + OH oxidation product
Oxidation products from all ozonolysis experiments			
31		CH ₂ OH ⁺	formaldehyde
45		C ₂ H ₄ OH ⁺	acetaldehyde
47		CH ₂ O ₂ H ⁺	formic acid
59		C ₃ H ₆ OH ⁺	acetone
61		C ₂ H ₄ O ₂ H ⁺	acetic acid
3-carene			
81, 82, 137, 138 ^b		C ₁₀ H ₁₆ H ⁺ , C ₆ H ₉ H ⁺	monoterpene, fragments and isotopes
71, 73, 87, 89, 97, 107, 111 ^c , 113 ^c , 115, 123 ^c , 125, 127, 141 ^c , 151, 167, 169 ^d			unidentified oxidation products
α-terpinene			
81, 82, 137, 138		C ₁₀ H ₁₆ H ⁺ , C ₆ H ₉ H ⁺	monoterpene, fragments and isotopes
73, 87, 89, 107, 109, 113 ^c , 115, 123 ^c , 125, 127, 139, 141 ^c , 143, 151, 155 ^c , 157, 167, 171, 183, 185, 201			unidentified oxidation products
β-caryophyllene			
67, 68, 81, 82, 95, 109, 121, 137, 149, 205, 206		C ₁₅ H ₂₄ H ⁺	sesquiterpene, fragments, and isotopes
71, 73, 87, 115, 127, 133, 139, 151, 153, 159 ^c , 177, 197, 219, 223, 237, 253			unidentified oxidation products
α-humulene			
67, 81, 82, 95, 96, 97, 103, 109, 110, 121, 123, 135, 137, 149, 205, 206,		C ₁₅ H ₂₄ H ⁺	sesquiterpene, fragments, and isotopes
71, 73, 115, 125, 127, 129, 141 ^c , 197, 219, 221			unidentified oxidation products
α-pinene			
81, 82, 137, 138		C ₁₀ H ₁₆ H ⁺ , C ₆ H ₉ H ⁺	monoterpene, fragments and isotopes
71, 72, 107, 108, 123 ^c , 151, 152, 169, 170		C ₁₀ H ₁₆ O ₂ H ⁺	uncalibrated oxidation product: pinonaldehyde, fragments, and isotopes ^e
73, 75, 79, 87, 97, 111 ^c , 113 ^c , 115, 117, 125, 127, 129, 133, 139, 141 ^c , 143, 147, 155 ^c , 165, 167, 171, 183, 185			unidentified oxidation products
Terpinolene			
81, 82, 137, 138		C ₁₀ H ₁₆ H ⁺ , C ₆ H ₉ H ⁺	monoterpene, fragments and isotopes
71, 73, 87, 93, 109, 111 ^c , 113 ^c , 115, 125, 127, 129, 141 ^c , 143, 157, 167			unidentified oxidation products
β-pinene			
81, 82, 137, 138		C ₁₀ H ₁₆ H ⁺ , C ₆ H ₉ H ⁺	monoterpene, fragments and isotopes
97, 103, 121, 122, 139, 140, 141 ^c		C ₉ H ₁₄ OH ⁺ , C ₉ H ₁₂ H ⁺	calibrated oxidation product: nopinone, isotopes and fragments
107, 109, 111 ^c , 113, 119, 123 ^c , 125, 129, 153, 155 ^c , 169 ^c , 171, 185			unidentified oxidation products
Myrcene			
81, 82, 137, 138		C ₁₀ H ₁₆ H ⁺ , C ₆ H ₉ H ⁺	monoterpene, fragments and isotopes
71, 73, 75, 79, 93, 97, 111 ^c , 113 ^c , 115, 127, 139			unidentified oxidation products
Methyl chavicol			
149, 150		C ₁₀ H ₁₂ OH ⁺	oxygenated terpene and isotope
109, 115, 121, 125, 137, 151 ^c , 152, 163			unidentified oxidation products
Linalool			
81, 82, 137, 138, 155, 156		C ₁₀ H ₁₈ OH ⁺ , C ₁₀ H ₁₆ H ⁺	oxygenated terpene, fragments, and isotopes
73, 75, 93, 111 ^c , 113 ^c , 115, 127, 128, 129, 130			unidentified oxidation products

^aMasses associated with cyclohexane listed in bold font were >10% of the parent ion *m/z* 85.

^bAll monoterpenes occur predominantly on the parent *m/z* 137 and the fragment *m/z* 81 ions, with a small fraction (<20%) occurring on the ¹³C isotope with *m/z* (138, 82).

^cAsterisks following unidentified oxidation products represent unidentified ions that were observed in the canopy air of a coniferous forest in California by PTR-MS [Holzinger et al., 2005].

^dUnidentified oxidation products in bold font represent ions with >5% yield (on a mole basis) from the parent terpene.

^eFragments were determined from correlations with *m/z* 151 (the dominant pinonaldehyde ion), and agreed well with fragmentation patterns reported elsewhere for pinonaldehyde [Wisthaler et al., 2001].

Table 2. Initial Conditions and SOA Yields Obtained From This Study Compared With Results From Other Dark Ozonolysis Experiments

Temperature, K	RH, %	Δ H _C , ppb	Δ M _o , $\mu\text{g m}^{-3}$	OH Scavenger	SOA Mass Yield, % ^a	Reference
3-carene						
293	6.5	90 ± 3	271 ± 4	cyclohexane	54 ± 2	this work
306			63	2-butanol	13	[Yu <i>et al.</i> , 1999a]
306–310			6–64	2-butanol	8–13	[Griffin <i>et al.</i> , 1999]
290			390	none	76	[Hoffmann <i>et al.</i> , 1997]
α-terpinene						
293	3.4	61 ± 1	164 ± 1	cyclohexane	47 ± 1	this work
β-caryophyllene						
293	6.2	88 ± 4	336 ± 3	cyclohexane	45 ± 2	this work
287–290						
α-humulene						
293	4.5	111 ± 6	415 ± 3	cyclohexane	45 ± 3	this work
α-pinene						
292	4.1	186 ± 8	417 ± 5	cyclohexane	41 ± 2	this work
306–308			40–65	2-butanol	16–19	[Yu <i>et al.</i> , 1999a]
306–308			none	none	16	[Winterhalter <i>et al.</i> , 2003]
303–310			8–65	2-butanol	8–19	[Griffin <i>et al.</i> , 1999]
319–322			38–154	none	14–23	[Hoffmann <i>et al.</i> , 1997]
289			341	none	67	[Hoffmann <i>et al.</i> , 1997]
terpinolene						
293	5.5	112 ± 3	124 ± 2	cyclohexane	20 ± 1	this work
β-pinene						
293	6.3	180 ± 4	174 ± 3	cyclohexane	17 ± 1	this work
306–307			11–19	2-butanol	4–8	[Yu <i>et al.</i> , 1999a]
306–308			12–80	2-butanol	0–5	[Griffin <i>et al.</i> , 1999]
292			97	none	32	[Hoffmann <i>et al.</i> , 1997]
293–295			none	none	26	[Jaoui and Kamens, 2003] ^c
myrcene						
293	6.7	98 ± 3	61 ± 2	cyclohexane	11 ± 1	this work
methyl chavicol						
292	4.5	101 ± 3	40 ± 2	cyclohexane	6 ± 0.4	this work
linalool						
292	4.0	106 ± 5	8 ± 2	cyclohexane	1 ± 0.2	this work
290			39.5	none	8	[Hoffmann <i>et al.</i> , 1997]

^aSOA yields are expressed on a percent mass basis, using the ratio of $\mu\text{g organic aerosol m}^{-3}$ to $\mu\text{g terpene m}^{-3}$, and assuming an aerosol density of 1.25 g cm^{-3} .

^bPercent molar yield from 16 July 2000 experiment, with air temperatures most similar to the work reported here.

^cThese experiments were performed in the daylight in the presence of NO_x .

conditions used for the different experiments. The effect of temperature on SOA production is well known, with higher SOA yields resulting from experiments conducted at lower temperature, however, the compounding effects of temperature, RH, hydrocarbon consumption, and scavenger use make it difficult to compare SOA yield with other experiments. Recently, UV radiation was found to reduce SOA yield from α-pinene ozonolysis by a constant absolute reduction of ~0.03, or 3% [Presto *et al.*, 2005a], which does not affect comparisons with other dark ozonolysis experiments, but is expected to reduce the SOA yield of α-pinene, and perhaps other terpenes, in the ambient atmosphere. Additionally, high NO_x levels in α-pinene ozonolysis experiments were shown to dramatically reduce SOA yields as the $\text{VOC}:\text{NO}_x$ ratio decreased [Presto *et al.*, 2005b], however, its significance to the real atmosphere is site-dependent and may not be applicable to forested or remote regions with low NO_x concentrations.

[18] Jaoui *et al.* [2003] reported a lower SOA yield of 39% from the ozonolysis of β-caryophyllene, without the use of an OH scavenger under slightly lower air temperatures and higher RH (80–85%) than used here. These conditions are both expected to increase SOA yield compared to the yield we observed, however, those experiments

were conducted so that O_3 concentrations were depleted and approached 0 ppm, which may not have allowed for the further oxidation of the reported gas-phase oxidation products that still contained a double bond, suggesting the important contribution of second generation products in SOA yield. Thus perhaps the incomplete ozonolysis of all the gas-phase oxidation products resulted in the lower SOA yield observed by Jaoui *et al.* [2003].

[19] It is notable that the photo-oxidation of sesquiterpenes has been reported to result in a very high SOA yield, even when the photo-oxidation occurred at very high air temperatures. The photo-oxidation of β-caryophyllene resulted in >100% SOA yields at temperatures ranging from 316–322 K [Hoffmann *et al.*, 1997], and SOA yields from β-caryophyllene and α-humulene were ~30–80% under temperatures ranging from 306–310 K [Griffin *et al.*, 1999]. The shorter lifetime of sesquiterpenes with respect to ozone (~1 min at 50 ppb O_3) than OH (30–40 min at $2 \times 10^6 \text{ molecules cm}^{-3}$ OH) suggests that sesquiterpene ozonolysis experiments may be more relevant to the atmosphere since ozone oxidation is likely to be the dominant loss process. The SOA yields from sesquiterpenes presented here, and reported by Jaoui *et al.* [2003], suggest that the ozonolysis of β-caryophyllene results in high (~45%), but not extraordinarily high (~100%), yield

Table 3. Gas-Phase Molar Yields and Carbon Balance (%) for the Ozonolysis Experiments

Terpene	Formaldehyde,% Yield	Acetaldehyde,% Yield	Formic Acid,% Yield	Acetone,% Yield	Acetic Acid, % Yield	UnID, ^a % Yield	C Balance, ^b %
3-carene	25 ± 2	3.9 ± 0.4	11 ± 1	9.5 ± 1	14 ± 1	19 ± 1	55 ± 2
α-terpinene	4 ± 2	1 ± 0.3	9.6 ± 2	6.3 ± 1	9.5 ± 2	31 ± 2	58 ± 4
β-caryophyllene ^c	76 ± 20	0.9 ± 0.3	3.9 ± 1	1.1 ± 0.3	20 ± 5	6.4 ± 0.8	39 ± 2
α-humulene ^c	3.5 ± 1.1	0.9 ± 0.3	0.4 ± 0.2	1.2 ± 0.4	12 ± 1	9.5 ± 0.8	33 ± 2
α-pinene ^d	28 ± 3	2.9 ± 0.3	7.5 ± 0.7	5.9 ± 0.5	8 ± 0.9	15 ± 1	67 ± 3
terpinolene	29 ± 3	9 ± 0.8	4 ± 0.4	44 ± 4	5.8 ± 0.6	81 ± 9	77 ± 13
β-pinene ^d	65 ± 6	2.4 ± 0.2	4 ± 0.4	3.6 ± 0.3	8.6 ± 0.9	20 ± 1	54 ± 3
myrcene	51 ± 5	15 ± 2	3.9 ± 0.4	23 ± 2	5.3 ± 0.5	92 ± 10	69 ± 14
methyl chavicol	61 ± 5	· · ·	11 ± 1	1.1 ± 0.1	2.2 ± 0.3	50 ± 7	55 ± 8
linalool	34 ± 3	14 ± 1	2.5 ± 0.3	16 ± 1	5.1 ± 0.5	92 ± 9	63 ± 13

^aSum of the yields of all product ions (m/z) listed in Table 1.

^bThe carbon balance (%) from identified gas-phase products (formaldehyde, formic acid, acetaldehyde, acetone, nopinone, and pinonaldehyde), plus the yield of the unidentified compounds, assuming a conservative number of C for each observed ion, and from the particle-phase, assuming the SOA is 60% C. The pinonaldehyde yield used for the C balance calculation was the lower-limit yield of 19%.

^cSeed aerosol was not used in the sesquiterpene experiments.

^dFrom α-pinene ozonolysis, the percent molar yield of pinonaldehyde was estimated to range from 19 ± 2% to 34 ± 3% (see text) and the molar yield of α-pinene oxide was 5.4 ± 0.6%. From β-pinene ozonolysis the yield of nopinone from was 17 ± 2%.

of SOA, and may not be considerably higher than the SOA yield from monoterpenes.

3.2. Gas-Phase Yields of Low Molecular Weight Products

[20] Molar yields of gas-phase products are shown in Table 3, and a comparison with yields obtained in other studies is shown in Table 4. Yields were calculated as the slope of the least squares regression between the change in concentration of oxidation product and the change in concentration of the parent hydrocarbon. The uncertainty estimates presented in Table 3 are the standard errors of the estimated slope of the regression that also include the systematic uncertainties described in the Experimental section. For the oxidation products that peaked and decreased with time resulting from further oxidation or partitioning into the particle phase, the linear least squares regressions excluded data points after the peak in concentration. From this work, the highest yields of formaldehyde were observed from the ozonolysis of β-caryophyllene, β-pinene, myrcene, and methyl chavicol. β-caryophyllene, β-pinene, and methyl chavicol each have an external double bond, while myrcene is acyclic, with three double bonds. Conversely, very low formaldehyde yields were observed from α-humulene (3.5 ± 1%) and α-terpinene (4 ± 2%), both with multiple internal double bonds. Yields of acetaldehyde, formic acid, and acetic acid were <20% for all terpene compounds. Formic acid yields from terpene oxidation by OH were reported at <10% [Orlando *et al.*, 2000], however, we are not aware of other studies reporting yields of formic acid, acetic acid, or acetaldehyde from terpene ozonolysis. Acetone yields ranged from 1% from methyl chavicol and β-caryophyllene to 44% from terpinolene. Acetone yields have been reported from several different terpene compounds [Reissell *et al.*, 1999; Orlando *et al.*, 2000], and from β-pinene [Jaoui and Kamens, 2003] and linalool [Shu *et al.*, 1997], and are in reasonable agreement with yields obtained here (Table 4).

[21] Different analytical methods were used to determine the concentrations and yields of the low molecular weight oxidation products from different studies. The concentrations reported here were obtained using calibrations performed on the PTR-MS, however, because compounds are

detected by the PTR-MS according to their mass to charge ratio (m/z), compounds with the same molecular weight are indistinguishable. The calibrations of the parent terpenes and the identified oxidation products (except pinonaldehyde), which used SilcoSteel tubing of a similar length as the tubing used for chamber sampling, corrected for potential losses of sticky compounds, such as the sesquiterpenes, or low molecular weight acids, in the tubing. Thus underestimation of calibrated compounds due to loss in the tubing should be minimal, and concentrations and yields of calibrated compounds reported here should be considered an upper limit, as we operate on the assumption that the entire signal comes from the expected compound without interference. This assumption is likely valid for the parent terpenes and the low molecular weight oxidation products, as relatively few compounds, that might be expected from these oxidation experiments, share the same m/z as formaldehyde (m/z 31), acetaldehyde (m/z 45), formic acid (m/z 47), acetone (m/z 59), and acetic acid (m/z 61). For the larger oxidation products, reported according to their m/z , we cannot determine if one particular compound completely represents an observed oxidation product mass, because different oxidation products can share the same molecular weight, as seen with m/z 153 and 155 from β-pinene ozonolysis (Table 4). Thus the yields observed in this study of unidentified oxidation products, reported according to their m/z , are lower limits of the actual yields of a given m/z . Additionally, the inability to calibrate the higher molecular weight oxidation products against known standards means fragmentation patterns are not fully known, and implies that sticky oxidation products, such as the higher molecular weights acids, might be lost in the tubing and thus underestimated, affecting our ability to close the carbon mass balance of the system (Table 3). Interference by cyclohexane and its oxidation products on several m/z also inhibits our ability to detect terpene oxidation products occurring at those m/z .

[22] Generally, higher partitioning of oxidation products into the particle phase should be balanced by lower partitioning of oxidation products in the gas phase. Table 3 lists the molar yields of unidentified oxidation products and shows the expected general trend of higher molar yields of unidentified gas-phase products from terpenes with lower

Table 4. Comparison of Gas Phase Oxidation Product Yields, on a Percent Mole Basis, Observed in This Study With Results From Other Terpene Ozonolysis Experiments Conducted in the Dark

Product	Product Yield, %, This Work	Product Yield, %, Other Studies	Reference
3-carene			
Acetone	9.5	10	[Orlando et al., 2000]
Acetone	9.5	22–23	[Reissell et al., 1999]
<i>m/z</i> 169	0.3	trace ^a	[Hakola et al., 1994]
α -terpinene			
Acetone	4.4	2–3	[Reissell et al., 1999]
β -caryophyllene			
Formaldehyde	76	80	[Grosjean et al., 1993]
α -pinene			
Acetone	5.9	3	[Orlando et al., 2000]
Acetone	5.9	6–8	[Reissell et al., 1999]
Pinonaldehyde	19–34 ^b	6–18	[Yu et al., 1999a]
Pinonaldehyde	19–34 ^b	14	[Alvarado et al., 1998]
Pinonaldehyde	19–34 ^b	16	[Baker et al., 2001]
Pinonaldehyde	19–34 ^b	19	[Hakola et al., 1994]
Pinonaldehyde	19–34 ^b	23 (dry)	[Warscheid and Hoffmann, 2001]
Pinonaldehyde	19–34 ^b	32 (higher RH)	[Berndt et al., 2003]
Pinonaldehyde	19–34 ^b	42 (lower RH)	[Berndt et al., 2003]
Pinonaldehyde	19–34 ^b	53 (RH ~ 60%)	[Warscheid and Hoffmann, 2001]
<i>m/z</i> 153	5.4 \pm 0.6 ^c	2.1 ^d	[Alvarado et al., 1998]
<i>m/z</i> 153	5.4 \pm 0.6 ^c	3 ^d	[Berndt et al., 2003]
<i>m/z</i> 155	0.3 \pm 0.1	1.1–2.4 ^c	[Yu et al., 1999a]
<i>m/z</i> 171	0.1 \pm 0.02	2.2–9.8 ^f	[Yu et al., 1999a]
<i>m/z</i> 185	0.05 \pm 0.02	0.6–6.6 ^g	[Yu et al., 1999a]
Terpinolene			
Acetone	44	50	[Orlando et al., 2000]
Acetone	44	48–50	[Reissell et al., 1999]
<i>m/z</i> 111, 93	53 \pm 9 ^h	40	[Hakola et al., 1994]
β -pinene			
Formaldehyde	65	42	[Grosjean et al., 1993]
Formaldehyde	65	65 (higher RH)	[Winterhalter et al., 1999]
Formaldehyde	65	77	[Jaoui and Kamens, 2003]
Formaldehyde	65	84 (dry)	[Winterhalter et al., 1999]
Acetone	3.6	0.9	[Orlando et al., 2000]
Acetone	3.6	2–7	[Reissell et al., 1999]
Acetone	3.6	5	[Jaoui and Kamens, 2003]
Nopinone	17	16 (dry)	[Winterhalter et al., 1999]
Nopinone	17	16–17	[Yu et al., 1999a]
Nopinone	17	21	[Jaoui and Kamens, 2003]
Nopinone	17	22	[Grosjean et al., 1993]
Nopinone	17	23 (5% RH)	[Hakola et al., 1994]
Nopinone	17	35 (higher RH)	[Winterhalter et al., 1999]
Nopinone	17	40	[Hatakeyama et al., 1989]
<i>m/z</i> 153	6.1 \pm 1	1.9–4.5 ⁱ	[Jaoui and Kamens, 2003]
<i>m/z</i> 153	6.1 \pm 1	2–8 ^j	[Yu et al., 1999a]
<i>m/z</i> 155	4.7 \pm 1	5.3–8.1 ^k	[Jaoui and Kamens, 2003]
<i>m/z</i> 155	4.7 \pm 1	7–8 ^l	[Yu et al., 1999a]
<i>m/z</i> 171	0.1 \pm 0.03	4.6–14.3 ^f	[Yu et al., 1999a]
<i>m/z</i> 185	1.1 \pm 0.3	0.4–0.6 ^g	[Yu et al., 1999a]
Myrcene			
Formaldehyde	51	26	[Ruppert et al., 1997]
Acetone	23	21	[Reissell et al., 2002]
Acetone	23	25	[Orlando et al., 2000]
Acetone	23	29	[Ruppert et al., 1997]
<i>m/z</i> 75	16 \pm 4 ^m	33–38	[Reissell et al., 1999]
<i>m/z</i> 75	16 \pm 4 ^m	19	[Ruppert et al., 1997]
<i>m/z</i> 111 + 93	49 \pm 8 ⁿ	70	[Reissell et al., 2002]
Linalool			
Formaldehyde	34	36	[Shu et al., 1997]
Acetone	16	21	[Shu et al., 1997]
<i>m/z</i> 127	11 \pm 2	12.6 ^o	[Shu et al., 1997]
<i>m/z</i> 129, 111, 93	50 \pm 9 ^p	85 ^q	[Shu et al., 1997]

^aYield of caronaldehyde.^bEstimated yield (see text).^cUpper limit yield of α -pinene oxide based on the calibrated concentration calculated from *m/z* 153.^dYield of α -pinene oxide.^eYield of norpinonaldehyde.^fYield of norpinonic acid.^gYield of pinonic acid.^hYield of 4-methyl-3-cyclohexenone (C₇H₁₀O = 110 amu).ⁱSum of molar yields of reported products with molecular weight of 152, i.e., 3-oxonopinone, β -pinene oxide, and myrtenol.

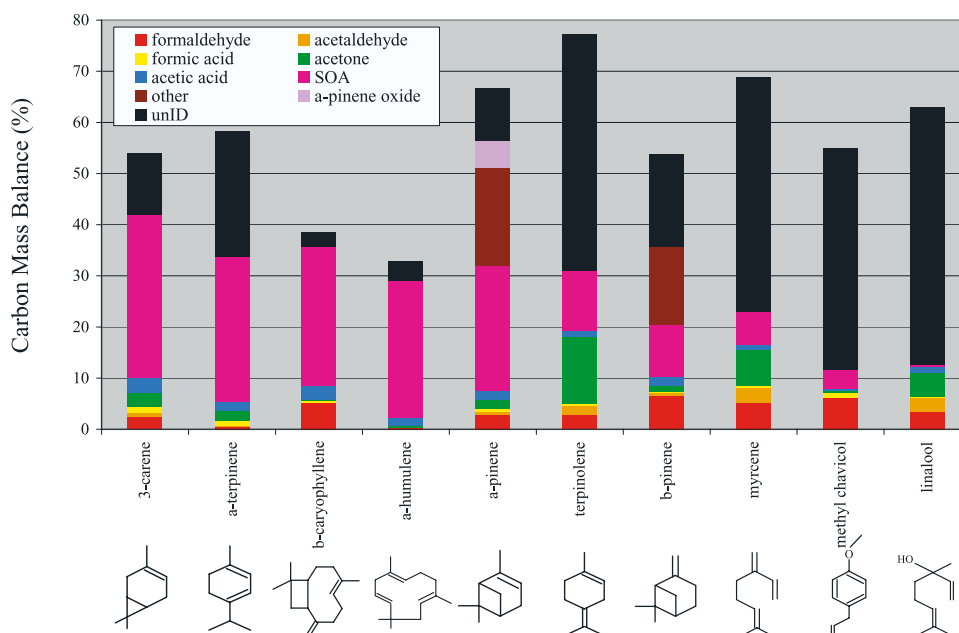


Figure 2. Carbon mass balance for each experiment. SOA was assumed to be 60% C, and carbon numbers were assumed for each unidentified product ion listed in Table 1. For α -pinene, “other” refers to the lower-limit yield of pinonaldehyde, and for β -pinene, “other” refers to nopinone.

SOA yields. The notable exceptions are α - and β -pinene, with low unidentified molar yields because of the identification of pinonaldehyde, α -pinene oxide, and nopinone, the dominant oxidation products, and β -caryophyllene and α -humulene, with very low unidentified m/z yields (<10%) because of fragmentation and loss of the higher molecular weight oxidation products. The carbon balance for each experiment (Table 3 and Figure 2) was calculated by summing the SOA yield, assuming the aerosol is 60% carbon, the yields of the calibrated oxidation products: formaldehyde, acetaldehyde, formic acid, acetone, acetic acid, nopinone and α -pinene oxide, and the estimated oxidation product: pinonaldehyde, and the yields of unidentified compounds, assuming the number of carbons for each oxidation product ion (Table 1). Without including the unidentified ions, we only accounted for 12–56% of the carbon from the reacted terpenes. With the unidentified compound ions included, the carbon balance only increased to 33–77%.

3.3. Gas-Phase Yields of High Molecular Weight Products

[23] We observed a nopinone yield of 17% from β -pinene ozonolysis, which agrees well with yields from other studies, which typically range from 16–22% (Table 4).

The initial reaction between ozone and β -pinene is known to form a primary ozonide (POZ) that decomposes into either a C_1 -Criegee intermediate (CI) + nopinone, or a C_9 -CI + formaldehyde [e.g., Winterhalter *et al.*, 1999, and references therein]. Thus nopinone and formaldehyde represent the only two possible channels for the decomposition of the POZ, and should sum to unity [Winterhalter *et al.*, 1999]. We observed a sum of the two carbonyls of $82 \pm 6\%$, suggesting that we may be underestimating yields of the sum of these two compounds by $\sim 20\%$.

[24] Pinonaldehyde yields from α -pinene ozonolysis were estimated by summing the calculated concentrations of pinonaldehyde-associated ions (Table 1) according to equation (1). The pinonaldehyde fragment ions were determined by finding the m/z that exhibited strong correlations ($R^2 > 0.8$) with m/z 151, the dominant pinonaldehyde ion. These fragment ions are listed in Table 1 and agree well with those described elsewhere [Wisthaler *et al.*, 2001]. Several of the ions reported by Wisthaler *et al.* [2001], m/z 43, 81, and 99 were not well correlated with m/z 151 because of interference from other compounds. Additionally, several ions listed in Table 1, m/z 71, 72, and 109, exhibited highly elevated slopes in the regression against 151 compared to those reported by Wisthaler *et al.* [2001]. Because the pressure of the reaction chamber in the PTR-MS determines

Notes to Table 4.

^jMolar yield of 3-oxonopinone.

^kSum of molar yields of reported products with molecular weight of 154, i.e., 1-hydroxynopinone (4.1%) and 3-hydroxynopinone (3.5%).

^lYield of the hydroxynopinones.

^mYield of hydroxyacetone ($C_3H_6O_2 = 74$ amu).

ⁿYield of 4-vinyl-4-pentenal ($C_7H_{10}O = 110$ amu).

^oYield of 5-ethenyldihydro-5-methyl-2(3H)-furanone ($C_7H_{10}O_2 = 126$ amu).

^pThe sum of m/z 129, 111, and 93 were used in the comparison with the 4-hydroxy-4-methyl-5-hexen-1-al yield and 2-ethenyl-2-methyl-5-hydroxytetrahydrofuran because of the likely dehydration of the hydroxyl and aldehyde groups from the parent (m/z 129) ion in the PTR-MS.

^qYield of 4-hydroxy-4-methyl-5-hexen-1-al ($C_7H_{12}O_2 = 128$ amu).

Table 5. Percent Yield, on a Mole Basis, of Oxidation Product Ions From Terpene Ozonolysis That Were Also Observed in Ambient Air Within a Ponderosa Pine Canopy in California

Terpene	<i>m/z</i> 111	<i>m/z</i> 113	<i>m/z</i> 123	<i>m/z</i> 141	<i>m/z</i> 151	<i>m/z</i> 155	<i>m/z</i> 159	<i>m/z</i> 169
3-carene	1.5 ± 0.3	1 ± 0.2	1.5 ± 0.3	2.4 ± 0.5	0.5 ± 0.1			
α-terpinene		1.3 ± 0.3	2.5 ± 0.6	1.4 ± 0.3	1 ± 0.3	1.2 ± 0.3		1.3 ± 0.3
<i>β-caryophyllene^a</i>							0.3 ± 0.1	
<i>α-humulene^a</i>				0.3 ± 0.1				
α-pinene	0.4 ± 0.1	0.6 ± 0.1		0.7 ± 0.2		0.3 ± 0.1		
Terpinolene	53 ± 9^b	2.8 ± 0.6		0.6 ± 0.1				
β-pinene	1.1 ± 0.3	0.4 ± 0.1	0.5 ± 0.3			4.7 ± 1		0.5 ± 0.1
Myrcene	50 ± 8^b	5.2 ± 1.2						
Methyl chavicol					25 ± 6			
<i>Linalool^a</i>	50 ± 9^c	1.5 ± 0.3						

^aThe terpenes listed in italics have not been measured in the air above the Blodgett Forest canopy. The short lifetime of the two sesquiterpenes, *β-caryophyllene* and *α-humulene* likely affect their detection in ambient air above the canopy, and linalool, typically associated with flowering citrus plants, may not be emitted at all from Blodgett Forest.

^bThe yield of *m/z* 111 represents the sum of the yields from *m/z* 111 and *m/z* 93. Yields listed in bold are yields greater than 10%, and all yields of unidentified product ions represent a lower limit because of lack of knowledge about fragmentation.

^cThe yield of *m/z* 111 represents the sum of the yields of *m/z* 129, 111, and 93.

the degree of fragmentation of the parent compound, we do not expect our fragmentation patterns to be identical to those reported by *Wisthaler et al.* [2001]. We operated the reaction chamber of the PTR-MS at a 2.1 mbar, higher than the 2.0 mbar used by *Wisthaler et al.* [2001]. Thus we expected increased fragmentation of pinonaldehyde, and we accordingly observed a lower proportion of *m/z* 169 to 151, and higher proportions of all other fragments listed in Table 1 to *m/z* 151. The lower-limit pinonaldehyde yield of 19 ± 2% was calculated by summing the concentrations of the ions, *m/z* 107, 108, 123, 151, 152, 169, and 170, that were within 2 times the fractions reported in *Wisthaler et al.* [2001]. The upper limit pinonaldehyde yield of 32 ± 3% includes *m/z* 71, 72, and 109, with proportions relative to *m/z* 151 that were more than three times larger than those reported by *Wisthaler et al.* [2001]. Including the contribution to the total pinonaldehyde signal from *m/z* 43, 81, and 99, using the proportions relative to *m/z* 151 [*Wisthaler et al.*, 2001], would increase the pinonaldehyde yield by ~2%. Our pinonaldehyde yield is quite uncertain, but should be in the range of 19–34%. Both the lower and upper limit yields are within the range of yields reported elsewhere (Table 4).

[25] Yields of pinonaldehyde from α-pinene + O₃ reactions were reported to be higher under high RH by *Warscheid and Hoffmann* [2001], and higher under drier conditions by *Berndt et al.* [2003]. However, pinonaldehyde yields were also found to be relatively independent of water over an RH range of 5–50%, and independent of the OH scavenger (cyclohexane versus 2-butanol) used [*Baker et al.*, 2001]. The experiments reported here were conducted under low RH (4% for α-pinene), relatively low temperatures (293 K), and intermediate starting concentrations of parent terpenes compared to other studies. While our initial conditions are most similar to those of *Yu et al.* [1999a], our estimated pinonaldehyde yield of 19–34% is more similar to the yields obtained under the dry conditions by *Warscheid and Hoffmann* [2001]. The lower-range pinonaldehyde yields reported by *Yu et al.* may be a result of the use of a denuder and derivatization techniques for gas-phase measurements, compared to the direct sampling and analysis using PTR-MS (this study), FT-IR [*Berndt et al.*, 2003], and APCI-MS [*Warscheid and Hoffmann*, 2001].

[26] Yields of the unidentified oxidation products reported according to their *m/z* can be tentatively compared with gas-

phase yields of carbonyls and carboxylic acids reported elsewhere (Table 4). The yields of ions associated with carbonyl compounds generally agree well those from other studies, but our yields of ions from carboxylic acids are lower than those reported elsewhere, likely because tubing losses. A few studies have observed carbonyl, hydroxyl-carbonyl, and acidic monoterpene oxidation products in the gas and particle phase collected from ambient air of a forested environment [*Yu et al.*, 1999b; *Kavouras et al.*, 1999]. Recently *Holzinger et al.* [2005] reported on measurements of oxidation products in the forest canopy using PTR-MS. They identified several ions exhibiting diurnal cycles and vertical profiles in the canopy that are suggestive of oxidation products that partition into the particle phase (nopinone and pinonaldehyde, and *m/z* 105, 123, 155, and 159), or that are formed from rapid oxidation of primary terpene compounds within the forest canopy at Blodgett Forest (e.g., *m/z* 111, 113, 123, and 141) [*Holzinger et al.*, 2005]. Many of these ions were also observed from these terpene ozonolysis experiments, and are followed by an asterisk in Table 1. Of these unidentified compounds in the forest canopy, *m/z* 113 was dominant, with typical mixing ratios of 0.5 ppb at a height of 6–8 m, which was directly above the canopy. The mixing ratios of *m/z* 111 were highest within the forest canopy, typically reaching 0.14 ppb. Table 5 shows that percent yields, on a mole basis, were highest of *m/z* 111 + *m/z* 93 from terpinolene and myrcene, 53 ± 9% and 50 ± 8%, respectively. Yields of *m/z* 113 were much lower, ranging from 1 to 5% from the six different terpenes (Table 5). Although the higher yields of *m/z* 111 than *m/z* 113 from myrcene and terpinolene seems to contradict the higher mixing ratios of *m/z* 113 than 111 observed at Blodgett Forest, the time evolution of these two compounds (Figures 3 and 4) shows that *m/z* 111 was not a stable product, but underwent further oxidation, whereas *m/z* 113 was stable over the course of the experiment, suggesting that *m/z* 111 produced in the canopy would quickly undergo further oxidation, leading to lower mixing ratios in the canopy than expected on the basis of the maximum gas-phase yield. Of the three terpenes with high yields of *m/z* 113, terpinolene, myrcene, and α-terpinene have been reported from Blodgett Forest, but represent a small fraction of the monoterpene emissions measured above the canopy [*Lee et al.*, 2005]. However, above-canopy

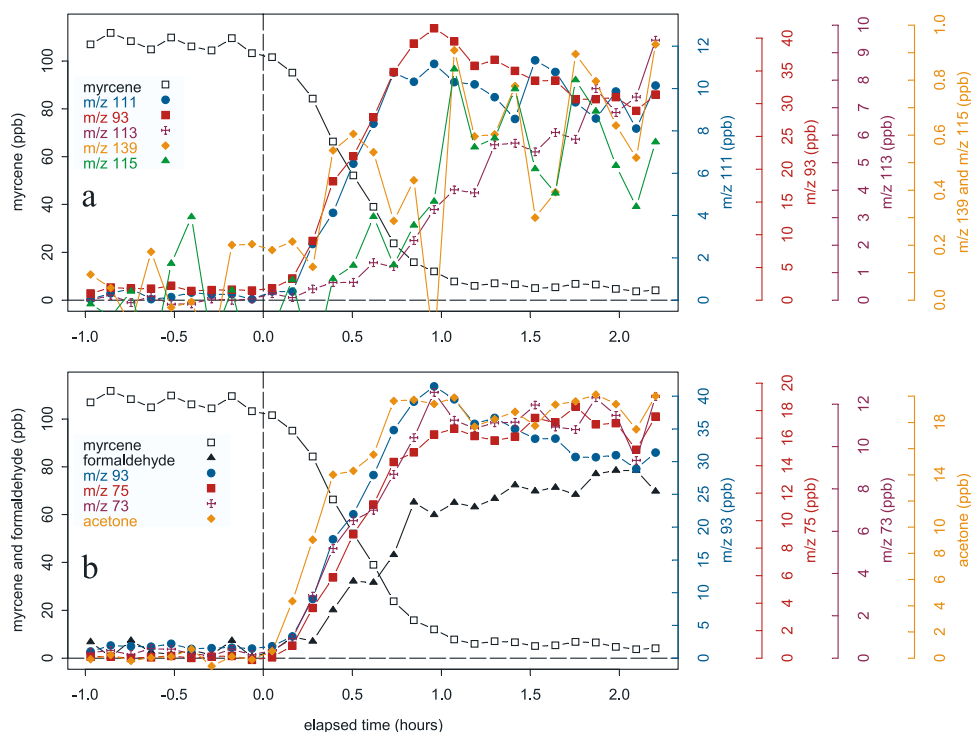


Figure 3. (a) Time series of myrcene ozonolysis and oxidation products for which structures are proposed (Figure 6). (b) Additional product ions, m/z 75 and 73, are also formed quickly, but unlike m/z 93, did not decrease over the course of the experiment.

measurements of concentration and flux only detect the terpene compounds that escape the forest canopy without undergoing within-canopy oxidation. Thus product ions detected inside the forest canopy likely come from the

oxidation of terpene compounds that do not escape the forest canopy, or perhaps escape in small quantities and are detected above the canopy at low mixing ratios. Comparisons between the gas-phase yields of unidentified

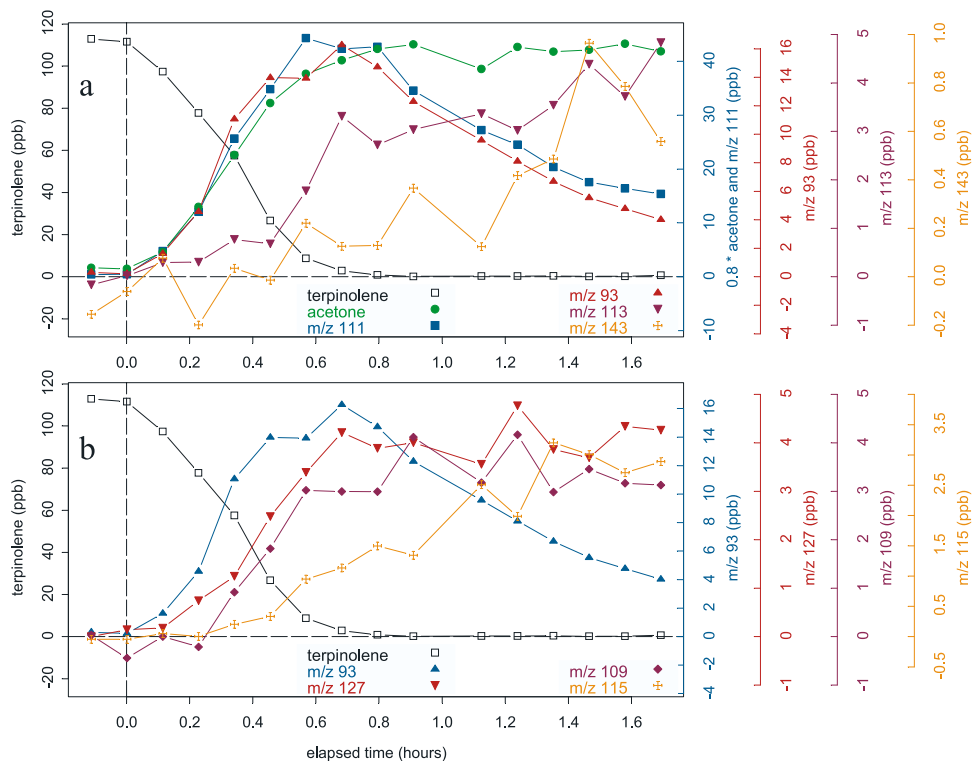


Figure 4. (a) Time series of terpinolene ozonolysis and oxidation product ions for which structures are proposed (Figure 7). (b) Additional product ions, m/z 127, 109, and 115, are formed later than m/z 93.

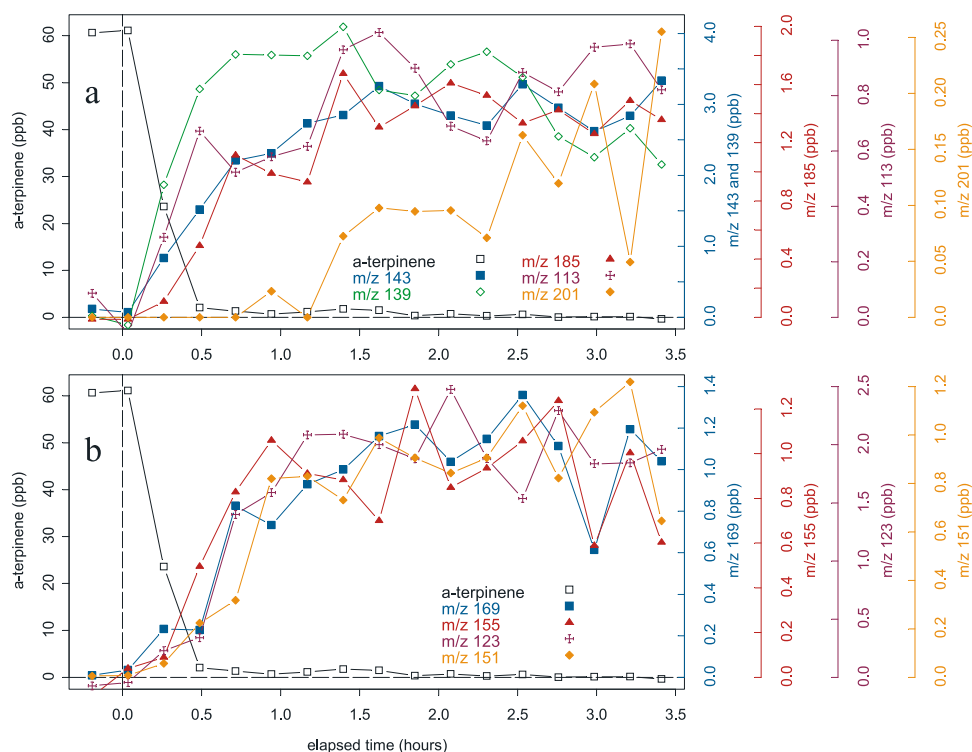


Figure 5. (a) Time series of α -terpinene ozonolysis and oxidation product ions for which structures are proposed (Figure 8). (b) Additional product ions were observed at low concentrations that continued to increase after complete consumption of α -terpinene.

oxidation products observed from these experiments and concentrations of product ions in the forest canopy cannot be quantified without knowledge of the actual emission rates of all terpene compounds in the absence of oxidative chemistry. However, the information in Table 1 of the product ions detected from these ozonolysis experiments, can be qualitatively compared with ions observed in the forest canopy to suggest that those compounds observed in the forest canopy are likely oxidation products from terpene oxidation, and the information in Table 5 can quantitatively confirm that the 10–50% yield estimate used by *Holzinger et al.* [2005] to calculate the original emission rate of precursor terpenes was reasonable. However, a better constrained estimate of the emission rate requires knowledge of the actual mix of very reactive terpene compounds emitted from the forest, since yields of identified and unidentified oxidation products vary significantly between different terpene species (Tables 3 and 5).

[27] Because many oxidation mechanisms and products have been described in detail elsewhere [e.g., *Winterhalter et al.*, 1999; *Baker et al.*, 2001; *Jaoui et al.*, 2003; *Docherty et al.*, 2005], we will focus the time series data on myrcene, terpinolene, and α -terpinene. These monoterpenes are more reactive with O_3 than OH ($\tau_{\text{myrcene}} \sim 28$ min, $\tau_{\text{terpinolene}} \sim 7$ min, and $\tau_{\alpha\text{-terpinene}} \sim 0.6$ min with respect to 50 ppb O_3), were observed in a forested atmosphere [*Lee et al.*, 2005], produced oxidation products with mass to charge ratios that were observed at the same site by *Holzinger et al.* [2005], and represent the spectrum of low, middle, and high yields of SOA. The partial oxidation mechanisms shown for these three compounds are not

intended to be an exhaustive presentation of all oxidation product ions reported in Table 1, nor do they include all possibilities for Criegee intermediates, but rather focus on the dominant oxidation product ions, and the ions that were observed by *Holzinger et al.* [2005].

3.4. Time Evolution of Gas-Phase Products

[28] Figures 3–5 show the time series graphs of myrcene, terpinolene, and α -terpinene, and represent 8–15 min averages of data collected by PTR-MS, depending on the scan time of the particular experiment. Figures 3a, 4a, and 5a show the loss of the parent terpene compound and the rise in concentration of oxidation products for which reasonable structures and mechanisms are suggested in Figure 6–8. Figures 3b, 4b, and 5b show the production of other interesting oxidation product ions for which structures or formation mechanisms could not readily be determined.

3.4.1. Myrcene

[29] The time series of myrcene ozonolysis (Figure 3a) shows multistep oxidation processes in real time: many products are formed quickly (acetone, m/z 111, 93, and 139) and other products are formed more slowly (formaldehyde, m/z 113 and 115). The similar change with time in the concentration of m/z 111 and 93 (linear least squares regression $R^2 = 0.99$), and their 18 amu mass difference, suggest that m/z 93 is a dehydrated fragment of m/z 111. Proposed structures for these product ions are shown in Figure 6. The production of 4-vinyl-4-pentenal (MW = 110 amu) from myrcene oxidation has been reported elsewhere, with a yield, corrected for secondary reactions

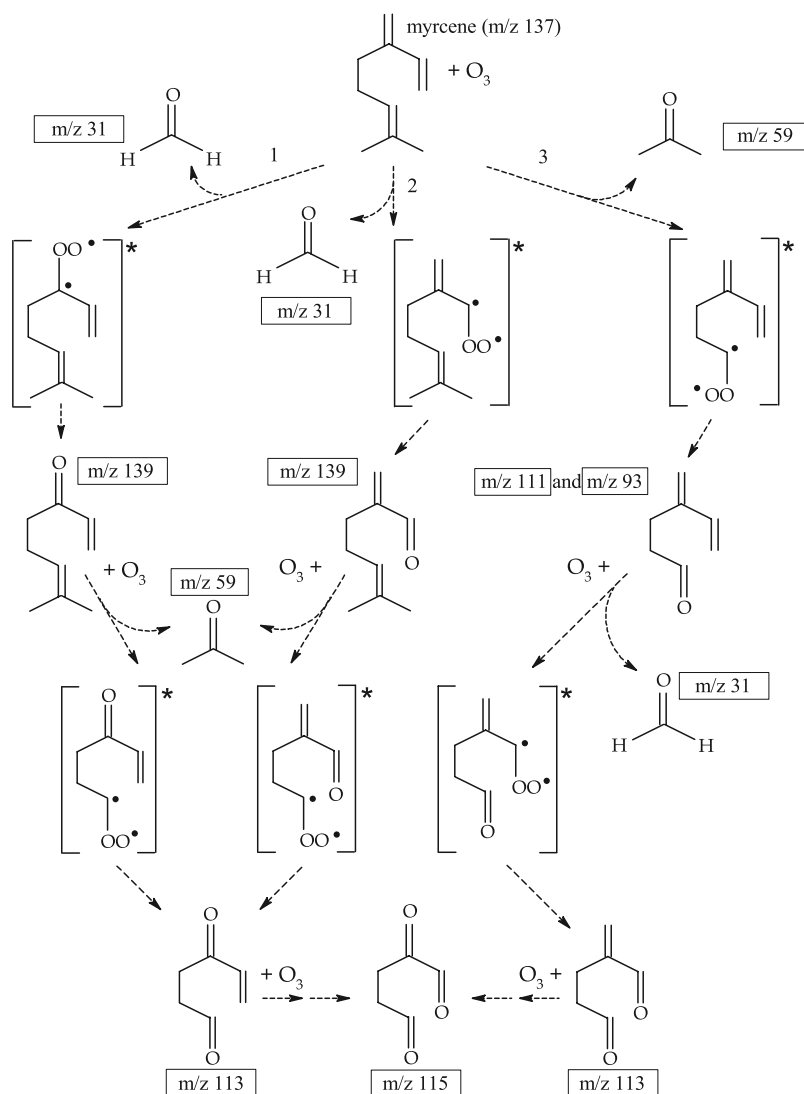


Figure 6. Partial mechanisms and proposed structures of selected oxidation products observed from myrcene ozonolysis. All boxed product ions were observed by PTR-MS. Dotted arrows represent multistep processes that, for clarity, are not illustrated here. Many other product ions were formed (Table 1), but we focus on the dominant products or products observed in ambient air by *Holzinger et al.* [2005].

with ozone, of $70 \pm 13\%$ [Reissell *et al.*, 2002], and corresponds to the structure proposed for m/z 111 + 93 in Figure 6. Corrections for the reactions of 4-vinyl-4-pentenal with ozone [Atkinson *et al.*, 1982] increased our calculated yield by 2%, however, because the rate constant of 4-vinyl-4-pentenal with ozone is assumed and not known, we do not apply this small correction to any of our data. The concentrations of m/z 111 + 93 are significantly higher than of m/z 139, suggesting that the dominant oxidation pathway is ozone attack at the double bond between carbons 6 and 7 (following pathway 3 in Figure 6). Acetone is formed more quickly than m/z 111 + 93 suggesting that the formation of acetone and the C₇-CI from the POZ (Figure 6, pathway 3) dominates over the formation of a C₃-CI and 4-vinyl-4-pentenal. 4-vinyl-4-pentenal can be formed from two pathways: the stabilization of the C₇-CI (Figure 6), and as the primary carbonyl partner in the formation of the C₃-CI (alternative CI from pathway 3 in

Figure 6, not shown). However, an OH yield from myrcene has been reported to be 0.63 [Aschmann *et al.*, 2002], suggesting that the hydroperoxide channel may be favored over stabilization for most of the Criegee intermediates, potentially resulting in less formation of 4-vinyl-4-pentenal from the C₇-CI. Formaldehyde is formed later than acetone and other product ions (Figure 3), suggesting that it is formed from the ozonolysis of first-generation oxidation products. Although Figure 3a does not indicate m/z 113 undergoes further oxidation as suggested in Figure 6, the comparatively short timescale of this particular experiment likely prevented our observation of m/z 113 oxidation. Because m/z 115 was observed coincident with m/z 113, but at much lower concentrations (Figure 3a), the compound observed at m/z 115 likely does not come directly from the oxidation of m/z 113, but from a different, nondominant pathway. Other ions, m/z 73 and 75, are also formed quickly, but unlike m/z 111 and 93, do not decrease over the course

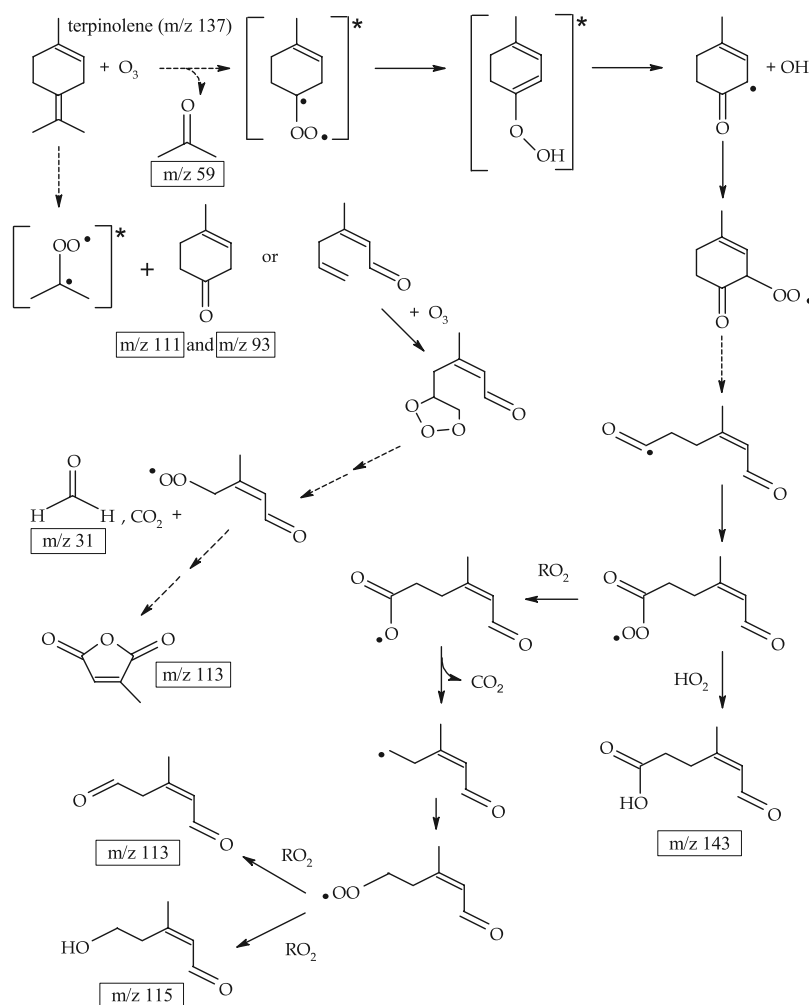


Figure 7. Partial mechanisms for the production of selected oxidation product ions from the ozonolysis of terpinolene. Additional Criegee intermediates and reaction pathways are possible but for clarity are not illustrated here.

of the experiment (Figure 3b). The concentrations of these product ions are significant, reaching 12–20 ppb, but oxidation products from the ozonolysis of myrcene with molecular weights of 72 and 74 amu are not readily determined.

3.4.2. Terpinolene

[30] Figure 4a shows that, like myrcene, ozonolysis of terpinolene produces ions occurring at m/z 111 and 93 that exhibit similar time structures ($R^2 = 0.99$), suggesting again that m/z 93 is the dehydrated fragment of m/z 111. The product 4-methyl-3-cyclohexen-1-one (MW = 110) has been identified from terpinolene oxidation [Hakola *et al.*, 1994]. The similar time series (Figure 4a) and yields of 4-methyl-3-cyclohexen-1-one ($53 \pm 9\%$) and acetone ($44 \pm 4\%$) suggest that acetone is only formed with 4-methyl-3-cyclohexen-1-one. The concentration of m/z 143 is low and highly variable (Figure 4a), suggesting that numerous other products resulted from the C₇-CI. The initial increase in concentration of m/z 113, from 0.2 to 0.6 hours, occurred more slowly than the increase of m/z 111 and 93, remained level from 0.6 to 1.2 hours, then increased again after 1.2 hours, suggesting that different oxidation

products from terpinolene ozonolysis share the same m/z , but were formed at different times. The first increase in m/z 113 may have resulted from the direct ozonolysis of terpinolene, while the second increase in m/z 113 may have resulted from further oxidation of m/z 111 (Figure 7). Potential structures for these product ions from Figure 4a are shown in Figure 7. Figure 4b shows that m/z 93, 109 and 127 all reach their maximum concentrations when terpinolene is fully consumed, but m/z 109 and 127 do not decrease over the course of the experiment. In contrast, m/z 115 continues to increase after all the terpinolene has been consumed. Although m/z 115 and 113 are fairly well correlated ($R^2 = 0.94$), m/z 115 does not show the same initial peak in mixing ratio at ~ 0.6 hours as m/z 113, possibly suggesting that one of the products contributing to m/z 113 is formed through a similar pathway as m/z 115 (Figure 7), whereas the other product is formed more quickly through a different pathway.

3.4.3. α -terpinene

[31] Numerous product ions were observed from α -terpinene ozonolysis (Table 1). Figure 5 shows that α -terpinene is rapidly oxidized (within 30 min), and many product ions

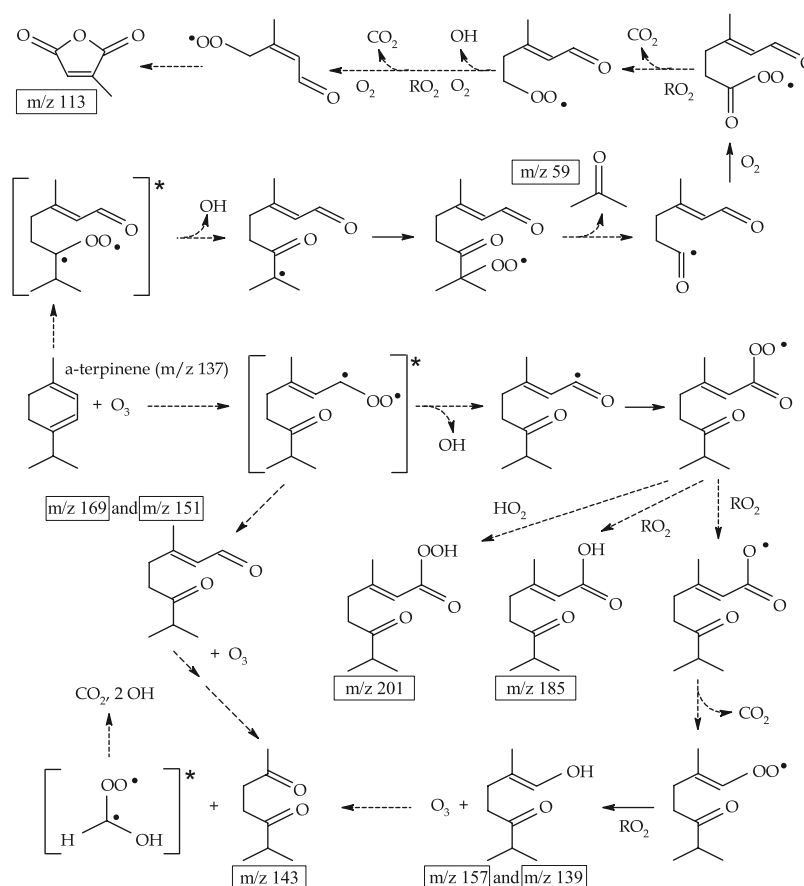


Figure 8. Partial mechanism for the ozonolysis of α -terpinene. Other possibilities for Criegee intermediates and reaction pathways exist but are not shown here.

are formed at low concentrations. Oxidation of α -terpinene is considerably more complicated than myrcene or terpinolene. The highest observed yield of a single ion occurred on m/z 139, with a yield of only $5.9 \pm 1.4\%$. With its two endo double bonds, the ozonolysis of α -terpinene should result in high yields of first generation products and produce low yields of second generation products. However, no product ions were observed at high yields, nor did any of the products, except m/z 139 which decreased by 50% in ~ 2 hours, decrease over the course of the 3.5 hour experiment, suggesting that the dominant first generation products were not detected, and that the observed product ions were likely second generation. Given its endo-double bonds, α -terpinene might be expected to initially form a keto-aldehyde, analogous to pinonaldehyde from α -pinene, that retains one double bond and occurs predominantly at m/z 169 and 151. In fact, m/z 169 and 151 were observed, but they continued to increase in concentration after all the α -terpinene was consumed, and did not decrease over the course of the experiment, suggesting that the observed m/z 169 and 151 were not product ions of “ α -terpinaldehyde”.

[32] Many different Criegee intermediates can be formed from α -terpinene, however, for simplicity we only illustrate three possibilities in Figure 8. In elucidating a mechanism for the formation of m/z 139 that retains a double bond, we could only find a compound occurring at m/z 139 as a

dehydrated fragment of m/z 157, which was observed, but not coincident with m/z 139. M/z 143 can be formed through different pathways from numerous other compounds (e.g., m/z 139, 169, 185, 201), but these secondary formation pathways for m/z 143 are not supported by the time series data. Simultaneous ozonolysis of the conjugated double bonds would form m/z 143 rapidly; however, the formation of a double POZ seems unlikely. The yields of all the gas-phase oxidation product ions are relatively low ($<10\%$), which is consistent with the high SOA yield observed from α -terpinene (Table 2). The observation of m/z 201 was particularly interesting because of its appearance after complete consumption of α -terpinene, and because of its high molecular weight which suggests it may participate in gas-to-particle partitioning. A structure for m/z 205 is suggested in Figure 8, however, the time evolution of m/z 201 and 185 suggest that they are not formed simultaneously, with the observation of m/z 201 occurring nearly one hour after m/z 185. A product occurring at m/z 113 was also observed (Figure 5a) at low concentrations (Table 5). The structure and formation mechanism for this compound is proposed in Figure 8, and is the same structure proposed for m/z 113 from terpinolene ozonolysis. The short lifetime of α -terpinene, its conjugated structure, its high SOA yield, and its production of numerous ions, many of which were observed in the forested atmosphere [Holzinger *et al.*, 2005], without straightforward formation mechanisms,

makes α -terpinene a particularly interesting and relevant monoterpene compound for further study.

4. Conclusions

[33] We conducted ozonolysis experiments on ten different terpene species to measure the time evolution and yields of gas-phase oxidation products and secondary organic aerosol. Yields of formaldehyde, acetone, and a few higher molecular weight oxidation products, such as nopinone, pinaldehyde, and related acids, have been reported in the literature for a limited number of terpenes, and generally are in good agreement with the yields obtained from our experiments. Yields of SOA are also in good agreement with those reported elsewhere from experiments under similar experimental conditions. In addition to yields of previously reported compounds, we report yields of formaldehyde, acetaldehyde, formic acid, acetone, acetic acid, nopinone, α -pinene oxide, pinaldehyde, and numerous other identified and unidentified compounds characterized by their mass to charge ratio, for the entire suite of ten terpene compounds. It is well known that the oxidation of any compound involves multiple steps, and the use of the PTR-MS in these experiments showed, in real time, the evolution of the different ions as first and second generation oxidation products.

[34] The PTR-MS is emerging as an important tool for the measurement of primary and secondary gas-phase compounds in field campaigns. Mass scans of ambient air will undoubtedly measure unidentified compounds, and concurrent or prior measurements of primary emissions at the given site will aid in narrowing the possible identities of the observed ions. Our results confirm that the product ions observed by Holzinger *et al.* [2005] are consistent with terpene ozonolysis reactions. Observations of unidentified products [Holzinger *et al.*, 2005] and knowledge of primary emissions [Lee *et al.*, 2005], together with the results reported here of the identified, tentatively identified, and unidentified oxidation products from primary terpene compounds, aid greatly in understanding the magnitude and significance of within-canopy oxidation. Because the detection of very reactive parent terpene emissions is difficult in ambient air, observations of the ions described in this study can serve as markers for within-canopy chemistry and reactivity. Thus these product ions are likely to be of significant interest to scientists conducting field measurements in atmospheric chemistry, biosphere-atmosphere exchange of volatile organic compounds, and secondary organic aerosol composition. Further experiments to identify the compounds contributing to the unidentified products are necessary and will be more useful to laboratory chemists and kineticists for the elucidation of more complete terpene oxidation mechanisms.

[35] In the real atmosphere, while ozonolysis may be the dominant loss process for some terpenes (i.e., α -terpinene, terpinolene, myrcene, β -caryophyllene, and α -humulene), photo-oxidation may dominate the loss of other terpenes. Thus, to accurately assess the impacts and gas-phase products of terpenes, photo-oxidation experiments were also performed and will be reported elsewhere (A. Lee *et al.*, Gas-phase products and secondary aerosol yields from the photo-oxidation of sixteen different terpenes, submitted to

Journal of Geophysical Research, 2006). The results from both the ozonolysis and photo-oxidation experiments can be used in future modeling efforts and field campaigns to better constrain the contribution of biogenic compounds to SOA production and their impacts on the oxidative capacity of the atmosphere, and to detect the photochemical signatures from emissions of very reactive biogenic VOCs.

[36] **Acknowledgments.** This material is based upon work supported by the National Science Foundation, under grants 0119510 and 0443448, and the California Air Resources Board (contract 00-732). A. Lee was supported by a Graduate Research Education Fellowship from the Department of Energy's Global Change Education Program. The Caltech Indoor Chamber Facility is supported by the U.S. Environmental Protection Agency Science to Achieve Results (STAR) Program, grant RD-83107501-0. The authors are grateful to Jesse H. Kroll for helpful discussions on oxidation mechanisms.

References

- Alvarado, A., E. C. Tuazon, S. M. Aschmann, R. Atkinson, and J. Arey (1998), Products of the gas-phase reactions of O(P-3) atoms and O-3 with alpha-pinene and 1,2-dimethyl-1-cyclohexene, *J. Geophys. Res.*, *103*(D19), 25,541–25,551.
- Aschmann, S. M., J. Arey, and R. Atkinson (2002), OH radical formation from the gas-phase reactions of O-3 with a series of terpenes, *Atmos. Environ.*, *36*(27), 4347–4355.
- Atkinson, R., and J. Arey (2003), Gas-phase tropospheric chemistry of biogenic volatile organic compounds: A review, *Atmos. Environ.*, *37*, S197–S219.
- Atkinson, R., S. M. Aschmann, W. P. L. Carter, A. M. Winer, and J. N. Pitts Jr. (1982), Alkyl nitrate formation from the NO_x-air photooxidations of C2-C8 n-alkanes, *J. Phys. Chem.*, *86*, 4563–4569.
- Atkinson, R., S. M. Aschmann, and J. Arey (1990), Rate constants for the gas-phase reactions of OH and NO₃ radicals and O-3 with sabinene and camphene at 296 ± 2-K, *Atmos. Environ., Part A.*, *24*(10), 2647–2654.
- Atkinson, R., S. M. Aschmann, J. Arey, and B. Shorees (1992), Formation of OH radicals in the gas-phase reactions of O₃ with a series of terpenes, *J. Geophys. Res.*, *97*(D5), 6065–6073.
- Bahreini, R., M. D. Keywood, N. L. Ng, V. Varutbangkul, S. Gao, R. C. Flagan, and J. H. Seinfeld (2005), Measurements of secondary organic aerosol (SOA) from oxidation of cycloalkenes, terpenes, and m-xylene using an Aerodyne aerosol mass spectrometer, *Environ. Sci. Technol.*, *39*, 5674–5688.
- Baker, J., S. M. Aschmann, J. Arey, and R. Atkinson (2001), Reactions of stabilized Criegee intermediates from the gas-phase reactions of O-3 with selected alkenes, *Int. J. Chem. Kinet.*, *34*(2), 73–85.
- Berndt, T., O. Boge, and F. Stratmann (2003), Gas-phase ozonolysis of α -pinene: Gaseous products and particle formation, *Atmos. Environ.*, *37*, 3933–3945.
- Calogirou, A., B. R. Larsen, and D. Kotzias (1999), Gas-phase terpene oxidation products: A review, *Atmos. Environ.*, *33*(9), 1423–1439.
- Ciccio, P., et al. (1999), Emission of reactive terpene compounds from orange orchards and their removal by within-canopy processes, *J. Geophys. Res.*, *104*(D7), 8077–8094.
- Cocker, D. R., R. C. Flagan, and J. H. Seinfeld (2001), State-of-the-art chamber facility for studying atmospheric aerosol chemistry, *Environ. Sci. Technol.*, *35*(12), 2594–2601.
- Di Carlo, P., et al. (2004), Missing OH reactivity in a forest: Evidence for unknown reactive biogenic VOCs, *Science*, *304*(5671), 722–725.
- Docherty, K. S., and P. J. Ziemann (2003), Effects of stabilized Criegee intermediate and OH radical scavengers on aerosol formation from reactions of beta-pinene with O-3, *Aerosol Sci. Technol.*, *37*(11), 877–891.
- Docherty, K. S., W. Wu, Y. B. Lim, and P. J. Ziemann (2005), Contributions of organic peroxides to secondary aerosol formed from reactions of monoterpenes with O-3, *Environ. Sci. Technol.*, *39*(11), 4049–4059.
- Faloon, I., et al. (2001), Nighttime observations of anomalously high levels of hydroxyl radicals above a deciduous forest canopy, *J. Geophys. Res.*, *106*(D20), 24,315–24,333.
- Fuentes, J. D., et al. (2000), Biogenic hydrocarbons in the atmospheric boundary layer: A review, *Bull. Am. Meteorol. Soc.*, *81*(7), 1537–1575.
- Geron, C., R. A. Rasmussen, R. R. Arnts, and A. B. Guenther (2000), A review and synthesis of monoterpene speciation from forests in the United States, *Atmos. Environ.*, *34*, 1761–1781.
- Goldstein, A. H., M. McKay, M. R. Kurpius, G. W. Schade, A. Lee, R. Holzinger, and R. A. Rasmussen (2004), Forest thinning experiment confirms ozone deposition to forest canopy is dominated by reaction with

- biogenic VOCs, *Geophys. Res. Lett.*, *31*, L22106, doi:10.1029/2004GL021259.
- Griffin, R. J., D. R. Cocker, R. C. Flagan, and J. H. Seinfeld (1999), Organic aerosol formation from the oxidation of biogenic hydrocarbons, *J. Geophys. Res.*, *104*(D3), 3555–3567.
- Grosjean, D., E. L. Williams, E. Grosjean, J. M. Andino, and J. H. Seinfeld (1993), Atmospheric oxidation of biogenic hydrocarbons—Reaction of ozone with beta-pinene, D-limonene and trans-caryophyllene, *Environ. Sci. Technol.*, *27*(13), 2754–2758.
- Hakola, H., J. Arey, S. M. Aschmann, and R. Atkinson (1994), Product formation from the gas-phase reactions of OH radicals and O₃ with a series of monoterpenes, *J. Atmos. Chem.*, *18*(1), 75–102.
- Hatakeyama, S., K. Izumi, T. Fukuwama, and H. Akimoto (1989), Reactions of ozone with a-pinene and b-pinene in air: Yields of gaseous and particulate products, *J. Geophys. Res.*, *94*, 13,013–13,024.
- Hoffmann, T., J. R. Odum, F. Bowman, D. Collins, D. Klockow, R. C. Flagan, and J. H. Seinfeld (1997), Formation of organic aerosols from the oxidation of biogenic hydrocarbons, *J. Atmos. Chem.*, *26*(2), 189–222.
- Holzinger, R., A. Lee, K. T. Paw U, and A. H. Goldstein (2005), Observations of oxidation products above a forest imply biogenic emissions of very reactive compounds, *Atmos. Chem. Phys.*, *5*, 1–9.
- Jang, M., and R. M. Kamens (1999), Newly characterized products and composition of secondary aerosols from the reaction of a-pinene with ozone, *Atmos. Environ.*, *33*, 459–474.
- Jang, M. S., N. M. Czoschke, S. Lee, and R. M. Kamens (2002), Heterogeneous atmospheric aerosol production by acid-catalyzed particle-phase reactions, *Science*, *298*(5594), 814–817.
- Jaoui, M., and R. M. Kamens (2003), Gas phase photolysis of pinonaldehyde in the presence of sunlight, *Atmos. Environ.*, *37*(13), 1835–1851.
- Jaoui, M., S. Leungsakul, and R. M. Kamens (2003), Gas and particle products distribution from the reaction of beta-caryophyllene with ozone, *J. Atmos. Chem.*, *45*(3), 261–287.
- Jenkin, M. E. (2004), Modelling the formation and composition of secondary organic aerosol from α - and β -pinene ozonolysis using MCM v3, *Atmos. Chem. Phys.*, *4*, 1741–1757.
- Kavouras, I. G., N. Mihalopoulos, and E. G. Stephanou (1999), Formation and gas/particle partitioning of monoterpenes photo-oxidation products over forests, *Geophys. Res. Lett.*, *26*(1), 55–58.
- Kesselmeier, J., and M. Staudt (1999), Biogenic volatile organic compounds (VOC): An overview on emission, physiology, and ecology, *J. Atmos. Chem.*, *33*, 23–88.
- Keywood, M. D., J. H. Kroll, V. Varutbangkul, R. Bahreini, R. C. Flagan, and J. H. Seinfeld (2004a), Secondary organic aerosol formation from cyclohexene ozonolysis: Effect of OH scavenger and the role of radical chemistry, *Environ. Sci. Technol.*, *38*(12), 3343–3350.
- Keywood, M. D., V. Varutbangkul, R. Bahreini, R. C. Flagan, and J. H. Seinfeld (2004b), Secondary organic aerosol formation from the ozonolysis of cycloalkenes and related compounds, *Environ. Sci. Technol.*, *38*(15), 4157–4164.
- Kroll, J. H., J. S. Clarke, N. M. Donahue, J. G. Anderson, and K. L. Demerjian (2001), Mechanism of HO_x formation in the gas-phase ozone-alkene reaction.1. Direct, pressure-dependent measurements of prompt OH yields, *J. Phys. Chem. A*, *105*(9), 1554–1560.
- Kurpius, M. R., and A. H. Goldstein (2003), Gas-phase chemistry dominates O₃ loss to a forest, implying a source of aerosols and hydroxyl radicals to the atmosphere, *Geophys. Res. Lett.*, *30*(7), 1371, doi:10.1029/2002GL016785.
- Lee, A., G. W. Schade, R. Holzinger, and A. H. Goldstein (2005), A comparison of new measurements of total monoterpene flux with improved measurements of speciated monoterpene flux, *Atmos. Chem. Phys.*, *5*, 505–513.
- Lindinger, W., A. Hansel, and A. Jordan (1998), Proton-transfer-reaction mass spectrometry (PTR-MS): On-line monitoring of volatile organic compounds at pptv levels, *Chem. Soc. Rev.*, *27*(5), 347–354.
- Ng, N. L., J. H. Kroll, M. D. Keywood, R. Bahreini, V. Varutbangkul, R. C. Flagan, J. H. Seinfeld, A. Lee, and A. H. Goldstein (2006), Contribution of first- versus second-generation products to secondary organic aerosols formed in the oxidation of biogenic hydrocarbons, *Environ. Sci. Technol.*, in press.
- Orlando, J. J., B. Noziere, G. S. Tyndall, G. E. Orzechowska, S. E. Paulson, and Y. Rudich (2000), Product studies of the OH- and ozone-initiated oxidation of some monoterpenes, *J. Geophys. Res.*, *105*(D9), 11,561–11,572.
- Pandis, S. N., S. E. Paulson, J. H. Seinfeld, and R. C. Flagan (1991), Aerosol formation in the photooxidation of isoprene and beta-pinene, *Atmos. Environ., Part A*, *25*(5–6), 997–1008.
- Presto, A. A., K. E. Huff Hartz, and N. M. Donahue (2005a), Secondary organic aerosol production from terpene ozonolysis. 1. Effect of UV radiation, *Environ. Sci. Technol.*, *39*, 7036–7045.
- Presto, A. A., K. E. Huff Hartz, and N. M. Donahue (2005b), Secondary organic aerosol production from terpene ozonolysis. 2. Effect of NO_x concentration, *Environ. Sci. Technol.*, *39*, 7046–7054.
- Reissell, A., C. Harry, S. M. Aschmann, R. Atkinson, and J. Arey (1999), Formation of acetone from the OH radical- and O-3-initiated reactions of a series of monoterpenes, *J. Geophys. Res.*, *104*(D11), 13,869–13,879.
- Reissell, A., S. M. Aschmann, R. Atkinson, and J. Arey (2002), Products of the OH radical- and O-3-initiated reactions of myrcene and ocimene, *J. Geophys. Res.*, *107*(D12), 4138, doi:10.1029/2001JD001234.
- Ruppert, L., et al. (1997), Product and aerosol formation from the ozonolysis of monoterpenes, in *Workshop on Biogenic Hydrocarbons in the Atmospheric Boundary Layer*, edited by J. D. Fuentes, pp. 127–130, Univ. of Va., Charlottesville.
- Schade, G. W., and A. H. Goldstein (2003), Increase of monoterpene emissions from a pine plantation as a result of mechanical disturbances, *Geophys. Res. Lett.*, *30*(7), 1380, doi:10.1029/2002GL016138.
- Shu, Y. H., and R. Atkinson (1995), Atmospheric lifetimes and fates of a series of sesquiterpenes, *J. Geophys. Res.*, *100*(D4), 7275–7281.
- Shu, Y., E. S. C. Kwok, E. C. Tuazon, R. Atkinson, and J. Arey (1997), Products from the gas-phase reactions of linalool and OH radicals, NO₃ radicals, and O₃, *Atmos. Environ.*, *31*(3), 896–904.
- Warscheid, B., and T. Hoffmann (2001), On-line measurements of a-pinene ozonolysis products using an atmospheric pressure chemical ionization ion-trap mass spectrometer, *Atmos. Environ.*, *35*, 2927–2940.
- Went, F. W. (1960), Blue Hazes in the Atmosphere, *Nature*, *187*(4738), 641–643.
- Winterhalter, R., P. Neeb, D. Grossmann, A. Kolloff, O. Horie, and G. Moortgat (1999), Products and mechanism of the gas phase reaction of ozone with beta-pinene, *J. Atmos. Chem.*, *35*(2), 165–197.
- Winterhalter, R., R. Van Dingenen, B. R. Larsen, N. R. Jensen, and J. Hjorth (2003), LC-MS analysis of aerosol particles from the oxidation of a-pinene by ozone and OH radicals, *Atmos. Chem. Phys. Disc.*, *3*(1), 1–39.
- Wisthaler, A., N. R. Jensen, R. Winterhalter, W. Lindinger, and J. Hjorth (2001), Measurements of acetone and other gas phase product yields from the OH-initiated oxidation of terpenes by proton-transfer-reaction mass spectrometry (PTR-MS), *Atmos. Environ.*, *35*(35), 6181–6191.
- Yu, J. Z., D. R. Cocker, R. J. Griffin, R. C. Flagan, and J. H. Seinfeld (1999a), Gas-phase ozone oxidation of monoterpenes: Gaseous and particulate products, *J. Atmos. Chem.*, *34*(2), 207–258.
- Yu, J. Z., R. J. Griffin, D. R. Cocker, R. C. Flagan, J. H. Seinfeld, and P. Blanchard (1999b), Observation of gaseous and particulate products of monoterpene oxidation in forest atmospheres, *Geophys. Res. Lett.*, *26*(8), 1145–1148.
- Zhang, S. H., M. Shaw, J. H. Seinfeld, and R. C. Flagan (1992), Photochemical aerosol formation from alpha-pinene and beta-pinene, *J. Geophys. Res.*, *97*(D18), 20,717–20,729.

R. Bahreini, R. C. Flagan, S. Gao, M. D. Keywood, N. L. Ng, J. H. Seinfeld, and V. Varutbangkul, Department of Environmental Science and Engineering, California Institute of Technology, Pasadena, CA 91125, USA.

A. H. Goldstein and A. Lee, Department of Environmental Science, Policy and Management, University of California, Berkeley, CA 94720-3114, USA. (alee@nature.berkeley.edu)

Appendix J

Gas-Phase Products and Secondary Aerosol Yields from the Photooxidation of 16 Different Terpenes^{*}

^{*} This chapter is reproduced by permission from “Gas-Phase Products and Secondary Aerosol Yields from the Photooxidation of 16 Different Terpenes” by A. Lee, A. H. Goldstein, J. H. Kroll, N. L. Ng, V. Varutbangkul, R. C. Flagan, J. H. Seinfeld, *Journal of Geophysical Research-Atmosphere*, 111, D 17305, doi: 10.1029/2006JD007050, 2006. Copyright 2006, American Geophysical Union.



Gas-phase products and secondary aerosol yields from the photooxidation of 16 different terpenes

Anita Lee,¹ Allen H. Goldstein,¹ Jesse H. Kroll,² Nga L. Ng,²
Varuntida Varutbangkul,² Richard C. Flagan,² and John H. Seinfeld²

Received 4 January 2006; revised 18 April 2006; accepted 16 May 2006; published 7 September 2006.

[1] The photooxidation of isoprene, eight monoterpenes, three oxygenated monoterpenes, and four sesquiterpenes were conducted individually at the Caltech Indoor Chamber Facility under atmospherically relevant HC:NO_x ratios to monitor the time evolution and yields of SOA and gas-phase oxidation products using PTR-MS. Several oxidation products were calibrated in the PTR-MS, including formaldehyde, acetaldehyde, formic acid, acetone, acetic acid, nopinone, methacrolein + methyl vinyl ketone; other oxidation products were inferred from known fragmentation patterns, such as pinonaldehyde; and other products were identified according to their mass to charge (*m/z*) ratio. Numerous unidentified products were formed, and the evolution of first- and second-generation products was clearly observed. SOA yields from the different terpenes ranged from 1 to 68%, and the total gas- plus particle-phase products accounted for ~50–100% of the reacted carbon. The carbon mass balance was poorest for the sesquiterpenes, suggesting that the observed products were underestimated or that additional products were formed but not detected by PTR-MS. Several second-generation products from isoprene photooxidation, including *m/z* 113, and ions corresponding to glycolaldehyde, hydroxyacetone, methylglyoxal, and hydroxycarbonyls, were detected. The detailed time series and relative yields of identified and unidentified products aid in elucidating reaction pathways and structures for the unidentified products. Many of the unidentified products from these experiments were also observed within and above the canopy of a Ponderosa pine plantation, confirming that many products of terpene oxidation can be detected in ambient air using PTR-MS, and are indicative of concurrent SOA formation.

Citation: Lee, A., A. H. Goldstein, J. H. Kroll, N. L. Ng, V. Varutbangkul, R. C. Flagan, and J. H. Seinfeld (2006), Gas-phase products and secondary aerosol yields from the photooxidation of 16 different terpenes, *J. Geophys. Res.*, *111*, D17305, doi:10.1029/2006JD007050.

1. Introduction

[2] Biogenic emissions of terpene compounds influence atmospheric chemistry through the formation of tropospheric ozone (O₃) and the production of secondary organic aerosol (SOA). Terpenoids (or isoprenoids) encompass several wide classes of compounds, including hemiterpenes (isoprene, C₅H₈), monoterpenes (C₁₀H₁₆), sesquiterpenes (C₁₅H₂₄), and oxygenated terpenes (e.g. C₁₀H₁₈O, C₁₀H₁₂O). Terpenoids are emitted from deciduous and evergreen trees as a function of temperature, or of both temperature and light [Kesselmeier and Staudt, 1999]. Terpenes, with their unsaturated carbon bonds, are reactive with OH, O₃, and NO₃, the common atmospheric oxidants, with lifetimes that range

from minutes to hours [Atkinson and Arey, 2003]. Several monoterpene oxidation products are known to undergo gas-particle partitioning, including nopinone, pinonaldehyde, pinic acid, and pinonic acid, and have been observed in ambient air in the gas and particle phases [Yu *et al.*, 1999; Kavouras *et al.*, 1999].

[3] Experiments examining terpene oxidation have been conducted since F. W. Went first suggested the blue haze in forested regions were products of these reactions. Early experiments determined rate constants for the reaction of many different terpenes with the major atmospheric oxidants [e.g., Atkinson *et al.*, 1989; Shu and Atkinson, 1994], and yields of SOA [e.g., Pandis *et al.*, 1991; Hoffmann *et al.*, 1997]. Experiments also examined gas-phase products from the oxidation of isoprene [Tuazon and Atkinson, 1990] and common monoterpene species, such as α - and β -pinene [Grosjean *et al.*, 1992; Arey *et al.*, 1990; Hakola *et al.*, 1994], as well as a broader suite of monoterpenes [Shu *et al.*, 1997; Reissell *et al.*, 1999; Orlando *et al.*, 2000]. SOA yield from isoprene has been long thought to be negligible [Pandis *et al.*, 1991]. However, recent observations of tetro

¹Department of Environmental Science, Policy, and Management, University of California, Berkeley, Berkeley, California, USA.

²Department of Environmental Science and Engineering and Department of Chemical Engineering, California Institute of Technology, Pasadena, California, USA.

compounds with an isoprene skeleton [Claeys *et al.*, 2004; Kourtchev *et al.*, 2005] and isoprene oxidation products [Matsunaga *et al.*, 2005] in ambient aerosol suggest that isoprene does contribute to ambient SOA production. Additionally, the high global isoprene emission rate (500 Tg year⁻¹) [Guenther *et al.*, 1995] and the 1–3% SOA yield obtained from the photooxidation of isoprene at lower temperatures and initial isoprene concentrations [Kroll *et al.*, 2005], also suggest that isoprene oxidation may represent an important contribution to global SOA production.

[4] The HC:NO_x ratio has been shown to impact SOA production. Pandis *et al.* [1991] showed that increasing the HC:NO_x ratio increased SOA yield when the ratio was <~10–15 ppb HC: ppb NO_x, but decreased SOA yield at higher ratios. From isoprene photooxidation under high NO_x, SOA yield decreased with increasing NO_x [Kroll *et al.*, 2006]. Experiments with HC:NO_x ratios >8 were reported to increase SOA production from *m*-xylene [Song *et al.*, 2005]. Additionally, higher NO_x levels in the chamber increase O₃ formation, which may impact SOA yield due to possible O₃ reactions. Low HC:NO_x ratios (~3–6 ppb HC: ppb NO_x) are generally representative of ambient air observed above Blodgett Forest, a Ponderosa pine plantation in the Sierra Nevada, California, where typical NO_x concentrations are ~1–2 ppb [Day *et al.*, 2002] and the sum of mixing ratios of all typically measured biogenic and anthropogenic VOCs in ambient air, that have a lifetime on the order of the time scale of these experiments, is ~5–6 ppb [Lamanna and Goldstein, 1999]. Thus, chamber experiments conducted at low HC:NO_x ratios (i.e., high NO_x) may be more applicable to the real atmosphere in forested environments.

[5] Recent studies provide observational support that terpenes can be oxidized within a forest canopy before detection by above-canopy flux techniques. In an orange grove in Spain, β-caryophyllene, a reactive sesquiterpene, was observed in branch enclosures but not in simultaneous measurements above the canopy, suggesting that β-caryophyllene was oxidized within the canopy [Ciccioli *et al.*, 1999]. At Blodgett Forest, chemical O₃ flux to the ecosystem scaled exponentially with temperature in a similar manner as monoterpenes [Kurpius and Goldstein, 2003], and from the same site, elevated monoterpene fluxes to the atmosphere from the mastication of Ponderosa pine trees [Schade and Goldstein, 2003] resulted in increased chemical O₃ flux to the ecosystem [Goldstein *et al.*, 2004], suggesting a linkage between chemical O₃ loss in the canopy and terpene emissions. In subsequent work, Holzinger *et al.* [2005] observed large quantities of previously unmeasured oxidation products above the same pine forest canopy. In a northern Michigan forest, elevated nighttime OH concentrations correlated with O₃ mixing ratios, suggesting that OH was produced from reactions between O₃ and unmeasured terpenes [Faloona *et al.*, 2001]. From the same forest, higher than expected OH reactivity was observed and scaled exponentially with temperature in a similar manner as biogenic emissions [Di Carlo *et al.*, 2004]. Taken together, these results provide convincing evidence of chemical loss of reactive compounds within the forest canopy through oxidation by OH and O₃.

[6] Previously, we reported the yields of SOA and gas-phase products from the ozonolysis of ten terpene com-

pounds [Lee *et al.*, 2006]. Here, we report the results from a series of chamber photooxidation experiments conducted on 16 terpene compounds in the presence of OH, NO_x, hν, and secondarily-produced O₃. Yields of SOA and gas-phase products are presented, as well as the time evolution of selected calibrated gas-phase oxidation products, and gas-phase oxidation products identified by their mass to charge ratio (*m/z*). A more detailed analysis of the contribution of first and second-generation oxidation products to SOA production is presented elsewhere [Ng *et al.*, 2006]. The goal of the PTR-MS measurements of gas-phase oxidation products from the ozonolysis and photooxidation of terpenes is to confirm if ions observed at Blodgett Forest are consistent with terpene oxidation, and to provide a guide to future studies using PTR-MS to monitor secondary gas-phase compounds in ambient air. Here, we present the yields of the observed oxidation product ions, and focus on the two product ions that were dominant at Blodgett Forest, *m/z* 113 and 111.

2. Experiment

[7] The photooxidation experiments were conducted at the Caltech Indoor Chamber Facility, which has been described in detail elsewhere [Cocker *et al.*, 2001; Keywood *et al.*, 2004]. Briefly, the facility consists of two suspended 28 m³ flexible Teflon chambers that maintain atmospheric pressure at all times. For the monoterpene, isoprene, and oxygenated terpene experiments, ammonium sulfate seed aerosol was added to act as a surface for the condensation of oxidation products, contributing to the measured yield of secondary organic aerosol. For the sesquiterpene experiments, no initial seed aerosol was used because nucleation from sesquiterpene oxidation would result in two aerosol modes, making data analysis, particularly the wall loss correction, difficult. The starting concentration of seed aerosol was about 20,000 particles cm⁻³, with a mean diameter of 80–100 nm. SOA yields were calculated from each experiment from the ratio of the amount of SOA formed (assuming density of 1.25 g cm⁻³) and the amount of hydrocarbon reacted. The hydrocarbon to NO_x ratio (HC:NO_x) for all experiments ranged from 0.7–2.2 ppb HC: ppb NO_x. O₃, produced from the photolysis of NO₂ inside the chamber, was measured using an ambient O₃ monitor (Horiba APOA-360, Irvine, CA), and calibrated using an internal O₃ generator and N₂ as zero air.

[8] Microliter volumes of individual liquid monoterpenes and oxygenated terpenes were injected into a 250 mL glass bulb and gently heated as a stream of clean air passed through the bulb, vaporizing the terpene and carrying it into the chamber. The radical precursor used was nitrous acid (HONO), prepared by dropwise addition of 2 mL of 1% NaNO₂ into 15 mL of 10% H₂SO₄ in a glass bulb attached to the chamber. A stream of dry air was passed through the bulb, introducing HONO into the chamber. A NO_x monitor (Horiba APNA-360, Irvine, CA) measured NO and NO₂, which were formed as side products in the preparation of HONO. HONO was detected by the PTR-MS at *m/z* 30, the dehydrated fragment of HONOH⁺, but not at the parent ion *m/z* 48, and also appeared to be detected by the NO_x monitor. However, HONO calibrations were not per-

Table 1. Parent Terpene Compounds, Listed in Order of Decreasing Aerosol Yield

Compound	Structure	Formula (<i>m/z</i>)	k_{OH}^{a} $\text{cm}^3 \text{ molec}^{-1} \text{ s}^{-1}$	Compound	Structure	Formula (<i>m/z</i>)	k_{OH}^{a} $\text{cm}^3 \text{ molec}^{-1} \text{ s}^{-1}$
β -caryophyllene		$\text{C}_{15}\text{H}_{24}$ (205)	2.0×10^{-10}	α -pinene		$\text{C}_{10}\text{H}_{16}$ (137)	5.3×10^{-11}
α -humulene		$\text{C}_{15}\text{H}_{24}$ (205)	3.0×10^{-10}	terpinolene		$\text{C}_{10}\text{H}_{16}$ (137)	2.3×10^{-10}
longifolene		$\text{C}_{15}\text{H}_{24}$ (205)	4.8×10^{-11}	β -pinene		$\text{C}_{10}\text{H}_{16}$ (137)	7.7×10^{-11}
limonene		$\text{C}_{10}\text{H}_{16}$ (137)	1.7×10^{-10}	γ -terpinene		$\text{C}_{10}\text{H}_{16}$ (137)	1.8×10^{-10}
myrcene		$\text{C}_{10}\text{H}_{16}$ (137)	2.1×10^{-10}	α -terpinene		$\text{C}_{10}\text{H}_{16}$ (137)	3.6×10^{-10}
methyl chavicol		$\text{C}_{10}\text{H}_{12}\text{O}$ (149)		verbenone		$\text{C}_{10}\text{H}_{14}\text{O}$ (151)	
3-carene		$\text{C}_{10}\text{H}_{16}$ (137)	8.7×10^{-11}	linalool		$\text{C}_{10}\text{H}_{18}\text{O}$ (155)	1.6×10^{-10}
aromadendrene		$\text{C}_{15}\text{H}_{24}$ (205)		isoprene		C_5H_8 (69)	9.9×10^{-11}

^aRate constants were obtained from *Atkinson and Arey* [2003, and references therein].

formed, so its concentration in the chamber was not well-constrained.

[9] When the seed, parent hydrocarbon, and NO_x concentrations stabilized, turning on the blacklights started the reactions. The indoor chambers were equipped with 276 GE350BL fluorescent blacklights centered at 354 nm, efficiently photolyzing HONO to OH and NO. To minimize temperature increases ($1\text{--}2^\circ\text{C}$ over the course of the experiment), 10% of the lights were used. Between experiments, the chambers were continuously flushed with clean compressed air that passed through four scrubbing cartridges containing activated carbon, silica gel, Purafil, and molecular sieve, respectively, and a HEPA filter before entering the Teflon chambers. The chambers were flushed for at least 36 h before the start of an experiment, which reduced O_3 and particle concentrations to below 1 ppb and 100 particles cm^{-3} , respectively. Hydrocarbon concentrations inside the chamber, before the injection of the terpene, were below detection limit for all parent terpenes.

2.1. Terpene Compounds and Gas-Phase Measurements

[10] Sixteen different terpenoid compounds were reacted in these experiments: isoprene, eight monoterpenes (α -pinene, β -pinene, 3-carene, terpinolene, α -terpinene, myrcene, limonene, γ -terpinene), four sesquiterpenes (α -humulene, β -caryophyllene, longifolene, and aromadendrene), and three oxygenated terpenes (methyl chavicol, also known as 4-allylanisole, linalool, and verbenone). Table 1 lists the structures and molecular weights of the parent terpenes used and the rate constants for their reactions with OH (k_{OH}). Gas-phase concentrations of the parent terpene were monitored using two instruments: a Hewlett

Packard gas chromatograph with a flame ionization detector (GC-FID) using a 60 m \times 0.32 μm DB-5 column (J&W Scientific, Davis, CA), and a proton transfer reaction mass spectrometer, or PTR-MS (Ionicon Analytik, Innsbruck, Austria) [Lindinger *et al.*, 1998]. Air from the reaction chamber was sampled using SilcoSteel (Restek Corporation, Bellafonte, PA) tubing, and pulled through a 2 μm pore size PTFE particulate filter (Pall Corporation, East Hills, NY) before analysis by PTR-MS, which measured parent terpenes as well as gas-phase oxidation products. The PTR-MS is a quadrupole mass spectrometer that uses hydronium ions (H_3O^+) to chemically ionize the compound of interest through a proton transfer reaction. Thus, any compound that has a proton affinity higher than that of water can be detected by the PTR-MS, and is identified by its mass to charge ratio (*m/z*). Because compounds are identified by their molecular weight plus 1 (H^+), the PTR-MS is unable to distinguish between different compounds with the same molecular weight. However, because of the controlled nature of these laboratory chamber experiments, where one terpene at a time is photooxidized, increasing count rates of certain ions are indicative of oxidation products from these reactions. Knowledge of the structures of the parent terpene allows for the deduction of possible identities of the oxidation products from reasonable oxidation mechanisms. However, structurally different oxidation products that have the same mass cannot be distinguished from one another by PTR-MS.

2.2. PTR-MS Calibrations and Concentrations

[11] For calibrations, each pure terpene compound was diluted in cyclohexane and injected into a Teflon bag filled to a final volume of 50 L. Cyclohexane, all parent terpene

Table 2. Molecular Weights Associated With Calibrated Oxidation Products and Sesquiterpenes Detected by PTR-MS

Compound	<i>m/z</i> (mass + 1)	Structure	Description
primary signal	21	H ₂ ¹⁸ OH ⁺	isotope of primary ion
	37	H ₂ OH ₂ OH ⁺	primary ion water cluster
oxidation products	31	CH ₂ OH ⁺	formaldehyde
	45	C ₂ H ₄ OH ⁺	acetaldehyde
common to all photooxidation experiments	47	CH ₂ O ₂ H ⁺	formic acid
	59	C ₃ H ₆ OH ⁺	acetone
β-caryophyllene	61	C ₂ H ₄ O ₂ H ⁺	acetic acid
	67, 68, 81^a, 82, 95, 109, 121, 137, 149, 205, 206 85, 113 ^{c*} , 141, 147, 153, 165, 167, 175, 177, 179, 181, 183, 189, 191, 197, 201, 207, 209, 217, 219, 223, 235, 237, 253 ^b	C ₁₅ H ₂₄ H ⁺	sesquiterpene, fragments, and isotopes unidentified oxidation products
α-humulene	67, 81, 82, 95, 96, 97, 103, 109, 110, 121, 123, 135, 137, 149, 150, 205, 206 57, 71, 73, 75, 83, 85, 87, 89, 99, 101, 115, 125, 127, 129, 133, 139, 141, 151 [*] , 153, 155 [*] , 157, 159 [*] , 161, 169 [*] , 175, 179, 183, 191, 193, 209, 219, 223	C ₁₅ H ₂₄ H ⁺	sesquiterpene, fragments, and isotopes unidentified oxidation products
	longifolene	81, 82, 95, 96, 103, 109, 110, 121, 123, 124, 135, 136, 149, 150, 205, 206, 207 71, 73, 75, 85, 87, 89, 99, 101, 113 [*] , 115, 129, 201, 203, 207, 219, 220^d, 221, 223, 235	C ₁₅ H ₂₄ H ⁺
aromadendrene	95, 96, 103, 109, 110, 121, 123, 124, 135, 136, 149, 150, 163, 205, 206, 207 73, 75, 82, 85, 87, 89, 99, 101, 103, 127, 139, 163, 165, 189, 190^d, 191, 203, 207, 209, 219, 221, 222^d, 223	C ₁₅ H ₂₄ H ⁺	sesquiterpene, fragments, and isotopes unidentified oxidation products

^aIons associated with parent terpenes listed in bold font represent ions >20% of the unfragmented parent terpene.

^bUnidentified oxidation products in bold font are ions with >5% yield (on a mole basis) from the parent terpene.

^cUnidentified oxidation products with asterisks represent ions that were observed at Blodgett Forest using PTR-MS [Holzinger *et al.*, 2005].

^dEven mass-to-charge ratio oxidation products that are not carbon isotopes of other oxidation products are likely gas-phase nitrogen containing products, e.g., organic nitrates.

compounds, and nopinone were obtained from Fluka Chemicals through Sigma-Aldrich (St. Louis, MO). The monoterpenes were calibrated from the same Teflon bag simultaneously by GC-FID and PTR-MS, and the sesquiterpenes and oxygenated terpenes were only calibrated using PTR-MS. Calibration curves were generated from measurements at three different terpene concentrations. Three different cylinder standards (Scott-Marrin Inc., and Apel-Riemer Environmental Inc.) containing ppm-level concentrations of acetaldehyde, acetone, isoprene, methyl vinyl ketone, methacrolein, and 3-methyl furan were diluted at varying flow rates into the inlet air stream sampling clean compressed air for calibrations of the PTR-MS at three concentration levels ranging from ~50–150 ppb. Three low molecular weight oxidation products: formaldehyde, formic acid, and acetic acid, and nopinone, a higher molecular weight oxidation product from β-pinene oxidation, were calibrated in the PTR-MS using Teflon bags. Nopinone was diluted in cyclohexane before injection into the bag, and the other three oxidation products were diluted in ultrapure water prepared by the Millipore Milli-Q system (Billerica, MA). Two different Teflon bags were used for the calibrations to separate cyclohexane-based and water-based solutions. Cyclohexane and its potential impurities are discussed in more detail by Lee *et al.* [2006]. However, because cyclohexane was only used in the standard calibrations, and not used directly in these photooxidation experiments, no interferences from cyclohexane + OH oxidation products are expected. The standard error of the slope of the calibration curves was <6% for formaldehyde, acetaldehyde, 3-methylfuran, 3-carene, and β-pinene, and <3% for

all other terpene compounds and calibrated oxidation products from cylinder standards and Teflon bags. Additional sources of error include the accuracies of the syringe, the volumetric flask used for the terpene dilutions, and the flow controller, together contributing an uncertainty of 3–5%.

[12] The concentrations of compounds for which pure commercial standards were not available were estimated based on the rate constant (*k*) of the proton transfer reaction, according to the equation [Lindinger *et al.*, 1998]:

$$[R] = \frac{[RH^+]}{[H_3O^+]_0 kt} \quad (1)$$

where *[R]* is the unknown concentration of the compound of interest, and *[RH⁺]* is the signal of the protonated compound, *[H₃O⁺]* is the primary ion signal, and *t* is the reaction time in the drift tube. Because the proton transfer reaction rate constants are not known for all compounds, an estimated rate constant (*k*) of 2 × 10⁻⁹ cm³ molecule⁻¹ s⁻¹ was used for those compounds without a measured rate constant. The rate constants for the proton transfer reaction of most compounds are generally within ±20% of the estimated *k*.

[13] Because a pinonaldehyde standard was not available, concentrations were calculated according to Equation (1). Fragments and isotopes associated with pinonaldehyde (Table 2) were determined from correlations with *m/z* 151 (the dominant pinonaldehyde fragment of the unfragmented *m/z* 169), and were compared with the fragments reported by Wisthaler *et al.* [2001]. Because our experiments were conducted at a higher drift tube pressure than Wisthaler *et*

Table 3a. Molecular Weights Associated With the Monoterpenes Detected by PTR-MS

Compound	<i>m/z</i> (mass + 1)	Structure	Description
limonene	69, 81 ^a , 82, 95, 96, 137 , 138 ^b	C ₁₀ H ₁₆ H ⁺ , C ₆ H ₉ H ⁺	monoterpene, fragments and isotopes
	107 ^c , 108, 123 ^{d*} , 124, 133, 151 [*] , 152, 169 [*] , 170	C ₁₀ H ₁₆ O ₂ H ⁺	uncalibrated oxidation product: limononaldehyde, fragments, and isotopes
	139, 140	C ₉ H ₁₄ OH ⁺	uncalibrated oxidation product: limonaketone and isotope
	57, 69, 70, 71, 73, 75 , 77, 83, 85, 87, 89, 93, 97, 99, 101, 103, 109, 111 [*] , 113 [*] , 115, 121, 125, 127, 129, 131, 135, 141 [*] , 143, 149, 153, 155 [*] , 156, 157, 165, 167, 171, 181, 183, 185, 187, 200 ^d , 218 ^d		unidentified oxidation products
myrcene	81 , 82, 137 , 138	C ₁₀ H ₁₆ H ⁺ , C ₆ H ₉ H ⁺	monoterpene, fragments and isotopes
	57, 64 ^c , 65, 71 , 73, 75 , 77, 83 , 85 , 87, 89, 93 , 97, 99, 101, 103, 111 [*] , 113 [*] , 115, 125, 127, 129, 139 [*] , 141, 143, 145, 153, 155 [*] , 159 [*]		unidentified oxidation products
3-carene	81 , 82, 137 , 138	C ₁₀ H ₁₆ H ⁺ , C ₆ H ₉ H ⁺	monoterpene, fragments and isotopes
	107 , 108, 123 [*] , 124, 133, 151 [*] , 152, 169 [*] , 170	C ₁₀ H ₁₆ O ₂ H ⁺	uncalibrated oxidation product: caronaldehyde, fragments, and isotopes
	71, 73, 75, 77, 79, 83, 85, 87, 89, 93 , 94, 97, 99, 101, 103, 107 , 109, 111 [*] , 113 [*] , 115, 121, 123 [*] , 124, 125, 127, 129, 133, 135 , 139 [*] , 141 [*] , 142, 151 [*] , 153 , 155 [*] , 157, 167, 169 [*] , 181, 183		unidentified oxidation products
α -pinene	81 , 82, 137 , 138	C ₁₀ H ₁₆ H ⁺ , C ₆ H ₉ H ⁺	monoterpene, fragments and isotopes
	71 , 72, 99, 107 , 108, 109 , 123 [*] , 151 , 152, 169, 170 ^f	C ₁₀ H ₁₆ O ₂ H ⁺	uncalibrated oxidation product: pinonaldehyde, fragments, and isotopes
	69, 73, 75, 83, 85, 87, 89, 94 ^d , 97, 101, 103, 111 [*] , 113 [*] , 115, 121, 125, 127, 129, 131, 139, 141 [*] , 153, 155 [*] , 157, 165, 167, 171, 183, 185, 200 ^e		unidentified oxidation products

^aIons associated with parent terpenes listed in bold font represent ions >20% of the unfragmented parent terpene.

^bAll monoterpenes occur predominantly on the parent *m/z* 137 and the fragment *m/z* 81 ions, with a small fraction (<20%) occurring on the ¹³C isotope with *m/z* (138, 82).

^cUnidentified oxidation products in bold font are ions with >5% yield (on a mole basis) from the parent terpene.

^dUnidentified oxidation products with asterisks represent ions that were observed in the canopy air of a coniferous forest in California by PTR-MS [Holzinger *et al.*, 2005].

^eEven mass-to-charge ratio oxidation products that are not carbon isotopes of other oxidation products are likely gas-phase nitrogen containing products, e.g., organic nitrates.

^fFragments were determined from correlations with *m/z* 151 (the dominant pinonaldehyde ion) that also agreed well with fragment ions reported elsewhere for pinonaldehyde [Wisthaler *et al.*, 2001]. Additional fragment ions reported by Wisthaler *et al.* [2001], *m/z* 43 and 81, were excluded from the pinonaldehyde concentration due to interference by other compounds.

al. [2001] (~2.2 mbar versus ~2.0 mbar), we expect to observe more fragmentation than reported by Wisthaler *et al.* [2001]. The fragment ions we observed were similar to Wisthaler *et al.* [2001], but *m/z* 151, 152, 169, and 170 represented a smaller proportion of the total pinonaldehyde signal, and *m/z* 43, 72, 99, 108, and 123 represented a larger fraction of the total pinonaldehyde signal. The contribution of the ions *m/z* 71 and 107 were similar to Wisthaler *et al.* [2001]. We did not include the small contribution from *m/z* 81 reported by Wisthaler *et al.* [2001], which was 10% of *m/z* 151, or 3.6% of the total pinonaldehyde signal, because of the interference from α -pinene fragmentation. Additionally, *m/z* 43, 71, and 72 showed time evolutions that deviated from *m/z* 151 towards the end of the experiment, when pinonaldehyde concentrations were decreasing due to further oxidation, suggesting that additional, non-pinonaldehyde compounds were interfering on those mass to charge ratios. Because of the difficulty in determining the pinonaldehyde concentration given the number of fragments and the possibility of interfering compounds, we calculated concentrations in three different ways to estimate a range of likely

pinonaldehyde concentrations. The upper limit mixing ratio, which is likely overestimated, is calculated from the sum of concentrations of all pinonaldehyde-associated ions listed in Table 2. The midrange mixing ratio excludes a contribution from *m/z* 43, 71, and 72, which exhibit time evolutions that significantly deviated from *m/z* 151 as pinonaldehyde decreased. The lower-limit mixing ratio, which is probably underestimated, only includes ions (*m/z* 107, 151, 152, 169, 170) that showed the same rate of decrease in signal as *m/z* 151 during the period when pinonaldehyde was undergoing further oxidation. Thus, pinonaldehyde mixing ratios and yields contain a great deal of uncertainty, which is evidenced in the upper and lower-limit range presented in Tables 6 and 9b. Yields of keto-aldehyde compounds from 3-carene, limonene, α -terpinene, and γ -terpinene were determined similarly, from correlations of other product ions with *m/z* 169 and 151. Similar fragment ions were observed (Tables 3a and 3b).

[14] High background counts from the blank chamber air were observed for the low molecular weight oxidation products, resulting in higher detection limits for those

Table 3b. Molecular Weights Associated With the Monoterpenes Detected by PTR-MS

Compound	<i>m/z</i> (mass + 1)	Structure	Description
terpinolene	81^a , 82, 137 , 138 65, 71, 73, 75, 77, 83, 85, 86 ^d , 87^b , 89, 93 , 97, 98 ^d , 99 , 101, 103, 107, 109, 111^{c*} , 113*, 115, 123, 125, 126, 127, 129, 135, 141*, 143, 149, 159, 167, 169, 183	C ₁₀ H ₁₆ H ⁺ , C ₆ H ₉ H ⁺	monoterpene, fragments and isotopes unidentified oxidation products
β-pinene	81 , 82, 137 , 138 83, 93, 97, 103, 121 , 122, 139 , 140, 141* 69, 71, 73, 79, 83, 85, 89, 93, 99, 101, 107, 108 ^d , 109, 111*, 113*, 115, 123*, 125, 127, 129, 135, 142, 149, 151*, 153, 155*, 157, 165, 167, 169*, 171, 183, 184 ^d , 185, 198 ^d	C ₁₀ H ₁₆ H ⁺ , C ₆ H ₉ H ⁺ C ₉ H ₁₄ OH ⁺ , C ₉ H ₁₂ H ⁺	monoterpene, fragments and isotopes calibrated oxidation product: nopinone, isotopes and fragments unidentified oxidation products
γ-terpinene	81 , 82, 137 , 138 107 , 123* , 124, 151* , 152, 169* , 170 57, 69, 71, 73, 74, 75, 77, 83, 85, 87 , 89, 93 , 97, 99, 101, 102, 103, 105, 107, 109, 111*, 113*, 115 , 125, 127, 129, 131, 133, 135 , 139, 141*, 143, 149, 153, 155*, 157, 159*, 165, 167, 171, 181, 183, 185, 199, 230 ^d	C ₉ H ₁₄ OH ⁺ , C ₉ H ₁₂ H ⁺ C ₁₀ H ₁₆ O ₂ H ⁺	monoterpene, fragments and isotopes uncalibrated oxidation product: γ-terpinaldehyde, fragments, and isotopes unidentified oxidation products
α-terpinene	93, 95, 81 , 82, 135, 137 , 138 107 , 123* , 124, 151* , 152, 169* , 170 65, 69, 71, 73, 75, 77, 87, 89, 97, 99, 101, 103, 109, 111*, 113*, 115, 125, 127, 129, 131, 135, 139 , 141*, 143 , 145, 153, 155*, 157, 158, 159*, 165, 167, 171, 178 ^d , 181, 183, 184 ^d , 185, 199, 201, 202 ^d , 229, 230 ^d	C ₁₀ H ₁₆ H ⁺ , C ₆ H ₉ H ⁺ C ₁₀ H ₁₆ O ₂ H ⁺	monoterpene, fragments and isotopes uncalibrated oxidation product: α-terpinaldehyde, fragments, and isotopes unidentified oxidation products

^aIons associated with parent terpenes listed in bold font represent ions >20% of the unfragmented parent terpene.

^bUnidentified oxidation products in bold font are ions with >5% yield (on a mole basis) from the parent terpene.

^cUnidentified oxidation products with asterisks represent ions that were observed in the canopy air of a coniferous forest in California by PTR-MS [Holzinger *et al.*, 2005].

^dEven mass-to-charge ratio oxidation products that are not carbon isotopes of other oxidation products are likely gas-phase nitrogen containing products, e.g., organic nitrates.

compounds. The detection limit ($1\sigma_{\text{background counts/sensitivity}}$) for the monoterpenes was ~70 ppt, for the sesquiterpenes: ~50 ppt, for the oxygenated terpenes: <50 ppt, for nopinone: 20 ppt, for acetaldehyde and acetone: <0.5 ppb, for formic acid: 1.5 ppb, acetic acid: <1 ppb, and for formaldehyde: 6 ppb. Starting concentrations for formaldehyde and formic acid, *m/z* 31 and 47, respectively, were <10 ppb, calculated from count rate divided by the sensitivity of the PTR-MS to those compounds. The background count rate on *m/z* 31 does not result from formaldehyde, but rather from interference from other ions, such as the ¹⁵N isotope of NO⁺. Additionally, back reactions between protonated formaldehyde (CH₂OH⁺) and H₂O make PTR-MS measurements of formaldehyde in ambient air difficult due to low formaldehyde mixing ratios and high water content of ambient air. Formaldehyde was calibrated up to a concentration of ~80 ppb, which was only exceeded in the myrcene (formaldehyde ~110 ppb) and isoprene (formaldehyde >300 ppb) experiments. Thus, our calculated yields of formaldehyde from myrcene and isoprene are subject to significant errors. Mixing ratios of all other oxidation products, from all experiments, were within the calibrated range. Starting concentrations for acetaldehyde, acetone, and acetic acid were <5 ppb. Background counts were subtracted from the signal for ions monitored. Concentrations of the calibrated oxidation products should be considered upper-

limit values, as other products with the same molecular weight may occur on the *m/z* of the calibrated products. Thus, the formation of, e.g., glycolaldehyde, is indistinguishable from acetic acid, as they both occur at *m/z* 61.

3. Results and Discussion

[15] Table 1 shows the structures and OH rate constants for the 16 terpenes used. The ions (*m/z*) associated with each parent terpene and their oxidation products are detailed in Tables 2–4. Initial conditions are listed for each experiment in Table 5. The HC:NO_x ratios are reported in Table 5 as ppb C: ppb NO_x, and in Table 6 as ppb HC: ppb NO_x. Hydrocarbon oxidation was initiated primarily by OH, formed from the photodissociation of HONO. Other oxidants, O₃ and NO₃, were also formed, but only later in the experiment, after much of the initial NO is depleted (from reactions with peroxy radicals). This typically occurred after almost all (~80%) of the parent hydrocarbon was depleted, so for most experiments O₃ and NO₃ did not react appreciably with the parent hydrocarbon. Possible exceptions were the sesquiterpenes, β-caryophyllene and α-humulene, which react very rapidly with O₃ [Shu and Atkinson, 1994]. Figure 1 shows the time series for O₃, NO, NO₂, and NO_x for a typical experiment (myrcene), where O₃ increases when most of the initial terpene has been depleted, and an

Table 4. Molecular Weights Associated With Other Terpenes Detected by PTR-MS

Compound	<i>m/z</i> (mass + 1)	Structure	Description
methyl chavicol	149^a , 150 65, 71, 73, 75, 85, 89, 97, 99, 101, 103, 109^b , 113, 121 , 123 ^{c*} , 124 ^d , 125, 129, 131, 137 , 151[*] , 153, 163, 165, 168 ^d , 170 ^d , 182 ^d	C ₁₀ H ₁₂ OH ⁺	oxygenated terpene and isotope unidentified oxidation products
verbenone	109 , 110, 123, 133, 151 , 152 69, 71 , 73, 75, 77, 83, 85, 87, 89, 93, 94, 97, 99, 100, 101, 107, 111 [*] , 113[*] , 115, 123 [*] , 124, 125 , 127, 129, 130, 141 [*] , 143, 144, 145, 151 [*] , 152, 153, 159 [*] , 167, 169 [*] , 185, 230 ^d	C ₁₀ H ₁₄ OH ⁺	oxygenated terpene, fragments, and isotopes unidentified oxidation products
linalool	81 , 82, 137 , 138, 155, 156, 60, 69 , 71, 72, 73, 74, 75 , 77, 79, 83 , 85, 87, 89, 93 , 97, 99, 101 , 107, 111[*] , 113 [*] , 115, 123 [*] , 124, 125, 127 , 129 , 141 [*] , 143, 145, 151 [*] , 153, 159 [*] , 167, 169 [*] , 185, 187, 188 ^d	C ₁₀ H ₁₈ OH ⁺ , C ₁₀ H ₁₆ H ⁺	oxygenated terpene, fragments, and isotopes unidentified oxidation products
isoprene	69 , 70 71 , 72 83, 84 57, 63, 65, 73, 75, 77, 79, 85, 86, 87, 89, 97, 99, 101, 103, 105, 113 [*] , 115, 117, 129, 133	C ₅ H ₈ H ⁺ C ₄ H ₆ OH ⁺ C ₅ H ₆ OH ⁺	isoprene and isotope MVK + MACR 3-methyl furan unidentified oxidation products

^aIons associated with parent terpenes listed in bold font represent ions >20% of the unfragmented parent terpene.

^bUnidentified oxidation products in bold font are ions with >5% yield (on a mole basis) from the parent terpene.

^cUnidentified oxidation products with asterisks represent ions that were observed in the canopy air of a coniferous forest in California by PTR-MS [Holzinger *et al.*, 2005].

^dEven mass-to-charge ratio oxidation products that are not carbon isotopes of other oxidation products are likely gas-phase nitrogen containing products, e.g., organic nitrates.

atypical experiment (β -caryophyllene), where O₃ increases after all of the initial terpene has been depleted. The two reactive sesquiterpenes, β -caryophyllene and α -humulene, both show the atypical profile for O₃. This may suggest that the atypical case of delayed O₃ production resulted from titration of O₃ by the parent sesquiterpene and/or first generation oxidation products, which still contain C = C double bonds. For all VOCs, O₃ and NO₃ are expected to react only with unsaturated hydrocarbon oxidation products. Because these products have generally received little study, it is difficult to estimate the relative contributions of OH, O₃, and NO₃ to such chemistry. However, it will be shown for selected terpenes that the formation of most of the major observed oxidation products can be explained using OH chemistry, suggesting that the roles of O₃ and NO₃ reactions are minimal.

[16] Numerous oxidation product ions were produced, many of which have been observed in ambient air within and above Blodgett Forest [Holzinger *et al.*, 2005]. The yields of the oxidation product ions observed in these photooxidation experiments that were also observed by Holzinger *et al.* [2005] are listed in Table 7. In ambient air, *m/z* 113 and 111 were dominant ions, and these ions were observed at low concentrations from all terpenes (*m/z* 113), and from all monoterpenes and a few oxygenated terpenes (*m/z* 111). Yield of *m/z* 113 was highest from myrcene (32%), and yield of *m/z* 111 was highest from terpinolene (29%) and linalool (20%), while aromadendrene did not produce any ions that were observed at Blodgett Forest. The number of oxidation ions observed from these photooxidation experiments is significantly larger than the number of oxidation ions observed from the ozonolysis experiments we conducted previously [Lee *et al.*, 2006]. The mean number of oxidation product ions observed from ozonolysis reactions was 14 ± 5 (mean ± SD) and the mean number of ions observed from photooxidation reactions was

33 ± 6. The PTR-MS was operated under similar conditions for both sets of oxidation experiments, with a drift tube pressure ~2.2 mbar, suggesting that the difference in the number of ions observed is not a result of increased fragmentation of products in the photooxidation experiments. Given the greater versatility of OH attack on the parent terpenes, a greater number of different products formed by photooxidation compared to ozonolysis are expected.

[17] Yields of SOA and gas-phase oxidation products will be discussed according to terpene classification, i.e., sesquiterpenes, monoterpenes, and other terpenes (oxygenated terpenes and isoprene). The gas-phase yields reported in Tables 6–10 were calculated as the slope of the linear least-squares fit of the regression between the product and the parent hydrocarbon. This method was used for both first- and second-generation products. For first-generation products that were further oxidized, only the linear, increasing portion of the regression was considered. Yields of second-generation oxidation products were calculated from a regression line based on an individually-selected time period that most appropriately reflected the production of the individual ion. Although stoichiometric yields of second-generation products are more precisely quantified against their parent compound (the first-generation product oxidized to produce the second-generation product), because first-generation products are generally unidentified, and because the parent terpenes are more commonly and easily measured than first-generation products in the real atmosphere, we report yields of second-generation products as a function of the parent terpenes, rather than their first-generation precursors. The carbon balance was calculated for each experiment as a function of time, and is represented in Figure 2 as an average for a 30–60 minute snapshot at the middle or end of each experiment for the purpose of carbon counting, and does not represent overall the stoi-

Table 5. Comparison of SOA Yields Obtained From This Study With Results From Other Photooxidation Experiments

Terpene	Temp, K	RH, %	ΔHC , ppb	ΔM_o , $\mu\text{g m}^{-3}$	HC:NO_x , ppbC/ppb	SOA Mass Yield, ^g %	Reference
β -caryophyllene	295	56	37 ± 3	212 ± 2	19	68 ± 7	This work
	319 ^d			845, 998	9	103, 125	[Hoffmann et al., 1997]
	308, 309			17–82	3, 8	37–79 ^b	[Griffin et al., 1999]
α -humulene	294	53	46 ± 1	254 ± 2	20	65 ± 1	This Work
	308, 307			13–59	3	32–85 ^b	[Griffin et al., 1999]
longifolene	293	49	34 ± 2	186 ± 2	9	65 ± 1	This work
limonene	294	45	120 ± 2	394 ± 4	11	58 ± 1	This Work
	313, 309			10–120	2, 5	8.7–34	[Griffin et al., 1999]
Myrcene	294	53	112 ± 2	272 ± 3	9	43 ± 1	This Work
	311, 312			3.5, 57.5	2, 4	5.6–6.8	[Griffin et al., 1999]
methyl chavicol	294	49	79 ± 2	194 \pm 2	8	40 ± 1	This work
3-carene	294	52	109 ± 2	236 ± 3	8	38 ± 1	This work
	319, 312 ^d			143, 161	10	23, 27	[Hoffmann et al., 1997]
	310, 312			2.5–99.7	3, 7	2–18 ^b 0.5 ^f	[Griffin et al., 1999]
aromadendrene	294	47	34 ± 1	107 ± 2	21	37 ± 2	This work
α -pinene	293	43	109 ± 1	199 ± 3	12	32 ± 0.1	This work
	298			not given		4–40 ^c	[Noziere et al., 1999]
	?			?		43	[Hatakeyama et al., 1991]
	309–324			1–96	7–15 ^a	43 1–12 ^d ~32–45 ^e	[Hoffmann et al., 1997] [Jaoui and Kamens, 2001]
terpinolene	294	50	110 ± 5	190 ± 4	11	31 ± 2	This Work
	313, 316			25–133	3, 4	1.5–4.1	[Griffin et al., 1999]
β -pinene	293	50	170 ± 5	293 ± 4	21	31 ± 1	This work
	307–317			153	9 ^a	30	[Hoffmann et al., 1997]
	297–304				21.1	20.9	[Jaoui and Kamens, 2003b]
	316, 313			7–141	7, 6	3–27 ^b 1.8 ^f	[Griffin et al., 1999] [Larsen et al., 2001]
γ -caryophyllene	294	48	118 ± 6	193 ± 3	11	29 ± 2	This Work
α -terpinene	312, 311	47	103 ± 1	21, 66	5, 4	9.8–16	[Griffin et al., 1999]
	293			20, 74	3, 5	8.2–17.5	[Griffin et al., 1999]
Verbenone	294	46	105 ± 2	127 ± 2	11	19 ± 0.4	This work
linalool	295	40	124 ± 2	104 ± 4	10	13 ± 0.3	This work
	320, 318 ^d			19, 137	11, 9	4.2, 9.8	[Hoffmann et al., 1997]
	312			26.7	2	5.6	[Griffin et al., 1999]
isoprene	294	54	506 ± 33	26 ± 1	9	2 ± 0.1	This work
	~293			25–500	0.5–30	0.1–1.8	1–3

^aThe reported hydrocarbon to NO_x ratio includes propene, used as the photochemical initiator.

^bThe range reported here represent the lowest and highest yields from a series of experiments, with the corresponding temperatures, ΔM_o , and hydrocarbon to NO_x ratios.

^cAssumed aerosol density of 1 g cm^{-3} . The range of aerosol yield results from several different experiments with higher yields observed from higher initial α -pinene concentrations.

^dFrom nine different experiments. Average of reported range of temperatures.

^eAerosol yields are reported as the maximum carbon yield (19–27%). To convert to total SOA mass yield for comparison with other experiments, we assumed the aerosol was 60% carbon.

^fPercent molar yield of identified carboxylic acids and carbonyls in the aerosol phase.

^gSOA yields are expressed on a percent mass basis, using the ratio of $\mu\text{g organic aerosol m}^{-3}$ to $\mu\text{g parent terpene m}^{-3}$, assuming an aerosol density of 1.25 g cm^{-3} .

chiometric yields (Tables 6–10). The estimated carbon balance from all experiments ranged from $52 \pm 5\%$ to $138 \pm 55\%$, with considerable uncertainties associated with the assignment of carbon number for each unidentified ion, as well as uncertainty from the calibration of parent terpenes and oxidation products, and the collisional rate constant. Although we assumed SOA was 60% carbon (based on the %C of pinic acid), this number is uncertain and may vary for each experiment, and likely affected the total carbon balance by elevating it, resulting in carbon balances for some experiments $>100\%$. The carbon balances for each experiment are shown in Figure 2, and because of the large uncertainty associated with the mass balance, reflect a qualitative assessment of the ability of the PTR-MS to

detect the unidentified compounds according to their m/z . Clearly, the products formed from sesquiterpene photooxidation are not as readily detected by PTR-MS as the products from the photooxidation of other terpenes.

[18] Product yields from other studies are also compared with the results obtained from these experiments (Tables 8 and 9a–9c), however, other experiments often use different radical precursors, such as CH_3ONO , NO_2 , or H_2O_2 , which may impact gas-phase and SOA yields. Thus, these comparisons are included to simply present the range of yields observed elsewhere under different experimental conditions. In addition to carbonyls and acids, these photooxidation experiments in the presence of NO_x should be expected to produce organic nitrates. Theoretical calculations have sug-

Table 6. Gas-Phase Yields From Terpene Photooxidation Experiments

Terpene	$\frac{HC}{NO_x}$ ^a	CH ₂ O ^b % Yield	C ₂ H ₄ O % Yield	CH ₂ O ₂ % Yield	C ₃ H ₆ O % Yield	C ₂ H ₄ O ₂ % Yield	UnID ^c % Yield	Total C Balance, ^d %
β-caryophyllene	1.3	42 ± 10	0.6 ± 0.2	6.2 ± 2	1.5 ± 0.4	8.7 ± 2	22 ± 1	62 ± 5
α-humulene	1.4	—	0.2 ± 0.1	6.1 ± 0.8	2.4 ± 0.3	7.5 ± 0.7	54 ± 3	77 ± 9
longifolene	0.8	25 ± 3	3.7 ± 0.4	31 ± 3	3.8 ± 0.3	15 ± 1	30 ± 2	62 ± 7
limonene	1.1	43 ± 5	0.7 ± 0.1	5.0 ± 0.6	0.4 ± 0.1	3.2 ± 0.4	61 ± 3 ^e	113 ± 17
myrcene	0.9	74 ± 8^f	0.7 ± 0.1	4.5 ± 0.5	22 ± 2	3.9 ± 0.4	134 ± 10	100 ± 17
methyl chavicol	0.8	52 ± 6	0.7 ± 0.1	7.9 ± 1	0.7 ± 0.1	25 ± 2^g	121 ± 11	101 ± 20
3-carene	0.8	35 ± 4	1.6 ± 0.2	5.4 ± 0.6	9.3 ± 0.9	5.1 ± 0.6	95 ± 5 ^h	138 ± 55
aromadendrene	1.4	65 ± 8	2.9 ± 0.3	12 ± 2	4.8 ± 0.5	4.1 ± 0.4	69 ± 7	74 ± 14
α-pinene	1.1	16 ± 2	1.4 ± 0.2	4.5 ± 0.5	6.3 ± 0.6	3.4 ± 0.4	91 ± 14 ⁱ	100 ± 7
terpinolene	1.1	23 ± 3	0.7 ± 0.1	3.5 ± 0.7	20 ± 2	1 ± 0.2	109 ± 8	87 ± 18
β-pinene ^j	2.1	49 ± 6	0.6 ± 0.1	8.2 ± 0.7	7.9 ± 0.7	1.4 ± 0.1	26 ± 1	52 ± 5
γ-terpinene	1.1	17 ± 2	1.2 ± 0.2	8.3 ± 0.8	5.3 ± 0.5	4.5 ± 0.5	130 ± 10 ^k	112 ± 28
α-terpinene	1.0	7.8 ± 2	0.7 ± 0.1	6.1 ± 1	3.1 ± 0.4	2 ± 0.3	61 ± 4 ^l	123 ± 40
verbenone	1.1	32 ± 2	2.1 ± 0.3	8 ± 0.8	13 ± 1	6.9 ± 0.6	92 ± 4	79 ± 17
linalool	1.0	43 ± 5	1.1 ± 0.1	3.2 ± 0.4	25 ± 2	17 ± 2 ^g	144 ± 11	104 ± 25
isoprene ^m	1.8	160 ± 19^f	1.9 ± 0.3	4.6 ± 0.6	0.4 ± 0.1	5.7 ± 0.7 ^g	15 ± 1	101–114 ± 22

^aInitial hydrocarbon (ppb parent terpene) to NO_x (ppb NO + NO₂) ratio of the experiment.

^bGas-phase yields of CH₂O (formaldehyde), C₂H₄O (acetaldehyde), CH₂O₂ (formic acid), C₃H₆O (acetone), and C₂H₄O₂ (acetic acid), are expressed on a percent mole basis. Product yields >20% are listed in bold.

^cUnidentified molar yields does not include the identified but uncalibrated ions associated with the dominant aldehydes formed from limonene, 3-carene, α-pinene, α-terpinene, and γ-terpinene (Table 2).

^dTotal carbon balance calculated from the sum of the gas-phase products and SOA, assuming aerosol is 60% carbon. See text for explanation of uncertainty estimates.

^eYield of limononaldehyde was 68 ± 7%.

^fSubject to significant error due to concentrations beyond range of calibrations.

^gLikely includes a contribution from glycolaldehyde (C₂H₄O₂, MW = 60).

^hMolar yield of caronaldehyde was 77 ± 8%.

ⁱThe midrange pinonaldehyde yield was used in the calculation.

^jThe nopinone yield from β-pinene photooxidation was 17 ± 2%.

^kYield of γ-terpinaldehyde was 57 ± 6%.

^lYield of α-terpinaldehyde was 19 ± 2%.

^mMVK + MACR yield was 60–87 ± 11% and 3-methylfuran yield was 3.6 ± 0.4%.

gested that OH oxidation of α-pinene produces a 19% yield of organic nitrates in chamber experiments, and a 13% yield in the real atmosphere [Peeters *et al.*, 2001]. Laboratory experiments have suggested that abstraction from aldehydic H on pinonaldehyde produces high yields (81%) of a PAN analogue under high NO_x conditions [Nozière and Barnes, 1998]. Table 10 lists the molar yields of the even *m/z* product ions (characteristic of a N-containing compound), which were produced from ten of the terpene compounds at extremely low yields. The PTR-MS observed a 1% yield of organic nitrates from α-pinene, suggesting that perhaps these organic nitrates were thermally unstable in the PTR-MS, fragmented in the PTR-MS on odd *m/z*, which are not typically associated with N-containing compounds, were lost to tubing walls, or were not formed at high yields in these experiments. If these organic nitrates are high carbon number compounds, such as the PAN analogue from pinonaldehyde oxidation, then the poor detection of these compounds by PTR-MS should affect the carbon mass balance of the experiments. Poor carbon balances were obtained for β-pinene and the sesquiterpenes, and undetected organic nitrates may be responsible. However, due to the high degree of uncertainty in the carbon mass balance, a 20% yield of undetected organic nitrates are within the uncertainty estimates of many of the experiments, and may not represent a significant and detectable carbon loss.

[19] Time series graphs and production mechanisms for selected ions from selected terpenes will be presented, and

will focus primarily on *m/z* 113 and 111. The production mechanisms for many of the product ions are very straightforward, however, in order to generate compounds that correspond with the observed product ions and time series, many of the production mechanisms represent pathways that seem less likely or straight-forward. In the following sections, we suggest possible mechanisms and products for a limited number of terpenes and their observed ions that correspond best to the observed data, focusing primarily on the ions observed in a ponderosa pine forest canopy [Holzinger *et al.*, 2005], while also addressing the inconsistencies between expected and observed ions. Aerosol yields and comparisons with other studies are presented in Table 5, but a more detailed analysis of the contribution of first- and second-generation oxidation products to SOA production from these photooxidation experiments, and ozonolysis experiments performed in 2003 [Lee *et al.*, 2006], is presented elsewhere [Ng *et al.*, 2006].

3.1. Sesquiterpenes

[20] SOA yields were highest from β-caryophyllene (68%), α-humulene (65%), and longifolene (65%), with an intermediate SOA yield of 37% from aromadendrene (Table 5). The relatively few experiments conducted on sesquiterpene oxidation have focused primarily on β-caryophyllene and α-humulene, thus no data was found in the existing literature on longifolene and aromadendrene photooxidation. High SOA yields for β-caryophyllene and α-humulene have been observed by other studies [e.g.,

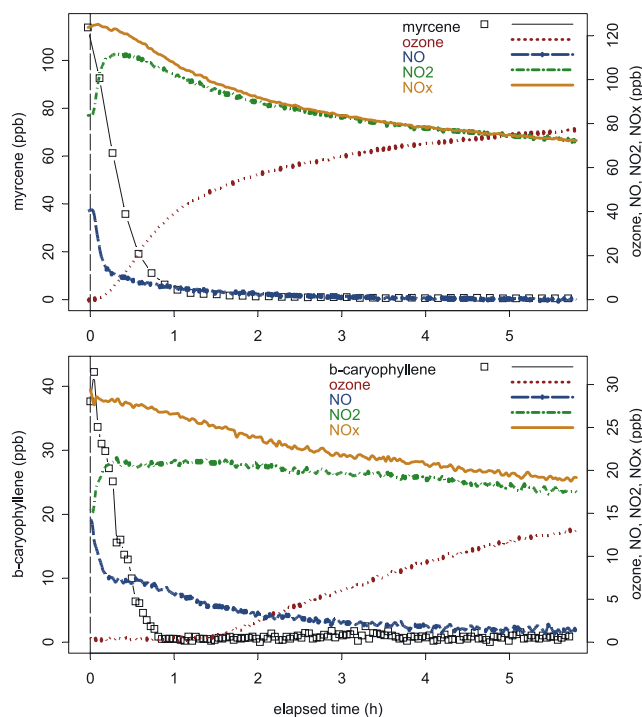


Figure 1. Time series plots of O₃, NO, NO₂, and NO_x for myrcene, which was fairly representative of all experiments, and β-caryophyllene, which was similar to α-humulene, but atypical compared to all other experiments. Red dotted lines represent O₃. Blue dashed lines represent NO. Green dotted and dashed lines represent NO₂. Orange solid lines represent NO_x.

Hoffmann et al., 1997; Griffin et al., 1999]. Gas-phase yields of low molecular weight oxidation products (Table 6) varied for the sesquiterpenes, with high formaldehyde yields from aromadendrene, β-caryophyllene, and longifolene, all with

an external double bond, and relatively low yields of acetaldehyde, acetone, and acetic acid. High formic acid yields were observed from longifolene, but not from β-caryophyllene or aromadendrene, all with external double bonds. The carbon mass balances for all four sesquiterpenes are relatively low compared to most other monoterpenes, ranging from 62–77%. The poor mass balances for the sesquiterpenes suggests that the observed unidentified products are underestimated or that additional gas-phase products were formed that were not measured by PTR-MS.

3.1.1. Aromadendrene and Longifolene

[21] The photooxidation of aromadendrene produced high yields of *m/z* 207 and 189 (47 ± 7%), which are likely the dominant product ions of the ketone formed from OH addition at the terminal carbon of the external double bond. The formation of this product would also produce formaldehyde, which also accounts for the high formaldehyde yield observed (65 ± 8%). In contrast, the photooxidation of longifolene, which is similar in structure to aromadendrene, produced low yields of *m/z* 207 (2 ± 0.4%), and *m/z* 189 was not observed. Yields of formic acid were greater than formaldehyde, and the dominant unidentified ion produced was *m/z* 203, at a yield of only 5 ± 1%, suggesting that the photooxidation of longifolene is more complex than that of aromadendrene, with several different pathways that produce lower gas-phase yields of many different products and higher yields of SOA, which is surprising given that the similar, and comparatively simple structures of these two sesquiterpenes would suggest similar oxidation pathways and yields.

3.1.2. α-Humulene

[22] The photooxidation of α-humulene, with no external double bonds, did not produce formaldehyde, and produced low yields of the other calibrated oxidation products. Initial oxidation of any one of the three internal double bonds would produce a high molecular weight C₁₅ multifunctional species (e.g., a C₁₅H₂₄O₂ keto-aldehyde occurring at *m/z*

Table 7. Percent Yield (Slope of Regression ± Standard Error of Slope) on a Mole Basis, of Product Ions From Terpene Photooxidation That Were Also Observed in the Ambient Air Within a Ponderosa Pine Canopy in California

Terpene	<i>m/z</i> 111	<i>m/z</i> 113	<i>m/z</i> 123	<i>m/z</i> 141	<i>m/z</i> 151	<i>m/z</i> 155	<i>m/z</i> 159	<i>m/z</i> 169
<i>β-caryophyllene</i> ^a		0.4 ± 0.1		0.4 ± 0.1				
<i>α-humulene</i> ^a		1.1 ± 0.3		1.1 ± 0.2	1.5 ± 0.3		0.3 ± 0.1	0.5 ± 0.2
<i>longifolene</i>		0.7 ± 0.1						
limonene	1 ± 0.2	1 ± 0.2	21 ± 4 ^b	1.3 ± 0.3	13 ± 3	0.7 ± 0.2	0.1 ± 0.02	4.6 ± 1
myrcene	9.3 ± 2 ^c	32 ± 7	5.5 ± 1	0.6 ± 0.2		1.1 ± 0.3	0.1 ± 0.02	
3-carene	1.7 ± 0.4	2 ± 0.4	26 ± 6	4.5 ± 1	19 ± 4	0.8 ± 0.2		6.9 ± 2
methyl chavicol		0.9 ± 0.1	0.5 ± 0.04		23 ± 0.4			
α-pinene	1 ± 0.2	0.9 ± 0.2	3.6 ± 0.7	1 ± 0.2	24 ± 5	0.8 ± 0.2		2.4 ± 0.5
terpinolene	29 ± 6 ^d	2.8 ± 0.6	1.7 ± 0.4	1.7 ± 0.4				
β-pinene	0.7 ± 0.2	0.4 ± 0.1	1.1 ± 0.2		1.4 ± 0.3	0.8 ± 0.2		
γ-terpinene	0.4 ± 0.1	1 ± 0.2	17 ± 4	2.2 ± 0.5	14 ± 3	0.7 ± 0.1	0.1 ± 0.02	14 ± 3
α-terpinene	0.6 ± 0.1	0.6 ± 0.2	7.2 ± 2	0.9 ± 0.4	4.6 ± 1	3.4 ± 1	0.1 ± 0.03	2.7 ± 1
verbenone ^a	3.2 ± 0.7	6.5 ± 1		1.8 ± 0.4		1.5 ± 0.3	0.2 ± 0.04	0.4 ± 0.1
<i>linalool</i> ^f	20 ± 4 ^e	2.5 ± 0.5	0.7 ± 0.1	0.5 ± 0.1	0.4 ± 0.1		0.04 ± 0.02	0.3 ± 0.1
<i>isoprene</i>		0.6 ± 0.1						

^aThe terpenes listed in italic font have not been measured in the air above the Blodgett Forest canopy. The short lifetime of the two sesquiterpenes, β-caryophyllene and α-humulene likely affect their detection in ambient air above the canopy, and linalool, typically associated with flowering citrus plants, may not be emitted at all from Blodgett Forest. Verbenone, an oxygenated terpene associated with plant-insect interactions, has not been specifically targeted for measurements at Blodgett Forest.

^bYields listed in bold are yields greater than 10%, and all yields of unidentified product ions represent a lower limit due to lack of knowledge about fragmentation.

^cYield of *m/z* 111. The sum of yields of *m/z* 111 and 93 is 41 ± 7% (see text).

^dYield of *m/z* 111. Sum of yields of *m/z* 111 and 93, the dehydrated fragment of *m/z* 111, was 43 ± 7%.

^eYield of *m/z* 111. The sum of yields of *m/z* 129, 111 and 93 is 75 ± 10%.

Table 8. Comparison of Gas-Phase Oxidation Product Yields From Sesquiterpenes, Isoprene, and Oxygenated Terpenes, on a Percent Mole (ppb/ppb) Basis, Observed in This Study With Results From Other Terpene Photooxidation Experiments

Terpene	Product	Product Yield, % This Work	Product Yield, % Other Studies	Reference	
α -humulene	<i>m/z</i> 219	3 ± 0.5	9.5 ^a	[Jaoui and Kamens, 2003a]	
linalool	acetone	25	51	[Shu et al., 1997]	
	<i>m/z</i> 127	8.1 ± 2	6.8 ^b	[Shu et al., 1997]	
isoprene	<i>m/z</i> 129, 111, 93	75 ± 10	46 ^c	[Shu et al., 1997]	
	formaldehyde	160 ^d	63 ± 10	[Tuazon and Atkinson, 1990]	
	MVK + MACR		60–87 ± 11	57 ± 6	[Miyoshi et al., 1994]
				61	[Paulson et al., 1992]
				55 ± 6	[Zhao et al., 2004]
				54	[Tuazon and Atkinson, 1990]
	3-methylfuran		3.6 ± 0.4	54	[Miyoshi et al., 1994]
				4.4 ± 0.6	[Atkinson et al., 1989]
		<i>m/z</i> 85	1.5 ± 0.3	4 ± 2	[Paulson et al., 1992]
		<i>m/z</i> 87	1.3 ± 0.3	<2	[Sprengnether et al., 2002]
	<i>m/z</i> 101	0.5 ± 0.1	8.4 ± 2.4 ^e	[Zhao et al., 2004]	
			3.3 ± 1.6 ^f	[Zhao et al., 2004]	
			~15% ^g	[Baker et al., 2005]	
			19.3 ± 6.1 ^h	[Zhao et al., 2004]	

^aSum of yields of 3-seco- α -humulone aldehyde and 7-seco- α -humulone aldehyde, and α -humulal aldehyde, all with MW = 236. We did not observe *m/z* 237, but did observe *m/z* 219, its dehydrated fragment.

^bYield of 6-methyl-5-hepten-2-one (C₈H₁₄O = 126 amu).

^cYield of 4-hydroxy-2-methyl-5-hexen-1-al and its cyclized isomer (C₇H₁₂O₂ = 128 amu).

^dLikely overestimated due to calibration issue.

^eYield of *m/z* 85 measured by PTR-MS and attributed to a C₅ carbonyl (C₅H₈O = 84 amu).

^fYield of *m/z* 87 measured by PTR-MS and attributed to a C₄ hydroxycarbonyl (C₄H₆O₂ = 86 amu).

^gEstimated yield of two C₅ hydroxycarbonyls.

^hYield of *m/z* 101 measured by PTR-MS and attributed to a C₅ hydroxycarbonyl (C₅H₈O₂ = 100 amu).

237), however, this ion was not observed from α -humulene photooxidation, suggesting that this species was not detected because it was rapidly oxidized, partitioned directly into the particle phase, or fragmented completely in the PTR-MS. Additionally, higher yields of lower molecular weight unidentified ions, e.g., *m/z* 87, 99, 101, and 125 were observed, indicating ring-opening did occur with cleavage at multiple internal double bonds. Despite the higher yields of comparatively low molecular weight ions, SOA yield from α -humulene was still high. The gas- and particle-phase products from the photooxidation of α -humulene was studied elsewhere [Jaoui and Kamens, 2003a] using denuder and filter sampling with sample derivatization and analysis by GC-MS and HPLC. By accounting for nine different oxidation products in the gas and particle phases, Jaoui and Kamens [2003a] obtained a carbon balance of ~44%, suggesting that the use of surrogate standards underestimated yields, or that additional products may be produced. In the gas-phase, carbon yields of 3-seco- α -humulone aldehyde, 7-seco- α -humulone aldehyde, and α -humulal aldehyde (all MW = 236) dominated, and summed to 9.5% [Jaoui and Kamens, 2003a]. Although we did not observe a product ion at *m/z* 237, we did observe *m/z* 219, which is expected to be the dehydrated fragment of *m/z* 237. Our observed yield of *m/z* 219 (3 ± 0.5%) was lower than the sum of the three C₁₅ products observed by Jaoui and Kamens [2003a], which is expected as these compounds likely produce additional fragments or are otherwise lost to tubing walls. Our carbon mass balance for α -humulene was 77 ± 9%, suggesting that the gas-phase compounds observed by PTR-MS as 32 product ions, though underestimated, likely include additional products besides the nine identified by Jaoui and Kamens [2003a].

3.1.3. β -Caryophyllene

[23] Figure 3 shows the time series of β -caryophyllene photooxidation, indicating that the production of *m/z* 207 occurs quickly, corresponding to OH addition to the terminal C of the external double bond (Figure 4). Oxidation products with MW = 236 and 252 have been proposed for β -caryophyllene ozonolysis [Calogirou et al., 1997], and represent first-generation oxidation products from O₃ attack at the internal double bond. Although OH attack at the internal double bond would also likely result in first-generation products occurring at *m/z* 237 and 253 (Figure 4), the observed time evolution and mixing ratio of *m/z* 237 suggest that this ion corresponds to a non-dominant, late-forming (perhaps third-generation) product. It is possible that the first-generation keto-aldehyde product corresponding to *m/z* 237 was formed but not observed in the gas-phase because it partitioned directly into the particle phase. The formation of oxidation products at *m/z* 253 and 235 is observed but delayed compared to *m/z* 207 and 189 (Figure 3). While *m/z* 189 may be the dehydrated fragment of *m/z* 207, the time series of the two ions are not identical (Figure 2) and the correlation coefficient is low (R² = 0.3), suggesting that *m/z* 189 is a different product, or that the very low mixing ratios observed for *m/z* 189 and 207 makes a correlation difficult to detect. Figure 4 shows partial mechanisms for the initial production and further oxidation of *m/z* 207. For comparison, the first-generation products corresponding to MW = 236 and 252, proposed by Calogirou et al. [1997], that are not likely the products observed in these photooxidation experiments, are illustrated in grey. The further oxidation of *m/z* 207 may produce the observed oxidation ions *m/z* 219, 237, the dehydrated fragments of *m/z* 255 (Figure 4). Although the

Table 9a. Comparison of Gas-Phase Oxidation Product Yields From Monoterpenes, on a Percent Mole (ppb/ppb) Basis, Observed in This Study With Results From Other Terpene Photooxidation Experiments

Terpene	Product	Product Yield, % This Work	Product Yield, % Other Studies	Reference
limonene	Formaldehyde	43	92 ^a	[Librando and Tringali, 2005]
	formic acid	7	36 ± 5 ^a	[Larsen et al., 2001]
			54 ± 10 ^a	[Larsen et al., 2001]
	Acetone	0.4	54 ^a	[Librando and Tringali, 2005]
	<i>m/z</i> 139 ^b	4.9 ± 1	<0.03	[Reissell et al., 1999]
			not detected	[Larsen et al., 2001]
<i>m/z</i> 169 ^d	68 ± 7	39 ± 15 ^c	[Larsen et al., 2001]	
		20 ± 3	[Hakola et al., 1994]	
		17 ± 3	[Arey et al., 1990]	
		29 ± 6 ^c	[Hakola et al., 1994]	
myrcene	Formaldehyde	74 ^f	28	[Arey et al., 1990]
			not detected	[Larsen et al., 2001]
	formic acid	5	30 ± 6	[Orlando et al., 2000]
	Acetone	22	5 ± 2	[Orlando et al., 2000]
	<i>m/z</i> 111	9.3 ± 2	36 ± 5	[Orlando et al., 2000]
			41	[Reissell et al., 1999]
3-carene	Formaldehyde	35	19 ± 4 ^g	[Reissell et al., 2002]
			21 ± 4	[Orlando et al., 2000]
	formic acid	5	12 ± 3	[Larsen et al., 2001]
			20 ^a	[Librando and Tringali, 2005]
	Acetone	9	30 ± 3 11 ^a	[Larsen et al., 2001]
			11 ^a	[Librando and Tringali, 2005]
Acetone <i>m/z</i> 169	77 ± 8 ^h	8 ± 2	[Orlando et al., 2000]	
		15 ± 3	[Orlando et al., 2000]	
		15 ± 3	[Reissell et al., 1999]	
		15 ± 5	[Larsen et al., 2001]	
<i>m/z</i> 169	77 ± 8 ^h	34 ± 8 ⁱ	[Hakola et al., 1994]	
		31 ⁱ	[Arey et al., 1990]	
			14 ± 5 ⁱ	[Larsen et al., 2001]

^aFrom experiments where the photolysis of H₂O₂ was used as the OH source.

^bSum of *m/z* 139 and 121.

^cYield of limona ketone.

^dSum of yields of *m/z* 169, 170, 151 (the dehydrated fragment of *m/z* 169), 152, 133, 123, 124, 107, and 108.

^eYield of endolim, also called limononaldehyde.

^fSubject to significant error due to concentrations beyond range of calibrations.

^gYield of 4-vinyl-4-pental.

^hSum of *m/z* 169, 170, 151 (the dehydrated fragment of *m/z* 169), 152, 133, 123, 124, 107, and 108.

ⁱYield of caronaldehyde.

production of a keto-keto-aldehyde from further oxidation of *m/z* 207 at the remaining internal double bond, with a molecular weight of 238 (*m/z* 239) seems likely, the ions *m/z* 239 and 221, which are shown for reference in Figure 4, were not observed from these experiments. It should also be noted that many products, particularly the acids, may also be produced from ozonolysis reactions.

[24] We conducted dark ozonolysis experiments of β-caryophyllene and α-humulene in 2003 [Lee et al., 2006], and in comparison, the photooxidation of these two sesquiterpenes produced higher SOA yields than ozonolysis. Because the lifetime of these two sesquiterpenes from O₃ reaction is considerably shorter compared to OH oxidation, the lower SOA yields of ~45% from ozonolysis may be atmospherically relevant.

3.2. Monoterpenes

[25] SOA yields from monoterpenes ranged from 25% to 58% (Table 5). Yields are generally expected to be higher from terpenes with internal double bonds, because oxidation does not necessarily result in carbon loss. This trend is generally observed, with several terpenes with internal double bonds, such as limonene, 3-carene, α-pinene, and

terpinolene, producing higher SOA yields than β-pinene, the only single external double bond monoterpene tested. However, high SOA yields were observed from myrcene, which is acyclic, and low SOA yields were observed from α- and γ-terpinene, both with two internal double bonds.

3.2.1. Limonene

[26] The 58% SOA yield from limonene was highest of all monoterpenes (Table 5). High yields of formaldehyde were also observed from limonene, whereas yields of acetaldehyde, formic acid, acetone, and acetic acid were low. Limononaldehyde (C₁₀H₁₆O₂) has been reported as a limonene oxidation product [Hakola et al., 1994], and the PTR-MS observed high yields of the ions we determined to be associated with limononaldehyde (Table 3a), with a total yield of 68 ± 7%. In comparison to other studies (Table 9a), we observed a very high yield of limononaldehyde and low yields of limonaketone, formaldehyde, and formic acid. The time series of limonene photooxidation is shown in Figure 5. Limononaldehyde and limonaketone were observed simultaneously, but higher yields of limononaldehyde suggest OH preferentially attacks limonene at the internal double bond. Other ions are subsequently produced, and are likely oxidation products of limononaldehyde, such

Table 9b. Comparison of Gas-Phase Oxidation Product Yields From Monoterpenes, on a Percent Mole (ppb/ppb) Basis, Observed in This Study With Results From Other Terpene Photooxidation Experiments

Terpene	Product	Product Yield, % This Work	Product Yield, % Other Studies	Reference
α -pinene	formaldehyde	16	23 \pm 9	[Noziere et al., 1999]
			19 \pm 5	[Orlando et al., 2000]
	formic acid	5	16 ^a	[Librando and Tringali, 2005]
			8 \pm 1 ^b	[Noziere et al., 1999]
			8 \pm 1 ^a	[Larsen et al., 2001]
			28 \pm 3	[Larsen et al., 2001]
	acetone	6	13 ^a	[Librando and Tringali, 2005]
			7 \pm 2	[Orlando et al., 2000]
			15 \pm 2	[Wisthaler et al., 2001]
			11 \pm 3	[Reissell et al., 1999]
			11 \pm 3 ^a	[Larsen et al., 2001]
			11 \pm 3	[Aschmann et al., 1998]
			9 \pm 6	[Noziere et al., 1999]
			7 \pm 2 ^b	[Noziere et al., 1999]
			5 \pm 2	[Orlando et al., 2000]
			87 \pm 20	[Noziere et al., 1999]
pinonaldehyde	63 (range 47–83) ^c 30 \pm 0.3 ^d	56 \pm 4	[Hatakeyama et al., 1991]	
		37 \pm 7 ^b	[Noziere et al., 1999]	
		34 \pm 9	[Wisthaler et al., 2001]	
		31 \pm 15	[Vinckier et al., 1998]	
		31–34 ^c	[Jaoui and Kamens, 2001]	
		29	[Arey et al., 1990]	
		28	[Hakola et al., 1994]	
		28 \pm 5	[Aschmann et al., 2002]	
		6 \pm 2 ^a	[Larsen et al., 2001]	
		1.4–1.8 ^{f, g}	[Jaoui and Kamens, 2001]	
		4–6.4 ^{f, h}	[Jaoui and Kamens, 2001]	
0.2 \pm 0.05	[Jaoui and Kamens, 2001]			
3.9–4.2 ^{f, i}	[Jaoui and Kamens, 2001]			
0.3 \pm 0.1	[Jaoui and Kamens, 2001]			
6.1–16.9 ^{f, j}	[Jaoui and Kamens, 2001]			
19 ^w	[Aschmann et al., 2002]			
terpinolene	formaldehyde	23	29 \pm 6	[Orlando et al., 2000]
	formic acid	4	8 \pm 2	[Orlando et al., 2000]
	acetone	20	39 \pm 5	[Orlando et al., 2000]
	m/z 111 and 93	43 \pm 7	36–45	[Reissell et al., 1999]
			26 \pm 6 ^k	[Hakola et al., 1994]
			26 \pm 5	[Reissell et al., 1999]
			24	[Arey et al., 1990]
	m/z 169	—	19 \pm 4 ^l	[Reissell et al., 2002]
10			[Arey et al., 1990]	

^aFrom experiments where the photolysis of H₂O₂ was used as the OH source.

^bConducted in the absence of NO_x.

^cSee Experiment section for description of the pinonaldehyde yield calculation.

^dSum of m/z 169, 170, 151 (the dehydrated fragment of m/z 169), and 152.

^eA II yields reported by Jaoui and Kamens [2001] are % carbon yields. The yields listed above are converted from % carbon to % total mass yields for comparison with yields obtained from this and other studies.

^fAll yields reported by Jaoui and Kamens [2001] are % carbon yields. The yields listed above are converted from % carbon to % total mass yields for comparison with yields obtained from this and other studies.

^gYield of α -campholenal (MW = 152).

^hYield of norpinonaldehyde (MW = 154).

ⁱSum of norpinonic acid (MW = 170) and pinalic4-acid (MW = 170) yields, with yields of pinalic-4-acid roughly 12 times larger than yields of norpinonic acid.

^jSum of pinonic acid (MW = 184) and 1-hydroxypinonaldehyde (MW = 184) yields, with pinonic acid yields roughly 4–8 times larger than 1-hydroxypinonaldehyde.

^kYield of 4-methyl-3-cyclohexen-1-one (MW = 110).

^lYield of 4-vinyl-4-pentanal (MW = 110).

as m/z 171, 153, and 143. A partial mechanism for the formation of these ions is shown in Figure 6. Other ions are formed even later, such as m/z 218, which is likely an organic nitrate compound produced at a low observed yield of <1% (Table 10), and m/z 113, which was the dominant ion observed at Blodgett Forest. Molar yields of other unidentified ions totaled 61%, and the carbon mass balance at the end of the experiment was 113 \pm 17%, suggesting that the concentrations of unidentified oxidation products to the carbon balance are overestimated and may have resulted

from incorrect assignments of carbon number to the product ions or from overestimating the %C in the SOA formed.

3.2.2. Myrcene

[27] The photooxidation of myrcene, an acyclic terpene, produced relatively high yields of SOA (43%) compared to other monoterpenes, in contrast to the low yields (~12%) obtained from myrcene ozonolysis [Lee et al., 2006]. The lifetimes of myrcene with respect to 50 ppb O₃ or 2 \times 10⁶ molecules OH cm⁻³ are similar (28 minutes and 39 minutes, respectively), suggesting that ozonolysis and photooxida-

Table 9c. Comparison of Gas-Phase Oxidation Product Yields From Monoterpenes, on a Percent Mole (ppb/ppb) Basis, Observed in This Study With Results From Other Terpene Photooxidation Experiments

Terpene	Product	Product Yield, % This Work	Product Yield, % Other Studies	Reference
β -pinene	formaldehyde	49	54	[Hatakeyama <i>et al.</i> , 1991]
			45 \pm 8	[Orlando <i>et al.</i> , 2000]
			23 \pm 2	[Larsen <i>et al.</i> , 2001]
	formic acid	8.2	31 ^a	[Librando and Tringali, 2005]
			30.3	[Jaoui and Kamens, 2003b]
			38 \pm 4 ^a	[Larsen <i>et al.</i> , 2001]
			5 ^a	[Librando and Tringali, 2005]
	acetone	7.9	2 \pm 1	[Orlando <i>et al.</i> , 2000]
			16 \pm 2	[Wisthaler <i>et al.</i> , 2001]
			11 \pm 3 ^a	[Larsen <i>et al.</i> , 2001]
			8.5 \pm 2	[Aschmann <i>et al.</i> , 1998]
			6.5	[Jaoui and Kamens, 2003b]
	nopinone	17	2 \pm 2	[Orlando <i>et al.</i> , 2000]
			79 \pm 8	[Hatakeyama <i>et al.</i> , 1991]
			27 \pm 4	[Hakola <i>et al.</i> , 1994]
30 \pm 5			[Arey <i>et al.</i> , 1990]	
25 \pm 5 ^a			[Larsen <i>et al.</i> , 2001]	
25 \pm 3			[Wisthaler <i>et al.</i> , 2001]	
15.2			[Jaoui and Kamens, 2003b]	
0.9			[Jaoui and Kamens, 2003b]	
<i>m/z</i> 151	1.4 \pm 0.3	0.9	[Jaoui and Kamens, 2003b]	
<i>m/z</i> 153	2.8 \pm 0.6	1.9 ^b	[Jaoui and Kamens, 2003b]	
<i>m/z</i> 155	0.8 \pm 0.2	5.3 ^c	[Jaoui and Kamens, 2003b]	
<i>m/z</i> 171	0.1 \pm 0.03	<0.1 ^d	[Jaoui and Kamens, 2003b]	
<i>m/z</i> 185	0.1 \pm 0.02	0.5 ^e	[Jaoui and Kamens, 2003b]	
γ -terpinene	acetone	5	10 \pm 3	[Reissell <i>et al.</i> , 1999]
α -terpinene	acetone	3	\sim 10	[Reissell <i>et al.</i> , 1999]

^aFrom experiments where the photolysis of H₂O₂ was used as the OH source.

^bSum of yields of β -pinene oxide (1%) and 3-oxonopinone (0.9%). A trace amount of myrtenol was reported but not quantified and is not included in the sum.

^cSum of yields of 1-hydroxynopinone (3.1%) and 3-hydroxynopinone (2.2%).

^dYield of 3,7-dihydroxynopinone.

^eYield of pinonic acid.

tion are both important loss processes in the real atmosphere. High yields of formaldehyde (74%) and acetone (22%), and low yields of formic and acetic acid (<5%) were observed. Our yield of acetone is slightly lower than the 36% reported by Orlando *et al.* [2000] and the 41% yield reported by Reissell *et al.* [1999]. While our yield of formic acid is the same as the yield obtained elsewhere [Orlando *et al.*, 2000], our yield of formaldehyde is much higher than the 30% yield of Orlando *et al.* [2000]. Because the formaldehyde mixing ratios in the chamber (\sim 110 ppb) were beyond the range of the calibrated linear response, the formaldehyde yield from myrcene is subject to considerable error.

[28] Numerous compounds can be produced from myrcene due to the many possible sites for OH attack. Many product ions were detected, with highest molar yields from *m/z* 93 (32 \pm 6.8%) and 113 (32 \pm 6.7%). The product 4-vinyl-4-pentenal (MW = 110) was identified from other studies [Reissell *et al.*, 2002], and was observed from myrcene ozonolysis at *m/z* 111 and 93 [Lee *et al.*, 2006]. However, from these photooxidation studies, *m/z* 111 and 93 were not well correlated ($R^2 = 0.5$) and exhibited different loss rates with time (Figure 7) where *m/z* 93 was oxidized completely, as expected given that 2 two double bonds remain in the structure, whereas *m/z* 111 was not, suggesting that other compounds likely interfered on *m/z* 111. Additionally, *m/z* 111 correlated well with other ions, e.g., *m/z* 71 ($R^2 = 0.96$), 83 ($R^2 = 0.97$), 97, 113, and 139 (all $R^2 = 0.93$). These correlations were not observed from

the ozonolysis studies [Lee *et al.*, 2006], and may indicate that these ions are fragments of the same compound, or that these ions represent different compounds that are produced and consumed at similar rates. 4-vinyl-4-pentenal is likely detected at both *m/z* 111 and 93, but another product or

Table 10. Yields of Organic Nitrate Oxidation Products^a

Terpene	<i>m/z</i>	Yield, %
longifolene	220	0.8 \pm 0.2
	200	0.1 \pm 0.02
limonene	218	0.2 \pm 0.04
	64	0.1 \pm 0.03
myrcene	124	0.4 \pm 0.1
	168	0.5 \pm 0.1
methyl chavicol	170	0.3 \pm 0.1
	180	0.5 \pm 0.1
	182	0.1 \pm 0.03
	94	0.9 \pm 0.2
α -pinene	200	0.2 \pm 0.04
	108	1.9 \pm 0.4
β -pinene	184	0.1 \pm 0.05
	198	0.2 \pm 0.04
	230	0.1 \pm 0.02
γ -terpinene	178	0.05 \pm 0.02
	184	0.1 \pm 0.05
α -terpinene	202	0.1 \pm 0.03
	230	0.2 \pm 0.04
	230	0.1 \pm 0.02
	188	0.2 \pm 0.05
verbenone	230	0.1 \pm 0.02
linalool	188	0.2 \pm 0.05

^aReported yields are limited to those oxidation products with even mass-to-charge ratios that are unambiguously not carbon isotopes of the preceding *m/z*.

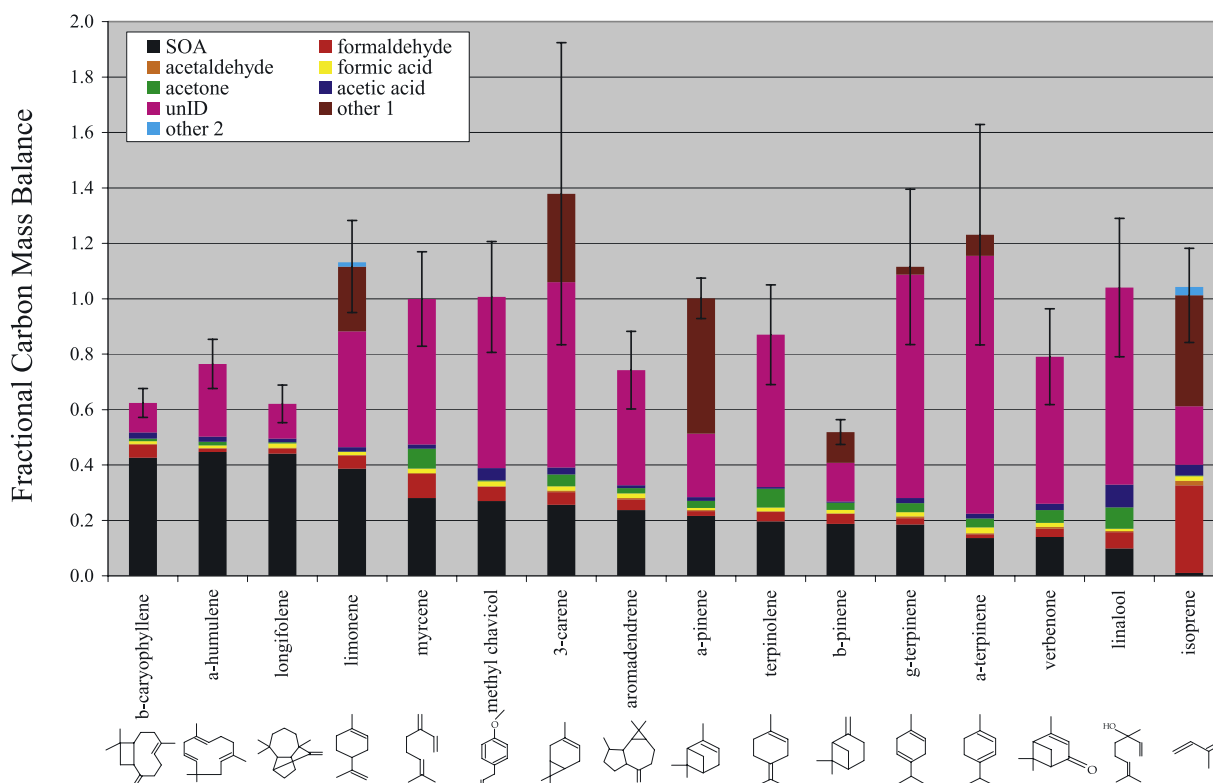


Figure 2. Carbon mass balance of SOA (assuming aerosol is 60% carbon) and gas-phase oxidation products, represented as a 30–60 minute snapshot in time at the middle or end of the experiment for the purpose of carbon accounting, and does not represent overall stoichiometric yields. The “other 1” category represents the calibrated products nopinone and MACR + MVK from β -pinene and isoprene, respectively, and the uncalibrated products limononaldehyde, caronaldehyde, pinonaldehyde, γ -terpinaldehyde, and α -terpinaldehyde, from limonene, 3-carene, α -pinene, γ -terpinene, and α -terpinene, respectively. The “other 2” category represents limonaketone from limonene and 3-methyl furan from isoprene. Aerosol molar yields ($\mu\text{g aerosol m}^{-3}/\mu\text{g terpene m}^{-3}$) were calculated assuming an aerosol density of 1.25 g cm^{-3} .

products might interfere on m/z 111. Thus, our reported yield of 4-vinyl-4-pentenal of 41% (Table 9a) is likely overestimated, but by no more than 9%. The total gas-phase carbon balance for myrcene was $100 \pm 17\%$.

[29] Figure 7 shows the time series plots for selected ions. Acetone and the compounds occurring on m/z 71, 93, 111, 113, and 139 are clearly first-generation oxidation products, as their concentrations peak as myrcene becomes completely oxidized. All of these compounds decreased in concentration after myrcene was fully consumed. In contrast, the product occurring on m/z 115 was clearly a second-generation product, as its concentration continued to increase after complete consumption of myrcene. Figure 8 shows potential structures for some of the ions shown in Figure 7. The production of m/z 113 from myrcene photooxidation as a first-generation product, and at a high molar yield, is surprising because it was formed as a second-generation product in myrcene ozonolysis [Lee *et al.*, 2006], suggesting that different products from photooxidation and ozonolysis contribute to observations of m/z 113 in ambient air. A product with m/z 113 can be formed simply from oxidation of 4-vinyl-4-pentenal (m/z 111), as suggested for myrcene ozonolysis [Lee *et al.*, 2006], however, as shown in Figure 8, production of m/z 113 as a first-generation

product directly from myrcene photooxidation is more complicated and may involve the co-production of a compound with m/z 89 and a dehydrated fragment of m/z 71. A possible alternative to the exotic cyclization step shown in Figure 8 is the formation of the acyclic tricarbonyl species by internal rearrangement of a peroxy radical [Vereecken and Peeters, 2004], which may oxidize multiple double bonds in a single oxidation step. Myrcene photooxidation was the dominant source of m/z 113 observed from all photooxidation and ozonolysis experiments.

3.2.3. 3-Carene, α -Pinene, and β -Pinene

[30] Compared to the other terpenes discussed here, 3-carene, α -pinene and β -pinene have been relatively well studied, and thus, we will not present a detailed discussion of the photooxidation of these compounds. SOA yields obtained here from 3-carene photooxidation (38%) are higher than those obtained elsewhere [Hoffmann *et al.*, 1997] and [Griffin *et al.*, 1999], which is generally consistent with the lower temperature of our experiment. From 3-carene ozonolysis, SOA yields (54%) were higher than from photooxidation. Our formaldehyde yield was higher than those observed elsewhere, and yields of formic acid and acetone were lower than other studies (Table 9a), but the sum of all caronaldehyde-associated ions (Table 3a)

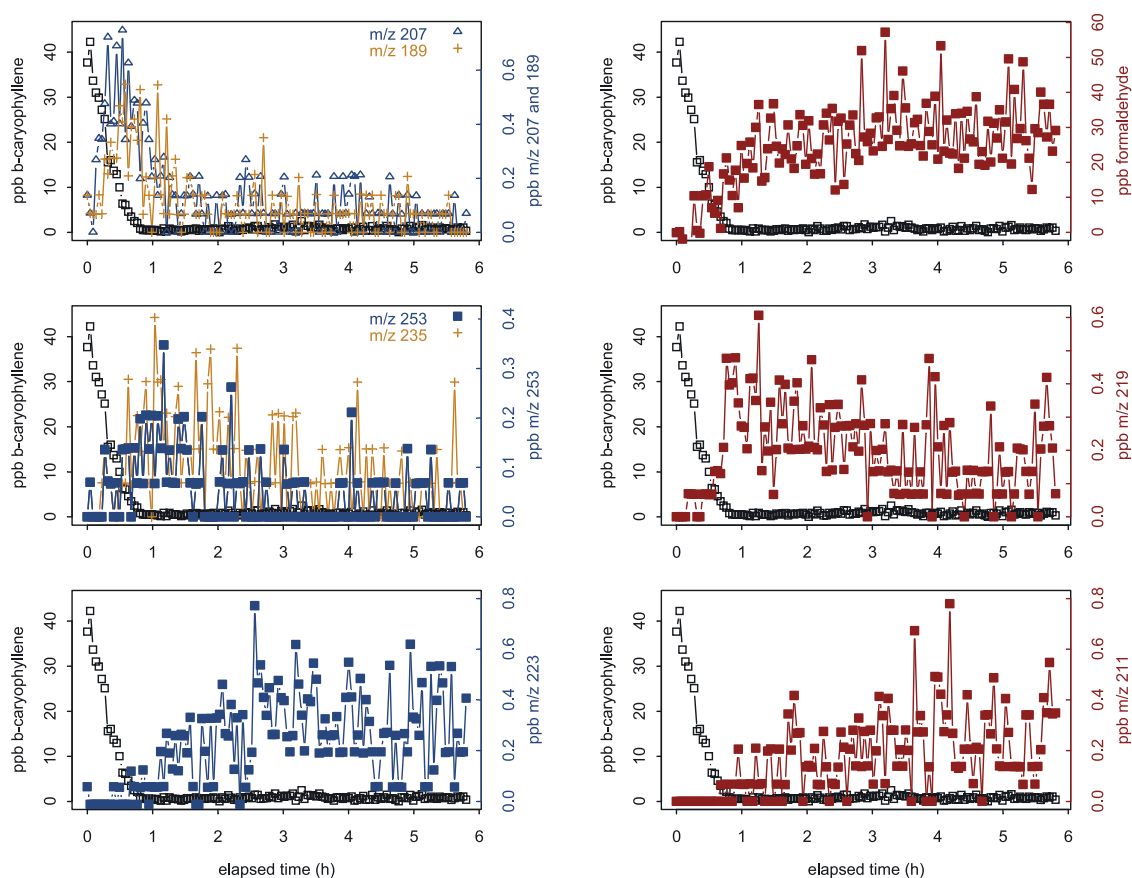


Figure 3. Photooxidation of β -caryophyllene shows the production of primary (m/z 207, 189), secondary (m/z 253, 235, 219), and perhaps delayed secondary or tertiary (m/z 223, 211) oxidation products.

produced much higher yield (77%) than yields observed from other studies (Table 9a). In contrast, caronaldehyde was produced at very low yields from the ozonolysis of 3-carene (<1%). The high SOA yield and low caronaldehyde yields from 3-carene ozonolysis, and the lower SOA yield and higher caronaldehyde yield from 3-carene photooxidation suggest that caronaldehyde does not readily partition into the particle phase. Caronaldehyde was not calibrated in the PTR-MS, and the calculated yield of this product is based on the sum of all ions (Table 3a) that are well correlated with m/z 169 and 151, the dominant caronaldehyde ions. The very high yield of caronaldehyde observed from these photooxidation experiments compared to other work may suggest that this correlation method overestimates caronaldehyde yields by incorrectly attributing certain ions to caronaldehyde. This method was also used for pinonaldehyde from α -pinene, which agreed well with many of the previous experiments when only m/z 151, 152, 169, and 170 were accounted for, but was within the higher range of other results when all ions that correlated well with m/z 151 and 169 were included (Table 9b). The yield of limonaldehyde from limonene was also higher than previous results, further suggesting that some of the ions we found to be correlated with m/z 151 and 169 from the keto-aldehyde produced from attack at the internal double bond, and were reported as fragments from a pinonaldehyde standard by [Wisthaler *et al.*, 2001] may

not be fragments of the keto-aldehyde, or, more likely, may suffer from interference from other compounds.

[31] SOA yield from α -pinene photooxidation agrees relatively well with other studies [Nozriere *et al.*, 1999] and [Jaoui and Kamens, 2001]. Compared to other terpenes, α -pinene was not a significant source of the low molecular weight products (Table 6) and yields of these products are slightly lower than those observed elsewhere (Table 9b). Our pinonaldehyde yield is generally higher, but within the range of those observed elsewhere. A theoretical study was conducted on the OH oxidation of α -pinene and predicted higher yields of pinonaldehyde ($\sim 60\%$ versus $\sim 36\%$) under lower NO (normal atmospheric conditions) compared to the higher NO conditions of many laboratory chamber experiments [Peeters *et al.*, 2001].

[32] SOA yield from β -pinene was 31%, similar to the yield obtained by Hoffmann *et al.* [1997] and Griffin *et al.* [1999], obtained under a lower HC:NO_x ratio and higher temperatures, and was higher than the 21% SOA yield obtained by Jaoui and Kamens [2003b] under a similar HC:NO_x ratio and slightly higher temperatures (Table 5). The observed yields of formaldehyde, formic acid, and acetone (Table 9c) were similar to those observed elsewhere [Hatakeyama *et al.*, 1991; Orlando *et al.*, 2000; Jaoui and Kamens, 2003b; Aschmann *et al.*, 1998]. However, Larsen *et al.* [2001] observed a lower yield of formaldehyde, and significantly higher yields of formic acid in experiments

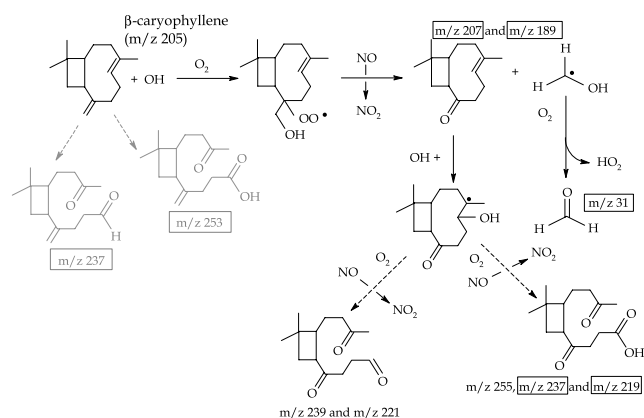


Figure 4. Partial mechanisms for β -caryophyllene photooxidation. The boxed product ions represent observed ions, and the gray structures were products observed from β -caryophyllene ozonolysis, but were not observed by PTR-MS as gas-phase photooxidation products.

conducted under low NO_x levels, which is suggestive of the favored production of formic acid over formaldehyde after OH addition to the terminal carbon of the exo double bond under low NO_x .

[33] Nopinone has been reported to be the dominant product from the ozonolysis and photooxidation of β -pinene, and our observed photooxidation yield of 17% is

comparable to the 15.2% yield reported by *Jaoui and Kamens* [2003b], but low compared to most other studies, which range from 25–27%, with a highest reported yield of 79% (Table 9c). Numerous other products have been reported, including β -pinene oxide, oxonopinone, hydroxynopinones, and pinonic acid [*Jaoui and Kamens*, 2003b]. Our yields of ions corresponding with previously reported products are comparatively low for the hydroxynopinones and pinonic acid, but high for the sum of β -pinene oxide and 3-oxonopinone (m/z 153). Our low carbon mass balance of $52 \pm 5\%$ from β -pinene photooxidation suggests that yields of nopinone, or other high molecular weight oxidation products, were underestimated, or not detected.

3.2.4. Terpinolene

[34] Terpinolene photooxidation produced an SOA yield of 31% and high molar gas-phase yields (43%) of the oxidation product ions at m/z 111 and 93, the dehydrated fragment of 111 ($R^2 = 0.96$), corresponding to the identified product 4-methyl-3-cyclohexen-1-one [*Hakola et al.*, 1994] produced from primary OH attack at the exocyclic double bond. Our observed yield of 4-methyl-3-cyclohexen-1-one is higher than reported elsewhere, whereas we observed very little production of m/z 169 (0.5%), the C_{10} keto-aldehyde formed from OH attack at the endocyclic double bond, which has been observed at a 10% yield elsewhere [*Arey et al.*, 1990]. Our measured yields of formaldehyde (23%), formic acid (4%), and acetone (20%) are lower than yields reported elsewhere of $\sim 30\%$, 8%, and $\sim 40\%$, respectively (Table 9b). The yield of m/z 111 + 93 was

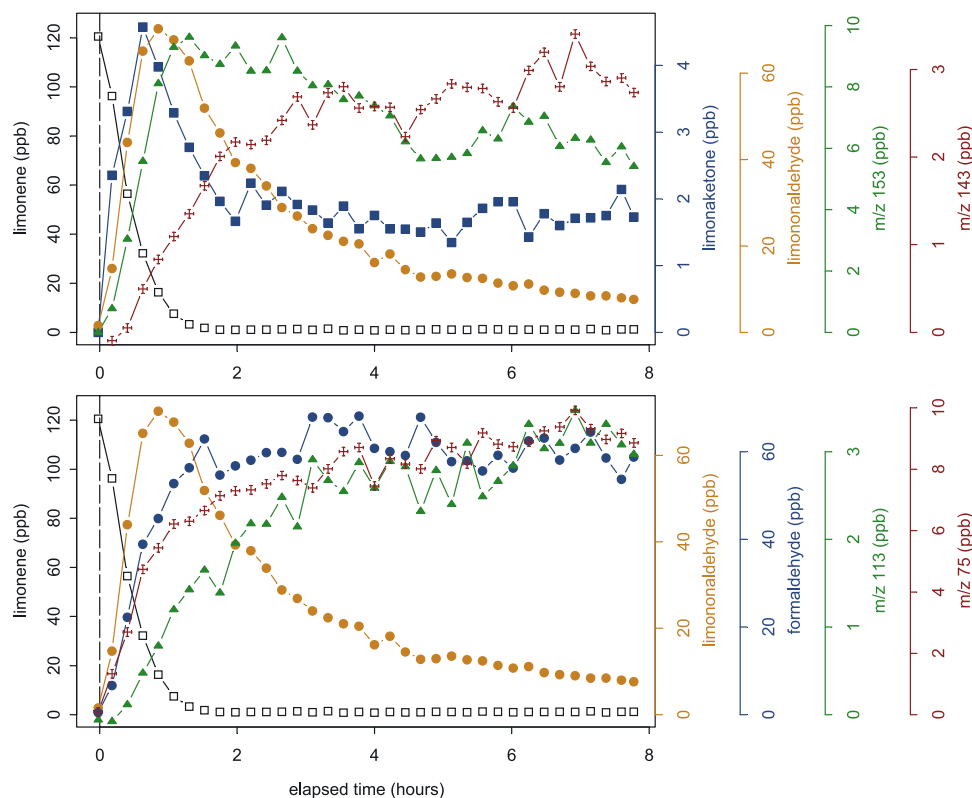


Figure 5. Time series of selected products from limonene photooxidation. Blue squares represent limonaketone (top) or formaldehyde (bottom). Orange circles represent limononaldehyde (top and bottom). Green triangles represent m/z 153 (top) or 113 (bottom). Red crosses represent m/z 143 (top) or 75 (bottom).

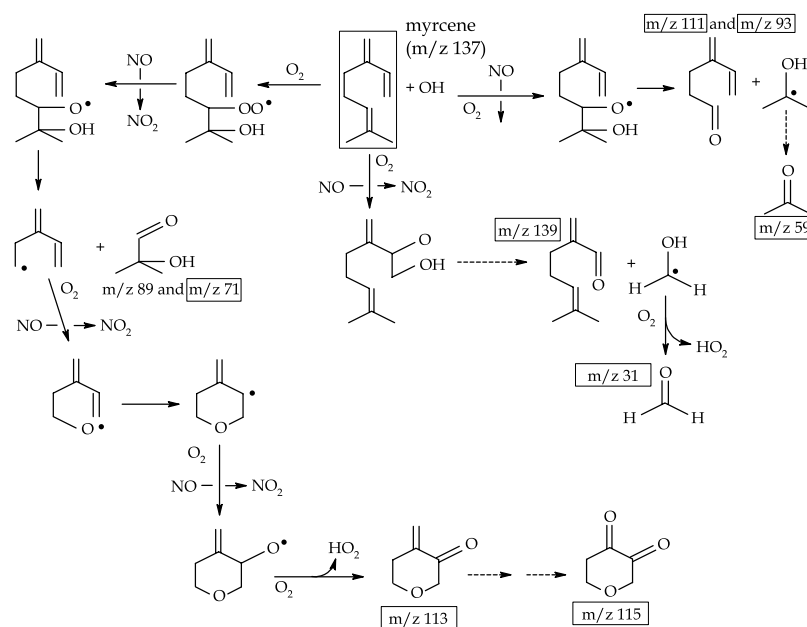


Figure 8. Partial mechanisms for the production of selected ions from myrcene photooxidation. Because we focus on major product ions, or the product ions that were also observed by in ambient air by *Holzinger et al.* [2005], for clarity, other likely pathways and products are not shown. Note that the compounds occurring on m/z 113 and 115 can be produced as second and third-generation products from the further oxidation of m/z 111, however, the time series data (Figure 7) clearly show that m/z 113 is produced as a first-generation product. A possible alternative to the exotic cyclization step shown is the formation of the acyclic tricarbonyl species by internal rearrangement of a peroxy radical [*Vereecken and Peeters*, 2004], which may oxidize multiple double bonds in a single oxidation step.

4-methyl-3-cyclohexen-1-one at the remaining internal double bond was also rapid, and likely led to the production of m/z 143 (a C₇ keto-keto-aldehyde), 99, and 113. The C₇ keto-keto-aldehyde (m/z 143) was oxidized further (Figure 9) and likely led to the production of other product ions, including m/z 115 (Figure 10). Numerous other reaction pathways and products are likely to be formed from oxidation of m/z 143, however, for simplicity, only one pathway, leading to the production of m/z 115, is shown in Figure 10. Hydrogen abstraction from 4-methyl-3-cyclohexen-1-one (m/z 111) by OH can also lead to the production of a compound with m/z 113 (Figure 10), which was observed as a second-generation product (Figure 9).

[36] Terpinolene has been observed in ambient air at Blodgett Forest, but does not represent a dominant monoterpene measured above the canopy [*Lee et al.*, 2005]. However, its shorter lifetime with respect to O₃ compared to OH oxidation, and the relatively high yields of m/z 111 and 113, suggest that terpinolene may contribute to the chemical O₃ deposition [*Kurpius and Goldstein*, 2003] and high in-canopy mixing ratios of m/z 111 and 113 observed at Blodgett Forest [*Holzinger et al.*, 2005].

3.2.5. γ -Terpinene

[37] Yields of SOA, as well as yields of the calibrated low molecular weight oxidation products from γ -terpinene are low compared to other monoterpenes. In contrast, the molar yield (ppb product/ppb terpene) of m/z 169 and the ions associated with this C₁₀ keto-aldehyde (γ -terpinaldehyde), of which there are two possible isomers resulting from the oxidation of either double bond, was $57 \pm 6\%$, and the

molar yield of all product ions (excluding those associated with γ -terpinaldehyde) was $130 \pm 10\%$, suggesting that many other unidentified products are formed from γ -terpinene. γ -terpinaldehyde was formed quickly as a first-generation oxidation product and upon further oxidation of either isomer of m/z 169, m/z 69 + 87 and 115 would also be formed quickly. Other oxidation products are formed as second-generation products, including m/z 103 + 85, 131 + 113, and 101. Oxidation of γ -terpinene by 2×10^6 molecules OH cm⁻³ is faster than by 50 ppb O₃ (47 minutes versus 95 minutes), suggesting that OH oxidation of γ -terpinene in the real atmosphere likely dominates, and contributes to the observations of m/z 123, 151, and 169 in ambient air (Table 7).

3.2.6. α -Terpinene

[38] Like γ -terpinene, yields of SOA and low molecular weight products from α -terpinene are low. The photooxidation of α -terpinene was rapid and α -terpinaldehyde, with two possible isomers at m/z 169 (Table 3b), m/z 125, 157 + 139, and 185 + 167 were the first products observed, and thus appear to be first-generation products. However, these ions do increase in concentration after complete consumption of α -terpinene, suggesting that multiple products occur on these masses, or that these ions are not first-generation products. Other ions are clearly formed as second-generation products, including formaldehyde, acetone, and m/z 99, 115, and 143. Yields of α -terpinaldehyde ($19 \pm 2\%$) and m/z 143 ($13 \pm 3\%$) were dominant. Excluding the ions associated with α -terpinaldehyde, the molar yield of unidentified products was $\sim 60\%$, suggesting that many other important

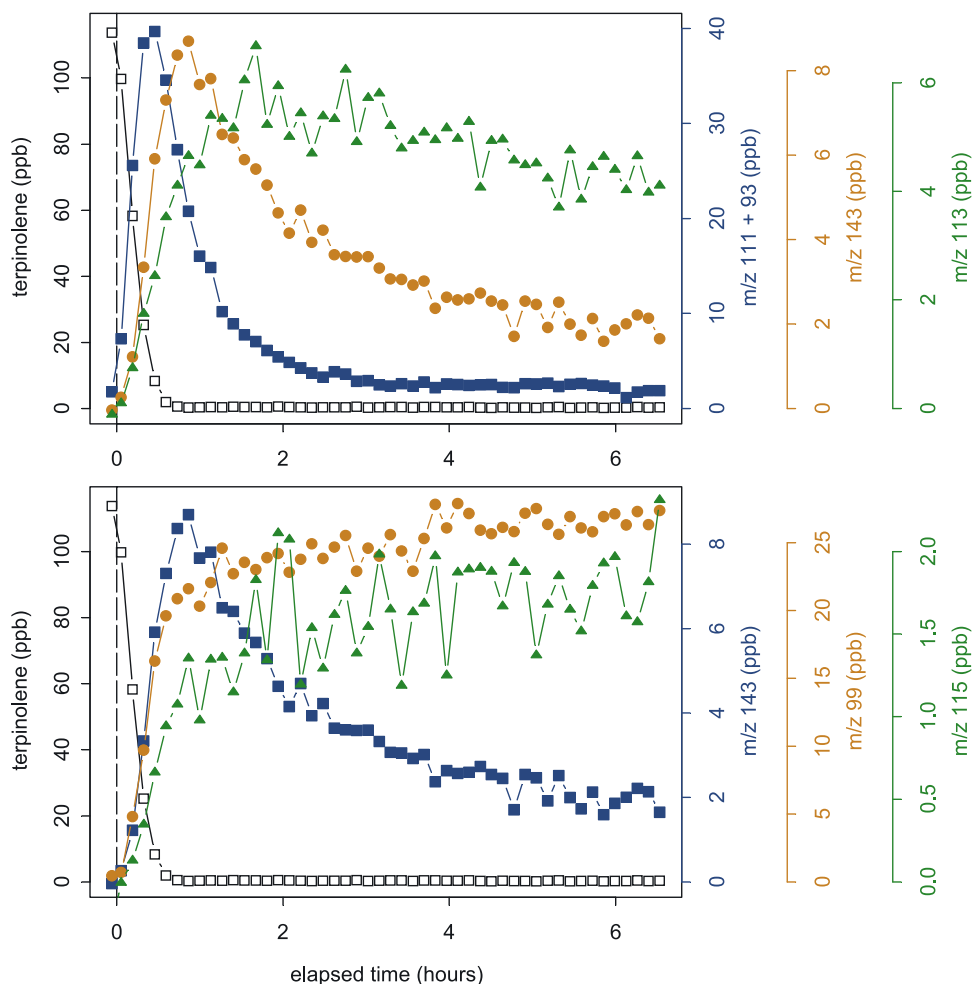


Figure 9. Time series of selected products from terpinolene photooxidation. Blue squares represent m/z 111 + 93 (top) or 143 (bottom). Orange circles represent m/z 143 (top) or 99 (bottom). Green triangles represent m/z 113 (top) or 115 (bottom).

products were formed, including four potential organic nitrate products occurring at m/z 178, 184, 202, and 230 (Table 10). Despite the rapid oxidation of α -terpinene and the uncertainty over observing first-generation products, the carbon mass balance was $123 \pm 40\%$, suggesting we have overestimated the %C in the SOA formed or the amount of gas-phase products observed.

3.3. Oxygenated Terpenes and Isoprene

3.3.1. Methyl Chavicol

[39] SOA yield from methyl chavicol was highest of all oxygenated terpenes (40%), and also considerably higher than the SOA yield obtained from methyl chavicol ozonolysis [Lee *et al.*, 2006]. High yields of formaldehyde ($52 \pm 6\%$) were also observed, as expected due to its external double bond, and acetic acid was also produced at high yield ($25 \pm 2\%$). OH addition to the terminal carbon of the external double bond can result in the formation of an aldehyde with m/z 151 ($C_9H_{10}O_2$) plus formaldehyde, or an aldehyde with m/z 137 ($C_8H_8O_2$) plus glycolaldehyde (hydroxyl acetaldehyde), with m/z 61. The observations of m/z 61 were likely glycolaldehyde, not acetic acid. The C_9

compound on m/z 151 was observed at a yield of $23 \pm 5\%$, while the C_8 compound on m/z 137 was produced at a yield of $42 \pm 9\%$. All of these dominant ions were first-generation products. Glycolaldehyde was not calibrated in the PTR-MS, however, calculation of glycolaldehyde yield can be approximated by the sum of m/z 61 and 43, or from the calibration of acetic acid, assuming they behave similarly in the PTR-MS. The sum of yields of m/z 61 + 43 was $37 \pm 5\%$, higher than the 25% yield using the acetic acid calibration factor. The higher yield is in better agreement as a co-product of m/z 137. The yield of formaldehyde is $\sim 20\%$ higher than the yield of m/z 151, suggesting that the compound occurring at m/z 151 may be underestimated due to fragmentation. Five potential organic nitrate compounds were also produced at low observed yields of $<1\%$ (Table 10).

3.3.2. Verbenone

[40] SOA yield from verbenone, and oxygenated terpene with a similar structure to α -pinene, was low (19%). A high yield of formaldehyde (32%) was observed, which was not expected, given its endo double bond. Numerous oxidation product ions were observed, but yields were generally low

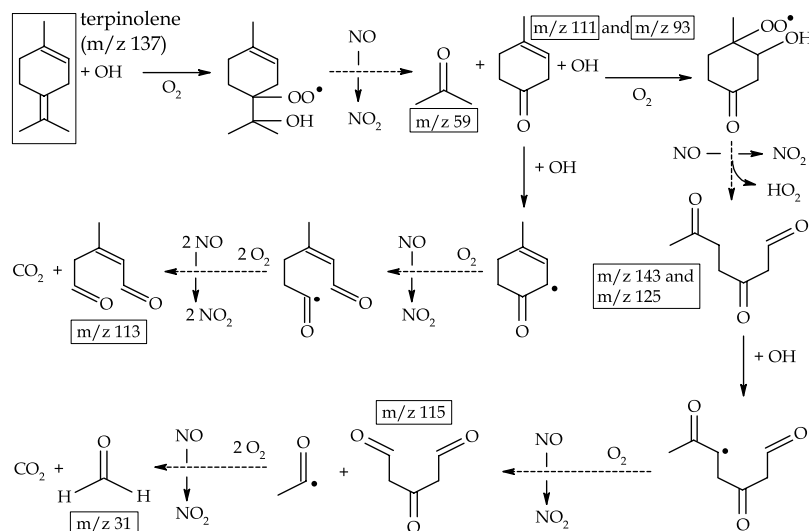


Figure 10. Partial mechanisms for the production of selected ions from terpinolene photooxidation. Because we focus on major product ions, or the product ions that were also observed by in ambient air by Holzinger *et al.* [2005], for clarity, other likely pathways and products are not shown.

for all ions, with the highest yield observed on m/z 71, at $12 \pm 3\%$. The carbon mass balance ($79 \pm 17\%$) was low compared to other C_{10} terpenes, suggesting that product ions were underestimated, possibly due to losses in tubing.

3.3.3. Linalool

[41] Linalool photooxidation produced SOA in substantially higher yield (13%) than from ozonolysis (1%) [Lee *et al.*, 2006]. As expected from its structure, linalool produced high yields of formaldehyde (43%) and acetone (25%). Numerous other product ions were observed. The dominant product was the C_7 compound, formed with acetone from OH attack on the internal double bond, occurring on m/z 129 and its dehydrated fragments m/z 111 ($R^2 = 0.97$) and 93 ($R^2 = 0.98$), formed at a yield of $75 \pm 10\%$. A product with MW = 128 has been reported elsewhere as 4-hydroxy-4-methyl-5-hexen-1-al and its cyclized isomer, with a yield of 46% [Shu *et al.*, 1997], which is nearly 1.6 times smaller than our observed yield (Table 8). OH attack at the internal double bond is expected to dominate over addition to the terminal double bond with a ratio of $\sim 77\%/23\%$ [Shu *et al.*, 1997]. This ratio is roughly consistent with our 75% yield of 4-hydroxy-4-methyl-5-hexen-1-al, but inconsistent with the 46% yield observed by [Shu *et al.*, 1997]. The formation of this product should also lead to the co-production of acetone, however, our low acetone yield, which is also low compared to the 51% reported elsewhere [Shu *et al.*, 1997], suggests that our acetone yield may be underestimated. Alternatively, our yield of 4-hydroxy-4-methyl-5-hexen-1-al may also be overestimated as a result of interference of other compounds on m/z 93, 111, or 129. Because of the good correlations between m/z 93 and 111 with m/z 129, and because of the good agreement in our 75% yield of the product formed from OH attack at the internal double bond with the expected branching ratio reported by [Shu *et al.*, 1997], we believe that our yield of 4-hydroxy-4-methyl-5-hexen-1-al is reasonable, but cannot find an explanation for the low yields we observed of the acetone co-product. Shu *et al.* [1997] also observed that OH attack at the terminal

double bond produces 6-methyl-5-hepten-2-one ($C_8H_{14}O$, MW = 126), with a yield of 6.8%, with the co-production of glycolaldehyde ($C_2H_4O_2$, MW = 60), which was not observed by Shu *et al.* [1997]. We observed a comparable yield of 8% for m/z 127, and yield of 17% for m/z 61, which may be dominated by glycolaldehyde but may still include some contribution from acetic acid. Numerous ions produced at high yields were observed in addition to the dominant C_7 product, including m/z 75, 99, 101, and 127, and were produced as different generational products, suggesting that the photooxidation of linalool results in numerous different products formed through a variety of mechanistic pathways. The carbon balance for linalool was $104 \pm 25\%$.

3.3.4. Isoprene

[42] SOA yield from isoprene photooxidation was low (2%), as has been shown from previous studies [Pandis *et al.*, 1991; Kroll *et al.*, 2005]. A high molar yield of formaldehyde (160%) contributed to $<30\%$ of the total carbon. The yields of methacrolein (MACR) and methyl vinyl ketone (MVK) could not be differentiated because they occur on the same m/z , thus we report the sum of the two products, whose yield ranged from $60\text{--}87 \pm 11\%$. The reported range results from uncertainty in the use of individual calibration factors for MACR and MVK in obtaining a concentration of the sum of the two compounds. The lower yield of MACR + MVK was calculated from a calibration factor that was the weighted average of individual calibrations factors for MVK:MACR of 1.45:1, based on reported yields of MVK and MACR from previous studies [Atkinson and Arey, 2003] and references therein. The higher yield of MACR + MVK was calculated from a calibration factor from a cylinder standard containing a mix of MVK and MACR in a ratio of 1.04:1 (MVK:MACR). Our observed yields of MACR + MVK were higher, but near the range of those obtained previously (Table 8). The yield of formaldehyde from isoprene oxidation that we obtained was extremely high compared to other studies.

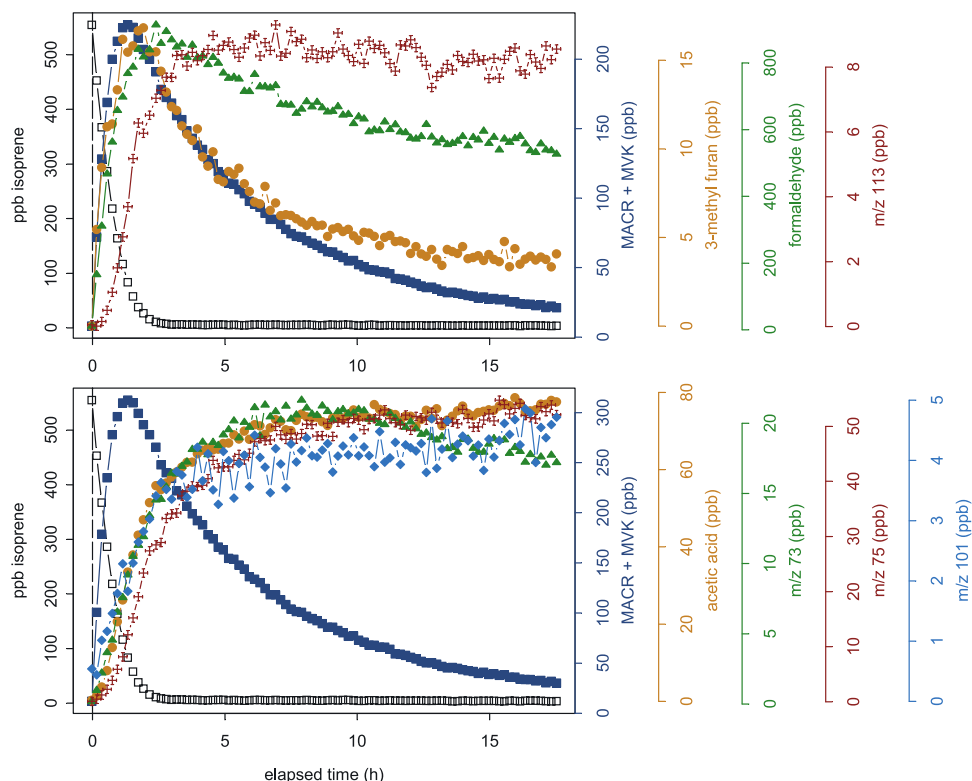


Figure 11. Time series of selected products from isoprene photooxidation. Blue squares represent MACR + MVK (top and bottom). Orange circles represent 3-methylfuran (top) or acetic acid (m/z 61) (bottom). Green triangles represent formaldehyde (top) or m/z 73 (bottom). Red crosses represent m/z 113 (top) or m/z 75 (bottom). The light blue diamonds represent m/z 101 (bottom).

Because the starting concentration of isoprene was high (~ 500 ppb), mixing ratios of formaldehyde were also high and well beyond the range of the calibrated linear response. Thus, the formaldehyde yield from isoprene is subject to significant error.

[43] Previously reported yields of MACR + MVK range from 54–61%, which is similar to our yield based on the weighted average of individual MACR and MVK calibration factors, suggesting that for isoprene oxidation, the PTR-MS is sensitive to the identities of the products that occur on m/z 71. In contrast to the high yields observed for formaldehyde and MACR + MVK, our yield of 3-methylfuran is similar to those reported elsewhere (Table 8). The carbon balance for isoprene was $101\text{--}114 \pm 22\%$. Other products identified by their m/z , including m/z 73, 75, 85, 99, 101 and 113, contributed to 20% of the carbon during the period when MACR + MVK and formaldehyde were co-dominant ($\sim 2.5\text{--}3$ hours).

[44] The time series for isoprene oxidation product ions show that several products are first-generation, including MACR + MVK and 3-methylfuran, and other products are second-generation, including m/z 113, and the ions m/z 61, 73, and 75 (Figure 11). The observed signal on m/z 61, reported as acetic acid ($\sim 6\%$ yield), may result from the production of glycolaldehyde, and m/z 73 and 75, likely corresponding to methylglyoxal and hydroxyacetone. Several ions were observed from isoprene photooxidation, including m/z 113, a dominant ion observed in ambient air

[Holzinger *et al.*, 2005], and m/z 101 (Table 8), which has also been observed by PTR-MS in ambient air above a tropical rain forest [Warneke *et al.*, 2001] and a tropical savanna [Holzinger *et al.*, 2002], and may be the C_5 hydroxycarbonyls reported by Zhao *et al.* [2004] and Baker *et al.* [2005].

[45] The production of hydroxycarbonyls from OH oxidation of isoprene were reported by Kwok *et al.* [1995], but were not quantified due to the lack of standards for those compounds. Using PTR-MS, Zhao *et al.* [2004] reported yields of C_5 hydroxycarbonyl products, based on the detection of m/z 101, of $19 \pm 6\%$, similar to the estimated combined yield of $\sim 15\%$ of two C_5 hydroxycarbonyls [Baker *et al.*, 2005]. These two yields are much larger than our observations of m/z 101 (Table 8). If m/z 101 is indeed a C_5 hydroxycarbonyl, we expect the compound to dehydrate and produce a fragment at m/z 83, and possibly m/z 65. The dominant ion produced from 3-methylfuran, however, also occurs on m/z 83, thus production of the C_5 hydroxycarbonyl would likely interfere and overestimate yields of 3-methylfuran. The yield of m/z 65 was only $\sim 30\%$ of m/z 101 ($R^2 = 0.91$). Because our observed yield of 3-methylfuran is similar to those reported elsewhere, and because m/z 101 and 65 were observed at such low mixing ratios, it is likely that the C_5 hydroxycarbonyls were not well detected by the PTR-MS, due to the production of other unknown fragments besides m/z 83 or 65. Additionally, Zhao *et al.* [2004] did not report the pressure in the PTR-MS reaction

chamber or the observed fragments of the C₅ hydroxycarbonyls, nor did they report yields of 3-methyl furan, thus it is unclear whether significant fragmentation of *m/z* 101 occurred, and whether they attributed their observations of *m/z* 83 to the C₅ hydroxycarbonyl instead of 3-methyl furan, or if the yield of the C₅ hydroxycarbonyl is based solely on *m/z* 101 and yields of 3-methyl furan are not reported for a different reason.

[46] Many ions, including *m/z* 113, 101, 75, 73, and 61 (acetic acid + glycolaldehyde) were clearly observed as second-generation products. Second- (or later-) generation products were found to contribute significantly to the SOA formed in this experiment [Ng *et al.*, 2006], and glycolaldehyde, hydroxyacetone, and methylglyoxal have recently been observed in the gas and particle phases in two forested environments in the United States [Matsunaga *et al.*, 2005]. However, other laboratory experiments have shown that SOA composition analyzed with an aerosol mass spectrometer from isoprene oxidation is very similar to SOA from MACR oxidation [Kroll *et al.*, 2006], and that MVK oxidation does not result in SOA production [Kroll *et al.*, 2005], suggesting that MACR oxidation products contributed to the SOA growth observed from isoprene photooxidation.

3.4. Relevance to Ambient Observations of Product Ions

[47] Observations of *m/z* 123, 151, and 169 can result from the oxidation of many different terpenes with endo double bonds, including α -pinene, 3-carene, γ -terpinene, α -terpinene, and limonene (Table 7), suggesting that these ions may not be unique indicators of rapid, within-canopy oxidation reactions, because they are formed from both slow and fast reacting terpenes. The ambient observations of *m/z* 111 and 113 suggested formation within the forest canopy from rapid oxidation of reactive terpenes [Holzinger *et al.*, 2005]. From these experiments, *m/z* 111 was observed at high yields from myrcene, terpinolene, and linalool. *m/z* 113 was observed as a product ion from all 16 terpenes, but was only formed at significant yields, and observed as a first-generation product, from myrcene photooxidation, suggesting that myrcene may be the dominant contributor to production of *m/z* 113 in ambient air. If concentrations of OH are elevated inside the canopy, as recently suggested [Goldstein *et al.*, 2004; Farmer *et al.*, 2005], the lifetime of myrcene may decrease enough, relative to the canopy mixing time, to contribute to the rapid chemistry suggested by Holzinger *et al.* [2005]. The better carbon mass balance obtained from the C₅ and C₁₀ experiments compared to the C₁₅ experiments suggest that additional uncertainty exists in the detection and quantification of sesquiterpene oxidation products. Additionally, the reactivity of β -caryophyllene and α -humulene with O₃, and the resulting difficulty in measuring their emission rates, suggest that these compounds or similar compounds are likely important for SOA production and rapid-within canopy chemistry, but their emissions are still poorly characterized and require further study. The results from these photooxidation experiments, and previous ozonolysis experiments [Lee *et al.*, 2006] confirm that the ions observed by Holzinger *et al.* [2005] are consistent with terpene oxidation products. Although the identities of these products and their precursor terpenes remain uncertain,

these experiments aid in identifying the important ions that can serve as markers for terpene reactivity and resulting SOA production in the real atmosphere.

4. Conclusions

[48] We conducted photooxidation experiments on 16 different terpenes to measure the time evolution and yields of gas-phase oxidation products and secondary organic aerosol. Yields of formaldehyde, acetone, and a few higher molecular weight oxidation products, such as nopinone, pinonaldehyde, and related acids, have been reported in the literature for a limited number of terpenes, and generally are in good agreement with the yields obtained from our experiments. Yields of SOA are also in good agreement with those reported elsewhere from experiments under similar experimental conditions. In addition to yields of previously reported compounds, we report yields of formaldehyde, acetaldehyde, formic acid, acetone, acetic acid, nopinone, pinonaldehyde, MACR + MVK, and numerous other identified and unidentified compounds characterized by their mass to charge ratio, for the entire suite of 16 terpene compounds. It is well known that the oxidation of any compound involves multiple steps, and the use of the PTR-MS in these experiments showed, in real time, the evolution of the different ions as first and second-generation oxidation products. These detailed time series, in conjunction with observed yields, aid in understanding and elucidating likely reaction pathways and structures for the unidentified products.

[49] The PTR-MS is emerging as an important tool for the measurement of primary and secondary gas-phase compounds in field campaigns. Mass scans of ambient air will undoubtedly measure unidentified compounds, and concurrent or prior measurements of primary emissions at the given site will aid in narrowing the possible identities of the observed ions. Our results confirm that the product ions observed by [Holzinger *et al.*, 2005] are consistent with terpene photooxidation reactions. Many different oxidation products likely contribute to the ions observed in ambient air. Observations of unidentified products [Holzinger *et al.*, 2005] and knowledge of primary emissions [Lee *et al.*, 2005], together with the results reported here of the identified, tentatively identified, and unidentified oxidation products from primary terpene compounds, aid greatly in understanding the magnitude and significance of within-canopy oxidation. Because the detection of very reactive parent terpene emissions is difficult in ambient air, observations of the ions described in this study can serve as markers for within-canopy chemistry and reactivity, and thus of SOA production. Observations of these product ions are likely to be of significant interest to scientists conducting field measurements in atmospheric chemistry, biosphere-atmosphere exchange of volatile organic compounds, and secondary organic aerosol composition. Further experiments to identify the compounds contributing to the unidentified products are necessary and will be more useful to laboratory chemists and kineticists for the elucidation of more complete terpene oxidation mechanisms.

[50] **Acknowledgments.** This material is based upon work supported by the National Science Foundation under grants 0119510 and 0443448.

Additional support was provided by the California Air Resources Board (contract 00-732). A. Lee was supported by a Graduate Research Education Fellowship from the U.S. Department of Energy's Global Change Education Program. The Caltech Indoor Chamber Facility is supported by the U.S. Environmental Protection Agency Science to Achieve Results (STAR) Program grant RD-83107501-0, and the U.S. Department of Energy grant DE-FG02-05ER63983. The authors are grateful to R. Holzinger for help in transporting and installing the PTR-MS in the Caltech Indoor Chamber Facility. We also thank the two anonymous reviewers for their thorough review and helpful comments.

References

- Arey, J., R. Atkinson, and S. M. Aschmann (1990), Product study of the gas-phase reactions of monoterpenes with the OH radical in the presence of NO_x, *J. Geophys. Res.*, *95*(D11), 18,539–18,546.
- Aschmann, S. M., A. Reissell, R. Atkinson, and J. Arey (1998), Products of the gas phase reactions of the OH radical with alpha- and beta-pinene in the presence of NO, *J. Geophys. Res.*, *103*(D19), 25,553–25,561.
- Aschmann, S. M., R. Atkinson, and J. Arey (2002), Products of reaction of OH radicals with alpha-pinene, *J. Geophys. Res.*, *107*(D14), 4191, doi:10.1029/2001JD001098.
- Atkinson, R., and J. Arey (2003), Gas-phase tropospheric chemistry of biogenic volatile organic compounds: A review, *Atmos. Environ.*, *37*, S197–S219.
- Atkinson, R., S. M. Aschmann, E. C. Tuazon, J. Arey, and B. Zielinska (1989), Formation of 3-methylfuran from the gas-phase reaction of OH radicals with isoprene and the rate-constant for its reaction with the OH radical, *Int. J. Chem. Kinet.*, *21*(7), 593–604.
- Baker, J., J. Arey, and R. Atkinson (2005), Formation and reaction of hydroxycarbonyls from the reaction of OH radicals with 1,3-butadiene and isoprene, *Environ. Sci. Technol.*, *39*(11), 4091–4099.
- Calogirou, A., D. Kotzias, and A. Ketrup (1997), Product analysis of the gas-phase reaction of b-caryophyllene with ozone, *Atmos. Environ.*, *31*(2), 283–285.
- Ciccioli, P., et al. (1999), Emission of reactive terpene compounds from orange orchards and their removal by within-canopy processes, *J. Geophys. Res.*, *104*(D7), 8077–8094.
- Claeys, M., et al. (2004), Formation of secondary organic aerosols through photooxidation of isoprene, *Science*, *303*(5661), 1173–1176.
- Cocker, D. R., R. C. Flagan, and J. H. Seinfeld (2001), State-of-the-art chamber facility for studying atmospheric aerosol chemistry, *Environ. Sci. Technol.*, *35*(12), 2594–2601.
- Day, D. A., P. J. Wooldridge, M. B. Dillon, J. A. Thornton, and R. C. Cohen (2002), A thermal dissociation laser-induced fluorescence instrument for in situ detection of NO₂, peroxy nitrates, alkyl nitrates and HNO₃, *J. Geophys. Res.*, *107*(D6), 4046, doi:10.1029/2001JD000779.
- Di Carlo, P., et al. (2004), Missing OH reactivity in a forest: Evidence for unknown reactive biogenic VOCs, *Science*, *304*(5671), 722–725.
- Faloona, I., et al. (2001), Nighttime observations of anomalously high levels of hydroxyl radicals above a deciduous forest canopy, *J. Geophys. Res.*, *106*(D20), 24,315–24,333.
- Farmer, D. K., P. J. Wooldridge, and R. C. Cohen (2005), Biosphere-atmosphere exchange of reactive nitrogen oxides over a midelevation Sierra Nevada forest, *Eos Trans. AGU*, *86*(52), Fall Meet. Suppl., Abstract A44B-01.
- Goldstein, A. H., M. McKay, M. R. Kurpius, G. W. Schade, A. Lee, R. Holzinger, and R. A. Rasmussen (2004), Forest thinning experiment confirms ozone deposition to forest canopy is dominated by reaction with biogenic VOCs, *Geophys. Res. Lett.*, *31*, L22106, doi:10.1029/2004GL021259.
- Griffin, R. J., D. R. Cocker, R. C. Flagan, and J. H. Seinfeld (1999), Organic aerosol formation from the oxidation of biogenic hydrocarbons, *J. Geophys. Res.*, *104*(D3), 3555–3567.
- Grosjean, D., E. L. Williams, and J. H. Seinfeld (1992), Atmospheric oxidation of selected terpenes and related carbonyls - Gas-phase carbonyl products, *Environ. Sci. Technol.*, *26*(8), 1526–1533.
- Guenther, A. B., et al. (1995), A global model of natural volatile organic compound emissions, *J. Geophys. Res.*, *100*, 8873–8892.
- Hakola, H., J. Arey, S. M. Aschmann, and R. Atkinson (1994), Product formation from the gas-phase reactions of OH radicals and O₃ with a series of monoterpenes, *J. Atmos. Chem.*, *18*(1), 75–102.
- Hatakeyama, S., K. Izumi, T. Fukuyama, H. Akimoto, and N. Washida (1991), Reactions of OH with alpha-pinene and beta-pinene in air: Estimate of global CO production from the atmospheric oxidation of terpenes, *J. Geophys. Res.*, *96*(D1), 947–958.
- Hoffmann, T., J. R. Odum, F. Bowman, D. Collins, D. Klockow, R. C. Flagan, and J. H. Seinfeld (1997), Formation of organic aerosols from the oxidation of biogenic hydrocarbons, *J. Atmos. Chem.*, *26*(2), 189–222.
- Holzinger, R., E. Sanhueza, R. von Kuhlmann, B. Kleiss, L. Donoso, and P. J. Crutzen (2002), Diurnal cycles and seasonal variation of isoprene and its oxidation products in the tropical savanna atmosphere, *Global Biogeochem. Cycles*, *16*(4), 1074, doi:10.1029/2001GB001421.
- Holzinger, R., A. Lee, K. T. Paw U, and A. H. Goldstein (2005), Observations of oxidation products above a forest imply biogenic emissions of very reactive compounds, *Atmos. Chem. Phys.*, *5*, 1–9.
- Jaoui, M., and R. M. Kamens (2001), Mass balance of gaseous and particulate products analysis from alpha-pinene/NO_x/air in the presence of natural sunlight, *J. Geophys. Res.*, *106*(D12), 12,541–12,558.
- Jaoui, M., and R. M. Kamens (2003a), Gas and particle products distribution from the photooxidation of a-humulene in the presence of NO_x, natural atmospheric air and sunlight, *J. Atmos. Chem.*, *46*, 29–54.
- Jaoui, M., and R. M. Kamens (2003b), Mass balance of gaseous and particulate products from beta-pinene/O₃/air in the absence of light and beta-pinene/NO_x/air in the presence of natural sunlight, *J. Atmos. Chem.*, *45*(2), 101–141.
- Kavouras, I. G., N. Mihalopoulos, and E. G. Stephanou (1999), Formation and gas/particle partitioning of monoterpenes photo-oxidation products over forests, *Geophys. Res. Lett.*, *26*(1), 55–58.
- Kesselmeier, J., and M. Staudt (1999), Biogenic volatile organic compounds (VOC): An overview on emission, physiology, and ecology, *J. Atmos. Chem.*, *33*, 23–88.
- Keywood, M. D., V. Varutbangkul, R. Bahreini, R. C. Flagan, and J. H. Seinfeld (2004), Secondary organic aerosol formation from the ozonolysis of cycloalkenes and related compounds, *Environ. Sci. Technol.*, *38*(15), 4157–4164.
- Kourtchev, I., T. Ruuskanen, W. Maenhaut, M. Kulmala, and M. Claeys (2005), Observation of 2-methyltetrols and related photo-oxidation products of isoprene in boreal forest aerosols from Hyytiälä, Finland, *Atmos. Chem. Phys.*, *5*, 2761–2770.
- Kroll, J. H., N. L. Ng, S. M. Murphy, R. C. Flagan, and J. H. Seinfeld (2005), Secondary organic aerosol formation from isoprene photooxidation under high-NO_x conditions, *Geophys. Res. Lett.*, *32*, L18808, doi:10.1029/2005GL023637.
- Kroll, J. H., N. L. Ng, S. M. Murphy, R. C. Flagan, and J. H. Seinfeld (2006), Secondary organic aerosol formation from isoprene photooxidation, *Environ. Sci. Technol.*, *40*, 1869–1877.
- Kurpius, M. R., and A. H. Goldstein (2003), Gas-phase chemistry dominates O₃ loss to a forest, implying a source of aerosols and hydroxyl radicals to the atmosphere, *Geophys. Res. Lett.*, *30*(7), 1371, doi:10.1029/2002GL016785.
- Kwok, E. S. C., R. Atkinson, and J. Arey (1995), Observation of hydroxycarbonyls from the OH radical-initiated reaction of isoprene, *Environ. Sci. Technol.*, *29*(9), 2467–2469.
- Lamanna, M. S., and A. H. Goldstein (1999), In situ measurements of C₂–C₁₀ volatile organic compounds above a Sierra Nevada ponderosa pine plantation, *J. Geophys. Res.*, *104*(D17), 21,247–21,262.
- Larsen, B. R., D. Di Bella, M. Glasius, R. Winterhalter, N. R. Jensen, and J. Hjorth (2001), Gas-phase OH oxidation of monoterpenes: Gaseous and particulate products, *J. Atmos. Chem.*, *38*(3), 231–276.
- Lee, A., G. W. Schade, R. Holzinger, and A. H. Goldstein (2005), A comparison of new measurements of total monoterpene flux with improved measurements of speciated monoterpene flux, *Atmos. Chem. Phys.*, *5*, 505–513.
- Lee, A., A. H. Goldstein, M. D. Keywood, S. Gao, V. Varutbangkul, R. Bahreini, N. L. Ng, R. C. Flagan, and J. H. Seinfeld (2006), Gas-phase products and secondary aerosol yields from the ozonolysis of ten different terpenes, *J. Geophys. Res.*, *111*, D07302, doi:10.1029/2005JD006437.
- Librando, V., and G. Tringali (2005), Atmospheric fate of OH initiated oxidation of terpenes: Reaction mechanism of alpha-pinene degradation and secondary organic aerosol formation, *J. Environ. Manage.*, *75*(3), 275–282.
- Lindinger, W., A. Hansel, and A. Jordan (1998), Proton-transfer-reaction mass spectrometry (PTR-MS): On-line monitoring of volatile organic compounds at pptv levels, *Chem. Soc. Rev.*, *27*(5), 347–354.
- Matsunaga, S. N., C. Wiedinmyer, A. B. Guenther, J. J. Orlando, T. Karl, D. W. Tooney, J. P. Greenberg, and Y. Kajii (2005), Isoprene oxidation products are a significant atmospheric aerosol component, *Atmos. Chem. Phys. Discuss.*, *5*, 11,146–11,156.
- Miyoshi, A., S. Hatakeyama, and N. Washida (1994), OH radical-initiated photooxidation of isoprene: An estimate of global CO production, *J. Geophys. Res.*, *99*(D9), 18,779–18,787.
- Ng, N. L., J. H. Kroll, M. D. Keywood, R. Bahreini, V. Varutbangkul, R. C. Flagan, J. H. Seinfeld, A. Lee, and A. H. Goldstein (2006), Contribution of first- versus second-generation products to secondary organic aerosols formed in the oxidation of biogenic hydrocarbons, *Environ. Sci. Technol.*, *40*, 2283–2297.
- Noziere, B., and I. Barnes (1998), Evidence for formation of a PAN analogue of pinonic structure and investigation of its thermal stability, *J. Geophys. Res.*, *103*(D19), 25,587–25,597.

- Noziere, B., M. Spittler, L. Ruppert, I. Barnes, K. H. Becker, M. Pons, and K. Wirtz (1999), Kinetics of the reactions of pinonaldehyde with OH radicals and with Cl atoms, *Int. J. Chem. Kinet.*, *31*(4), 291–301.
- Orlando, J. J., B. Noziere, G. S. Tyndall, G. E. Orzechowska, S. E. Paulson, and Y. Rudich (2000), Product studies of the OH- and ozone-initiated oxidation of some monoterpenes, *J. Geophys. Res.*, *105*(D9), 11,561–11,572.
- Pandis, S. N., S. E. Paulson, J. H. Seinfeld, and R. C. Flagan (1991), Aerosol formation in the photooxidation of isoprene and beta-pinene, *Atmos. Environ., Part A*, *25*(5–6), 997–1008.
- Paulson, S. E., R. C. Flagan, and J. H. Seinfeld (1992), Atmospheric photooxidation of isoprene. 1. The hydroxyl radical and ground-state atomic oxygen reactions, *Int. J. Chem. Kinet.*, *24*(1), 79–101.
- Peeters, J., L. Vereecken, and G. Fantechi (2001), The detailed mechanism of the OH-initiated atmospheric oxidation of alpha-pinene: A theoretical study, *Phys. Chem. Chem. Phys.*, *3*(24), 5489–5504.
- Reissell, A., C. Harry, S. M. Aschmann, R. Atkinson, and J. Arey (1999), Formation of acetone from the OH radical- and O₃-initiated reactions of a series of monoterpenes, *J. Geophys. Res.*, *104*(D11), 13,869–13,879.
- Reissell, A., S. M. Aschmann, R. Atkinson, and J. Arey (2002), Products of the OH radical- and O₃-initiated reactions of myrcene and ocimene, *J. Geophys. Res.*, *107*(D12), 4138, doi:10.1029/2001JD001234.
- Schade, G. W., and A. H. Goldstein (2003), Increase of monoterpene emissions from a pine plantation as a result of mechanical disturbances, *Geophys. Res. Lett.*, *30*(7), 1380, doi:10.1029/2002GL016138.
- Shu, Y. G., and R. Atkinson (1994), Rate constants for the gas-phase reactions of O₃ with a series of terpenes and OH radical formation from the O₃ reactions with sesquiterpenes at 296 ± 2-K, *Int. J. Chem. Kinet.*, *26*(12), 1193–1205.
- Shu, Y. H., E. S. C. Kwok, E. C. Tuazon, R. Atkinson, and J. Arey (1997), Products of the gas-phase reactions of linalool with OH radicals, NO₃ radicals, and O₃, *Environ. Sci. Technol.*, *31*(3), 896–904.
- Song, C., N. Kwangsam, and D. R. Cocker (2005), Impact of hydrocarbon to NO_x ratio on secondary organic aerosol formation, *Environ. Sci. Technol.*, *39*, 3143–3149.
- Sprengnether, M., K. L. Demerjian, N. M. Donahue, and J. G. Anderson (2002), Product analysis of the OH oxidation of isoprene and 1,3-butadiene in the presence of NO, *J. Geophys. Res.*, *107*(D15), 4268, doi:10.1029/2001JD000716.
- Tuazon, E. C., and R. Atkinson (1990), A product study of the gas-phase reaction of isoprene with the OH radical in the presence of NO_x, *Int. J. Chem. Kinet.*, *22*(12), 1221–1236.
- Vereecken, L., and J. Peeters (2004), Nontraditional (per)oxy ring-closure paths in the atmospheric oxidation of isoprene and monoterpenes, *J. Phys. Chem. A*, *108*(24), 5197–5204.
- Vinckier, C., F. Comperolle, A. M. Saleh, N. Van Hoof, and I. Van Hees (1998), Product yields of the alpha-pinene reaction with hydroxyl radicals and the implication on the global emission of trace compounds in the atmosphere, *Fresenius Environ. Bull.*, *7*(5–6), 361–368.
- Warneke, C., et al. (2001), Isoprene and its oxidation products methyl vinyl ketone, methacrolein, and isoprene related peroxides measured online over the tropical rain forest of Surinam in March 1998, *J. Atmos. Chem.*, *38*, 167–185.
- Wisthaler, A., N. R. Jensen, R. Winterhalter, W. Lindinger, and J. Hjorth (2001), Measurements of acetone and other gas phase product yields from the OH-initiated oxidation of terpenes by proton-transfer-reaction mass spectrometry (PTR-MS), *Atmos. Environ.*, *35*(35), 6181–6191.
- Yu, J. Z., R. J. Griffin, D. R. Cocker, R. C. Flagan, J. H. Seinfeld, and P. Blanchard (1999), Observation of gaseous and particulate products of monoterpene oxidation in forest atmospheres, *Geophys. Res. Lett.*, *26*(8), 1145–1148.
- Zhao, J., R. Zhang, E. C. Fortner, and S. W. North (2004), Quantification of hydroxycarbonyls from OH-isoprene reactions, *J. Am. Chem. Soc.*, *126*, 2686–2687.

R. C. Flagan, J. H. Kroll, N. L. Ng, J. H. Seinfeld, and V. Varutbangkul, Department of Environmental Science and Engineering and Department of Chemical Engineering, California Institute of Technology, Pasadena, CA 91125, USA.

A. H. Goldstein and A. Lee, Department of Environmental Science, Policy, and Management, University of California, Berkeley, Berkeley, CA 94720-3114, USA. (ahg@nature.berkeley.edu)